Ministry of Earth Sciences
(Government of India)

ENVIRONMENTAL IMPACT STATEMENT

Environmental conditions and likley impact in the area selected for nodule collection trials at the Indian PMN site in the Central Indian Ocean Basin

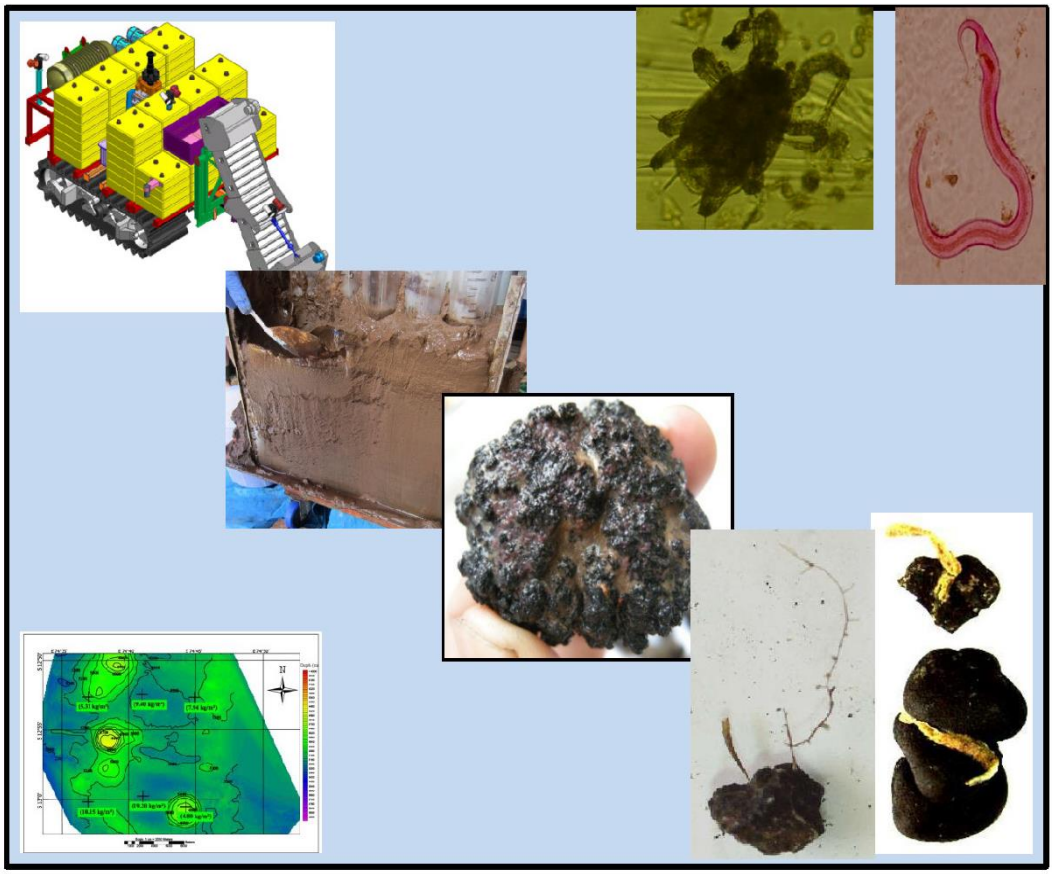

Report submitted to

The International Seabed Authority, Jamaica

Jan 2020

List of contributors

Coordinated and compiled by :	Dr. Rahul Sharma and Dr. B. Nagender Nath
With contributions from:	
Dr. Rahul Sharma	Chief Scientist (Retd.), CSIR-National Institute of Oceanography, Goa
Dr. B. Nagender Nath	Chief Scientist (Retd.), CSIR-National Institute of Oceanography, Goa
Dr. Baban Ingole	Chief Scientist (Retd.), CSIR-National Institute of Oceanography, Goa
Dr. V.S.N Murty	Chief Scientist (Retd.), CSIR-National Institute of Oceanography, Goa
Dr. N.H. Khadge	Senior Principal Scientist, CSIR-National Institute of Oceanography, Goa
Dr. Maria Brenda Mascarenhas – Pereira	Principal Scientist, CSIR-National Institute of Oceanography, Goa
Dr. M T Babu	Principal Technical Officer (Retd.), CSIR-National Institute of Oceanography, Goa
Dr. Mani Murali	Senior Scientist, CSIR-National Institute of Oceanography, Goa
Mr. S. Jai Sankar	Senior Technical Officer, CSIR-National Institute of Oceanography, Goa
Mr. Jayesh Patil	Project Assistant II, CSIR-National Institute of Oceanography, Goa
Mr. Virsen Gaikwad	Project Assistant II, CSIR-National Institute of Oceanography, Goa
Dr. MA Atmanand	Director, National Institute of Ocean Technology, Chennai
Dr. GA Ramadass	Scientist G, National Institute of Ocean Technology, Chennai
Mr. Gopkumar K	Scientist F, National Institute of Ocean Technology, Chennai
Dr Vijay Kumar	Advisor, Ministry of Earth Sciences, New Delhi
Dr. T.R.P. Singh	Hon. Advisor, Ministry of Earth Sciences, New Delhi

Contents

Executive Summary

The Ministry of Earth Sciences (Government of India) proposes to conduct technical trials for demonstration of its nodule collector pre-prototype machine in the Indian contract area of Central Indian Ocean Basin (CIOB) during 2021. The objective of the trial is to test the capability of the machine in terms of locomotion, crushing, pumping and discharge within a limited area on the seabed. It is also proposed to collect environmental data before and after the trials as well as over a period of time to assess the extent of impact on physico-chemical and biological conditions.

During the trial, nodule collector with two pickup units of 0.8 m width each mounted on two moving tracks on either side will be operated over a cumulative distance of 1000 m and collect nodules from sediment layer down to 15-30 cm. In the initial trial, the nodules collected through the pickup unit will be crushed to 1-20 mm size and released behind the collector; whereas in the subsequent trial, the same will be pumped up to ~80m above and released in the near bottom water column. The collector speed is expected to be 0.15 m/sec and the pumping will be carried out at a maximum rate of 80 cum/hour.

As per the ‘Recommendations for the guidance of contractors for assessment of possible environmental impacts arising from exploration for marine minerals in the Area’ (ISBA/25/LTC/6), section VI B identifies ‘(b) testing of collection systems and equipment’ as one of the activities ‘requiring environmental impact assessment’andas per Para 34 of the same guidelines, the contractor is mandated to submit a‘prior environmental impact assessment (EIA) report’to the International Seabed Authority (ISA)before the activitytakes place. Accordingly this report is submitted. It initially describes the background information as well as the project history and the scope. Later, the report provides a general description of the area and mineral resource, as well as technical information of the proposed nodule collection systems (as per Para 38 of ISBA/25/LTC/6) which includes the mineral collection technique, expected depth of penetration, running gear, methods of separation of mineral resource and sediment on the seafloor, processing and crushing, and methods for transporting, separation on the vessel, and those dealing with abraded fines and sediment, followed by the plan of work for sea trials.

Based on extensive baseline environmental data collected during several expeditions, the existing physico-chemical environment comprising of bathymetry, sediment properties, water column and meteorological data, as well as biological environment comprising of water column

biology, benthic faunal communities, nodule associated fauna and community structure are described for their spatial, temporal and seasonal variability on a regional scale over several years as well as local conditions within the Impact Reference Zone (IRZ) and Preserved Reference Zone (PRZ) in the Central Indian Basin.

India was one of the few entities to conduct a Benthic Impact Experiment (BIE) called the Indian Deep-sea Environment Experiment (INDEX) in 1997, which was similar to those conducted by National Oceanography and Atmosphere Administration (NOAA-BIE), Japan (JET), InterOceanMetal (IOM-BIE), besides Germany that had conducted the Disturbance and Recolonization (DISCOL) study. During INDEX, a Deep-Sea Sediment Resuspension System (DSSRS) was used to simulate conditions similar to deep-sea mining, albeit on a small scale, at 5100 m depth in the nodule area of CIOB for a period of 9 days resuspending ~580 tons of (dry) sediment into the near bottom waters. The impact analyzed using core samples, sediment trap and current data, photographic records as well as water samples, showed vertical mixing of sediments, lateral migration of sediment plume, changes in physico-chemical characteristics of sediment and reduction in biomass immediately after the experiment. However, long term monitoring showed that the influence of natural variability was evident in most parameters and that the initial impact of the experiment had waned off to a large extent suggesting that over a period of time, the natural environmental variability masks the effect of disturbance.

Estimates of the proposed collection trials show that the maximum impact is expected over a direct area of 4600 m^2, impacting 690m^3 by volume or 828kg by weight of sediment, of which the sediment picked along with nodules could be 1600 kg (20% by weight of nodule) considering 50% efficiency of the collector. In terms of scale, the overall impact of the collection trials would be $\leq$1 % of the Benthic Impact Experiment (INDEX) conducted by India in 1997, which in itself was considered to be extremely small in comparison to commercial mining. The report further describes the potential impacts on physico-chemical and biological environment due to the nodule collection trials, that are expected to be extremely minor considering that the trials are restricted to a track of maximum of 1000 m in length, which will be conducted for a couple of hoursduring 2-3 deployments.

Due to such small scale activity, it is expected that no serious harm is expected to be caused to the seafloor environment or in the near bottom water column. Small scale impacts due to compaction during locomotion of the collector, or due to nodule removal, sediment

redeposition and bio-geochemical alteration are expected that would get restored within a short span of time in view of the weak currents and recolonisation by biological communities from adjacent areas. No permanent damages, however, are expected to affect the gene flow and biogeochemical continuity. It is also proposed to monitor various environmental parameters in the proposed IRZ and PRZ indicative of restoration of pre-operation conditions as well as natural variability. It is expected that the results of this study will provide useful information on impacts of such small scale activities and develop protocols for monitoring of large scale mining. Moreover, the nodule collection trials would help in improving / upscaling the systems for further development of proto type as well as commercial mining systems in future.

1. Introduction

1.1 Background of the project

In its endeavor to develop deep-sea polymetallic nodules as an alternative source for metals in future, India has been consistently conducting activitiesin all the four components of deep-sea mining, viz. exploration and resource evaluation, mining system development, metallurgical processing as well as environmental impact assessment (Fig. 1.1.1).

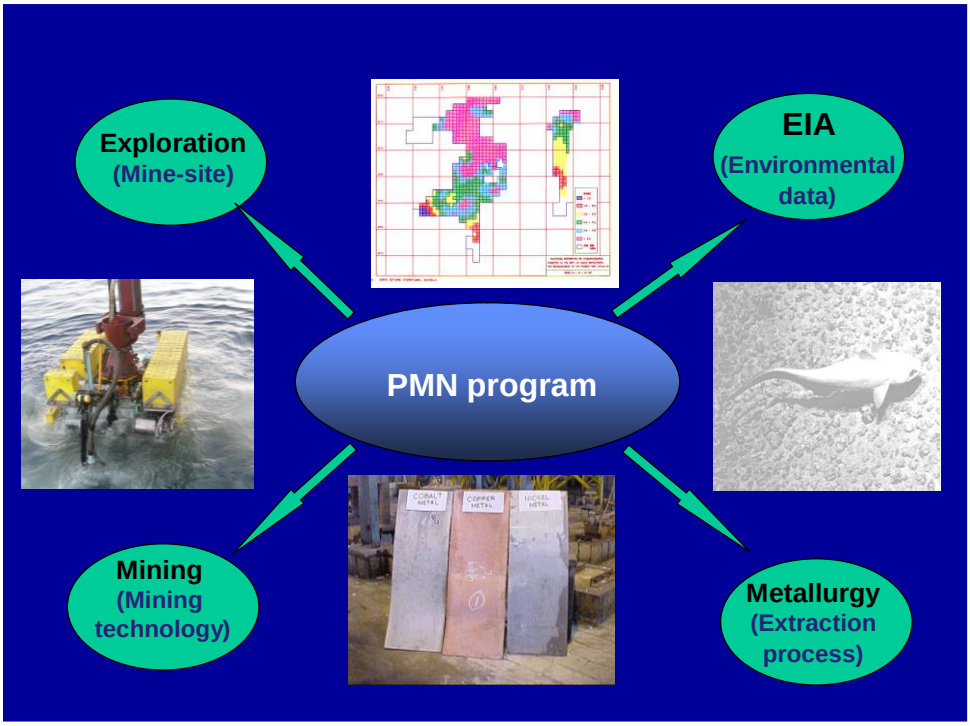

Fig. 1.1.1: Components of Indian Polymetallic Nodules Program

India embarked on its mission for exploration of deep-sea minerals with the recovery of the first polymetallic nodule samples by the Indian Research Vessel Gaveshani on the 26 of January 1981. This was followed by the formulation of a national Polymetallic Nodules (PMN) program with concerted efforts that led to India being given the Pioneer Investor status with exploration rights over an area of 1,50,000 sq km. (Fig. 1.1.2) in Central Indian Ocean Basin (CIOB) under the UN Convention on Law of the Sea (UNCLOS). Subsequently, through periodic relinquishments, an area of 75,000 km^2 has been retained by India as per the contract with the International Seabed Authority (ISA). Based on nodule abundance, grade and bathymetry, a

block of ~13.875 km x 13.875 km is demarcated as the Impact Reference Zone (IRZ) for conducting the proposed trials of the nodule collector.

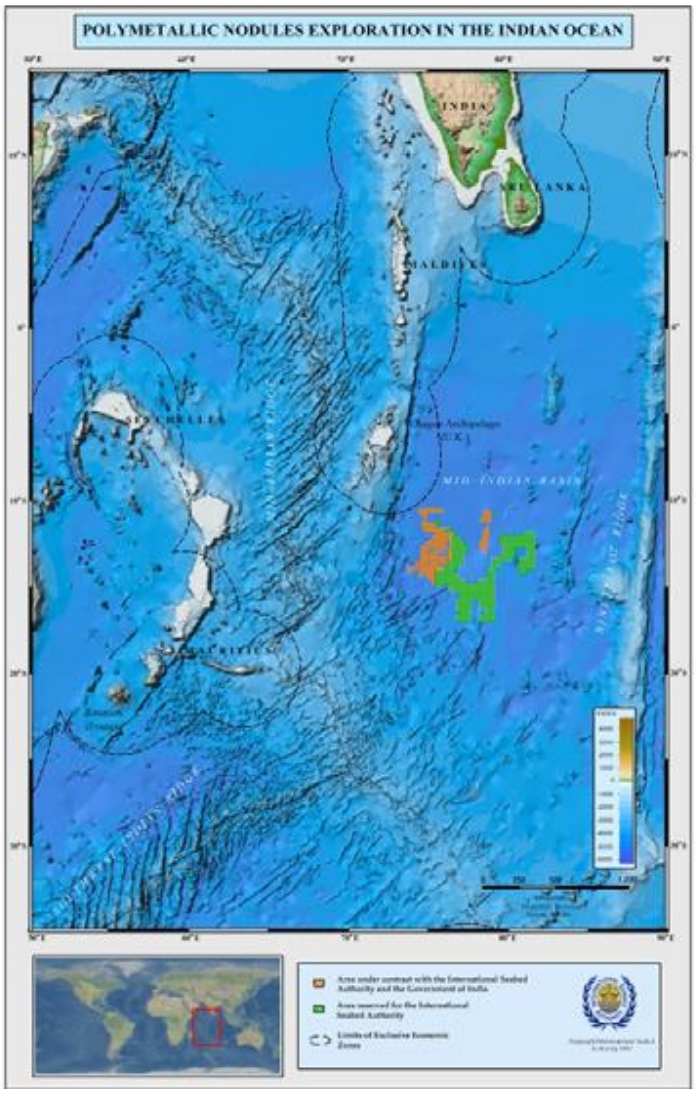

Fig. 1.1.2: Pioneer area and reserved area in Central Indian Ocean Basin
(Source: www.isa.org.jm)

Arising from the need for evaluation of environmental data for prediction of potential impact of mining on marine ecosystem, the project on 'EIA studies for nodule mining in CIOB' was initiated in 1996. The program was funded by Ministry of Earth Sciences (erstwhile Dept. of Ocean Development), Govt. of India and implemented by CSIR-National Institute of Oceanography (NIO, Goa), a constituent laboratory of Council of Scientific and Industrial Research (CSIR-NIO).

The objectives of the program included:

- To establish baseline conditions of marine environment in the area
- To assess the potential impact of nodule mining on marine ecosystem by simulating a benthic disturbance
- To understand the processes of restoration and re-colonisation of benthic environment
- To provide scientific inputs for mitigation of environmental impact due to deep-sea mining operations

The project was being conducted in following phases

Phase I: 1995-1997 - Baseline data collection for identification of experimental disturbance site (EDS-Test area) and preservation reference site (PRS-Reference area)

Phase II: 1997-2005- Benthic impact experiment and long-term monitoring of impact and restoration of environmental conditions in EDS and PRS

Phase III: 2003-2012 - Environmental variability data collection and creation of database

Phase IV: 2012-2015 - Comprehensive analysis of environmental conditions in Contract area

Phase V: 2015 onwards - Environmental data collection and monitoring in Impact Reference Zone (IRZ) and Impact Reference Zone (PRZ)

Simultaneously, India has also been working on developing deep sea mining technology in a phased manner. To minimize developmental costs and associated risks, initial efforts were focused on realization and qualification of machinery for long term operations in shallow waters, followed by further development of machinery for deeper waters.An initial study was carried out on the various deep sea mining concepts and the flexible riser concept was chosen for further development.

It is proposed to carry out the trials of thepre-prototype nodule collector system in the CIOB during 2021. As per the ISA guidelines, it is required to prepare a prior-EIA report which is required to be submitted to ISA in advance. This report, based on the environmental data collected so far both on regional and local scale, presents the baseline conditions in the proposed area of operation and an assessment of environmental data and the likely impacts in area selected for collection trials of nodules in Central Indian Ocean Basin.

1.2 Project history

1.2.1 Exploration program

A timeline of major activities under the PMN program is shown in Table 1.2.1.1.

Table 1.2.1.1: Major milestones under exploration in the CIOB

January 26,1981	First nodule sample collected by Indian scientists on
April, 1982	India recognized as Pioneer Investor
August 1982-87	3 million sq.km area explored
August 1987	Pioneer Area Allocation to India (150,000 sq.km)
July 1994	First relinquishment of 20% area
October 1996	Second relinquishment of 10% area
2002	Third and final relinquishment of 20% area
2008	First Generation Mine Site Identified
2013	Test Mine Site (Impact Reference Zone) identified

During the course of the exploration program, the quantum of data collection is given in Table 1.2.1.2.

Table 1.2.1.2: Quantum of data collected and major outputs during PMN exploration

Area Surveyed	~3 Million Sq.km
Nodule sampling (by free fall grab, photo grab, Van veen grab, Okean grab etc).	Over 2500 locations with 5-7 operations in each station.
Total number of sampling operations	~ 10,900
Grid of sampling	Completed 0.125° (~14 km) km grid in entire Pioneer area, and 0.0625° (~7 km) grid in a part of the area measuring approximately 18,400 km^2
Total Bulk nodules Collected (by Dredging)	300 tons
Seabed photographs	>50,000
Echosounding (12 and 3.5 Khz echosounder)	500000 lkm
Multibeam Swath bathymetry	300000 sq.km
High resolution Multibeam swath bathymetry	12,000 lkm
Sediment Coring (Box/spade cores)	~ 50 stations.
No of expeditions	76
Ships used (8)	RV Gaveshani, ORV Sagarkanya, MV Farnella, DSV Nand Rachit ,MV GA Reay, MV Skandi Surveyor, RV AA Sidorenko, Akademik Boris Petrov
Scientific Publications (in national and international journals)	>350 (>25 Ph.D.s)

The sampling gird for quantification of nodule resources and subsequent relinquishments is shown in Fig. 1.2.1.1

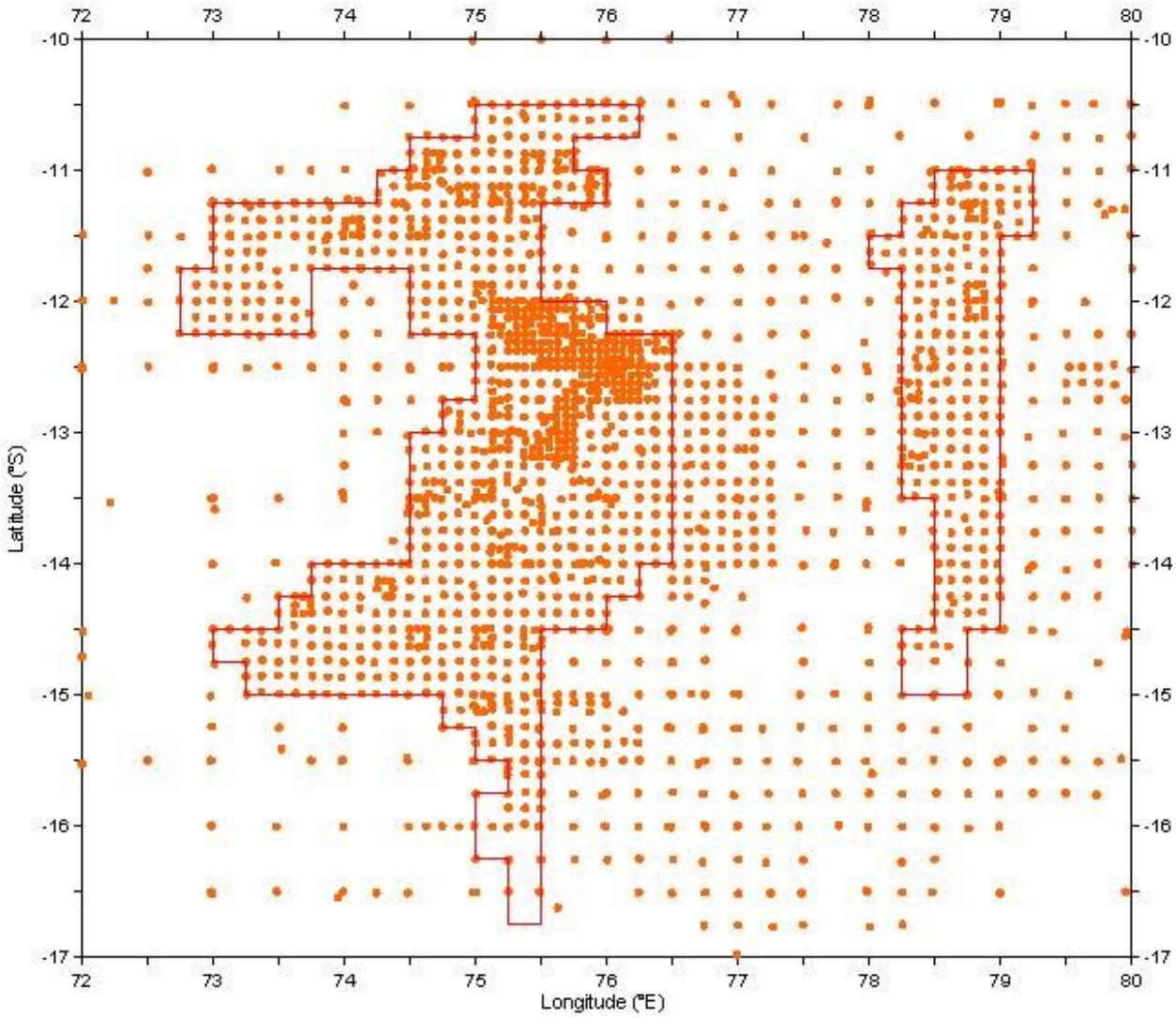

Fig. 1.2.1.1: Sampling grid for nodule estimation

Besides sampling a detailed high resolution mapping of the seafloor was undertaken using multi-beam system (Fig. 1.2.1.2).

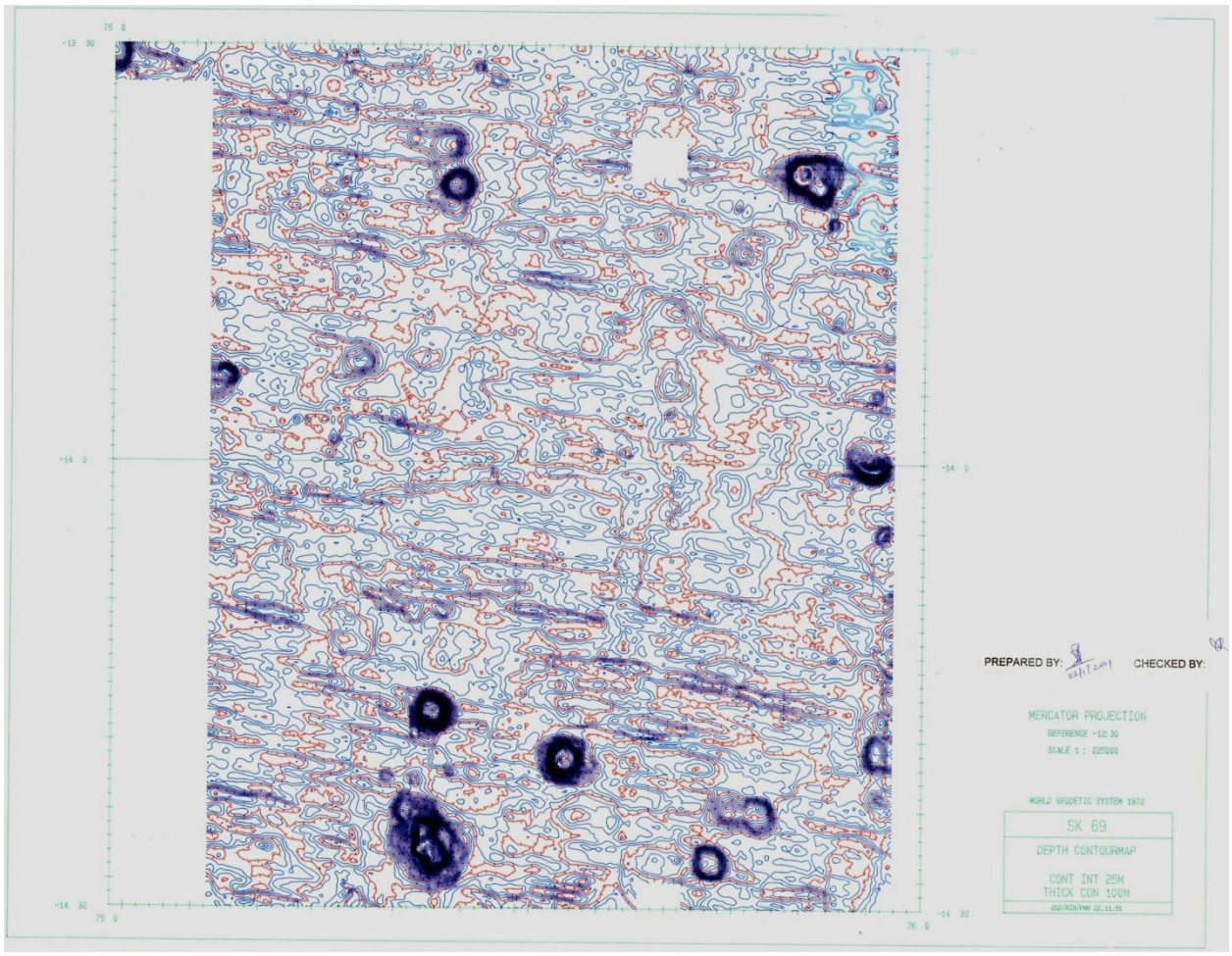

Fig. 1.2.1.2: Sample multi-beam bathymetry map of CIOB

Based on nodule abundance (Fig.1.2.1.3), grade and bathymetry, areas for relinquishment were identified (Fig. 1.2.1.4).

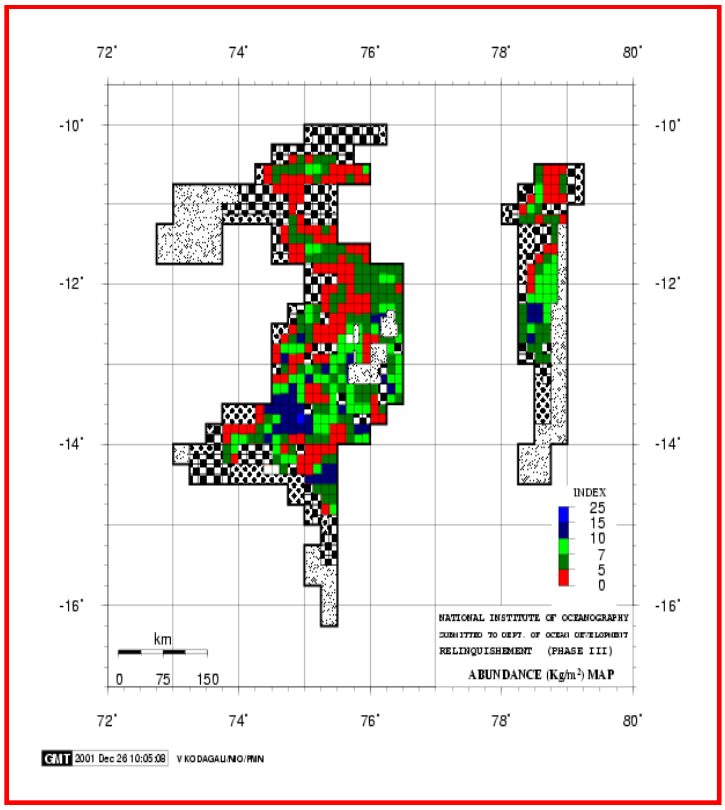

Fig. 1.2.1.3: Abundance map of Indian retained area

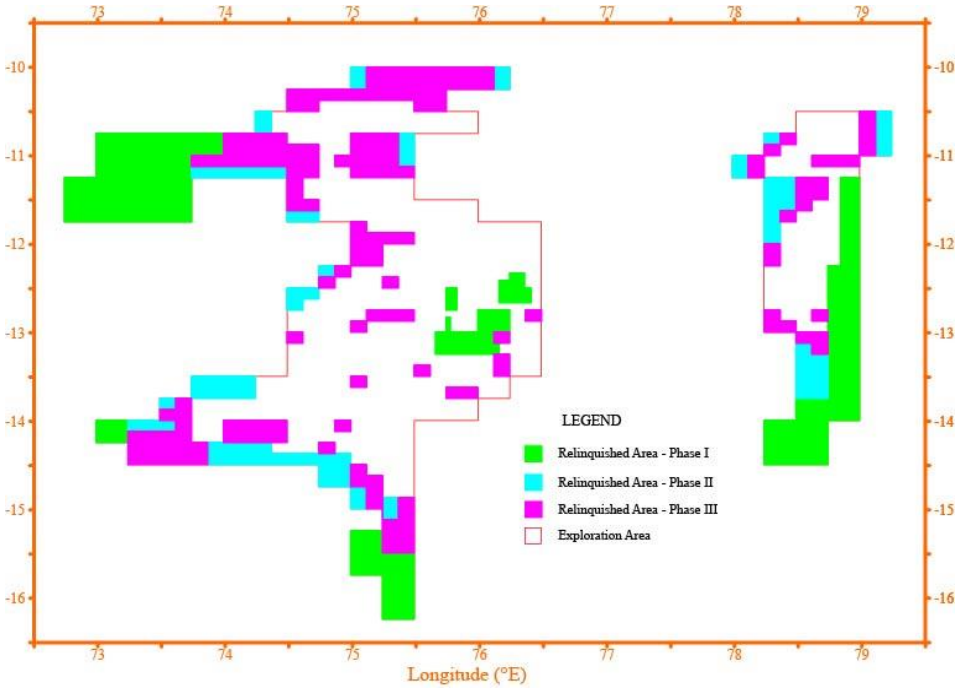

Fig. 1.2.1.4: Relinquishment phases in CIOB

The estimated resource (MMT) in the Indian area during different phases is given in Table 1.2.1.3

Table 1.2.1.3: Estimated resources (in MMT) during different phases of relinquishment

Resource	Pioneer Area (150,000 km^2)	Retained Area after Phase I (120,000 $km^{2)}$	Retained Area after Phase II (105,000 km^2)	Exploration Area (75,000 km^2)
Nodules (Dry)	607	490	455	382.8
Mn	144.5	120	113	95.17
Co	0.87	0.66	0.59	0.418
Ni	7.0	5.9	5.5	4.509
Cu	6.34	5.5	5.3	4.455
Total Metal	158.71	132.06	124.39	104.552

1.2.2 Environmental studies

The environmental studies for nodule mining have been conducted since 1995 to establish baseline conditions in nodule areas, assess potential environmental impact of mining, and understand processes of restoration / recolonisation and providing environmental inputs for nodule mining.

Subsequently, the International Seabed Authority has issued the 'Recommendations for guidance of the contractors for assessment of possible environmental impacts arising from exploration for marine minerals in the Area (ISBA/19/LTC/8, July 2013)' that require the following information from a Contractor:

- Baseline data in the proposed mining area
- Test and reference sites for environmental monitoring
- Results of simulated impact experiment
- Expected environmental impact due to mining
- Critical parameters for monitoring impacts
- Proposed measures to minimize the effects

The major activities conducted under the EIA program are described in Table 1.2.2.1. Data collected on different environmental parameters during these phases is shown in Table 1.2.2.2.

In order to achieve this, 14 expeditions using 6 research vessels have been conducted for collecting environmental data a variety of techniques such as sediment sampling, sounding, camera profiles, CTD profiles with water sampling and moorings (Table 1.2.2.3).

Table1.2.2.1: Schedule of major activities for environmental studies in CIOB.

Period	Activity
1995-1997	Baseline data in EDS* and PRS*
1997-2005	Benthic impact experiment and monitoring the impact in EDS* and PRS*
2003-2012	Collection of environmental variability data
2012-2015	Comprehensive analysis of environmental conditions in Contract area
2015-2022	Baseline environmental studies at IRZ*& PRZ* and evaluation of impact of collector test

*EDS-Experimental disturbance site, PRS-Preservation reference site, IRZ-Impact Mining Zone, PRZ –Preserved Reference Zone

Table 1.2.2.2: Key parameters analyzed under multi-disciplinary environmental studies

Discipline	Parameters analysed
Physical	Bathymetry, sediment thickness, currents, temperature, salinity, turbidity
Chemical	pH, Eh, nitrate (NO_2), nitrite (NO_3), phosphate (PO_4), silicate (SiO_2), DO
Sediment characteristics (i) Basic properties of sediments (ii) Geochemistry of sediments & pore water	Grain size (sand, silt, clay %). Moisture content, Specific gravity, Wet density, Shear strength. Organic carbon and trace metals in sediments and pH& nutrients in pore water
Biological communities (i) Seafloor communities (ii) Biochemistry & microbiology (iii)Biological character of water	Macrofauna density, total meiofauna, Protein, Carbohydrates, Lipids, AODC, ATP Chlorophyll, Primary productivity
Sedimentation	Settling fluxes, quantum, nature and composition

Table 1.2.2.3: Data collection in different phases of the project (EDS=Experimental Disturbance Site, PRS=Preservation Reference Site, N=Nodule area)

Phase	Ship	Cruise#	Year	Sediment sampling stations			Sounding(Km)			Cameraprofiles		CTD + water stations			Current meter Moorings		
				EDS	PRS	N	EDS	PRS	N	EDS	PRS	EDS	PRS	N	EDS	PRS	N
Baseline	Sidorenko	12	1995														3
	Sidorenko	16	1996	26	26		600	600									
	Sidorenko	17	1996	13			300										
	Sidorenko	18	1996														4
	Sagar Kanya	120	1997											28			
	Yuzhmorgeol	3A	1997											6			
	Yuzhmorgeol	3B	1997											2			
Pre-disturbance	Yuzhmorgeol	3A	1997	17						7					10		
	Yuzhmorgeol	3B	1997									2					
Post-disturbance	Yuzhmorgeol	3B	1997	16						7		2					
Monitoring – I	Sidorenko	34	2001	14	5					5	1	2					
Monitoring – II	Sidorenko	46	2002	11	2												
Monitoring – III +EVD-I	Sidorenko	61	2003	12	3	26											
Monitoring – IV +EVD-II	Boris Petrov	04	2005	5	3	25											
EVD-III	Boris Petrov	26	2007			22											
EVD-IV	Boris Petrov	38	2009			2								2			
Env. Data in IRZ, PRZ	Sindhu Sadhana	13	2015	5	5	3	50	50				1	1	1			
Total	Ships= 6	14		119	44	78	950	650		19	1	7	1	39			17

Environmental data generated has been archived in several databases generated for the activity (Table 1.2.2.4).

Table 1.2.2.4: Databases generated during environmental studies

Database*	Phases included	Parameters included	Contents
PMN-EIA database - I	Baseline, Pre-disturbance, Post-disturbance	All parameters of water column and benthic environment	EIA metadata (MS Word) EIA analyzed data tables (MS Access) EIA reports (Multipage compressed Tiff)
PMN-EIA database-II	Monitoring-I, Monitoring-II, Monitoring-III, Monitoring-IV	All parameters of benthic environment	EIA metadata (MS Word) EIA analyzed data tables (MS Access) EIA reports (MS Word)
PMN-EIA database-III	EVD-I, EVD-II, EVD-III EVD-IV	All parameters of benthic environment	EVD metadata tables (MS Word) EVD analyzed data tables (MS Access) EVD reports (Adobe Acrobat)

*All data submitted to ISBA

The findings during each of the phases of the environmental program are described in different sections of this report.

1.2.3 Development of underwater mining system

An underwater mining system for operations and the flexible riser concept was validated in the Indian seas at 410 m water depth jointly by National Institute of Ocean Technology (NIOT) and InstitutfürKonstruktion (IKS) of University of Siegen, Germany. The tests instilled confidence to carry out further studies that led to modifications in the mining system and mother vessel subsequently. The results from the tests were analyzed and it was decided to augment the mother vessel with Dynamic Positioning System (DPS) and Launch and Recovery Systems (LARS) to facilitate long term operations. The underwater system was completely dismantled and the condition of components was analyzed. The system was augmented with increased buoyancy packs, provided with fins for increased cooling rate, and distributed pressure compensated systems for enhanced performance. The modified system was tested for long-term operations at 451 m depth off Goa coast during March 2006. During the next phase, the underwater collector and crushing systems were developed, the solids pump modified for large solids handling capability, chassis widened to accommodate the slurry pump in between the tracks of the mining machine, hydraulics systems enhanced to

provide fluid power for collector and crusher, electronics, instrumentation and control systems upgraded. Artificial nodules were developed having the same aggregate impact index as that of manganese nodules. A remotely operable artificial nodule laying system was developed to create a nodule carpeted tracks at 500 m depth and tested off Chennai coast in 2007. The mining machine was integrated and tested in the test pond in March 2010 followed by sea trials during September.- October 2010.

A remotely operated deep-sea in-situ soil tester has been developed and successfully tested at 5200 m depth in the CIOB. The results from the trials done on the Underwater Collection and Crushing systems at 512 m depth during October 2010 gave confidence for undertaking the main project involving development of integrated mining system using flexible riser concept. A project has been undertaken for accomplishment of this major task with the objective of designing and developing a new crawler based mining machine capable of collecting and pumping nodules from water depth of ~6000m and to develop a flexible riser system for transporting nodules from the ocean floor to the mother ship/barge.

1.3 Credentials of the proponent

The Ministry of Earth Sciences (MoES), (formerly, the Department of Ocean Development), Government of India, through a host of national institutes, has been carrying out activities related to different components of deep-sea mineral exploration since 1982 as follows:

- CSIR-National Institute of Oceanography – Survey and exploration (since 1982)
- CSIR-Institute for Materials and Metals Technology, CSIR-National Metallurgical Laboratory and others – Metallurgical processing (since 1982)
- CSIR-National Institute of Oceanography - Environmental studies (since 1995)
- ESSO-National Institute of Ocean Technology - Mining technology development (since 1996)

The progress of activities under each of these components has been reported to ISA through periodic as well as annual reports regularly. Moreover the results obtained under the components have been published in and presented at international journals and conferences and well received by their peers.

MoES and the International Seabed Authority (ISA) entered into a Contract for Exploration of Polymetallic Nodules on 25th March 2002 covering an approved work plan for the contract period for a period of 15 years. Subsequently, along with the review of work carried out during second five year period of the contract, a supplementary report was submitted to the

Authority by MoES proposing the work plan for the third five year period which was also approved by the Authority. At the completion of the contract period, MoES and ISA have entered into an agreement for extension of contract for further a further period of 5 years until March 2022.

1.4 Scope and structure of the report

1.4.1 Scope of the report

As part of the mining technology development, it is proposed to conduct trials for nodule collection, crushing and local pumping along with locomotion by using a seabed crawler in a limited area within the IRZ during 2021. In accordance with the 'Recommendations for guidance of contractors for assessment of possible environmental impact arising from exploration marine minerals in the Area which states that testing of collection systems and equipment require prior environmental impact assessment as well as an environmental monitoring programprag to be carrieds out during and after the activity (ISBA/25/LTC/6), consequently MoES/Government of India is expected to submit an EIA report to ISA for conducting these trials.

The scope of this report is to describe the existing / baseline environmental conditions in the Impact Reference Zone where the trials will be conducted as well as Preservation Reference Zone within the context of regional environmental setting in the Contract area. The report further includes an evaluation of likely environmental impacts of the proposed activity of nodule collection trials**.**

1.4.2 Structure of the report

The report is structured under the following sections:

Section 1-describes the background and provides a summary of main activities of the project, followed by the project history, credentials of the proponent, and scope and structure of the report.

Section 2-describes the policy, legal and administrative context of the project

Section 3 - describes the proposed activity including location of the general area as well as IRZ and PRZ, mineral resource in the area; technical information of nodule collection system, methods for separation of the mineral resource and the sediment, mineral crushing methods; methods for transporting the material to the surface, processing and discharge (if any), plan of work for sea trials of collection system, duration of the test and test plans. This

information will be useful in evaluating the likely impacts of the tests on seafloor environment.

Section 4 - describes the existing physico-chemical environment (bathymetry, meteorology, water column, sediment properties) in the area.

Section 5 - describes the existing biological environment (megafauna, macrofauna, meiofaunaand nodule associated fauna) in the area.

Section 6–describes the types of impacts that could occur due to different activities related to deep-sea mining. It further deals with the results of the benthic impact experimentconducted by India (INDEX) as well as development of sediment plume model, and salient outcomes of these studies.It also provides the estimation of area, volume, and weight of nodules and sediment to be disturbed during nodule collection trials followed by prediction of the likely physico-chemical impacts of nodule collection trials on the seafloor.

Section 7-describes the potential impacts on biological environment based on available baseline, environmental variability and experimental data.

Section 8-deals with the plans of environmental impact assessment and monitoring of the proposed activity.

2. Policy, legal and administrative context

2.1 International

The present study on environmental impact assessment (EIA) for conducting the trials for pre-prototype nodule collector is proposed to be conducted in "the Area" which is defined by the 1982 United Nations Convention of the Law of the Sea (UNCLOS), ‘as the seabed and ocean floor and subsoil thereof beyond the limits of national jurisdiction’. The International Seabed Authority (ISA) is designated with the responsibility of regulating all activities in the Area particularly with respect to the seabed resources in accordance with the legal regime established in Part XI of the Convention (Implementing Agreement) and Part XII of the Convention, respectively.

The proposed activity will be conducted in the Indian contract area located in the international waters of the Central Indian Ocean Basin situated between 10 and 15° S latitudes and 77 and 77^{o} E longitudes. An agreement for exploration for polymetallic nodules was signed between the ISA and the Ministry of Earth Sciences (MoES, erstwhile Department of Ocean Development) on behalf of Government of India in 2002 for a period of 15 years, which was subsequently extended in 2017 for a period of 5 years.

The ongoing studies in the Indian contract area are being planned as per the following regulations issued by the International Seabed Authority:

(i) Recommendations for the guidance of contractors for the assessment of the possible environmental impacts arising from exploration for marine minerals in the Area (ISBA/25/LTC/6)section VI B requires‘prior environmental impact assessment’, as well as ‘environmental monitoring programme’ to be submitted by a contractor to ISA for ‘Testing of collection systems and equipment’.

(ii) Draft *Regulations on Exploitation of Mineral Resources in the Area* (ISBA/24/LTC/WP.1).

According to the draft regulations, Annexure IV provides an outline for the preparation of and Environmental Impact Statement, as also a draft template for the same (ISBA/24/LTC/WP.1/Add.1)

In addition to these, the guidelines issued by the International Maritime Organization (IMO) that deals with use of vessels at sea, international shipping, safety, and ship-based marine pollution prevention obligations will apply to this activity.

2.2 National

The activity will be conducted under the Polymetallic nodules program of the Ministry of Earth Science (MoES), which is the designated representative of the Government of India at the International Seabed Authority. The Minstry of Earth Sciences, who is authorized to sign the contracts with ISA on behalf of Government of India, will be responsible for all compliance with the applicable national and international regulations. Moreover, for any activity being conducted within the EEZ of the country, all maritime as well as environmental regulations issued by the Government of India will be applicable.

3. Area of operation and description of the proposed collector test

3.1 General description of area, geological setting and polymetallic nodules

3.1.1 Location

The Indian application area for nodule exploration is located in the Central Indian Ocean Basin, one of ten major abyssal basins/plains in the Indian Ocean region (Fig. 3.1.1.1), located to the south of Sri Lanka. The Indian Ocean covers approximately one-fifth of the total world ocean area. It is the youngest and physically most complex of the world's five major oceans. The Central Indian Ocean Basin is open to Bay of Bengal in the north. The Central Indian Ocean Basin is approximately 6,000 km long and 1,600 km wide, and its depth reaches 6,090 m. The northern part, as far south as 8°–10° S is plain sloping gently, while in south there are hills and mountains. Afanasiy Nikitin seamount in the central part of the basin is well known for cobalt crust deposits (Glasby et al., 2010), which reaches a maximum height of 1,549 m (Krishna, 2003). The Central Indian Ocean Basin between Central Indian Ridge and Ninety East Ridge, bounded in the south by the South Eastern Indian Ridge and the Indian Ocean Triple Junction, has a complex evolutionary pattern as it might have been affected by the evolution of the triple junction, the slower spreading CIR and the medium rate spreading SEIR (Tapscott et al., 1980).

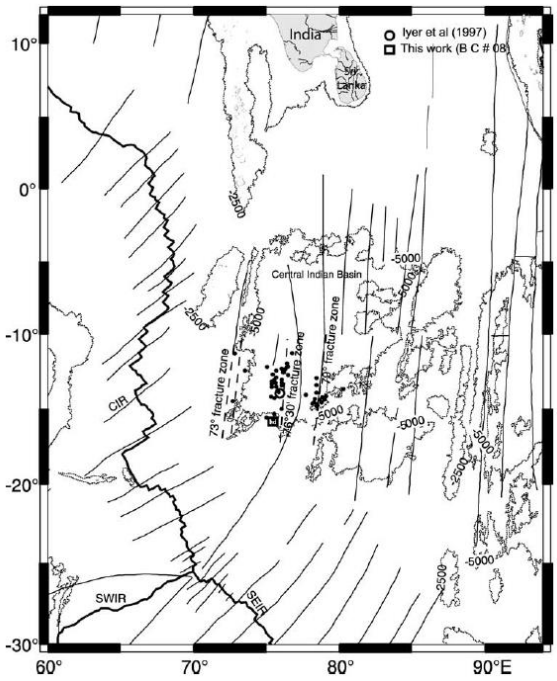

Fig. 3.1.1.1: Tectonic map of CIOB (modified from Nath et al., 2008)

3.1.2 Age of CIOB crust and evolution

The evolution of Indian Ocean starts from the Cretaceous period in the geological time. The evolution of Indian Ocean closely relates to the destruction of the Tethys Sea and formation of the Himalayan mountain ranges (Sclater et al., 1971, 1973; Curray et al., 1981). The opening of western Indian Ocean and seafloor spreading started by the breakup of Gondwanaland in the Late Jurassic time (anomaly M22, ~152 Ma). The separation of Antarctic-Australian plate from India-Madagascar-Seychelles plate started around ~133 Ma (Early Cretaceous, Ramana et al., 1994). Initial separation of Indian continent from Gondwanaland began around ~127 Ma and this spreading continued N-S until 90 Ma (Curray et al., 1981). The northward journey (90-53 Ma) of the Indian continent occurred between two great transform faults: Ninety East Ridge on the east and Chagos – Laccadive ridge on the west. The breakup of Madagascar from India started in Late Cretaceous time. The drifting of India from Madagascar is suggested to have commenced at about 86.5 Ma (Yatheesh et al., 2006). Seychelles rifted from the Indian continent and gave birth to the Carlsberg Ridge around the time of spreading anomaly 28 (~68 Ma) (McKenzie and Sclater et al., 1971).The Reunion hotspot had created the Deccan flood basalts on western Indian Shield around 66-68 Ma (Fisk et al., 1989).The soft collision between India and Asia was about 53 Ma (early Eocene Period; Sclater et al., 1974) paved the way for initial formation of mighty Himalayas. The next phase of evolution took place from 53 to 33 Ma. During this period the separation of Australian plate from the Antarctic plate by SEIR started. During the same time Ninety East Ridge became inactive and Indian and Australian plates became single Indo-Australian plate and separation from Antarctic plate continued to Present (Sclater et al., 1974). The latest event in the history of Indian Ocean is the formation of Red Sea and Gulf of Aden, which separates Arabia from Africa.

The magnetic anomalies of Late Cretaceous and Cenozoic age are reported on both sides of the South West Indian Ridge (SWIR), South East Indian Ridge (SEIR) and Central Indian Ridge (CIR) (Segoufin et al., 1981; Patriat, 1987; Royer et al., 1988). Anomaly 29 is the oldest reported magnetic anomaly mapped in the western Central Indian Ocean Basin. Kameshraju et al. (1989) reported magnetic anomalies numbered 21, 22, 23, 24 and 25 (Early and Middle Eocene / ~43-56 Ma) in the southern part of CIOB trending in an east-west direction associated with the 79°E fracture zone. The seafloor-spreading model studies indicate a variable spreading rate of 3.6 cm/yr between anomalies 21 and 23 (Middle Eocene) and 8.0 cm/yr between anomalies 23 and 25 (Early Eocene), these rates are approximately the same as reported earlier for the SEIR (McKenzie and Sclater et al., 1971; Sclater et al., 1974;

Sclater et al., 1976). Patriat et al. (1988) proposed the reconstructions of evolution of 79°E fracture zone originated as a result of the ridge jump along the CIR during the middle Eocene time of anomalies 22 to 20. The observed and modelled magnetic lineations (anomalies 21 to 25) from the west of the suggested triple junction trace are assumed as these anomalies have been originated from the SEIR (Kameshraju et al., 1989). Sclater et al. (1974) have found that these anomalies have been originated from an ancient east-west trending SEIR. Sclater et al. (1976) identified a fracture zone south of 27°S trending N45°E between 82° and 85°E which appears to change its direction to N10°E due to the reorientation of the SEIR from east-west to northwest-southeast between the anomalies 18 and 15 (~43 to 39 Ma).

The CIR near the triple junction has been spreading symmetrically at a nearly constant half rate of 2.7 cm/yr over the last 4 Ma, where as the SEIR prolongs the CIR as a medium rate spreading center (~ 3.0 cm/yr half-rate) while the SWIR is a slow spreading ridge (0.8 cm/yr; Tapscott et al., 1980).

Deep sea drilling in the eastern Indian Ocean shows that the oceanic crust off Western Australia is approximately 140 million years old and becomes younger to the west; this dates the initial opening of the Indian Ocean (James et al., 1973). Müller et al. (1997) illustrate the age of CIOB around 40-80Ma. (Fig. 3.1.2.1)

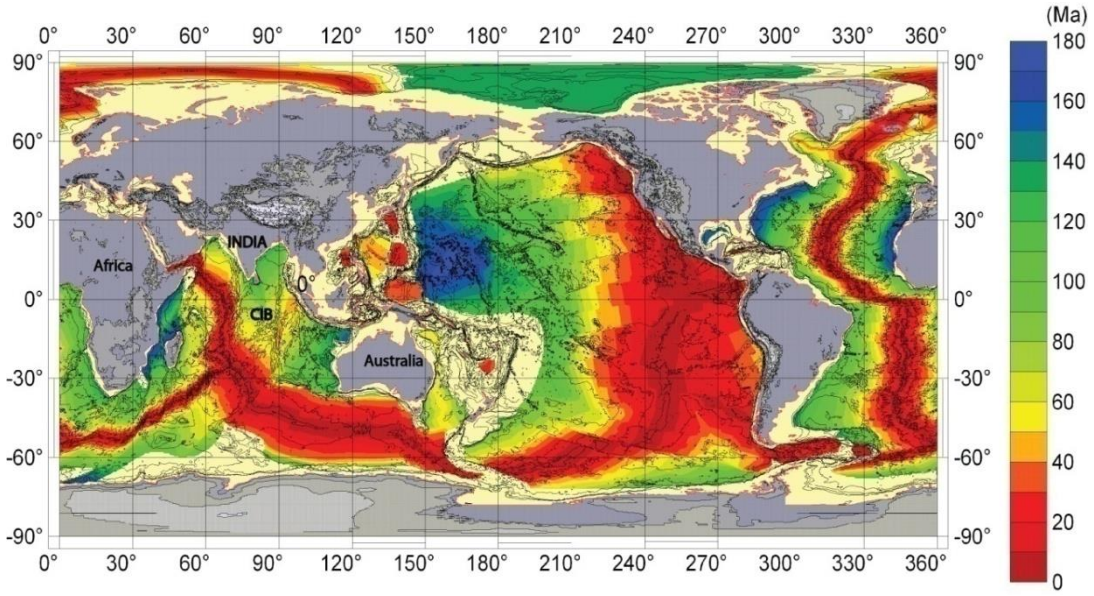

Fig. 3.1.2.1: Schematic map showing the ages of the ocean crust in the world ocean (Müller et al., 1997).

3.1.3 Petrology of rocks

All the topographic highs including the abyssal hills and seamounts and parts of the abyssal plain are floored by volcanic rocks, the majority of them being Normal Mid-ocean Ridge

basalts (N-MORB), ferrobasalts (Fe-Ti rich), spilites (albitised basalts), and rhyolitic volcanics mainly composed of drift pumice (Iyer et al., 2007). The pumice recovered from deeper parts of CIOB occurs in various shapes and sizes, uncoated or coated by ferromanganese oxides and the pumice field in CIOB covers an area of 600,000 km^2, approximately encompassing one-ninth of the basinal area (Iyer et al., 1993a). X-ray diffraction studies of pumice revealed cryptocrystalline quartz to be the dominant mineral followed by plagioclase. Indurated slabs of zeolites were recovered from the abyssal depths of the ClOB, which have shown the characters similar to harmotome-rich scorias of the Society Ridge and phillipsite slabs in the Pacific Ocean and have been described as zeolitites by Iyer et al. (1993b). They contain dominantly the phillipsite-harmotome group of minerals and were considered to have formed from volcanic precursors.

3.1.4 Sediment distribution

The sediment distribution in CIOB varies from north to south (Fig. 3.1.4.1). The northern part of the CIOB is covered with terrigenous sediments (up to 5°S latitude), from 5° to 14.5°S the major sediment type is siliceous oozes with sporadic calcareous patches found at around 12-14°S latitude and 82.5-83.5°E longitudes. The southern part of the basin (south of latitude 14.5°S) is covered with red clay (Nath et al., 1989). The continental source indicators like illite- kaolinite- chlorite abundance are decreasing from north to south in CIOB and montimorllionite content is highest in red clays of southern part and may have been derived from ridge basalt weathering (Rao et al., 1988).

Nath et al. (1992) have summarized the sediments in the CIOB into five different groups:

1) Northern most part of the CIOB floored with illite-kaolinite-chlorite rich (90%) terrigenous sediments mostly derived from Himalayan river input, transported through the turbiditic channels in the Bengal Fan.

2) Siliceous oozes/clays containing radiolarian skeletons in the northern central part of CIOB, without any manganese nodule deposits and are affected by terrigenous sedimentation (Nath et al., 1989).

3) Siliceous oozes/clays in the south central part of the CIOB with large nodule deposits (Sudhakar, 1989) with low sedimentation rate 2mm/ka (Banakar et al., 1991).

4) Calcareous sediments from shallow areas (Nath et al., 1992) on the flanks of the basin and the seamount tops (Nath et al., 2012).

5) Pelagic red clays in the southern most part of the CIOB, which are derivates of wind-derived material from distal sources such as Australia and also the altered sediments from local volcanics (e.g., Nath et al., 2012) and can contain manganese nodules.

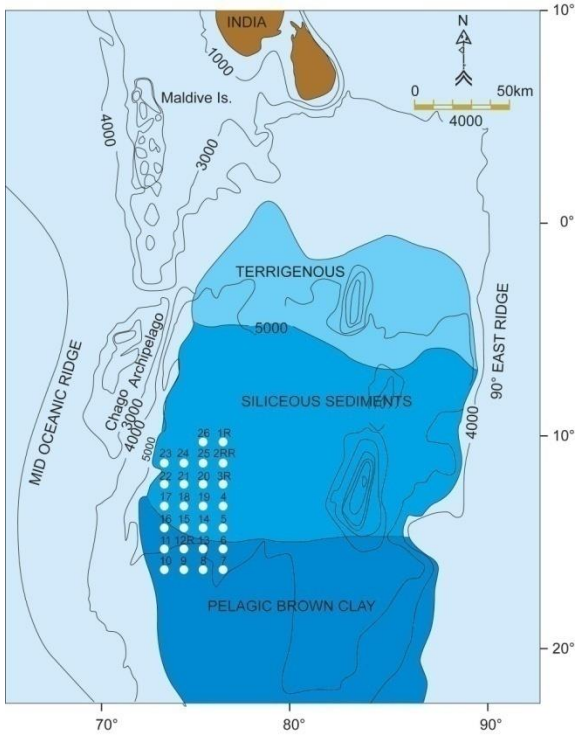

Fig. 3.1.4.1: Major sediment domains in the Central Indian Ocean Basin

3.1.4.1 Major sediment components

The CIOB sediments are dark yellowish brown to dark brown in color (Fig. 3.1.5.1) and predominantly clayey silt in texture. The sediments mainly from the siliceous ooze domain show features of bioturbation (Fig. 3.1.5.1). The coarse (sand) fraction components include siliceous skeletons of radiolarians, sponge spicules, volcanic glass, altered volcanics such as palagonites, authigenic silicates such as zeolites and manganese micronodules. The pelagic clays in southern area also contain foraminferal keels in small quantities. The major mineralogy is quartz and feldspars. Differential thermal analyses, Infra-red spectroscopy and the X-ray diffraction analyses of fine-grained size fractions of sediments from the CIOB has shown 2 smectite minerals (montmorillonite and Fe-rich montmorillonite), illite, chlorite and kaolinite (Rao et al., 1988). While the latter 3 minerals have been identified as the detrital products from Ganges and Brahmaputra, montmorrilonite is derived from the weathering of ridge and basinal rocks and the Fe-rich montmorrilonite is a product of early diagenetic process. Chemically, the sediments contain abundant biogenic silica/opal derived from the skeletons of siliceous microfossils. The maximum biogenic silica content can go upto 35%

(Pattan et al., 1992). Sediments retrieved from the flanks of a seamount in a fracture zone complex have shown signatures of hydrothermal alteration and metalliferous nature (Mascarenhas-Pereira et al., 2010). The sediments were ferruginous, had REE patterns similar to those from the hydrothermal vent field and the hydrothermal alteration features included 1) the depleted sedimentary organic carbon,2) dissolution features of radiolarian skeletons, 3) the presence of altered minerals such as smectite and zeolites and 4) distinctly different magnetic properties in the altered sediments (Nath et al., 2008). Predominant influence of neutral chloride type hydrothermal fluids was inferred from the geochemical data.

Fig. 3.1.4.1.1: A & D. Vertical section of sediment core showing fine-grained light to dark brown colored deep-sea sediments; B. Subcore showing clear signs of bioturbation at subsurface depths; C. Box core with sediments overlain by nodules before the subsampling.

Volcanic tephra, predominantly of bubble wall shards with the co-occurrence of platy and blocky types were found to be widespread in CIOB sediments (Fig. 3.1.5.2). Rarity of vesicles in the shards suggests that they are formed in depths deeper than 4000 m, below the volatile fragmentation depth (VFD). Geochemical analyses have shown that the tephra have SiO_2 contents ranging from~74 to 77% suggesting that they are mainly rhyolitic and formed

from melts of siliceous composition (e.g., Mascarenhas-Pereira et al., 2006). Some of the sediment cores in CIOB have yielded five volcanic horizons, in the top 30 cm, of which four have visual and dispersed shards. Rhyolitic glass shards of bubble wall, platy, angular and blocky types were retrieved from various stratigraphic horizons in the cores. The five volcanogenic horizons correspond to ages of ~34, 70–75, ~85, 107–109 and142–146 ka (Mascarenhas-Pereira et al., 2016).

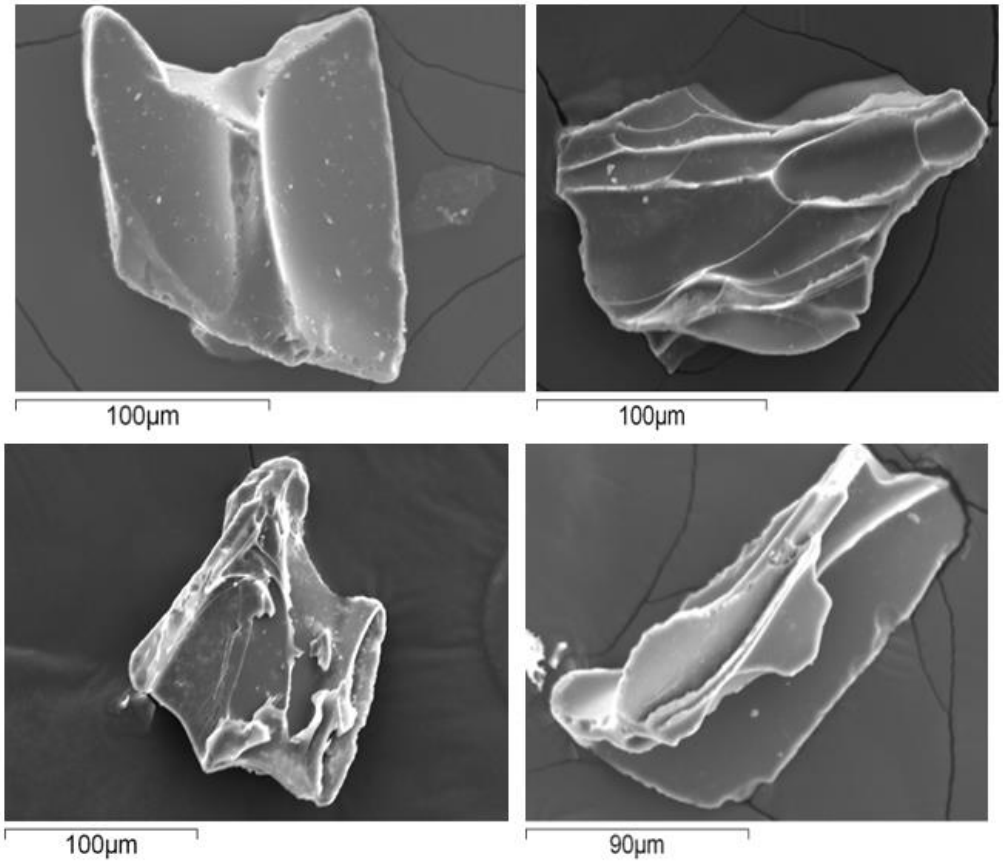

Fig. 3.1.4.1.2: Different types of volcanic tephra in CIOB sediments

3.1.4.2 Sedimentation rates

As the water depth in most of the CIOB is below the CCD, the major sediment types are non-carbonates which do not allow the ^{14}C dating. Thus, the principal techniques used in dating the sediments have either been the radiolarian biostratigraphy or the radiometric dating using $^{230}Th_{excess}$ method. The sedimentation rates in CIOB in general are very low (0.32 mm/ka to 4.6 mm/ka) with the slowest sedimentation rates being found in pelagic clays and the sediments depositing on flanks and tops of seamounts possibly because of erosion. A compilation of sedimentation rates published so far as presented in the Table 3.1.6.1 below.

Table 3.1.4.2.1: Compilation of sedimentation rates estimated for the Central Indian Ocean Basin from the literature

Core	Lat (°S)	Long (°E)	Depth (m)	Sed. rate ($mm.ky^{-1}$)	Reference
SK/247	5°	76°	5170	4.2	Borole (1993)
NR/54	7°	78° 15'	5200	2.5	Gupta (1991)
226	13° 08'	75° 01'	5270	2.0	Borole (1993)
SK/657	14° 00'	76° 00'	5050	2.0	Mudholkar et al. (1993)
F200B	12°	76° 30'	5450	2.0	Borole (1993)
F88B	12 °42'	77°	5430	0.8	Borole (1993)
SS667	12°30'	76°	5250	1.5	Borole (1993)
SK183	06°	76°	5170	0.8	Borole (1993)
NR-1	9.99	77.92	5250	1.6	Banakar et al. (1991)
NR-35	11.97	78.49	5450	2.2	Banakar et al. (1991)
NR-21	11	78.49	5325	4.6	Banakar et al. (1991)
AAS61/BC-14	14 00.231	75 30	5145	2.69	Mascarenhas-Pereira et al. (2016)
AAS61/BC-20	12 00.066	75 23	5200	2.29	Mascarenhas-Pereira et al. (2016)
AAS61/BC-25	10 59.964	75 30	5300	2.33	Mascarenhas-Pereira et al. (2016)
ABP4/BC37	16°06.031′	75°26′,	4252	0.62	Nath et al. (2013)
AAS61/BC 8	15 59.981	76 30.	5010	0.32	Mascarenhas-Pereira et al. (2006)
AAS-05/GC-2	13◦03′	74◦44′	5099	4.55	Pattan et al. (2005)

3.1.5 Polymetallic nodules

Polymetallic nodules cover an area of approximately $54x10^6$ km^2 in the world oceans. The most extensive nodule fields are found in the Pacific Ocean. The nodules are spread about $23x10^6$ km^2 in the Pacific Ocean. The Atlantic Ocean has the lowest distribution, with an area of about $8x10^6$ km^2. Indian Ocean has a nodule field spread over $10\text{-}15x10^6$ km^2.

In the Indian Ocean, the nodules are distributed in the Crozet basin, the Wharton basin, the Somali basin and the CIOB, and richest among them are found in the CIOB. The nodules in the CIOB vary in size, shape and surface texture. The size of CIOB nodules ranges from less than 1 cm to more than 10 cm in diameter and smaller nodules <4 cm are common in CIOB (Valsangkar et al., 1989). Smaller nodules (< 4cm) dominate the entire basin with nodules of 0-2cm size class dominating the eastern part of the basin, northern side of the study area and small patches on the seamount tops. Other class of smaller nodules (2-4 cm size range) is the dominant size class in CIOB, in eastern and southern part of the study area except deep basins. Larger nodules (>4 cm) dominate in the areas of deep basins. Among these, 4-6 cm sized nodules are abundant in the north western part of the CIOB, while those between 6 and 8 cm are limited to central deep basins only (Vineesh et al., 2009). Irrespective of the size class they belong to, irregular shaped nodules predominate in the entire CIOB. Smaller nodules are comparatively more rounded, subrounded or spheroidal. Larger nodules have shown irregular, elongated, tabular, triangular and mammillated shapes. The shapes of most nodules were found to be closely related to the substrate or nucleus in which they grew. Irregular shaped nodules were generally found to have altered basalt as nucleus. Deep basins in between the seamounts chains with pumice as the major nucleus type shows increasing degree of roundness. The dominant surface texture of the CIOB nodules was found to be rough (see Vineesh et al., 2009 for details). Eastern part of the area between 10-13°S shows smooth and mixed surface texture (Fig. 3.1.5.1). The central part of the basin (74.5° E to 78°E) shows abundant rough textured nodules (Fig. 3.1.5.2) which may be due to the presence of more number of seamounts with a rugged topography (Mukhopadhyay et al., 1995; Kodagali, 1995). Spheroidal and ellipsoidal nodules with rough surface are more common among smaller nodules in CIOB (Jauhari et al., 2000).

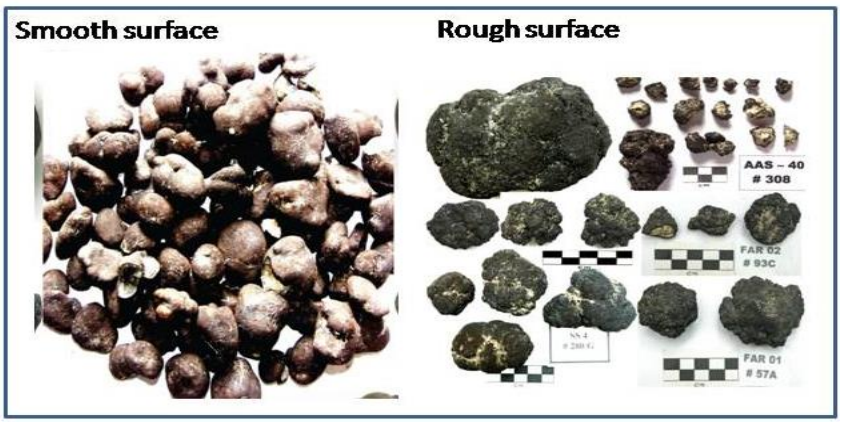

Fig. 3.1.5.1: Typical smooth and rough surface nodules from the CIOB (modified from Vineesh, 2012)

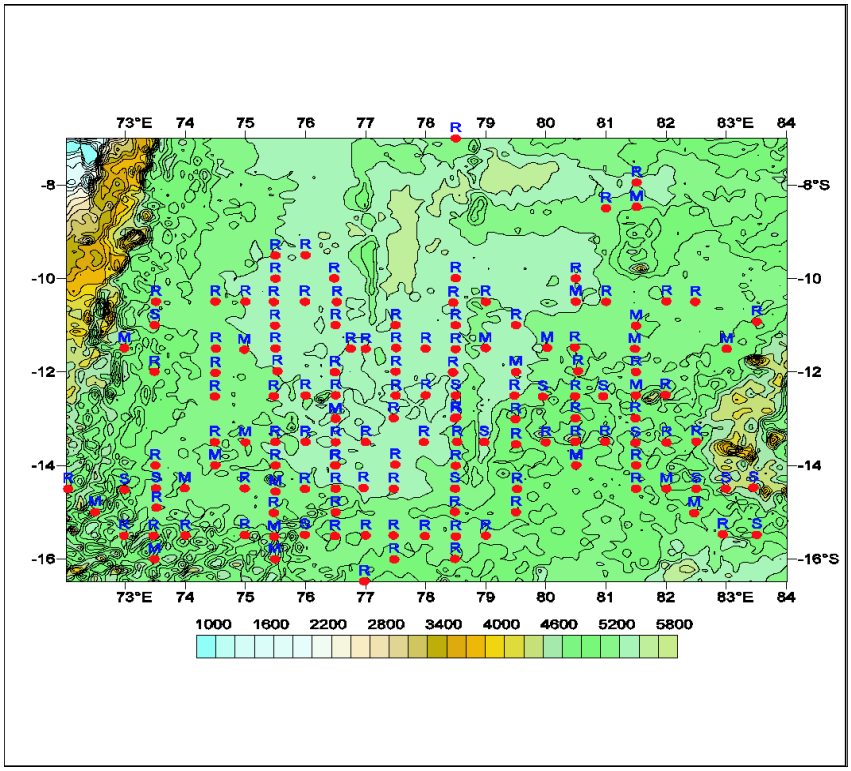

Fig. 3.1.5.2: Regional distribution pattern of surface texture of manganese nodules in CIOB. R, S and M indicate rough, smooth and mixed type texture (Vineesh et al., 2008)

The average abundance of manganese nodules in CIOB is 4.51 kg/m^2 (Mukhopadhyay et al., 2002) which is less than that in other contract areas in the Pacific. After the 3-phase relinquishment, the retained area of 75,000 km^2 contained 382 million tons of nodules with the metal grade given in Table 3.1.5.1 (Shyam Prasad, 2005).

Table 3.1.5.1: Metal grades in polymetallic nodules in CIOB

Metal	Range
Manganese	22-30%
Iron	5-11%
Nickel	1-1.7%
Copper	0.9-1.5%
Cobalt	0.08-0.12%
Grade (Cu+Ni+Co)	2.2-3.3%

3.2. Impact Reference Zone (IRZ) and Preservation Reference Zone (PRZ)

3.2.1 Selection of IRZ and PRZ

The Pioneer Area of 1,50,000 sq.km. was divided into blocks of 1/4°x1/4° which were sequentially numbered. These were later subdivided into blocks of 1/8°x1/8° as shown in the Contract area of 75,000 sq.km. which is retained by India after relinquishment (Fig. 3.2.1.1).

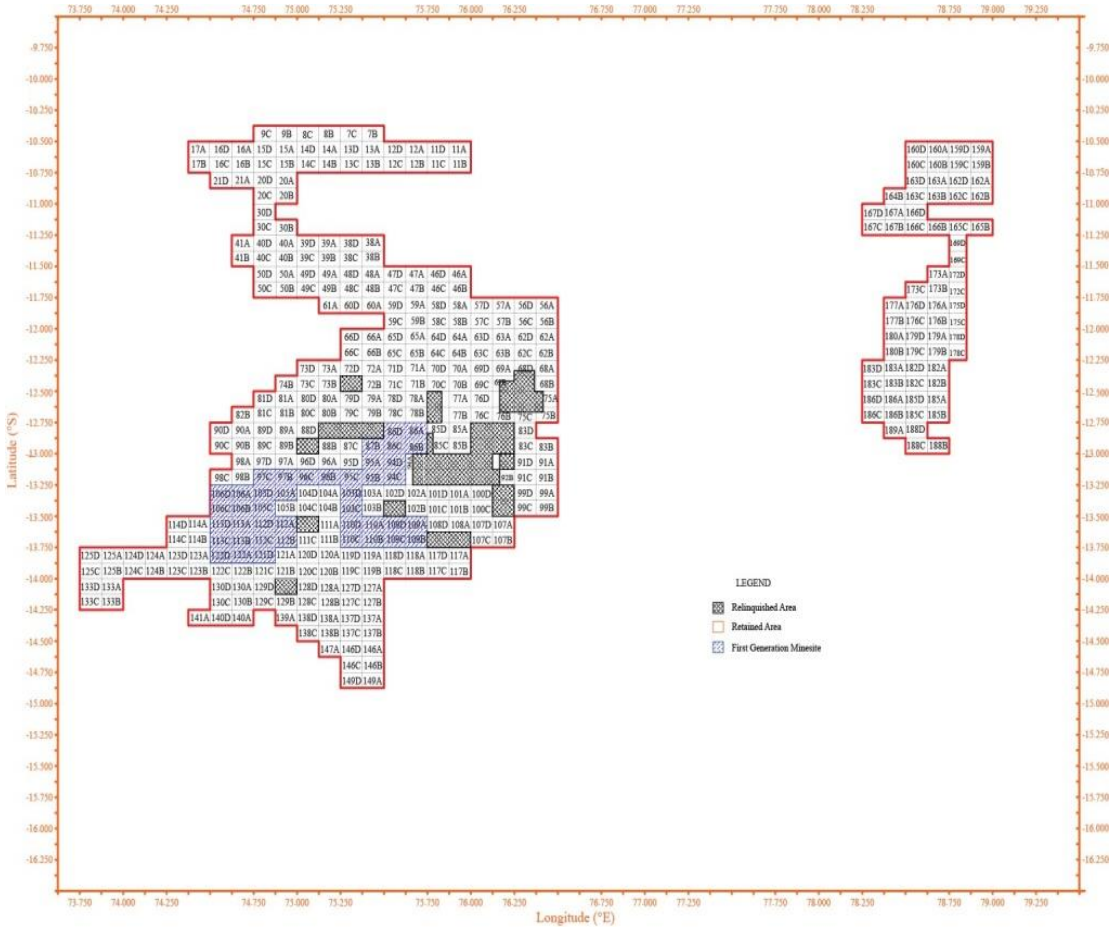

Fig. 3.2.1.1: Indian contract area with blocks of 1/8°x1/8°

Within the Contract area, two nodule-rich areas viz., the Impact Reference Zone (IRZ) and Preservation Reference Zone (PRZ) have been identified (marked PRZ and IRZ (Fig. 3.2.1.2). IRZ which corresponds to block no. 109D measuring 1/8°x1/8° (7.5x7.5 nautical miles) was selected for the purpose of conducting the nodule collector trial; whereas Preservation Reference Zone (PRZ) which corresponds to block 90C also measuring 1/8°x1/8° (7.5 x 7.5 nautical miles) was selected as a reference area to study the natural environmental variability. The boundary co-ordinates of both the areas are presented in Table 3.2.1.1.

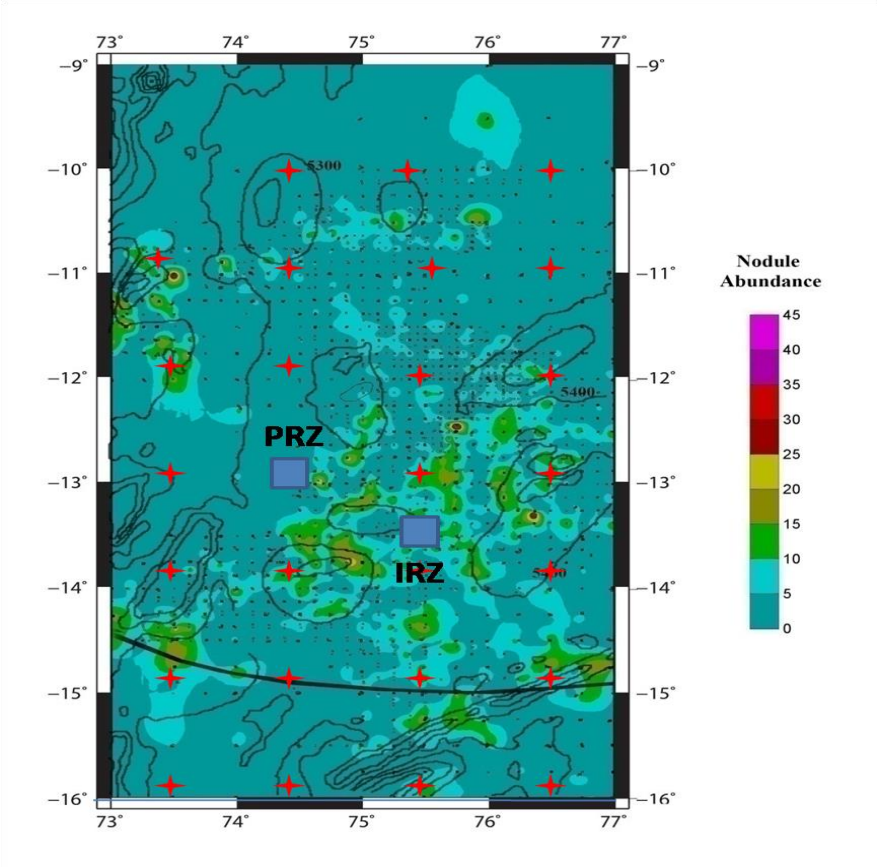

Fig. 3.2.1.2: PRZ and IRZ locations in a regional bathymetric map. Colour codes indicate the nodule abundance (kg/m^2). Dots represent the sampling stations

The basis for selection of IRZ was the abundance, grade and bathymetry of the block for conducting the nodule collection trials, whereas PRZ was selected on the basis of similar nodule abundance and grade, and availability of detailed environmental data over four seasons at a location BC 18 which is close to PRZ (23 km) and would be useful for assessing the natural variability in the area. The IRZ and PRZ are separated by ~60 nautical miles, and lie within a similar sedimentary domain and seafloor bathymetry configuration.

Table 3.2.1.1: Co-ordinates of IRZ and PRZ

IRZ (Block 109D)		PRZ (Block 90B)	
Long (°E)	Lat (°S)	Long (°E)	Lat (°S)
75.5000 -	13.5000	74.6250 -	12.8750
75.6250 -	13.5000	74.7500 -	12.8750
75.6250 -	13.6250	74.7500 -	13.0000
75.5000 -	13.6250	74.6250 -	13.0000
75.5000 -	13.5000	74.6250 -	12.8750

3.2.2 Nodule resources of IRZ and PRZ

Manganese nodule resources viz., the abundance and grade data of two blocks IRZ and PRZ are presented in this section. Abundance is estimated from the gripping surface area of the sampler. For example, the freefall grab used in major part of Indian exploration program has a gripping surface area of 0.13 m^2. The weight of nodules obtained in a grab is extrapolated to one square meter. As the sampling density increases and the grid size narrows down, the confidence in estimates of regional variability in abundance increases. As described in earlier sections, the metal grade considered here, is the combined metal percent of 3 elements namely the copper, cobalt and nickel. Both IRZ and PRZ are relatively richer blocks (Tables 3.2.2.1 and 3.2.2.2) both in terms of abundance and grade. The abundance presented for each station (Tables 3.2.2.1 and 3.2.2.2 and Figs. 3.2.2.1 to 3.2.2.4) represents an average of 2-7 sampling locations occupied in each station. According to the estimates made during the year 2019, the kriged abundance and the grade for IRZ are 9.419 kg/m^2 and 2.45% and for PRZ are 11.203 kg/m^2 and 2.35%, respectively.

Table 3.2.2.1: Abundance and grade of IRZ (refers to exploration BLOCK NO. 109D) stations.

Ship/cruise	Station	Latitude (°S)	Long (°E)	Depth (m)	Abundance (kg/m^2)	Grade (%)
SKA009	598	13.500	75.626	5250	10.15	2.94
SKA017	859	13.622	75.607	5280	10.65	2.41
FAR001	044	13.500	75.498	5191	14.08	2.13
SKY020	223	13.626	75.496	5216	06.38	2.59
AAS040	318	13.500	75.627	5200	00.00	NA
AAS040	319	13.497	75.495	5230	13.60	2.22
SSD048	043	13.500	75.562	5217	11.40	NA
SSD048	044	13.562	75.500	5230	09.56	NA
SSD048	045	13.562	75.562	5156	06.67	NA
SSD048	046	13.562	75.625	5173	02.87	NA
SSD048	047	13.624	75.562	5232	01.53	NA
SSD048	048	13.500	74.812	5117	12.80	NA

NA - Not analyzed

Table 3.2.2.2: Abundance and grade of PRZ (refers to exploration BLOCK NO. 90B) stations

Ship/cruise	Station	Latitude (°S)	Long (°E)	Depth (m)	Abundance (kg/m^2)	Grade (%)
SKA05	0313	13.008	74.737	5217	4.80	2.84
SKY20	0228	13.003	74.616	5096	10.15	2.58
SKY20	0230	12.877	74.616	4739	5.31	2.13
SKY20	0231	12.877	74.748	5057	7.94	2.72
AAS38	0240	12.996	74.684	5310	19.20	NA
AAS38	0242	12.874	74.682	5305	9.40	1.64

The station-wise variability in abundance and grade of nodules in area IRZ are shown in figures 3.2.2.1 and 3.2.2.2. Except for 3 stations, all other stations show high abundance. The eastern corner of the area shows large variability possibility representing the local variability. The metal grade in the area mostly falls in para-marginal category.

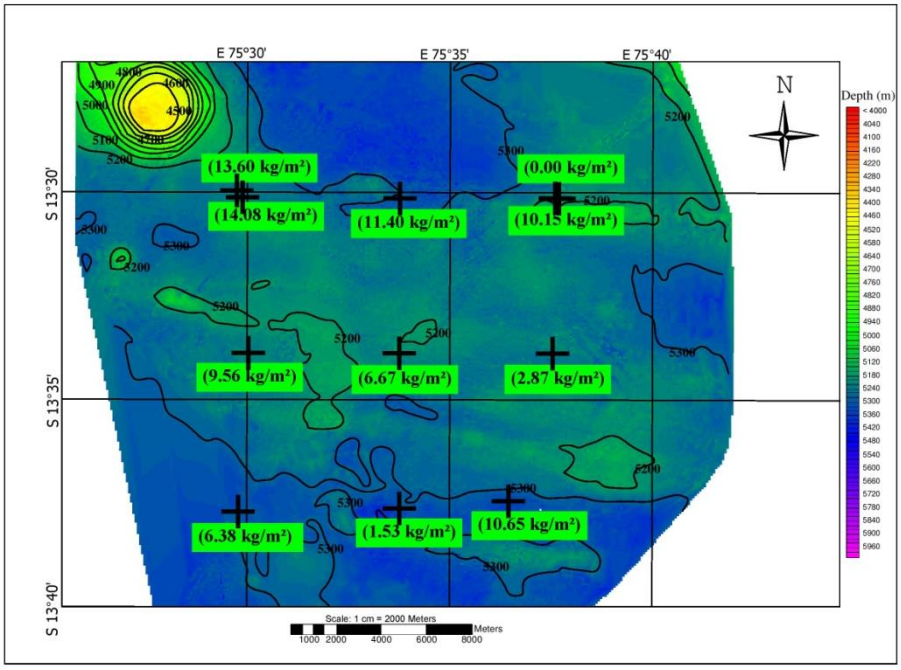

Fig. 3.2.2.1: Station-wise nodule abundance in IRZ

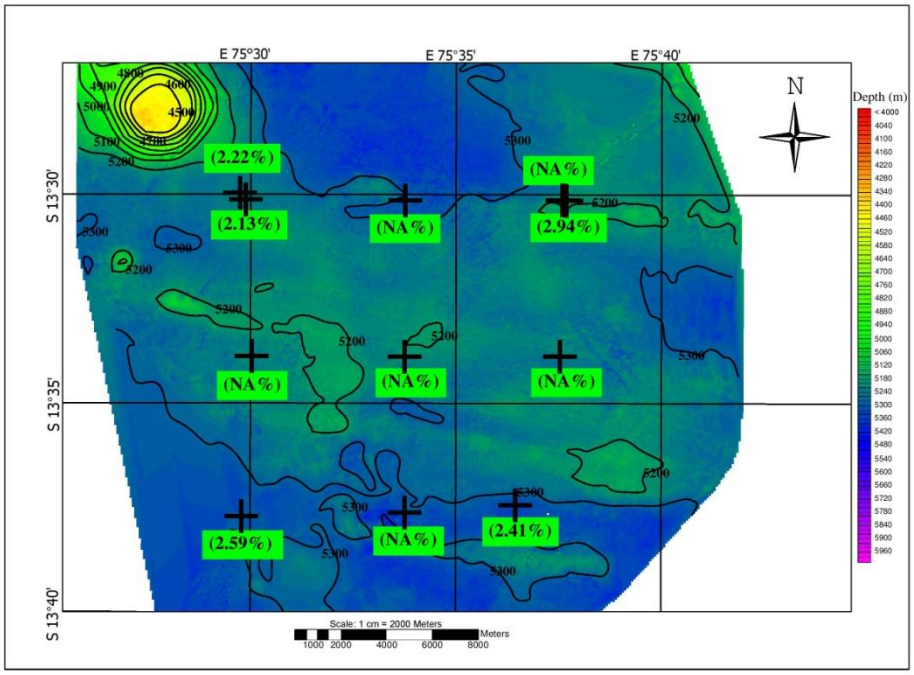

Fig. 3.2.2.2: Station-wise metal grade in IRZ

The station-wise variability in abundance and grade of nodules in area PRZ are shown in figures 3.2.2.3 and 3.2.2.4. Relatively, the abundance in PRZ is lesser than that found in IRZ. Lower abundances are seen at the base of topographic elevations. The metal grade in the area ranges from sub-marginal to para-marginal category.

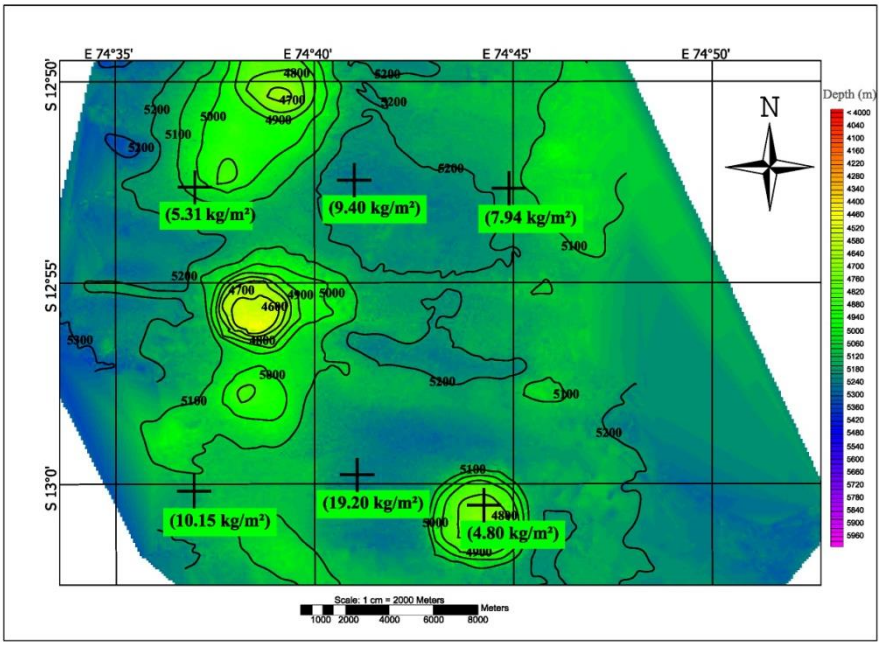

Fig. 3.2.2.3: Station-wise nodule abundance in PRZ

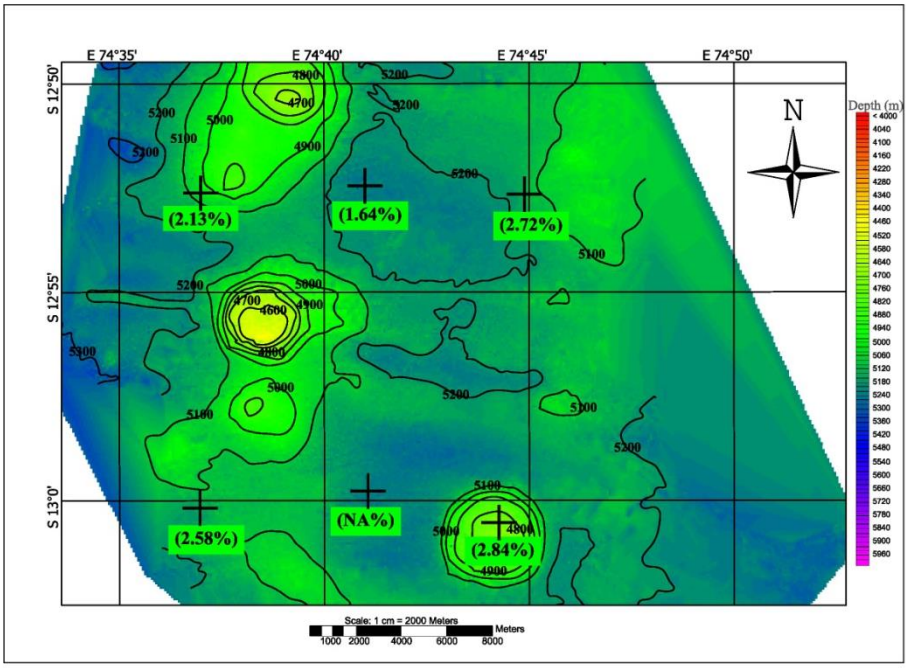

Fig. 3.2.2.4: Station-wise metal grade in PRZ

3.3 Technical information of nodule collector system

The information provided in this section is as per no. VIC Para 38 of ISBA/25/LTC/6 (i.e. Information and measurements to be provided by the contractor performing an activity requiring an environmental impact assessment during exploration).

The salient details of the mining machine-nodule collector system are as follows:

(i)	Locomotion by caterpillar type tracks	Total contact area - 4.5 m^2
(ii)	No. of Nodule Pick-ups	Two, with each of working breadth of 0.8 m
(iii)	Location of Pick-ups	In front
(iv)	Locomotion Speed	Nominal speed of 0.15 m/s and maximum of 0.30 m/s
(v)	Seabed Soil Penetration	Nodule collector rake: 150-300 mm
(vi)	Weight in Air	about 14 t
(vii)	Weight Underwater	Less than 4 t
(viii)	Powering	Electro-hydraulic

(a) Mineral collection technique

The nodule collection-pickup system is a moving comb type rake (Fig. 3.3.1), which sieves up solid pieces greater than 10 mm in size. Soil and smaller objects due to relative combs' motion would fall back through the gaps to the seabed. The nodules after pick-up are moved up to the crusher unit by a conveyor system. Each pickup unit has a total width

of 0.80m with a depth of penetration of 100-300mm from the seabed surface. The travel speed of advance would be at a nominal speed of 0.15 m/s. During the proposed trials, two nodule collection-pickup systems would be fitted on the front of the mining machine.

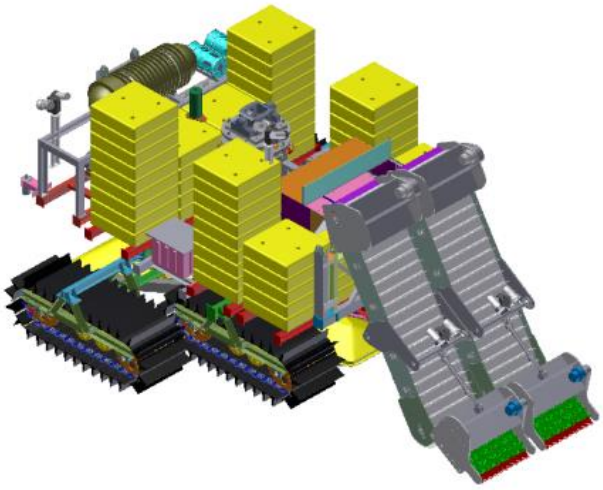

Fig. 3.3.1: Nodule collection system with comb-type rake

(b) Expected depth of penetration into the seabed would be about 150-300mm from the seabed surface.

(c) Running gear of the seabed mining machine (skis, wheels, caterpillars, Archimedes screws, bearing plates, water cushion, etc.) which contacts the seabed would be caterpillar type tracks, with a total contact area of 4.5 m^2.

(d) Methods for separation on the sea floor of the mineral resource and the sediment, including washing of the minerals, concentration and composition of sediment mixed with water in the operational plume created at the seabed, height of discharge above the sea floor, modelling of particle size dispersion and settlement, and estimates of depth of sediment smothering with distance from the mining activity.

The nodule collection-pickup system is a moving comb type rake which sieves up solid pieces greater than 10 mm in size. Soil and smaller objects due to relative combs' motion would fall back through the gaps to the seabed. The nodules after pick-up are moved up to the crusher unit by a conveyor system. In this manner, soil particles adhering to the collected nodules will be washed off before crushing and local pumping.

(e) Processing methods at the seabed

No processing of the minerals will be undertaken on the seabed or underwater.

(f) Mineral crushing methods

A lumped crusher would be used to reduce the nodules to sizes in the range of ~~1~~ minus 20 mm

(g) Methods for transporting the material to the surface.

In the planned experiment, there is no pumping of the crushed nodules to the surface. To test and validate the pumping system, it is planned to pump a limited quantity of the crushed nodule slurry at a concentration of less than 8% by volume up a 100-200 flexible lay flat hose, clamped to the umbilical cable. The hose discharge would be approximately at a height of about 80 m above the seabed at a rate of less than 80 m^3/hr.

(h) Separation of the mineral resource from the fines and the sediment on the surface vessel

Slurry will not be pumped to the surface.

(i) Methods for dealing with the abraded fines and sediment.

Slurry will not be pumped to the surface.

(j) Volume and depth of discharge plume, concentration and composition of particles in the discharged water and chemical and physical characteristics of the discharge

The crushed nodules slurry will be pumped to depths of approx. 80 m above the seabed to validate the system. The slurry is expected to have a nodule particles distribution of top size 20 mm. The slurry concentration is expected to be less than 8% by volume at a flow rate of 80 m^3/hr.

(k) Mineral resource processing on the surface vessel.

Slurry will not be pumped to the surface vessel.

(l) Location of the mining test and boundaries of the test area

Collector test site known as the Impact Reference Zone is located in a block of 7.5x7.5 nautical miles area in the CIOB between the following coordinates:

Lat (°S)	Long (°E)
-13.5000	75.5000
-13.5000	75.6250
-13.6250	75.6250
-13.6250	75.5000

3.4 Plan of work for sea trials of collector system

The planned trials intends to test and validate the seabed locomotion with nodule collection, nodule collection efficiency and stage one slurry pumping by the mining machine system. The trials are thus planned in stages as follows:

Trial-1, Locomotion & Nodule Collection Efficiency Test: The mining machine would be positioned on the seabed and once the initial attitude of the mining machine has been established (location, sinkage, trim and direction), locomotion with nodule collection would be initiated in a straight line over steps of 20 m. The nodules picked up would be collected in a collection basket with underwater load cells to actively estimate the amount of nodules collected by the mining system. The cumulative distance planned is about 100 m at 0.15 m/s nominal speed. Once the collection basket fills up (approx. 300 kg), the excess collected nodules would spill over back to the seabed. The operations would be monitored visually through underwater camera system. The mining machine with the 300 kg nodules collected would be thereafter brought up to the surface with the mining machine.

Trial-2, Nodule Collection, Crushing and Local Pumping Test: For this test, a nodule crusher unit would be fitted in place of the nodule collecting box and integrated with a slurry pump. The nodules collected would be crushed to smaller sized pieces-particles (top size 20 mm) and pumped as seawater slurry to the rear of the mining machine, as the seabed system advances forward. The objective of the test is to establish the underwater working of the crusher unit with actual nodule supply and its integration with the pumping system. A cumulative distance of approx. 500 m would be traversed in steps during the trials at 0.15 m/s nominal speed.

Trial-3, Nodule Collection, Crushing and Pumping up a Slurry Hose: For this test, the systems would be same as in Trial-2 above with a flexible slurry hose connected to the discharge of the slurry pump. The flexible hose would be clamped to the umbilical cable and the slurry discharge into the sea would be about 80 m above the seabed. The objective of the trials is to establish slurry pumping through the hose, the performance parameters and the associated loads on the mining machine affecting its locomotion, if any. A cumulative distance of approx. 500 m would be traversed in steps during the trials at 0.15 m/s nominal speed.

(a) Probable duration of the test

The trials of the mining machine and nodule collector would be conducted within the Disturbed Area, within the IRZ at 2-3 sites, up to 3 hours at each site, during which the nodule collector would be operated several times to collect nodules for short durations as brought out above.

(b) Test plans

Tests are planned to be conducted within the Disturbed Area in the IRZ at 2-3 sites as brought out above. A cumulative distance of about 1000 m is planned to be transversed during the trials at a nominal speed of 0.15 m/s with a maximum speed of 0.30 m/s.

3.5 Risks Associated with the Planned Trials

Ser	Emergency-Failure	Management Strategy
(a)	Deteriorating weather conditions and Tropical Cyclones	The period chosen for the trials during Jan-Feb 2021 has greater probability for fair weather conditions and lesser for Tropical cyclones, as observed from weather forecast models. Daily and weekly weather forecast and ship board information systems would provide the required intimation in planning for the mining operations.
(b)	Ship Failures - Discharges from ship	Accidental or intentional discharges from the ship are not envisaged. The ship systems and operations are IMO compliant.
(c)	Ship's DP failure	The ship has adequate safeguards and back-ups systems in respect of power, navigation equipment and number of thrusters, being DP Class-II certified. Notwithstanding, if the problem still occurs, stop all operations and lift the mining machine off the seabed, to prevent dragging and/or anchoring. Drain the slurry from the flexible hose, in case pumping was in progress. In case the defect cannot be quickly rectified and DP restored, retrieve the deployed system progressively.
(d)	Total power failure onboard ship	Ship's crew would make efforts to restore power and provide supply to the umbilical winch at the EARLIEST to lift up the mining machine off the seabed. Retrieve the system in case total power supply requirements, especially for the DP cannot be restored.

(e)	Failure of A-Frame	Ship systems are being checked comprehensively and load testing undertaken before proceeding for the trials. In the event of the defect, and repair not possible, and winch umbilical load cannot be taken on the A-frame, umbilical to be severed on deck and the subsea system recovered subsequently by separate arrangements.
(f)	Umbilical winch control failure	Abort trials and attempt resetting the system. In case system not restored, retrieve system using the 'Emergency Mode'.
(g)	Hydraulic Oil leakage from subsea system	System checked comprehensively in hyperbaric test chamber before employing at sea. If problem still occurs during use, abort operations and retrieve on deck. Hydraulic Oil quantity less than 1 m^2.
(h)	Low insulation in umbilical cable, mining machine or shipboard switchboard	If fault cannot be identified and localised for repair, abort the trials and retrieve the system to deck.
(j)	Conductor failure of the umbilical cable or loss in communication	Abort trials and carefully retrieve the system.
(k)	Severing of the umbilical cable	The subsea system would land/remain on the seabed and will be recovered by separate arrangements.
(l)	Malfunction of HiPaP or acoustic pingers	Proceed with dead reckoning if mining machine compass and DVL operational.
(m)	Ingress of water into instrumentation or transformer enclosures	System checked comprehensively in hyperbaric test chamber before employing at sea. If problem still occurs during use, abort operations and retrieve on deck.

4. Baseline physico-chemical environment

4.1 Onboard and laboratory methods for collection of baseline data

As described in section 1.2.2, fourteen cruises have been conducted onboard 6 research vessels since 1995 for collection of environmental data in different phases of the program. This section describes the methods used during the cruise onboard RV Sindhu Sadhana (SSD 013) in July - August 2015. RV Sindhu Sadhana, an indigenously built research vessel in an Indian shipyard located on the west coast of India and was commissioned in 2014, which has an overall length of 80 m, breadth of 17.6 m, gross tonnage of 4170 tones (Fig. 4.1.1). The vessel is equipped with state of the art navigation, sampling and oceanographic data acquisition systems and can accommodate 57 scientists and crew members. During the cruise, environmental data was collected in IRZ and PRZ through systematic bathymetry survey, 5 sediment samples each for assessing benthic conditions and 1 station in each was occupied for water column characteristics. The parameters analyzed were same as those evaluated in the previous phases of the project. Detailed description of data collection methods is given in this section followed by an overview of the existing physico-chemical environment in the entire contract area as well as IRZ and PRZ.

Fig. 4.1.1: Indian Research vessel Sindhu Sadhana

4.1.1 Satellite Navigation

Global Positioning system (GPS) was used for vessel navigation during the cruise with Furuno DGPS Navigator (Fig. 4.1.1.1) and Kongsberg Dynamic Positioning system (K-POS-DP-11) for fixing of core sampling and CTD locations. The accuracy of the DP system was 1m. A repeater display was available in Data Acquisition Laboratory where Atlas Hydrosweep multibeam and Knudsen deep-sea Echosounder are installed for pinger synchronization. The Furuno Electrionic Chart Display Information System (ECDIS) installed on bridge was used for electronic display of hydrographic charts. Station locations and cruise track generated from this data is given in Fig. 4.1.1.2.

Fig. 4.1.1.1: Furuno Navigator

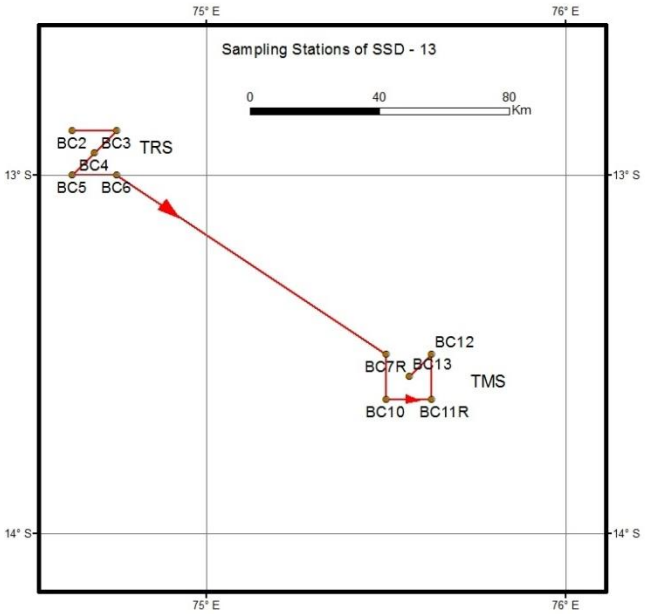

Fig. 4.1.1.2: Station locations in the IRZ and PRZ.

4.1.2 Deep sea Echo Sounder

The 1600 and 3200 series echo sounders were designed with a USB interface port to provide advanced remote control and signal data acquisition and recording capabilities. KEL has developed a pair of specialized PC applications that run under Windows to interface to these sounders: a client-side application and a server-side application. The server-side, EchoControlServer.exe, runs on the host PC (the one physically connected to the sounder) and communicates with the echo sounder's internal signal processing modules using the USB interface. It uses TCP/IP communications to receive control settings from the client which it passes to the sounder, and to send echogram data from the sounder to the client. It also interfaces to peripheral devices such as GPS receivers and heave sensors via the host PC's RS-232 ports. It acquires the sensor data and transfers it to the client and the sounder as necessary. The client-side application, EchoControlClient.exe can run on either the same host PC as the server-side or it can run on another PC on the same network. This client-side application allows the user to control the echo sounder, display in real-time grayscale graphic on the PC monitor (Fig. 4.1.2.1), capture envelope signal data, perform standard depth-logging, and record in real-time to a thermal recorder.

The system was used for underway monitoring of seafloor topography and as well as synchronizing pinger record during sampling.

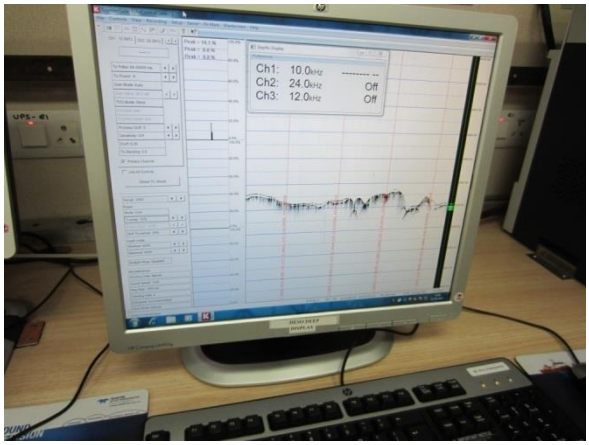

Fig 4.1.2.1: Computer display of Deep sea echo sounder

4.1.3Multibeam system

ATLAS PARASTORE multibeam system (Fig. 4.1.3.1), used during the cruise, provided an intuitive graphical user interface with parallel control of the data acquisition process by an online visualisation of recorded data. The recorded data is stored in a hybrid raw data format

(ASDF format) containing complete sounding profiles. Multibeam survey was carried out with N-S and E-W lines of about 15-20 km each in IRZ and PRZ for mapping of topographic features and contour maps were generated for IRZ and PRZ based on multi-beam data collected during the cruise (Fig. 4.1.3.2).

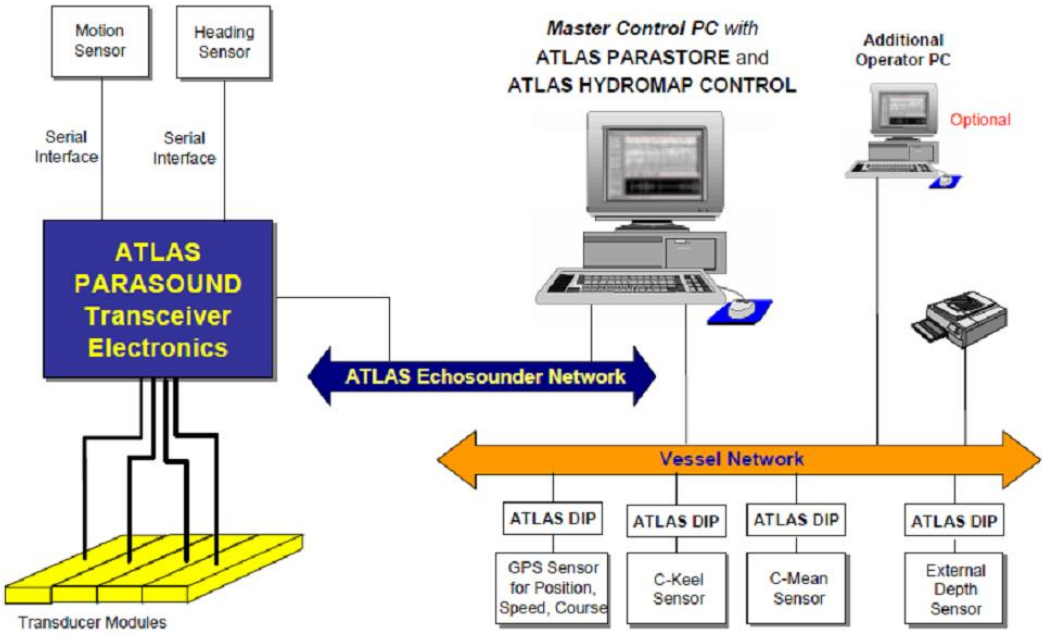

Fig 4.1.3.1: Configuration of Atlas Parastore System

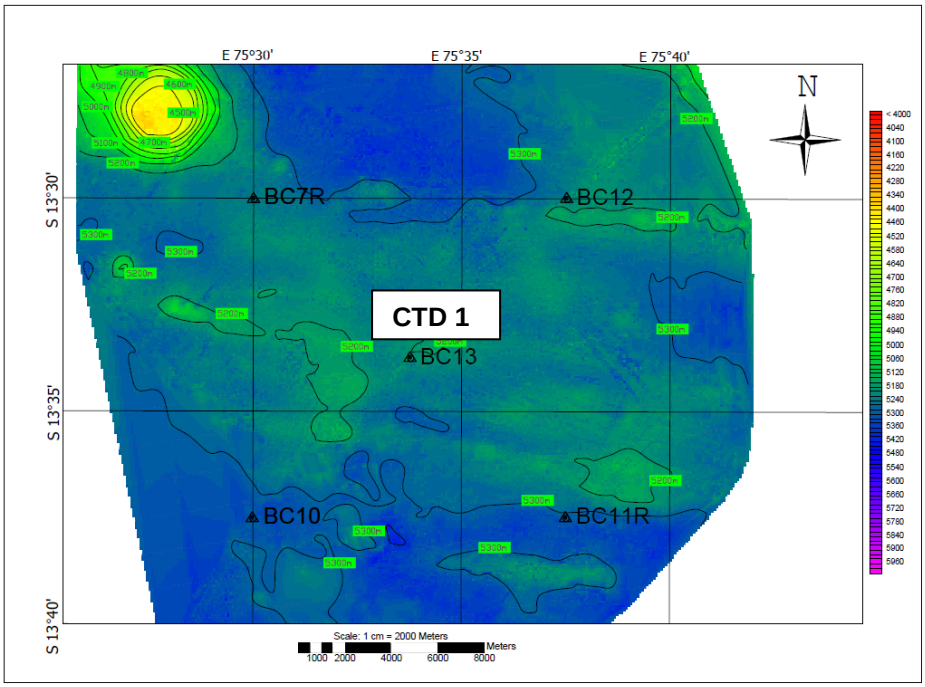

Fig 4.1.3.2a: Bathymetry map with sediment core and CTD locations in IRZ

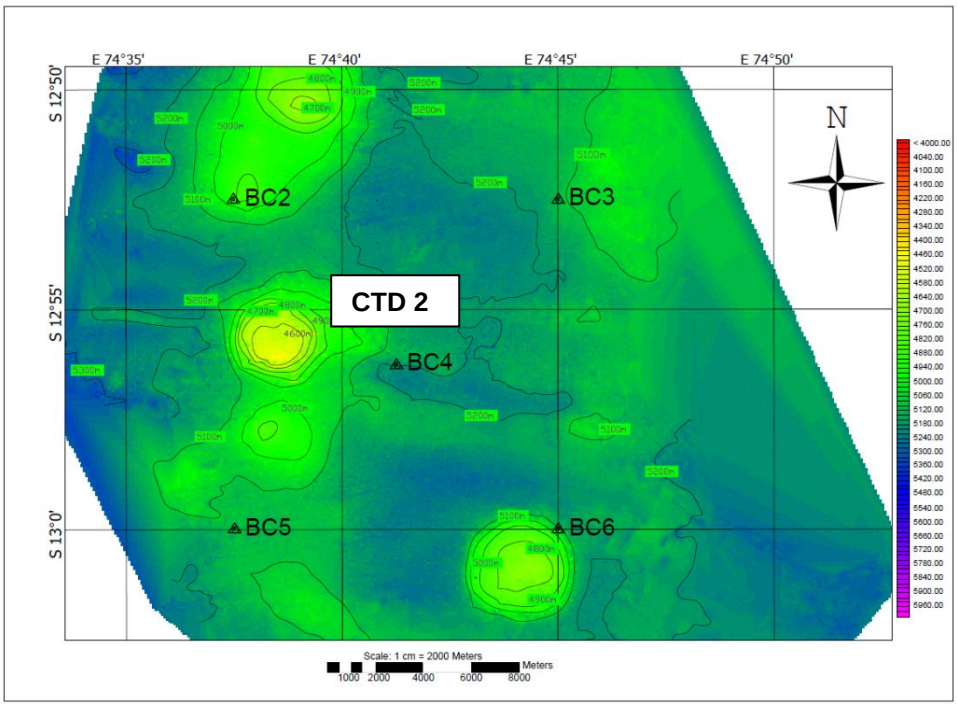

Fig 4.1.3.2b Bathymetry map with sediment core and CTD locations in PRZ

4.1.4 Autonomous Weather Station

The AWS installed on bow deck measures data on wind speed and direction, atmospheric temperature and pressure, relative humidity, sea surface temperature, solar radiation (Fig. 4.1.4.1) continuously with respect to ship's position. Real time data is received continuously on computer in Physics laboratory for recording of data at desired timings..

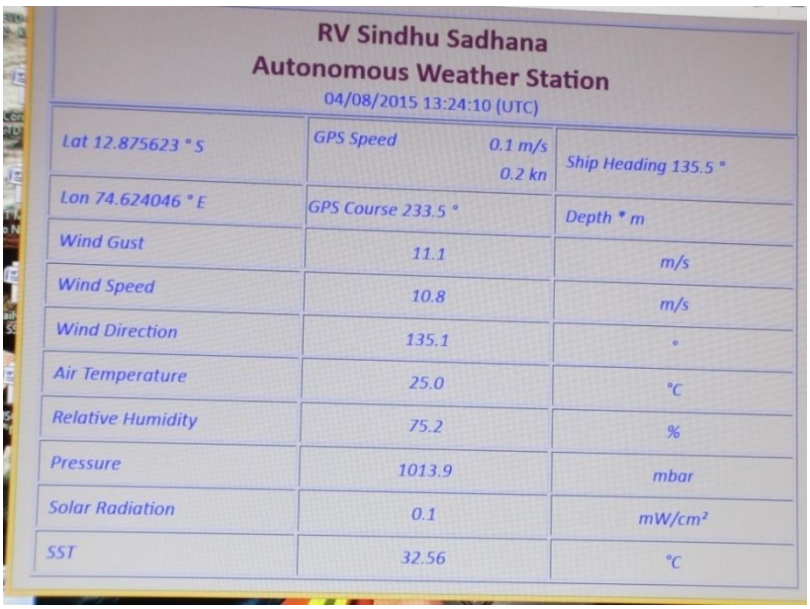

Fig. 4.1.4.1: Display of AWS with ship's position.

4.1.5 Seabed sample collection

Box / Spade corer measuring 50x50x50 cm was used for sediment sample collection (Fig. 4.1.5.1). A quadrant of 15x15 cm, acrylic core liners of small size (5.7 cm diameter) and PVC liners of large size (12.5 cm diameter) were inserted (Fig. 4.1.5.2) in each box core for sub sampling. Sediments were sub-sampled at 2cm interval down to 10 cm and at 5cm interval for the remaining depth of the core for most of the samples. Same sub-sampling intervals have been maintained so far in the EIA studies for comparing results from the earlier cruises. Sub-cores were collected for different studies and shared among the geological and biological disciplines, such as sedimentology, porewater chemistry, sediment geochemistry, geotechnical properties, macrofauna, meiofauna. Locations of sample collections are given in Table 4.1.5.1.

Fig 4.1.5.1: Box core used during the cruise.

Fig 4.1.5.2: Top view of box core after inserting liner and quadrant.

Table 4.1.5.1: Sampling locations in IRZ & PRZ for baseline data

S. No.	Station No.	Latitude (°S)	Longitude (°E)	Water depth (m)
1	BC-2/PRZ	12 52.534	74 37.446	4908
2	BC-3/PRZ	12 52.509	74 45.009	5094
3	BC-4/PRZ	12 56.216	74 41.217	5152
4	BC-5/PRZ	13 00.003	74 37.494	5055
5	BC-6/PRZ	13 00.014	74 44.998	4900
6	BC-7R/IRZ	13 29.999	74 29.982	5227
7	BC-10/IRZ	13 37.498	75 29.990	5280
8	BC-11R/IRZ	13 37.497	75 37.494	5252
9	BC-12/IRZ	13 29.995	75 37.493	5180
10	BC 13/IRZ	13 33.743	75 33.743	5187

4.1.6 Water column data collection

CTD system (SEA-BIRD Electronics Inc.,USA) was used for measuring water column parameters along with a rosette containing 12 Niskin water samplers of 10 L capacity (Fig.4.1.6.1) for water collection. CTD was operated at one location each in IRZ (CTD 1 at centre of IRZ) and PRZ (CTD 2 at centre of PRZ) (Table 4.1.6.1). All water samplers closed properly after firing from deck unit at different depths during the shallow (200 m) as well as deep (>5000 m) casts at all stations (Table 4.1.6.2). The CTD profiles for shallow cast and deep casts in IRZ and PRZ are shown in Figs. 4.1.6.2 and 4.1.6.3 respectively.

Table 4.1.6.1 Details of CTD and water sampling

S. No.	Station No.	Latitude (ºS)	Longitude (ºE)	Water depth (m)
1	CTD 1	13 33.747	75 33.742	5168
2	CTD 2	12 56.246	74 41.242	5090

Table 4.1.6.2CTD water sampling depths during the cruise

S. No.	CTD 1 (IRZ Centre) Water depth 5168m		CTD 2 (PRZ Centre) Water depth 5090m	
	Sampling depths (m)		Sampling depths (m)	
	Shallow cast	Deep cast	Shallow cast	Deep cast
1	200 (2)*	5156 (3)	150	5083
2	150 (2)	5146 (3)	100	5073
3	100 (2)	3500 (2)	93	3500
4	85 (2)	1000 (2)	50	1200
5	60 (2)	600 (2)	30	750
6	10 (2)	-	10	-

*Number in bracket shows No. of bottles used for water sample for all CTD stations.

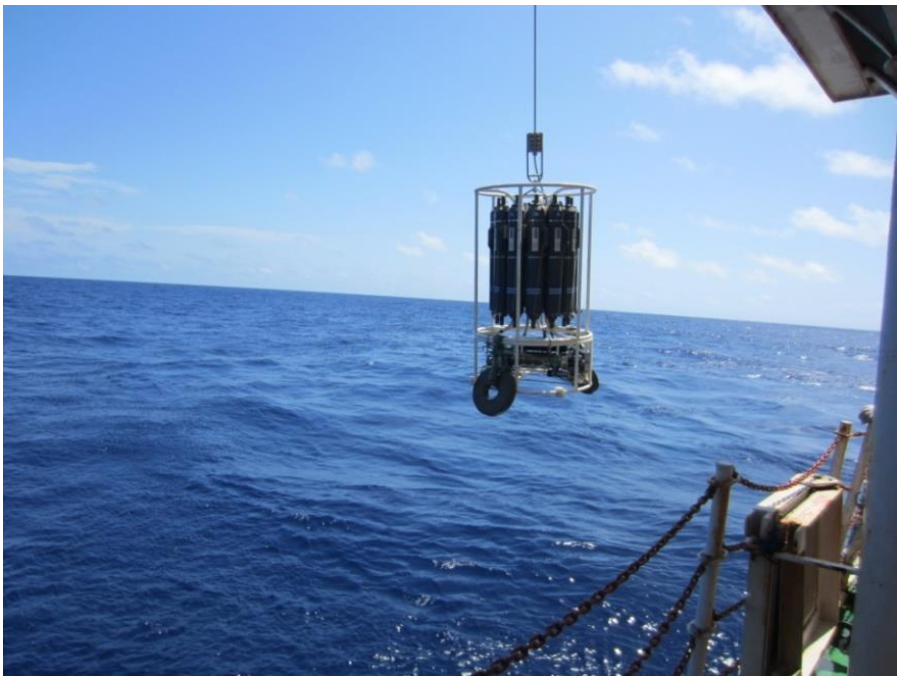

Fig 4.1.6.1: CTD being lowered with Niskin sampling bottles.

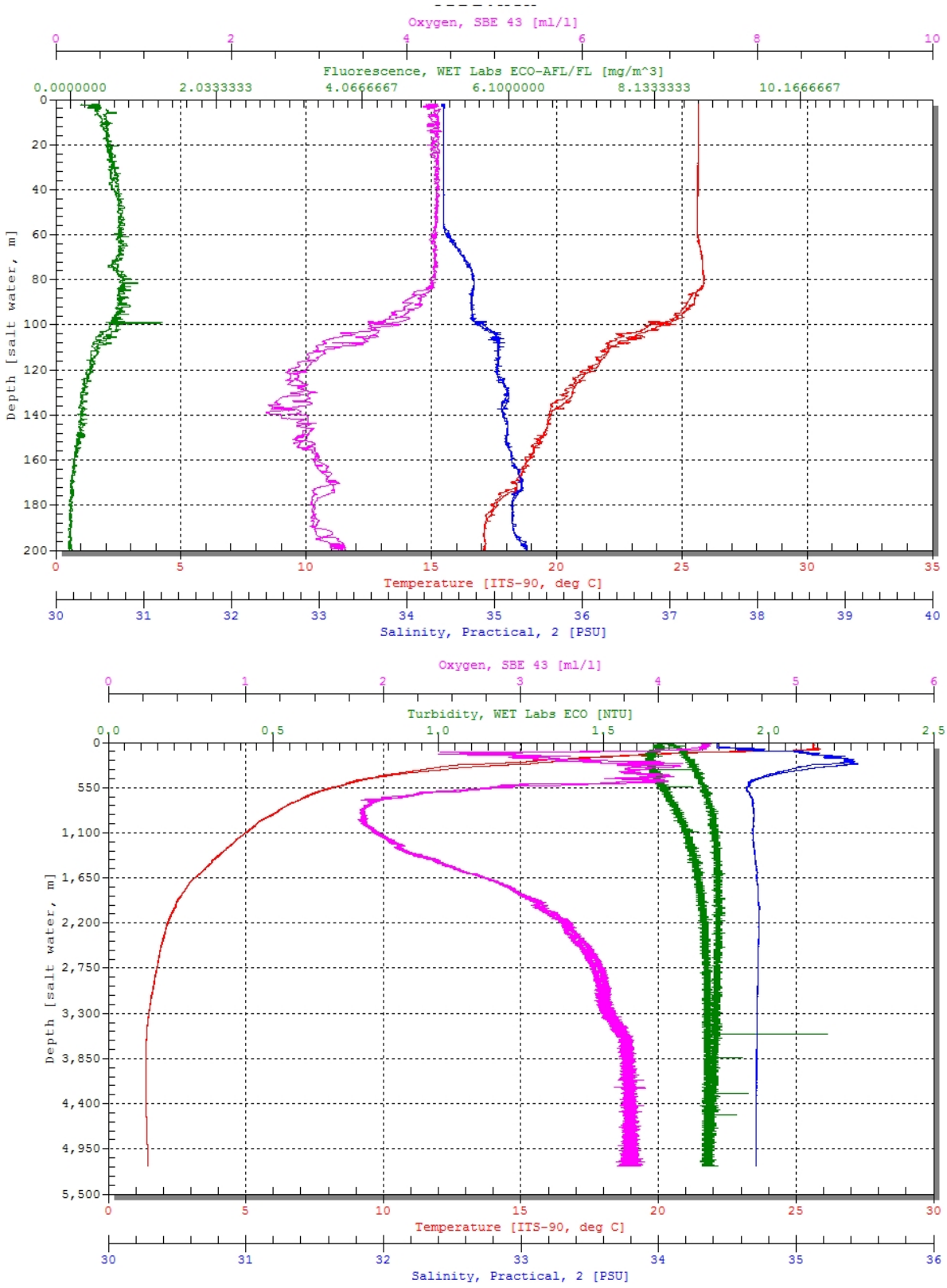

Fig. 4.1.6.2: CTD profiles in the IRZ

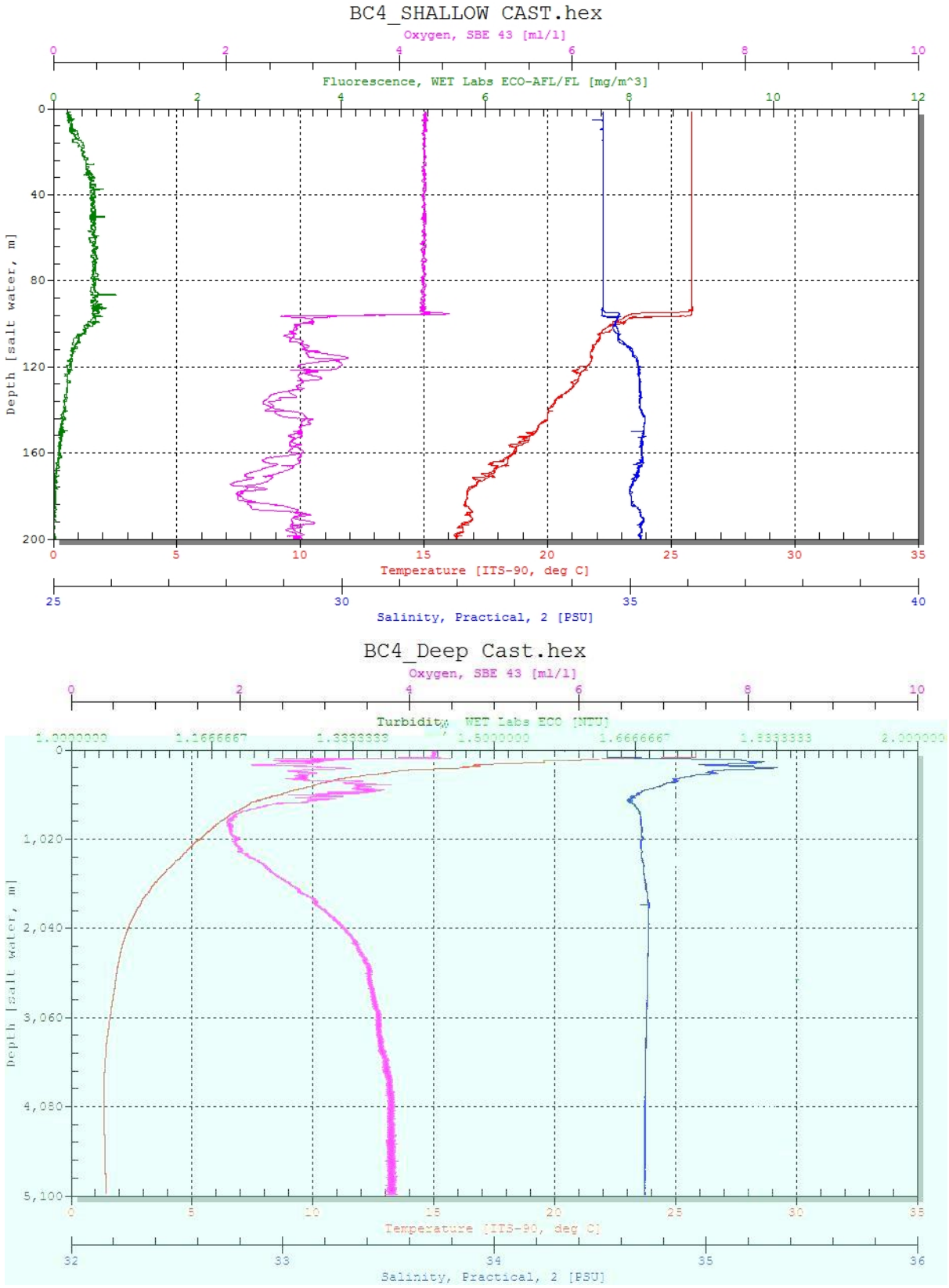

Fig. 4.1.6.3: CTD profiles in the PRZ

4.2 Bathymetry of the area

The northern part of CIOB is plain sloping gently, while in south there are hills and mountains (Fig. 4.2.1). Afanasiy Nikitin seamount in the northern part of the basin reaches a maximum height of 1549 m (Krishna, 2003). The CIOB is surrounded by two prominent north−south trending aseismic ridges: the Chagos–Laccadive Ridge (CLR, generated from the Reunion hot spot) to the west and the Ninetyeast Ridge (NER from Kerguelen hotspot) to the east. The Deformed Boundary Zone (DBZ) is located to the north of the CIOB while the Indian Ocean Ridge System (SWIR and SEIR) is located to its south (e.g. Mukhopadhyay et al., 2002). CIOB shows many morphotectonic features, such as seamounts, hills, ridge-normal lineaments and ridge-parallel lineations (Kameshraju, 1993; Mukhopadhyay et al., 2002; and references therein). The asymmetrical flexuring of seafloor in north and central CIOB (high spreading rate) is due to tensional stress and resulted in the formation of widely spaced faults, folds with low amplitude and large wavelength. The average water depth increases from west to east. The western part (71° to 74°E) is extremely rugged compared to the eastern part of the CIOB (79° to 82°E) which has moderately rugged topography, while the central CIOB (74° to 79°E) is almost a plain.

The CIOB has a slope angle between 0° and 3° (Kodagali, 1991) but the slope may be as high as 18° in seamount dominated areas (Mukhopadhyay et al., 1994). Mukhopadhyay et al. (1997) found that the bathymetric variation of the CIOB is related to the rate and direction of spreading and plate reorganisation. Ridge parallel lineations in the central and eastern parts of the CIOB trend 100–280° while the lineations are trending 145–325° found in the west of 73°E. The lineations trending ESE–WNW are in general, well spaced, show broad wavelength and low amplitude, and whereas those oriented approximately NW–SE are closely spaced with high amplitude (Small, 1998). The ridge parallel faults are common in CIOB and the density and number of faults increase from north to south and the faults are generally oriented between N80°E and N110°S. The length of faults varies from ~4 km in the older crust (north) to about 56 km on the younger crust (south). The throw along these faults varies between less than 50 m to more than 100 m. (Mukhopadhyay et al., 2002).

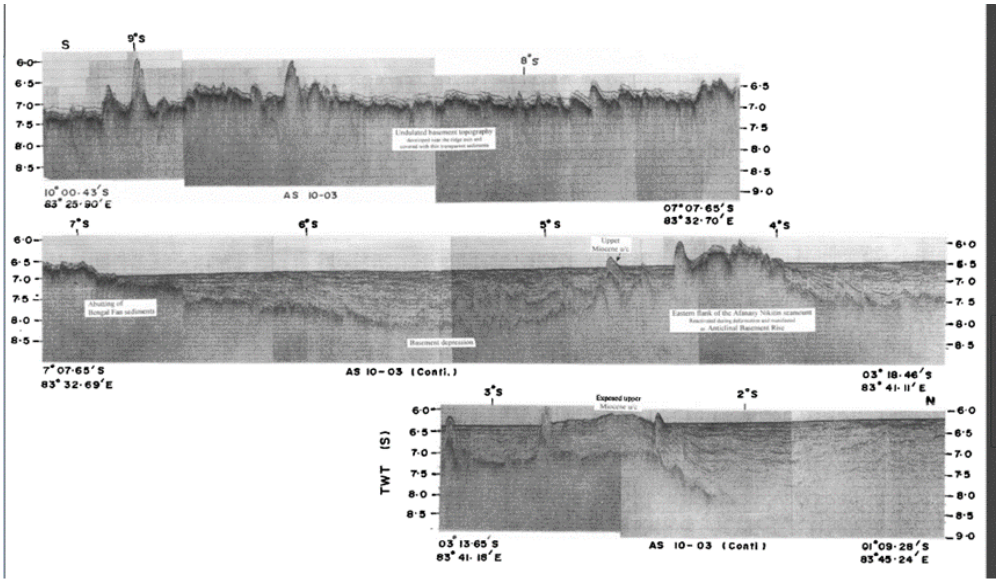

Fig. 4.2.1:Seismic profiles showing surface expression of seafloor from north to south in the eastern part of CIOB. The northern area, except at the Afanasiy Nikitin seamount, is flat as a manifestation of extension of Bengal Fan sedimentation and the southern area shows rugged topography with folding and topographic undulations (from Krishna etal., 1998)

4.2.1 Fracture zones

Three major fracture zones along 73ºE (Vishnu Fracture Zone), 76.5ºE (triple junction trace on the Indian plate-TJT-In) and 79ºE (Indrani) are identified trending almost north south in CIOB (Kameshraju, 1993). Analysis of magnetic data and bathymetry from the CIOB reveals the identification of the Cenozoic magnetic anomalies 21 to 24 on the N-S profile along 71°E. This confirms the presence of the 73°E fracture zone and suggests that the CIOB crust in this region was generated at the Southeast Indian Ridge spreading centre (Kameshraju, 1990). The elevated central portion of the Vishnu fracture zone shows many small abyssal hills with ESE–WNW orientation (Mukhopadhyay et al., 2002). The disposition of magnetic anomalies and the nature of ridge-parallel lineations in the surrounding areas suggest formation of Vishnu FZ from the east–west section of Central Indian Ridge at a half-rate of 80 mm/year between A26 and A23 and at 36 mm/year between A23 and A21. The fracture zone has offset the magnetic lineations of the same age right-laterally by about 70 km, the offset is larger in the eastern side than in the western side (Kameshraju, 1990). The fracture zone widens from ~14 km in the north to ~17 km in the south. The fine scale bathymetric variations reveal that the average amplitude and wavelength of the seafloor crenulations within the FZ are 233 m (range 40–530 m) and 22.5 km (range 8.1–38.2 km), respectively (Kessarkar, 1998).

The Indrani FZ (parallel to ~79°E) shows crest-trough topography with an elevation difference (300 m). The topography has steep gradients in the south and is gentler in the north. The seafloor along the western flank is shallower than that of the eastern flank. Seamounts along this fracture zone are mostly located in the south (Kameshraju et al., 1993). The lithospheric thickness of this fracture zone as deduced from the gravitational edge effect is 100 km and the thermal structure, considering the horizontal heat conduction, indicated the elastic limit of the lithosphere up to 23 km (Kameshraju et al., 1993).

The presence of a fracture zone at 75°45'E revealed by strike of the magnetic anomalies 21, 22, 23, 24 and 25 and trends N12°E, parallel to the fracture zones 73º and 79ºE. The evolution of the Indian Ocean Triple Junction might have caused the observed differential offsets in the magnetic anomalies across the 75°45'E fracture zone. This suggests that the evolution of the triple junction and the reorientation of the SEIR and CIR resulting in the major spreading direction changes in the CIOB during the Eocene are the major processes that have influenced the evolution of the ocean floor (Kameshraju et al., 1989).

4.2.2 Seamounts and abyssal hills

General topography of the basin varies with small abyssal hills to seamounts giving rough bottom morphology. Multibeam mapping of the CIOB reveals presence of abundant isolated seamounts and seamount chains sub-parallel to each other and closely related to the major fracture zones along 73° E, 79° E and 75°45′ E. Das et al. (2007) identified eight parallel seamount chains in CIOB that trend almost north–south and reflecting the north-ward motion of the Indian plate (Fig. 4.2.2.1). Around 200 seamounts are reported from CIOB (Mukhopadhyay and Khadge, 1990; Das et al., 2007 and references therein). The CIOB can be divided into two distinct regions, the highly deformed north (north of 9°S) and northeastern part and the relatively undeformed southern part (south of 9°S). Majority of the CIOB seamounts were formed during the period 61 to 52 Ma, and the formation of seamounts have peaked between 56 to 52 Ma (Das et al., 2007). This closely corresponds with the Indo-Eurasian collision event, during which time the spreading rate increased (95–55 mm/yr; Das et al., 2007). The seamounts are aligned in a line trending almost north south direction. The abundance of seamounts in CIOB is comparatively lesser than that of Pacific and Atlantic Ocean. On a basinal scale, the CIOB has an abundance of 976 seamounts/10^6 km^2 but on a finer scale this value varies from 500 to 1600 seamounts/10^6 km^2. Analyses of bathymetry, gravity and seismic reflection data of the diffusive plate boundary in the CIOB reveal a new kind of deformed structure besides the well-reported structures of long-wavelength anticlinal

basement rises and high-angle reverse faults (Krishna et al., 2002). General slope of the area trends towards southeastern part of the CIOB. All the seamounts are aligned in line trending almost north south direction. Eight parallel N-S trending seamount chains were identified and these reflect the motion of the Indian plate in the geologic past (Das et al., 2007). According to seamount morphology, Das et al. (2007) classified seamounts from CIOB into four different classes.

- Type 1: low height-width (HW) ratio < 0.08 indicates low slope angle (< 10°) and low flatness (< 0.12)
- Type 2: HW ratio of 0.081–0.16 shows variable slope angle (6°–15°) and flatness (0.08–0.3) indicates seamount complex indicates subsequent eruption
- Type 3: an intermediate HW ratio of 0.161–0.23 shows high slope angle (> 10°) and high flatness (> 0.2) represents older seamounts with collapse summits that formed through fissure eruption.
- Type 4: high HW ratio > 0.23 points to a high slope angle (>10°) and low to moderate flatness (< 0.2), indicates a point source of magma eruption indicates point source with flow of magma along the seamount slope.

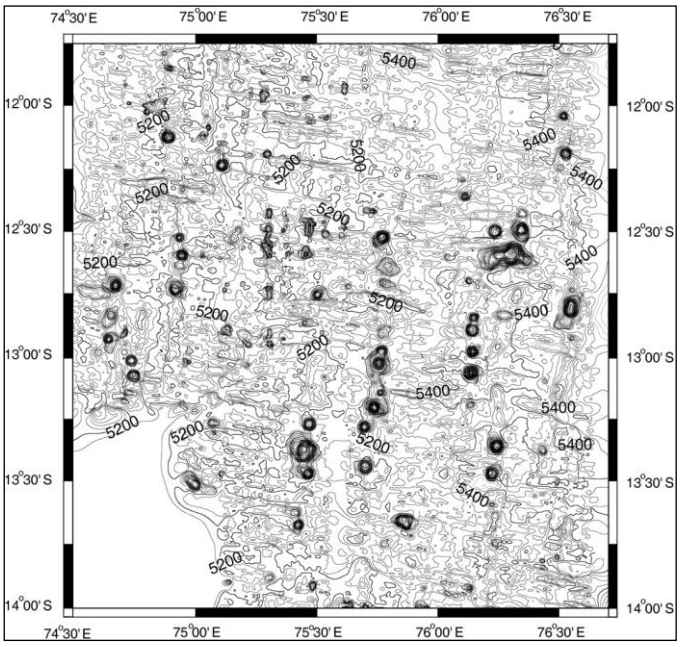

Figure 4.2.2.1: The N-S trending seamount chains in the central part of study area (Das et al., 2007)

Majority of seamounts in the CIOB were formed near the spreading ridge axis (e.g., Mukhopadhyay et al, 2002). Presence of fracture zones does not necessarily influence seamount density. The Triple junction traces in Indian plate appear to be magmatically

pronounced and have actively influenced the seamount abundance. Seamounts show multiple episodes of growth. The off-axis production of individual, isolated seamounts is far and few. Intraplate volcanism, which is of local and minor scale, mostly enlarged the dimensions of pre-existing near-axis seamounts (Fig. 4.2.2.2). It was found that the single-peaked seamounts are dominant (89%), multi-peaked are less (8%) and composite ones are rare (3%) and formed near the ridges, and their abundance depends on availability of magma (Iyer et al., 2012).

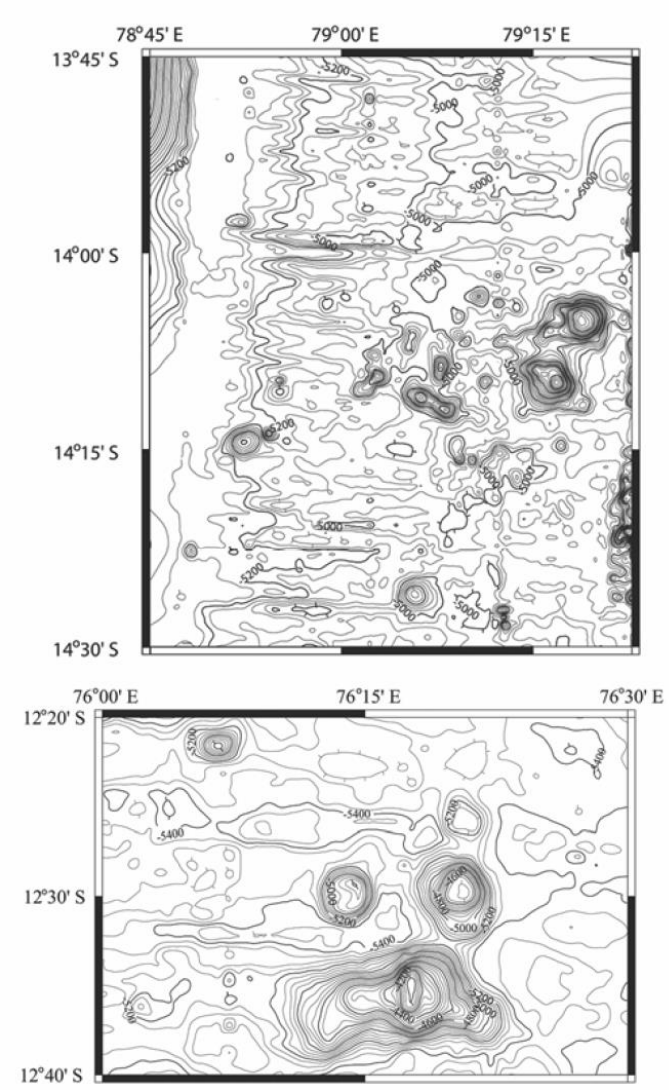

Fig. 4.2.2.2: Bathymetry of seamounts of variable morphology in CIOB (Iyer et al., 2012). Upper panel: Seamounts near the fracture zone that are less conical and have an elongated base. Lower panel: Mostly conical seamounts.

4.2.3 Intraplate deformation in the northern part

High present-day seismicity, abnormally high heat flow, intense tectonic deformations of sediments and basement, as well as other unusual geophysical characteristics (see e.g., Weissel et al., 1980) make the Central Indian Basin unique among oceanic

basins(Nephrochnov et al., 1988). The oceanic lithosphere in the central Indian Ocean has been deformed systematically by the concentration of compressional stresses related to the plate-boundary configuration and the ongoing collision of India with Asia (e.g., Krishna et al., 2001). The deformation has occurred on two major spatial scales: (1) long-wavelength (100–300 km) folding of the oceanic lithosphere and overlying sediments, and (2) reverse faulting of 5–20 km- wide blocks (Weissel et al., 1980; Neprochnov et al., 1988; Bull, 1990; Krishna et al., 1998). The drilling in the Basin indicated that significant deformation of the central Indian Ocean lithosphere began at ca. 8.0–7.5 Ma (Leg 116 Shipboard Scientific Party, 1987; Curray et al., 1989; Cochran, 1990) and the studies of seismic data have shown that deformation has occurred periodically (Krishna etal., 1998) (Fig. 4.2.3.1). The location of this deformation has been placed in a plate kinematic setting (Royer et al., 1997; Gordon et al., 1998) by splitting the traditionally defined Indo-Australian plate into the Indian, Australian, and Capricorn plates, with multiple, diffuse plate boundaries (Fig. 4.2.3.1).

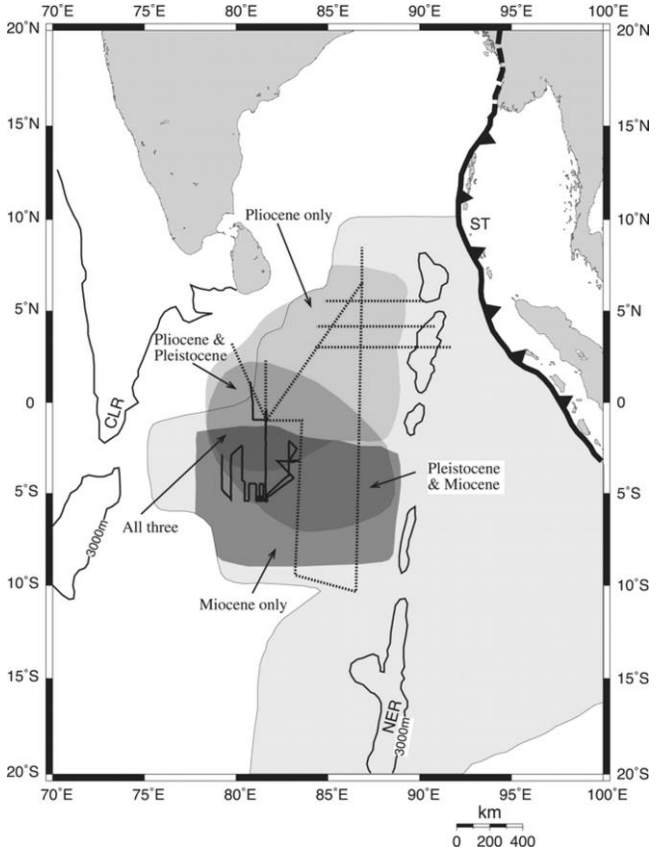

Fig.4.2.3.1: Deformation of oceanic lithosphere in space and time in central Indian Ocean. Shading shows position of diffuse plate boundary separating Capricorn, Indian, and Australian plates (Royer et al., 1997). Superimposed on this area are approximate spatial extents of long-wavelength folding at three different times (8.0–7.5, 5.0–4.0, 0.8 Ma) (Krishna et al., 2001).

The deformation is manifested by large scale folds and faults both in bathymetric and seismic maps. The lithosphere is systematically folded as crests and troughs (Fig.4.2.3.2). More than 500 high-angle reverse faults and small-scale folds were observed within the deformation zone (Krishna et al., 2001). At some locations, faulting has significantly modified the regular long-wavelength basement topography (Fig. 4.2.3.2) to produce a "sharp-crest–broad-trough" profile.

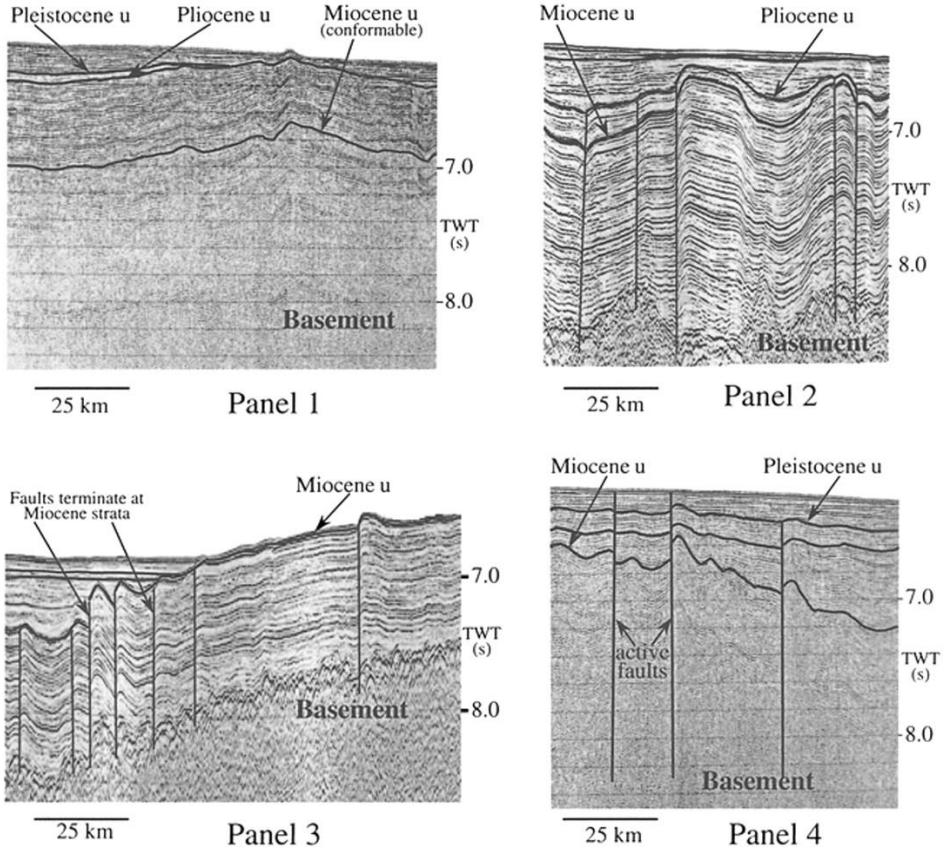

Fig. 4.2.3.2: Seismic reflection profile panels showing that the sediments clearly record major folding episodes and fault continuity in Miocene and Pleistocene time (Krishna et al., 2001).

4.2.4 Bathymetry of the contract area

As shown above, the CIOB has areas with rugged topography with seamounts and abyssal hills. In one of 3 phases of the relinquishment exercise carried out, the key parameter used was topography to eliminate areas with large slope angles and clustered seamounts and hills to facilitate the deployment of mining systems safely. The contract area with the multibeam bathymetry is presented in Fig. 4.2.4.1.

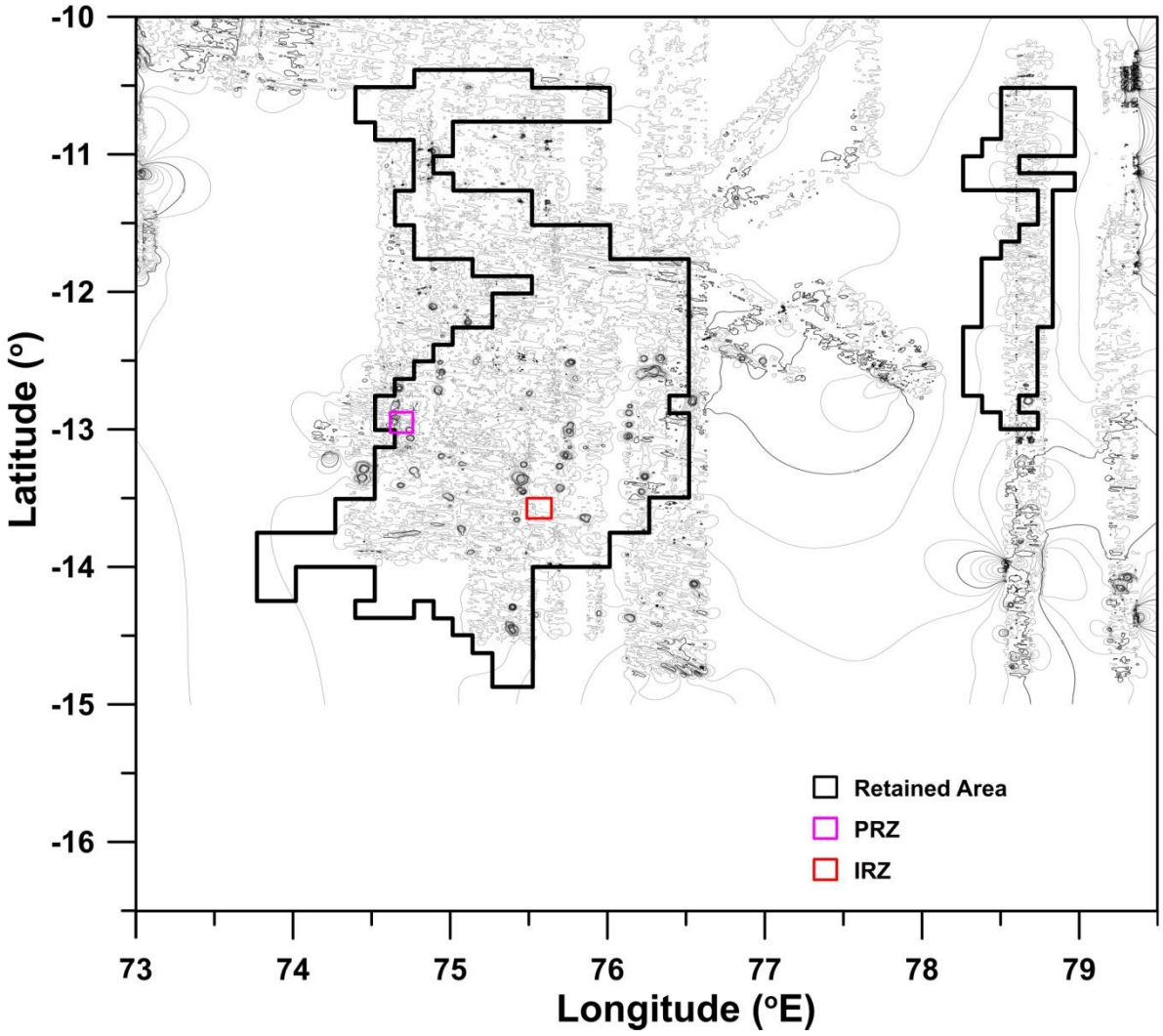

Fig. 4.2.4.1: Multibeam bathymetric map of surveyed area in CIOB. The boundaries of contract area after 3 phases of relinquishment is shown in the figure

4.2.5 Sediment thickness

While most the nodule bearing areas in CIOB has a thickness of about 100 m of sediments, the sub-bottom profiling systems help us assess the nature and variability of upper sediment layer thickness which could be acoustically transparent. As observed in seafloor photographs as well as grab and core samples collected from nodule areas, sediments seem to be associated with nodules at all locations and the presence of this sediment could play a major role in the operation of the collector on the seafloor as it could sink depending on its weight / buoyancy and physical characteristics of the sediment including thickness and geotechnical properties. Analysis of records from sounding data such as sub-bottom profiler show the sediment as acoustically transparent layer (ATL) having either homogenous or layered structure on the seafloor with variable thickness ranging from a few meters to several tens of meters (Fig. 4.2.5.1).

Correlation of ATL with different topographic settings suggests that at many of the locations (50%), its thickness is small (<10m) on the abyssal hills; whereas in the valleys, the majority of locations (>60%) have higher thickness (30-60 m) and slopes have variable thickness indicating that thickness of ATL is controlled by topographic features (Sharma et al., 2013). The study further shows that although nodule abundance does not have significant correlation with thickness of ATL, the sediment layer is responsible for partial to complete burial depending upon either size or abundance causing problems in estimating nodule populations from seafloor photographs as also observed in the Pacific Ocean (Fewkes et al, 1979; Felix, 1980).

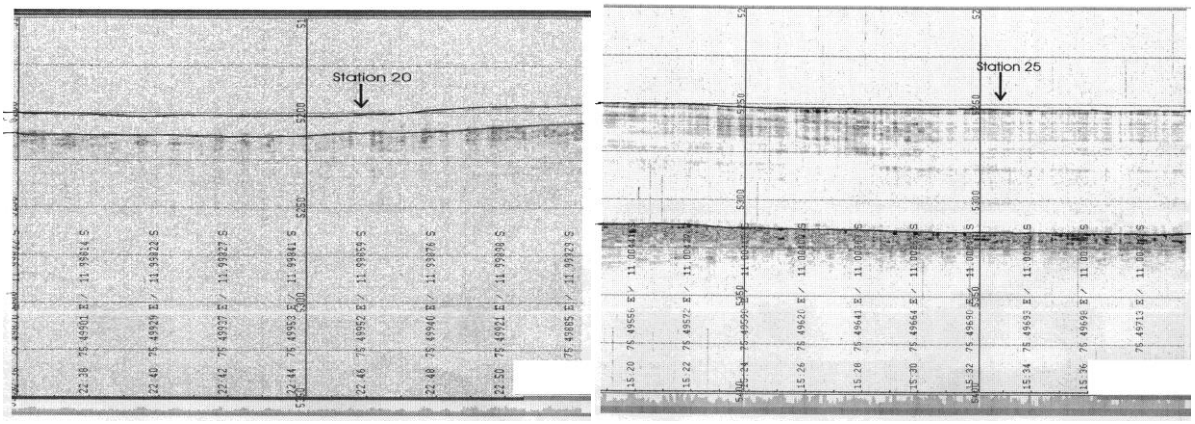

Homogenous sediment (thickness ~ 10 m) Layered sediment (thickness ~ 60 m)

Compact homogenous sediment Non reflecting basement

Fig. 4.2.5.1: Records of sub-bottom profiling

4.2.6 Regional variation of multibeam bathymetry and parasound data

In one of the expeditions to collect environmental variability data in the Indian contract area onboard RV Boris Petrov (March-May 2005), multibeam bathymetry and Parasound data were analyzed. Both the hydrosweep bathymetric and parasound system were operated simultaneously in the survey area. While the Hydrosweep system was useful in deciphering the

topographic features, Parasound was useful in deciphering the sediment thickness. The subbottom and bathymetric features were entirely different in the southern area as compared to the areas in the north. The survey was particularly useful in noticing features of about 20-25 m in height, which were seen to occur frequently in the areas surveyed during the cruise. Several small topographic features represented by the presence of numerous rocky outcrops in the area along the track, protruding through thick sediment piles were noticed. The nodule bearing areas had less uniform topography interspersed with several small topographic highs. Overall the area has several east-west trending lineations. The eastern area has deeper depths with signs of good sediment fill compared to the northern area occupied during the cruise. The recording of multibeam and Parasound data continued between all the stations and a depth contour map was generated.

4.2.7 Bathymetry and sediment thickness along the N-S transects

Two N-S transects (with some deviations during the sampling stations) covering a large distance between 10 and 16°S were surveyed (Fig.4.2.7.1). The seafloor depth and the sediment thickness are higher in the northern areas compared to the south, with the depth varying generally between 5200-5340 m in the north and between 4900-5230 m in the south. The sediment thickness from the Parasound was found to vary between 50-70 m in the north as compared to 10-15 m in the south. The depth and sediment thickness around the sampled locations alongthe transects are given in Table 4.2.7.1. A section of the transect between 10^{o} - 11^{o}S showing bathymetry and sediment thickness is given in Fig. 4.2.7.2

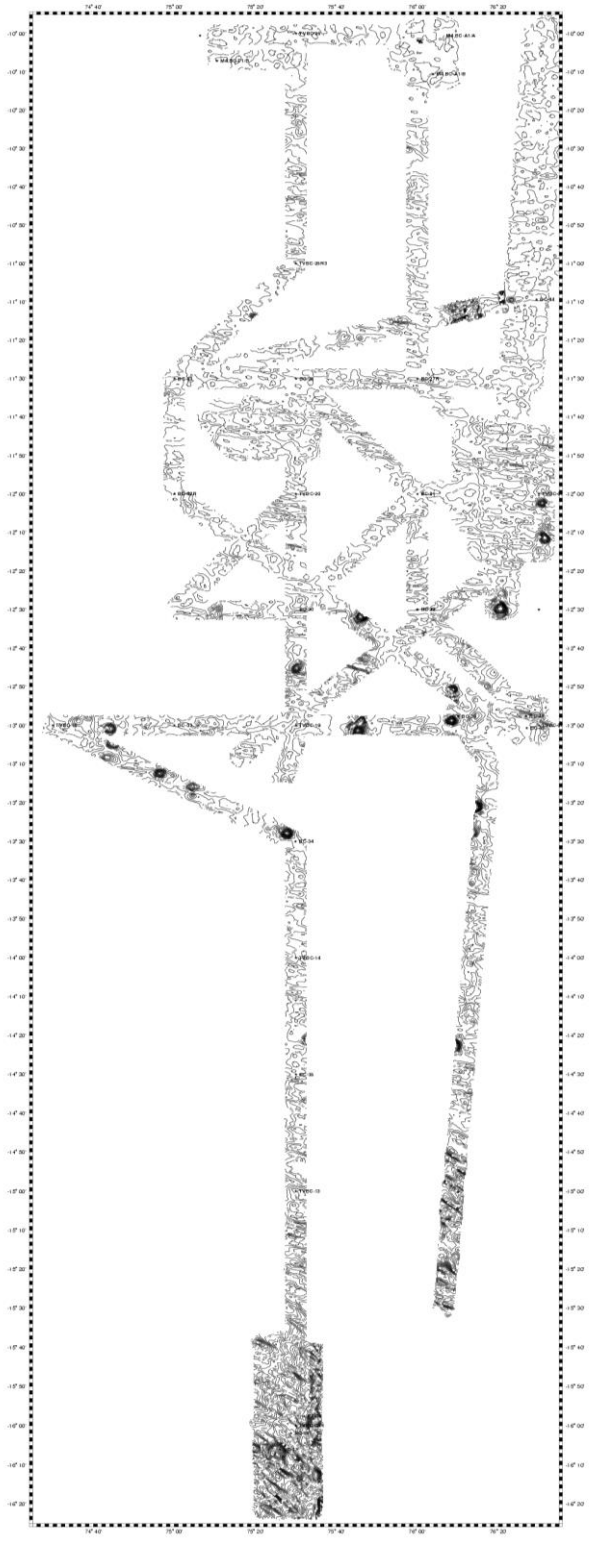

Fig. 4.2.7.1: Multibeam map of N-S transects in contract area

Table 4.2.7.1: Description of geomorphology of sampled stations

Sl.No.	Station Number	Depth (m)	Sediment thickness (m)
1.	TVBC 26	5338	70
2.	TVBC 25	5292	50
3.	BC 28	5266	30
4.	TVBC 20	5239	50
5.	BC 30	5180	-
6.	TVBC 19	5096	-
7.	BC 34	5225	10
8.	TVBC 14	5189	15
9.	BC 35	5237	10
10.	TVBC 13	4899	15
11.	TVBC 8	5201	10

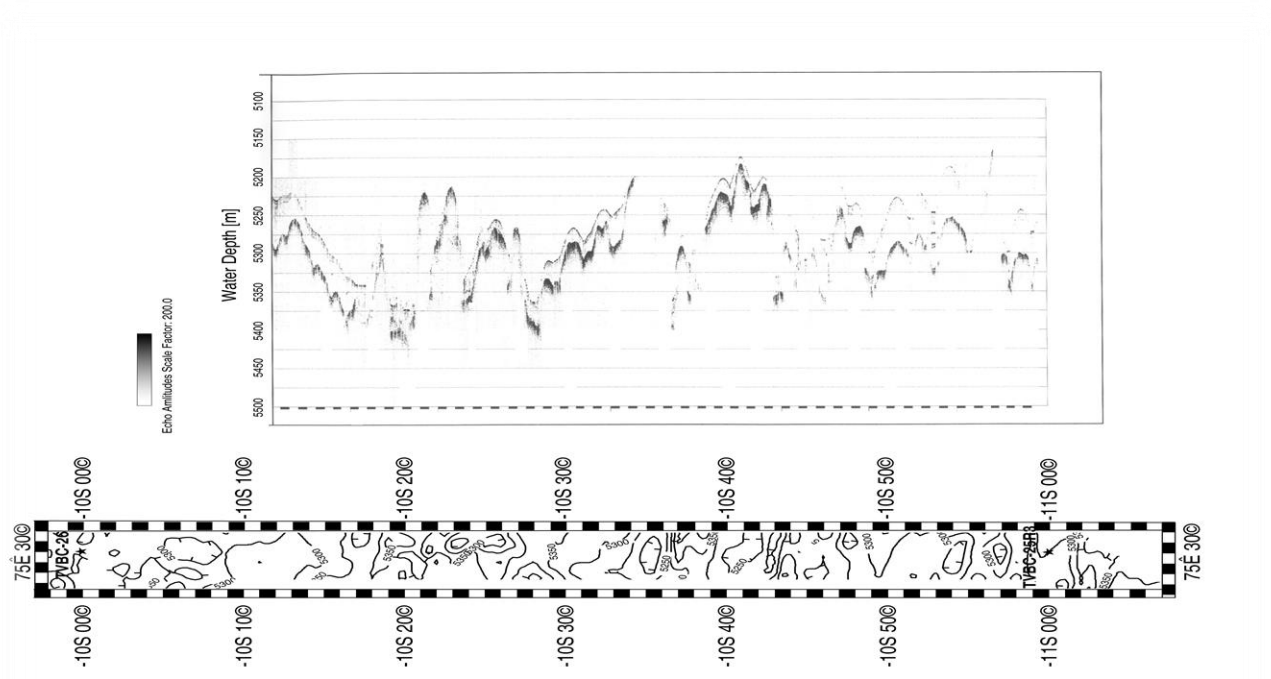

Fig. 4.2.7.2: Parasound and multibeam along N-S transect (75°30'E, 10° - 11°S)

4.2.8 Bathymetry and sediment thickness along an E-W transect

The general bathymetric variations and the sediment thickness along an east-west transect between 74°30' and 76°30'E along the 13°S latitude (Fig. 4.2.8.1) were assessed. It was found that the eastern section is deeper than the western section of the transect, the deepest contour on west is 5150 m, while in centre is 5250 m and the deepest part in the east is 5650 m. The sediment thickness was found to vary with the seafloor topography, with less thickness on peaks and higher thickness on slopes and valleys.

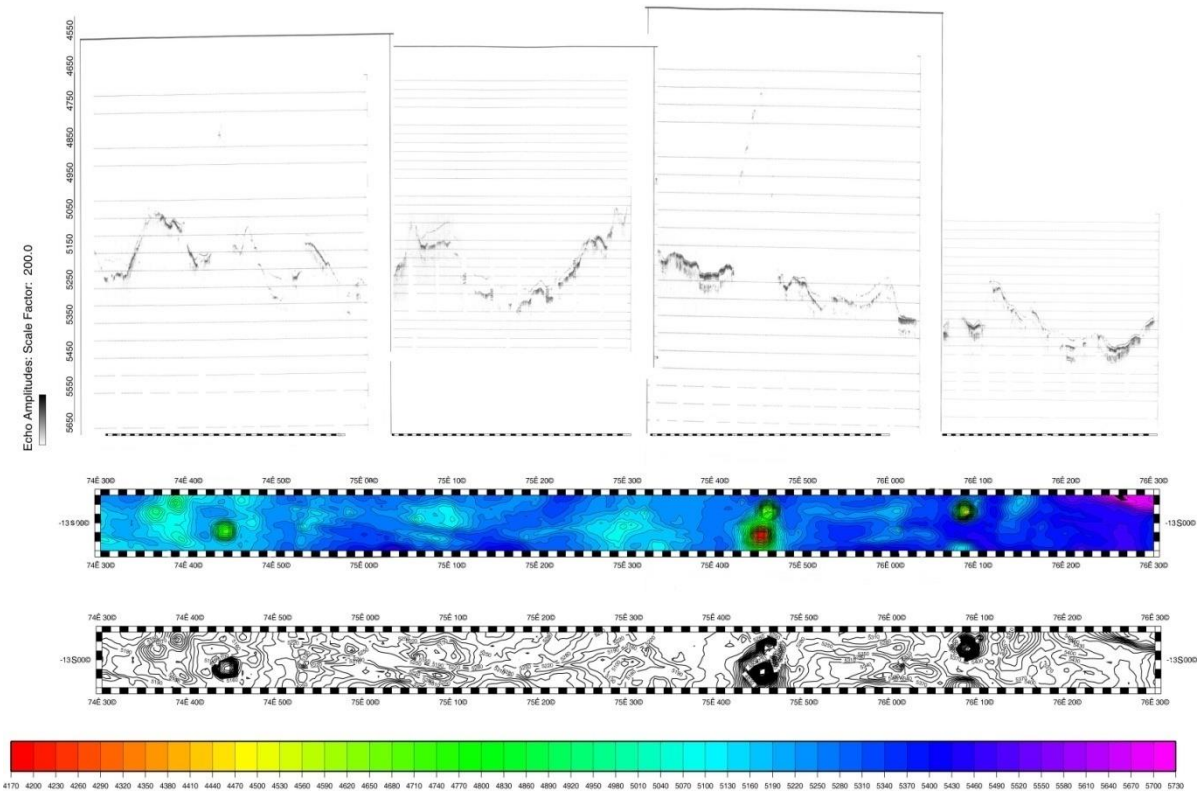

Fig.4.2.8.1: Parasound and multibeam along E-W transect (74°30' – 76°30'E, 13°S)

4.2.9 Nodule distribution characteristics in relation to bathymetry, sediment cover, its thickness and associated seafloor features

Nodule distribution in relation to its association with the seafloor features was analyzed from 20,000 seafloor photographs in the Indian Contract area. Typically nodules are found in varying coverages on the seafloor (1-90%) and are associated with substrates such as sediments and rock outcrops / ferromanganese crusts (Fig 4.2.9.1). Correlation of the distribution of nodules, sediments and rock shows that these are controlled by seafloor topography which in turn influences the burial of nodules within the upper sediment layers as well as exposure of rocks as sources of nucleus for the formation of nodules.

Dense nodules Sparse nodules with rocks

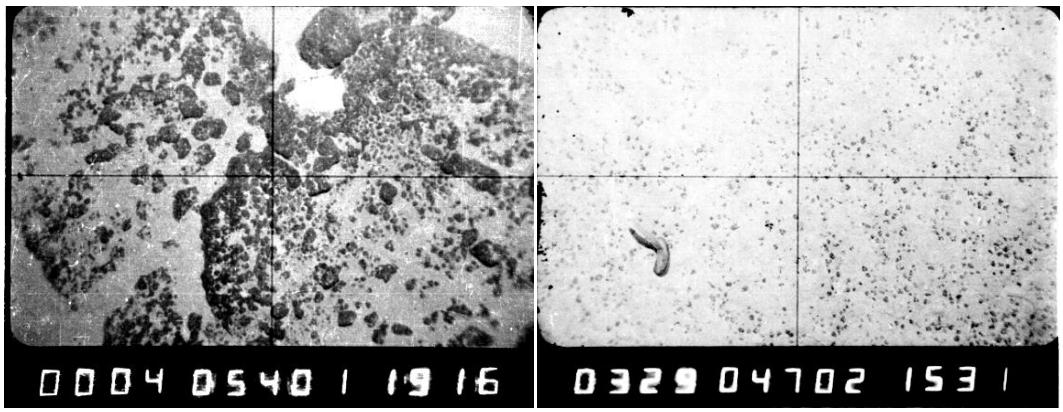

Nodules and crusts Nodules and benthic biota on sediment substrate

Fig. 4.2.9.1: Distribution of nodule coverage on the seafloor

An analysis of ~20,000 seafloor photographs from CIOB showed a majority (65%) of them having nil nodule coverage, some (17%) of them with low nodule coverage (<20%) and the remaining (18%) having moderate (20-50%) and high (50-80%) coverage (Sharma et al., 2010). However, physical sampling using grabs in the same area has shown average nodule abundance ranging from 3.84-8.23 kg/m^2 confirming the presence of nodules in the entire area implying that nodules at many locations in CIOB could be buried under the top 20-25 cm of sediment cover to which grabs can penetrate (Sharma et al., 2013).

4.2.10 Bathymetry and sediment thickness in IRZ and PRZ

During the expedition of RV Sindhu Sadhana (July-August 2015) to collect environmental data in the IRZ and PRZ, seafloor bathymetry data was generated with the multibeam mapping system onboard and maps were prepared for both the areas (Figs. 4.2.10.1a,b). While most of the IRZ area is deeper (5200 to little deeper than 5300m), the northwestern part of the area has an abyssal hill with the water depth at summit is ~4500 m. The depths in

PRZ are slightly shallower (5100 to 5200m), but have 3 abyssal hills with summit heights of 400 to 600m (water depths of ~4600, 4700 and 4800m respectively).

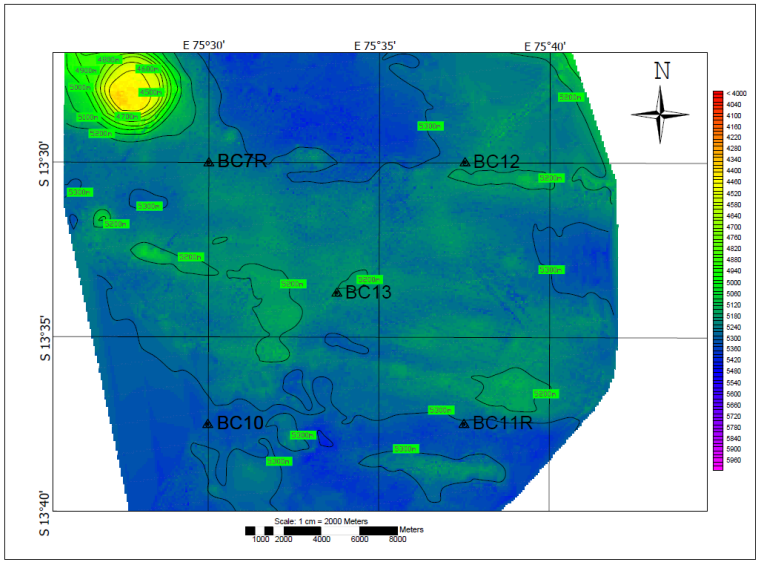

Fig. 4.2.10.1a: Bathymetric map with sediment core locations in IRZ

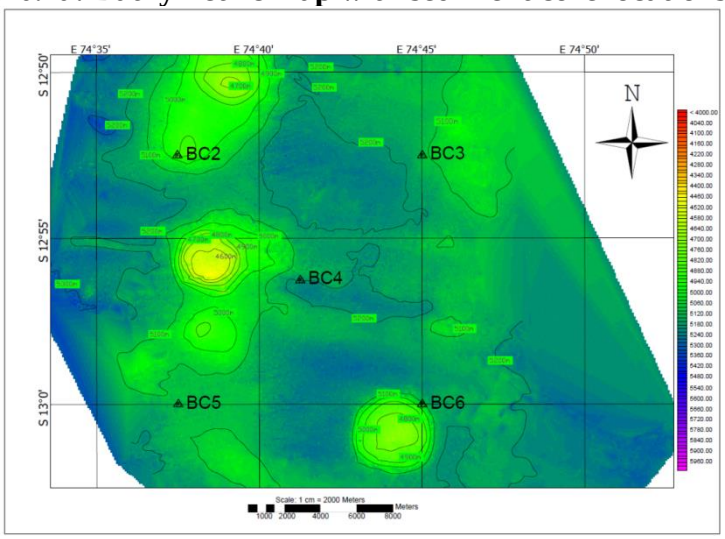

Fig.4.2.10.1b: Bathymetric map with sediment core locations in PRZ

Thickness of acoustically transparent sediment layer at the sampling locations was also evaluated from Parasounddata in both the areas (Table 4.2.10.1). The thickness of sediments as depicted by Parasound ranges between 10 and 80 m and the nature of sediments interpreted from these records is soft and sometimes compact. On a slope category scale of 1-4 (with increasing roughness), IRZ and PRZ fall in 2 and 4 categories respectively, with slope angles in IRZ mostly below 3°.

Table 4.2.10.1: Parasound record of nature and thickness of sediments at sampling stations in IRZ and PRZ

S. No.	Station No.	Type of seafloor	Thickness of top layer (m)
1	BC-2/PRZ	Uneven, homogenous sediment	50
2	BC-3/PRZ	Soft sediment, homogenous sediment	80
3	BC-4/PRZ	Uneven, soft sediment	-
4	BC-5/PRZ	Slightly compact, homogenous sediment	50
5	BC-6/PRZ	Soft bottom, homogenous sediment	50
6	BC-7R/IRZ	Parasound record not clear	20
7	BC-10/IRZ	Flat, soft sediment	50
8	BC-11R/IRZ	Parasound record not clear	60
9	BC-12/IRZ	Parasound record not clear	25
10	BC-13/IRZ	Parasound record not clear	10

4.3 Atmospheric and meteorological conditions

4.3.1 Historical data

Historical data for almost ten year periods for sea-surface temperature, wind speed and rainfall (1988-1998); cyclones (1997-2007) and waves (1953-1961) from global sources (Grass et al., 2000; www.metoffice.gov.uk; Hogben and Lumb, 1967) was analyzed for areas in and around the Central Indian Ocean Basin (Sharma, 2019).

4.3.1.1 Sea surface temperature

Sea surface temperature evaluated for the period (Table 4.3.1.3.1 Fig. 4.3.1.3.1) shows that average temperature between December and May is between 27^{o} and 29^{o}Celsius that corresponds to Austral summer, whereas the period from June to November has an average temperature between 24^{o} and 26^{o}Celsius corresponding with Austral winter. In terms of maximum and minimum, the temperatures are generally within the range of +/- 2^{o} Celsius (Grass et al., 2000). Hence, the temperature range in the area is very small throughout the year with no extreme temperatures that could have any serious effects on the deep sea mining operations.

4.3.1.2 Wind speed

Wind speed data collected during the period (Table 4.3.1.3.2, Fig. 4.3.1.3.2) shows that mean wind speed is relatively higher (6.8-8.4 m/s) from June to November with August and September recording the highest wind speeds (maximum of 9.39 m/s and 9.53 m/s respectively), whereas these are lower (4.8-6.5 m/s) from December to May with February and March having the lowest wind speeds (minimum of 3.38 and 3.88 m/s) during different years. Although in general, wind speeds are not very strong throughout the year, winds are responsible for generation of waves and can have serious impact on operations during the occurrence of cyclones and hurricanes (see section on cyclones).

4.3.1.3 Rainfall

Analysis of mean rainfall data for different months during the period (Fig. 4.3.1.3.3 and Table 4.3.1.3.3), shows that although the area does not appear to receive very heavy rains throughout the year, the months from January to April receive relatively higher average rainfall (5.679 - 6.577 mm/day) whereas July to October has lower average rainfall (2.327-3.311 mm/day) and the intervening months (May-June and November-December) have intermediate rainfall. However, there could be episodic heavy rainfall coinciding with the events of cyclones as described in the next section.

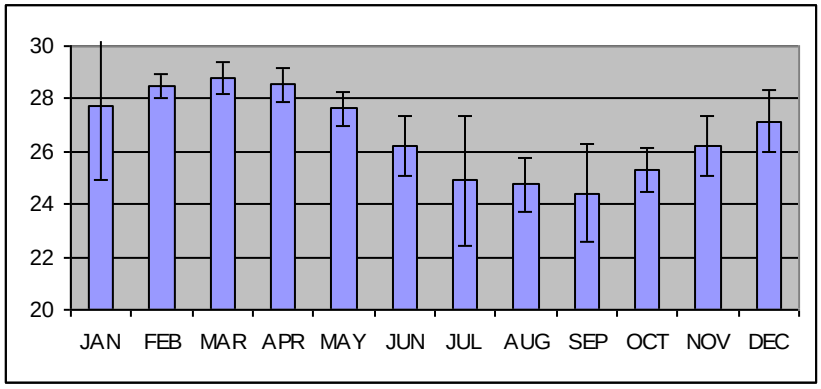

Fig. 4.3.1.3.1: Variation in average sea surface temperature for different months (in degree Celsius)

Table 4.3.1.3.1: Variation in sea surface temperature for different months (in degrees Celsius)

YEAR/ MONTH	JAN	FEB	MAR	APR	MAY	JUN	JUL	AUG	SEP	OCT	NOV	DEC
1988	28.35	29.29	29.43	29.5	28.10	26.4	25.41	25.93	21.71	26.24	26.35	26.95
1989	28.59	28.82	28.75	28.09	27.02	25.33	21.10	23.88	24.27	25.20	26.08	27.33
1990	28.66	28.20	28.93	28.12	27.48	25.73	25.23	24.49	24.76	25.39	26.40	27.26
1991	28.14	28.71	28.83	28.63	28.36	27.45	25.74	24.42	24.33	24.75	26.38	27.13
1992	28.34	28.61	28.76	28.74	27.63	25.94	25.08	24.78	24.44	25.00	25.55	26.52
1993	27.20	27.82	28.61	28.67	27.10	26.01	25.26	25.23	25.08	25.23	26.21	27.09
1994	27.28	27.91	28.31	27.86	27.26	25.15	25.00	24.70	24.91	25.52	26.36	27.74
1995	23.61	28.45	28.76	28.30	27.56	26.63	25.31	24.71	24.67	25.01	26.07	27.16
1996	28.00	28.46	28.65	28.28	27.64	26.72	25.28	24.56	24.74	25.06	26.42	27.33
1997	28.17	28.03	28.34	28.54	27.38	26.26	25.12	24.81	25.30	26.33	27.43	28.26
1998	29.07	28.96	29.48	29.16	28.33	26.90	25.53	24.63	24.44	24.74	25.18	25.92
Average	27.76	28.47	28.80	28.53	27.62	26.22	24.91	24.74	24.42	25.31	26.22	27.15
Minimum	23.61	27.82	28.31	27.86	27.02	25.15	21.10	23.88	21.71	26.33	25.18	25.92
Maximum	29.07	28.96	29.48	29.16	28.36	27.45	25.74	25.93	25.30	24.74	27.43	28.26
Std deviation	2.850	0.459	0.587	0.650	0.671	1.150	2.474	1.029	1.871	0.805	1.126	1.170

Table 4.3.1.3.2: Variation in mean wind speed for different months (in m/s)

Year/ Month	JAN	FEB	MAR	APR	MAY	JUN	JUL	AUG	SEP	OCT	NOV	DEC
1988	5.362	3.3895	3.881	3.93	5.897	6.219	7.755	7.223	7.156	7.306	6.625	7.306
1989	4.764	5.756	4.486	5.787	7.029	7.427	8.220	8.350	7.995	7.206	6.075	6.23
1990	5.480	4.257	5.072	5.398	6.201	7.270	6.654	7.866	8.275	7.164	6.690	5.869
1991	6.172	4.996	5.661	6.120	5.780	7.011	8.722	8.311	9.530	8.698	7.390	6.683
1992	4.755	6.202	4.599	5.073	6.803	7.540	8.245	8.719	8.371	8.447	7.423	6.600
1993	6.610	4.852	4.314	5.713	7.127	7.812	7.929	7.959	8.05	8.200	6.990	6.751
1994	6.027	4.900	5.328	6.212	6.381	7.681	8.983	9.39	8.004	7.830	7.610	6.277
1995	5.620	5.364	5.420	6.324	6.358	7.205	8.500	9.029	8.811	7.450	6.844	6.130
1996	5.690	5.915	5.536	6.753	6.185	7.740	7.933	8.580	8.035	7.847	6.740	5.039
1997	5.149	5.381	4.593	5.867	6.826	8.001	8.811	8.63	7.529	7.199	6.381	5.420
1998	5.567	5.199	4.166	5.101	6.990	7.922	8.227	8.68	9.05	8.708	6.502	7.483
Avg	5.563	5.110	4.823	5.661	6.507	7.438	8.179	8.430	8.255	7.823	6.842	6.344
Min	4.755	3.389	3.881	3.93	5.897	6.219	6.654	7.223	7.156	7.164	6.075	5.039
Max	6.610	5.915	5.661	6.753	7.127	8.001	8.983	9.39	9.530	8.708	7.610	7.483
SD	0.930	1.290	0.890	1.423	0.615	0.910	1.182	1.085	1.188	0.774	0.767	1.222

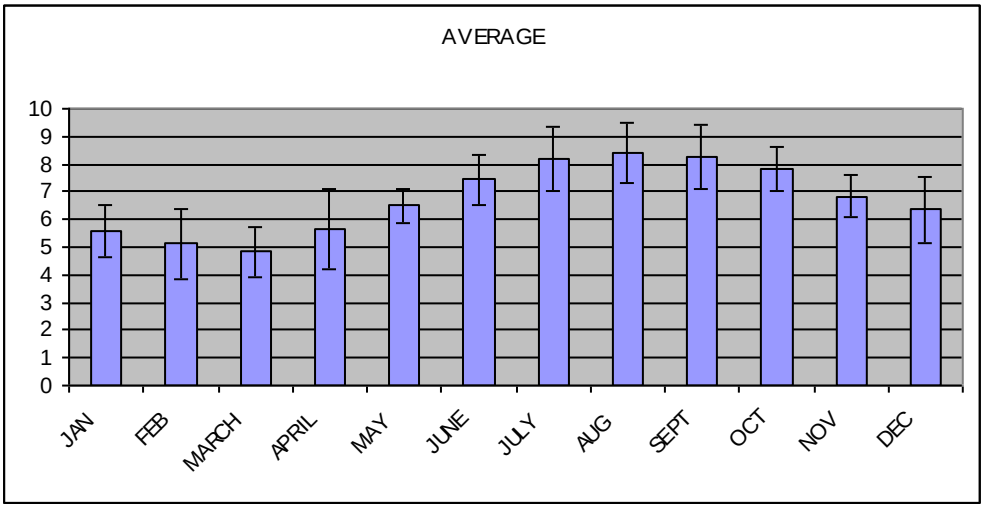

Fig. 4.3.1.3.2: Average wind speed for different months (in m/s).

Table 4.3.1.3.3: Variation in rainfall for various months (in mm/day)

YEAR/ MONTH	JAN	FEB	MAR	APR	MAY	JUN	JUL	AUG	SEP	OCT	NOV	DEC
1988	7.925	6.31	7.335	4.391	6.004	2.6875	2.62	2.0225	4.027	3.898	7.37	2.1285
1989	4.839	6.248	6.815	9.07	6.039	3.840	3.391	3.37	3.722	3.511	3.505	3.991
1990	4.32	3.435	8.135	5.732	3.901	5.148	2.421	4.003	4.033	2.6025	5.168	4.991
1991	6.885	6.6	2.472	6.335	4.880	5.136	4.273	1.611	4.572	1.709	6.71	7.57
1992	5.52	7.985	4.776	2.089	2.764	1.483	3.067	2.569	1.955	1.644	2.382	6.565
1993	6.975	5.71	6.79	6.995	3.350	3.384	3.541	1.855	2.5	1.371	3.179	4.605
1994	7.33	8.77	4.113	4.595	2.134	2.093	2.544	1.851	1.459	2.093	7.09	1.851
1995	4.599	6.85	7.8	5.249	3.346	1.784	2.04	2.284	1.818	2.467	5.44	3.076
1996	6.355	7.935	7.38	6.96	3.674	5.875	4.566	1.959	3.615	3.553	2.388	5.755
1997	6.475	7.989	6.32	5.112	2.364	6.12	4.656	2.10	2.54	3.112	3.654	6.145
1998	1.249	4.522	4.465	8.09	8.48	4.086	3.309	1.977	3.177	1.92	1.762	1.544
Average	5.679	6.577	6.036	5.874	4.266	3.785	3.311	2.327	3.038	2.541	4.422	4.383
Minimum	1.249	3.435	2.472	2.089	2.134	1.483	2.04	1.611	1.459	1.92	7.37	1.544
Maximum	7.925	8.77	8.135	9.07	8.48	6.12	4.656	4.003	4.572	3.898	1.762	7.57
Standard deviation	3.397	2.681	2.862	3.494	3.229	2.318	1.308	1.227	1.556	1.0115	2.805	3.014

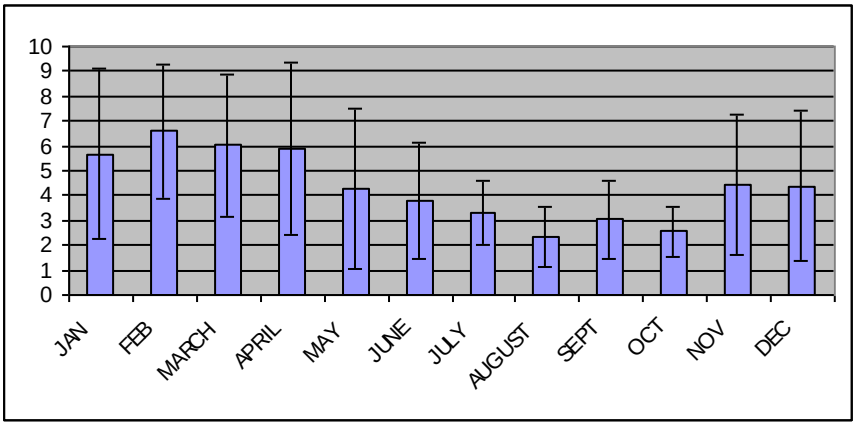

Fig. 4.3.1.3.3: Variation in average rainfall for various months (in mm/day)

4.3.1.4 Cyclones

Occurrence of cyclones has been analyzed in terms of frequency and speed for a ten year period (1997-2007) for the region. Cyclones are classified into four types on the basis of speed (www.metoffice.gov.uk), as follows:

i. Tropical depressions (<34 knots).
ii. Tropical Storms (34-63 knots).
iii. Hurricane/ Typhoon (64-127 knots)
iv. Severe hurricane/ Super typhoon (>127 knots)

Data for different types of cyclones in the Indian Ocean (Fig. 4.3.1.4.1, Table 4.3.1.4.1) shows that the months which are more prone to cyclones (more than 10 occurrences in a month of any type of cyclone described above) are January to March; whereas the months with lesser no. of cyclones (i.e. less than 10 occurrences in a month) are April to December. No cyclones were recorded in August and September,

Although, the most destructive category of cyclones, i.e. super hurricane did not occur during these years, hurricanes are more prominent during the months January to March, which have been also registered as the months having maximum number of cyclones. In the category of storms, although January and February witnessed the maximum number; April, June, July, October, November and December, also witnessed storms but in fewer numbers. Depressions are more in the months of March, April, October and November, but they do-not pose a serious threat in comparison to hurricanes and super hurricanes, which may cause severe damage to the mining platform. During August and September, there were no cyclones of any intensity in the area.

The months from April to December appear to be the most favourable months for carrying out the seabed mining operations, since these months are only subjected to none or low speed storms and depressions, without registering any major hurricanes. Hence, about a 90-100 day period between January and early April appears to be unfavourable in terms of total number of cyclones and hurricanes in the area. Cyclones play a major role in perturbing the stability of an off-shore platform as well as for conducting operations from the platforms due to adverse effects on working as well as structural parts. Moreover, analysis of cyclone tracks (Fig. 4.3.1.4.2) shows that most cyclones were concentrated in the western parts of the Indian Ocean, whereas very few cyclones actually crossed the Central Indian Ocean Basin, making it favourable area for deep-sea mining operations.

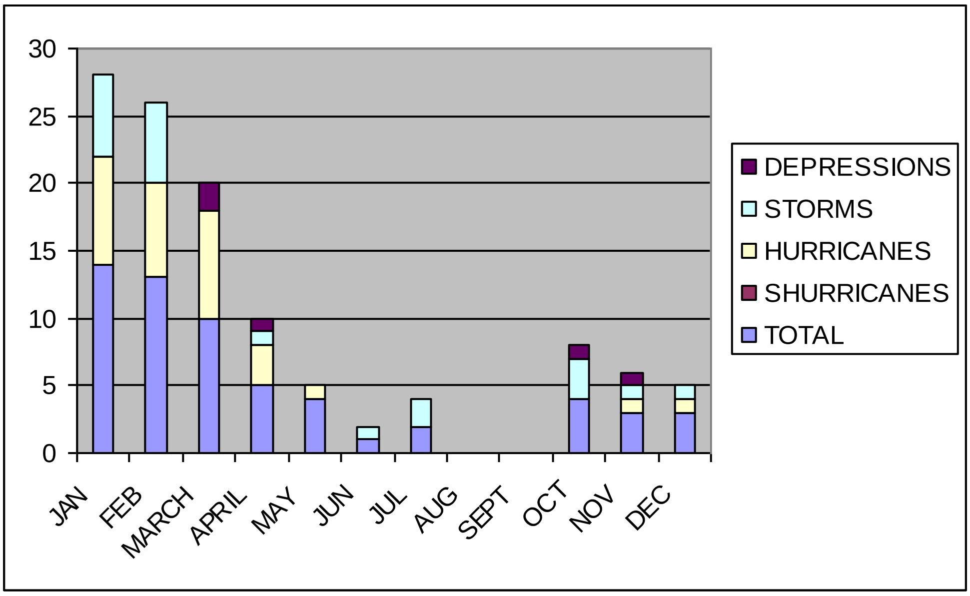

Fig.4.3.1.4.1: Occurrence of cyclones for different months between1997-2007

(Source : www.metoffice.gov.uk)

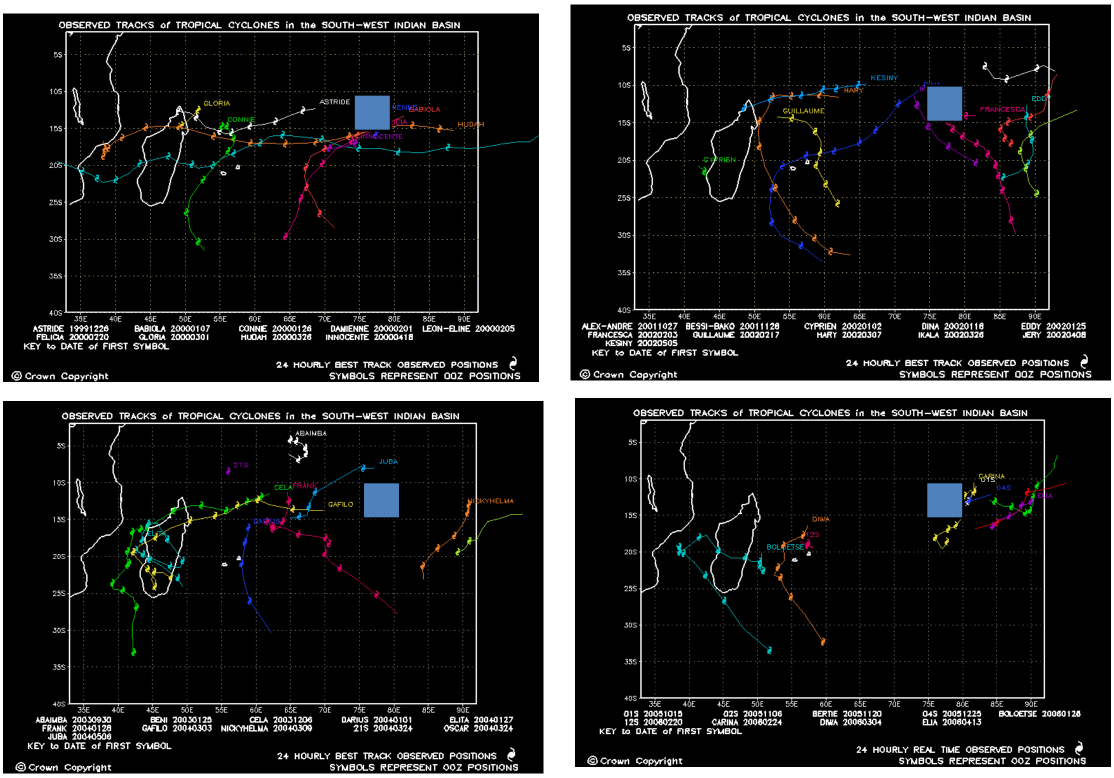

Fig. 4.3.1.4.2: Cyclone tracks during the study period: 1999-2000 (top left), 2001-2002 (top right), 2003-2004 (bottom left) and 2005-2006 (bottom right). Central Indian Ocean basin is marked with blue box.

Table 4.3.1.4.1: Frequency of occurrence and speed of cyclones during the years

MONTH/ YEAR	JAN		FEB		MAR		APR		MAY		JUN		JUL		AUG		SEP		OCT		NOV		DEC	
	N	Km	N	Km	N	Km	N	Km	N	Km	N	Km	N	Km	N	Km	N	Km	N	Km	N	Km	N	Km
1997	4	55, 45, 65, 115	3	90, 60, 125	1	75	0	0	3	nd	0	0	1	45	0	0	0	0	0	0	0	0	0	0
1999	1	55	2	40, 40	3	25, 90, 30	1	115	0	0	0	0	1	45	0	0	0	0	0	0	0	0	0	0
2001	3	100, 80, 105	0	0	1	75	2	30, 60	0	0	1	40	0	0	0	0	0	0	2	30, 55	1	35	1	nd
2003	2	75, 55	3	105, 80, 45	2	115, 140	1	65	1	65	0	0	0	0	0	0	0	0	1	45	1	105	1	65
2005	3	45, 100, 35	1	60	1	65	Nd	Nd	0	0	0	0	0	0	0	0	0	0	1	35	1	45	1	35
2007	1	65	4	115, 55,	2	105, 115	1	110	0	0														

				125, 70																				
Total number of cyclones	14		13		10		5		4		1		2		0		0		4		3		3	
Tropical depressions	0		0		2		1				0		0		0		0		1		1		0	
Tropical cyclones	6		6		0		1				1		2		0		0		3		1		1	
Hurricanes/typhoons	8		7		8		3		1		0		0		0		0		0		1		1	
Super Hurricanes/ Super typhoons	0		0		0		0				0		0		0		0		0		0		0	

4.3.1.5 Waves

Wave data was analysed from Ocean wave atlas (Hogben and Lumb, 1967) for block no. 35 (0^o-10^o S, 60^o-90^o E) in the Central Indian Ocean Basin. The data is classified into three seasons – North-east monsoon (December-February), South-west monsoon (May-September) and transition period (March-April, October-November). The maximum number (1000-1500 waves) recorded throughout the year irrespective of seasons were 1 m high, followed by < 1m and 1-2.5m (200-1000 waves) and very few (<100 waves) of 3-8 m height (Fig. 4.3.1.5.2 and Table 4.3.1.5.1). Similarly, maximum number (700-2000 waves) had a direction between 80^o and 160^o during the period from May to September followed by direction between 230^o and 280^o (400-500 waves) during the period from December to February, whereas very few (<300 waves) were recorded with directions ranging from 0 to 360 throughout the year (Fig. 4.3.1.5.3, Table 4.3.1.5.2).

In terms of wave period (the average of time interval between passages of successive crests or troughs of waves), the majority of waves were of the time period of 5 to 9 seconds. Very few waves have been reported with a time period >14 seconds. However, some waves with an interval of 10-13 seconds have been recorded. In case of the total number of waves recorded, the duration from May to September has witnessed the maximum number of waves, followed by transition months (Table 4.3.1.5.3, Fig. 4.3.1.5.4).

From the above observations, we can interpret that, wave heights are generally less than 2.5 m throughout the year with few waves having more heights (3-8 m). Also the wave direction varied between 80-160^o and 230-280^o during different seasons which will have to be considered during designing of the mining platform. Winds are responsible for initiating the waves, that is higher the wind velocity, higher the waves, and the time interval between the two successive crests (or troughs) of waves will be high.

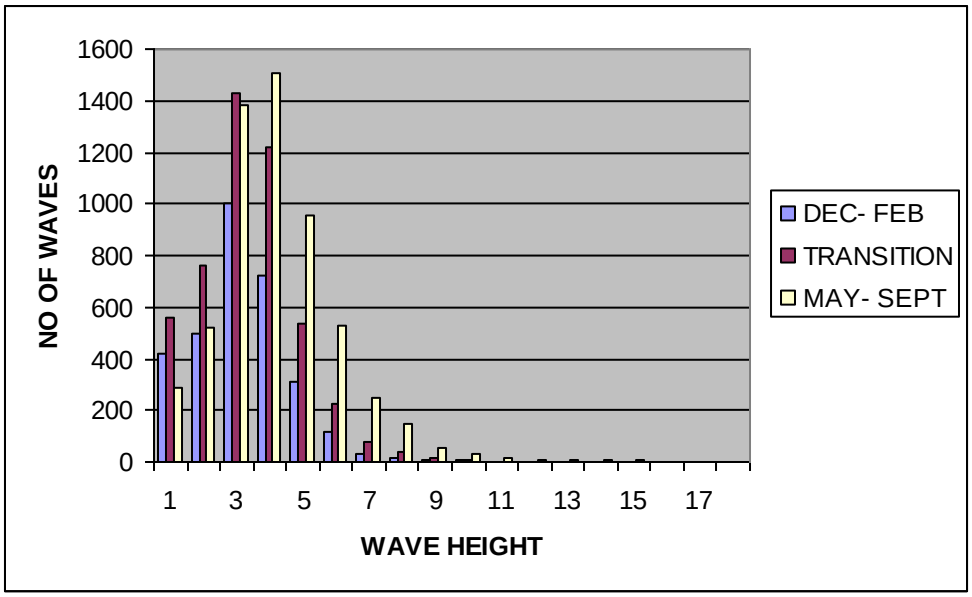

Fig.4.3.1.5.1: Number of waves of different heights for various seasons (in meters)

Table 4.3.1.5.1: Number of waves of different heights for various seasons

	December-February (North east monsoon)	March-April, October-November (Transition months)	May-September (South west monsoon)
Wave height (m)	Total no. of waves	Total no. of waves	Total no. of waves
0.25	420	556	284
0.50	494	765	520
1.00	1004	1432	1386
1.50	719	1223	1507
2.00	314	536	959
2.50	116	224	530
3.00	34	75	248
3.50	19	37	149
4.00	5	14	54
4.50	7	8	31
5.00	1	3	12
5.50	1	1	6
6.00	0	0	5

6.50	1	0	7
7.00	1	0	4
7.50	0	1	3
>8.00	0	0	3

Table 4.3.1.5.2: Number of waves in different directions for various seasons

	December-February (North east monsoon)	March-April, October-November (Transition months)	May-September (South west monsoon)
Wave direction (degrees)	Total no. of waves	Total no. of waves	Total no. of waves
350- 10	182	94	42
20- 40	135	111	38
50- 70	122	310	361
80-100	200	717	1441
110-130	266	831	1932
140-160	177	542	855
170- 190	131	255	290
200- 220	194	313	169
230- 250	429	511	150
260- 280	462	474	140
290- 310	325	208	48
320- 340	206	108	30

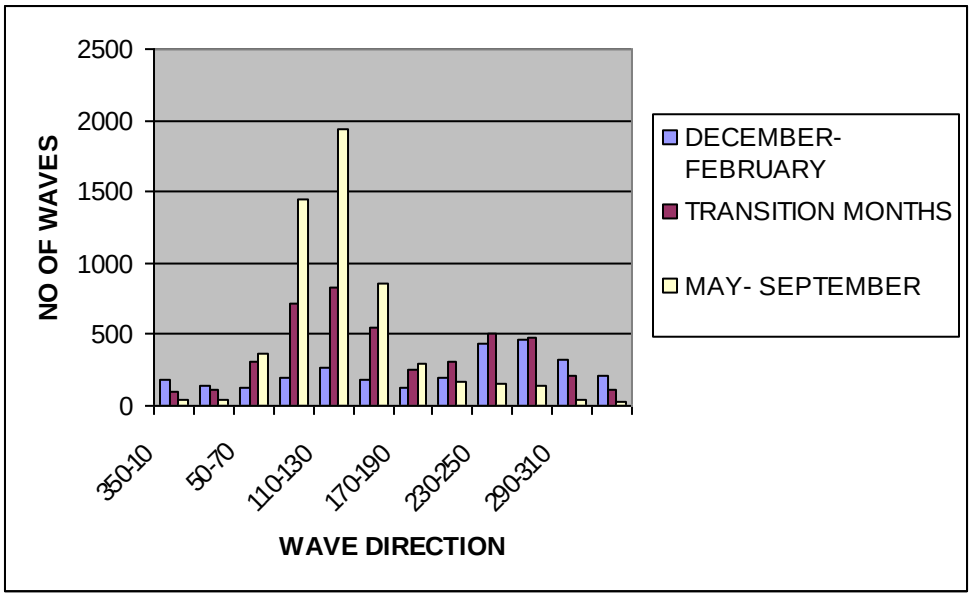

Fig.4.3.1.5.3: Number of waves in different directions (in degrees)

Table 4.3.1.5.3: Number of waves for different periods

	December-February (North east monsoon)	March-April, October-November (Transition months)	May-September (South west monsoon)
Wave period (secs)	Total no. of waves	Total no. of waves	Total no. of waves
CALM WAVES	307	401	212
5 OR LESS	1382	2083	1730
6 OR 7	825	1254	1727
8 OR 9	367	630	1192
10 OR 11	146	319	532
12 OR 13	42	108	215
14 OR 15	18	38	42
16 OR 17	4	6	22
18 OR 19	1	2	2
20 OR 21	3	5	2
OVER 21	41	29	32

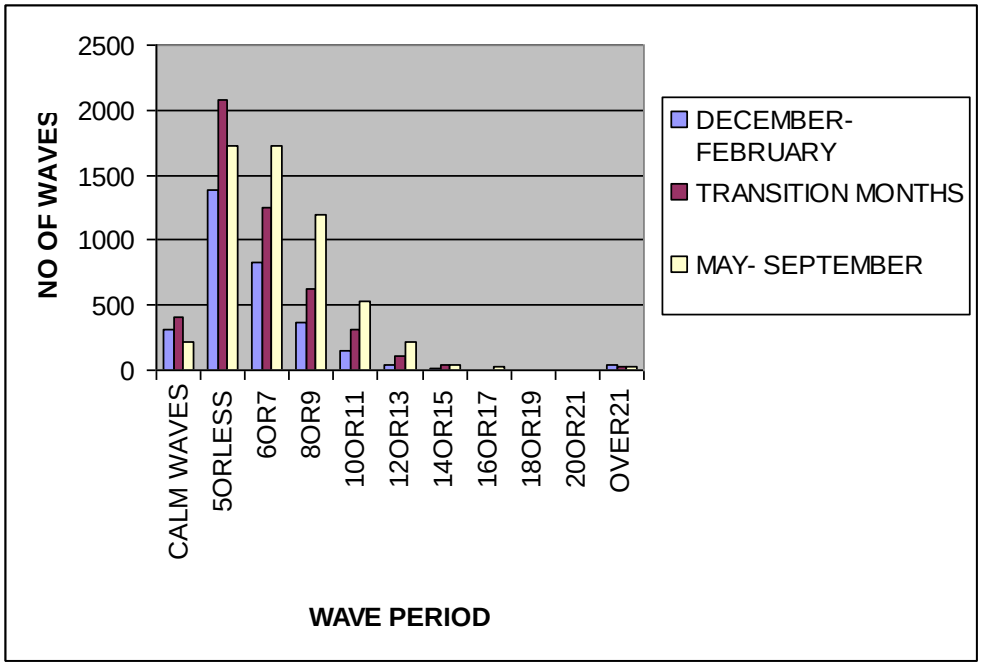

Fig.4.3.1.5.4: Number of waves for different of waves for different periods for various months (in seconds)

4.3.1.6 Summary of atmospheric and sea-surface factors

Atmospheric and sea-surface data evaluated for 10 year period (Table 4.3.1.6.1) shows average monthly sea surface temperature vary between a small ranges throughout the year (25-29^{o}), average wind speed is also not very severe (5-8 m/s or 18-29 km/hour) except in case of depressions, average rainfall is not very heavy (2-6 mm/day). Sea surface temperature and rainfall follow a similar pattern (high during December-February and low during May-September), whereas wind speed is the opposite. However, variable (seasonal) wind speed, can lead to variation in wave height, direction and period. Depressions are common throughout the year and more hurricanes occur during January to March, but no super hurricanes in the area giving it fairly comfortable working conditions except for a period of 90-100 days during January to March.

Table 4.3.1.6.1: Summary and implications of meteorological conditions for mining platform

Parameters	**Characteristics**
1.Surface – Temperature (monthly average)	25-29^{o} C
- Rainfall (monthly mean)	2-6 mm/day
- Wind speed (monthly mean)	5-8 m/s (18-29 km/hr)
2. Waves - height	Generally <2.5 m (Max.= 8m)
- Direction	Variable (0-360$^{o)}$
- Period	Generally < 10/sec
3. Cyclones – None	0 - August-September
- Depressions	<34 km/hr – Jan-Dec
- Storms	34-63 km/hr – Jan-Dec
- Hurricanes	64-127 km/hr – Jan-Mar
-Severe hurricanes	>127 km/hr – Nil

Source: 1. Grass et al. (2000), 2. Hogben and Lumb (1967), 3. www. metoffice.gov.uk

4.3.2 Regional observations

During one of the expeditions for collecting environmental variability data in CIOB onboard RV Boris Petrov (September-October 2009), physical parameters such as wind speed, wind direction, humidity, pressure and sea surface temperature were measured at intervals of 4 hrs on all days (Fig. 4.3.2.1). During the cruise, in general the wind speeds varied between 2 m/sec to 15 m/sec

with events of intermediate gusty winds with speeds exceeding >18 m/sec on a few occasions. During most of the cruise period, northerly winds were recorded. A significant change in the air temperatures was observed between northern and southern hemispheres. The air temperatures in the southern hemisphere were lower with an average value of 25^{o}C, while warmer air temperatures were observed in the northern hemisphere with values exceeding 30^{o}C. Sea Surface Temperatures showed an increasing trend from 24^{o}C at 12^{o}S towards the equatorial regions with values exceeding 29.5^{o}C. From 4^{o}N onwards the SSTs showed a decreasing trend towards 12^{o}N where the values were about 27^{o}C. Similarly,sea surface salinity showed an increasing trend from 34.5 ppt at 12^{o}S to 36 ppt at 4^{o}S.

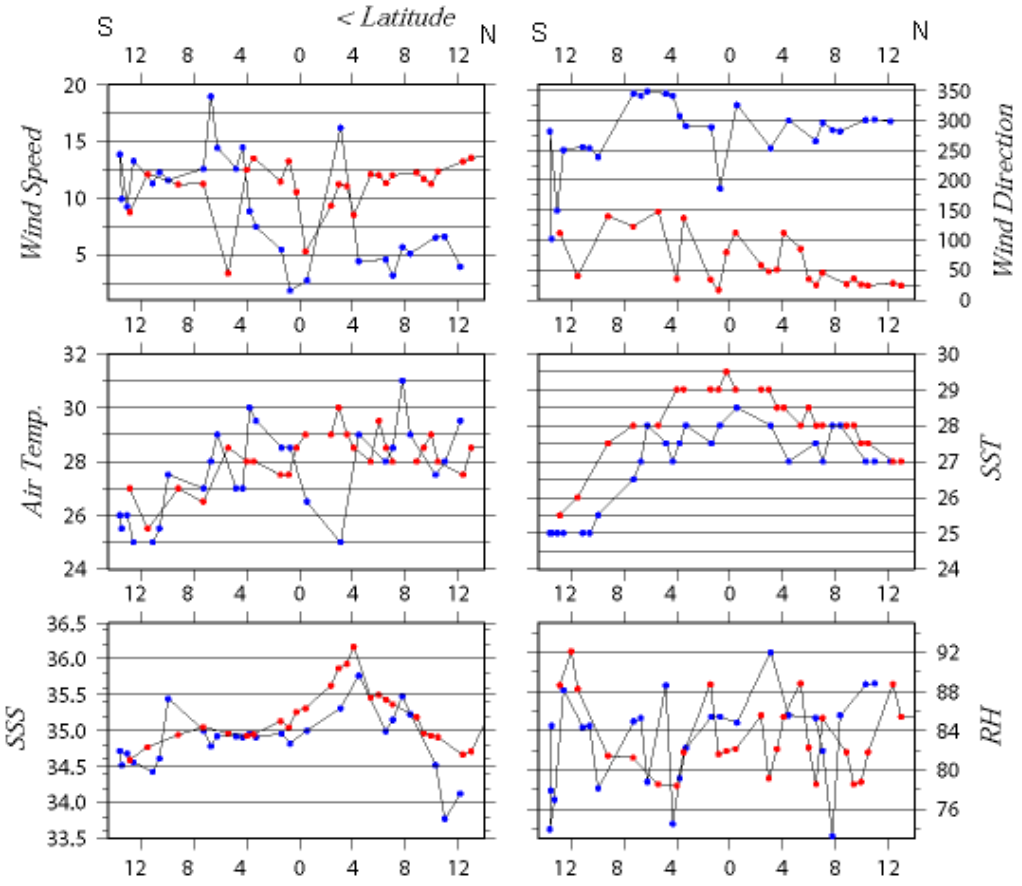

Fig 4.3.2.1: Distribution of surface meteorological parameters during 9 - 22 Sep 2009 (Red dots) and 23 Sep to 06 Oct 2009 (blue dots)

4.3.3 Local observations

Weather data was also collected during the cruise onboard RV Sindhu Sadhana in the months of July-August 2015 with daily observations at 8.00 hours shows that within the CIOB, wind speed ranged between 7.3-14.2 m/s, wind direction between 93-152^{o}, atmospheric temperature between

23-26.4ºC, relative humidity between 55-79%, atmospheric pressure between 1011.5-1018 Mbar and sea state between 4-7 (Table 4.3.3.1).

Table 4.3.3.1: Weather data collected daily at 0800 hrs during the cruise
(Readings highlighted in yellow only are from the Contract area).

S. N.	Date	Position (deg min)	Wind speed (m/s)	Wind direction (degree)	Air Temperature (ºC)	Relative humidity (%)	Air pressure (Mbar)	Sea state	Ship speed (kt) / hdg (deg.)
1	25.7.15	-	-	-	-	-	-	-	-
2	26.7.15	13 30.0N	8.6	165	26.6	86.8	1007.8	2	8.0/159
		74 26.3E							
3	27.7.15	10 49.8N	5.4	155	25.6	88.4	1010.0	1	8.6/161
		75 43.5E							
4	28.7.15	07 34.9N	3.4	289	27.3	82.7	1009.4	1	8.3/181
		76 17.6E							
5	29.7.15	04 09.3N	8.5	200	28.1	70.4	1009.6	1	9.0/182
		76 06.2E							
6	30.7.15	01 02.0N	9.4	189	28.2	76.7	1009.9	2	7.7/176
		75 56.3E							
7	31.7.15	02 04.2S	8.8	162.6	28.6	72.1	1009.3	3	7.1/176
		75 46.1E							
8	1.8.15	05 02.6S	8.6	171.9	27.0	78.7	1010	3	7.7/170
		75 54.3E							
9	2.8.15	06 59.9S	6.9	149.1	26.5	83.3	1011.2	4	0.1/148
		75 59.9E							

10	3.8.15	09 16.4S	14.2	141	26.4	79.3	1012.3	5	7.7/182
		75 44.9E							
11	4.8.15	12 11.4S	13.9	146	25.6	70.5	1014.3	5	7.7/193
		74 52.5E							
12	5.8.15	12 52.5S	9.3	116	25.2	69.1	1014	5	0.1/95
		74 45.0E							
13	6.8.15	12 59.9S	11.8	118	25.1	62.2	1012	5	0.1/278
		74 37.0E							
14	7.8.15	13 30.0S	13.1	92.8	23.2	77.3	1014.2	5	0.2/278
		75 30.0E							
15	8.8.15	13 29.7S	16.2	126	24.2	75.6	1014	7	2.5/88
		75 30.1E							
16	9.8.15	13 30.0S	14.4	130	23.9	77	1013.5	7	0.2/285
		75 37.5E							
17	10.8.15	14 45.9S	9.2	117	26	65	1013.9	7	5.9/254
		75 77.8E							
18	11.8.15	15 40.9S	11.6	108	25	50	1016	7	1.9/111
		75 17.1E							
19	12.8.15	16 00.0S	13.8	111	24.3	55.5	1018	7	0.1/106
		75 30.0E							
20	13.8.15	16 00.0S	12.0	130	23	68.2	1017	7	0.1/118
		75 30.0E							

21	14.8.15	15 00.0S	12	110	24.2	57.2	1015	6	0.2/120
		75 30.0E							
22	15.8.15	13 37.4S	11.4	127	24.8	62.5	1013	6	0.1/291
		75 29.9E							
23	16.8.15	13 37.5S	13	149	23.4	75.4	1012.6	5	0.2/315
		75 37.5E							
24	17.8.15	13 33.7S	10	152	23.7	62.4	1012	5	0.2/321
		75 33.7E							
25	18.8.15	12 56.2S	11	135	24.6	61.6	1011.5	5	0.2/288
		74 41.2E							
26	19.8.15	10 52.3S	7.3	121	24.9	77.8	1012.1	4	7.8/24
		75 22.5E							
27	20.8.15	07 40.8S	5.5	102	26.7	79.4	1011.4	2	8.1/9
		75 55.4E							
28	21.8.15	05 05.8S	5.2	102	28.2	77.1	1010.6	2	8.4/358
		75 52.2E							
29	22.8.15	01 47.5S	5.3	38	27.3	71.1	1008.9	2	8.4/358
		75 38.5E							
30	23.8.15	01 44.4N	4.2	355	27.9	69.0	1010	0	8.9/355
		75 23.9E							
31	24.8.15	04 56.1N	6.3	305	28.1	78.7	1009.5	1	8.3/350
		75 10.7E							

32	25.8.15	07 47.7N	10.5	334	28.4	75.7	1008.7	2	8.5/356
		7458.9E							
33	26.8.15	10 59.8N	12.2	329	27.8	74.7	1007.9	2	7.5/356
		74 45.5E							
34	27.8.15	13 44.9N	5.6	6.0	26.6	85.6	1005.9	2	7.1/334
		74 25.1E							

4.4 Water column conditions

4.4.1 Water column – Physical properties

Baseline data relating to water column was collected during 1996-1997 in nodule bearing area of CIOB using CTD system and water samplers at 36 locations are covering an area of 600x900 km (Fig.4.4.1.1). The study assessed the water column physical oceanographic parameters, namely, the potential temperature, salinity and potential density together with geostrophic circulation regime in the deeper depths of the basin (Babu et al., 2001). Most of the description in this section is reproduced from the published paper (Babu et al., 2001) adding literature from other sources. The hydrography data used in the present analysis were collected over a wide area of the western part of CIOB (71°–79°E; 9°–14°S) during austral summer (January 1997) from the Indian research vessel ORV Sagar Kanya at twenty-eight stations spaced at a 1°- latitude interval along meridional sections 79°E, 77°E, 75°E and 71°E, while during the austral winter season (June–July 1997), hydrographical stations were occupied by Russian research vessel R.V. Yuzhmorgeologia in the central part of CIOB (75°–77°E; 9°–11°S) where a benthic disturbance on experimental scale was carried out. The spatial variations in the physical parameters decreased below 3500m, inferring a restricted basin-scale deep circulation. Other published work is shown to represent the temperature structure in the northern part of CIOB.

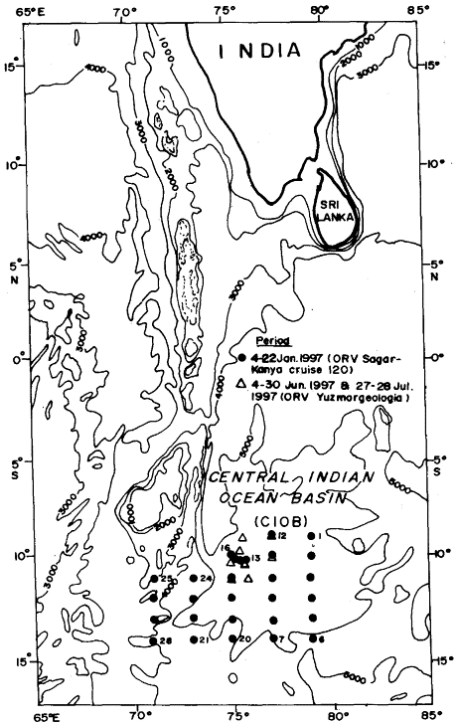

Fig. 4.4.1.1: Hydrographic stations for baseline water column data collection in the CIOB

4.4.1.1XBT studies - Vertical thermal section of top 250m along 75°E

During the cruise onboard RV Boris Petrov undertaken during Sept-Oct 2009 (EVD IV), 18 XBT stations were occupied and vertical temperature profiles were collected by deploying Ms.Sippican make T7 XBT probes, LM3A Hand Held Launcher and MK 130 Data Acquisition System. The vertical thermal section in the upper 250m water column along 75°E and between 13°N to 13°S is presented in Fig. 4.4.1.1.1. Sea surface temperatures (SSTs) varied between 24°C and >29.5°C with the presence of warmest waters in the equatorial regions. Temperatures in the upper 50m water column between 3°N and 3°S are much higher exceeding > 29.5°C when compared with other ends of the meridional section. Thermocline is seen up-sloping from 150m depth at 13°S to 50m depth at 13°N with tightly packed isotherms indicating strong north-south gradient. Downward tilt of isotherms close to the south eastern coast indicates the presence of equatorward currents. Below 200m depth no significant differences are seen in the thermal section.

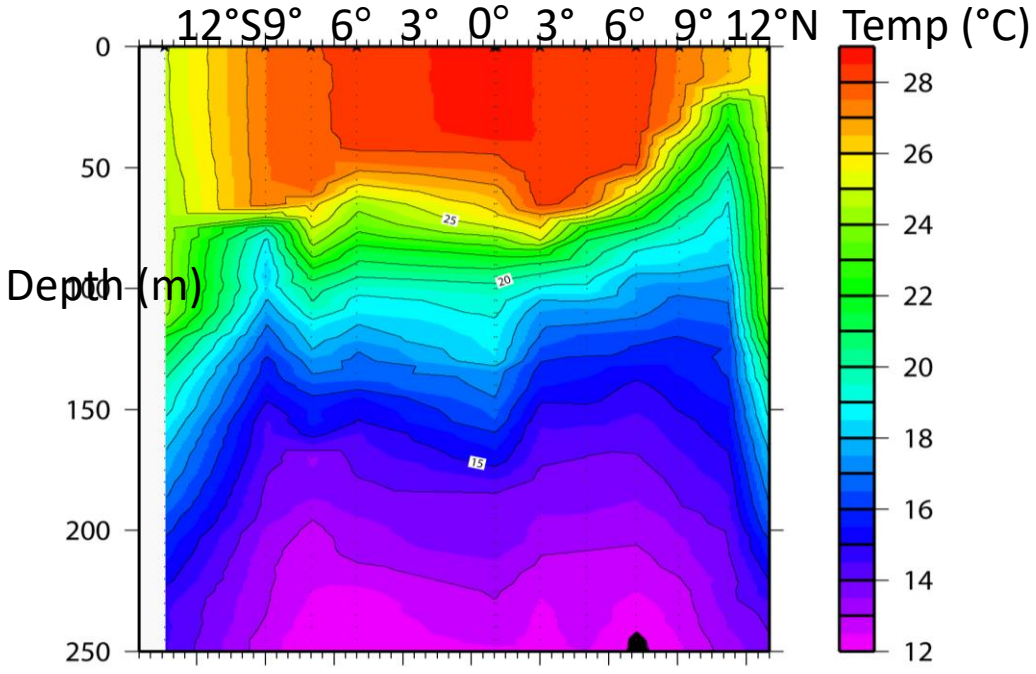

Fig. 4.4.1.1.1: Vertical thermal section during 09 – 25 Sep 2009

4.4.1.2 World Ocean Circulation Experiment Temperature Profile

The full depth temperature profile along an East-West transect at 8°S (Profile *I2*) covering the entire Indian Ocean but cutting across the CIOB is shown below (data and maps from http://www.ewoce.org). The temperature variations are large up to 2000m depth and reach up to 3° C (Fig. 4.4.1.2.1). The warmer water on the top layer 20-27°C reaches to a depth of about 200m in the *I2* profile and the depth of warmer pool is increasing continuously the

depth from equator to the study area. In the deeper levels almost same temperature (2-3°C) are shown along *I2*profile.

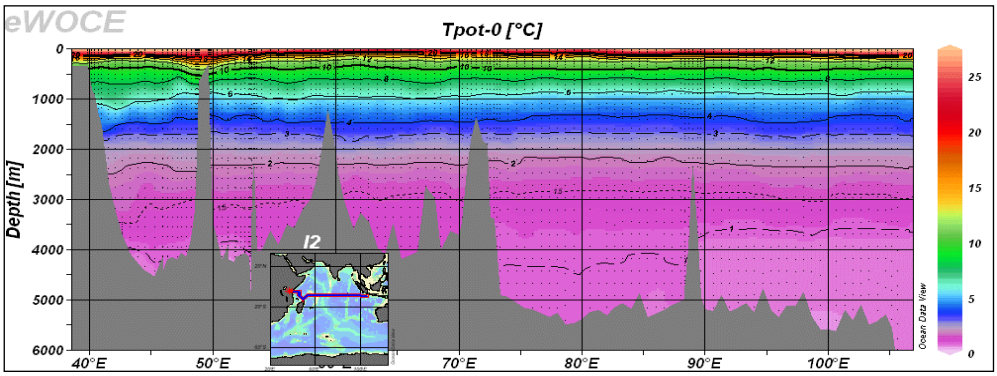

Fig. 4.4.1.2.1: Profile I2 shows the distribution of temperature in seawater on a W-E transect across the Indian Ocean at latitudes of 8°S. (www.ewoce.org)

4.4.1.3 CTD observations

Conductivity – temperature – depth records in the area have shown that water temperature ranges between 26°C (at the surface) to 1.0°C (at 5000 m depth), whereas salinity is constant at 34.7 ppm (+ 0.2 ppm) throughout the water column during different seasons (Babu et al., 2001).

4.4.1.3.1 Distributions of potential temperature, salinity and potential density during southern summer

4.4.1.3.1.1 Along 79°E longitude

In the upper layers of the water column, the thermocline has a trough shape, with maximum deepening around 11°–12°S (Fig. 4.4.1.3.1.1.1), suggesting that thermal flow across this section is characterized by an anti-clockwise circulation. North of 11°–12°S, the suggested flow is to the west, while to the south an eastward flow is inferred. The southward sloping of isotherms in the intermediate depth range of 800–1500m indicates a westerly flow across the entire section. The meridional down-sloping of isotherms is least around 2000m depth as compared to the slopes of isotherms above and below it. In deep waters (>4500m depth), the orientation of 1°C isotherm suggests westward flow concentrated around 10°S.

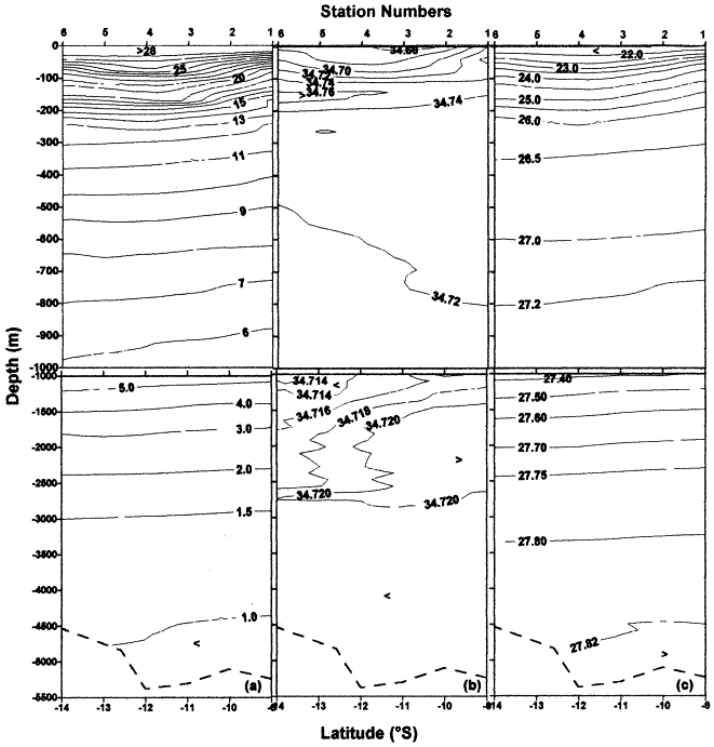

Fig. 4.4.1.3.1.1.1: Distribution of (a) potential temperature (°C), (b) salinity (psu) (c) potential density (kgm^{-3}) along 79°E during southern summer (January 1997)

Salinity distribution at 79°E (Fig. 4.4.1.3.1.1.1) shows the presence of low-salinity waters (<34.70psu) occupying the upper 100m, brought into the study area from the east by the South Equatorial Current (SEC). In intermediate depths around 1000m depth, fresher waters (<34.14psu) are encountered prominently in the south between the stations 4 and 6, pointing to the northward spreading of the Antarctic Intermediate Water mass (AIW). Below 3000m, the salinity is less than 34.72psu, with reduced gradients similar to those seen in the temperature field. The conspicuous presence of a weak salinity maximum (>34.718psu) in the depth range of 1500–3000m is due to southward spreading of the North Indian Deep Water (NIDW). The distribution of potential density (σ_θ (Fig. 4.4.1.3.1.1.1) at 79°E resembles more or less that of temperature with reduced gradients below 3000m depth. In very deep waters below 4500m, high potential density (>27.2kg m^{-3}) waters are confined around 10°S on account of relatively cold waters having potential temperatures less than 1°C.

4.4.1.3.1.2 Along 71°E longitude

Near the western boundary of the CIOB (71°E), the trough nature of thermocline seen in the east at 79°E is absent in the upper 300m. A general southward down-slope of isotherms infers

westerly flow in the upper layers across the entire section. Below 2500m depth the 1.5°C isotherm has a reverse slope suggesting a reverse flow towards east between 13° and 14°S.
The core salinity of intermediate low-salinity water mass around 1000m is seen reduced in its value to 34.708psu at 71°E compared to the higher core value of 34.714psu observed at 79°E. This east to west reduction in core salinity minimum of the AIW suggests of the dominance of zonal flow over the meridional flow in the intermediate depths, like in the upper layers. The reduction in core value of the NIDW is from 34.72 psu at 79°E to 34.71 psu at 71°E.
The distribution of potential density (σ_θ) has a profound influence of temperature rather than salinity, as the effect of a sub-surface high-salinity maximum around 250m is not seen in the density distribution. The isopycnals dip to the south in upper layer of 300m, while at deep waters greater than 2500 m they have the opposite slope, suggesting easterly flow.

4.4.1.3.2 Distributions of potential temperature, salinity and potential density at deeper depths during southern winter

Physical properties of the abyssal depths in a smaller central part of the CIOB between 75° and 77°E and 9° and 11°S were assessed using the CTD data collected during August 1997. Though the spatial variations are subtle, the presence of relatively cold waters in the east and southeast suggests an incursion in deeper parts of CIOB. Salinity distributions at these depths further also show the presence of relatively low-salinity waters in the east. The association of cold, low-salinity values in the east indicates an overflow of the Antarctic Waters across suspected gaps or saddles of the Ninety-east Ridge. The potential density field is more or less uniform, indicating sluggish motions below the sill-depth. This is similar to earlier observations (Warren and Johnson, 2002). Deep water in the Central Indian Basin is Circumpolar Deep Water from the South Australia Basin (Fig. 4.4.1.3.2.1 a). It enters the Central Indian Basin (Fig. 4.4.1.3.2.1 b) by two routes. Water flowing northwestward toward the junction between the Southeast Indian Ridge and the Ninetyeast Ridge near 33°S, 85°E splits, continuing northwestward along the eastern flank of the Southeast Indian Ridge. It proceeds northward as another boundary current, and turns westward to feed the deep western-boundary-current system of the West Australian Basin, along the Ninetyeast Ridge. Some of that water in turn spills over deep saddles on the Ninetyeast Ridge to form the colder, oxygen-richer, lower deep water of the Central Basin.

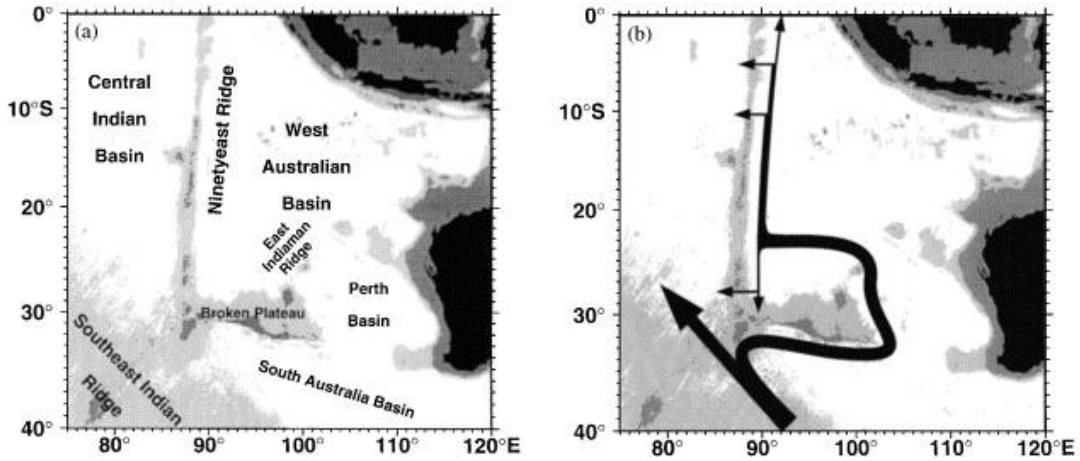

Fig. 4.4.1.3.2.1 (a and b): Schematic course of deep boundary currents and locations of deep overflows across the Ninetyeast Ridge supplying lower deep water to the Central Indian Ocean Basin (Warren and Johnson, 2002)

4.4.1.3.3 Near-bottom circulation during southern winter

The dynamic topography field at 5000 m relative to 2000 db surface in the central part of CIOB, representing the abyssal circulationis only of 0.02 dynamic meters, indicating a weak near-bottom flow regime chiefly characterized by southwesterly flow bounded by clockwise and anti-clockwise eddies on its northern and southern sides, respectively cyclonic and anti-cyclonic eddies on its right and left sides, respectively (Fig. 4.4.1.3.3.1; Babu et al., 2001).

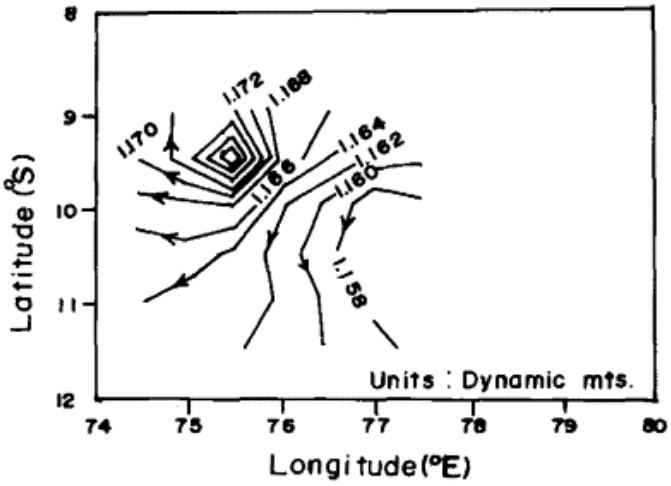

Fig.4.4.1.3.3.1: Dynamic depth (dynamic metres) of 5000-db pressure surface below the reference level of assumed no motion at 2000m during southern winter (Babu etal., 2001).

4.4.1.4Moorings and current data

In addition to the CTD measurements, mooring systems were deployed at three stations (MS-1, MS-2 and MS-3) forming a triangle in the CIOB area (Fig.4.4.1.4.1) for a period of 270 days between 1995 and 1997 to analyse regional currents at 3 levels in the area. Deployment at the three stations (moorings designated as MS-1, MS-2 & MS-3) was carried out during a first phase covering the period September 1995 to January 1996 and during a second phase from April 1996 to September 1996 (moorings designated as MS-1A, MS-2A & MS-3A). During a third phase, only one mooring was repeated at MS-1 station (designated as MS-1B) from November 1996 to April 1997. The details of the moorings at the three stations in all phases are given in Table 4.4.1.4.1. The bottom-most current meters were placed 80–137m above the sea floor during first and third phases and at a uniform 160m above sea floor during the second phase. The data acquired during this phase was processed, interpreted and published by Murty etal. (2001).

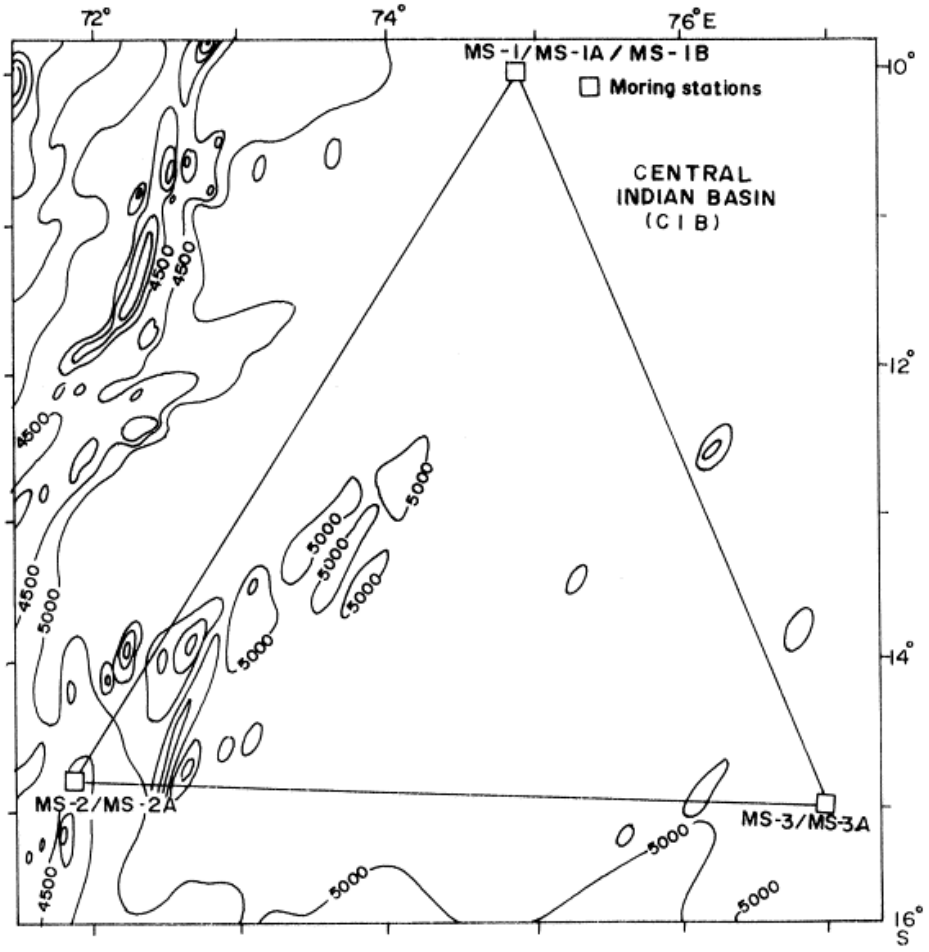

Fig. 4.4.1.4.1: Locations for current meter moorings in the area

Table 4.4.1.4.1: Details of the current-meter moorings in the Central Indian Ocean Basin

Phase-1			
Mooring Station	MS-1	MS-2	MS-3
Latitude (°S)	09°56.726′	14°46.143′	14°58.307′
Longitude (°E)	74°54.794′	71°54.843′	76°58.854′
Depth (m)	5180	4537	5236
Deployed on	29-09-1995	11-10-1995	13-10-1995
Recovered on	10-01-1996	19-01-1996	15-01-1996
Phase-2			
Mooring Station	MS-1A	MS-2A	MS-3A
Latitude (°S)	09°55.877′	14°47.120′	14°56.151′
Longitude (°E)	74°54.612′	71°55.253′	76°58.167′
Depth (m)	5260	4630	5210
Deployed on	06-04-1996	04-04-1996	02-04-1996
Recovered on	13-09-1996	21-09-1996	19-09-1996
Phase-3			
Mooring Station	MS-1B		
Latitude (°S)	09°57.26′		
Longitude (°E)	74°56.56′		
Depth (m)	5176		
Deployed on	02-11-1996		
Recovered on	04-05-1997		

Long term deployment of (~270 days) current meters at 3 locations and different depths ranging from ~500 m to 5000 m during 1995-1996 in the Central Indian Ocean Basin (Murty et al, 2001) revealed that mean current velocities at shallower depths (450-670 m) vary between 3.12 cm/s (during April-September) as against 5.23 cm/s (during September –

January) at the northern location (10°S, 75°E), whereas these were considerably low between 2.21 and 2.29 cm/s (during both deployments) at the southwestern location (15°S, 72°E) and still lower between 52 and 0.65 cm/s (during both deployments) at the south-eastern location (15°S, 77°E). At deeper depths, the mean current velocities recorded were very low (<1 cm/s) throughout the period for the entire water column (1200-5100m) at all the three locations with the exception of one deployment (September-January) at the northern location (10°S, 75°E) where it ranged between 1-2 cm/s (Table 4.4.1.4.2). In the northern basin, seasonal variability in the currents at 500m and 1200m depth has been attributed (Murty et al., 2001) to the seasonal north–south shift in the westward-flowing South Equatorial Current (SEC). Low-frequency (30–60 day) oscillation, superimposed on high-frequency (inertial, semi-diurnal and diurnal) fluctuations, is noticed at all the depths including near-bottom depth (5100m) where the U-component of current was dominant. The variability of the currents at the intermediate depth range (1150–1300m), encompassing the three stations of 500 km apart, indicates the existence of anticyclonic gyral circulation.

Table 4.4.1.4.2: Mean currents in Central Indian Ocean Basin

Station Period of measurements	Depth (m)	*V* (cm/s) [a]	*R* (°) [a]
MS-1 Sep 95 - Jan 96 (spring-summer)	500	5.23	329
	1200	2.93	269
	3500	1.28	271
	4900	1.72	240
MS-1A Apr 96 – Sep 96 (fall-winter)	500	3.12	106
	1200	0.46	149
	3500	0.21	93
	4900	0.15	132
	5100	0.08	170
MS-2 Sep 95 - Jan 96 (spring-summer)	600	2.21	76
	1300	1.23	117
	3600	0.07	132
	4400	0.11	277
MS-2A Apr 96 – Sep 96 (fall-winter)	670	2.29	184
	3670	0.02	84
	4270	0.07	100

	4470	0.56	107
MS-3 Sep 95 - Jan 96 (spring-summer)	1200 4900 5100	0.52 0.18 0.51	144 244 254
MS-3A Apr 96 – Sep 96 (fall-winter)	450 1150 3450	0.65 1.23 0.14	352 51 124

[a]*V* and *R* are the phase–mean current velocity and mean direction (Source: Murty et al., 2001)

The zonal (U) and meridional (V) components of the velocity vectors obtained from the initial time-series data (at 1h interval) at 5100m depth in the benthic layer at station MS-1B during summer–fall of 1996–97 (Fig. 4.4.1.4.2) show the superposition high-frequency oscillations on the low-frequency variation. The relatively large amplitude of U-component velocity variations highlights the predominantly east–west zonal flows at the abyssal depths, consistent with the large-scale circulation derived from the hydrographic data which shows predominant westward zonal flow at abyssal depths.

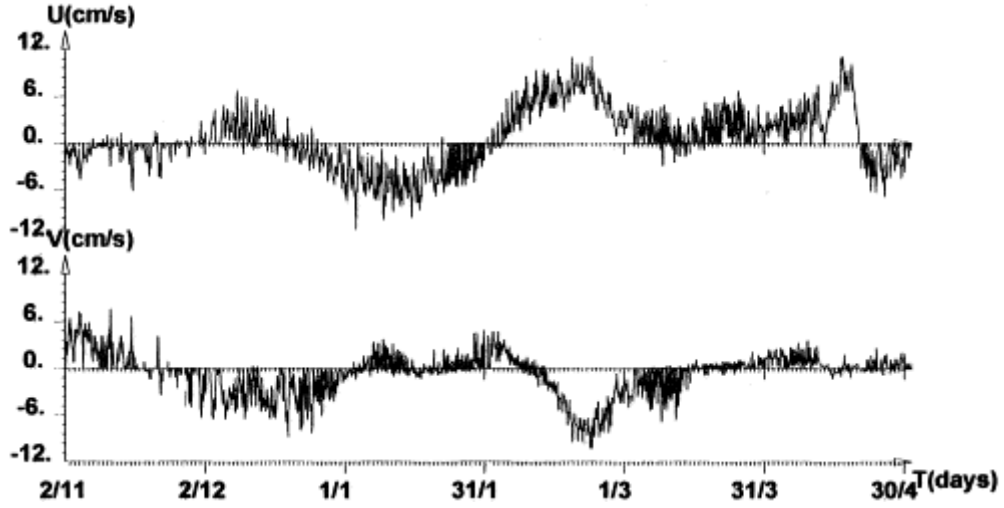

Fig.4.4.1.4.2: Temporal variation of (a) U-component and (b) V-component of velocity vector (initial series data) at 5100 m at station MS-1B during southern summer–fall season.

4.4.1.4.1 Bottom current moorings

In addition to the long term mooring at regionally spaced stations, short moorings with current meters at 7 levels were deployed at 10°01'S, 76°E in the CIOB to assess the abyssal currents. The current meters were deployed at 4, 8, 15, 30, 50, 100 and 500 metres above the

bottom during October 1996-April 1997 (Murty et al., 1999). Monthly mean currents showed low frequency variability with a 40-60 day period and a general SSE flow with a seasonal variability in the flow pattern with a reversal in January (Fig. 4.4.1.4.1.1). The mean flow is high at 50 mab and decreased above and below 50 mab. The decrease is followed by veering towards the seabed. A low frictional velocity was seen implying that the bed stress is usually low to cause local re-suspension of sediments.

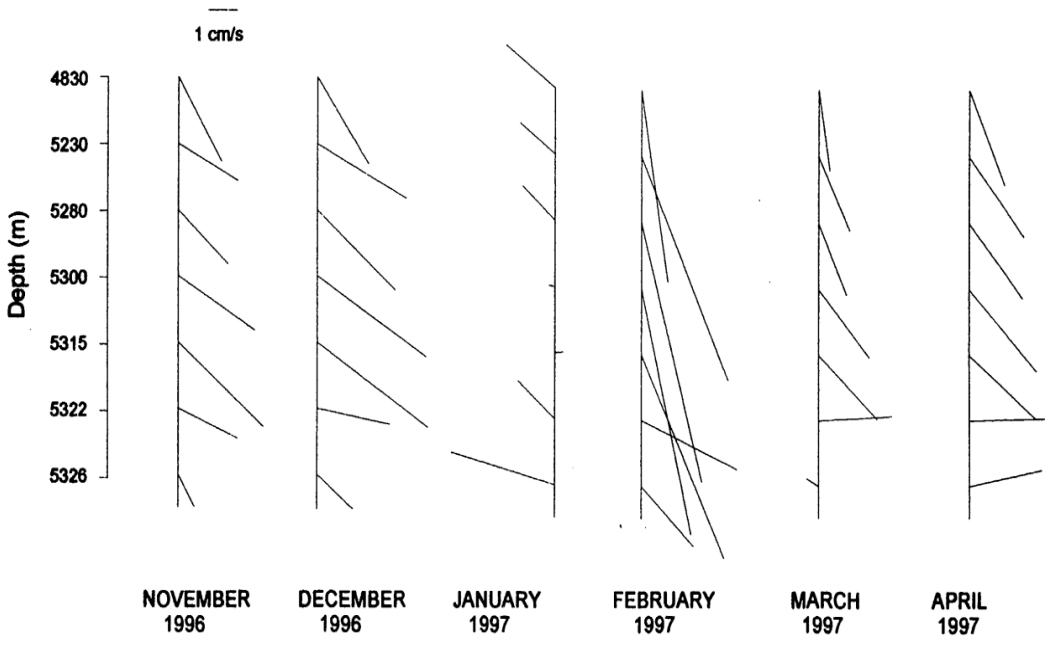

Fig. 4.4.1.4.1.1: Monthly variation of mean currents at various depths in the benthic layer(Murty etal., 1999)

4.4.1.5 Baseline water column physical oceanographic parameters in IRZ and PRZ

4.4.1.5.1 Temperature-salinity profiles in IRZ, PRZ

During RV Sindhu Sadhana cruise no. 13 during 17-18 August 2015, baseline temperature and salinity data was collected in IRZ (CTD 1 at 13° 33.747'S and 75° 33.742'E) and in PRZ (CTD 2 at 12°56.246'S 74° 41.242'E). Temperature and salinity profiles at CTD 1 and CTD 2 stations represent the austral winter (August) season of 2015. Similar temperature and salinity data collection was carried earlier during the 120th cruise of ORV Sagar Kanya during 4-22 January of 1997 in the entire CIOB from which temperature and salinity profiles at stations of CTD-19 and CTD-20 were compared with those of CTD 1 (which coincides with the location of CTD-20 of 1997) and CTD 2 (which coincides with that of CTD-19 of 1997).

In the present analysis, the vertical potential temperature profiles obtained in January 1997 represent austral summer and those of August 2015 represent austral winter.Comparison of profiles of potential temperature at stations CTD-2 (PRZ) and CTD-1(IRZ) during austral winter season of 2015 for the full water column (Fig. 4.4.1.5.1.1a), in the upper 1000 m (Fig.4.4.1.5.1.1 b) and for the depth range of 1000-5100 m layer (Fig. 4.4.1.5.1.1 c) showed high level consistency between these stations over the full water column (Fig.4.4.1.5.1.1 a), except in the thermocline depth range (90 – 400 m) where warm waters prevailed at station CTD- 1. At both the stations, the mixed layer is large up to ~90 m with uniform potential temperature of 26°C (clearly evident in Fig.4.4.1.5.1.1 b). There is much variation in potential temperature at both the stations in the 1000-abyssal layer (Fig. 4.4.1.5.1.1 c).

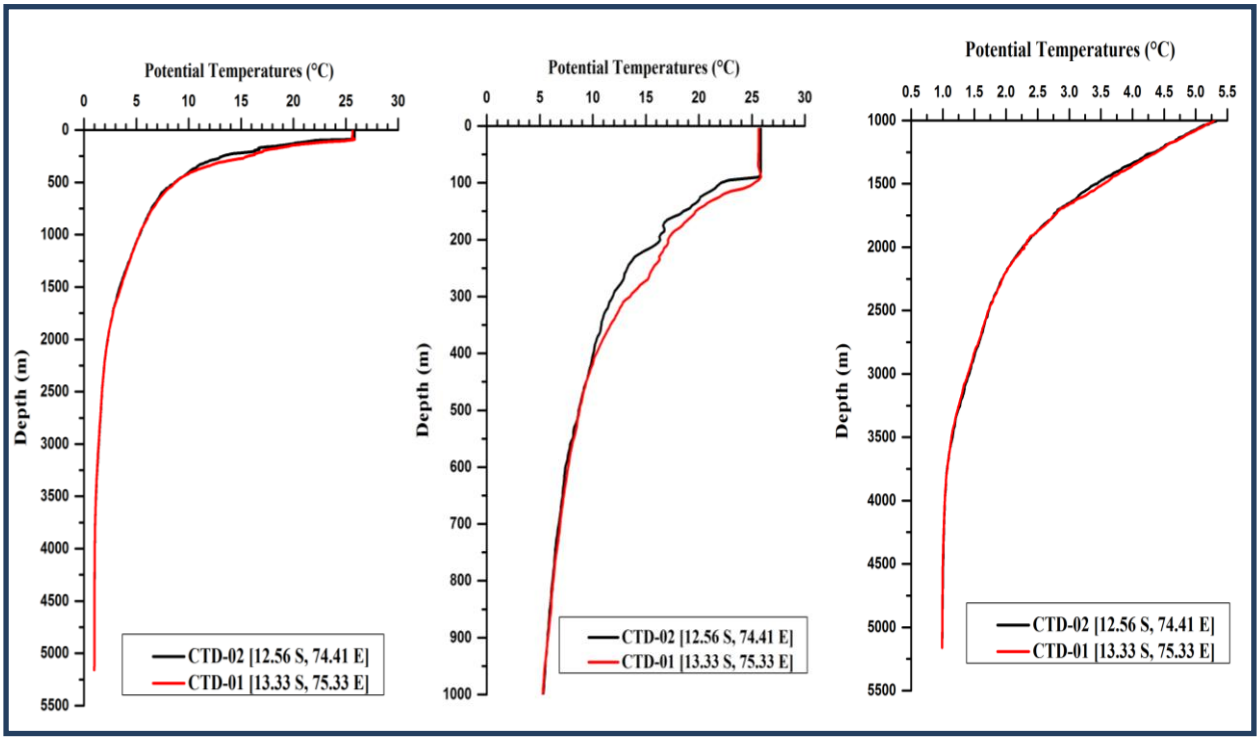

Fig. 4.4.1.5.1.1 Comparison of profiles of potential temperature (a) surface to abyssal depth, (b) surface to 1000 m layer and (c) 1000 m – abyssal depth range at stations CTD-2 (austral winter 2015) and CTD-1 (austral winter 2015) representing PRZ and IRZ respectively

Comparison of profiles of salinity at CTD-2 and CTD-1 in austral winter season of 2015 (Fig. 4.4.1.5.1.2 a) showed consistency in the profiles with the presence of low salinity waters in the mixed layer, subsurface higher salinity (35.0 – 35.5 psu) water in the thermocline depth range (100-400 m) corresponding to the southern tropical Indian Ocean subsurface high

salinity watermass (Fig. 4.4.1.5.1.2 b) and also high salinity watermass with weaker salinity maximum (34.72 – 37.74 psu) in the intermediate depth range (1500-3250 m) corresponding to the North Indian Ocean Deep watermass (Fig. 4.4.1.5.1.2 c).

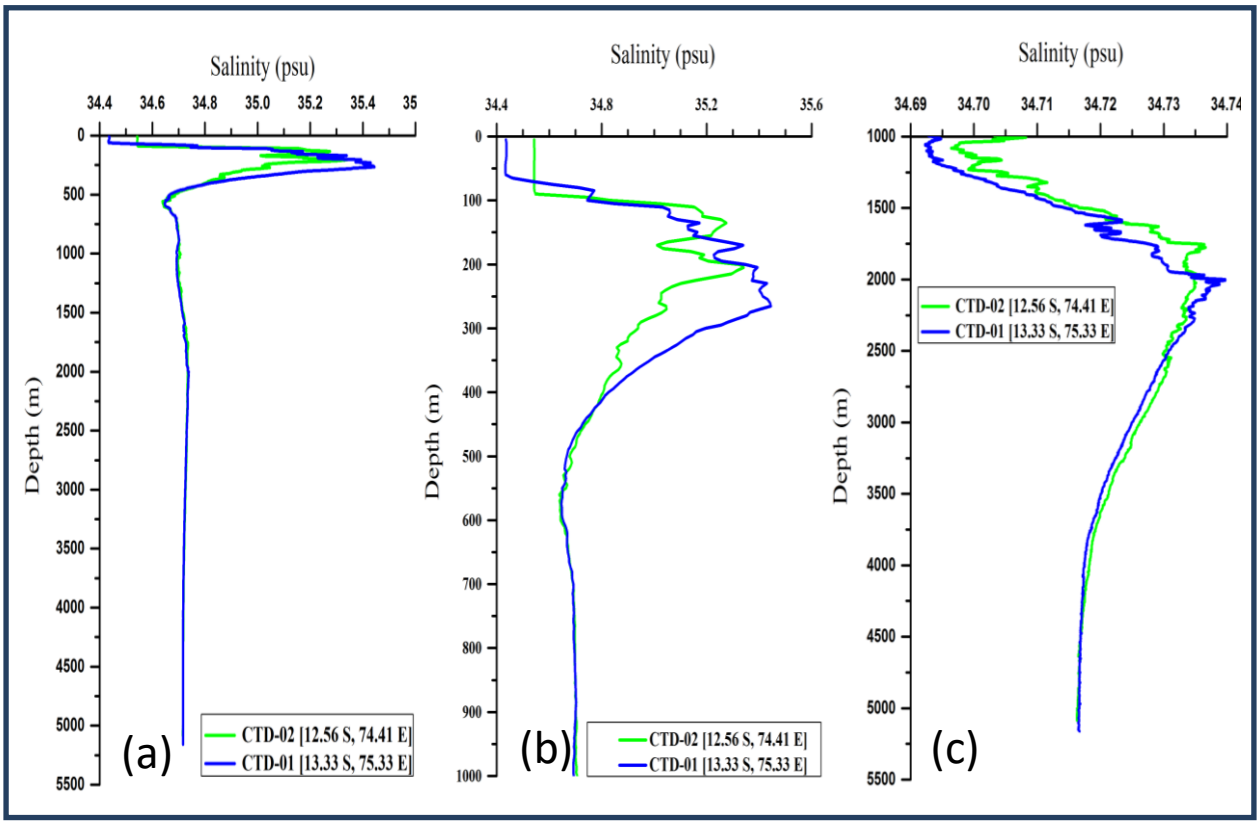

Fig. 4.4.1.5.1.2: Comparison of profiles of salinity (a) surface to abyssal depth, (b) surface to 1000 m layer and (c) 1000 m – abyssal depth range at stations CTD-2 (austral winter 2015) and CTD-1(austral winter 2015) representing PRZ and IRZ respectively

Comparison of profiles of potential temperature and salinity at stations CTD-1 and CTD-20 for the full water column (Fig. 4.4.1.5.1.3a), in the upper 1000 m (Fig. 4.4.1.5.1.3 b) and for the depth range of 1000-5100 m layer (Fig. 4.4.1.5.1.3 c) highlights both the seasonal variations and variability over the duration of 18 years. The salinity profiles at stations CTD-19 and CTD-20 (austral summer season) deviated more at the surface (<100 m) from those of CTD 2 and CTD 1 (austral winter season). However, the salinity profiles of CTD 2 and CTD 1 (austral winter season) are similar and show a consistency between the profiles and spatial variation in salinity between the stations.

The potential temperature profile in austral winter season shows a large (~80 m) mixed layer with uniform low (26°C) temperature at station CTD 1 (clearly evident in Fig. 4.4.1.5.1.3 b).

The potential temperature profile in austral summer season shows warmer sea surface temperature (29°C) and shallower mixed layer (~20 m) (clearly evident in Fig. 4.4.1.5.1.3 b). Between 40 m and 350 m depth range, warmer temperatures occur during austral winter season, compared to cooler waters in austral summer season (Fig.4.4.1.5.1.3 b). Below 350 m depth, there is no much seasonal variation in potential temperature till abyssal depths (Figs. 4.4.1.5.1.3 b, 4.4.1.5.1.3 c).

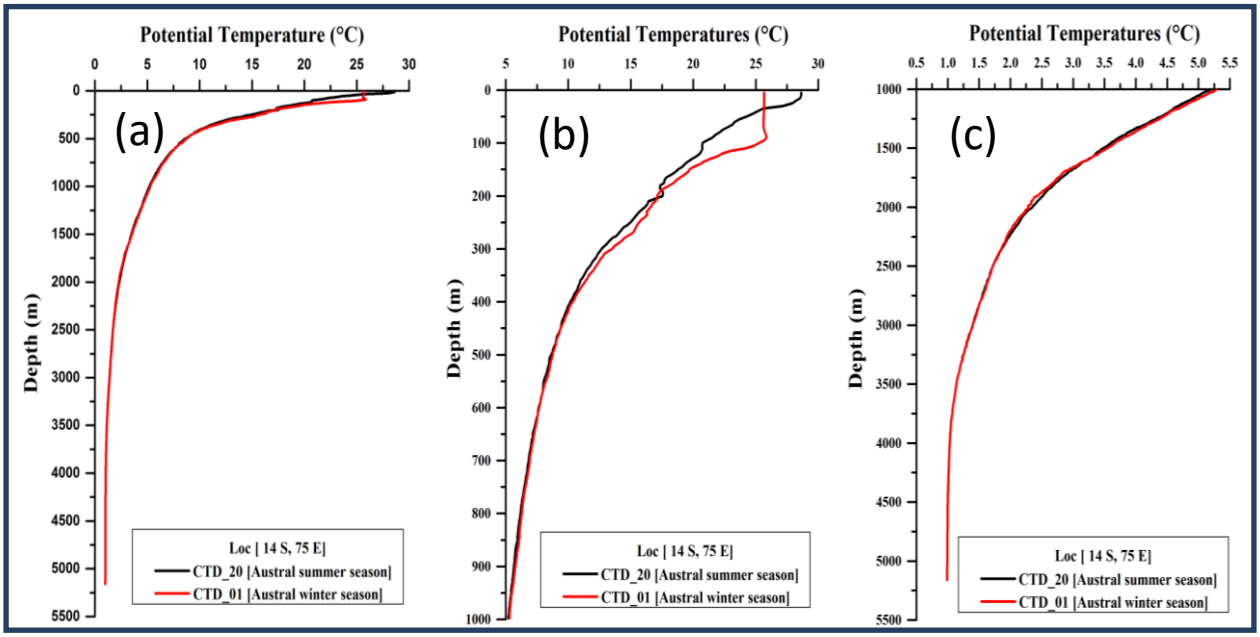

Fig. 4.4.1.5.1.3: Comparison of profiles of potential temperature (a) surface to abyssal depth, (b) surface to 1000 m layer and (c) 1000 m – abyssal depth range at stations CTD-1 (austral winter 2015) and CTD-20 (austral summer 1997) in IRZ

Comparison of profiles of potential temperature at stations CTD- 2 and CTD-19 for the full water column (Fig.4.4.1.5.1.4 a), in the upper 1000 m (Fig.4.4.1.5.1.4b) and for the depth range of 1000-5100 m layer (Fig. 4.4.1.5.1.4c) highlights both the seasonal variations and variability over the duration of 18 years. The salinity profiles of CTD 2 and CTD 1 (austral winter season) are compared to understand the consistency and spatial variation in salinity between the stations. The potential temperature profile in austral winter season shows a large (~80 m) mixed layer with uniform low (26°C) temperature at station CTD 1 (clearly evident in Fig.4.4.1.5.1.4b). The potential temperature profile in austral summer season shows warmer sea surface temperature (29°C) and shallower mixed layer (~10 m) (clearly evident in Fig. 4.4.1.5.1.4 b). Between 40 m and 350 m depth range, warmer temperatures occur during austral winter season, compared to cooler waters in austral summer season (Fig. 4.4.1.5.1.4b). Below 350 m depth, there is no much seasonal variation in potential temperature till abyssal depths (Figs.4.4.1.5.1.4b, 4.4.1.5.1.4c).

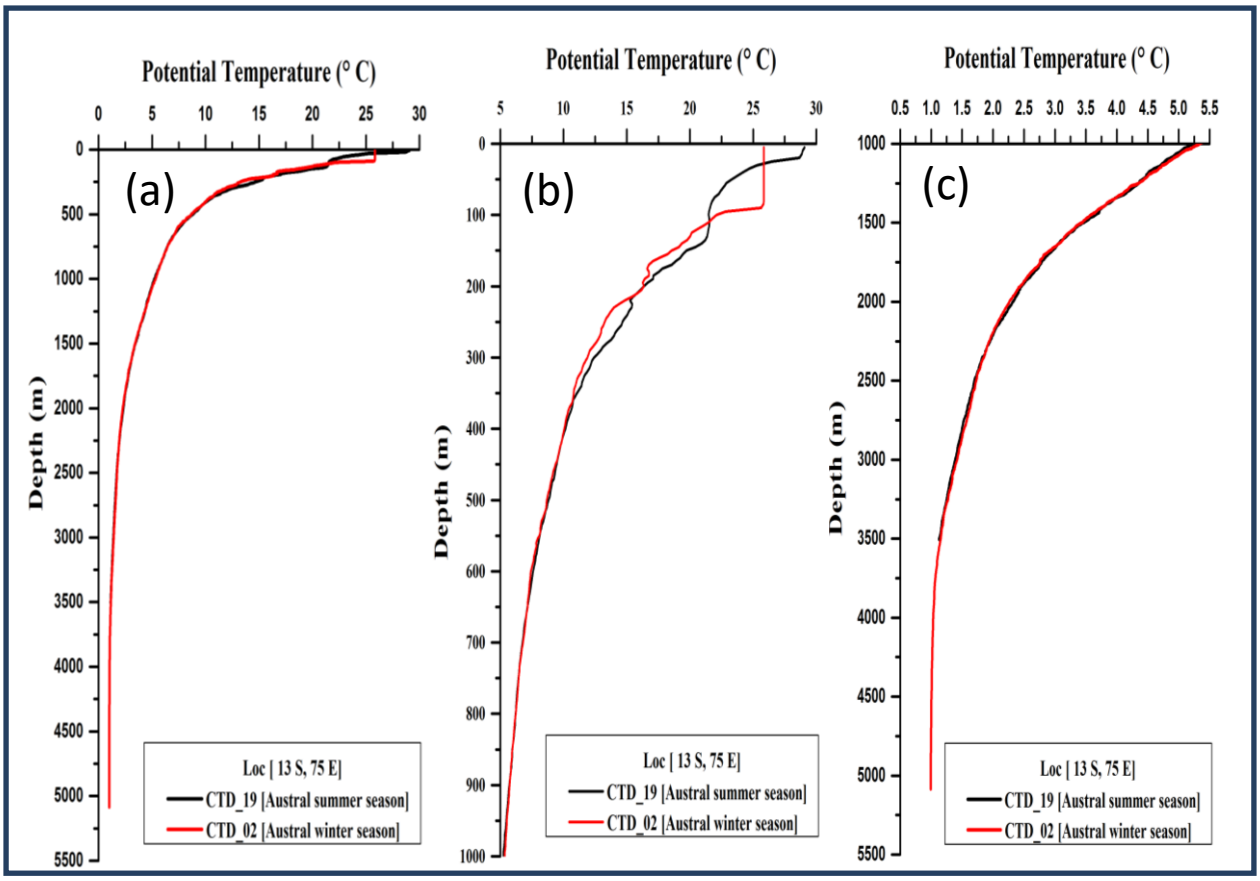

Fig. 4.4.1.5.1.4 Comparison of profiles of potential temperature (a) surface to abyssal depth, (b) surface to1000 m layer and (c) 1000 m – abyssal depth range at stations CTD-2 (austral winter 2015) and CTD-19 (austral summer 1997) in PRZ.

4.4.1.6 Satellite-data analysis of sea surface temperature in IRZ and PRZ

Satellite data for sea surface temperature and productivity in IRZ and PRZ were evaluated for Austral summer (January-February 2015) and Austral summer (July-August 2015) in order to understand the seasonal variability in these parameters. While the SST variability is presented here, chlorophyll and the primary productivity derived from that are presented in water column Biology section.

4.4.1.6.1 Sea Surface Temperature (SST)

Daily, high resolution (0.01 degrees x 0.01 degrees) SST data was taken from the web server (http://ourocean.jpl.nasa.gov/SST/). Global 1 km SST (G1SST) analysis uses satellite data from sensors that include the Advanced Very High Resolution Radiometer (AVHRR), the Advanced Along Track Scanning Radiometer (AATSR), the Spinning Enhanced Visible and Infrared Imager (SEVIRI), the Advanced Microwave Scanning Radiometer-EOS (AMSRE),

the Tropical Rainfall Measuring Mission Microwave Imager (TMI), the Moderate Resolution Imaging Spectroradiometer (MODIS), the Geostationary Operational Environmental Satellite (GOES) Imager, the Multi-Functional Transport Satellite 1R (MTSAT-1R) radiometer, and in situ data from drifting and moored buoys.

4.4.1.6.2 Austral Summer

The SST showed 28.4^{o}C in PRZ during January and February (Blue box in Fig. 4.4.1.6.2.1 a &4.4.1.6.2.1 b). While in IRZ, SST showed 28.6^{o}C during January and 28.2^{o}C during February (Red box in Fig.4.4.1.6.2.1 a &4.4.1.6.2.1 b). Cooling was more (~0.4^{o}C) in IRZ compared to PRZ.

To understand the temporal variations, time series of SST over the areas IRZ (black line) and PRZ (red line) have been plotted (Fig.4.4.1.6.2.2). In both the areas, SST showed comparable values during January; while during February SST showed relatively lower value in PRZ compared to IRZ (a seen in Fig.4.4.1.6.2.2) which indicates cooling is more prominent in PRZ as compared to IRZ.

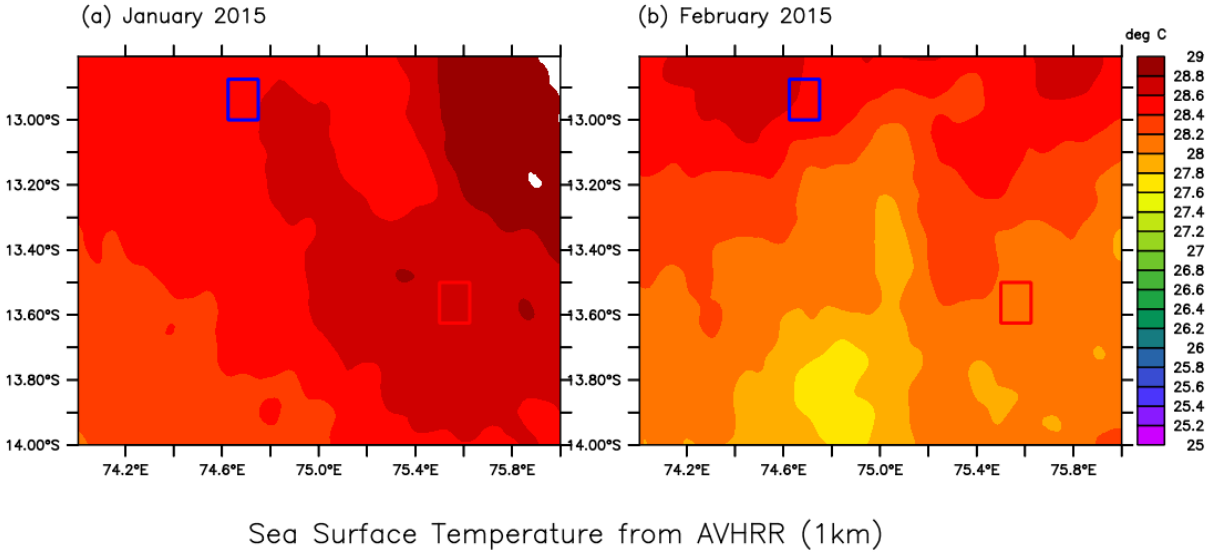

Fig. 4.4.1.6.2.1: Sea surface temperature (in deg C) during (a) January and (b) February. The blue box indicates PRZ and red box indicates IRZ.

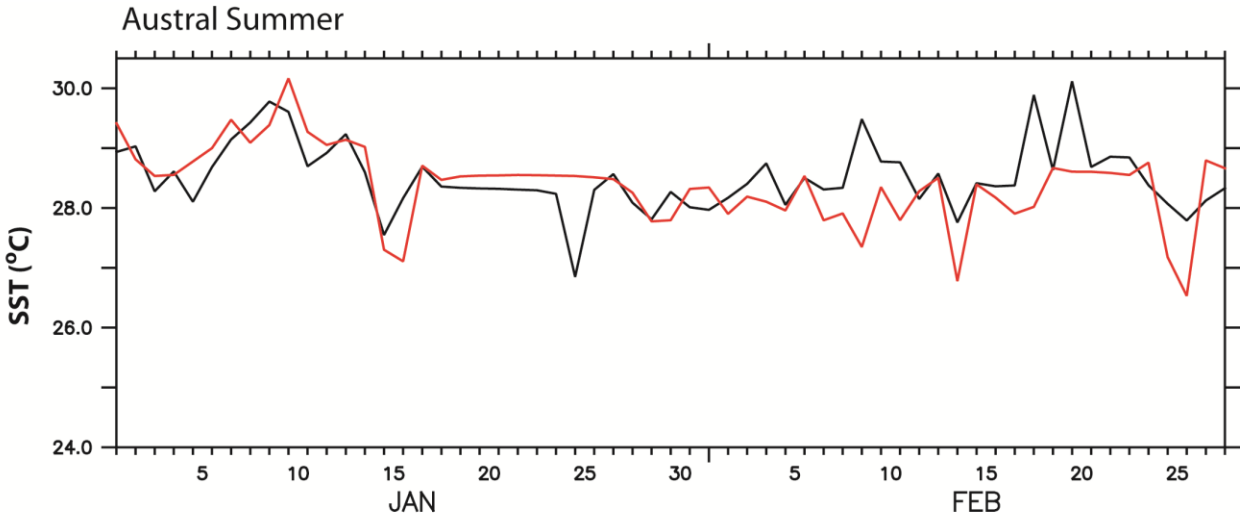

Fig. 4.4.1.6.2.2: Time series of Sea surface temperature (in deg C) during Austral Summer 2015 in the area IRZ (black line) PRZ (red line).

4.4.2Water column - Chemical properties

Water-column data were collected during the cruise no. 120 on the ORV *Sagar Kanya* (December 27, 1996 to January 31, 1997) at the CTD locations described in water column physics section. The water samples were collected with 10/30-l *General Oceanics samplers (Niskin/GO-FLO* type) fitted on a rosette along with the CTD. Dissolved oxygen was measured by the Winkler titration, pH by the multi-wavelength spectrophotometric method of Byrne and Breland (1989), phosphate by the method of Murphy and Riley (1962), while nitrate, nitrite and silicate were measured using an autoanalyser, *Skalar 5100/l* and the results are described in deSousa et al. (2001). The chemical properties of the water column show three equator-ward moving water masses (deSousa et al., 2001; Fig.4.4.2.1). The fastest moving water mass with subsurface salinity is maximum in the depth range 125-200 m, characterized by high salinity (34.74-34.77 psu) and oxygen minimum associated with weak maxima in nutrients. The second water mass with deep oxygen maximum (234-245 µM) in the depth range 250-750 m, associated with minima in nutrients and relatively high pH. The third water mass with salinity minimum water (34.714-34.718 psu) corresponding to the Antarctic Intermediate Water (AAIW) at depths 800-1200 m in the density (sigma-theta) range 27.2-27.5 (deSousa et al., 2001).

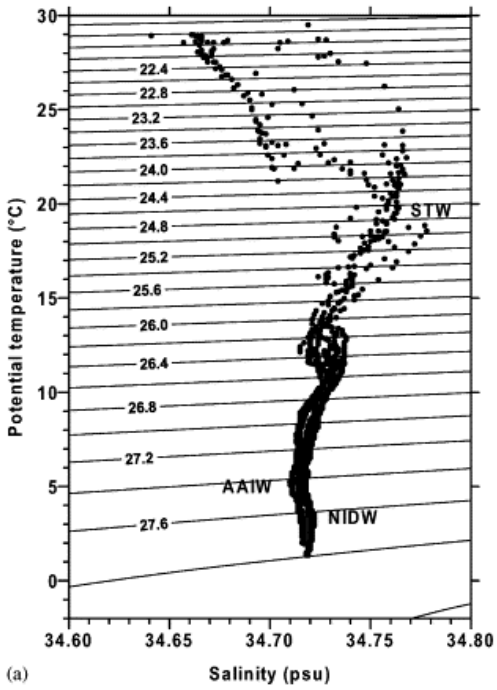

Fig. 4.4.2.1: Watermass structure in the CIOB along 79°E longitude and between latitudes 9° and 14°S. STW—subtropical water; AAIW—Antarctic Intermediate Water; NIDW—North Indian Deep Water

The average oxygen concentration of the high salinity near-surface water was found to be 251 µM at 32°S between longitudes 70°E and 80°E (Toole and Warren, 1993). A shallow oxygen minimum was associated with the subsurface salinity maximum and was found to be strongest in the north and weakened towards the south. In this layer, the average concentration of oxygen at 13°S was around 112 µM. This minimum is caused by the in situ consumption of oxygen by sinking detritus (Warren, 1981a,b).The dissolved oxygen content in the water column in the CIOB is examined along 8°S (*I2*).

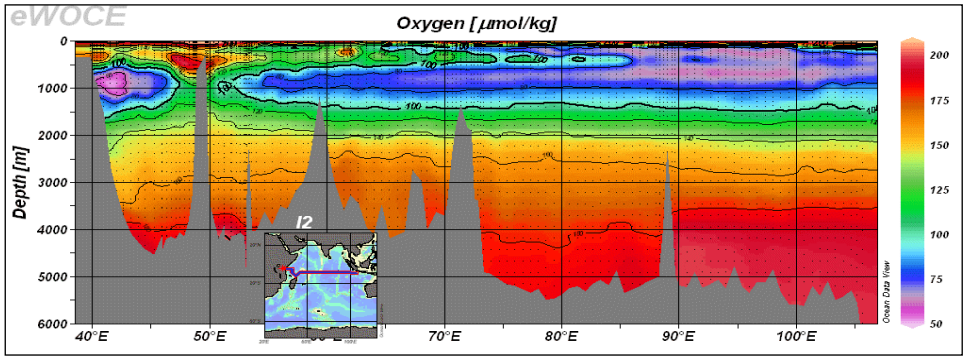

Fig.4.4.2.2: Profile I2 shows the distribution of dissolved oxygen in seawater on a W-E transect across the Indian Ocean at latitudes of 8°S. (www.ewoce.org).

The *I2* dissolved oxygen profile shows high oxygen content (200 µmol/kg) in the surface layers and decreases suddenly to form an oxygen minimum zone (200-1100m water depth)

(Fig.4.4.2.3). The dissolved oxygen content of this region is found to be 60 µmol/kg. Oxygen minimum zone (OMZ) is more prominent in the Wharton basin when compared to CIOB. In CIOB, OMZ shows two distinct layers 200-400 m top layer and 700-1100 m down layer separated by oxygen rich (120 µmol/kg) layer from 400-700 m. The dissolved oxygen content is increasing in the deeper layers, CIOB show oxygenated bottom waters (180µmol/kg) where as in Wharton basin oxygen content reaches up to 200µmol/kg. Bottom waters are oxygen rich as found in the *I2* profile. The shallow oxygen minimum was associated with the subsurface salinity maximum. It was strongest in the north and attenuated towards the south (Fig. 4.4.2.3). In this layer, the average concentration of oxygen at 13°S was around 112 µM. This minimum is caused by the in situ consumption of oxygen by sinking detritus (Warren 1981a, b as quoted in deSousa et al., 2001).

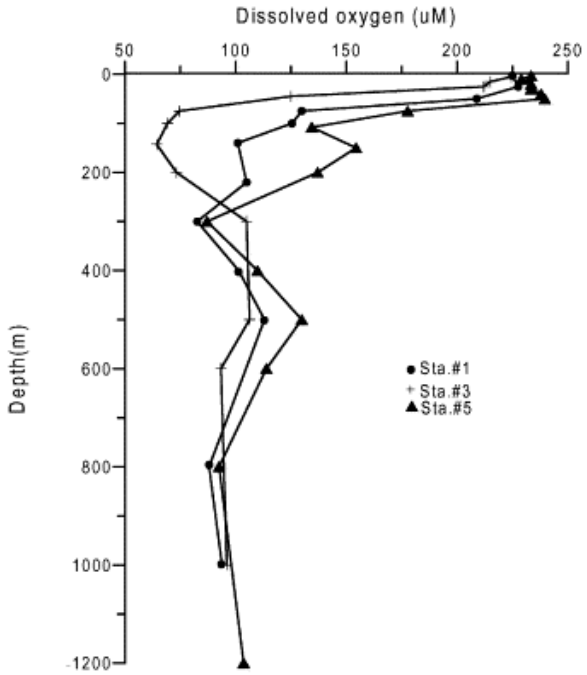

Fig. 4.4.2.3: Depth profiles of oxygen (µM) along 79°E longitude

The dissolved silicate concentration in CIOB waters are examined in the vertical profile, along 8°S (*I2*). It shows low silicate (0-5µmol/kg) layer from surface to 100m water depth. Deeper layers show continuous increase of silicate concentration with depth, the silicate rich (130µmol/kg) layers occurs below 3000 m water depth. Bottom layers show high silicate and more towards western side than the eastern side of CIOB (Fig. 4.4.2.4). The bottom waters show very high concentration throughout the CIOB suggesting benthic fluxes of silica to the seawater.

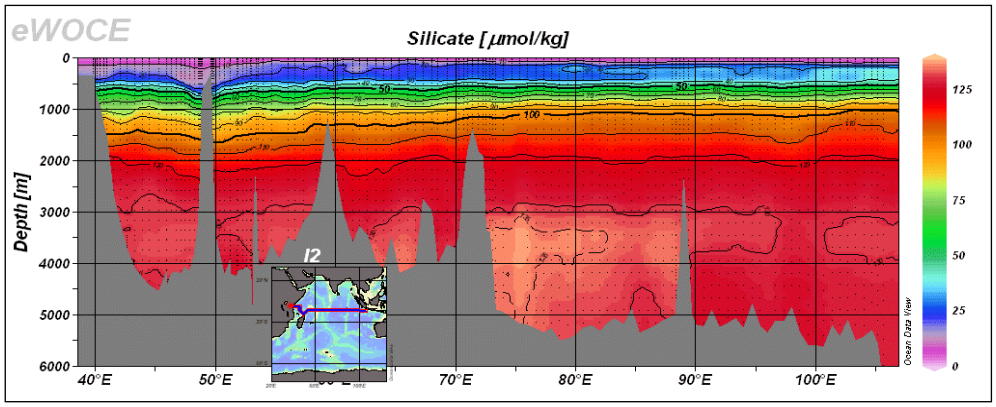

Fig. 4.4.2.4: Profile I2 shows the distribution of silicate in seawater on a W-E transect across the Indian Ocean at latitudes of 8°S. (www.ewoce.org).

deSousa et al. (2001) observed the surface mixed layer in CIOB, which was about 40 m thick, showed a northward shallowing trend and was characterized by low salinity (34.67 psu), high oxygen (223–245 µM), high pH (>8.2), and low nutrient contents . The concentration of nitrate was below 0.02 µM (deSousa et al., 2001). This low-salinity layer is caused by local excess of precipitation (Warren, 1981a), and/or by the influx of low-salinity Pacific water, as ‘‘Indonesian Through flow’’ (Warren, 1981a; Fieux et al., 1996). Between 10^{o} and 11^{o}S, a sharp salinity front, at 50 m depth separated the lower salinity waters (<34.67 psu), marking the influence of the Indonesian Through flow, from the higher salinity waters (>34.70 psu). The top of the thermocline was marked by a rapid fall in oxygen concentration from 225 to 100–125 µM and was associated with rapid increase in nutrient concentrations and decreased pH (deSousa et al., 2001). The deep water properties in CIOB remained almost constant below 3000 m depth (Fig. 4.4.2.5), except a gradual decrease of phosphate from 2.4 to 1.95 µM. The salinity of seawater varied within a very narrow range of 34.719–34.720 psu, but nitrate and silicate were varied within a range of 34.4–34.6 and 110–120 µM, respectively (deSousa et al., 2001). The deep waters in CIOB are believed to be of Antarctic origin carried northwards by circumpolar currents without any changes in its properties (Toole and Warren, 1993, Warren, 1981a, b, 1982).

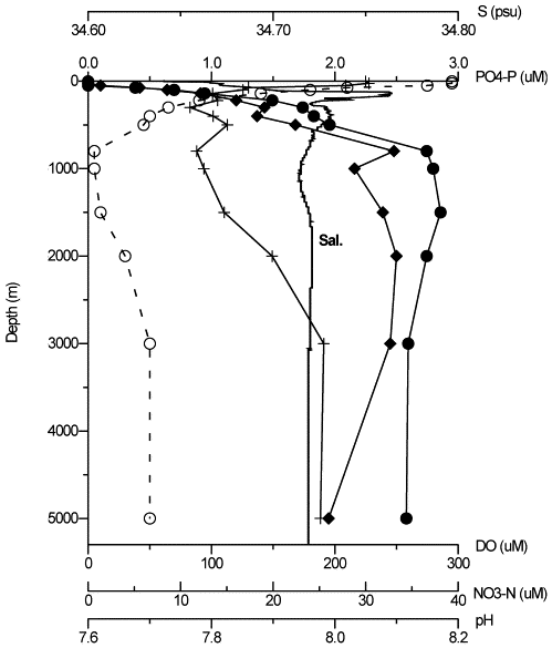

Fig. 4.4.2.5: Profiles of water properties at Sta.#3, pH (○), oxygen µM (+), nitrate µM (•), phosphate µM (♦) (Source: deSousa etal., 2001)

deSousa et al (2001) explained the entry of Sub-Antarctic Mode Water (SAMW) (Warren, 1981a) in to CIOB from the southwest. Below the subsurface salinity maximum layer, deep oxygen maximum (180 µM) layer is present at the depth range of 250–750 m. The maximum was intense in the western side of the basin and was associated with weak minima in nutrients (nitrate: 14–22 µM, phosphate: 0.6–2.2 µM and silicate: 12–22 µM and relatively high pH, >7.8). This relatively low concentration of nutrients and higher pH associated with SAMW also support the entrance of SAMW in the CIOB (deSousa et al., 2001). Antarctic Intermediate Water (AAIW) was seen as a 400m thick band in the depth range 800–1200 m and between 27.2 and 27.5 density levels also reported in CIOB (deSousa et al., 2001).

4.4.2.1 Dissolved organic carbon in the Central Indian Basin

Dissolved organic carbon (DOC) concentrations was measured in the vertical profiles of water column were studied at three locations from the Central Indian Basin and described in Sardessai and deSousa (2001). The observations were also taken close to the bottom to get the baseline information on this component of organic matter. The DOC concentrations in this area can be divided into three depth intervals. The subsurface layer (25–200m) shows highly variable distribution with concentrations ranging from 52 to 191 µM. Between 500 and 800m, DOC shows a minimum (41–57µM) and is associated with decreased oxygen. The bottom waters (3500–5300m) show decrease with little variability in the DOC concentrations

(41–64µM) suggesting its refractory nature in the deep ocean. The variable concentration of DOC with depth is related to the biochemical activity as well as to the chemical features of the water column. Vertical profiles of DOC, apparent oxygen utilisation (AOU) and oxygen in water columnat the three stations are shown in Fig. 4.4.2.1.1. Both high and low values of DOC with high AOU indicate no significant correlation between DOC and AOU and suggest simultaneous utilisation of oxygen for the oxidation of other species of organic matter in the water column.

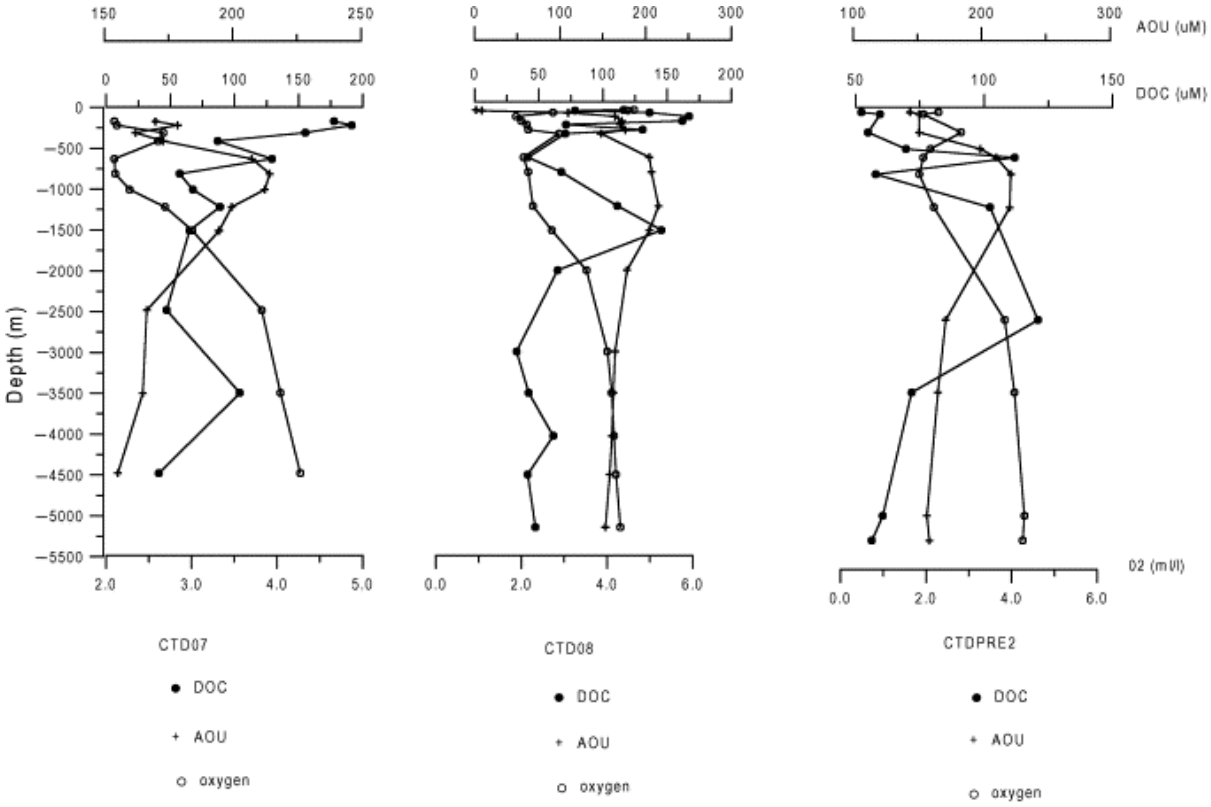

Fig. 4.4.2.1.1: Vertical profiles of DOC, AOU and oxygen at the three stations

4.4.2.2 Chemical properties in IRZ and PRZ

The baseline water column chemical oceanographic parameters in IRZ and PRZ were assessed in the year 2015. One CTD each was deployed in IRZ (CTD1) and PRZ (CTD2) (Fig. 4.4.2.2.1). Seawater was collected using Niskin bottles of 10L capacity fixed on a rosette and connected to the CTD system at desired depths while heaving the CTD. The depths of water sampling are determined from profiles of various sensors and CTD deck unit attached to the computer. Immediately after collection, pH of seawater was measured using pH meter by inserting the respective probes into the water samples. The seawater samples were analyzed for dissolved oxygen, and nutrients nitrite, phosphate and silicate, mostly on the same day. Basically, the methods used here are adopted from the standard seawater

analyses (Grasshoff et al., 1983). For filtration for Suspended Particulate Matter (SPM), 10 liter of seawater collected from selected depths were filtered using preweighed 0.45µm filter papers. The SPM along with the filter paper was stored for further analysis in the lab. In the shore laboratory, the filter papers were dried at ~40°C in the oven and weighed.

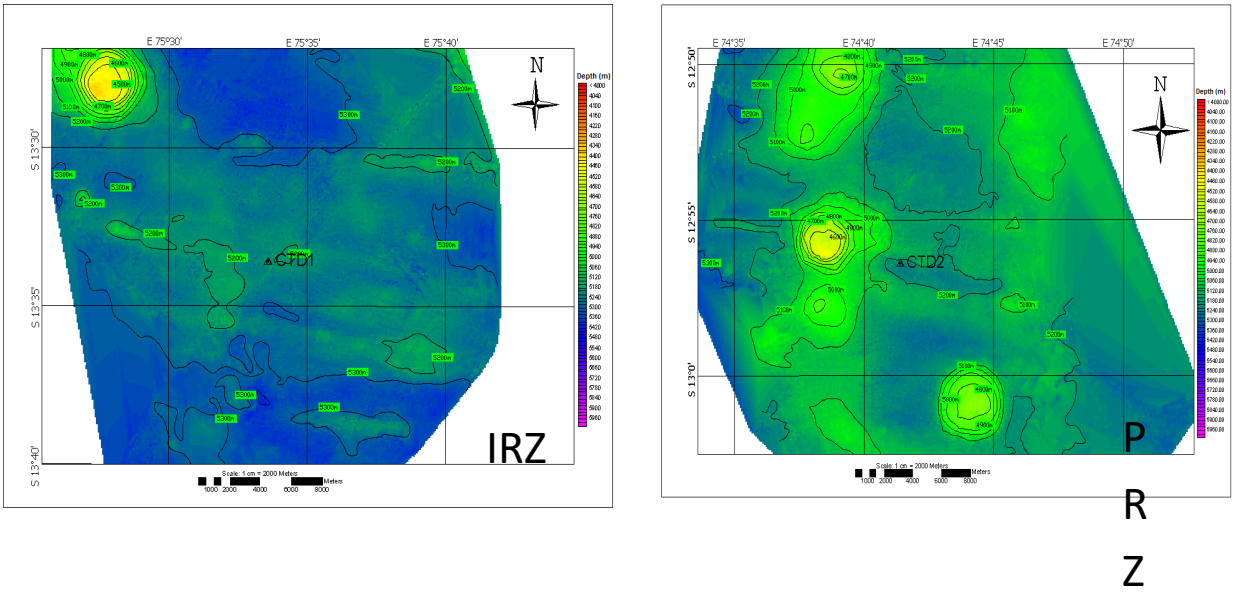

Fig. 4.4.2.2.1: Location map of CTD casts in the IRZ and PRZ

4.4.2.2.1 pH variation

The pH value of the station IRZ is within the range of 7.8 to 8.5 while in PRZ it is 7 to 8.5. High pH is seen in the surface waters at both locations (Fig. 4.4.11.1.1) which gradually decreases with increasing depth (about 1000 m). Further down the water column the pH gradually increases to about 8.2.

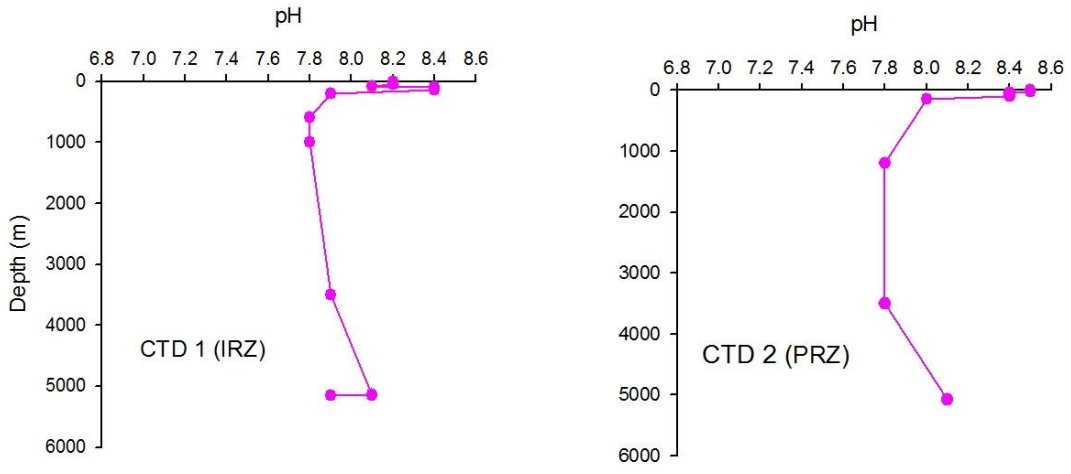

Fig. 4.4.2.2.1.1: Downcast variation in pH at the Impact Reference Zone (IRZ) and Preservation Reference Zone (PRZ)

4.4.2.2.2 Dissolved oxygen variation

Both the stations of IRZ & PRZ show almost similar pattern with DO values ranging from 1 to 5ml/L. High DO is seen in the surface waters at both locations which gradually decrease with increasing depth (about 50 m) with minimum (1-2 ml/L) at about 100-1000m. Further down the water column from about ~1000m, the DO gradually increases, reaching to about 4ml/L at ~4000 m water depth (Fig. 4.4.2.2.2.1). Low oxygen in intermediate waters may denote the local oxygen minimum zone which is also confirmed by CTD DO sensor data shown in Fig. 4.4.2.2.2.2 and Fig. 4.4.2.2.2.3. The sensor data, however, shows two minima, one at ~100m and the other between 600 to ~800m, the difference being due to resolution of sampling. While the overall pattern of high maximum, low intermediate and high bottom DO is similar in both the areas, the intensity of oxygen minima is varying locally.

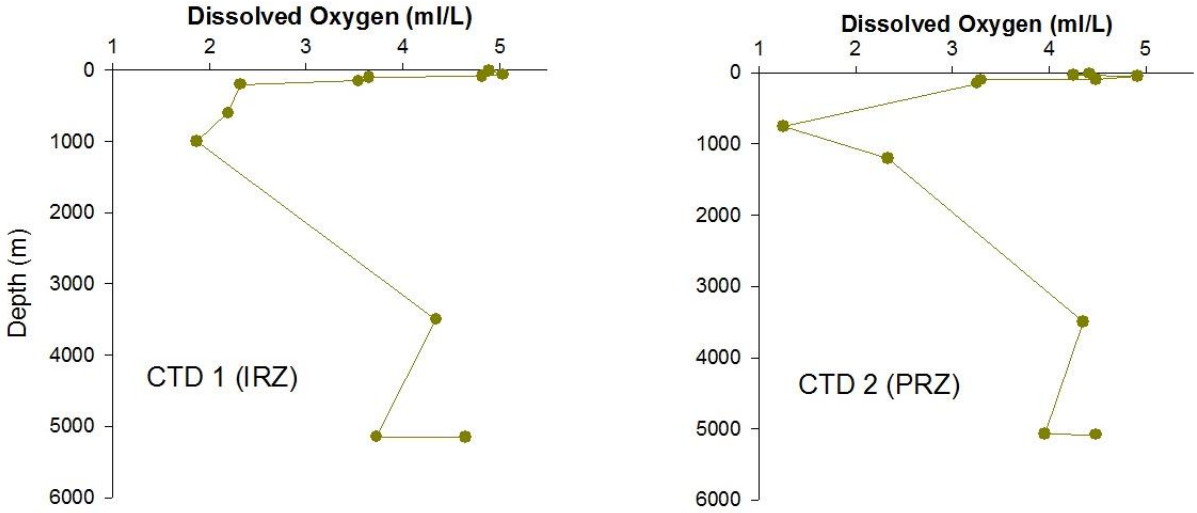

Fig. 4.4.2.2.2.1: Downcast variation in dissolved oxygen concentration at the Impact Reference Zone (IRZ) and Preservation Reference Zone (PRZ)

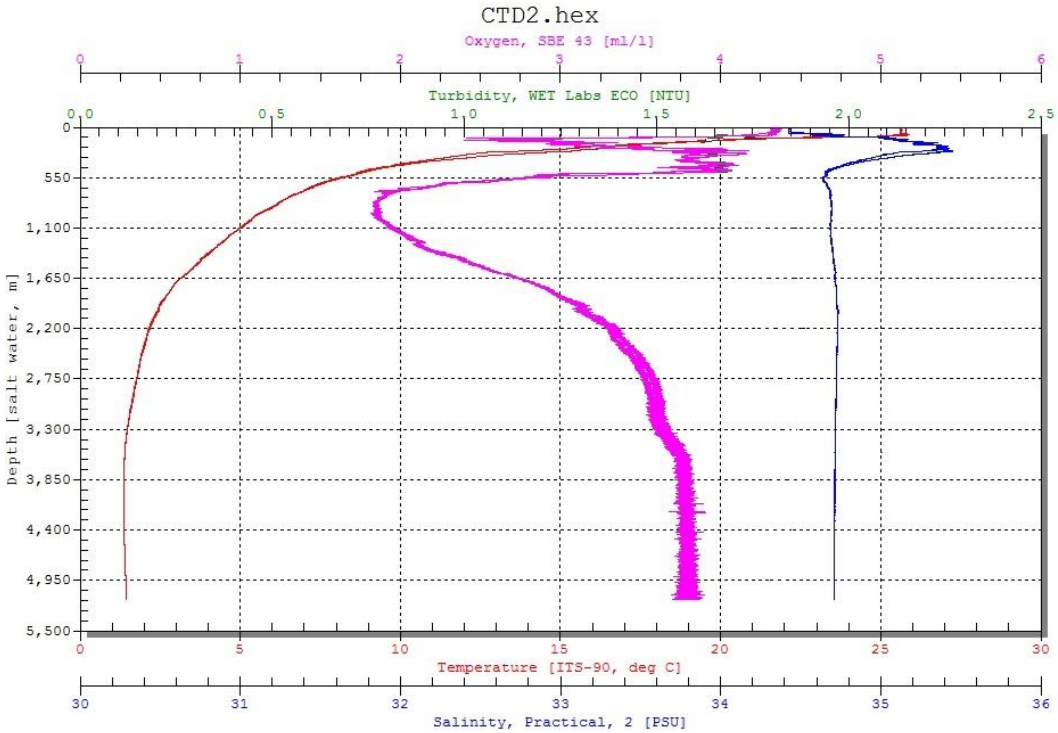

Fig. 4.4.2.2.2.2: CTD Profile at IRZ

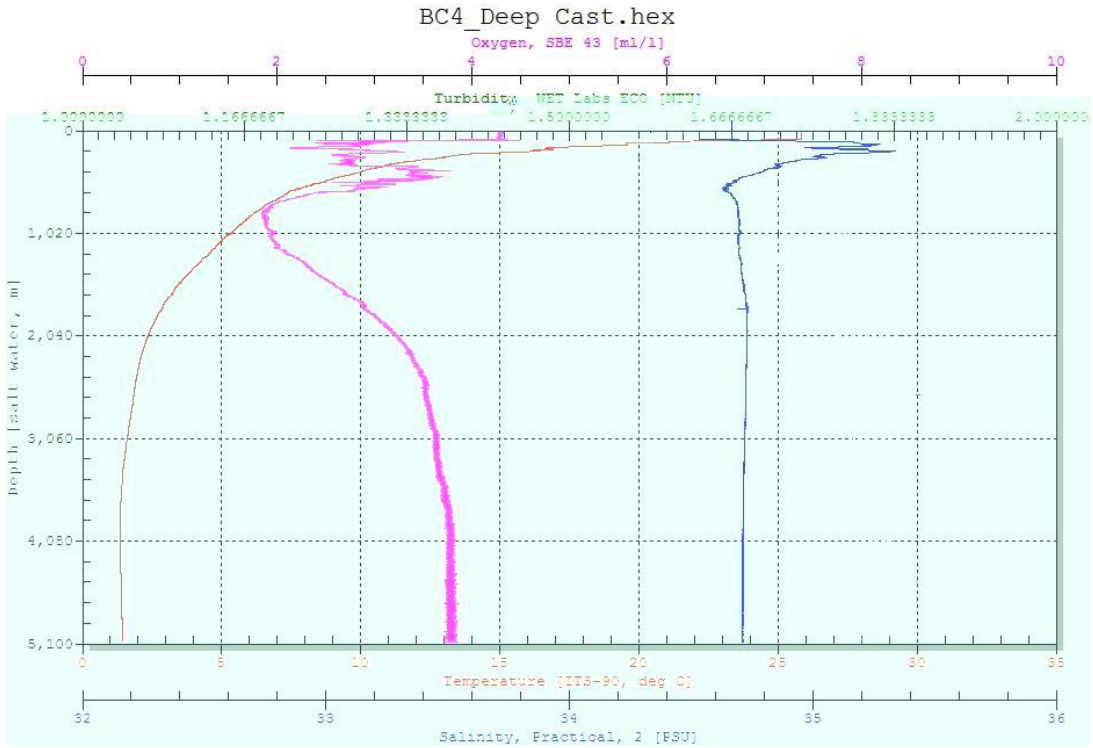

Fig.4.4.2.2.2.3: CTD Profile at PRZ

4.4.2.2.3 Nutrients in seawater

4.4.2.2.3.1 Phosphate

Both the CTD stations of IRZ and PRZ sampled at the central location of the area (CTD 1 and CTD 2 respectively), show almost similar pattern with lower phosphate concentration in the surface waters downto 1000m which gradually stabilize throughout the rest of the water column, the depth of phosphate increase coinciding with the end of intermediate oxygen minimum. PRZ however has higher phosphate concentration compared to the IRZ (Fig. 4.4.2.2.3.1.1).

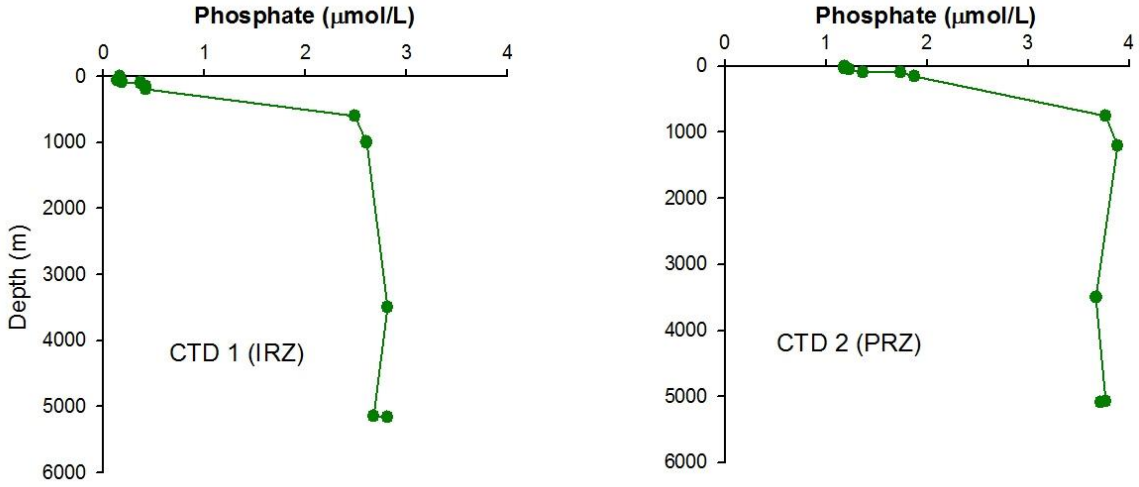

Fig. 4.4.2.2.3.1.1: Phosphate concentrations in seawater with depth at the Impact Reference Zone (IRZ) and Preservation Reference Zone (PRZ)

4.4.2.2.3.2 Nitrite

The nitrite concentration in both the areas ranges from below detection to 0.12 µmol/L, except for two points in each area (at about 100m). Both the stations of IRZ & PRZ show almost similar pattern with low concentration in the surface waters and with an intermediate high at about 100mts (Fig. 4.4.2.2.3.2.1). However the intermediate high at PRZ is substantially higher and nearly double compared to IRZ. High nitrite values at 100m coincide with the first oxygen minima and may indicate the reduction of nitrate in low oxygen waters.

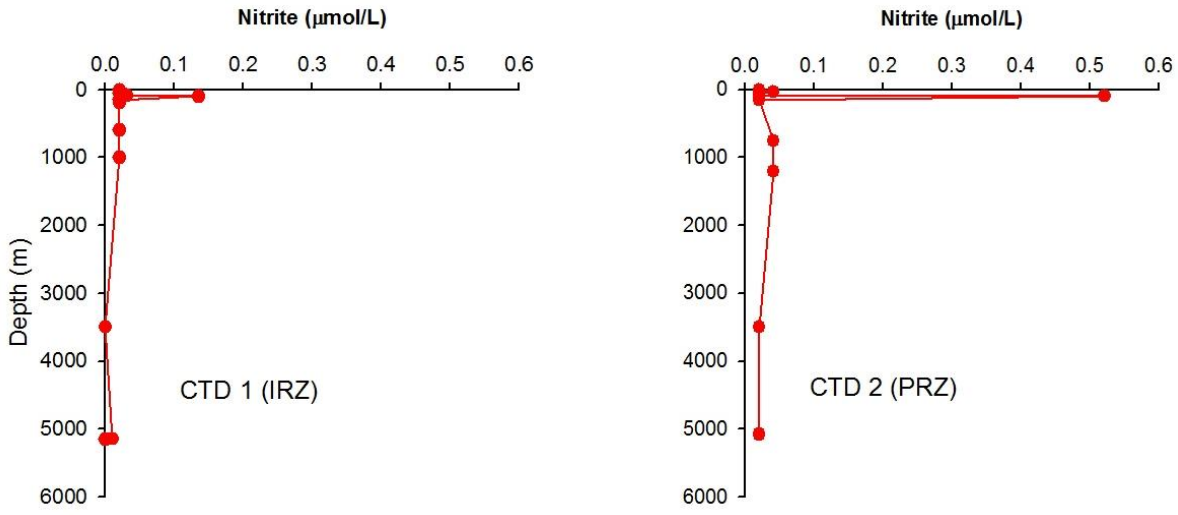

Fig. 4.4.2.2.3.2.1: Nitrite concentrations in seawater at the Impact Reference Zone (IRZ) and Preservation Reference Zone (PRZ)

4.4.2.2.3.3 Silicate

The silicate concentration in both the IRZ and PRZ ranges from 2.1 to 152 µmol/L shows nearly similar pattern in both the areas. Low values of silicate are seen in the surface waters (Fig. 4.4.2.2.3.3.1) which gradually increase throughout the length of the water column. Highest values of silicate concentration are seen near the bottom of the water column which was attributed before to the presence of Antarctic bottom waters (AABW). Silicate concentration is slightly higher in PRZ water column compared to IRZ.

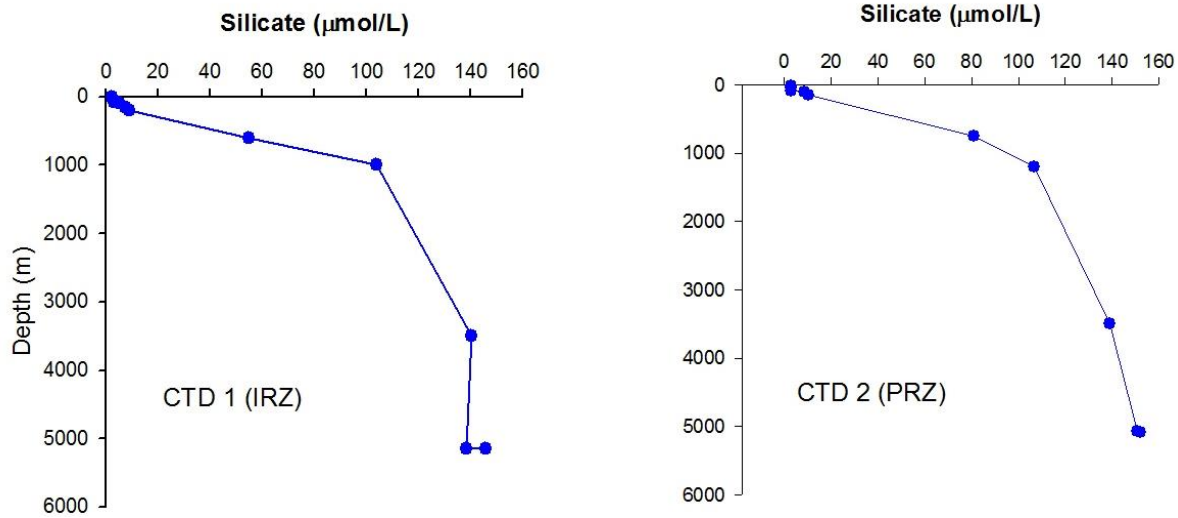

Fig. 4.4.2.2.3.3.1: Seawater silicate concentration at the Impact Reference Zone (IRZ) and Preservation Reference Zone (PRZ)

4.4.2.3 Suspended Particulate Matter (SPM) variation

The SPM values range between 0.06 and 0.011 gm/L. Both the stations of IRZ and PRZ show almost similar pattern with high variability in SPM concentration in the surface waters to a depth of about 500m (Fig. 4.4.2.3.1) probably related to higher biological activity. In the deeper depths, the variation of SPM content in both the locations is not significant. Both the stations show high bottom values probably due to resuspension.

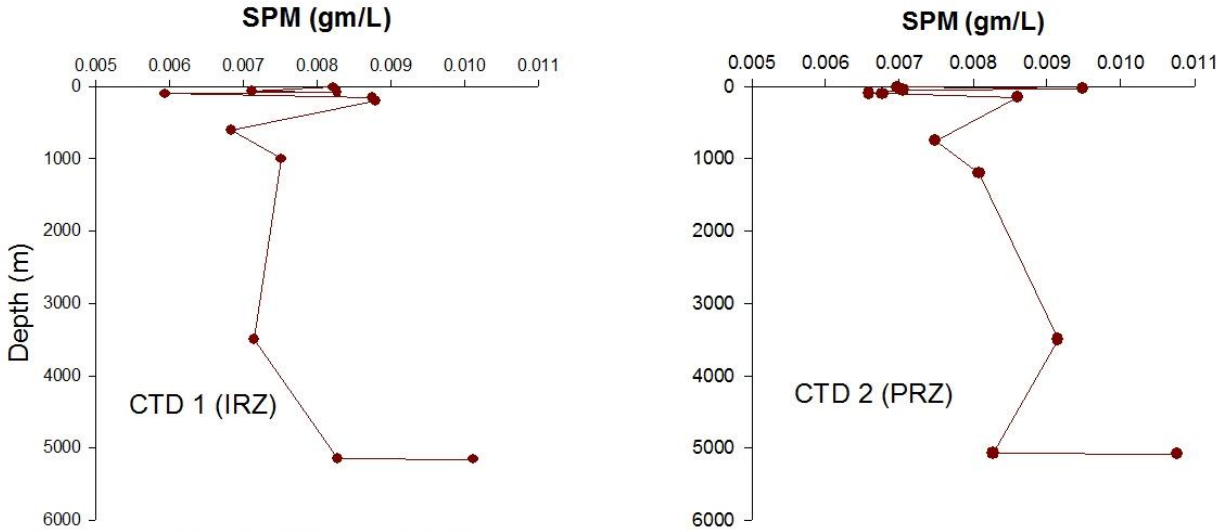

Fig. 4.4.2.3.1: Suspended particulate matter (SPM) content with depth at the Impact Reference Zone (IRZ) and Preservation Reference Zone (PRZ)

4.5 Physical properties of seabed sediments

The baseline grain-size and physical properties of CIOB sediments are presented here. For the regional variability, studies were carried out on sediment cores systematically sampled in a degree spacing between latitudes 10° and 16°S and longitudes 73°30' and 76°30'E in nodule bearing part of CIOB during the 61st expedition of A.A. Sidorenko (Fig. 4.5.1; Table 4.5.1). Earlier studies (Khadge, 2005, 2008) have shown that geotechnical properties vary with sediment type, and grain size varies with latitude (Valsangkar, 2011) in the CIOB sediments. The textural analyses of CIOB sediments were carried out to determine the distribution of sand, silt and clay. The sand fraction is retained on the sieve (while wet sieving) with a mesh size of 63µm. The silt and clay fractions were determined using the standard pipette analyses method (Folk 1968). Physical properties were measured following ASTM (1995), Das (1998), Bennett and Lambert (1971), Noorany (1985). Shear strength was measured using lab vane shear tester (AIMIL, India) on the CIOB sediments for assessing the sediment characteristics.

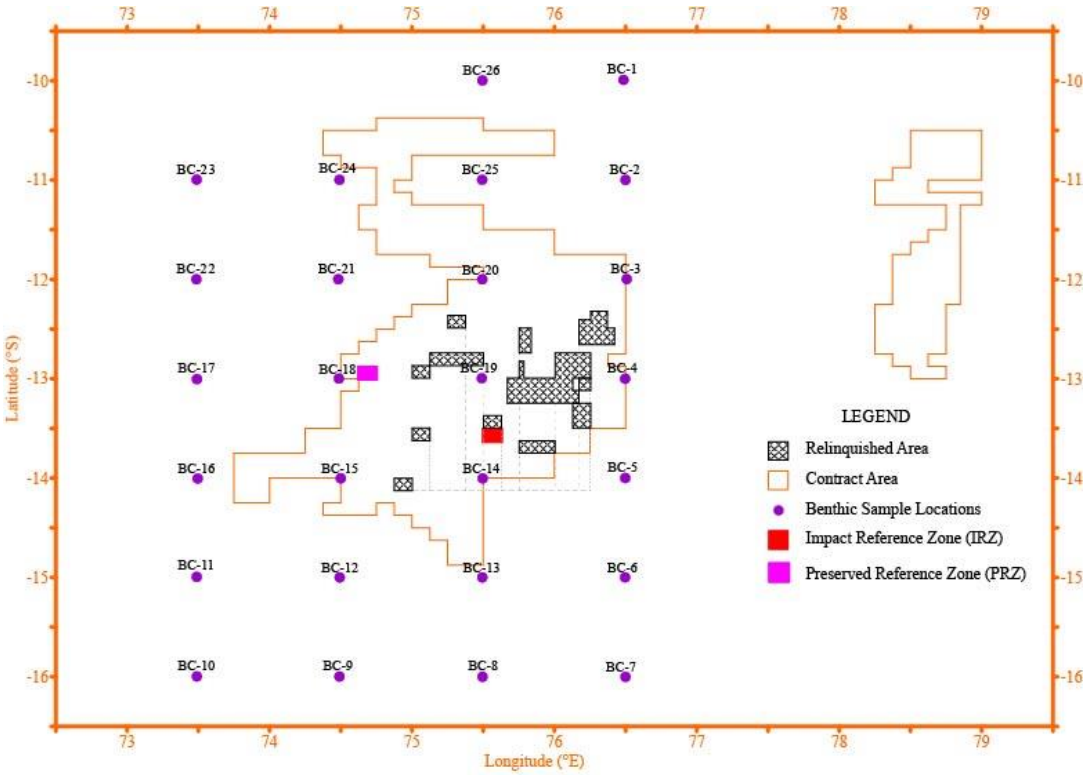

Fig. 4.5.1: Sediment coring locations for environmental variability studies.

Table4.5.1: Sediment sampling locations for regional environmental study in CIOB

Station No.	Latitude (S)	Longitude (E)	Water depth (m)
BC-1R	9° 59.661'	76° 29.220'	5355
BC-2RR	11° 00.033'	76° 30.038'	5320
BC-3R	11° 59.924'	76° 30.559'	5280
BC-4	13° 00.032'	76° 29.915'	5360
BC-5	13° 59.992'	76° 29.947'	5180
BC-6	14° 59.984'	76° 29.895'	4980
BC-7	16° 00.047'	76° 30.043'	5070
BC-8	15° 59.981'	76° 30.000'	5010
BC-9	15° 59.847'	74° 29.907'	5350
BC-10	15° 59.775'	73° 29.999'	4900
BC-11	14° 59.694'	73° 29.961'	5480
BC-13	15° 00.007'	75° 29.918'	4840
BC-14	14° 00.231'	75° 30.064'	5145
BC-15	14° 00.180'	74° 30.457'	5160
BC-16	14° 00.315'	73° 30.370'	5120
BC-17	13° 00.317'	73° 30.038'	4810
BC-18	12° 59.963'	74° 29.647'	5050
BC-19	12° 59.769'	75° 29.688'	5070
BC-20	12° 00.066'	75° 29.893'	5200
BC-21	11° 59.986'	74° 29.428'	5055
BC-22	12° 00.011'	73° 29.819'	4900
BC-23	10° 59.888'	73° 29.937'	5100
BC-24	10° 59.955'	74° 29.927'	5050
BC-25	10° 59.964'	75° 29.842'	5300
BC-26	9° 59.988'	75° 29.959'	5290

4.5.1 Surface sediments

The observations made on spatial changes in sediment properties and geotechnical parameters are described in the following sections.

4.5.1.1 Grain size distribution

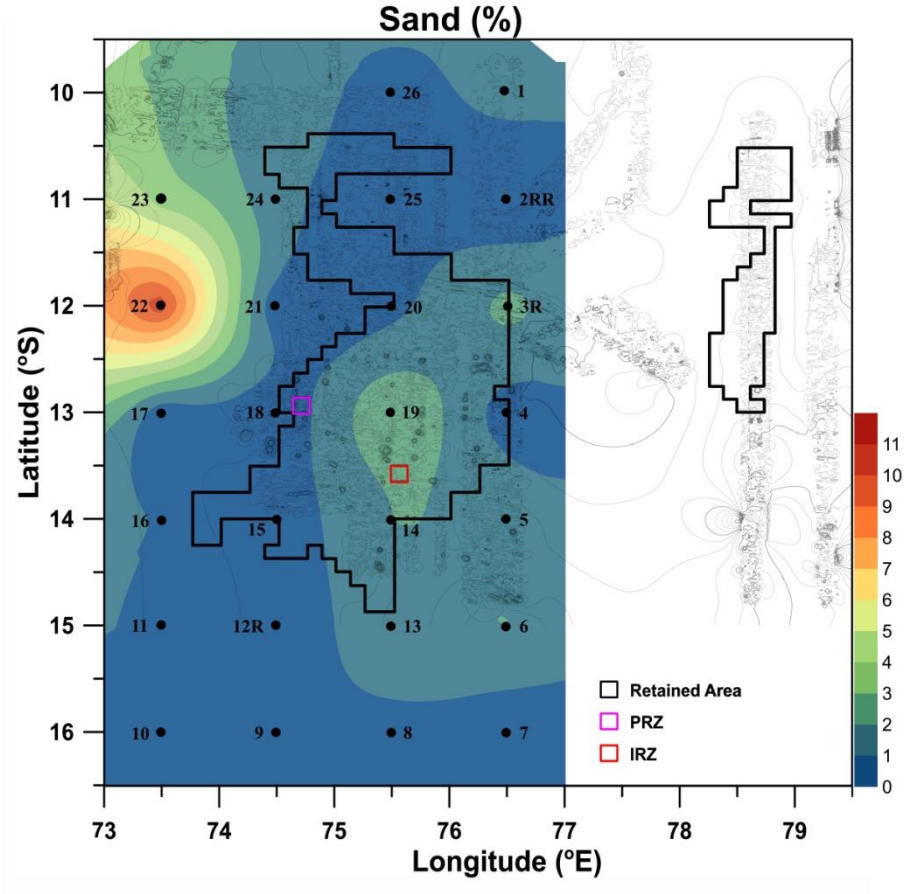

Fig. 4.5.1.1.1: Sand content (%) in the surface sediments in the CIOB.

The 26 locations cover mainly siliceous ooze with very few stations falling in pelagic clay south of 15ºS latitude. Spatial variations in sand, silt and clay content of surface sediments in the CIOB are observed. Although sand content in the CIOB is <5%, it shows southward reduction from 10º to 16ºS (Fig. 4.5.1.1.1). However, it does not have any specific latitudinal trend. One sample in the west, in 12°S transect, shows the highest value. The average sand content in the CIOB is 1.06% (Valsangkar, 2011).

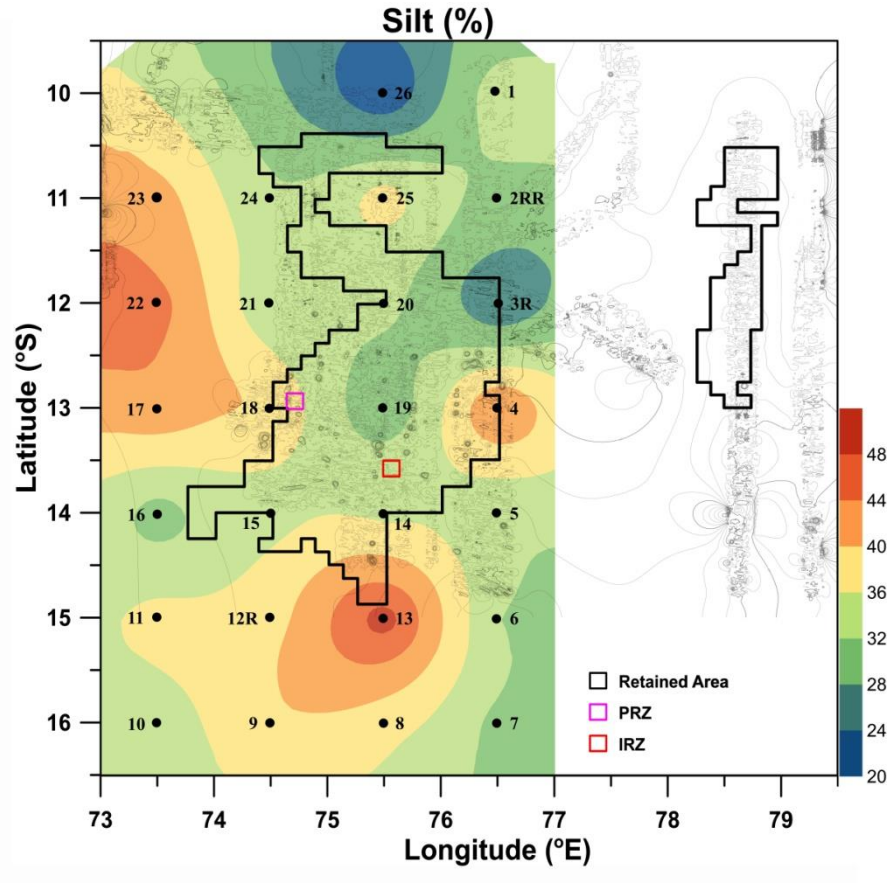

Fig. 4.5.1.1.2: Silt content (%) in surface sediments from the CIOB

The silt in the CIOB sediments varies from 20 to 46% (Fig. 4.5.1.1.2) with an average of 35% (Valsangkar, 2011). It increases from NE to SW with an area of high values in west (Fig. 4.5.1.1.2). The high silt content could be due to terrigenous influx of Ganga and Brahmaputra rivers from the Bay of Bengal to the CIOB (Nath et al., 1989).

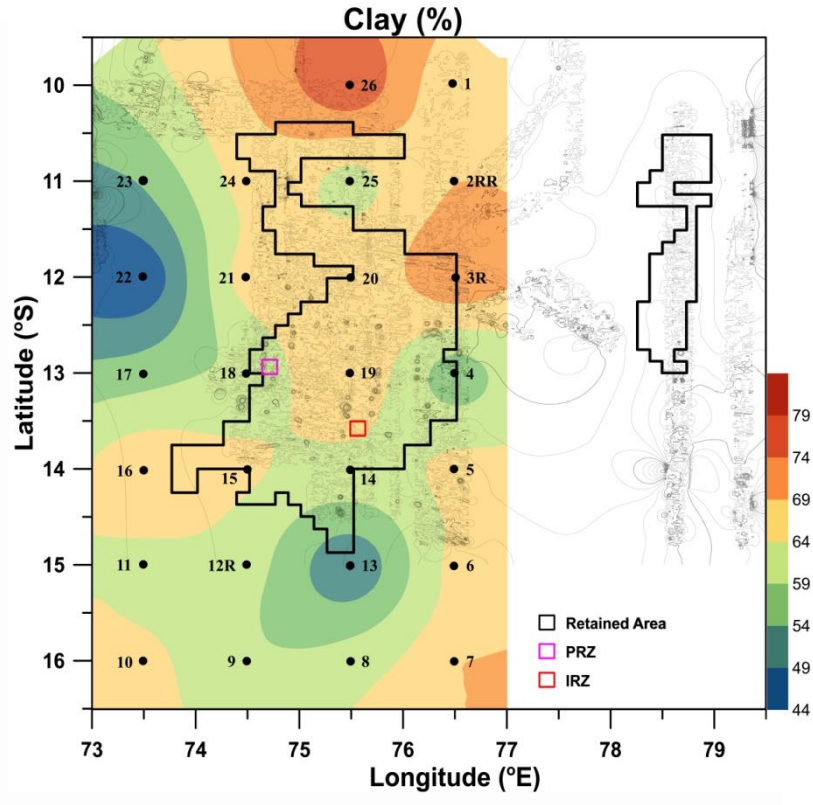

Fig. 4.5.1.1.3: Clay content (%) in surface sediments from the CIOB

Clay is dominant grain size in the surface sediments of the CIOB and it varies from 44 to 79%. The clay content decreases from north to south and also from east to west (Fig. 4.5.1.1.3), in a way reflecting the natural dispersal pattern of fine-grained sediments in the area The increase in clay at southern latitudes is due to additional source from the alteration of submarine basalts and other volcanic rocks (Kolla et al., 1976; Rao and Nath, 1988; Valsangkar, 2011). In general, the dominant texture of the CIOB sediments is silty clay.

4.5.1.2 Geotechnical properties

The natural water content (Fig. 4.5.1.2.1) of surface sediments collected from the CIOB varies from 490 to 790% (dry basis). Water content is the water holding capacity of sediments and depends on the pore spaces and clay minerals present in the sediment. The maximum value of 790% is seen mainly in the siliceous oozes around 10°S and 13°S. The water content decreases towards south around 16°S where pelagic clay is dominant. The mineralogical study (Valsangkar, 2011) of siliceous oozes/clays has shown high abundace of smectite, a clay mineral, with high water holding capacity. In addition, these sediments contain radialoarian tests, which can increase the porosity, helping retain more water

content.On the contrary, the southern sediments show high abundance of illite which has low water holding capacity.

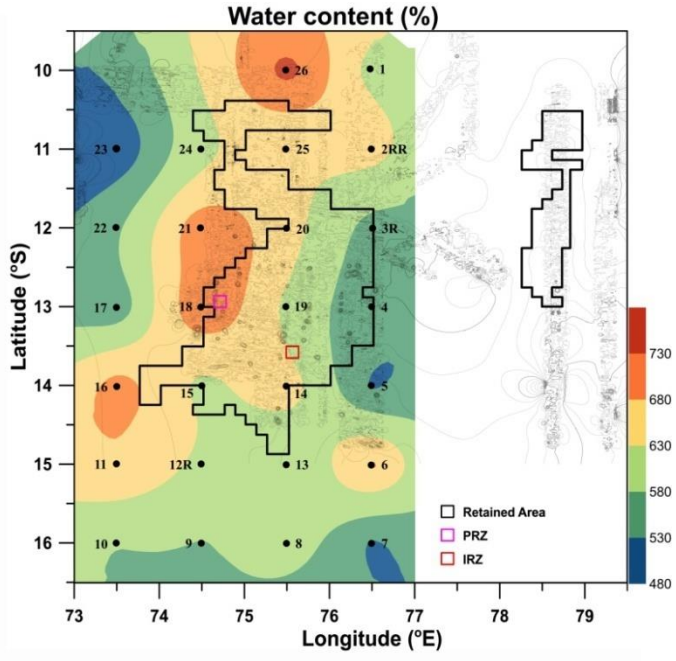

Fig. 4.5.1.2.1: Water content (% dry basis) in surface sediments from the CIOB

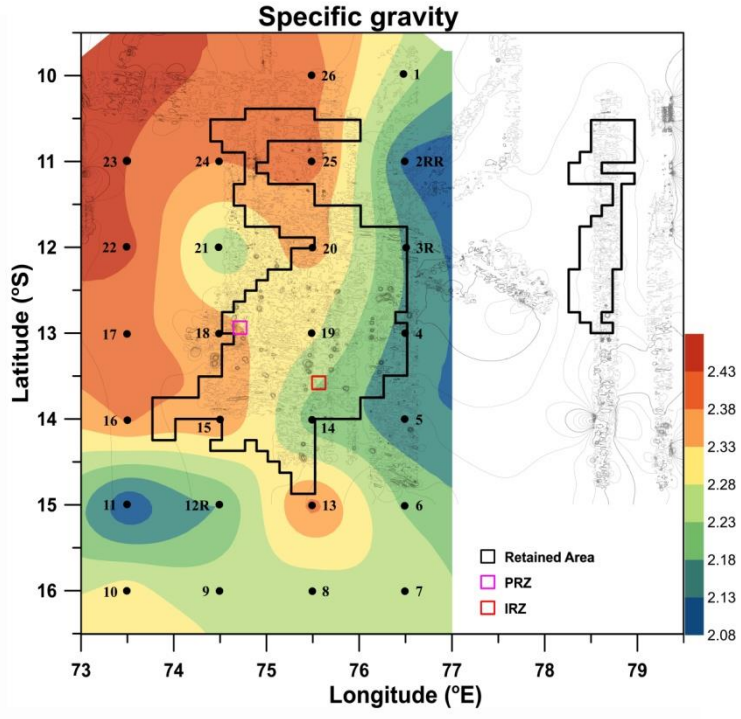

Fig. 4.5.1.2.2: Specific gravity of surface sediments from the CIOB

Specific gravity of the CIOB sediment (Fig. 4.5.1.2.2) varies between 2.0 to 2.5. It is distinctly less (2.0) in southern part (pelagic clays) and the eastern part of study area which

gradually increases towards north to 2.5. Distinctly, the western part of siliceous ooze domain has high specific gravity.

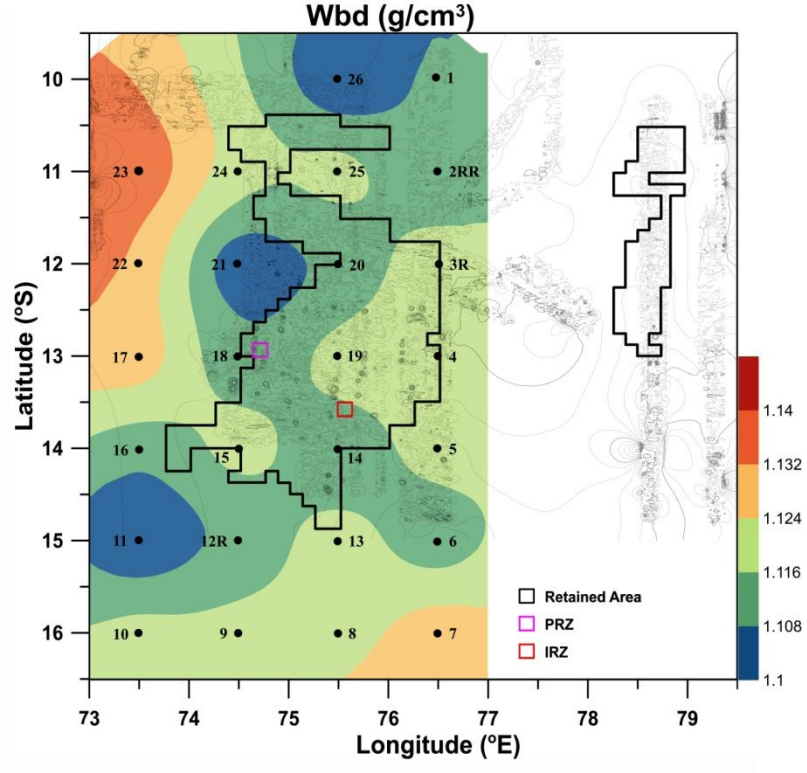

Fig. 4.5.1.2.3: Wet bulk density (g/cm^3) of surface sediments from the CIOB

Wet bulk density (Fig. 4.5.1.2.3) of the CIOB sediments varies from 1.10 (g/cm^3) to 1.14 (g/cm^3). Siliceous sediments are less dense than pelagic and calcareous clays due to low compaction and high water content. It increases from north to south of the study area. Interestingly, the nodule-abundant regions have near uniform wet bulk density.

Sediment porosity (Fig. 4.5.1.2.4) varies from 91% in the eastern part (core BC4) which increases to 95% at centre of study area (core BC18). The porosity is higher in siliceous oozes compared to that in pelagic clays in south.

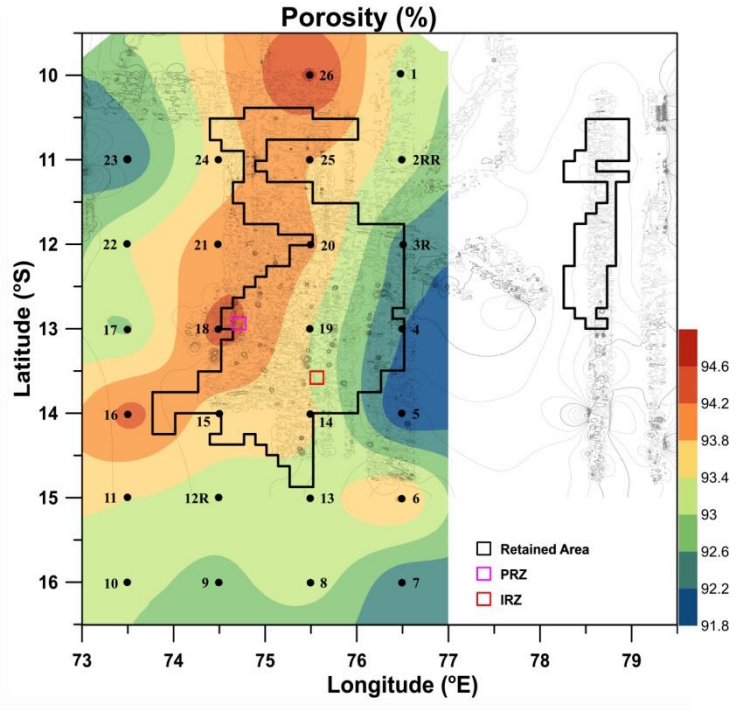

Fig. 4.5.1.2.4: Porosity (%) of surface sediments in the CIOB

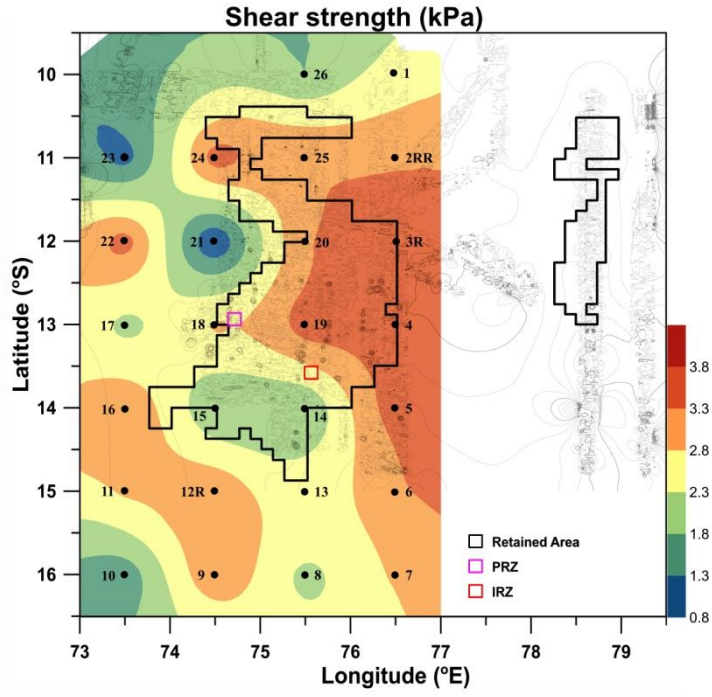

Fig. 4.5.1.2.5: Shear strength (kPa) of surface sediments in the CIOB

Shear strength of the surface sediments (Fig. 4.5.1.2.5) is < 2kPa. The high water content due to radiolarian tests and smectite dominance make sediments loose which leads to low shear strength. However, the shear strength increases in pelagic sediments and near seamount areas (BC4). Overall, the shear strength of sediments is high in the eastern part of the basin.

4.5.2Downcore variation

Downcore variation of grain size distribution and geotechnical properties were determined in all 26 box cores collected during EVD I in year 2003 (Fig. 4.5.10 to 4.5.12). . These cores were homogenous, soft in nature with subsurface features of lenses, mottling indicative of bioturbation. Sediments are moderate brown at top (0-10cm), with intercalations of moderate yellowish brown at middle (~10-20cm) and again moderate brown till bottom (~20-40cm) of cores. The core BC4 is entirely homogenous, without bioturbation and harder than all other cores, and located at the bottom of seamount area.

4.5.2.1 Grain size distribution

Fig. 4.5.2.1.1 shows the depth profiles of the sand, silt, clay content of 26 sediment cores presented in a manner in which they represent the geographic location, the top row representing the northernmost latitude they were sampled. While the sediment core locations cover a large nodule bearing area, about 9 stations fall in the Indian Retained Area where possible future nodule mining may take place.

Average sand content in sediments is < 2.5% which marginally increases with depth (Fig. 4.5.2.1.1). Silt percent varies from 16% to 60% with average of 35% in all the cores. It increases with depth in most of the cores.Clay percent in cores is dominating and varies widely from 35% to 81% (average 62%). However, in BC4, the clay content gradually reduces from 55% at surface to 35% at bottom of the core. All the cores are from siliceous domain except BC4 which is at bottom of a seamount. The sediments in this core are very homogenous without any bioturbation and somewhat harder compared to all the remaining.Locations of cores BC3, BC4, BC13, BC14, BC19 and BC20 fall on either side of the 76.5^{o}E fracture zone in the CIOB. It is reported that the higher clay content in these cores at the surface layers is due the additional supply of clay from the alteration of rocks from the fracture zone (Valsangkar, 2011). The alteration of rocks acts as additional source of clay to the basinal sediments.

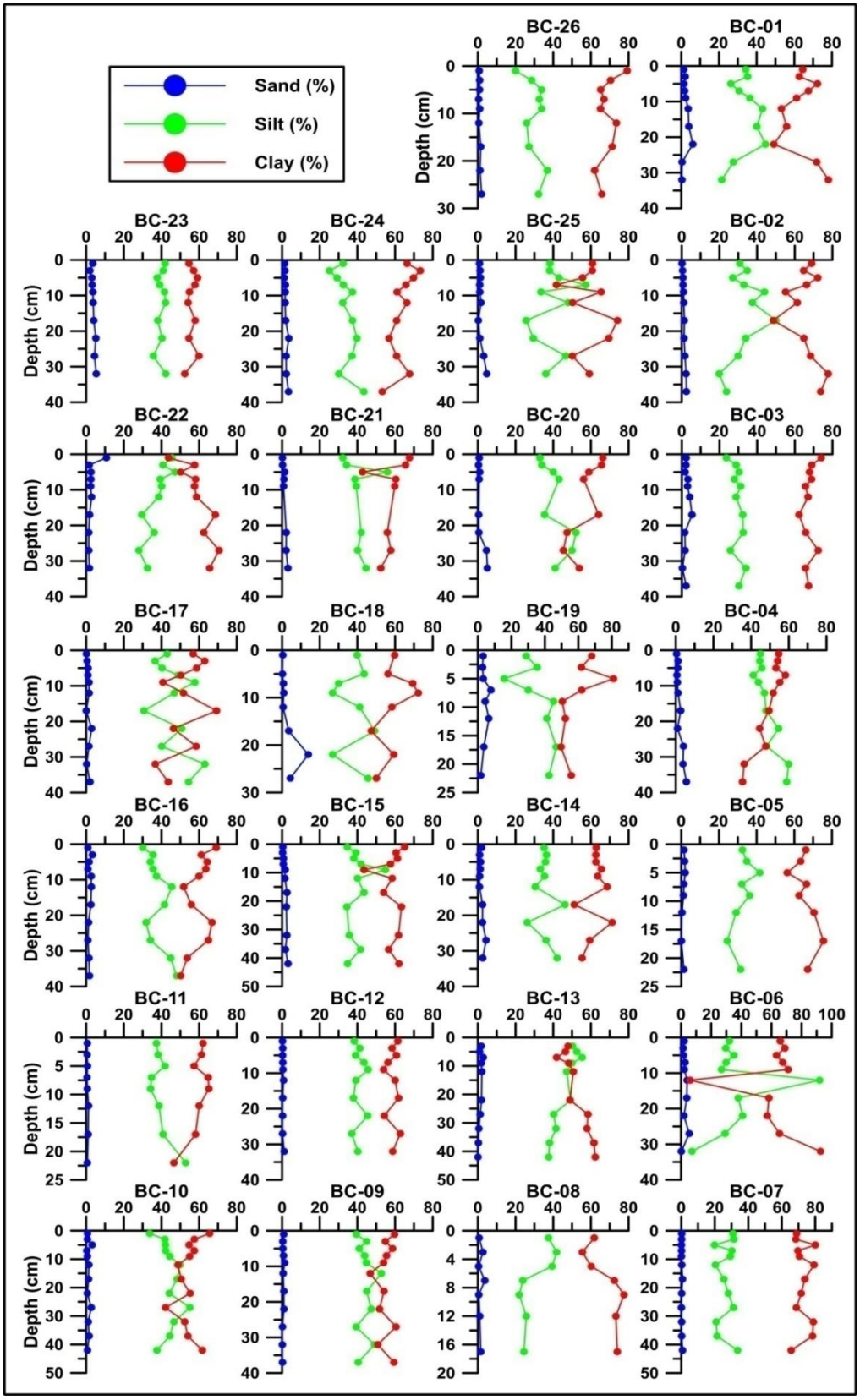

Fig. 4.5.2.1.1: Profiles of grain size distribution in CIOB sediments.

4.5.2.2 Geotechnical properties

Natural water content of sediments depends up on pore spaces and clay minerals present in them. The close coupling between water content, shear strength and meiobenthos in the Clarian-Clipperton Zone sediments from the Pacific Ocean have shown the significance of geotechnical parameters in environmental studies (Radxiejewska and Modlitba, 1999). The sediment properties are also known to be affected by the bioturbation in sediments (Richardson et al., 1985, Rowden et al. 1998). Siliceous sediments contain radiolarian tests that also lead to increase in water content. Fig. 4.5.2.2.1 indicates depth wise variation in water content in cores. It shows downward gradual reduction in water content. Water content of these cores varies in a broad range of 720% at the surface layer to 295% at subsurface layer implying consolidation of sediments with depth and bioturbation seen at middle of most of these cores. The sediment core BC4, from the base of seamount, has the lowest water content 545% at surface and 295% at 30-35cm layer due to hard nature of sediments as well as consolidation with depth.

Shear strength of the sediments (Fig. 4.5.2.2.2) is an important parameter for the design of nodule miner. It varies from 0.36kPa at 10cm in BC24 sediment layer to 3.59kPa at surface layer in BC4. Most of the cores show reduction in shear strength at middle depths where the bioturbation features are seen, possibly influenced by burrowing organisms. Over all, the shear strength increases with depth due to consolidation and lowering of water content. The sediments in BC4 are comparatively harder which is seen in low sediment recovery

The wet bulk density of the CIOB sediments (Fig. 4.5.2.2.3) varies from 1.11g/cm^3 to 1.19g/cm^3 and increases with depth.

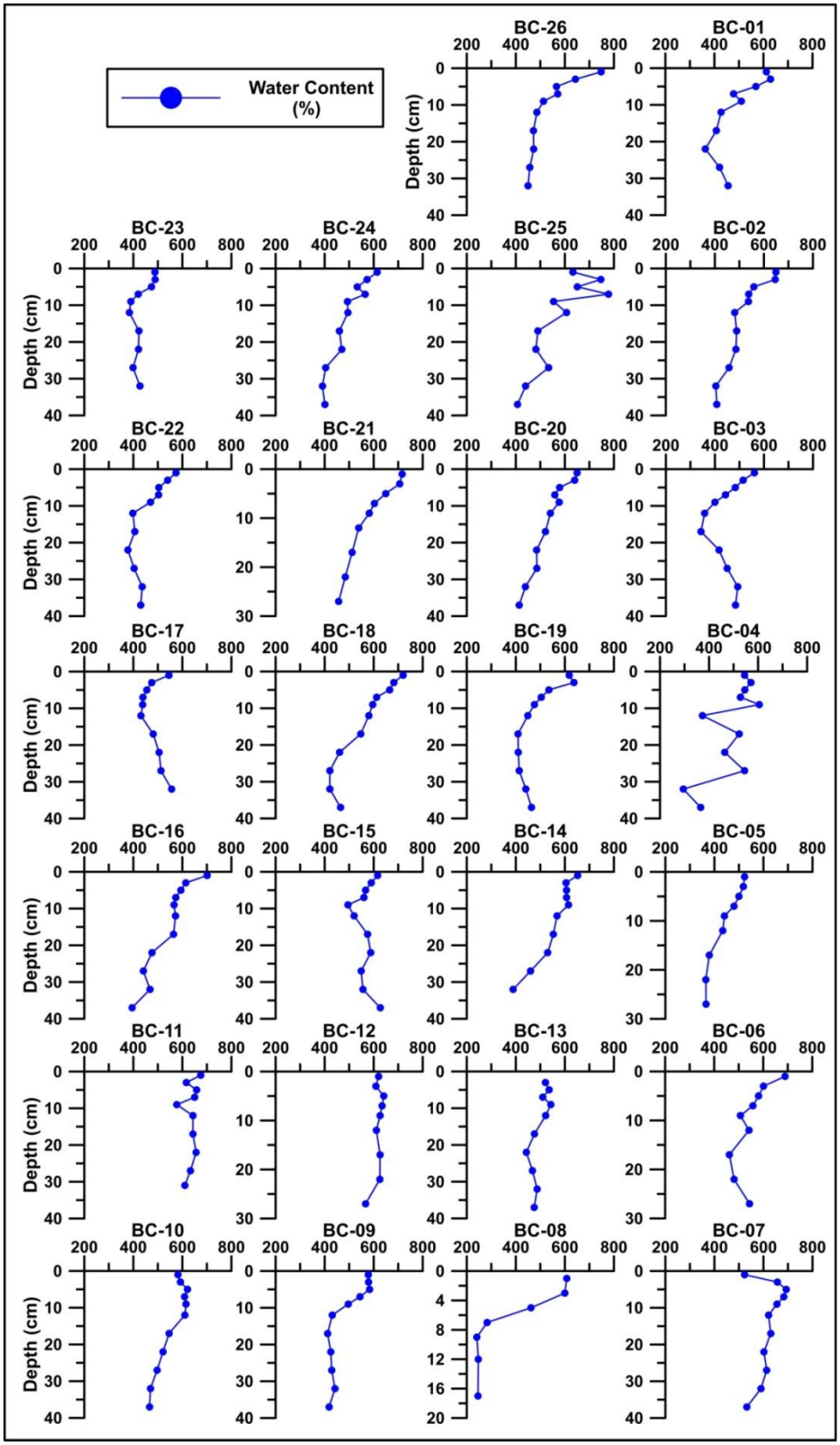

Fig. 4.5.2.2.1: Profiles of water content (dry %) in the CIOB sediments.

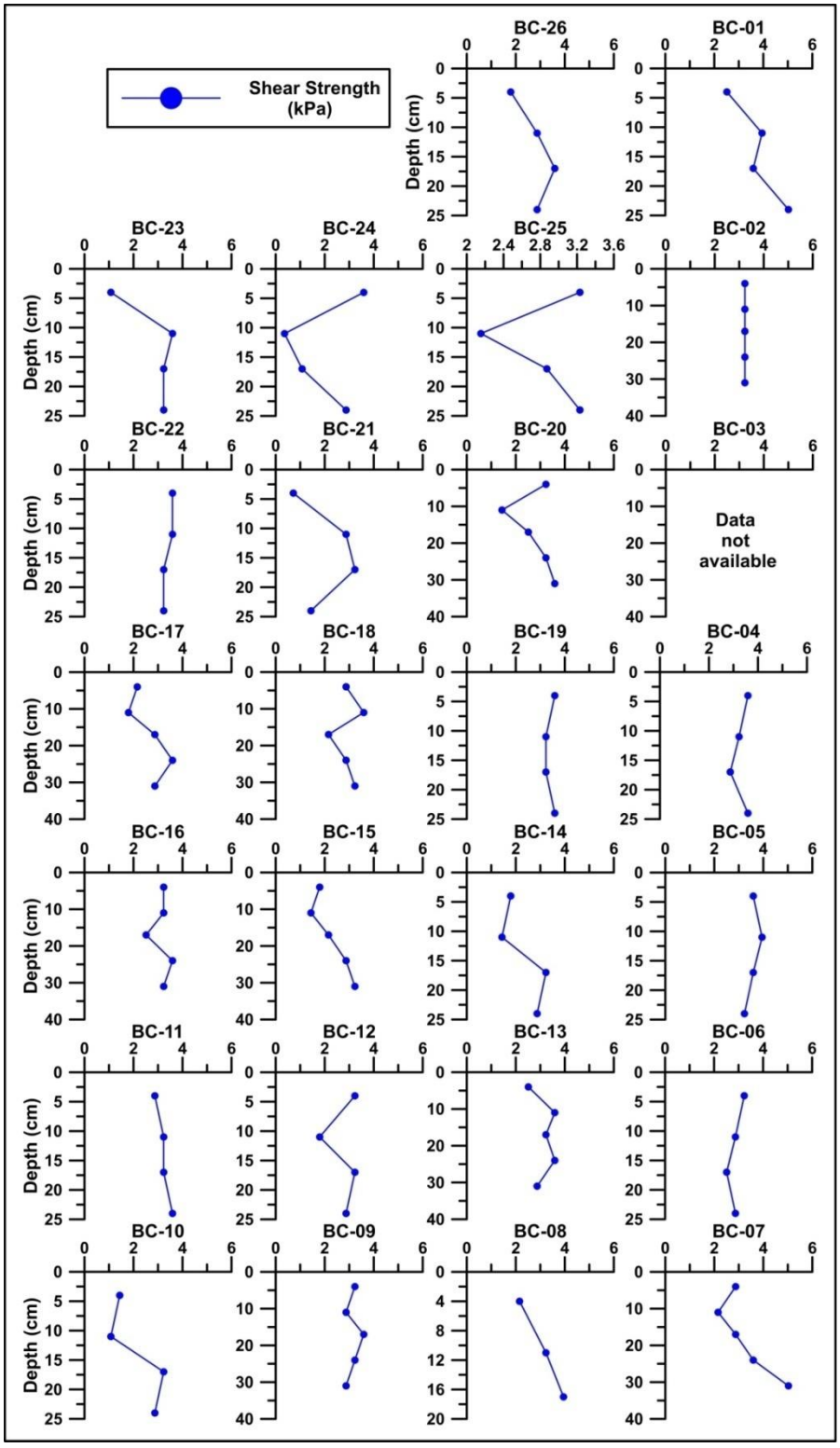

Fig. 4.5.2.2.2: Down core shear strength profiles of CIOB sediments

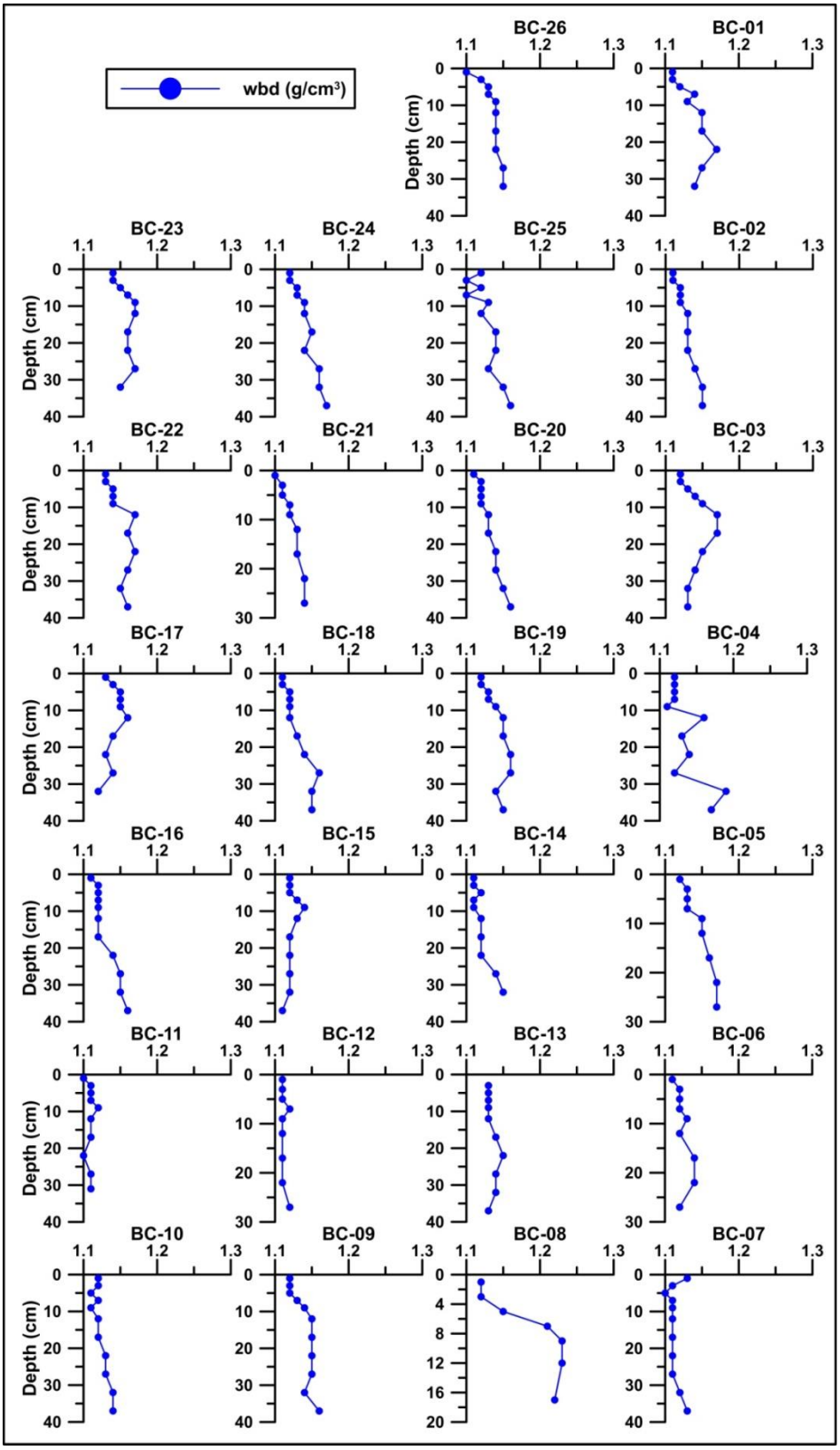

Fig. 4.5.2.2.3: Down core in wet bulk density in CIOB sediments

4.5.3Sediment properties in IRZ and PRZ

For the proposed activity of the project to conduct the nodule collector test, Impact Reference Zone (IRZ) and Preserved Reference Zone (PRZ) of 7.5 x 7.5 nm are identified within the contract area (Fig. 4.5.3.1). IRZ and PRZ areas are about 60 nm apart. During cruise # SSD 13 on board *RV Sindhu Sadhana*, sediment cores in IRZ and PRZ areas were collected for assessing the baseline conditions of sedimentary environment. For this, grain size, physical and geotechnical properties were studied (Table 4.5.3.1; Fig. 4.5.3.1). Various properties measured in these sediments would define the baseline conditions in the area and will be useful to assess the environmental impact and restoration processes after nodule collector tests. .

Table 4.5.3.1: Sampling locations in IRZ & PRZ for baseline data

S. No.	Station No.	Latitude (S)	Longitude (E)	Water depth (m)
1	BC-2/PRZ	12° 52.534'	74° 37.446'	4908
2	BC-3/PRZ	12° 52.509'	74° 45.009'	5094
3	BC-4/PRZ	12° 56.216'	74° 41.217'	5152
4	BC-5/PRZ	13° 00.003'	74° 37.494'	5055
5	BC-6/PRZ	13° 00.014'	74° 44.998'	4900
6	BC-7R/IRZ	13° 29.999'	74° 29.982'	5227
7	BC-10/IRZ	13° 37.498'	75° 29.990'	5280
8	BC-11R/IRZ	13° 37.497'	75° 37.494'	5252
9	BC-12/IRZ	13° 29.995'	75° 37.493'	5180
10	BC 13/IRZ	13° 33.743'	75° 33.743'	5187

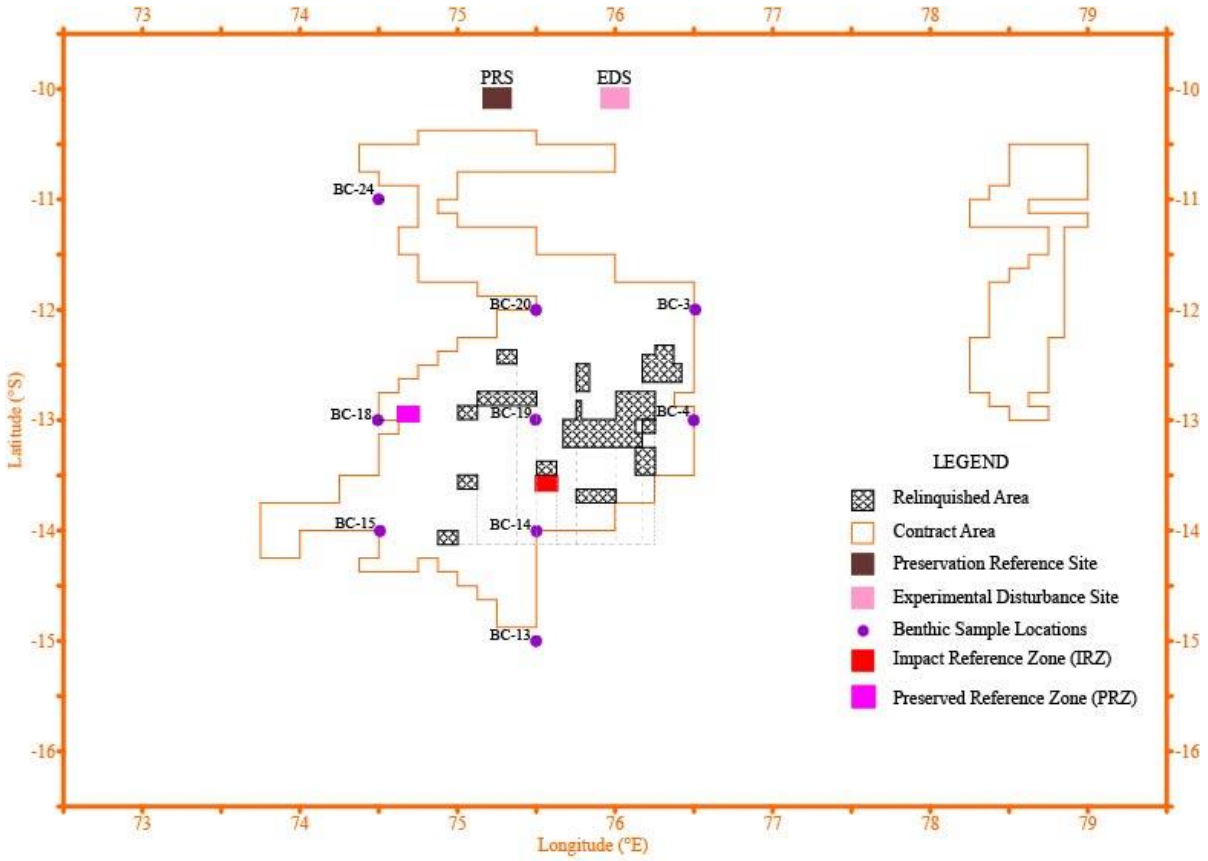

Fig. 4.5.3.1: Locations of Impact Reference Zone (IRZ) and Preserved Reference Zone (PRZ) in the CIOB.

4.5.3.1 Grain size analysis

The silt (63-4µm) and clay (<4µm) contents were measured following standard pipette analysis (Folk, 1968). Cores BC7R, BC10, BC11R, BC12 and BC13 were collected from the IRZ area (Fig. 4.5.3.1.2). Cores BC2, BC3, BC4, BC5 and BC6 were collected from the PRZ area (Fig. 4.5.3.1.1). These cores have moderate brown coloured sediments at the top followed by moderate yellowish brown to gray lenses and intercalations at the middle, and light brown sediments at the bottom. Bioturbation features are common at the middle part in most of the cores that are homogenous in nature. The core recovery varied from 34 cm to 43cm. The multibeam data shows that the IRZ has flat topography with water depth ranging from 5180m to 5280m, and the PRZ area water depth ranges between 4900m to 5152m (Fig. 4.5.3.1.1 and 4.5.3.1.2). In the PRZ sediment cores, sand varies from 7% to 25% (Fig. 4.5.3.2.1). Silt content varies from 15% to 43%, and clay from 45% to 72%. Similarly, in the IRZ sediments, sand percent varies widely from 1% to 25% (Fig. 4.5.3.2.4), silt content varies between 20% and 56% and clay from 41% to 71%. In both areas sand content varies in wide range due to changes in radiolarian fossil content.

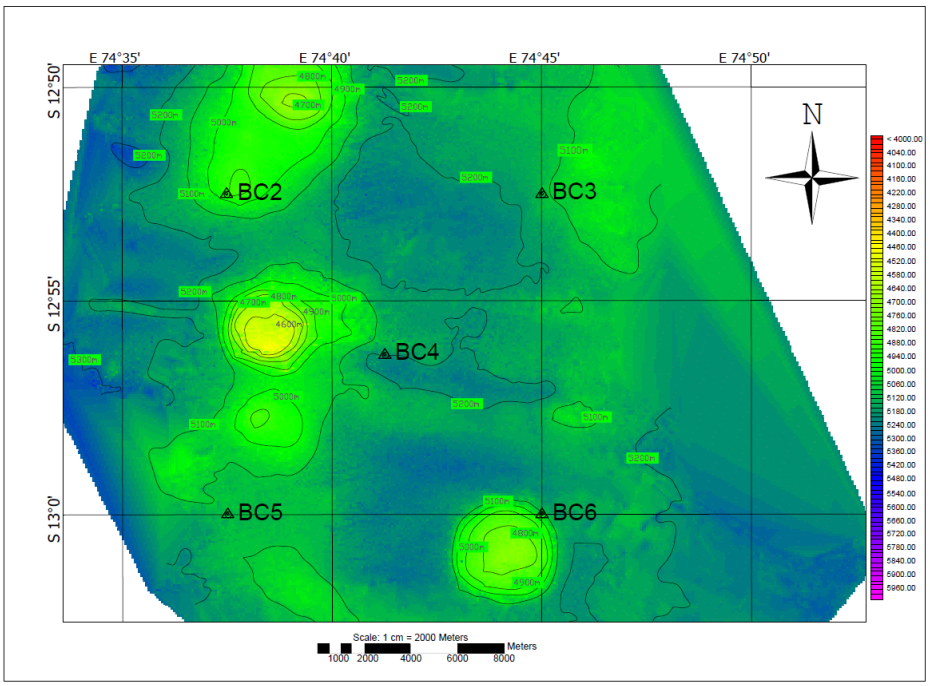

Fig. 4.5.3.1.1: Sampling stations and bathymetry in PRZ

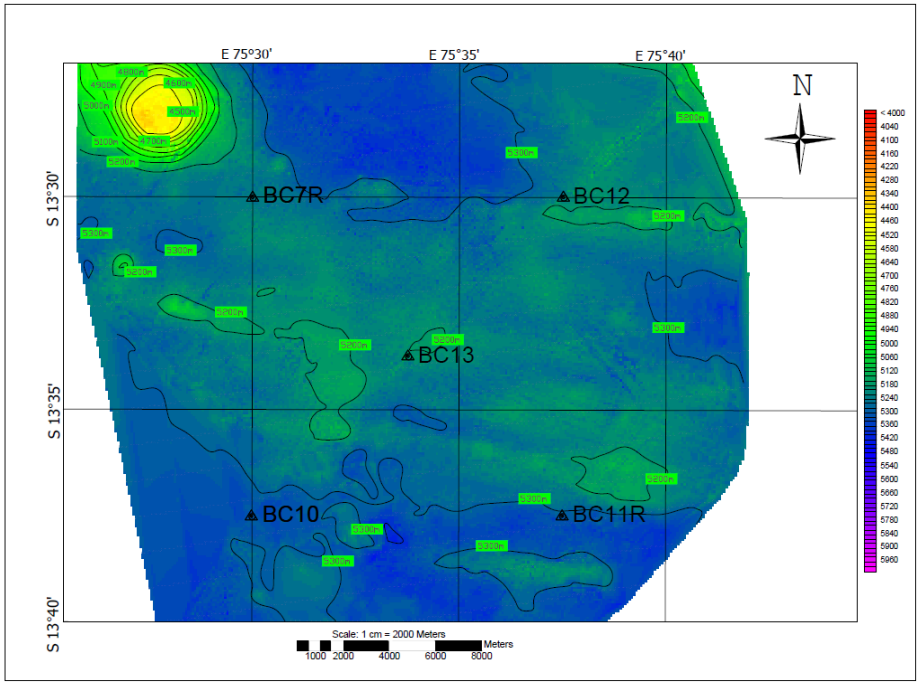

Fig. 4.5.3.1.2: Sampling locations and bathymetry in IRZ

4.5.3.2 Geotechnical properties

The water content in PRZ sediment cores variedbetween 301% and 693% (Fig. 4.5.3.2.2). Water content reduces with core depth in all cores due to compaction. Specific gravity varied from 1.65 to 2.21 (Table 4.5.3.2.1), and porosity from 86% to 93%. Wet bulk density of these sediments is in the range of 1.10g/cm^3 to 1.18g/cm^3. The high water content and high porosity is due to radiolarian fossil tests and the clay mineral smectite. The shear strength varies from 1.4kPa at the surface to 7.4kPa (Fig. 4.5.3.2.3) at the middle/bottom part of the cores.

In the IRZ, water content varies from 338% to 703% (Fig. 4.5.3.2.5). It reduces with core depth in all cores due to compaction. The specific gravity varies from 1.18 to 2.26, and porosity from 88% to 93% (Table 4.5.3.2.2). The wet bulk density of these sediments is 1.10 to 1.17 g/cm^3. These sediments are siliceous clays deposited with very low sedimentation (2mm/ka). The shear strength of these sediments varies from 0.7kPa at the surface to ~13kPa (Fig. 4.5.3.2.6) at the middle/bottom part of the cores. The shear strength increases with sediment core depth in all cores of the IRZ and PRZ.

Table 4.5.3.2.1: Range of sediment properties in PRZ

	Water Content (% dry)	**Specific gravity**	**Porosity (%)**	**Wet bulk density (g/cm^3)**	**Shear strength (kPa)**	**Sand (%)**	**Silt (%)**	**Clay (%)**
Minimum	301	1.65	86	1.1	1.43	7	15	45
Maximum	693	2.21	93	1.18	7.16	25	43	72
Average	407	1.98	90	1.13	4.34	13	30	57
Std. Dev.	79	0.14	1.7	0.02	1.15	4	5	6

Table 4.5.3.2.2: Range of sediment properties in IRZ

	Water Content (% dry)	Specific gravity	Porosity (%)	Wet bulk density (g/cm^3)	Shear strength (kPa)	Sand (%)	Silt (%)	Clay (%)
Minimum	338	1.8	88	1.1	0.716	1	15	42
Maximum	703	2.26	93	1.17	12.88	25	57	72
Average	473	2	90	1.13	5.23	12	31	57
Std. Dev.	75	0.11	1.4	0.02	3.18	4	6	6

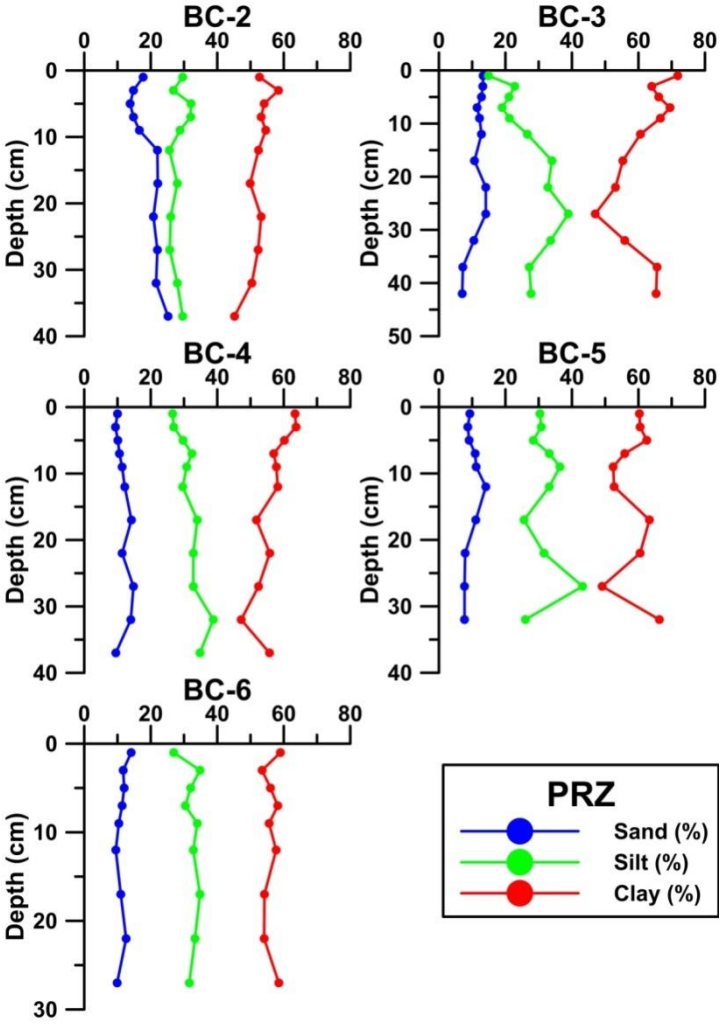

Fig. 4.5.3.2.1: Downcore variation in grain size in PRZ area

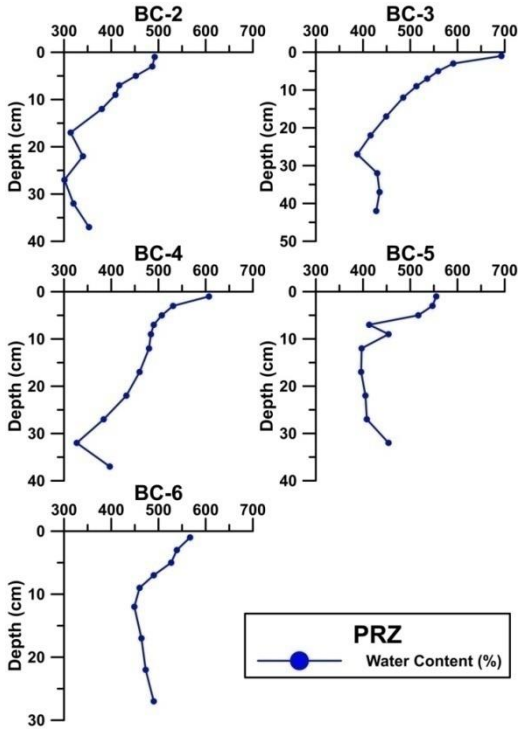

Fig. 4.5.3.2.2: Downcore variation of water content in the PRZ area

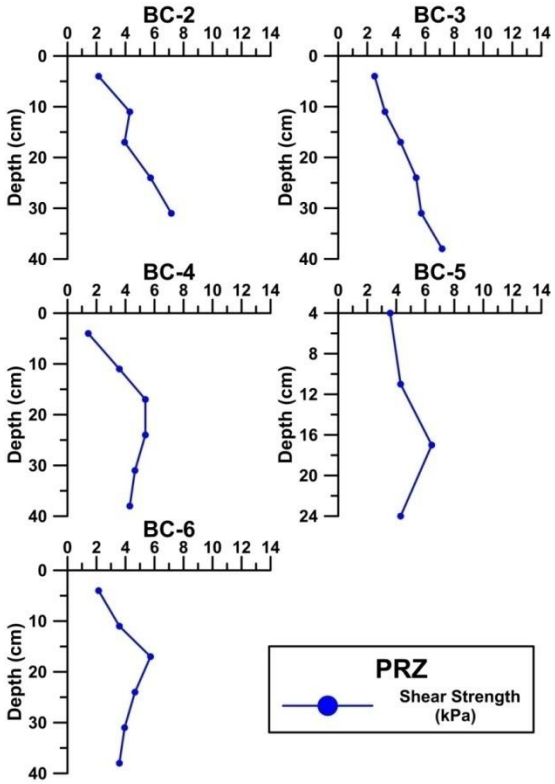

Fig. 4.5.3.2.3: Downcore variation in sediment shear strength from the PRZ area

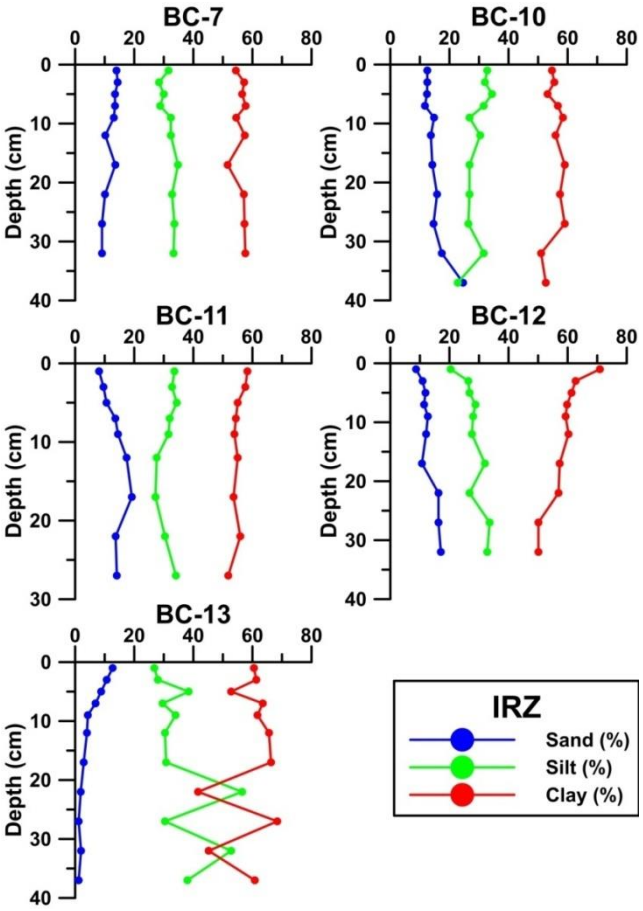

Fig. 4.5.3.2.4: Downcore variation in grain size distribution in sediments from the IRZ area

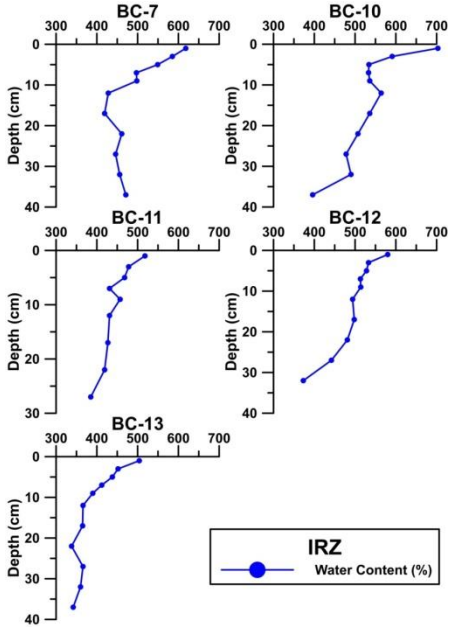

Fig. 4.5.3.2.5: Downcore variation of water content (% dry basis) in the IRZ area

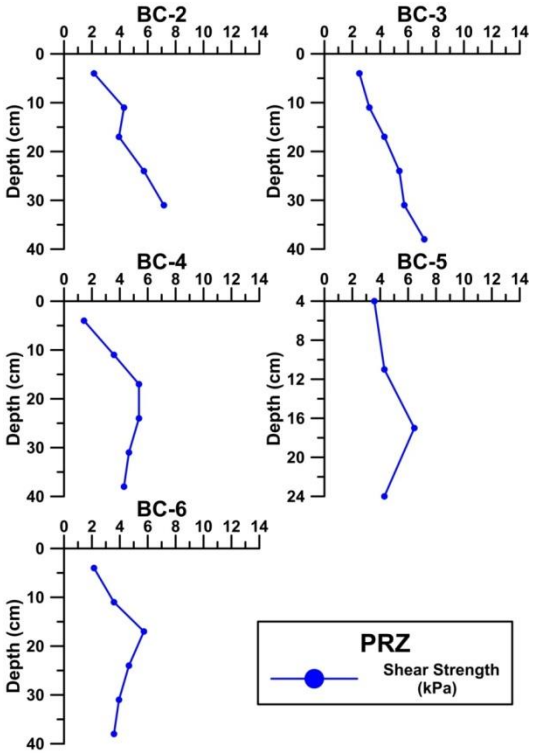

Fig. 4.5.3.2.6: Downcore variation in sediment shear strength from IRZ area

The study showed that the predominant texture of both PRZ and IRZ sediments are silty clays. They have high sand content (1%-25%) with low deviation with core depth. Silt content varies from 15% to 56%; and clay from 41% to 72%. The baseline data in IRZ and PRZ showed that the sediments in both areas have high water content with wide variation with core depth (301% to 703%). The shear strength of these sediments also varies widely (0.7kPa to 13kPa), and increases with core depth due to compaction. All parameters in IRZ and PRZ show similar trend with sediment depth.

4.6 Chemical properties of seabed sediments

In view of the role of organic matter diagenesis, through microbial and chemical processes, in controling the benthic biogeochemistry and the benthic ecosystem characteristics, geochemical parameters governing these processes were studied. Organic carbon reaches the seafloor through settling, it may either undergo degradation, through a sequence of reactions involving series of porewater oxidants (in the order of O_2, NO_3, NO_2, Mn oxide, Fe oxide, sulfate and so on), or may become buried. Since the sediment depth is a measure of time since deposition, sequence of organic carbon remineralization pathways create clear vertical gradients of both oxidants and products of the degradation process and is reflected in the porewater profiles. The porewater profiles can also be affected by the benthic burrowing and

bioturbation. As the benthic infauna burrows its way into sediments, solute exchange between the seawater and the porewater may take place because of irrigation effect. Most of these early diagenetic reactions associated with porewater diffusion and carbon mineralization takes place in top few tens of cms. It is with such a presumption that any disturbance by way of nodule mining would alter the existing depositional, decompositional biota sediment chemical relations, studies on a) porewater nutrients, and b) C, N and elemental variation in associated sediments were undertaken in all the phases of Indian program of Environmental studies for nodule mining. A regional study was undertaken mainly to create an environmental database for entire Indian Pioneer area by sampling in a systematic 1 degree by 1-degree grid pattern. Further, to study the downcore variation and lateral variation of benthic biogeochemistry and sediment dispersal patterns, sediments and porewaters from an area between 10° S to 16° S and from 73.5° to 75.5° E were sampled, with an overall goal of providing baseline data and to assess the natural benthic biogeochemical set-up and the dispersal pattern of fine-grained sediments. Porewater were studied for nitrite, phosphate and silicate and the solid phase was studied for elemental chemistry.

4.6.1 Regional porewater chemistry

The box cores of dimension 50 x 50 x 50 cm were used for retrieving sediment cores. PVC liners were inserted into the box core for sub-sampling for each discipline. Soon after the PVC liners were transferred to onboard laboratory, the first cores sub sampled were for Porewater Geochemistry and Microbiology/Biochemistry disciplines. The sub-sampling was carried out at 2 cm interval until 10 cm and 5 cm interval from 10 to 20 cm depth. Sediments were carefully transferred to the centrifuge tubes and were centrifuged at about 5000 rpm in a refrigerated centrifuge at about 2° C in order avoiding the effect of heating on porewater parameters. The supernatant water was siphoned off to the thoroughly cleaned plastic bottles. At the end of the separation, the porewaters were filtered with a Millipore filtration unit through 0.42 microns membrane filters. Immediately after filtration, pH was measured. The measurement of pH was possible only during the second phase of the cruise due to the non-functioning of pH meter during the first phase of cruise. Both the sub-sets were stored in the refrigerator/deep-freezer. The porewaters were analyzed for nutrients nitrite, phosphate and silicate, either on the same day or on the next day after extraction of porewaters. In addition, ammonia was measured in the porewaters in selected cores. The analytical methods used here for analyzing the porewater are adopted from the standard seawater analyses (Grasshoff et al., 1983)

4.6.1.1 Silica

Porewater silica concentrations in all the cores except two cores in the east and one in the south, are higher than the bottom water values of 130 µM reaching a maximum value of ~560 600 µM (Fig. 4.6.1.1.1). When the porewater silica concentrations in the surficial sediments are considered (0-2 cm), a distinct trend of high values in the northern (10° to 12°S) and central western (between 12° and 13°S latitudes and 73° and 75° E longitudes) areas of the study area (Fig. 4.6.1.1.2) is noticed. Distributional trend of surficial porewater contents is consistent with the benthic biomass distribution of the area. While the porewater silica reflects both the influence of biogenic productivity in the water column (diatom and radiolarian fluxes), and the dissolution of biogenic silica, benthic biomass is indicative of benthic ecosystem response to the settling organic matter fluxes. This suggests that the porewater silica is reflecting the benthic-pelagic coupling. Among the southern areas, porewater concentrations are distinctly lower probably because the influence of ITCZ related productivity influence is more dominant in northern latitudes. High silica values are due to the dissolution of biogenic silica, which is an abundant sediment component in this region. In some oceanic areas of high biological productivity, porewater silica profiles have local minima due to the pumping activity of benthic organisms and that could be the reason for surface highs in some stations.

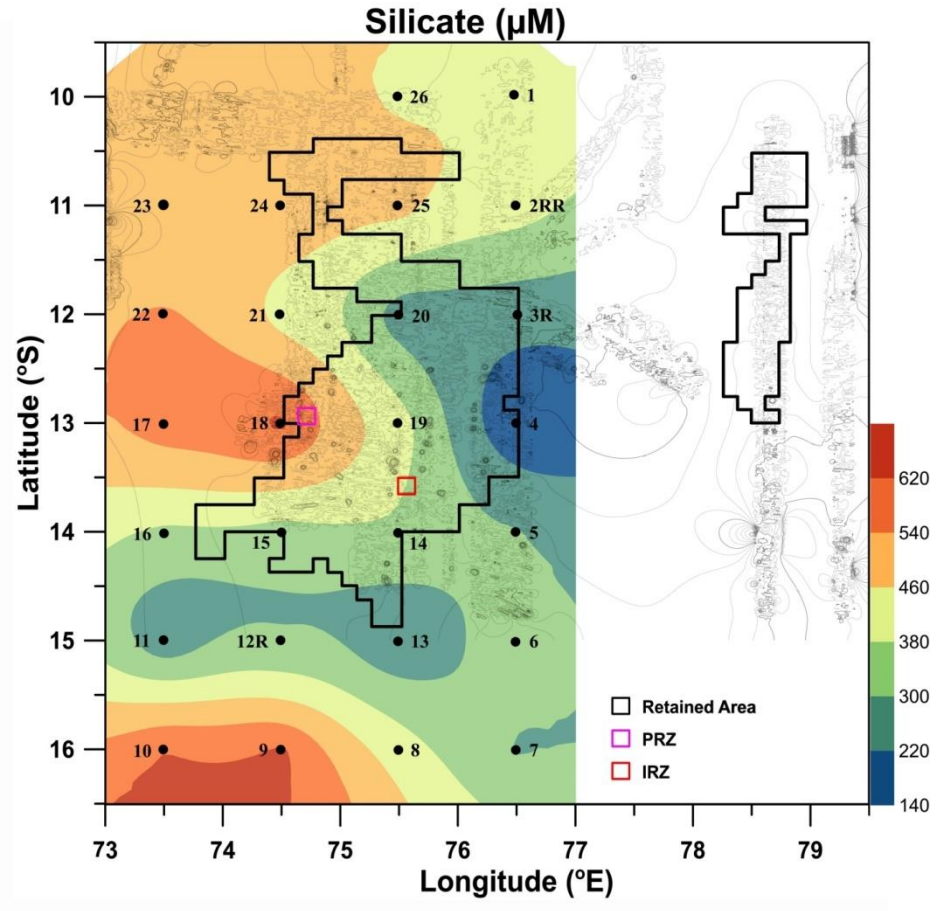

Fig. 4.6.1.1.1: Distribution of porewater silicate (µM) in surface sediments of CIOB.

Several cores show an increase with depth. Porewater silica values, considered for all the cases range from a maximum of 140 µM to a maximum of 600 µM, with intracore variation remaining in the range of 200 to 250 µM. Consistently high silica values (although less than the supersaturation limits of amorphous silica) and gradual decrease in silica values towards sediment water interface could indicate that the Central Indian Basin sediments are a substantial source of dissolved silica to the Indian Ocean. In general, the slopes in silica values are gradual. However, in some cores, change in profile is more prominent close to the surface and indicates that most biogenic silica dissolves integrally within the sediments, and not exclusively at the sediment-water interface. Bottom water instability may be controlling the opal dissolution and high silica values in this region. Rarely, these cores display asymptotic values in the depths considered (maximum 20 cm) indicating that the asymptotic values might be at deeper depths (>20 cm). Earlier work in this area has shown that the asymptotic values occur at depths of 20 to 25 cms (Nath and Mudholkar., 1989).

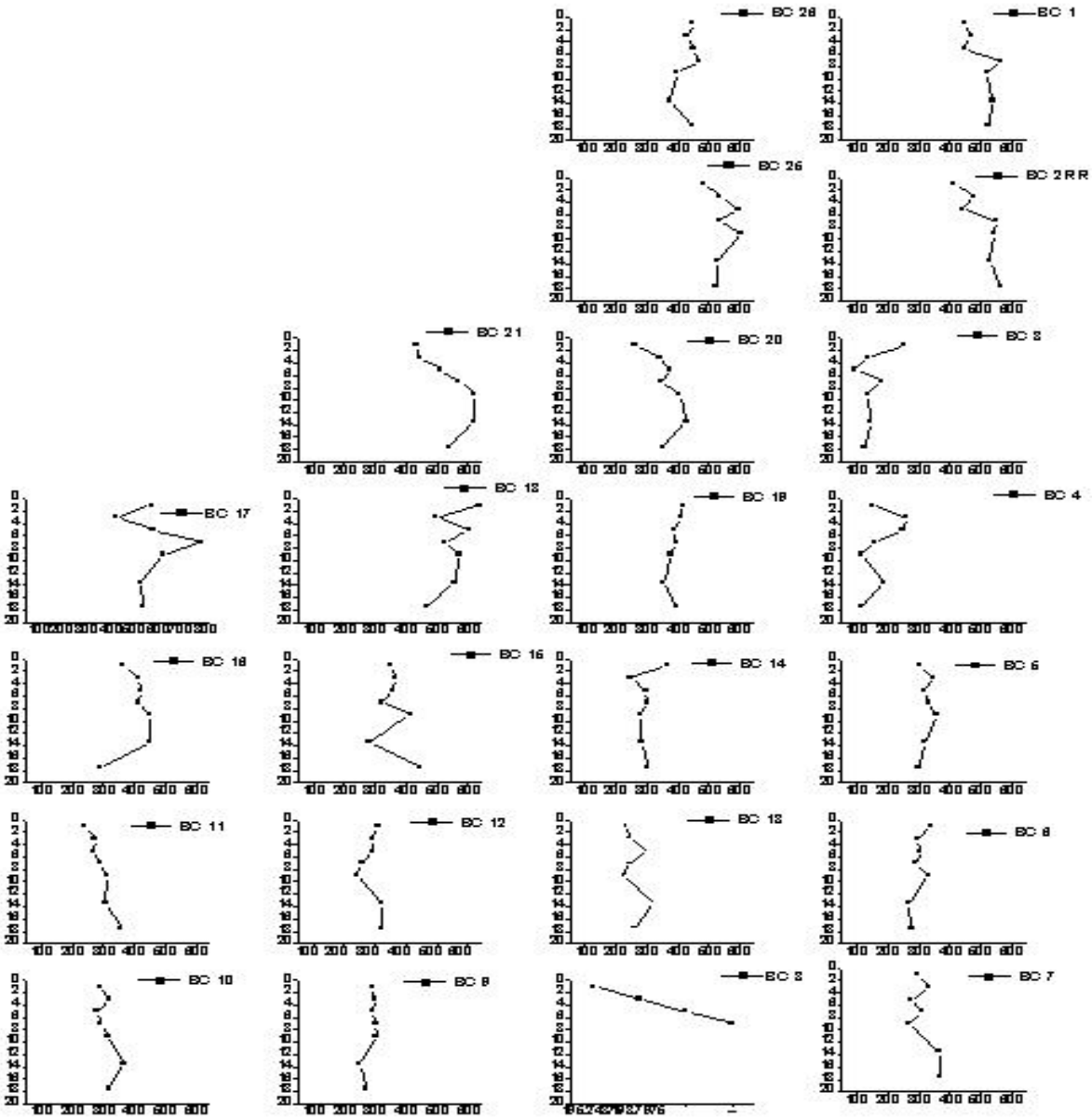

Fig. 4.6.1.1.2: Downcore distribution of porewater silicate (µM) in CIOB sediments

4.6.1.2 Phosphate

The porewater phosphate concentrations mostly hover between 1.5 and 2.5 µM. Compared to overlying water (between 0.7 and 1.5 µM), the porewater concentrations are higher (Fig. 4.6.1.2.1). Two stations in the eastern areas (BC 4 and 5) show low values (~0.5 µM) and correspond with lower silica and higher nitrite values. Higher porewater P contents in the surficial layers compared to the bottom water and lower values than the deeper sediment layers suggest phosphate fluxes out of sediment. Oxygen is considered often as to have an important regulatory effect on benthic phosphate fluxes. Since there is no significant variations in the bottom oxygen contents for the areas considered (Warren, 1982), area to area differences are minimal. The phosphate flux out of a sediment depends on the balance between the rate of phosphate production in the porewater during regeneration of organic matter and destruction of other carrier phases, and the sum rate of removal reactions in the sediment e.g., adsorption. Release of P adsorbed on Fe sites within the sediments may lead to their diffusion and mobility (Nath and Mudholkar, 1989). Lower values on the eastern area with rugged topography suggest an influence of bottom topography on the benthic biogeochemistry.

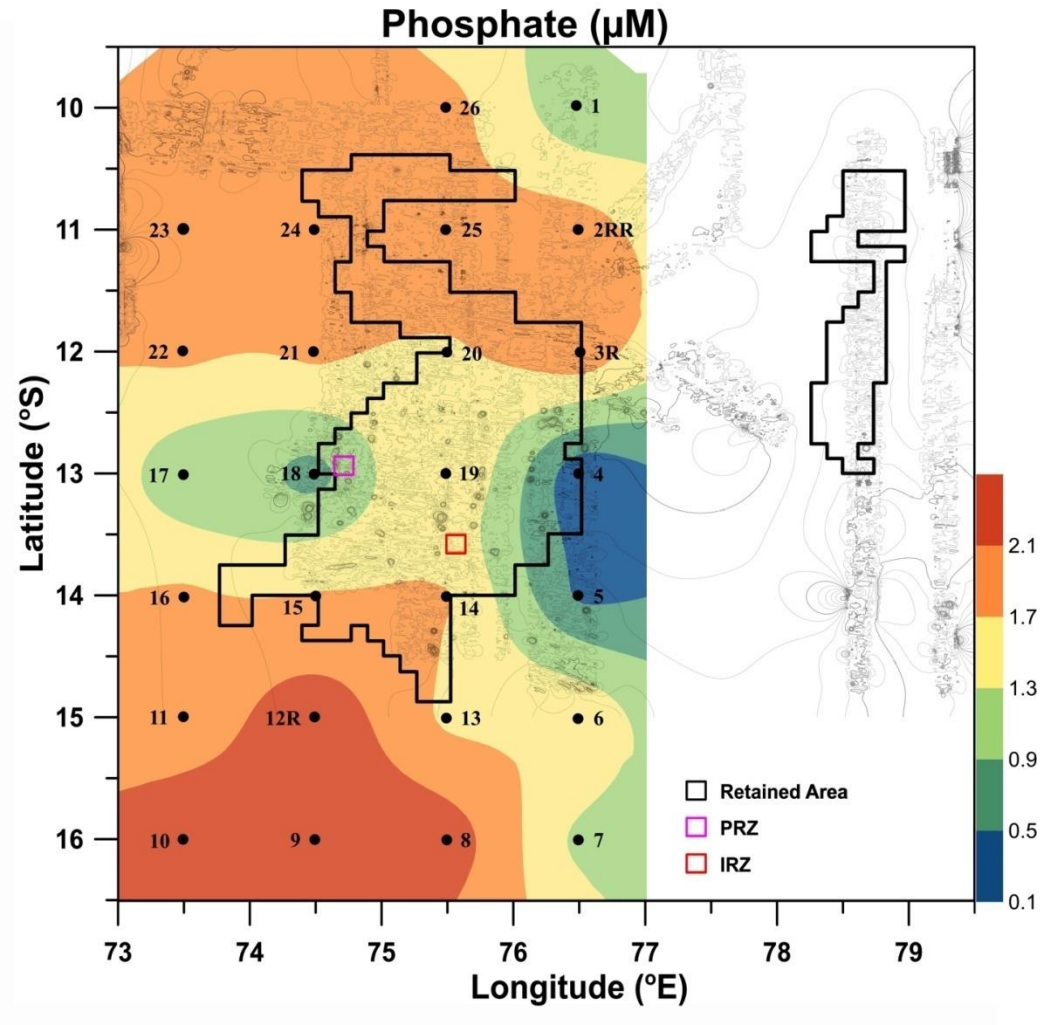

Fig. 4.6.1.2.1: Distribution of porewater phosphate (µM) in surface sediments of CIOB.

The porewater phosphate values measured in the investigated area (Fig.4.6.1.2.2) were of similar magnitude reported earlier for the CIOB (Nath and Mudholkar, 1989) but very low compared to continental margin sediments of the northern Indian Ocean (Linsy et al., 2018). The downcore gradient of phosphate concentrations in the porewater of the CIOB sediments can be attributed to the mobilization of iron oxyhydroxides. The relatively low values and constant depth profiles of porewater DIP in most of the stations indicate that the diagenetic remobilization of phosphate is currently not taking place actively in the study area. The low influx of C_{org} and highest adsorption of P by fine-grained particles hinder the remobilization of phosphate in the sediments of the CIOB and making them a sink of phosphate from the water column (Linsy et al., 2018).

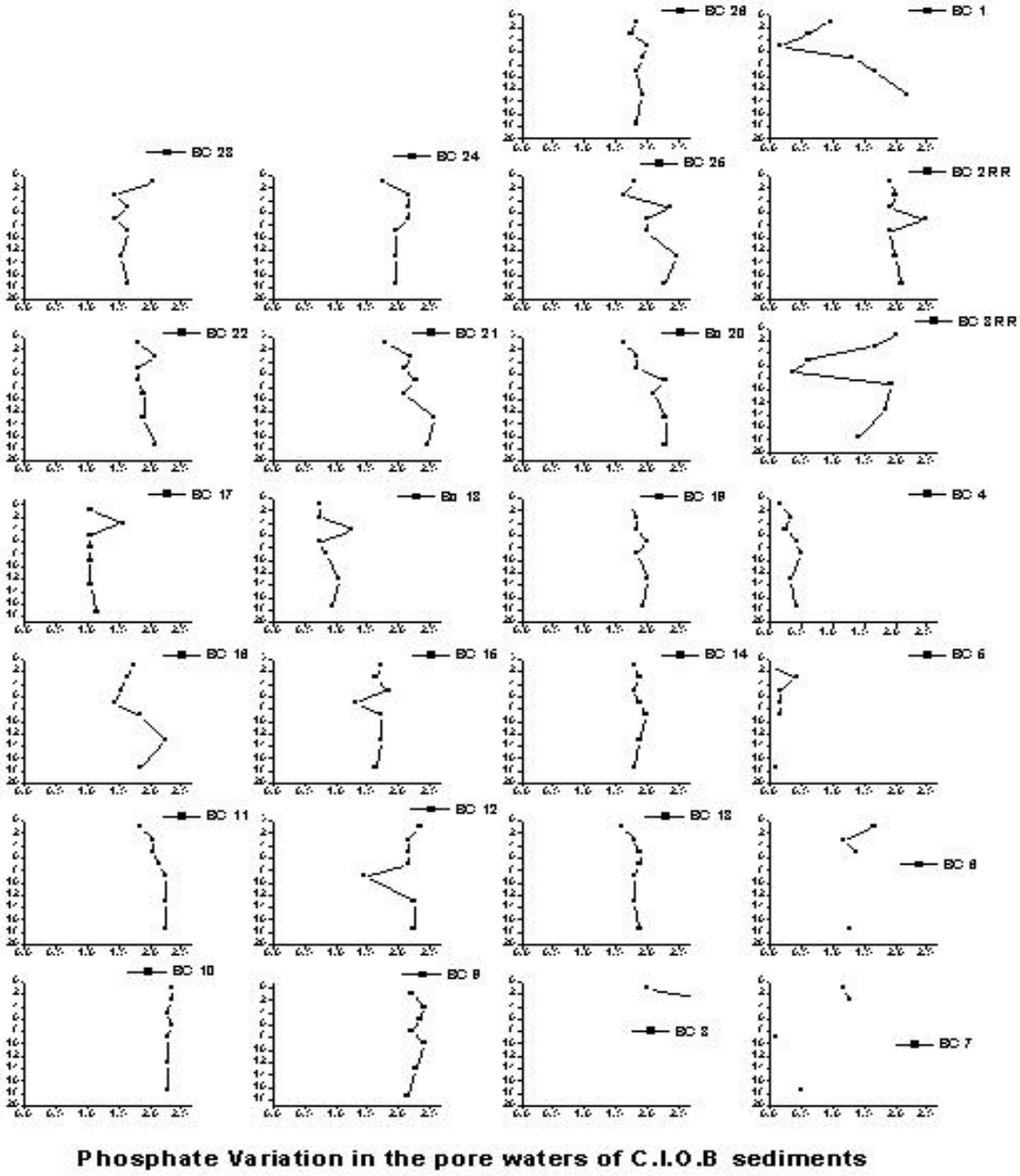

Fig. 4.6.1.2.2: Downcore distribution of porewater phosphate (µM) in CIOB sediments

4.6.1.3 Nitrite

Nitrite concentrations are generally low, rarely exceeding 1 µM (Fig. 4.6.1.3.1). Relatively, higher values are noticed only in one station (BC 22 in the west) and moderately high in one station in north (BC 26) and two stations in the east (BC 3 and 5). In remaining stations, values less than 0.7 µM are noticed in the surficial sediments (0-2 cm; Fig. 4.6.1.3.1). Nitrite increase in either seawater or porewater usually indicates either the oxidiation of ammonia and/or reduction of nitrate (Nath and Mudholkar, 1989 and references therein).

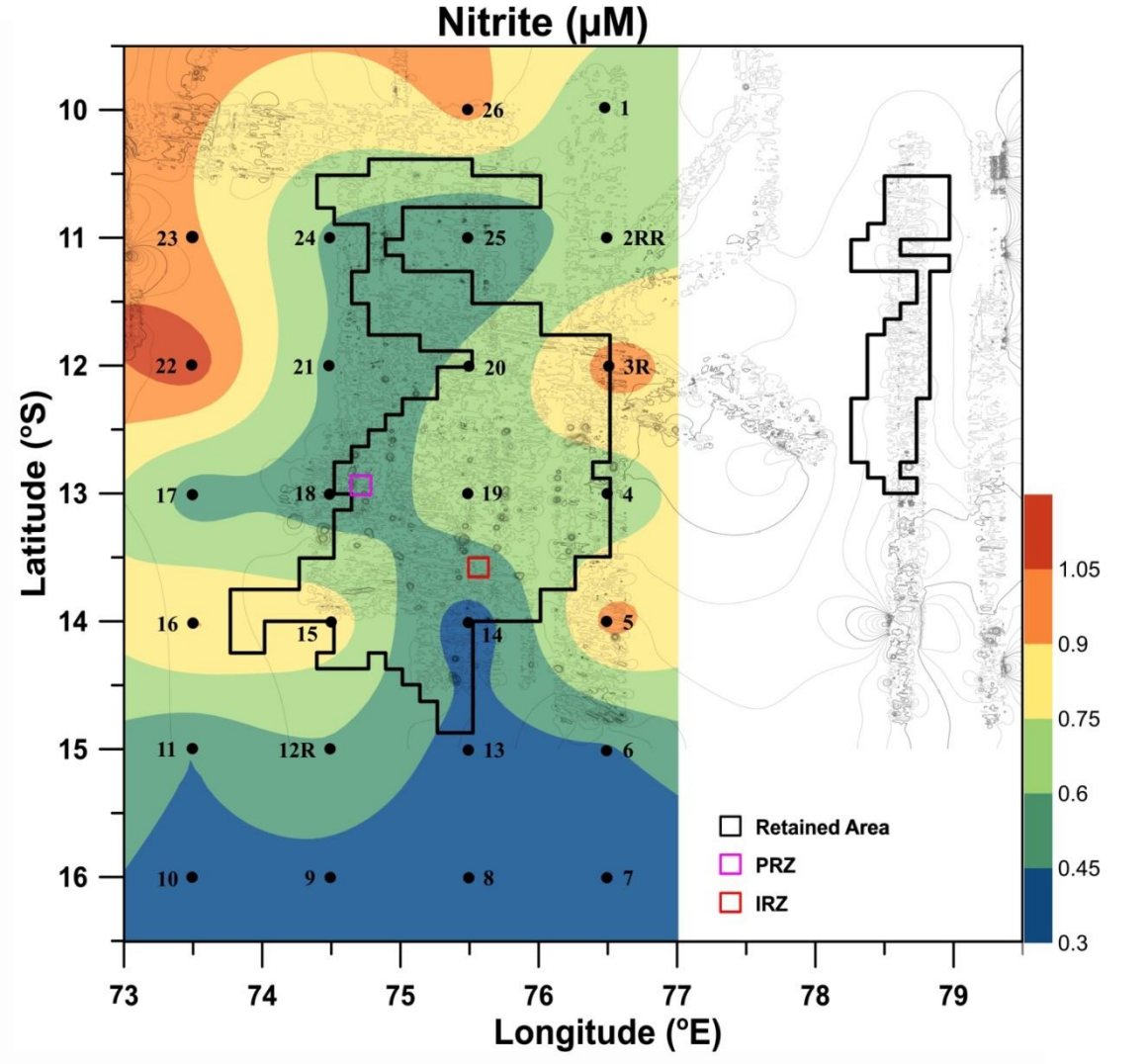

Fig. 4.6.1.3.1: Distribution of porewater nitrite (µM) in surface sediments of CIOB.

Downcore profiles at several stations show intermediate high values which is characteristic of Central Indian Basin, attributed to benthic burrowing, suboxic diagenesis and organic carbon mobility and the resultant micro-reducing zones within the sediments. Light green mottles are seen when the sediments are freshly recovered which turn into brown soon after coming in

contact with atmospheric oxygen. High nitrite values in subsurface depths of some cores might correspond to nitrate reductions or ammonia oxidation (Fig. 4.6.1.3.2).

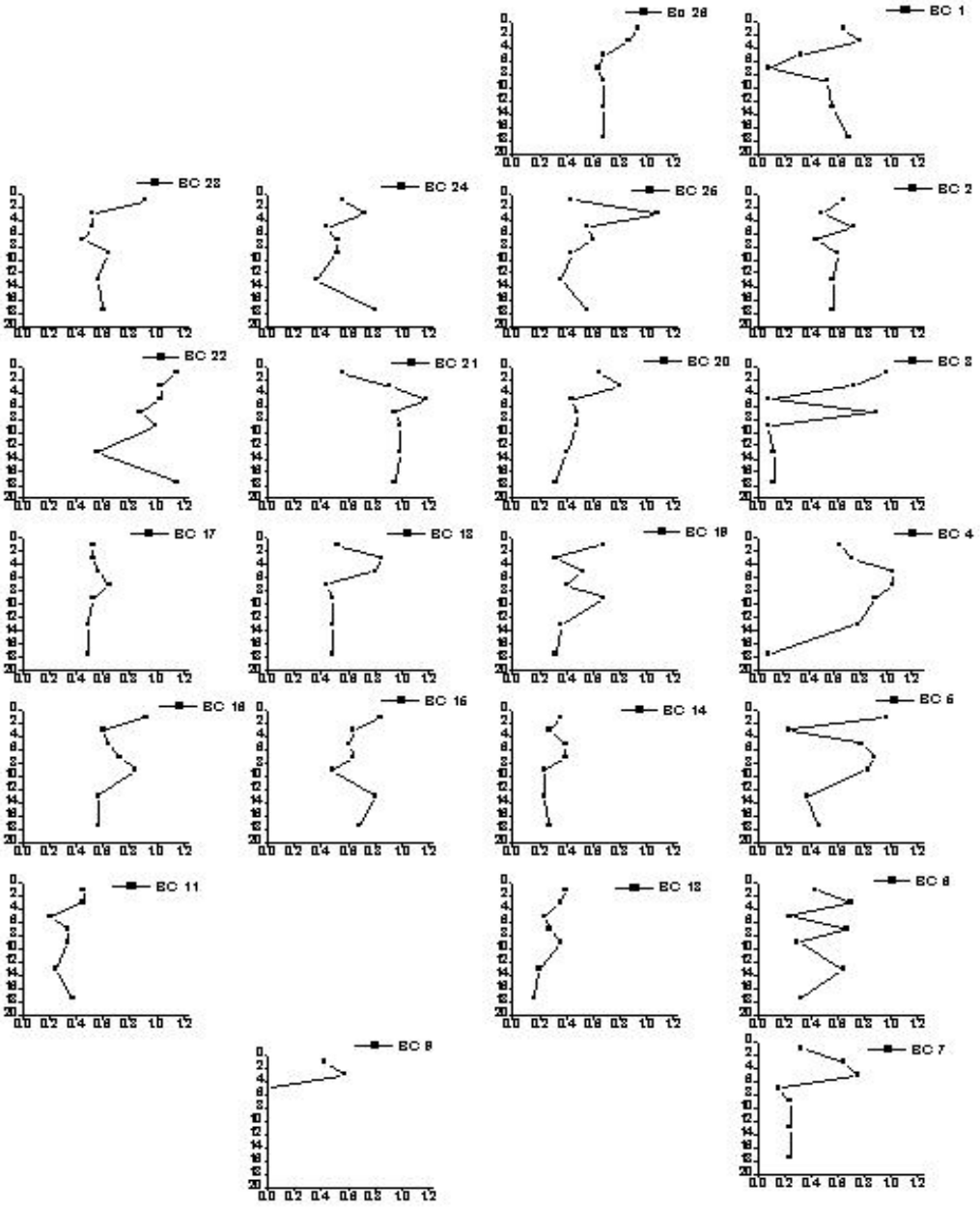

Fig. 4.6.1.3.2: Downcore distribution of porewater nitrite (µM) in CIOB sediments

4.6.2 Solid phase phemistry

4.6.2.1 Organic carbon

Sedimentary organic carbon values are less than 0.57% (Fig. 4.6.2.1.1) in all the cores studied here. When the surficial values are concerned, three patches of low values are seen in the northwestern, southwestern and southeastern corners. Low values are seen in the vicinity of large seamounts in the south. The variability in surface is relatively large in the south.

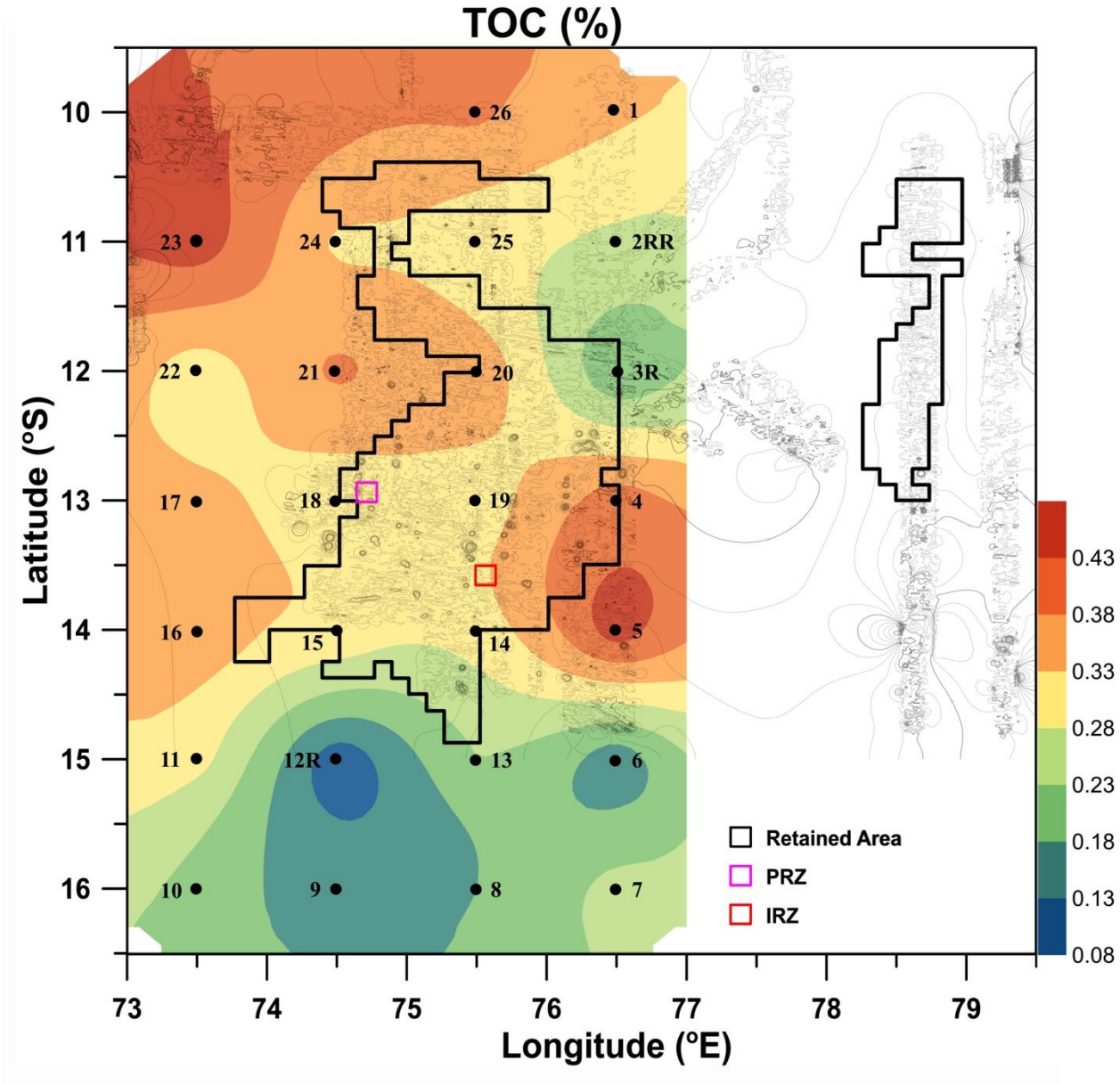

Fig. 4.6.2.1.1: Distribution of organic carbon (%) in surface sediments of CIOB.

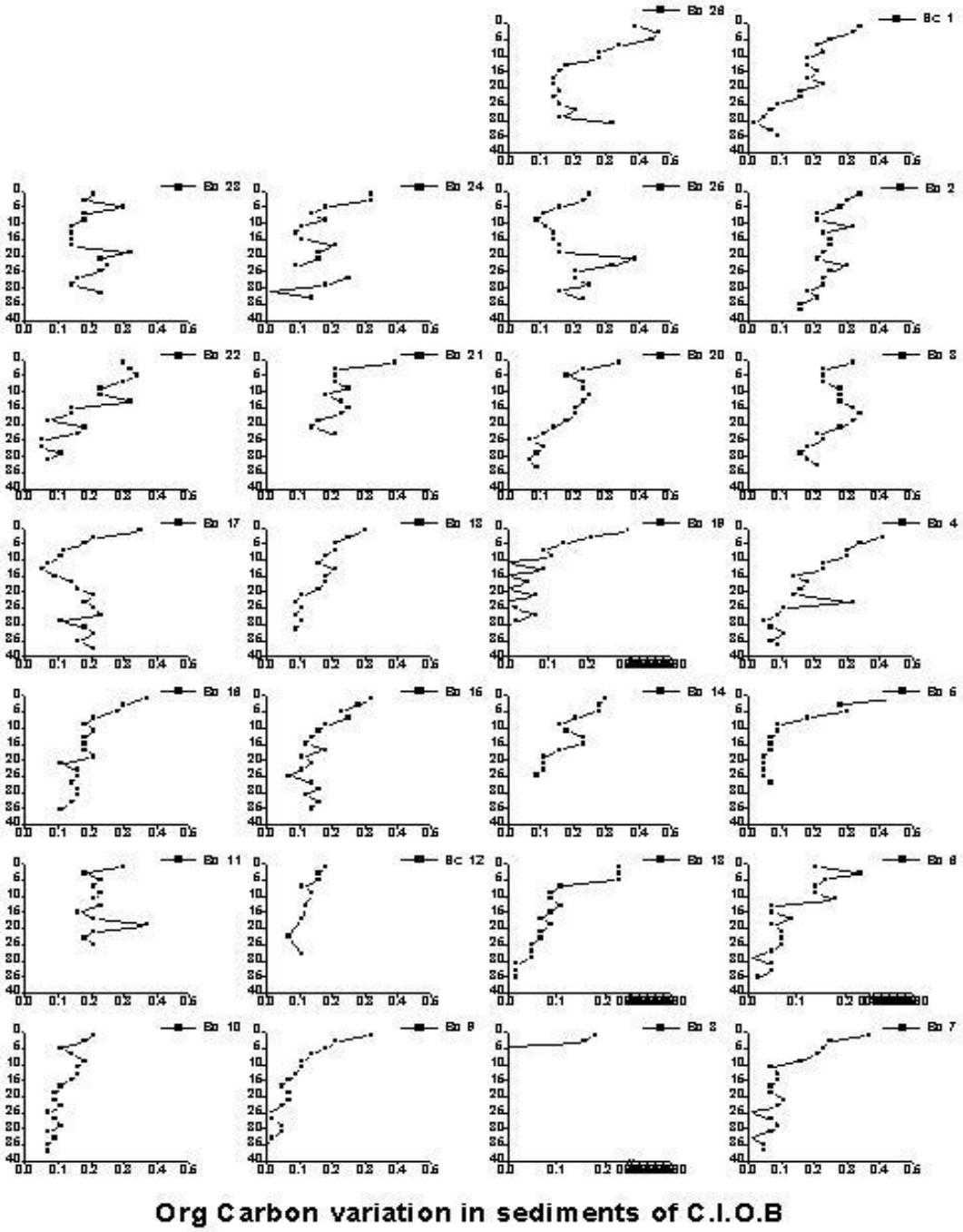

Fig. 4.6.2.1.2: Downcore variation of organic carbon (%) in CIOB sediments

In most of the cores, a surface enrichment is seen with a change in gradient at about 5 to 8 cms (Fig. 4.6.2.1.2). The gradient is relatively smooth in the surface 8 cms in some of the cores. Relatively smoother profiles in the surficial layers are seen in some cores, which probably may indicate mixing depth. When the downcore profiles are observed, subsurface

peaks are seen more in the northern areas compared to the southern areas. When downcore profiles of all the cores are plotted, there seems to be a regional trend of subsurface enrichment, which must be driven by lateral advection of porewaters in the intermediate depths. Like the different water masses in the oceans, stratification of porewater chemistry is possible. In addition to diffusion driven vertical transport of pore fluids, lateral movement in the subsurface depths is a possibility. More or less, a color change from sediments with dark yellowish brown homogenous nature underlain by sediments with intercalations and mottling indicating the influence of bioturbation and mixing features is seen in all the cores. This color change would probably limit the base of enriched organic C and may act as a boundary between preservation and decomposition and also probably due to the influence of surface and subsurface feeding by infauna and bioturbation activity (e.g. Nath and Mudholkar, 1989). Intermediate lows could also indicate the change in community structure with varying ratios in population of surface and suspension feeders to the burrowing organisms.

4.6.2.2 Sources and natural dispersal patterns of sediments

4.6.2.2.1 Terrigenous contribution to the sediment

In order to trace the dispersal of terrigenous material in the study area regional distributional plots of elements such as Al, Zr, Nb, Rb and Ti (Figs. 4.6.2.2.1.1, 4.6.2.2.1.2, 4.6.2.2.1.3, 4.6.2.2.1.4 and 4.6.2.2.1.5 respectively) contents which are refractory in nature were plotted. Al, Zr and Ti (Figs. 4.6.2.2.1.1, 4.6.2.2.1.2, 4.6.2.2.1.5), in marine sediments are primarily derived from aluminosilicate minerals from terrigenous sources. Zirconium (Zr) is another lithogenic element resistant to weathering and alteration processes. Zircons derived from Himalayan Rivers were also reported in turbiditic sediments in the northern part of basin. Therefore, zirconium would trace the resistant terrigenous material transported from north.

The elemental distribution plots show a similar trend in the study area with higher content in the northern and southern part of the basin (Figs 4.6.2.2.1.1, 4.6.2.2.1.2 and4.6.2.2.1.5). The similarity in the distributional patterns of these elements indicates a common source of derivation. Al content in the study area ranges from 4.18 to 7.31% (avg 5.43%); Zr content ranges from 99 to 409 ppm with an average of 142 ppm, while Ti content ranges from 0.19 to 0.43% (avg 0.23%). Rubidium content in the sediments showed an average value of 60 ppm. Zr, Nb and Ti contents show high concentration in the southern part of the study area (BC 8) where volcanic and hydrothermal alteration of sediments has been reported compared to the other sediments in the area (Figs. 4.6.2.2.1.2, 4.6.2.2.1.3 and 4.6.2.2.1.5). The lowest concentration of Nb (4.59 ppm) and Ti (0.21%) are found in central part of the study area,

which is underlain by siliceous ooze. The high content of these detrital elements in the north of the basin (north of 13°S supports the major detrital input to northern part of the CIOB. Earlier studies have reported terrigenous influence to the CIOB sediments north of 3°S indicated by the dominance of detrital clays. Some researchers have argued that the sediments derived from the Himalaya could reach south of Bengal Fan by the turbidity currents. Further, based on robust sediment mineralogical, surface sediment geochemical data and shale normalized REE pattern indicated the extent of terrigenous sedimentation in CIOB (Nath et al., 1989, 1992).

Rb gets accumulated into clay minerals and therefore its distributional pattern in marine environment could be used as an indicator of transportation pathways of fine–grained fraction of sediments along the bottom. Mechanical sorting of minerals that have tendency to get concentrated in finer fraction (eg. biotite) during transport greatly increases Rb/Sr ratio of clays relative to source rock but Rb may be leached from biotite during weathering, sediment reworking or exchange with saline solutions. Rb content (85 ppm) in the sediments is found to be highest in the northern area (BC–1) and decreases towards the west of the basin which reflects the pathway of terrigenous input to the basin, while relatively low concentration found in the southern part of the area (BC–8) may reflect local weathering of basinal rocks.

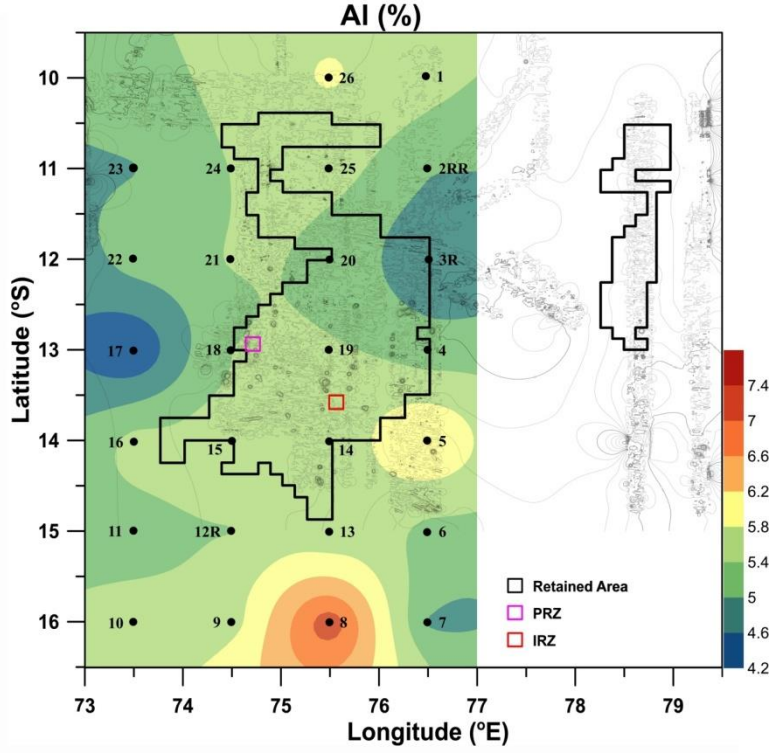

Fig. 4.6.2.2.1.1: Distribution of Al (%) in surface sediments of CIOB

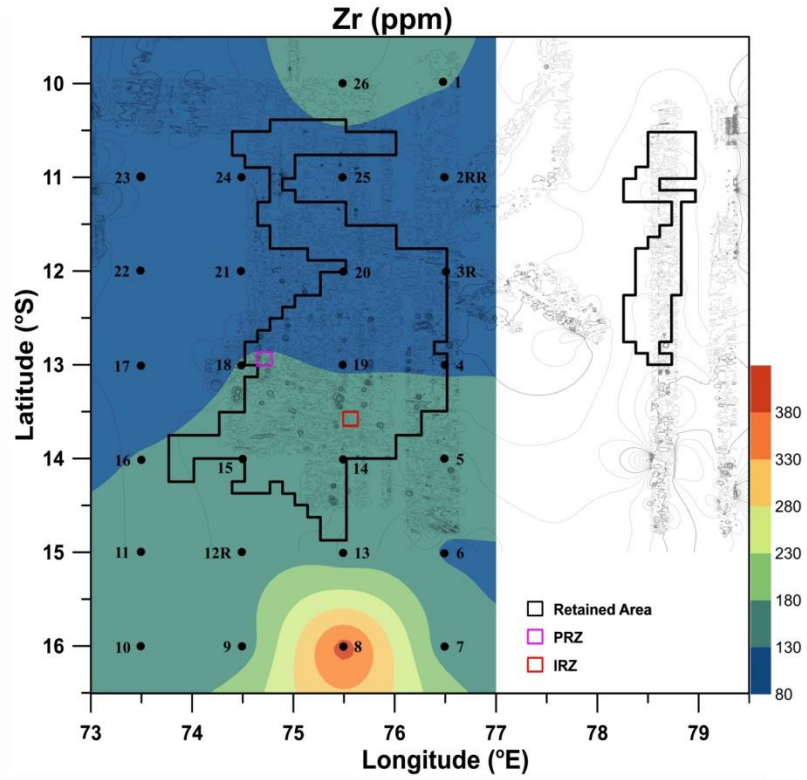

Fig. 4.6.2.2.1.2: Distribution of Zr (ppm) in surface sediments of CIOB

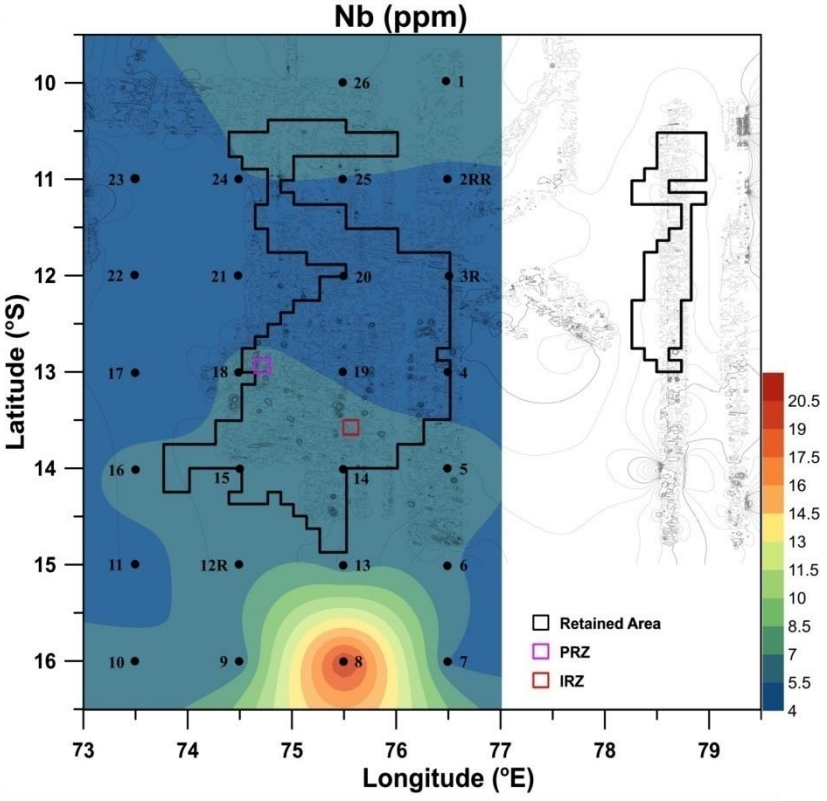

Fig. 4.6.2.2.1.3: Distribution of Nb (ppm) in surface sediments of CIOB

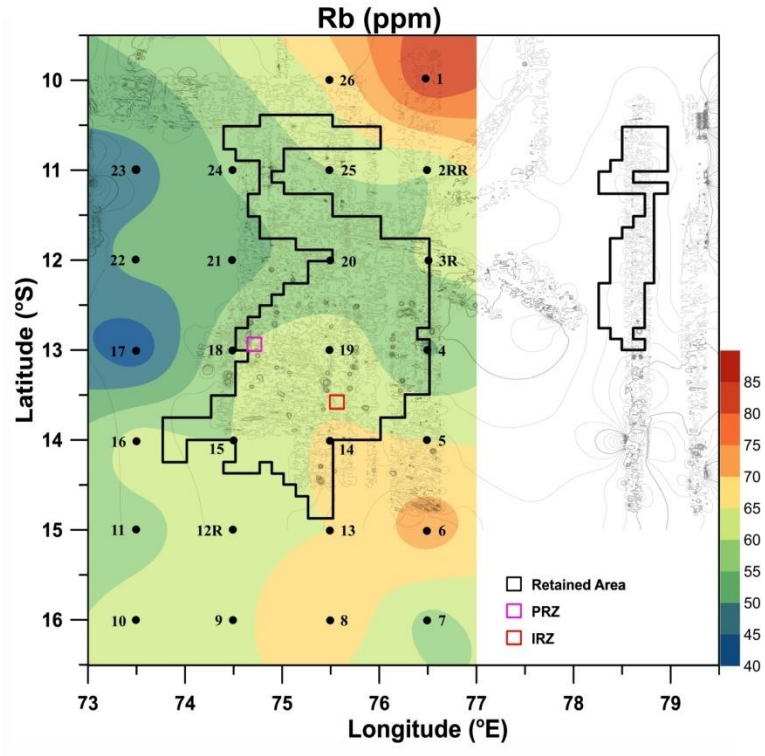

Fig. 4.6.2.2.1.4: Distribution of Rb (ppm) in surface sediments of CIOB

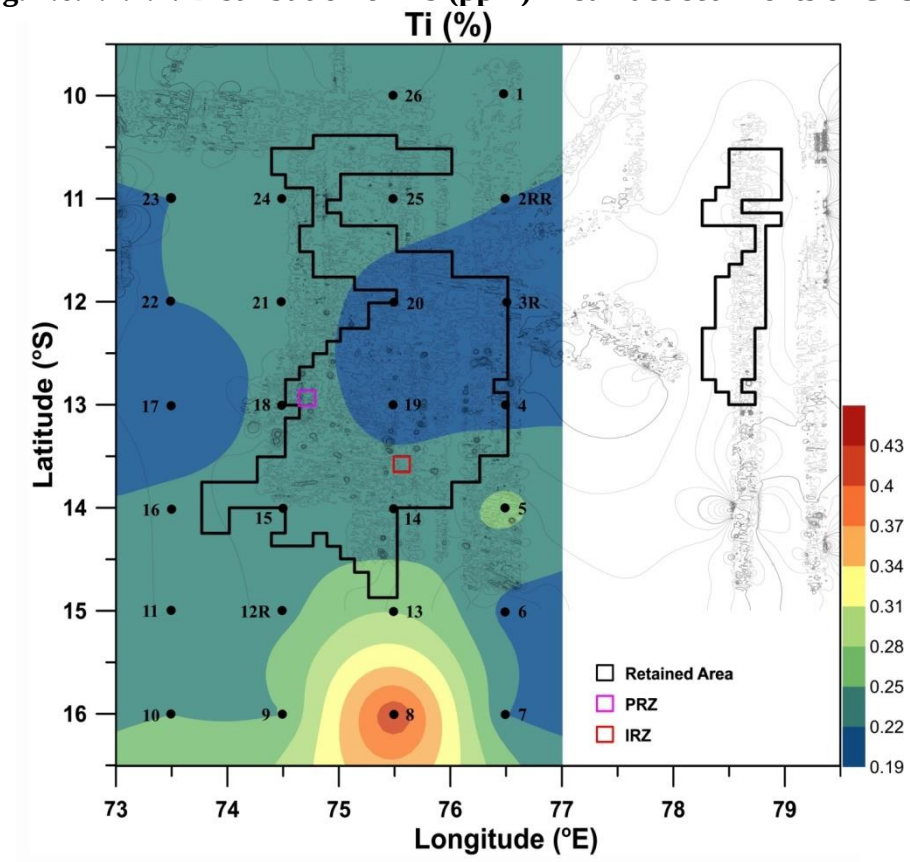

Fig. 4.6.2.2.1.5: Distribution of Ti (%) in surface sediments of CIOB.

4.6.2.2.2 Manganese and Iron – reflecting varying redox conditions

Manganese and iron in deep-sea sediments reflect a combined effect of supply from detrital sources as well as the deposition from water column and porewater through authigenic /insitu processes. Manganese in particular is sensitive to redox processes, dissolving when exposed to lower oxygenation conditions and precipitates at oxygenated settings. Additionally, both these elements can be enriched in sediments from hydrothermal processes. Both Mn and Fe show enrichment in the southwestern corner and in the center of the studied area (Fig. 4.6.2.2.2.1), the former probably reflecting the influence of hydrothermal processes operating in the area and the latter may be due to the redox influenced enrichment. Oxygenated water column and deeper depths in the latter area might promote the redox-induced precipitation of Fe and Mn.

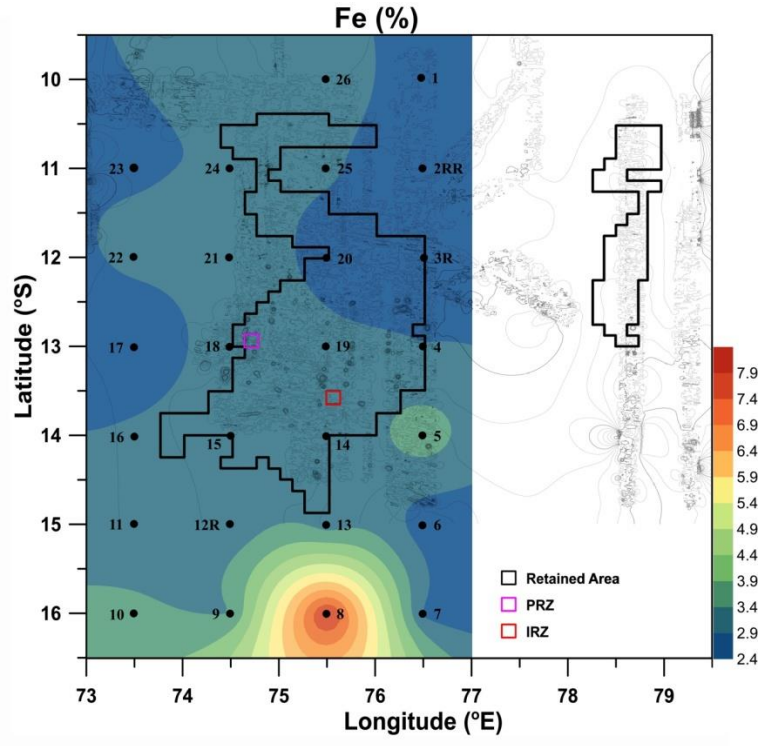

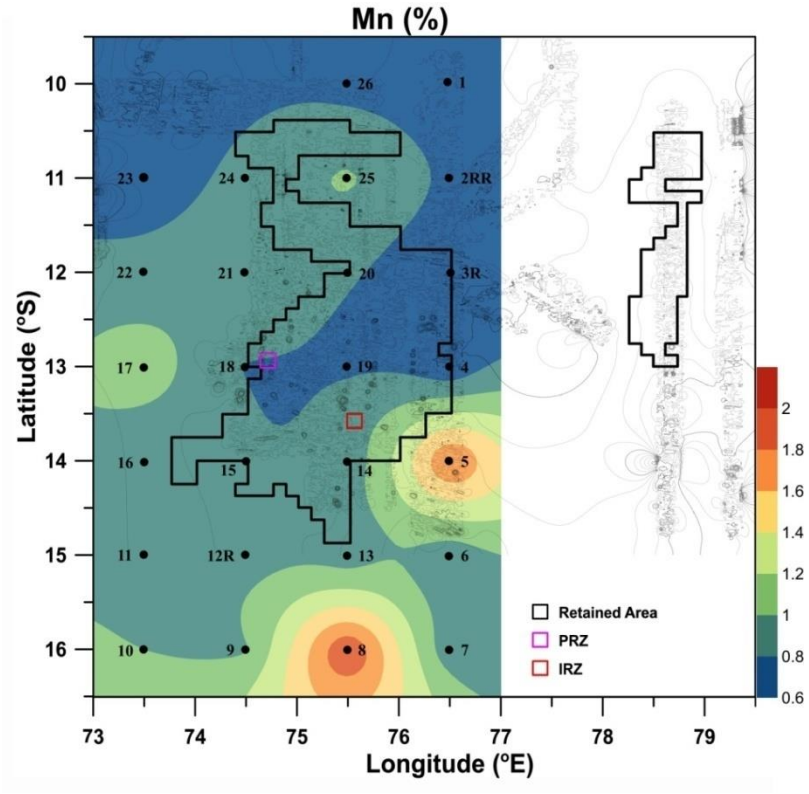

Fig. 4.6.2.2.2.1: Distribution of Fe and Mn (%) in surface sediments of CIOB.

4.6.3 Geochemical conditions in IRZ and PRZ

Sediment cores collected from five stations in IRZ and five stations in PRZ (Table 3.2.1.1), one each in four corners and the center of the block, were studied for geochemical properties of porewater and the solid phase. Elements recommended in ISA guidelines are measured in sediments. The downcore plots, of all the parameters studied in these cores, are placed in similar configuration of actual sampling. For example, the top left plot in the figure represents the core from northwestern area of IRZ.

4.6.3.1 Porewater chemistry

4.6.3.1.1 Phosphate

a) PRZ

Phosphate concentrations in all the five cores at PRZ range between 1.8 and 3.1 µmol/L. The downcore porewater phosphate concentrations of all the five cores are plotted in Fig. 4.6.3.1.1.1. The porewater phosphate values in core from the north western part of the area (core BC 2) are relatively lower than other cores. The top 6-8cm in all the cores tend to be low, most of them shows an intermediate high. The change coincides with the depth of color

change possibly related to Fe content which can control bound phosphate. The downcore patterns are not entirely similar in all the cores suggesting a local variability in benthic mixing and diagenetic processes.

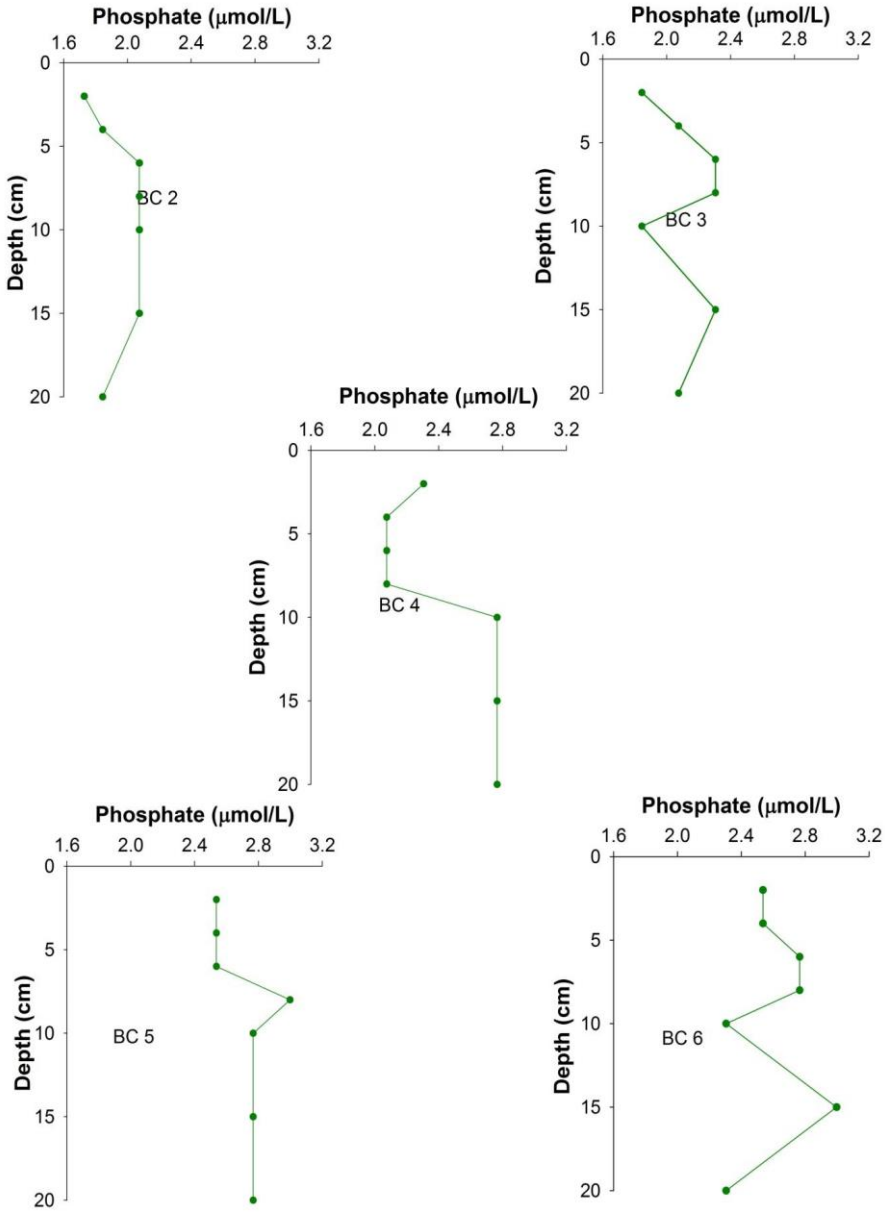

Fig. 4.6.3.1.1.1: Spatial variation in downcore porewater phosphate at PRZ

b) IRZ

Phosphate concentrations if all the cores at the Impact reference Zone (IRZ) range between 1.4 and 3.1µmol/L , with most of them falling between 2-2.4 µmol/L, and are in similar range as that seen in PRZ. Surface depletion is common in all the cores possibly due to seawater penetration (Fig. 4.6.3.1.1.2). But, they display higher values in subsurface depths >10cm bsf.

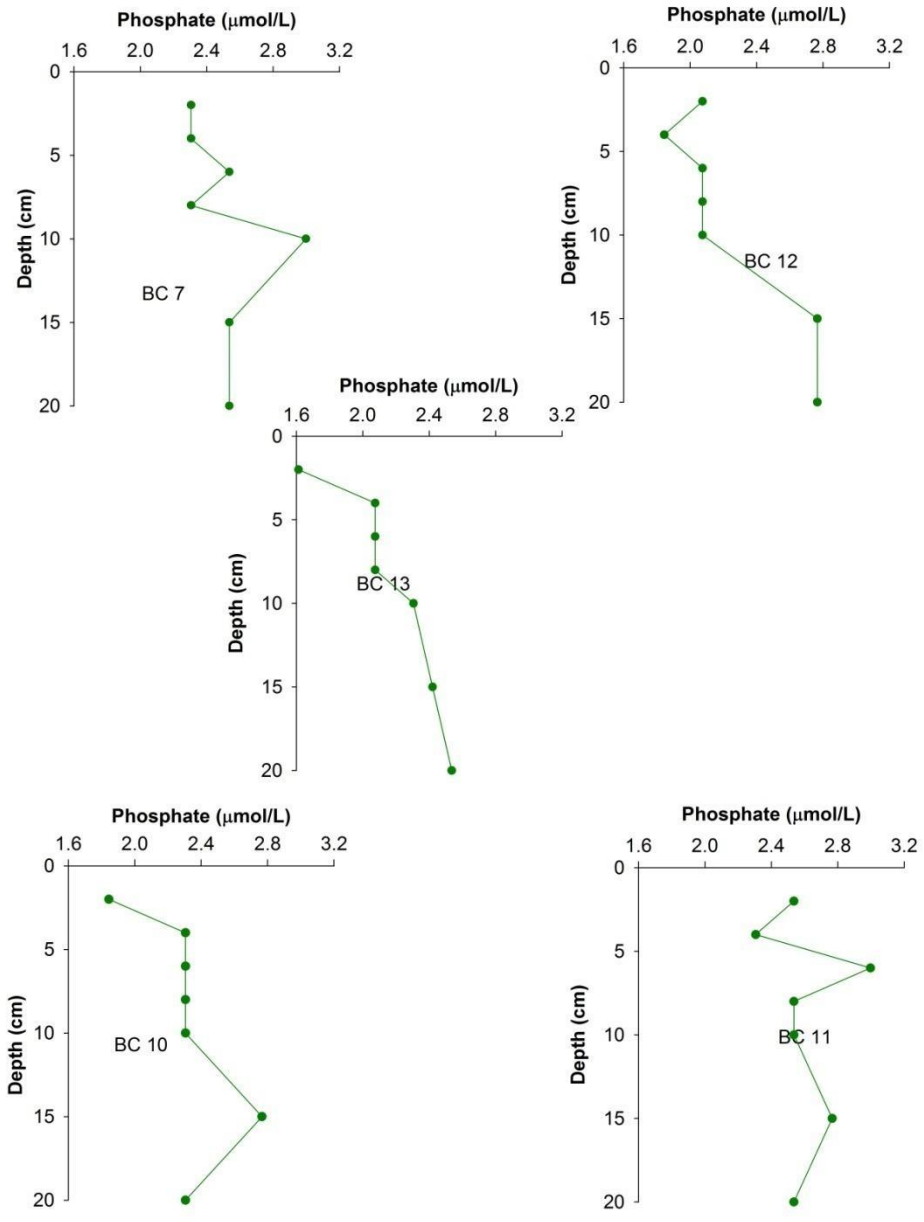

Fig. 4.6.3.1.1.2: Spatial variation in downcore porewater phosphate at the IRZ.

4.6.3.1.2 Nitrite

a) **PRZ**

Porewater nitrite of all the cores at the Preservation reference Zone (PRZ) are low and below 0.2 µmol/L (Fig. 4.6.3.1.2.1) typical of deep-sea sediments. Detected nitrite values may be due to the process of nitrification. Earlier studies have shown that this area has nitrifying bacteria and high porewater nitrate values.

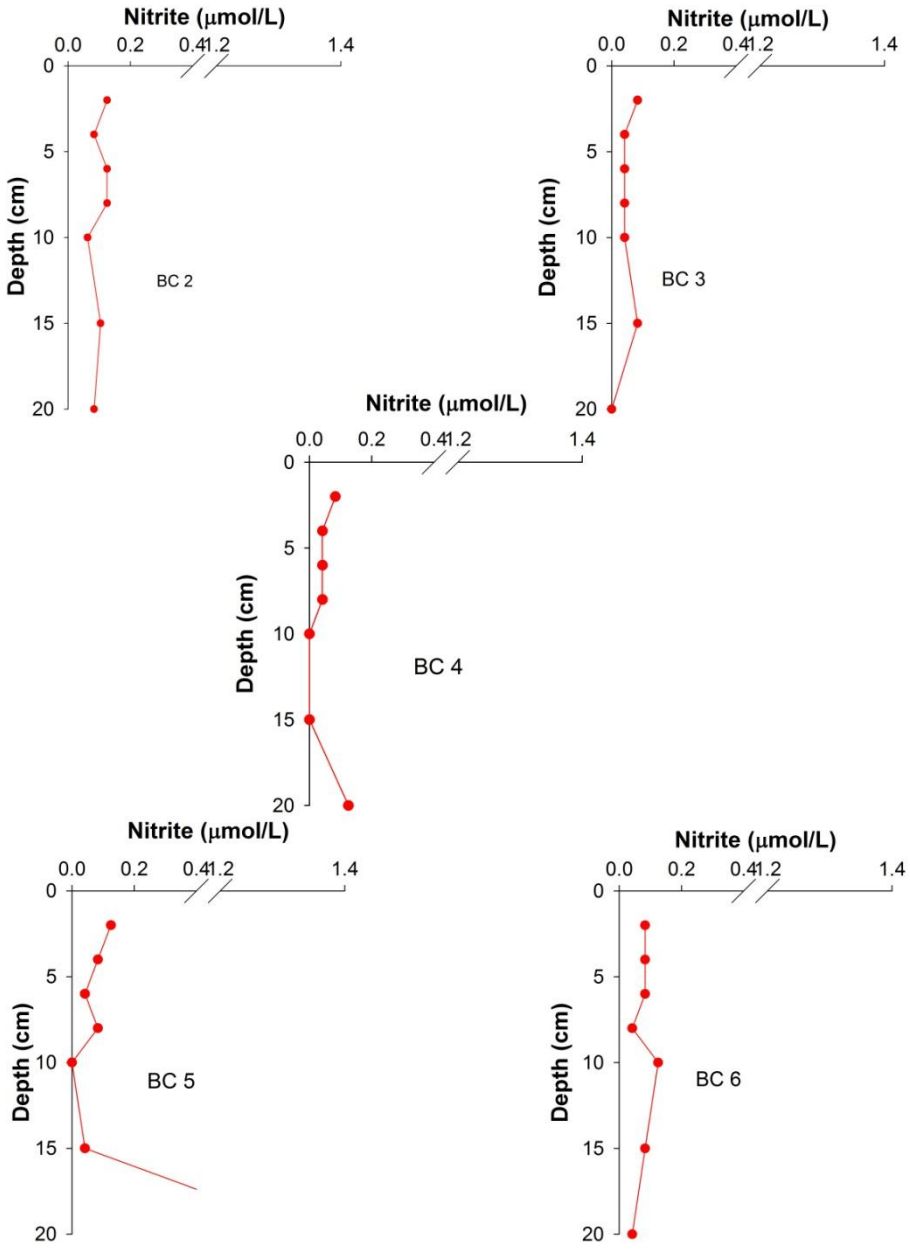

Fig. 4.6.3.1.2.1.: Spatial variation in downcore porewater nitrite at PRZ

b) **IRZ**

Porewater nitrite in cores from Impact reference Zone (IRZ) also is low (Fig. 4.6.3.1.2.2) similar to PRZ and their values are below 0.2 µmol/L, except for an intermediate in core BC 11 (1.2 µmol/L (Table).

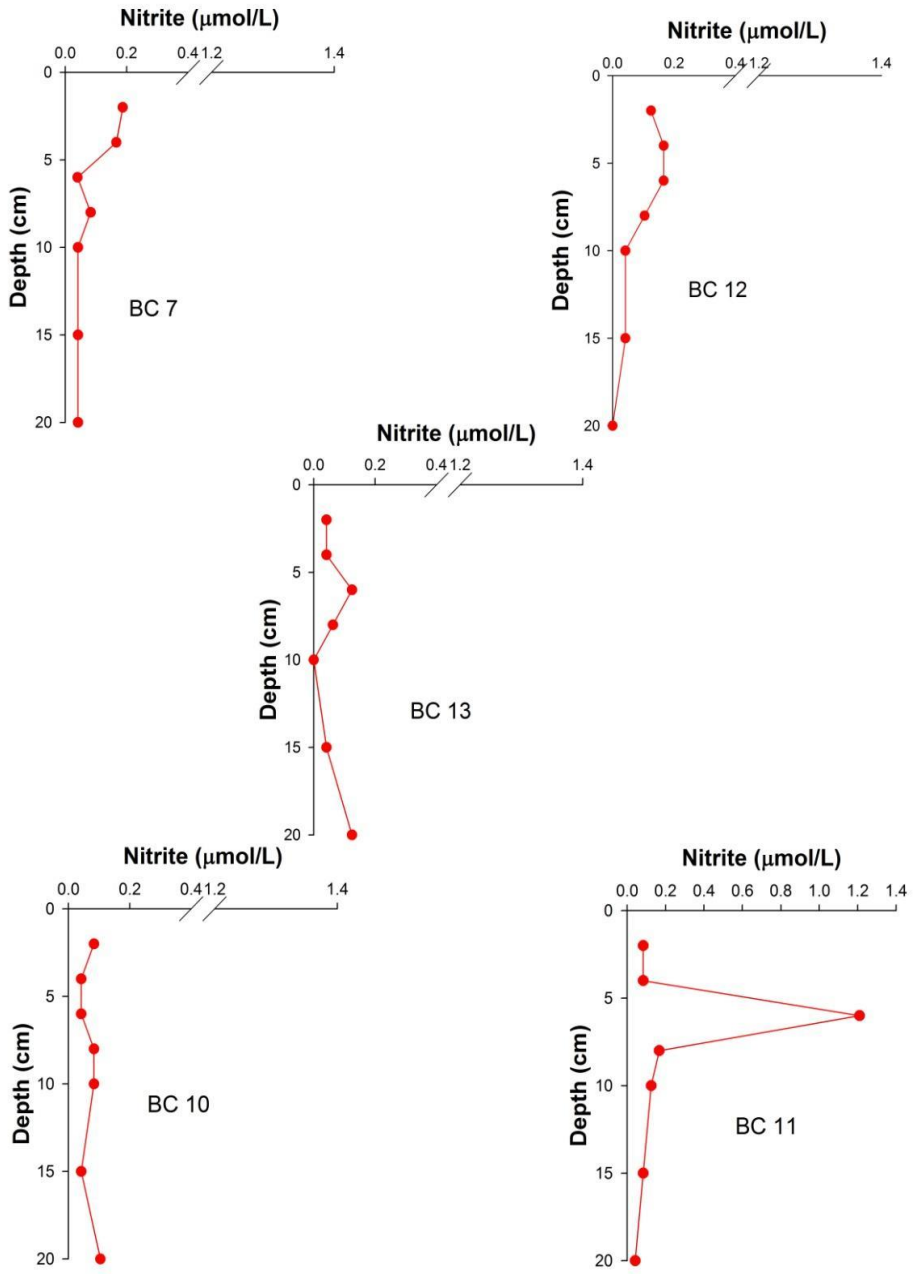

Fig. 4.6.3.1.2.2: Spatial variation in downcore porewater nitrite at IRZ.

4.6.3.1.3 Silicate

a) **PRZ**

In most of the cores, porewater silicate concentration are higher in deeper sections compared to the sediments at sediment-water interface and as well as the bottom waters (Fig. 4.6.3.1.3.1). Silicate in the core in center (BC 4) show a subsurface increase without kinks compared to other cores defining a smooth diffusional gradient from sediment to seawater. Northern cores are having lesser concentration compared to southern core and the center one showing a smooth trend suggesting a local variation.

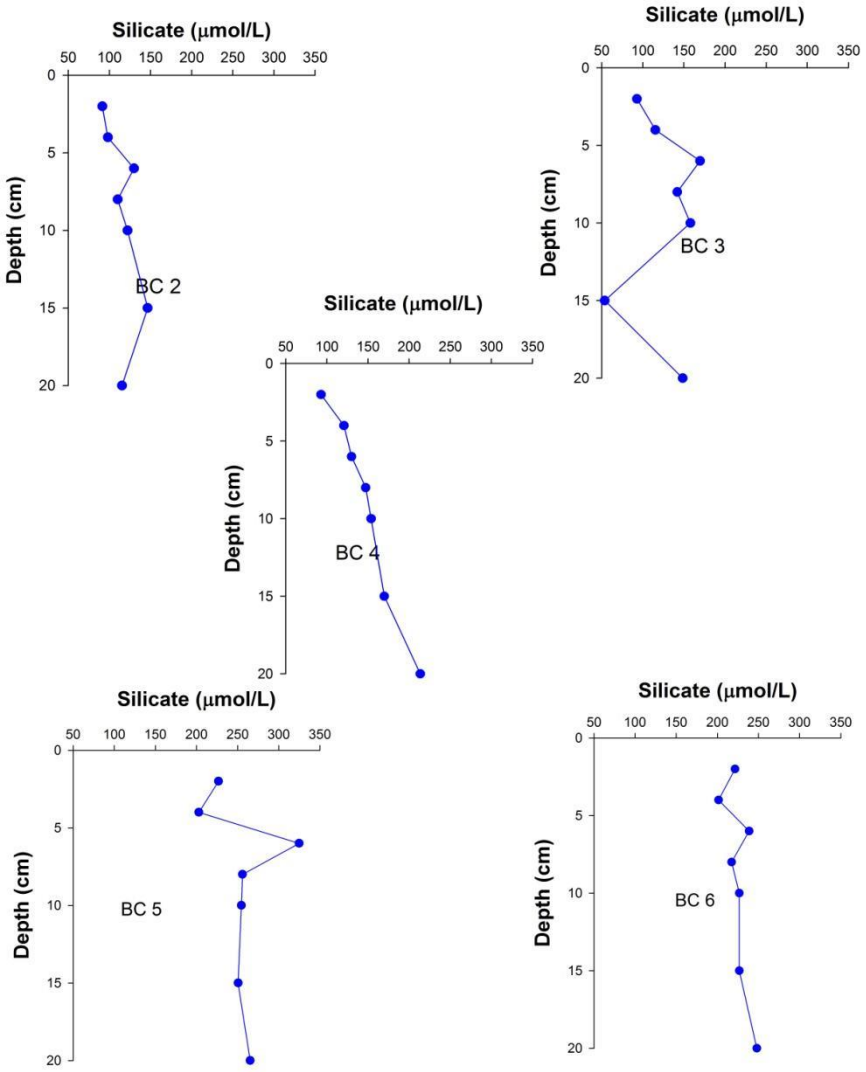

Fig. 4.6.3.1.3.1: Spatial variation in porewater silicate at PRZ

b) **IRZ**

Porewater silica concentrations of all cores in the IRZ are in the range between 150 and 300 µmol/L (Fig. 4.6.3.1.3.2). All cores are showing a downcore increase typical of Central Indian Ocean Basin. While the porewater silicate profiles in IRZ are relatively smoother, the PRZ cores show some subsurface kinks. A second difference is the higher porewater silicate values than the bottom water in all the cores of IRZ compared to some of the cores in PRZ.

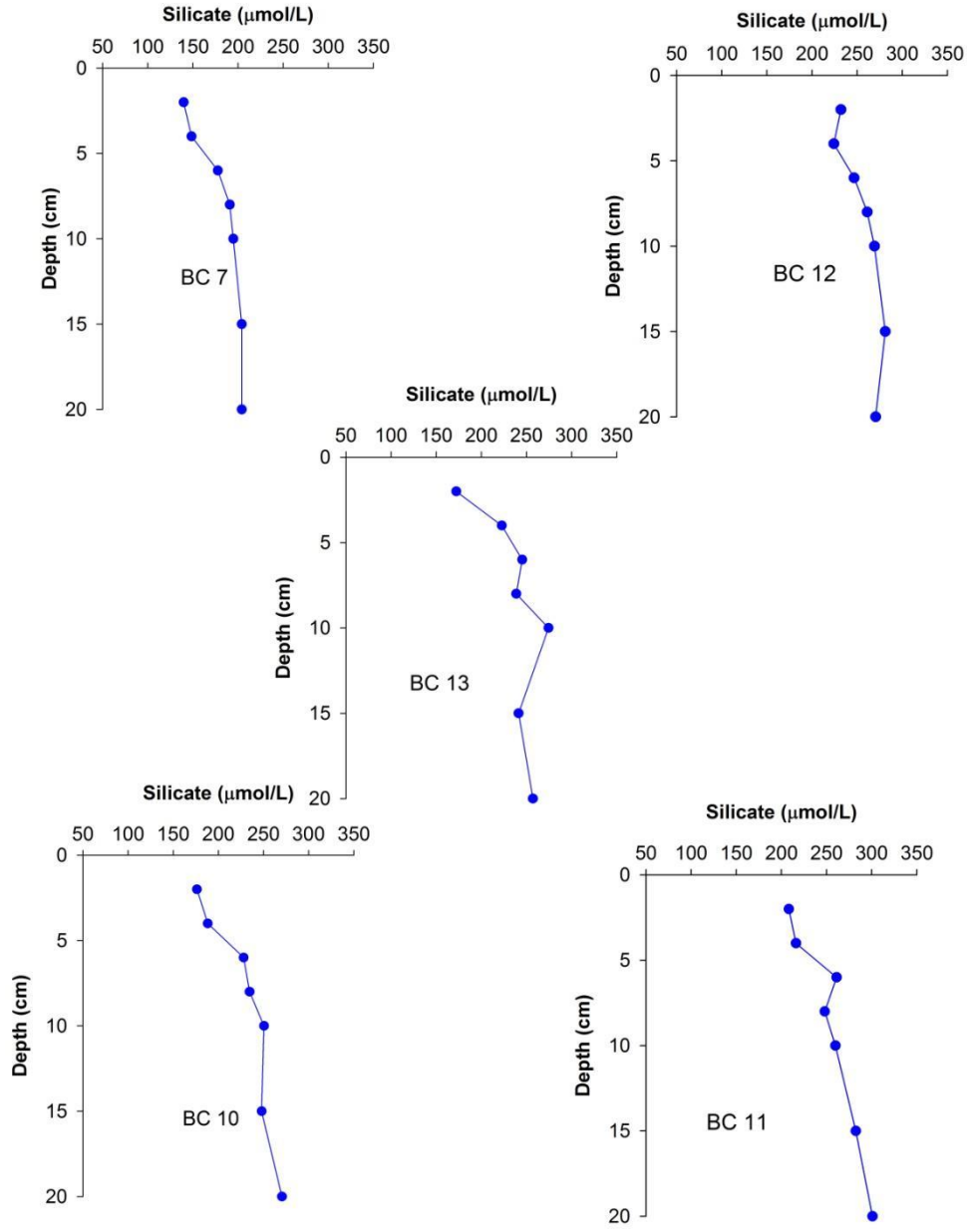

Fig. 4.6.3.1.3.2: Spatial variation in porewater silicate at IRZ

4.6.3.2 Solid phase chemistry

4.6.3.2.1 Organic carbon (%)

Organic carbon is an important chemical constituent for benthic ecosystem. Organic C content in the surface sediments of the core (BC 4) sampled in the Preservation reference Zone (PRZ) is nearly same as the sediment core (BC 13) sampled in the IRZ. The values are in general low and typical of deep-sea pelagic sediments. High organic carbon content is present in the surface sediments (0.6%) which gradually decrease to about 0.2% at 10cm bsf in BC 13 core, while the initial high organic content in surface layers is reduced to half at about 15 cm bsf in BC 4 core. The trend in both sites is same except for the magnitude. Reduction with depth may either be due to consumption by benthic biota or due to decomposition facilitated by longer oxygen exposure time. Sub bottom peaks are also seen in both areas.

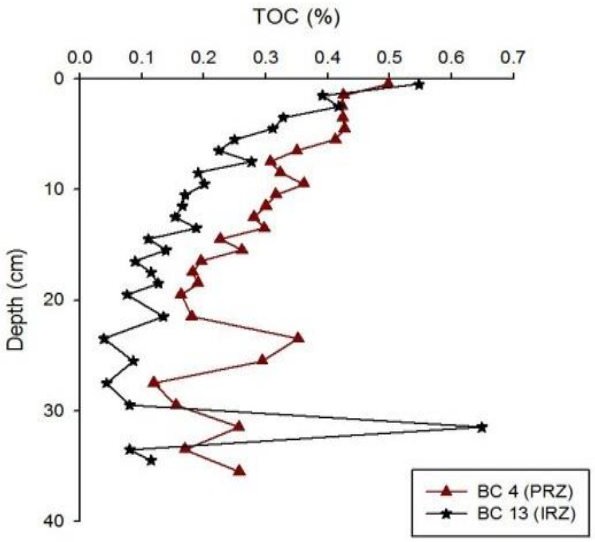

Fig. 4.6.3.2.1.1: Down core variation in organic carbon (%) at PRZ and IRZ

4.6.3.2.2 Elemental variation

The concentrations of V, Cr, Co, Ni, Cu, Zn and Pb in 10 sediment cores, 5 from the Preservation Reference Zone (PRZ) and 5 from the Impact Reference Zone (IRZ) were studied. The concentrations of V, Co, Ni, Cu and Pb in the cores BC-2, BC-3, BC-4, BC-5 and BC-6 sampled at PRZ are less compared to the cores i.e. BC-7, BC-10, BC-11, BC-12 and BC-13 sampled in the IRZ.

a) Vanadium

In general, vanadium concentrations are higher in IRZ than PRZ. In PRZ, V concentration display a narrow range of concentration between 35 to 55 ppm (i.e. in cores BC-2, BC-4, BC-5 and BC-6), however the concentrations in core BC-3 are higher (up to 80 ppm). In IRZ, generally the concentration range between 55 to 80 ppm. The mean V content in IRZ is 67 ppm.

In the PRZ, northern cores have more V concentration compared to rest of the area i.e. centre core and southern cores (Fig. 4.6.5.2.1). Northwestern (NW) core shows gradual decrease down the sediment depth from 69 to 40 ppm whereas in the northeastern (NE) core, the concentrations range between 65 to 80 ppm. In the core in centre, the V content is nearly similar down the core. Southwestern (SW) core shows low concentration (33 ppm) at the surface then increases up to 57 ppm at around 12-14cm, which further decrease down to 38 ppm till 20cm depth, whereas southeastern area (SE) shows similar concentration with slight decrease downcore from 54 to 41 ppm.

In IRZ, all the northern and southern cores show gradual decrease in the V concentration except the centre core. In the NE core, V is high (77 ppm) (Fig. 4.6.3.2.2.2) at the surface, then gradually decreases (59 ppm) down the core depth till 20 cm. The centre core shows gradual increase in the V from 59 ppm to 91 ppm. The SW core show gradual decrease down the core from 75 to 60 ppm whereas SE core show slight increase at the subsurface than surface followed similar range of concentration.

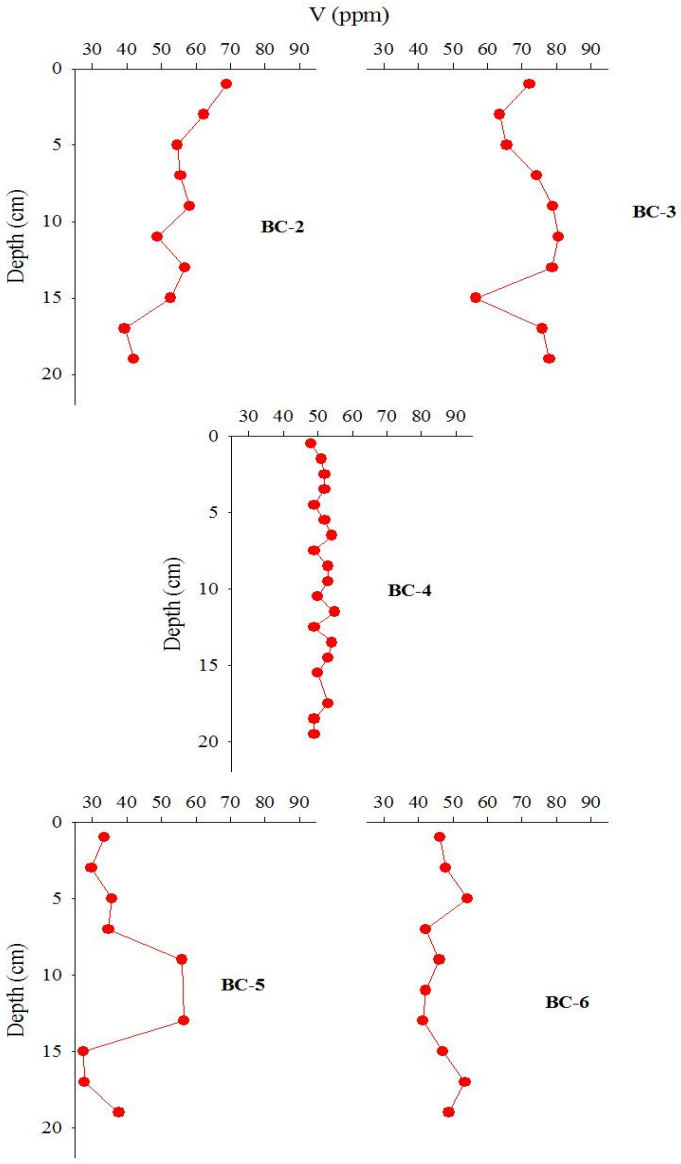

Regional variation of downcore Vanadium (V) concentration (ppm) at PRZ

Fig. 4.6.3.2.2.1: Down core variation in V concentration (ppm) at the Preservation Reference Zone

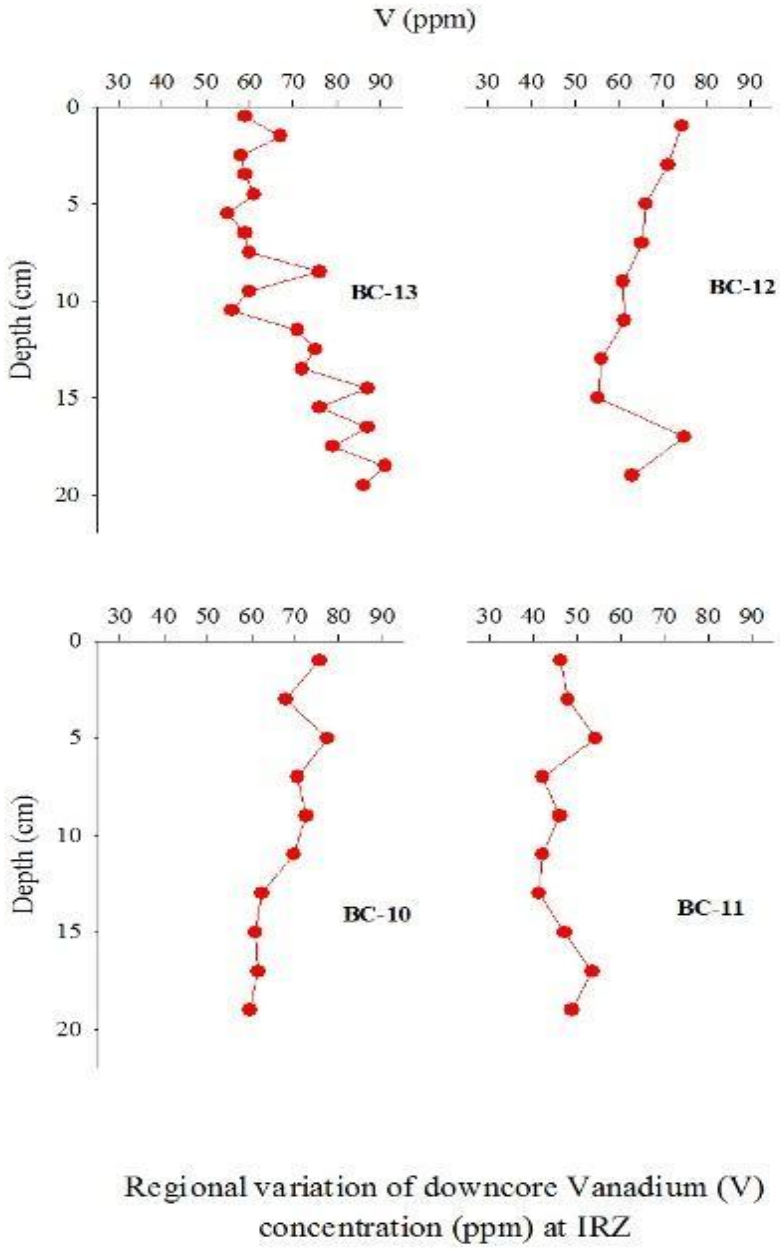

Fig. 4.6.3.2.2.2: Down core variation in V concentration (ppm) at the Impact Reference Zone

b) Chromium

Higher Cr concentrations are noticed in PRZ (mean - 43 ppm, range 17-170 ppm; Fig. 4.6.3.2.2.3) than IRZ (mean - 28 ppm, range 28-38 ppm; Fig. 4.6.3.2.2.3). Except for core BC-4 (in the centre with Cr concentration as high as 170ppm), the concentrations are <40ppm and are nearly similar in remaining four cores. In the PRZ, northern core has low (40 ppm) Cr concentration which gradually decreases down the core whereas the SW core show almost similar range of concentration and SE core shows drastic increase at 12 cm up to 72 ppm (Fig. 4.6.3.2.2.3). The centre core shows higher Cr concentration than any other core but with a large variability 40 ppm to 170 ppm.In the IRZ, all southern and northern cores show similar range of Cr concentration between 20 to 35 ppm (Fig. 4.6.3.2.2.4):

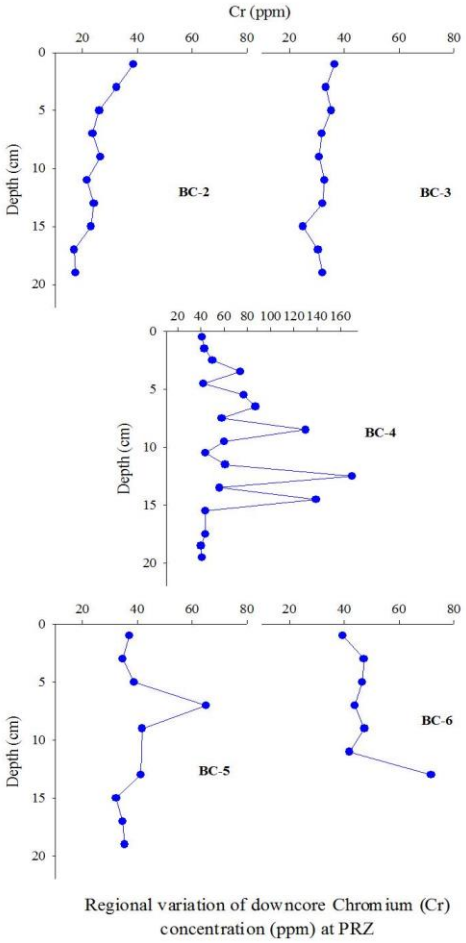

Fig. 4.6.3.2.2.3: Down core variation in Cr concentration (ppm) at the Preservation Reference Zone

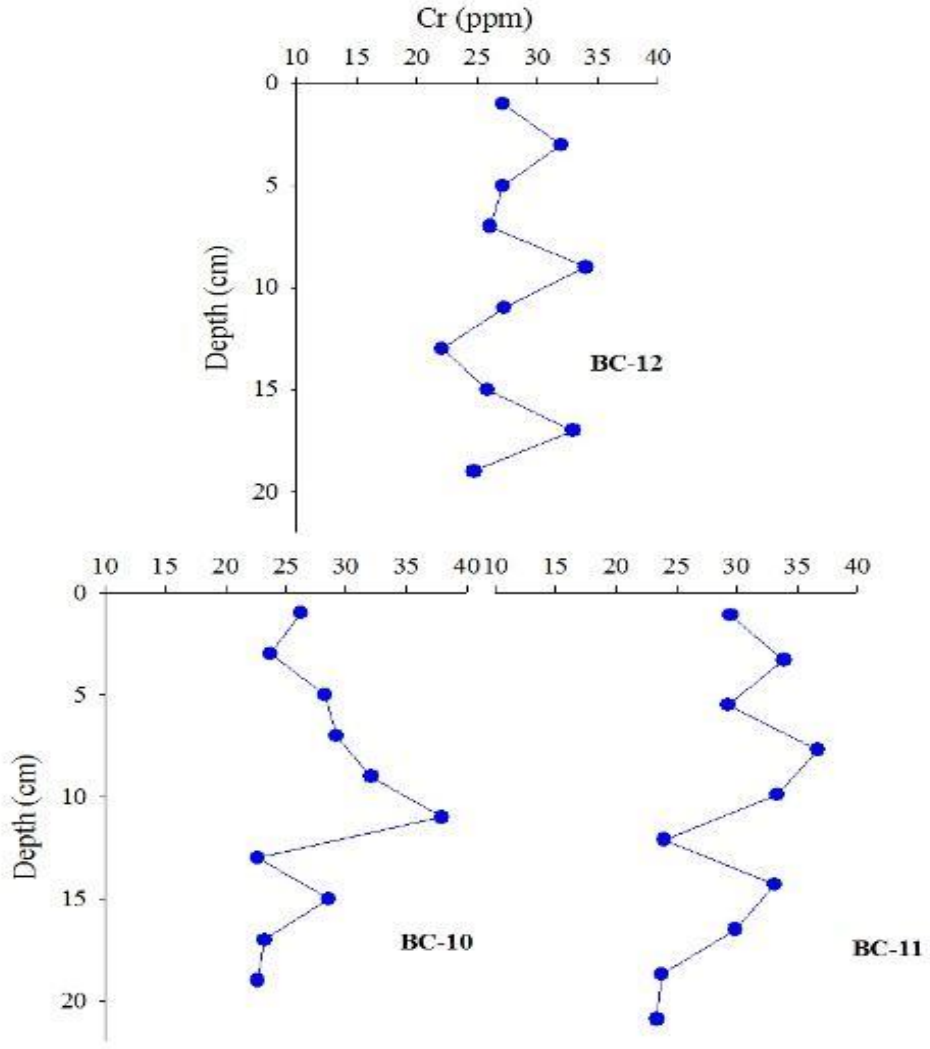

Regional variation of downcore Chromium (Cr) concentration (ppm) at IRZ

Fig. 4.6.3.2.2.4: Down core variation in Cr concentration (ppm) at the Impact Reference Zone.

c) Cobalt

Co concentrations in IRZ are higher than in PRZ sediments (Fig. 4.6.3.2.2.6 and Fig. 4.6.3.2.2.5). The concentration in PRZ are nearly similar and usually less than 60 ppm, whereas in IRZ a surficial enrichment is seen. In the PRZ, the NW core has higher Co concentration than NE core. In the NW core, a gradual downcore decrease in Co content is from 58 at top to 33 ppm at 20 cm whereas NE core show similar range of concentration between 19 to 25 ppm (Fig. 4.6.3.2.2.5). Also the centre core has the similar range of concentration between 36 to 48 ppm. The SW core has low concentration (< 40 ppm) than SE core (> 40 but <6 5 ppm) showing similar range of Co concentration.

In the IRZ, all the cores are showing gradual downcore decrease in the cobalt content. The NE core has higher concentration at the surface (120 ppm) then drastically decreased to 60 ppm at the subsurface depths (at about 3-4 cm) which is then followed by gradual decrease in concentration to 40 ppm (Fig. 4.6.3.2.2.6). Also in the centre core, the surface has about 80 ppm of Co, however increases to about 120 ppm (at 3-4 cm) which further decreases down core. The southern cores show similar range of Co with slight decrease till 20 cm.

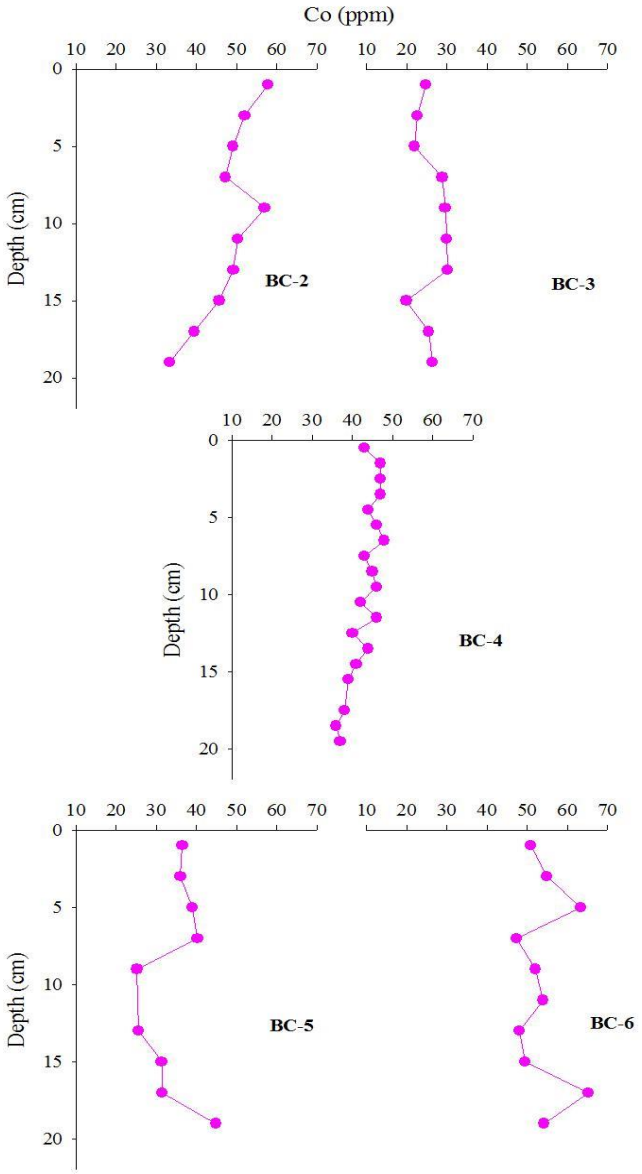

Fig. 4.6.3.2.2.5: Down core variation in Co concentration (ppm) at the Preservation Reference Zone

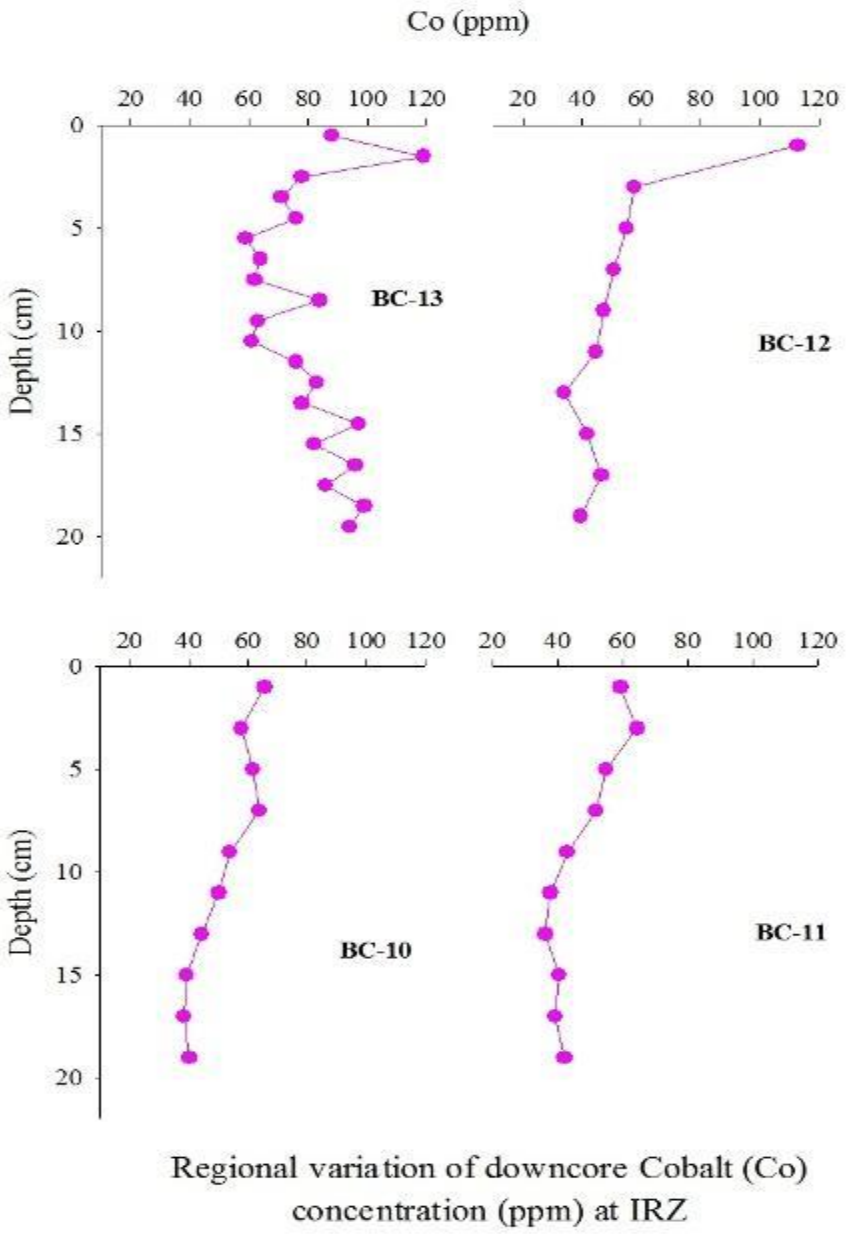

Fig. 4.6.3.2.2.6: Down core variation in Co concentration (ppm) at the Impact Reference Zone

d) Nickel

In the PRZ, the northern cores show similar (NW core ~ 200 ppm and NE core ~ 150 ppm) variation in Ni concentration (Fig. 4.6.3.2.2.7). In the southern cores, SW core has less (< 150 ppm) Ni concentration than SE core (>200 and <360 ppm).In the IRZ, all the cores display a downcore decrease in the Ni concentration. Compared to northern (412 ppm) and central (~600 ppm) cores, the concentrations in the southern stations (~200 to 250 ppm) are much less at the surface in the IRZ (Fig. 4.6.3.2.2.8), suggesting a large local variability. Ni content in IRZ cores is more than the PRZ cores at surface.

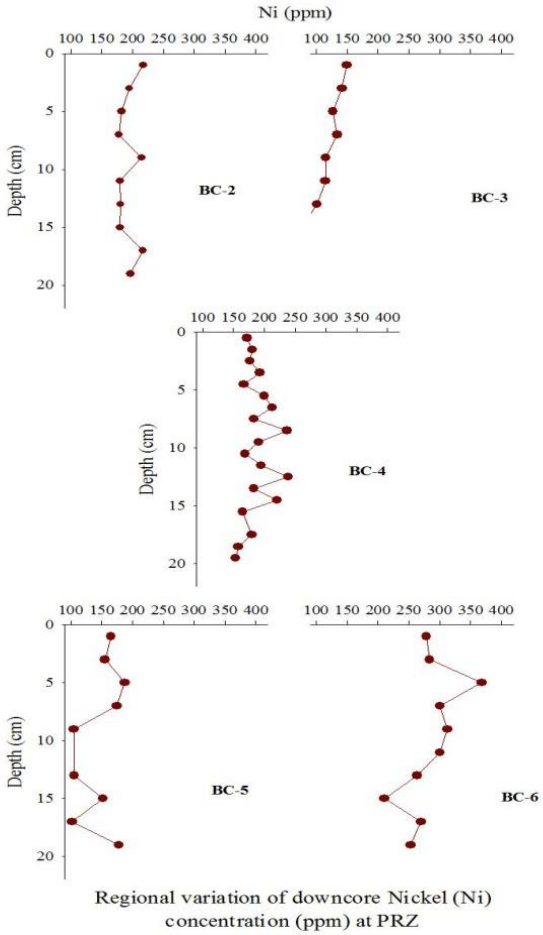

Fig. 4.6.3.2.2.7: Down core variation in Ni concentration (ppm) at the Preservation Reference Zone

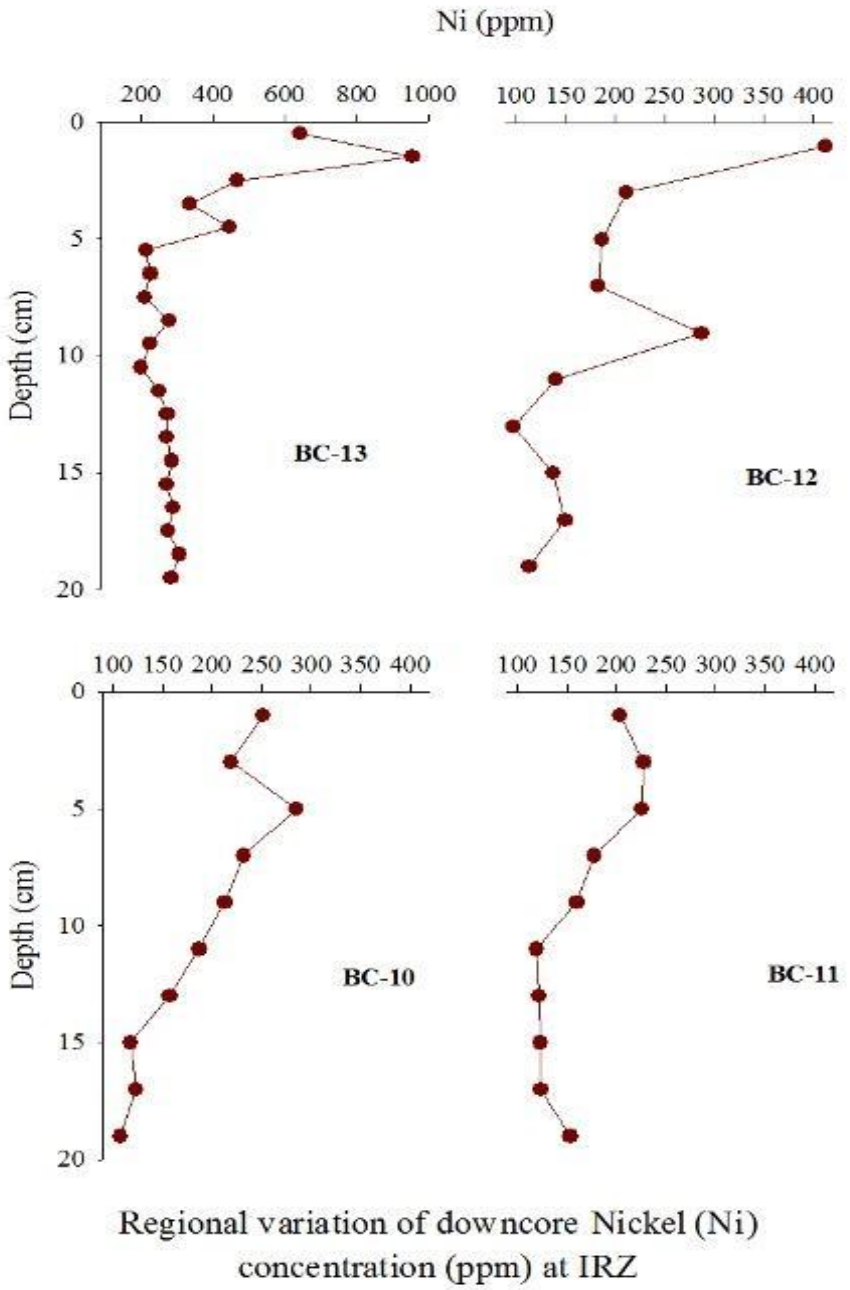

Fig. 4.6.3.2.2.8: Down core variation in Ni concentration (ppm) at the Impact Reference Zone

e) Copper

Cu concentrations in general are higher IRZ than PRZ (Figs. 4.6.3.2.2.10&4.6.3.2.2.9). The Cu concentrations are nearly similar in PRZ (~ 300 ppm) whereas the surface sample in centre core of IRZ shows very high concentration (892 ppm). The variability of Cu concentration in IRZ (86-892 ppm) is larger than PRZ (99-425 ppm) with averages being 244 and 299 ppm.

In the PRZ, the NW core has more Cu concentration (300 ppm) at the surface with a gradual decrease (minimum seen at about 12 cm) followed by an increase, whereas the Cu content being nearly similar in NE core (Fig. 4.6.3.2.2.9). Lack of significant gradient is also noticed in sediment cores in the centre and the SW corner, whereas a downcore increase is seen in the SE core.

In the IRZ, except for the NW core, all other cores show decrease with depth with the top 5 cm of the core in centre show a well defined significant downcore variation

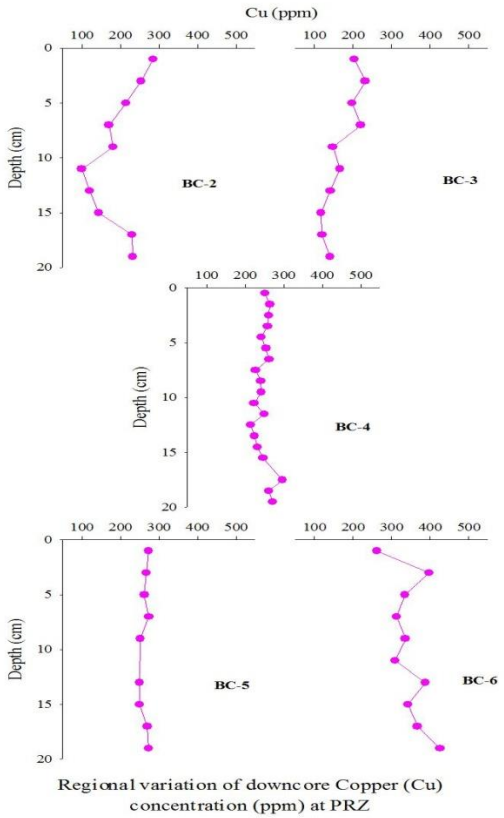

Fig. 4.6.3.2.2.9: Down core variation in Cu concentration (ppm) at the Preservation Reference Zone

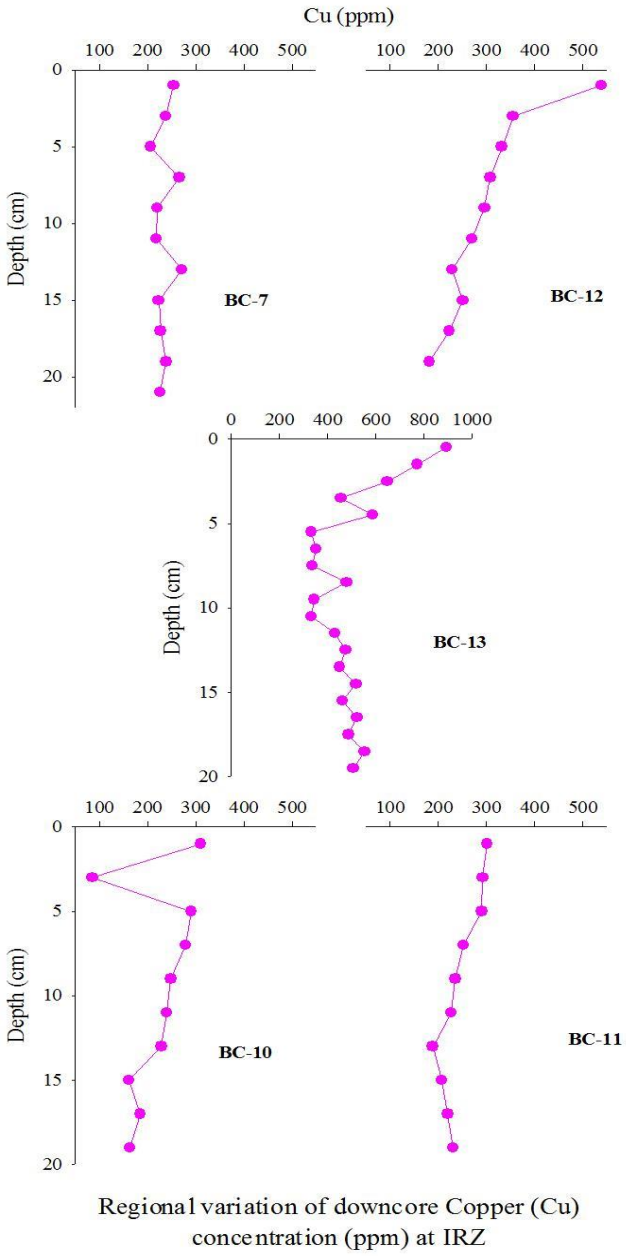

Fig. 4.6.3.2.2.10: Down core variation in Cu concentration (ppm) at the Impact Reference Zone

f) Zinc

Zn concentrations in general are slightly higher in PRZ (28-144 ppm; average 89 ppm) than IRZ sediments (47 to 216 ppm; average 87 ppm) (Figs. 4.6.3.2.2.11and4.6.3.2.2.12), and are about < =100 ppm except in core in the centre where very high concentrations are seen in the surface (216 ppm). In the PRZ, two northern cores show downcore changes (troughs and peaks) in concentrations while the central and southern cores either show little change or gradual change (Fig. 4.6.3.2.2.11).In the IRZ, all the cores have higher Zn at the surface which gradually decreases down (Fig. 4.6.3.2.2.12). The subsurface changes are more subtle (except the core in the centre) compared to the cores in PRZ.

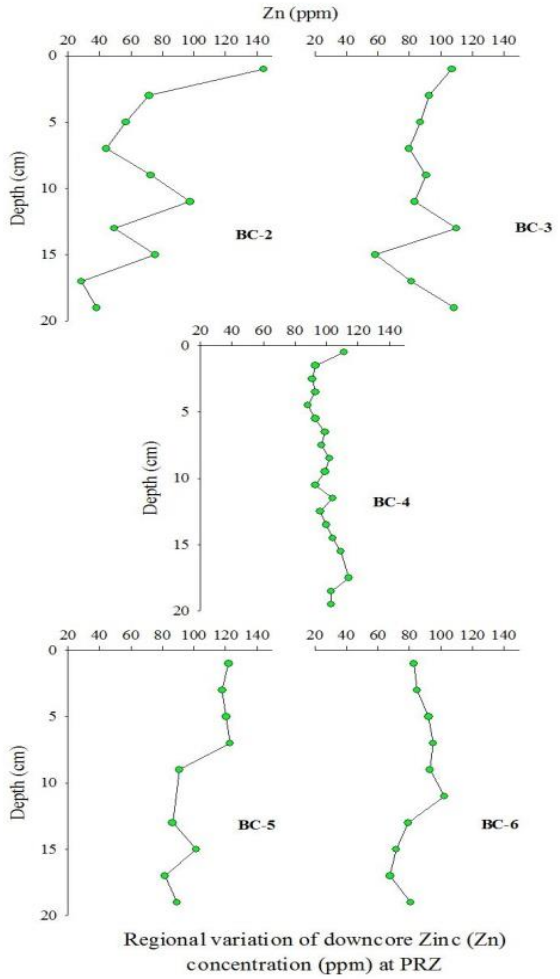

Fig. 4.6.3.2.2.11: Down core variation in Zn concentration (ppm) at the Preservation Reference Zone

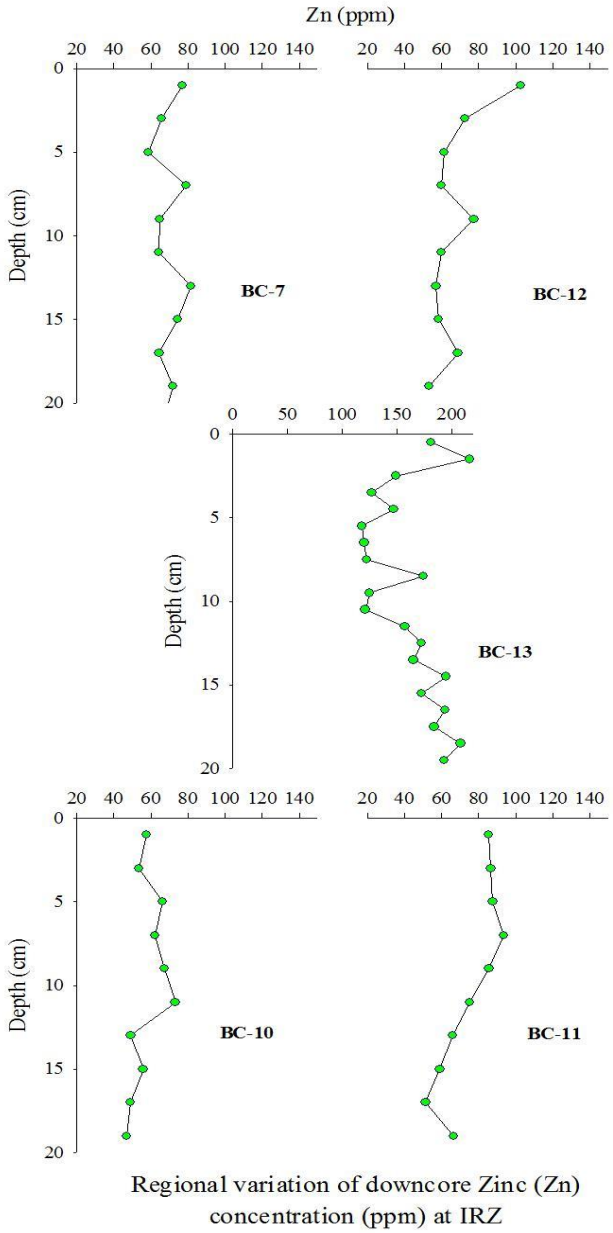

Fig. 4.6.3.2.2.12: Down core variation in Zn concentration (ppm) at the Impact Reference Zone

g) Lead

Pb concentrations are nearly similar in both PRZ (19 to 105 ppm; average 34 ppm) and IRZ (19-127 ppm; average 45 ppm) (Fig. 4.6.3.2.2.13 and Fig. 4.6.3.2.2.14). In the PRZ (Fig. 4.6.3.2.2.13), both the northern and southern cores have higher values at the surface which gradually decrease down the core from 55 to 20 ppm. The centre core shows similar (around 20 ppm) range of concentration till 15 cm after that there is drastic increase to 105 ppm.A downcore decrease is seen in Pb concentrations in all the IRZ cores (Fig. 4.6.3.2.2.14), except that a reverse is seen in the centre core

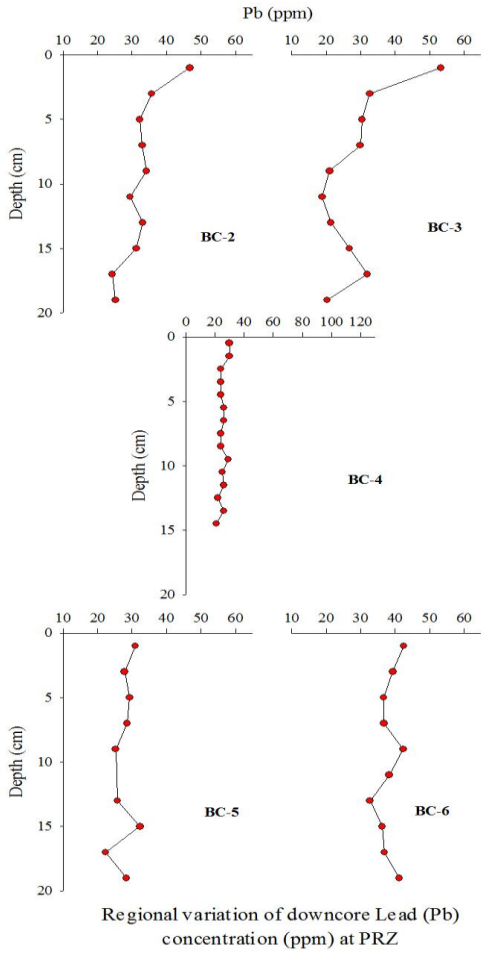

Regional variation of downcore Lead (Pb) concentration (ppm) at PRZ

Fig. 4.6.3.2.2.13: Down core variation in Pb concentration (ppm) at the Preservation Reference Zone

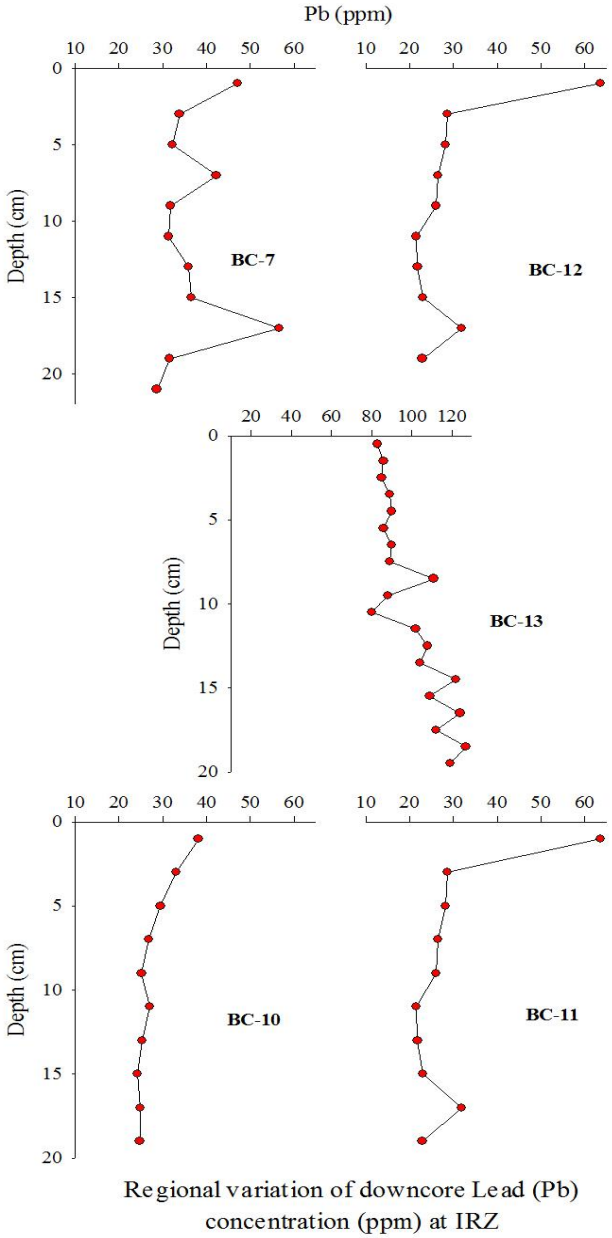

Fig. 4.6.3.2.2.14: Down core variation in Pb concentration (ppm) at the Impact Reference Zone

5. Baseline biological environment

5.1 Marine birds and mammals

Although dedicated studies for number and diversity of marine birds and mammals has not been commissioned, occasional sightings have been made during the several expeditions to the area during the exploration phase. Birds have rarely been sighted in and around the area and the few sightings have been mainly restricted to sea-gulls that either followed the vessel (or used it as its resting place) for a few days or encircled the vessel and disappeared. It is understood that these birds could be the predators for surface plankton, nekton and fish, but their rare appearance probably indicates the lack of sufficient quantities of preys on the surface in this area. Similarly, marine mammals were sighted mainly during the journey from Goa to the study area and very few were actually seen in the study area. Mostly whales and dolphins were sighted while the vessel was cruising, whereas sharks, turtles and flying fish were seen close to the vessel during operations probably in search of food.

5.2 Water column biology

5.2.1 Surface productivity

Detailed studies on surface productivity and associated environment have been carried during Sagar Kanya cruise (SK 120) to evaluate the surface phytoplankton and zooplankton abundance, biomass, taxonomy, primary productivity, and Photosynthetically Available Radiation (PAR) not only in the contract area but also around it at a systematic sampling interval of $1^{o}x1^{o}$ (Fig. 5.2.1.1), which has been reported by Matondkar et al., (2000). Studies on physico-chemical characteristics of water column in the area (Ramesh Babu et al., 2001; De'Sousa et al., 2001) have shown the presence of three water masses viz., (a) having sub-surface salinity maximum in the depth range of 125-200m, (b) with deep oxygen minimum at depth of 250-750m and (c) Antarctica Intermediate water (AIW) at depth of 800-1100m. These water masses are of great importance for biological productivity in CIOB. Earlier, Krey et al., (1976) had compiled *chlorophyll a* and primary productivity for CIOB region where *chlorophyll a* was $<0.05 mgm^{-3}$ at surface and 25m and 0.05-0.1mg m^{-3} at 50m indicating that *chlorophyll a* the phytoplankton community in the deep sea occurs on the typical physico-chemical environment where nutrients are very low. Some of these are described in the following sections.

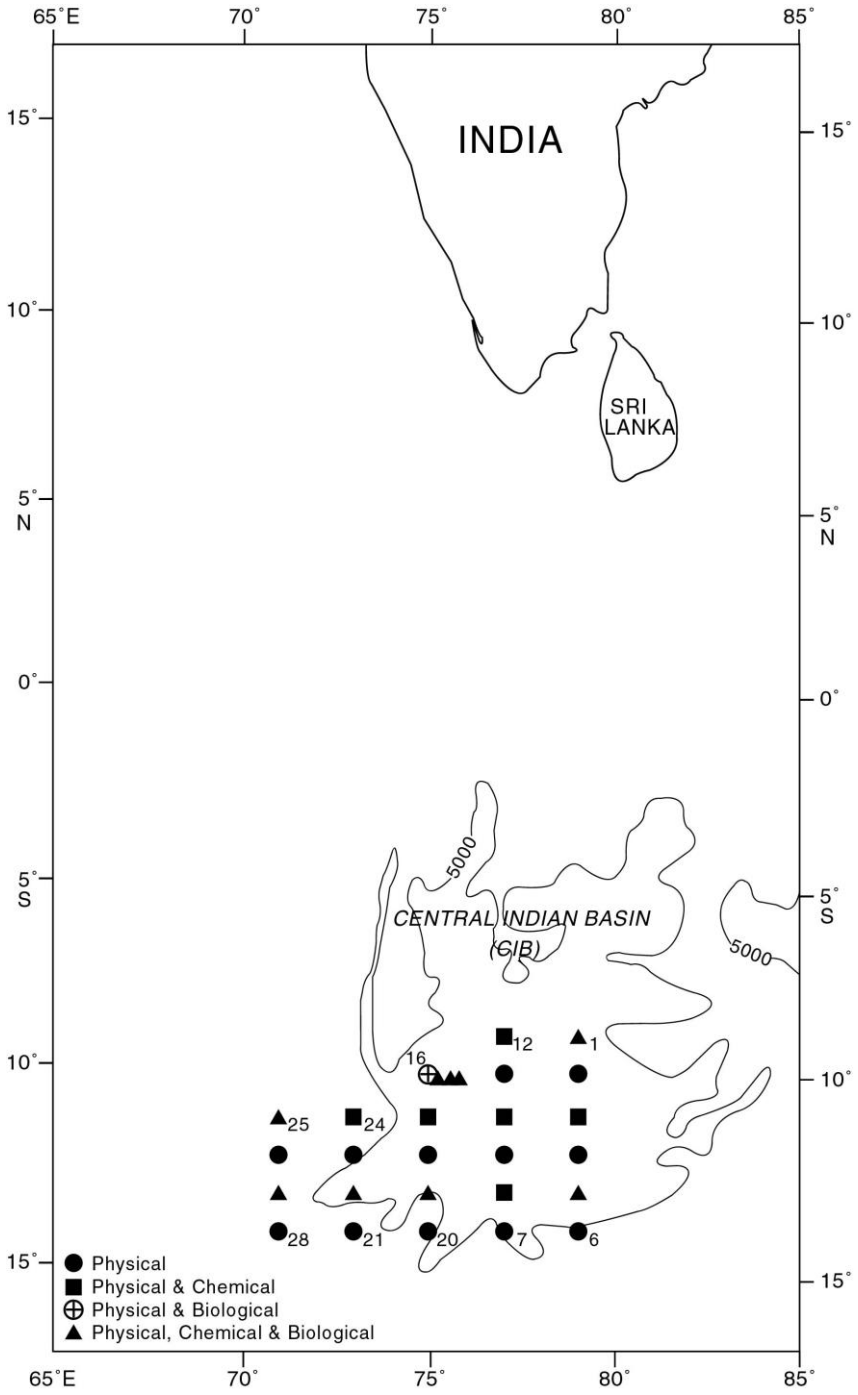

Fig. 5.2.1.1: Sampling locations for phytoplankton and zooplankton studies.

5.2.1.1 Solar radiation

The station-wise total Photosynthetically Active Radiation (PAR) is presented in Fig. 5.2.1.1.1a, b. The PAR decreased gradually down to 80m and it appears that the particulates from subsurface *chlorophyll a* maxima at 40-60m allow the PAR to reach lower depths of 80 - 90m. The PAR (at surface) along 79^{o} E was highest at 10^{o} S (Northern side) and decreased southwards while high PAR was recorded at 13^{o} S and 73^{o} E. Similar trend was observed at

75m in the study area , where minimum PAR was recorded below 80 m depth in all the stations. During the study period (December-January), the cloud cover and frequent rain considerably reduced the total PAR at the surface during sampling time. The low PAR at the surface (average 0.1085 $\mu Ecm^{-2}s^{-1}$), affected the surface primary production at most of the stations (except at station 9). The PAR at surface varied from 0.02-0.205 $\mu Ecm^{-2}s^{-1}$ and at 80m depth, it varied from nil-0.013 $\mu Ecm^{-2}s^{-1}$.

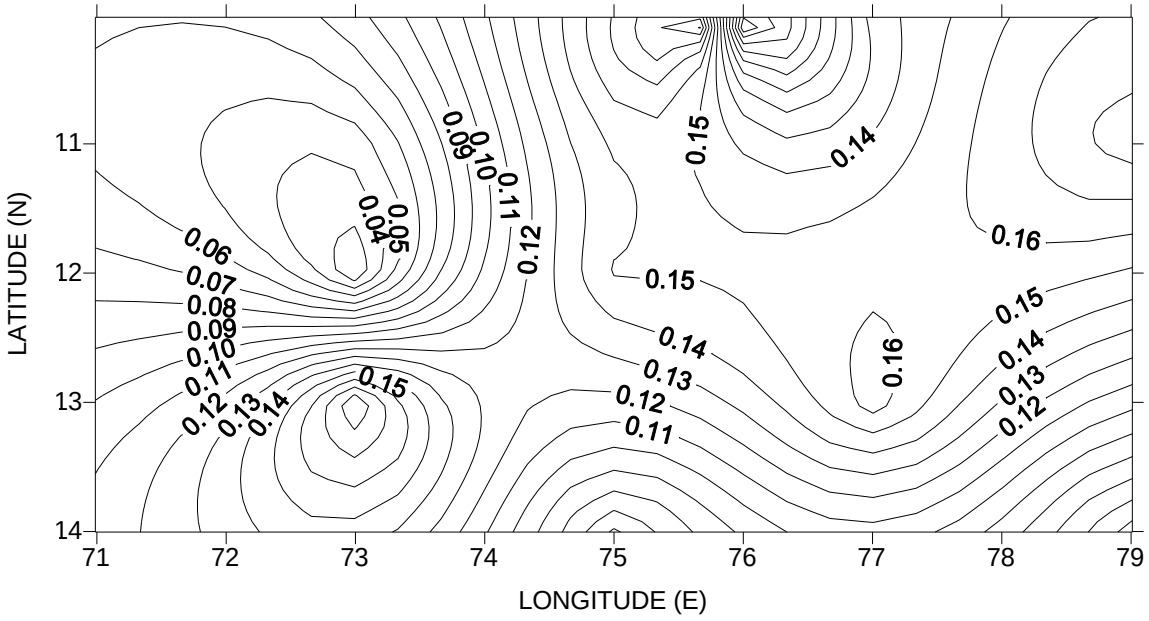

Fig. 5.2.1.1.1 a: PAR (μ E cm^{-2} s^{-1}) distribution at surface waters of Central Indian Ocean Basin

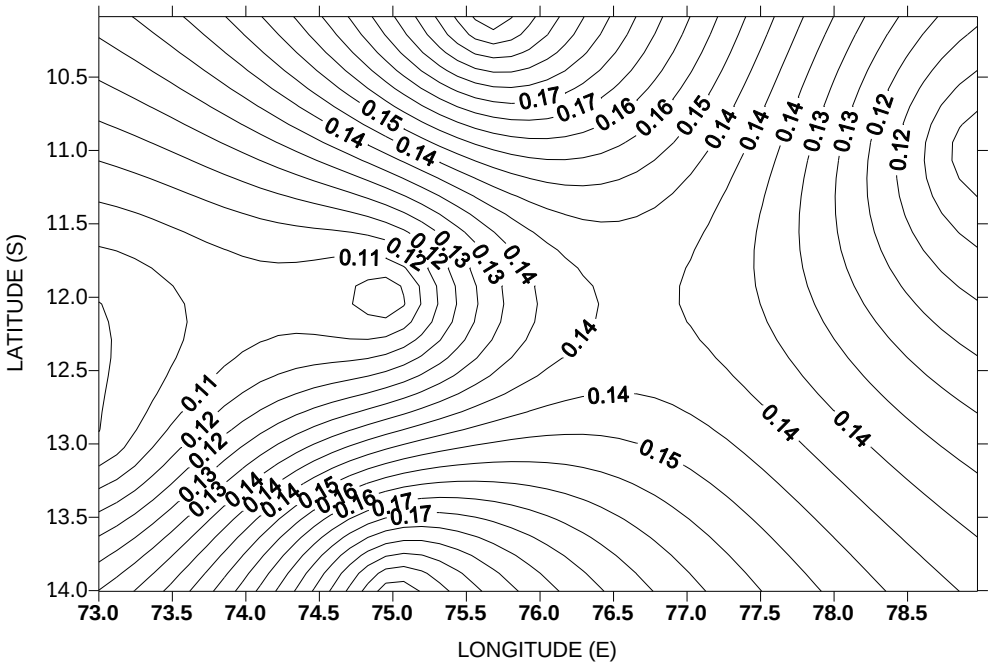

Fig. 5.2.1.1.1 b: PAR X 10^{-2} (μ E cm^{-2} s^{-1}) distribution at 70-80m depth in Central Indian Ocean Basin.

5.2.1.2 *Chlorophyll a* and primary production

Chlorophyll a was determined from surface to 150m at all the stations. The *chlorophyll a* concentrations were at low levels at all the stations in euphotic zone especially in mixed layer. Below the mixed layer**,** *chlorophyll a* increased to a maximum between 50-80m, where the concentration was 4 to 5 times higher than the surface concentration (Fig. 5.2.1.2.1). The *chlorophyll a* was detected down to 150m depth at most of the stations. The column *chlorophyll a* varied from 1.34 mg m^{-2} to 27.88 mg m^{-2} in the study area. The *chlorophyll a* maxima was invariably observed at 40-50m depth except at station13 where multiple maxima were observed, one at 35m depth and the other at 100m depth. The lowest *chlorophyll a* at surface was 0.043mgm^{-3} at station 3, which is at 79^{o} E and 11^{o} S latitude. The highest *chlorophyll a* at surface was 0.16 mgm^{-3} at station 18, which is at 75^{o} E and 11^{o} S latitude. The integrated *chlorophyll a* was highest at station 6 (27.8 mg m^{-2}) and lowest at station 20 (1.34 mg m^{-2}).

The data for simulated insitu primary production measured at daytime (12 hrs) is presented in Fig. 5.2.1.2.1. The surface productivity maximum was observed at most of the stations, except at station 9, where subsurface productivity maxima is noticed which coincided with subsurface *chlorophyll a* maxima. At station 3, station 11 and station 16, the secondary peak in the primary productivity coincided with *chlorophyll a* maxima at around 40-50m depth. The lowest primary productivity at surface was 0.12 mg C $m^{-3}d^{-1}$at station 9 and highest surface production was 9.72 mg C $m^{-3}d^{-1}$at station 6. The integrated column productivity varied from 9.06 mg C $m^{2}d^{-1}$ at station 9 to 103.4 mgC $m^{-2}d^{-1}$ at station14 in the study area, indicating a relatively high productivity around 10^{o} S and 75^{o} E. The high *chlorophyll a* at 75^{o} E and 12^{o} S latitude was found matching with high primary productivity and low *chlorophyll a* at 14^{o} S and 73^{o} E matched with low primary productivity in the same area (Fig. 5.2.1.2.2 a, b).

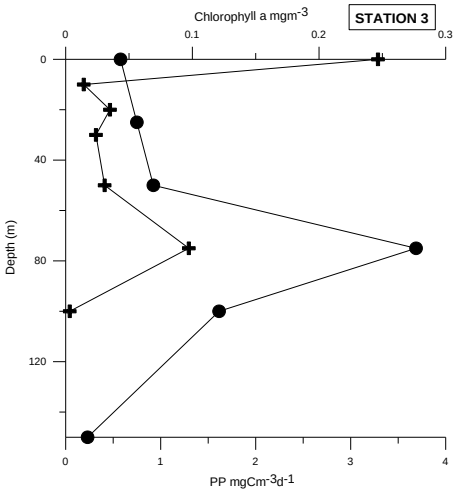
STATION 3
Chlorophyll a mgm-3
Depth (m)
PP mgCm-3d-1

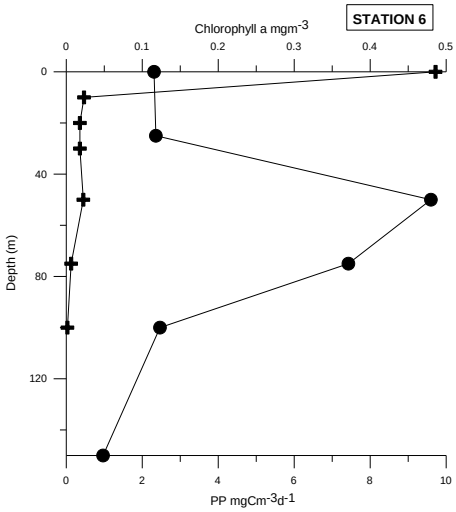
STATION 6
Chlorophyll a mgm-3
Depth (m)
PP mgCm-3d-1

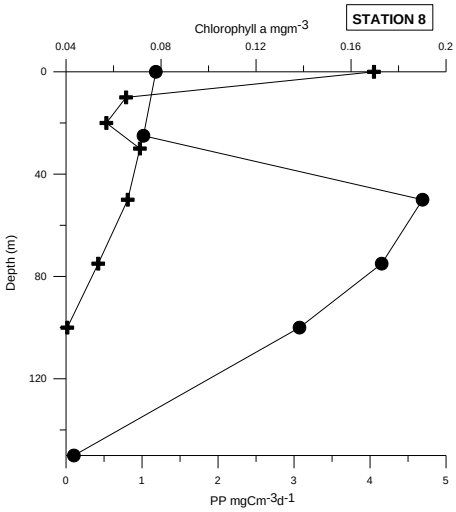
STATION 8
Chlorophyll a mgm-3
Depth (m)
PP mgCm-3d-1

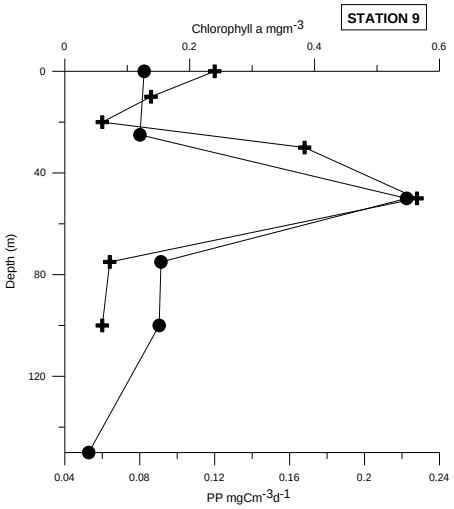
STATION 9
Chlorophyll a mgm-3
Depth (m)
PP mgCm-3d-1

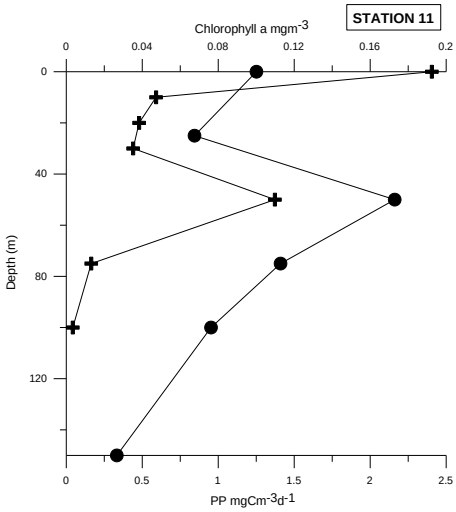
STATION 11
Chlorophyll a mgm-3
Depth (m)
PP mgCm-3d-1

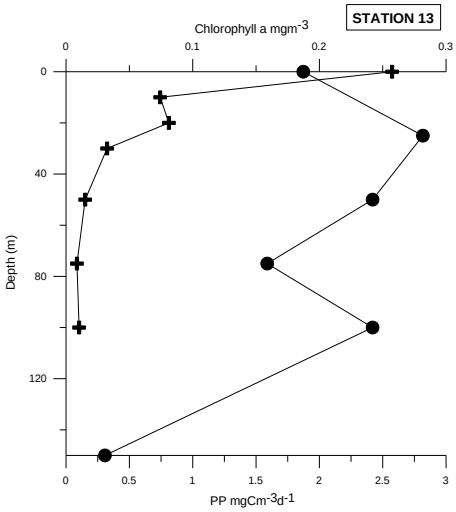
STATION 13
Chlorophyll a mgm-3
Depth (m)
PP mgCm-3d-1

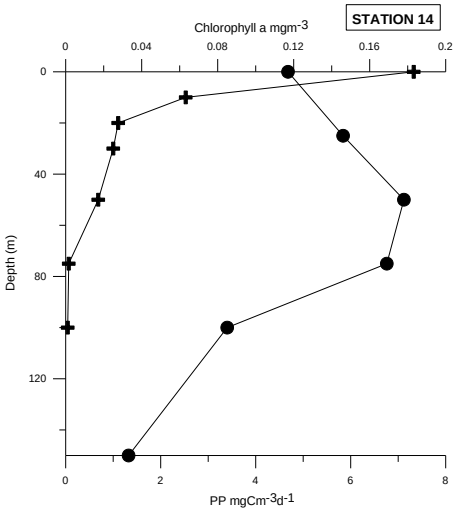
STATION 14
Chlorophyll a mgm-3
0
0.04
0.08
0.12
0.16
0.2
Depth (m)
0
40
80
120
0
2
4
6
8
PP mgCm-3d-1

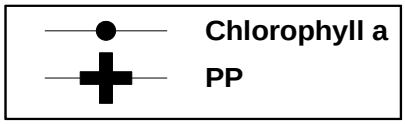
Chlorophyll a
PP

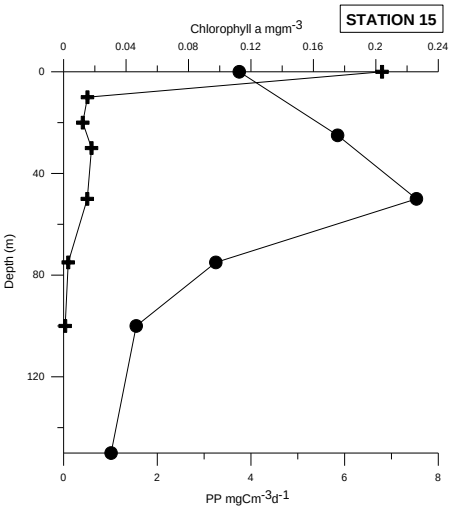
STATION 15
Chlorophyll a mgm-3
0
0.04
0.08
0.12
0.16
0.2
0.24
Depth (m)
0
40
80
120
0
2
4
6
8
PP mgCm-3d-1

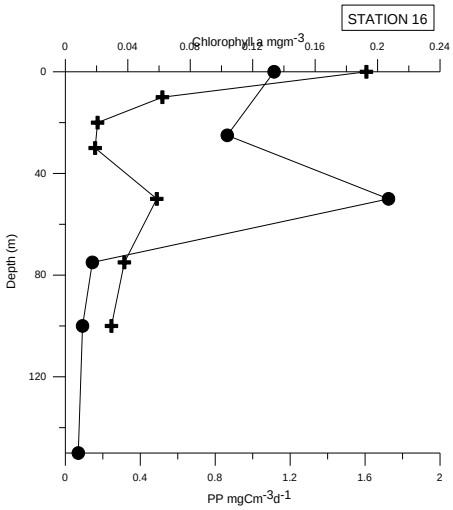
STATION 16
Chlorophyll a mgm-3
0
0.04
0.08
0.12
0.16
0.2
0.24
Depth (m)
0
40
80
120
0
0.4
0.8
1.2
1.6
2
PP mgCm-3d-1

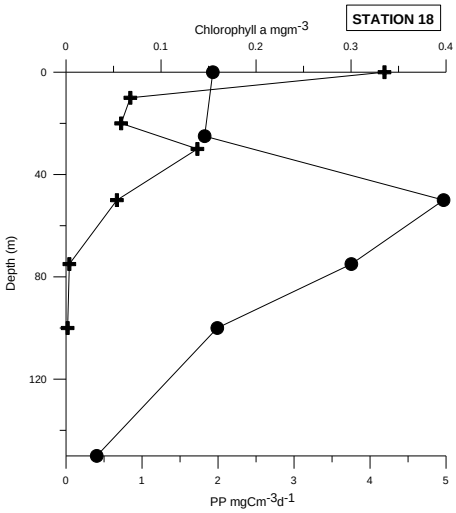
STATION 18
Chlorophyll a mgm-3
0
0.1
0.2
0.3
0.4
Depth (m)
0
40
80
120
0
1
2
3
4
5
PP mgCm-3d-1

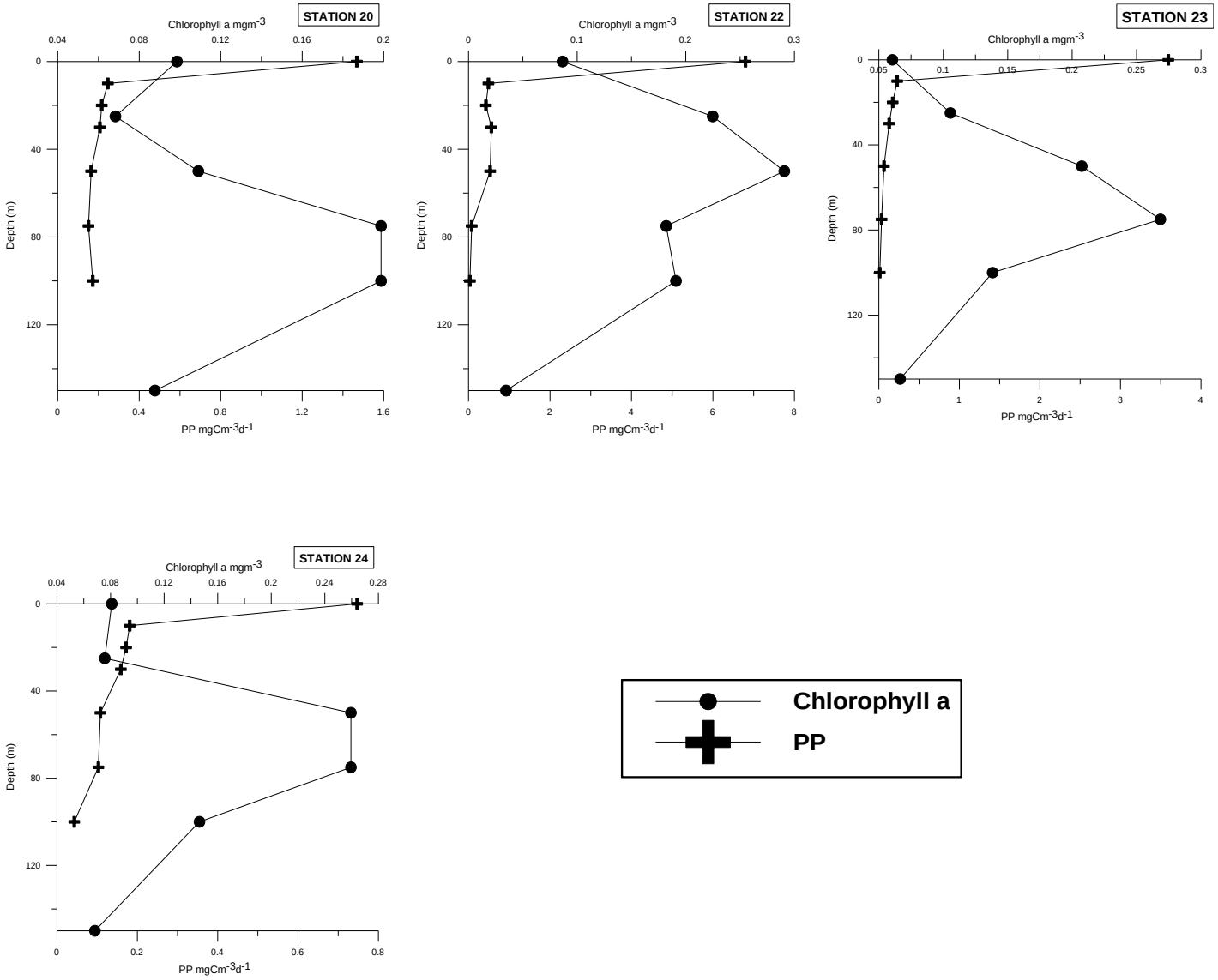

Fig. 5.2.1.2.1: *Chlorophyll a* (mgm^{-3}) and Primary productivity (mgCm^{-3}d^{-1}) distribution in Central Indian Ocean Basin.

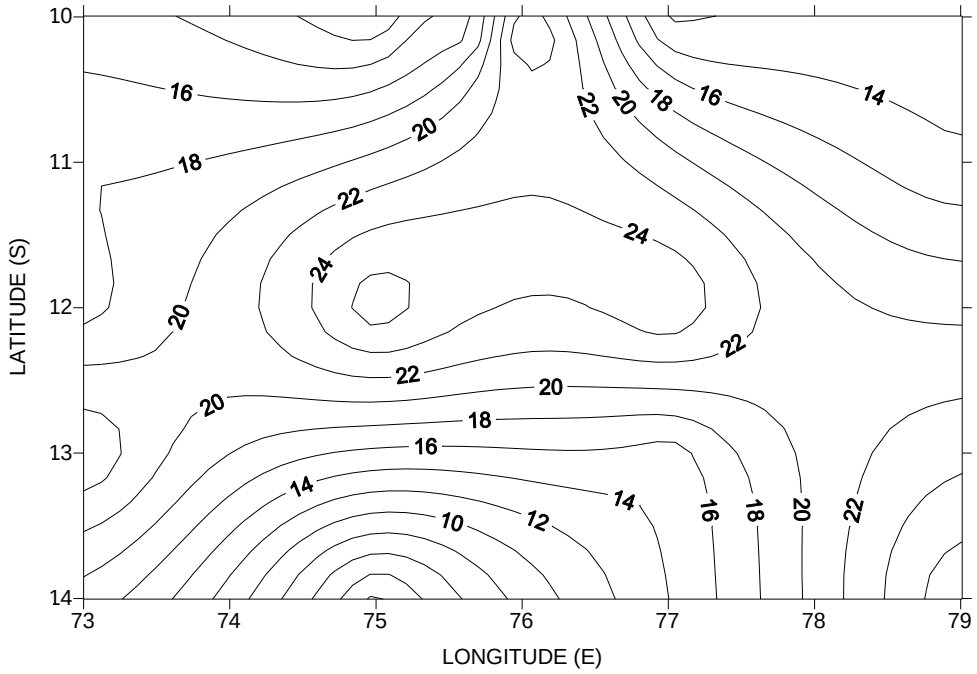

Fig. 5.2.1.2.2a: Column *chlorophyll a* (mgm^{-2}) distribution in Central Indian Ocean Basin.

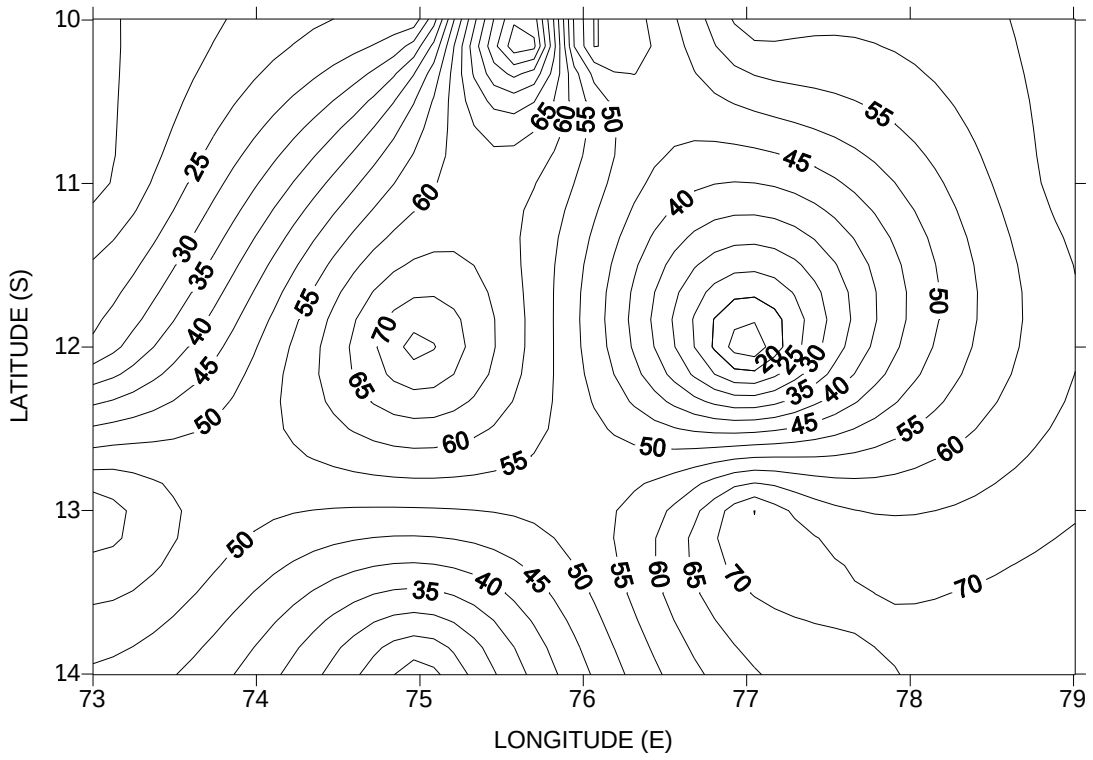

Fig. 5.2.1.2.2 b: Column Primary productivity (mgCm^{-3}d^{-1}) distribution in Central Indian Ocean Basin.

5.2.2 Phytoplankton

Diatoms and dinoflagellates were the main groups of organisms in the study area. The phytoplankton cell counts at surface were low, ranging from 0.12 to 1.18 x 10^4/l, where diatoms dominated the population. The high phytoplankton counts were seen in the areas east of 75° E longitude in northern part of the area and decreased in southern part. The phytoplankton distribution to the west of 75° E latitude had an opposite trend where counts were higher in the southern stations. The pattern of phytoplankton distribution remained same at surface, 25m and 75m depth in all the stations indicating homogeneity of the area. The population of phytoplankton at surface belonged to Coscinodiscus spp. Ceratium spp., Fragilaria spp. and Surirella spp. Taxonomic similarity was observed at surface, 25m and 75m water depths (Fig. 5.2.2.1, 5.2.2.2; 5.2.2.3) Lowest phytoplankton counts were recorded at station 18, which was 0.1674 x 10^4/l and highest counts at station 10 of the order of 1.4 x10^4/l of cells. The counts at 25m depth were higher than surface counts and supported by relatively high *chlorophyll a*values. At depth of 25m the Navicula spp., Rhizosolenia spp. and Thalassiothrix spp. were dominating the population. The phytoplankton cell counts at 75m depth were also high compared to surface counts and ranged from 0.06 x 10^4/l at station 24 to 1.5 x 10^4/l at station 3 and station 8, where *chlorophyll a* was also high. The dominant taxa at 75m depth were Chaetoceros spp., Fragilaria spp. and Nitzschia spp.

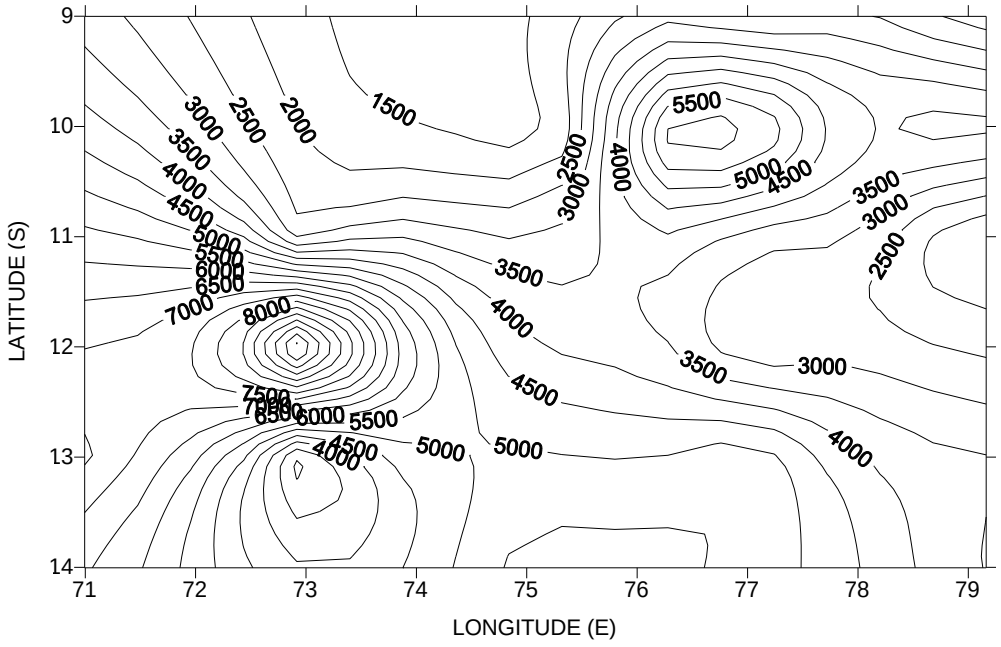

Fig. 5.2.2.1: Total phytoplankton counts (Cell nos.l^{-1}) distribution in the surface waters of Central Indian Ocean.

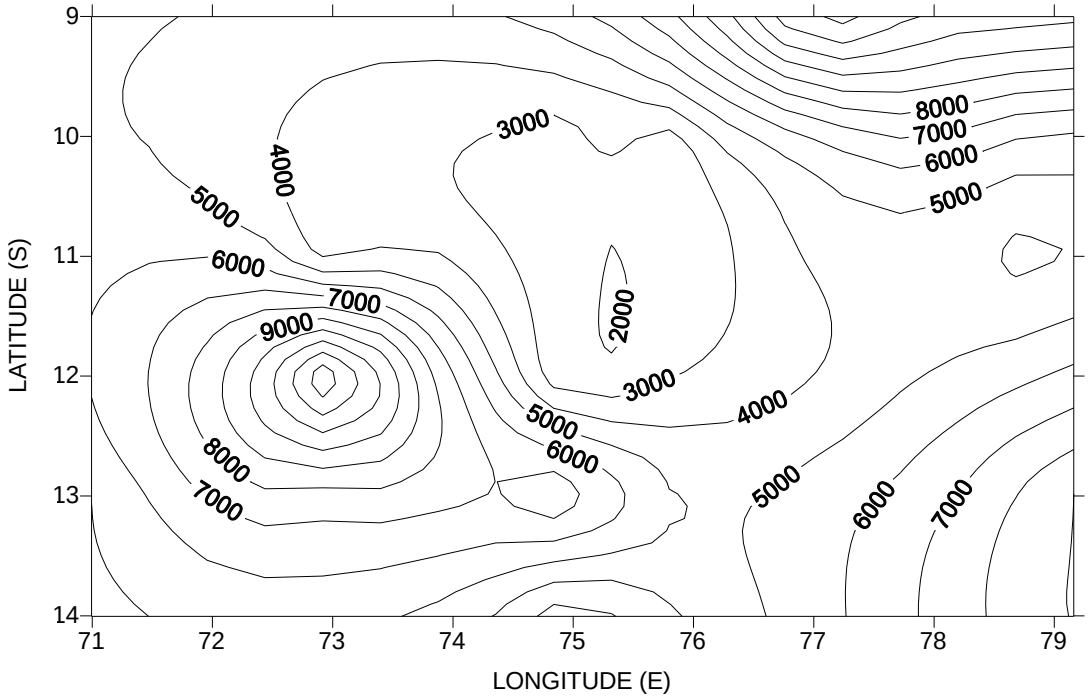

Fig. 5.2.2.2: Total phytoplankton counts (Cell nos.l^{-1}) distribution at 25 m depth in Central Indian Ocean.

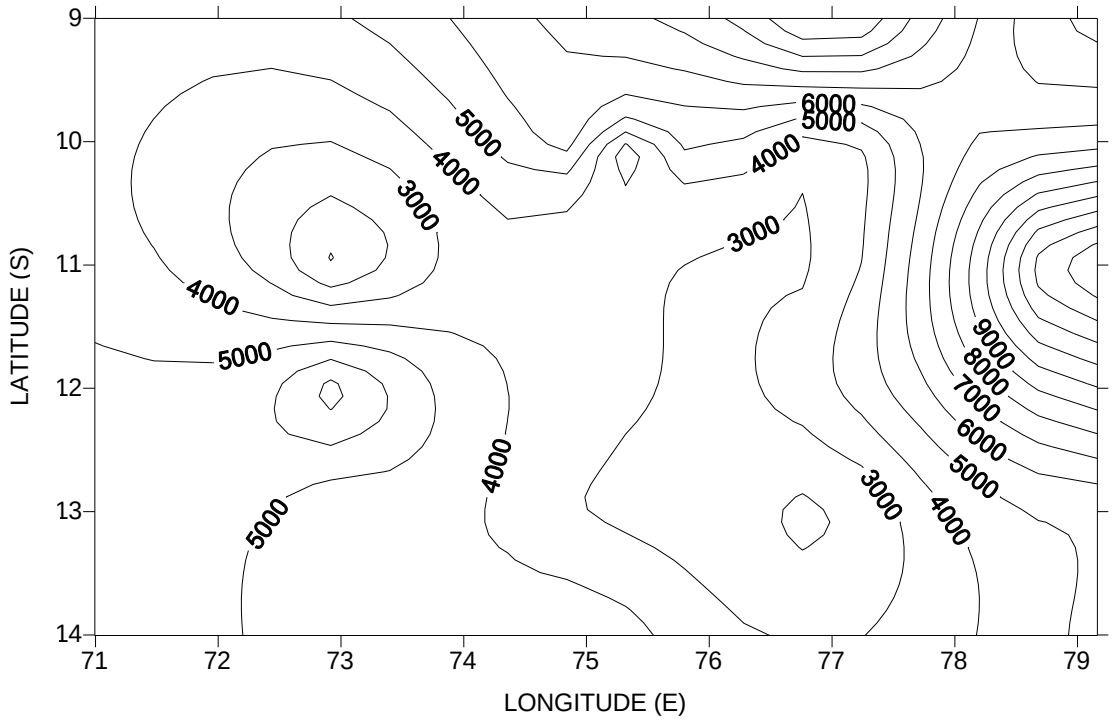

Fig. 5.2.2.3: Total phytoplankton counts (Cell nos.l^{-1}) distribution at 75 m depth in Central Indian Ocean.

5.2.3 Zooplankton

The zooplankton biomass in study area is presented in Fig. 5.2.3.1. In the isothermal layer (0-40m) the biomass ranged from 0.25 to 67ml/100m^3 and in thermocline layer (40 – 250m) from 2-23 ml/100m^3. Below the thermocline zooplankton biomass was 14ml/100m^3. The deeper layers of water, i.e. 300-500m and 500-1000m, were supporting low standing stocks of secondary producers, such as 0-3ml/100m^3 and 0-2.4 ml/100m^3 respectively. The study area has a rich and varied assemblage of zooplankton organisms with a total of 32 groups. Maximum abundance was at station 9 (92426 numbers/100 m^3) followed by station 15 (92373 numbers/100 m^3), the least at station 16 (710/100 m^3). At station 13, the high biomass 10ml/100m^3 mainly constituted of siphonophores.

The dominant groups of zooplankton in the study area were copepods (88%), cheatognaths (4.7%), ostracods (1.1%), decapod larvae (1.0%), amphipods (1%), molluscs (0.9%), euphausids (0.7%), fish larvae (0.3%) and fish eggs (0.2%). The remaining groups were widely distributed but low in abundance. Among the most dominant Copepod fauna, Calanus sp. constituted the bulk of population followed by Eucalanussp, Calocalanussp, Clausocalanussp, Pluromama sp. in the order of abundance. Decapod larvae were mostly of the deep sea Caridian prawn and most of the fish larvae were of Myctophids, Gonostomids, Trichunids, Scombrids and Carangids. Among the different water layers sampled, the upper mixed layer (0-50m) supported all the dominant groups and their percentage composition with respect to the lower layers sampled were Copepod (81%), Chaetognaths (72%), Ostracods (50%), euphasids (69%), amphipods (80%), and gastropods (73%), fish larvae (70%) and Fish eggs (56%). Below the mixed layer, the thermocline layer supported group-wise assemblages with similar trend in biomass concentrations. Copepod distribution at 0-50 m and 50-200 m is shown in Fig. 5.2.3.2 and 5.2.3.3.

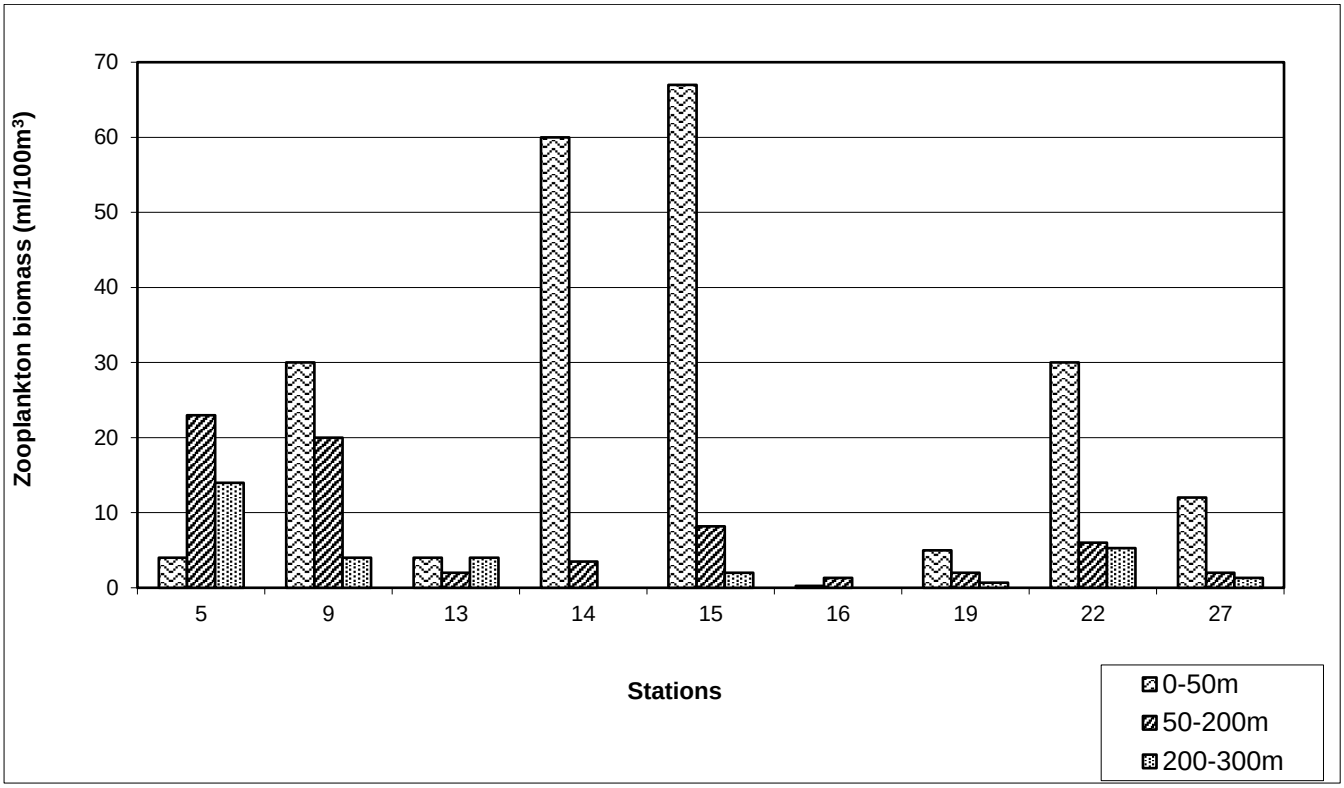

Fig. 5.2.3.1: Zooplankton biomass at 0-50, 50-200 and 200-300 m depth in the Central Indian Ocean Basin.

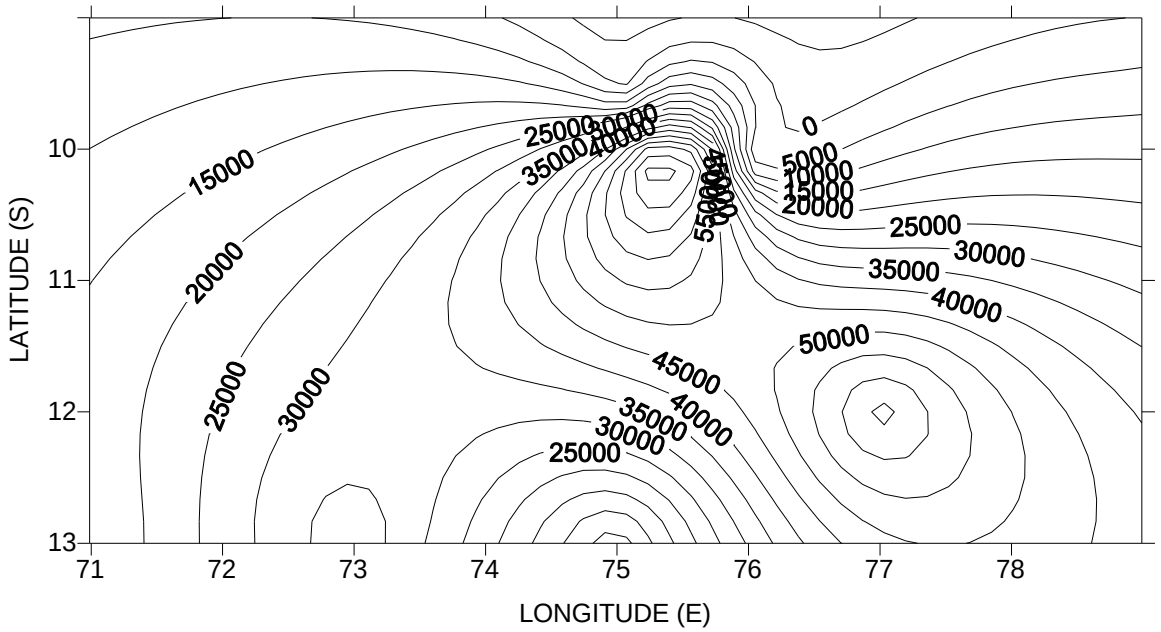

Fig. 5.2.3.2: Copepod distribution at 0-50m depth in Central Indian Ocean Basin.

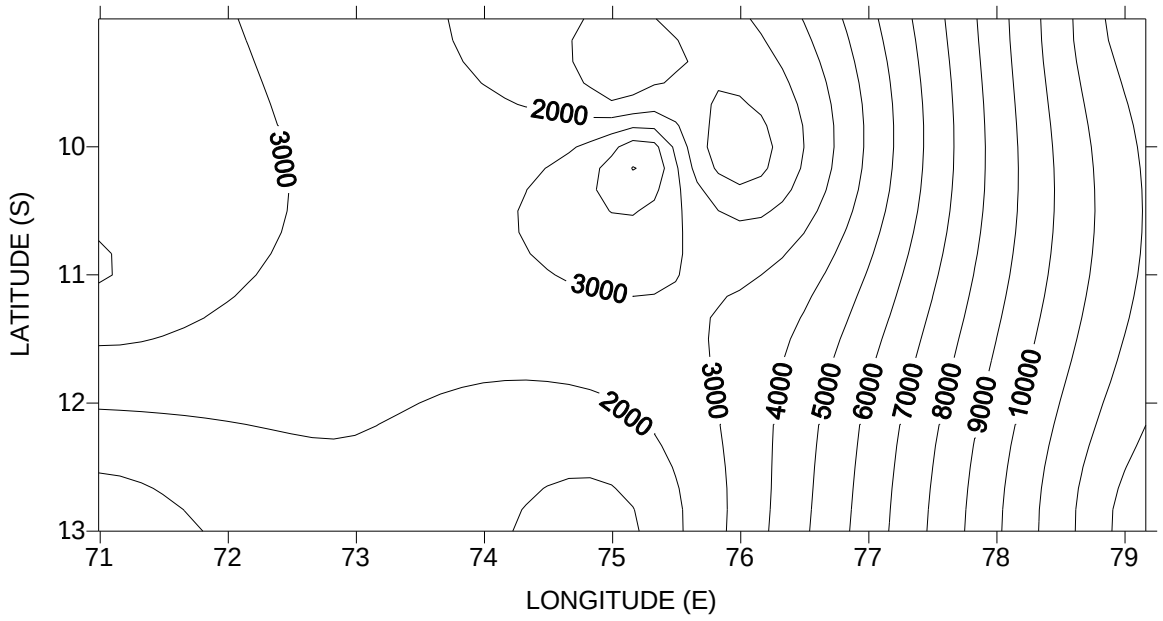

Fig. 5.2.3.3: Copepod distribution at 50-200m depth in Central Indian Ocean Basin.

5.2.4 Inter-relationship between surface biological parameters

As expected in the oligotrophic tropical and sub-tropical oceanic waters, the values for *chlorophyll a* were low. The average surface *chlorophyll a* (0.078 mg m^{-3}) and the average integrated value through the water column (17.75mgm^{-2}) are comparable with the value reported from the similar environments in the Pacific Ocean (El-Sayed and Taguchi, 1979; Malone 1971; Holmes 1961). The vertical distribution of *chlorophyll a* at most of the stations

occupied in CIOB was characterized by the presence of sub-surface maxima. It is well known that chlorophyll maxima occur over most of the tropical and subtropical waters of the world ocean (Eppley et al., 1973). It appears that deep *chlorophyll a* maxima is one of the features of the CIOB environment, which can be monitored during mining operation in the area. It is seen that there isspatial variability in the depth of *chlorophyll a* maxima layer, which is located either at 50m depth or at 80m depth. At station 13, *chlorophyll a*maxima was at 20m and 90m depth. The *chlorophyll a* maxima layer thus occurred at top of the pycnocline or middle of the pycnocline.

Interestingly, the phytoplankton cell counts also show a sub-surface maxima above and in the pycnocline. These *chlorophyll a* maxima correspond to 10 to 15% of surface light level during the study period. The depth of the chlorophyll maxima layer was also found to be closely associated with the distribution of nutricline, especially that of NO_3-N. In an earlier study from the tropical Pacific, *chlorophyll a* was equally low 0.06-0.17mgm^{-3} at surface and 10-20mg m^{-2} in column (El-Sayed and Taguchi, 1979), where the *chlorophyll a* maxima was located at 24-84m and depended on nutricline specially nitrate nitrogen. As reported from study of NE Pacific Ocean, the major factor in the maintenance of the *chlorophyll a* maxima layer in higher latitude is insitu rates of the photosynthesis (Jamart et al., 1977).

The primary productivity of the CIOB is very low, average being 51.23mg C m^{-2}d^{-1}. It is similar to the range of earlier reported value for CIOB (Kery, 1973; Krey and Babenerd, 1976) and from tropical pacific region (El-Sayed and Taguchi, 1979). Holmes (1961) and Ryther (1969) reported the productivity values of 150 mg C m^{-2}d^{-1} for deep sea region. Similarly, the column *chlorophyll a* rarely exceeded 25 mgm^{-2} and the maxima was located between 50-150m depth. El-Sayed and Taguchi (1979) and Malone (1971) reported primary productivity less than 10 mg C m^{-2}d^{-1}and *chlorophyll a* 9.8-21.0 mg m^{-2} for equatorial Pacific. In CIOB however, the patchiness in the phytoplankton cells were observed on 12^{o} S and 72-73^{o} E coinciding with pattern of *chlorophyll a* and primary production (Matondkar et al., 2000). The cell counts at 75m depth were lower than cell counts at surface and 25m depth.

Diatoms were most important groups of organisms and this shows that cell number at the surface, 25m and 75m sample was nearly equal, although productivity rates were considerably low in the sub-surface waters. Allen (1961) reported the presence of the coccolithophorids, dinoflagellates and diatoms in the Pacific Basin. Hasle (1959) also found Chaetoceros, Rhizosolenia and Nitzschia were important diatoms and Peridinium and Ceratium among dinoflagellates. The presence of similar phytoplankton taxa in CIOB confirms that the species found here are of typical deep ocean tropical environment type.

According to Holmes (1961),the zooplankton biomass in equatorial Pacific were low and ranged from 75 – 150ml/1000m^3 having significant of geographical variations. Thus, overall productivity of open ocean system at level of phytoplankton and zooplankton is low in CIOB. In the Central Pacific, Fryxell et al. (1979) reported equal importance of diatoms, coccolithophorids and dinoflagellates which were present in similar numerical density. In euphotic zone, however coccolithophorids were negligible in CIOB region. A spatial variation in the integrated value of the Fe in first 100m water column studied in CIOB was noticed. At station 8 the low concentration of Fe (154.74µg m^{-2}) was found affecting the primary productivity rates, which was 76.26 mg C $m^{-2}d^{-1}$ in euphotic zone. However, at station 14 the high content of column Fe (562.75µg m^{-2}) was found responsible to enhance the primary productivity rates (103.4mg C $m^{-2}d^{-1}$) in CIOB region (Matondkar et al., 2000). Since CIOB is totally isolated from the main land and therefore the source of Fe is only dust coming from islands or land masses around the Indian Ocean. Iron is generally required for the growth of the phytoplankton. Recently it is seen that externally added iron to the surface waters, stimulates the growth of phytoplankton in Southern Ocean indicating the role of iron as a phytoplankton growth-limiting factor.

5.3 Midwater fauna

As no major impacts in the midwater sections of the water column are expected due to the activity in the area, midwater fauna (zooplankton, mesopelagic, bathypelagic fish etc) have not been specifically studied in the area. We are also not aware of studies from other contractors or from literature highlighting the likely impacts on these during mining operations. In any case, our proposed activity is restricted to the seafloor and no impact is expected to any communities in this zone.

5.4 Benthic communities

The deep-sea floor contains a wide array of habitats such as sediment-covered slopes and plains, rocky mid-ocean ridges and seamounts, and island-like chemoautotrophic communities ranging from hydrothermal vents to whale falls. Communities in many of these habitats are likely to be very susceptible to anthropogenic disturbance due to low rates of productivity, growth, colonization, and delicate habitat structure. The benthic ecosystem of the abyssal depth is like a desert deprived of local primary production and is considered as food limited environment. Consequently the organisms living in abyssal habitats have to depend on supply of particulate organic matter (POM) from the surface waters.

5.4.1 Megafauna

In this study, the megafauna have been identified from underwater photographs. Photographic data of the deep-sea floor was collected using a specially developed photography system mounted on a frame and towed behind the ship, called as the deep towed system. Several transects with the deep towed system were conducted in the entire Indian area (Fig. 5.4.1.1) during which ~50,000 seafloor photographs were obtained. Out of these, ~300 images that showed the presence of megafauna (0.6% f the total photographs) were evaluated for this study. Megafauna were classified by using standard reference material available from literature as well as internet. In the study, a total of 8 Classes were identified and the most dominant among the megafauna was found to be the Holothurian constituting followed by the Hexactinellida, Actinopterygii, Asteroidea, Ascidiacea, Crustacean, Anthozoa and Xenophyophores respectively. The most dominant among the megafauna was Holothuria (63%) followed by Hexactinellida (19%), Actinopterygii (3%), Asteroidea (5%) and the Ascidiacea (2%), Crustacean (1%), Xenophyophores (2%) and Anthozoa (1%). The most dominant among the holothurians was the Benthodytes sp (21%), followed by Psychropotes sp. (20%), Peniagone sp. (4%), Mesothuria sp. (3%) and Enypiastes sp., Oneirophanta sp. and Psychronates sp. (1%). Hyalonema sp. constituted 12% followed by Euplectella constituting the 3% of the total Hexactinellida found in the study area. Of the total Actinopterygii, Typhlonus sp. constituted 2% and Bathysaurus sp. 1%. Hyphalaster sp. constituted 2% and Freyella sp. 1% of the total of the class Asteroidea in the present study area (Fig. 5.4.1.2).

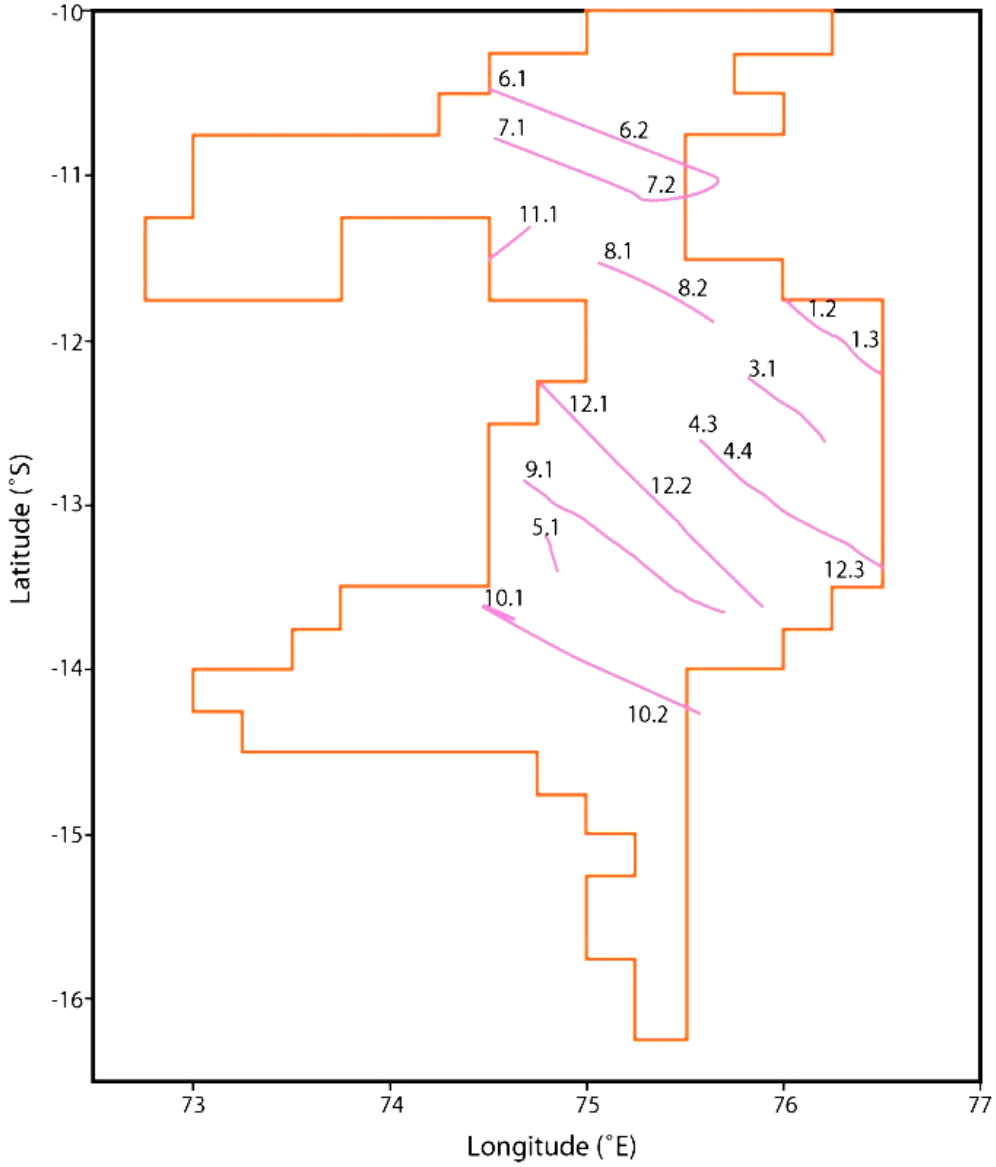

Fig. 5.4.1.1: Deep-tow photographic transects in CIOB

Faunal abundance assessed from the photographic data ranged from 22-103 no.100m^{-2} (49 ± 25SD). The least number of organisms were found at line number 3.1 (22 no.100m^{-2}) and the highest number of organisms were found at line number 12.3 (103 no.100m^{-2}) (Fig. 5.4.1.3). There is no significant variation in megabenthic density latitudinally (Fig.5.4.1.4). However, there is a slight increase in faunal abundance with increasing longitude though the increase is not very significant (Fig. 5.4.1.5).

The "S" value signifies the different groups that are present (Fig. 5.4.1.6), line number 12.3 has the most number of groups (11) followed by 12.2(10). The least number of groups (2) are found at line numbers 1.2 and 3.1. The abundance of species (N) is found to be highest at line number12.3 (103 no.100m^{-2}) and the least at line number 3.1 (22 no.100m^{-2}) as described earlier. The species richness (d) was found to be the least at line number 1.2 (0.2) and highest at line number 12.3 (Fig. 5.4.1.7). The evenness (J') of distribution of fauna is found to be

almost significant in all the line numbers respectively. The species diversity (H') was found to be highest at line number 12.3 (2.3) followed by 12.2 (2.2).

A distribution map (Fig. 5.4.1.8, 5.4.1.9) is plotted with respect to the latitude and longitude of the given area. It is observed that the holothurians are evenly distributed in the area and Benthodytes sp. are the most dominant among them followed by Psychropotessp., the other genus such as Peniagonesp., Mesothuriasp., Enypiastes sp. and Psychronates sp. are scarcely distributed over the area. Representative of all megafaunal groups identified are shown in Fig. 5.4.1.10 a & b. The fauna here is evenly distributed in which the Typhlonus sp. shows the highest density followed by the genus such as Hyalonemasp., Euplectella sp., Typhlonus sp. Bathysaurus sp. Hyphalaster sp. Freyella sp., Stannophyllum sp., Ascidacea, Decapoda, and Actinaria are scarcely distributed over the area.

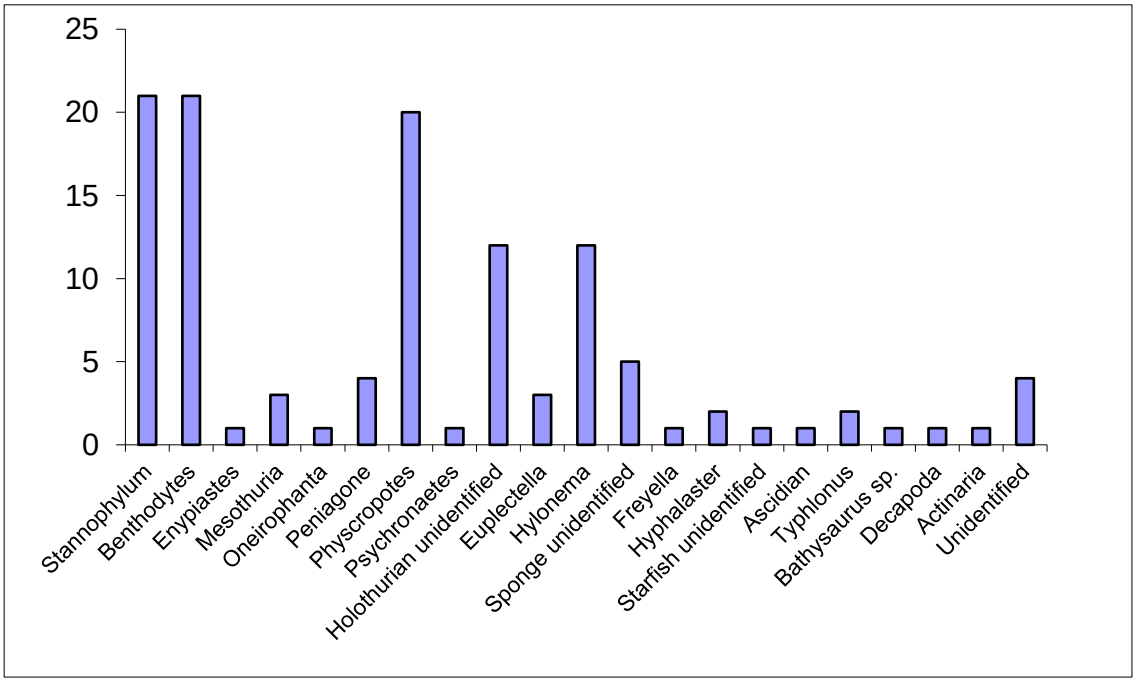

Fig. 5.4.1.2: Variation in density (no/100m^2) of megafauna

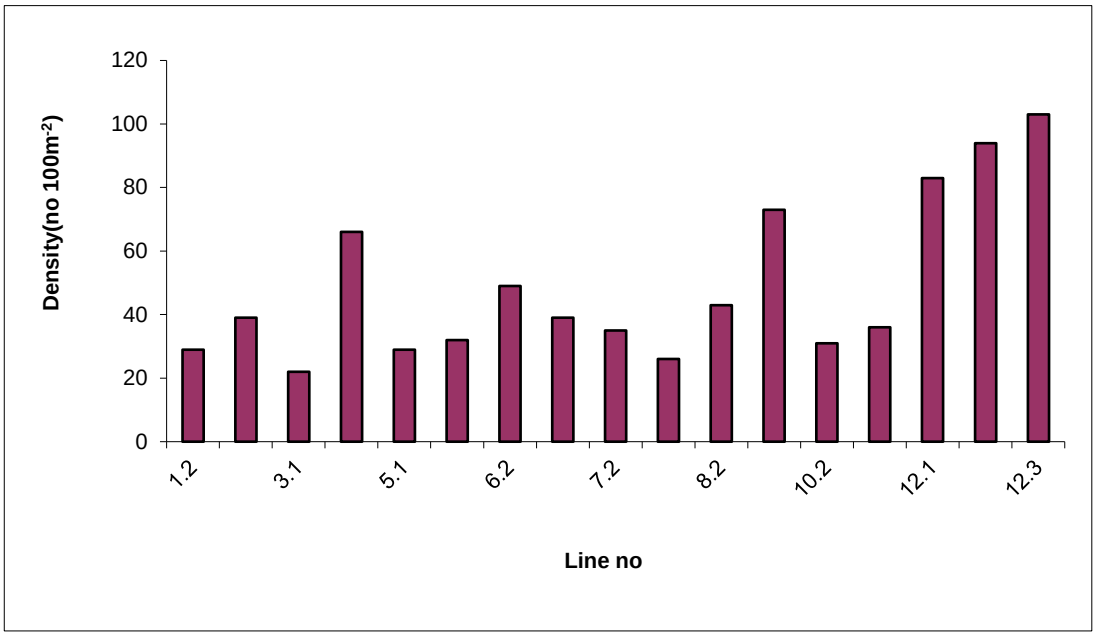

Fig. 5.4.1.3: Variation in density of Megafauna along different transects

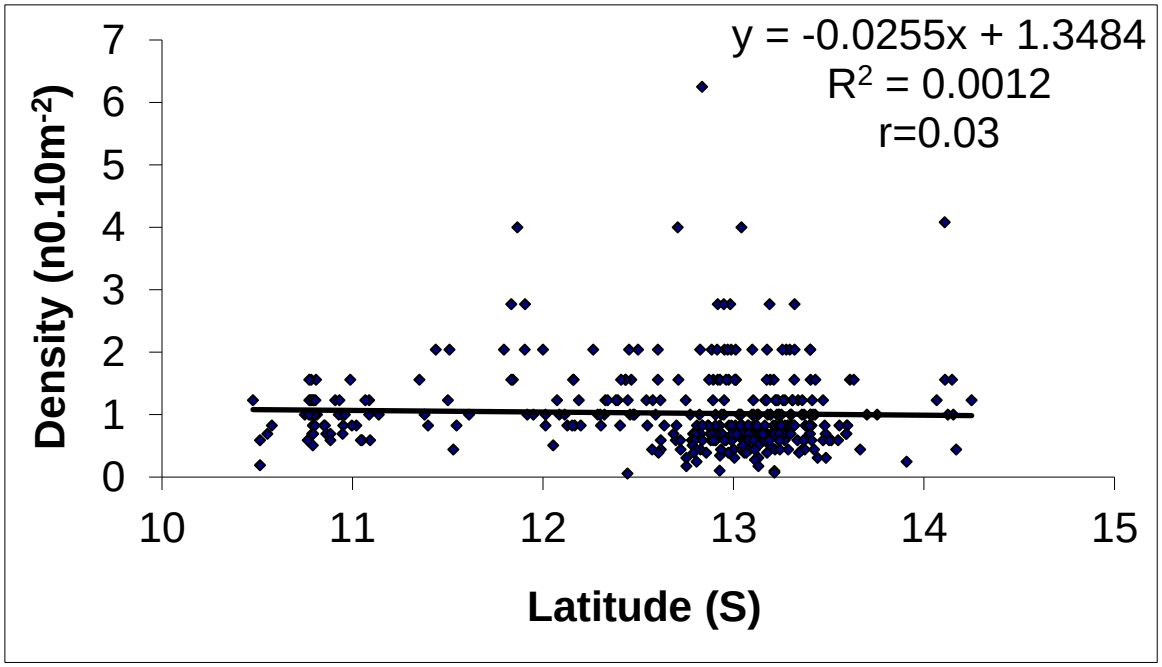

Fig. 5.4.1.4: Correlation between latitude and density of megabenthos.

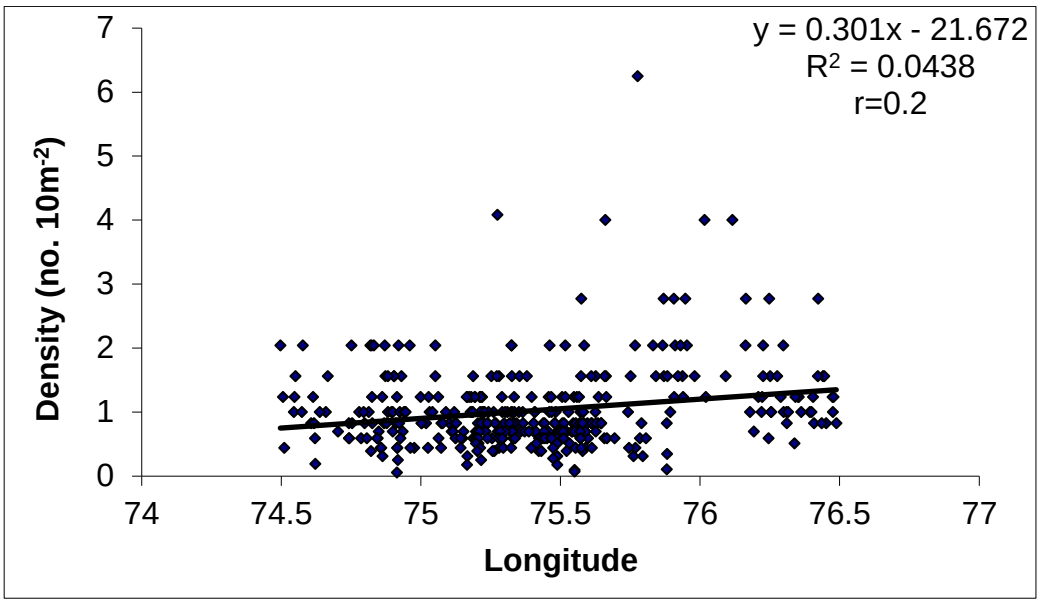

Fig. 5.4.1.5: Correlation between longitude and density of megabenthos.

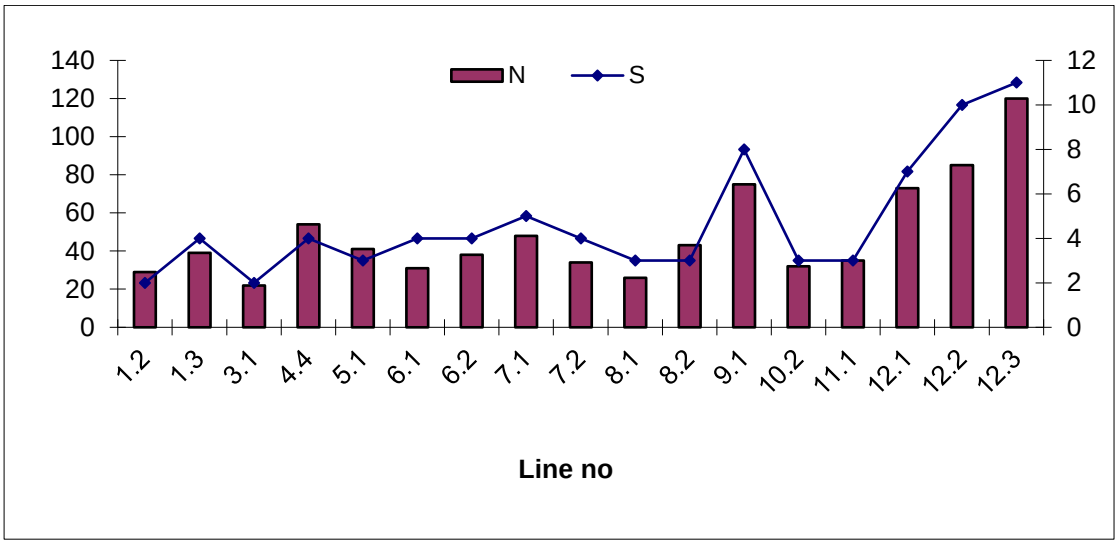

Fig. 5.4.1.6: Variation in megabenthic density (N) and number of species (S).

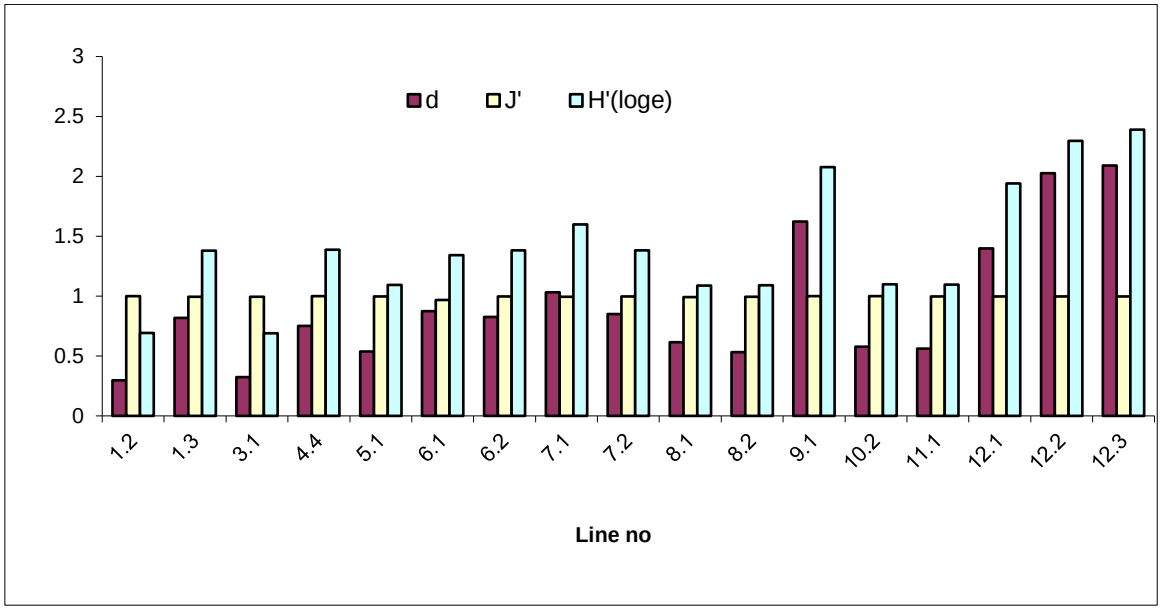

Fig. 5.4.1.7: Diversity of megafauna in the study area

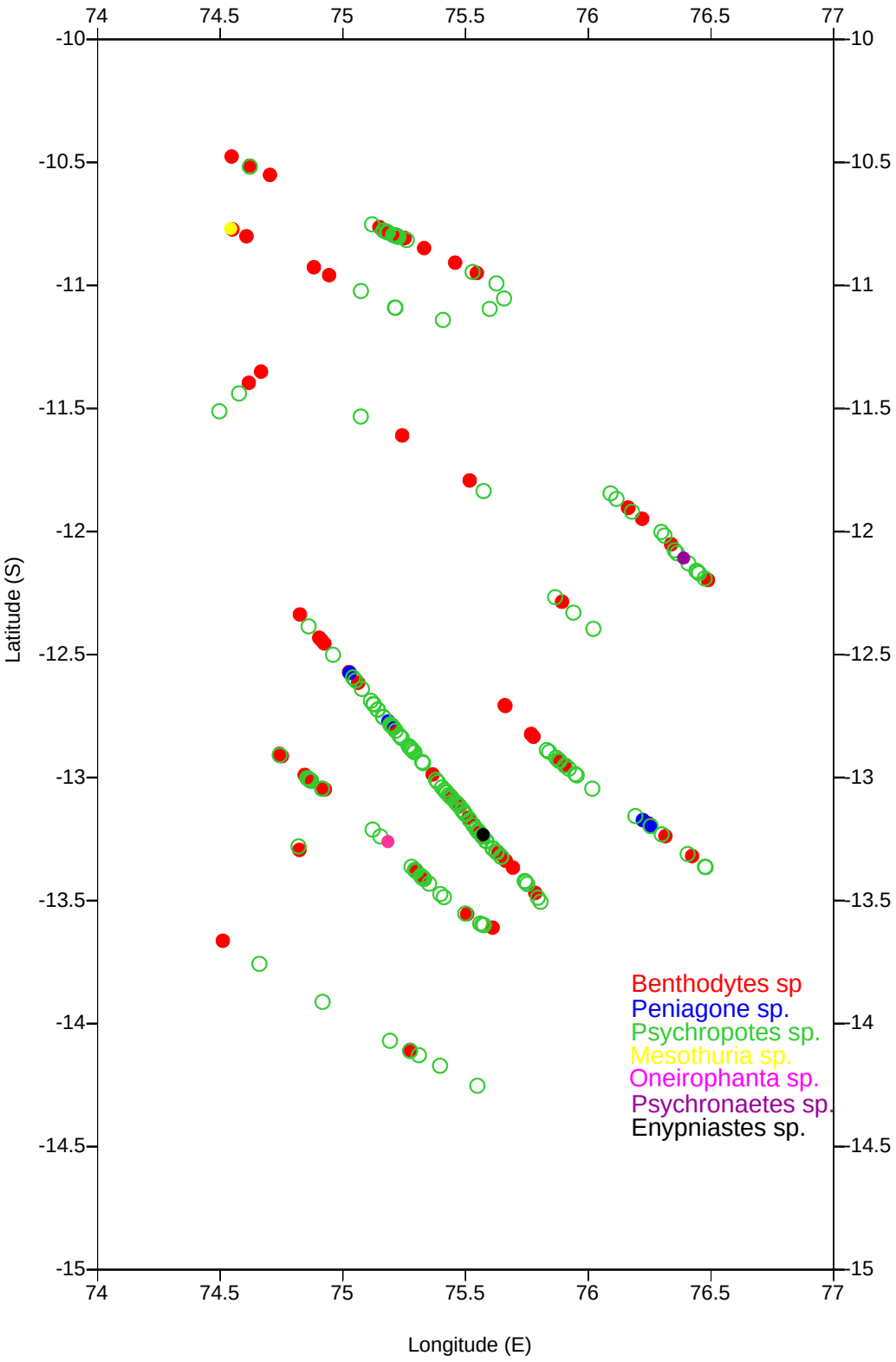

Fig. 5.4.1.8: Distribution of Class Holothuroidea in the study area.

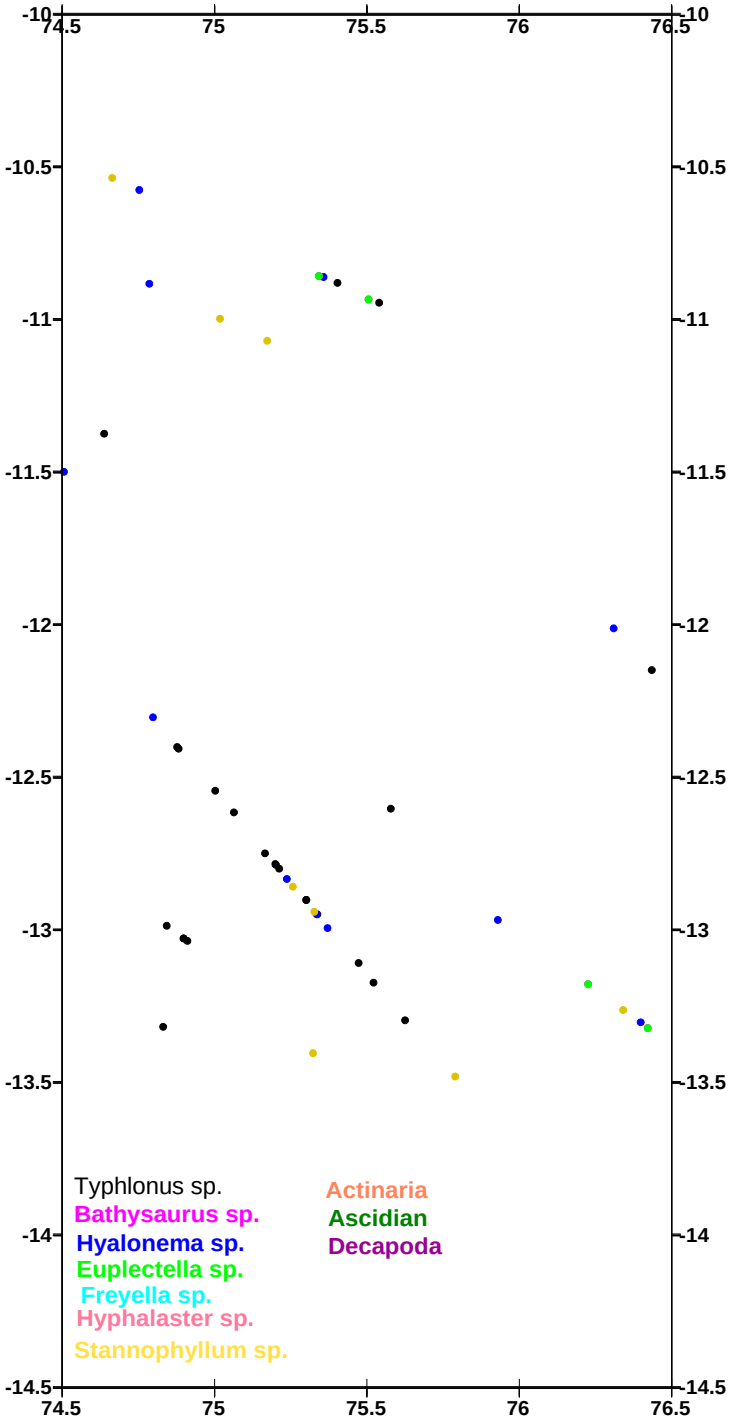

Fig. 5.4.1.9: Distribution of megabenthic taxa other than holothurians.

Fig. 5.4.1.10 a: Representative of megafauna caught in the grab samples (Hyalonema sp; Ophiura sp., Malpodonia sp., Hymenaster sp)

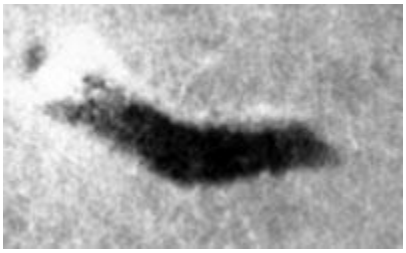

Stannophyllumsp

Euplectellasp.

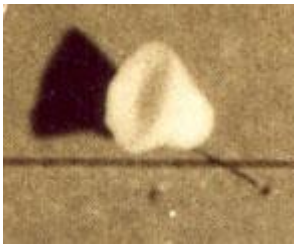

Hylonemasp

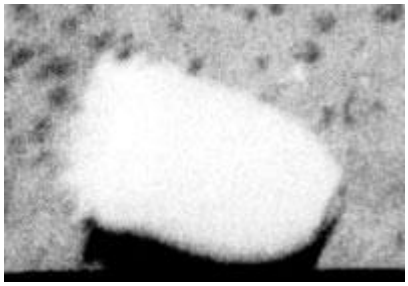

Actinaria

Benthodytessp

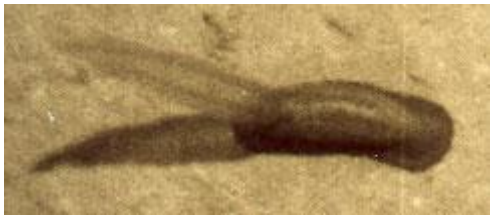

Psycropotessp

Psyronaetessp

Oneirophanta sp.

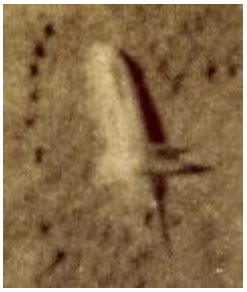

Peniagonesp

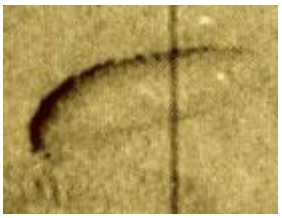

Mesothuriasp

Hyphalastersp.

Tunicates

Typhlonussp.

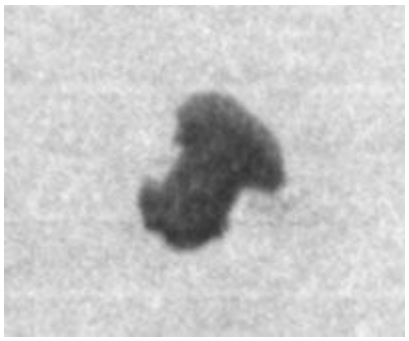

Enypiastessp

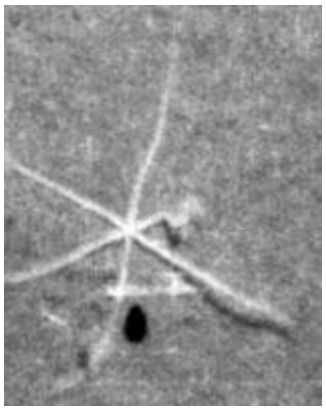

Freyellasp.

Decapoda

Bathysaurussp

Fig. 5.4.1.10 b: Representative pictures of Megafauna

5.4.2 Macrofauna

5.4.2.1 Composition

Macrofauna were evaluated from box core samples as well as quadrants in the box cores. A total of 11 major macrofaunal groups were observed in the CIOB (Fig. 5.4.2.1.1). Polychaete and Tanaidacea (26%) dominated in the faunal abundance followed by nematode (11%), harpacticoid (7%). Each group of sarcomastigophora, bivalve, ostracod, nemertina, isopod, larvae and unidentified were represented in the remaining 30% of the core sample. A total of 12 groups of macrofauna were identified in the quadrant samples (Fig. 5.4.2.1.2), of which polychaetes exhibit the highest abundance of 37% followed by nematode (21%), isopod (11%), tanaidacea (8%). Amphipod, bivalve, cyprid larvae, gastropod, glass sponge, halacarid, harpacticoid and unidentified larvae comprised 23% of the total fauna.

The dominant taxa of polychaeta comprise 10 families in the quadrant and core sample of CIOB (Fig. 5.4.2.1.3). They were as follows: Ampharetidae, Ariciidae, Eunicidae, Euphrosinidae, Flabelligeridae, Glyceridae, Maldanidae, Sebellidae, Spionidae, Syllidae. Core sample possess only four families but quadrant sample exhibit 10 families. Moreover these four families of Flabelligeridae, Ampharetidae, Ariciidae, and Syllidae were common and abundant in both the samples. The highest polychaete diversity was noticed in the longitude of 75.5 to 76.5°E.

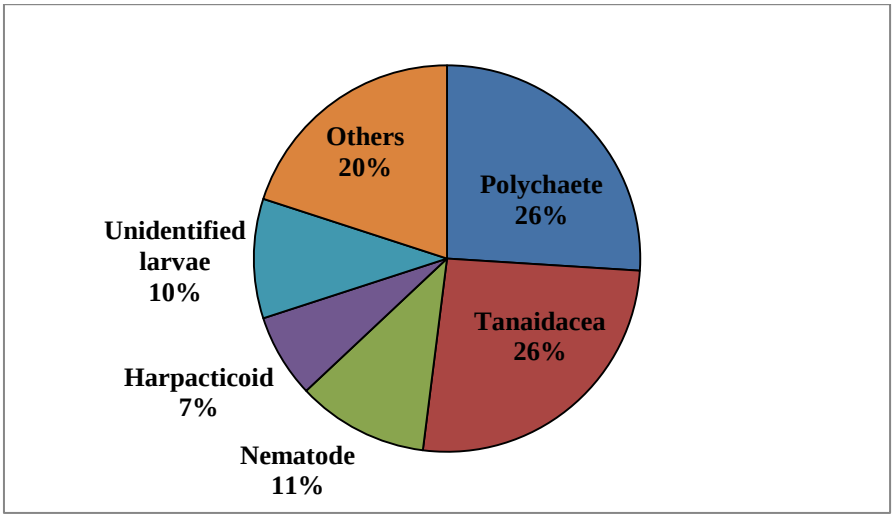

Fig. 5.4.2.1.1: Composition (%) of macrofauna in the core sample

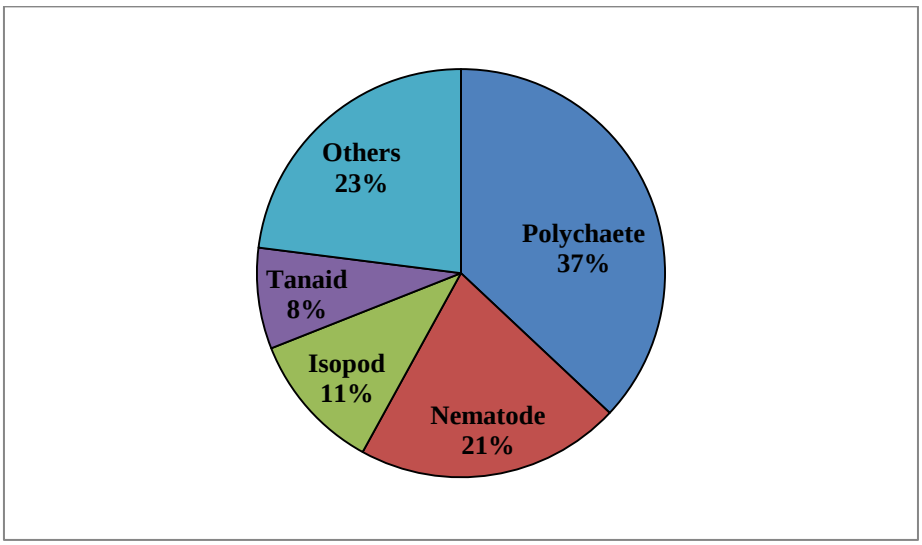

Fig. 5.4.2.1.2: Composition (%) of macrofauna in the quadrant sample

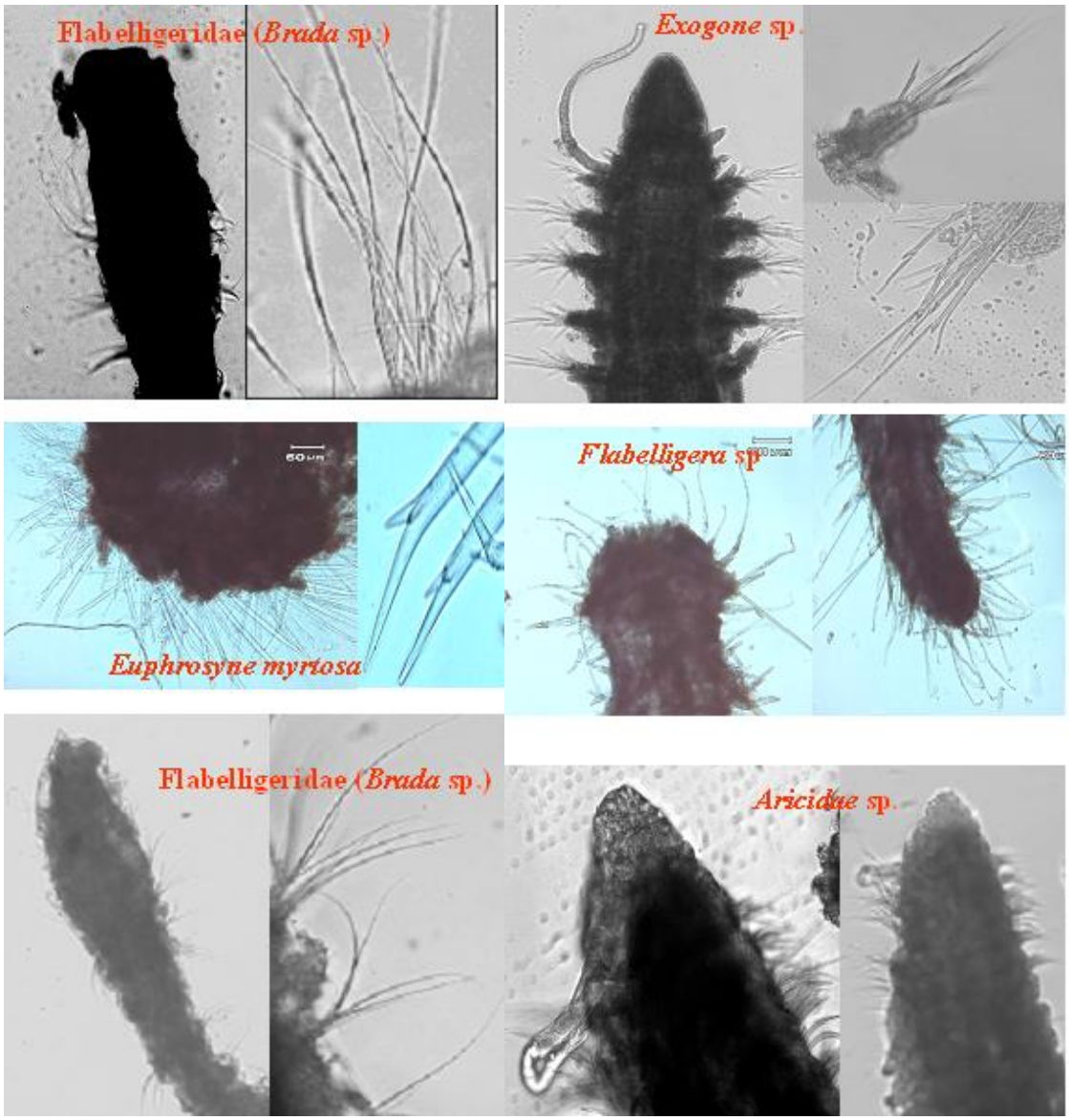

Fig. 5.4.2.1.3: Examples of macrofauna in the quadrant sample

5.4.2.2 Abundance

The abundance of macrofauna varied from 81 to 405 no. m^{-2} in a length of 40 cm core sample, whereas in the quadrant samples down to 15 cm, the average density ranged from 22 to 132 no. m^{-2} (mean: 55 no. $m^{-2} \pm 37$, n=25). Top core section of 0 to 5 cm contains 25.92% of the total macrofauna. The highest density was recorded at station BC-6 (132 no. m^{-2}) and lowest at station BC-24 (22 no. m^{-2}) (Fig. 5.4.2.2.1).The density data of macofauna suggests patchy distribution in the study area (Fig. 5.4.2.2.2). As compared to the Pacific and Atlantic Ocean, the Central Indian Ocean has low abundance of macrofauna (Veillette et al., 2007a, b; Ingole, 2003; Ingole and Koslow, 2005; Pavitran et al., 2009).

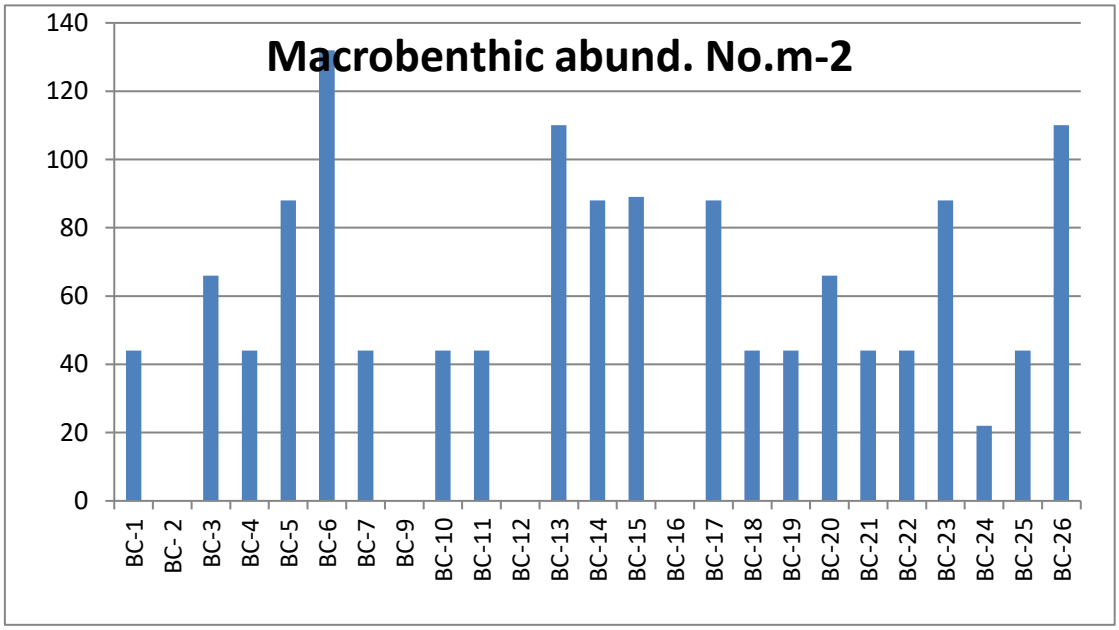

Fig. 5.4.2.2.1: Abundance of macrofauna (no. m^{-2}) in core samples.

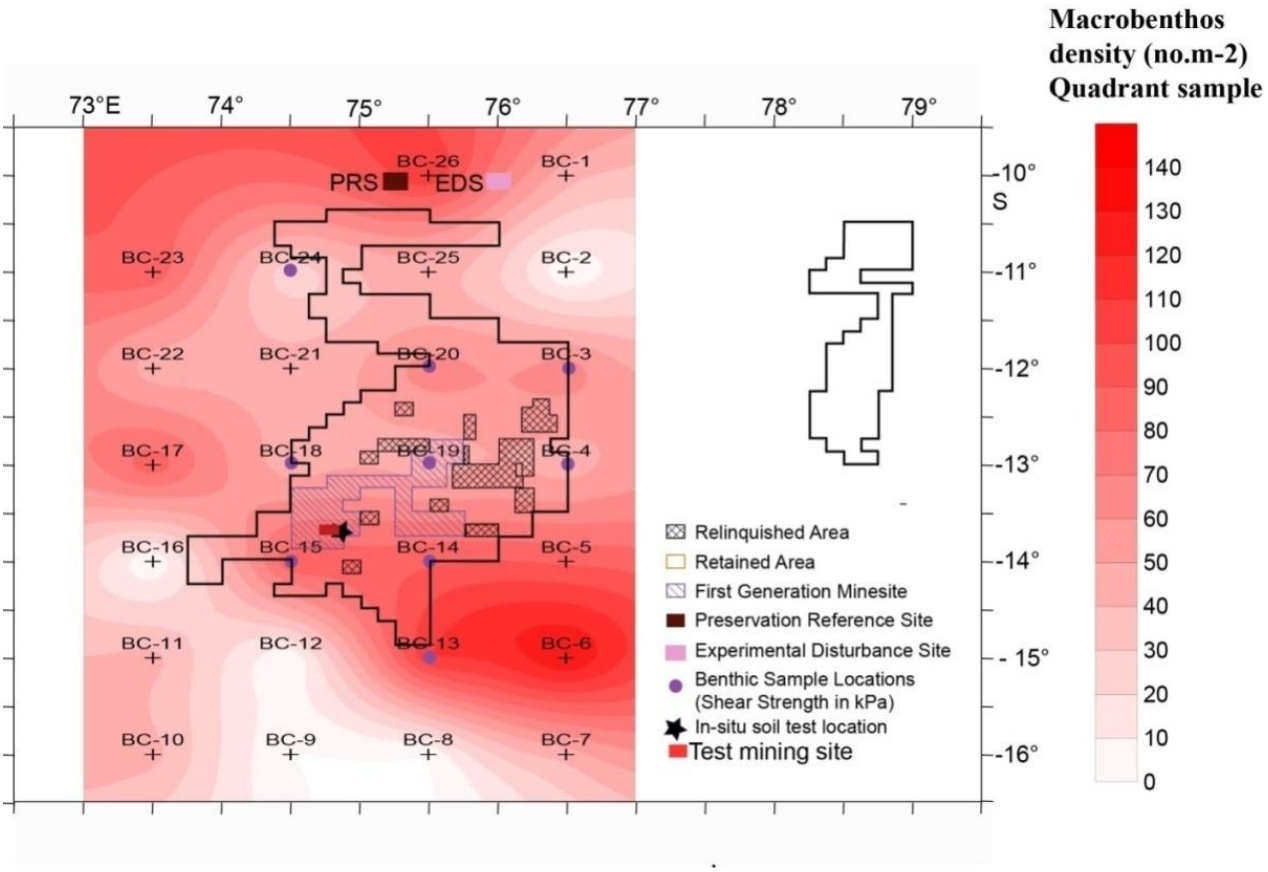

Fig. 5.4.2.2.2.: Distribution of macrofauna

5.4.2.3 Vertical distribution

Core samples were sectioned into 5cm interval to study the faunal distribution in the different depth intervals (Fig. 5.4.2.3.1). Vertically, the fauna was dominated in the 5-10cm section (41%) followed by the top section of 0-5cm (26%) of the total fauna. The third level of faunal abundance (18.52%) noticed at 10 to 15 cm section. The remaining down core of 15 to 40 cm showed their abundance steadiness of 4% of macrofauna in each interval of 5cm.

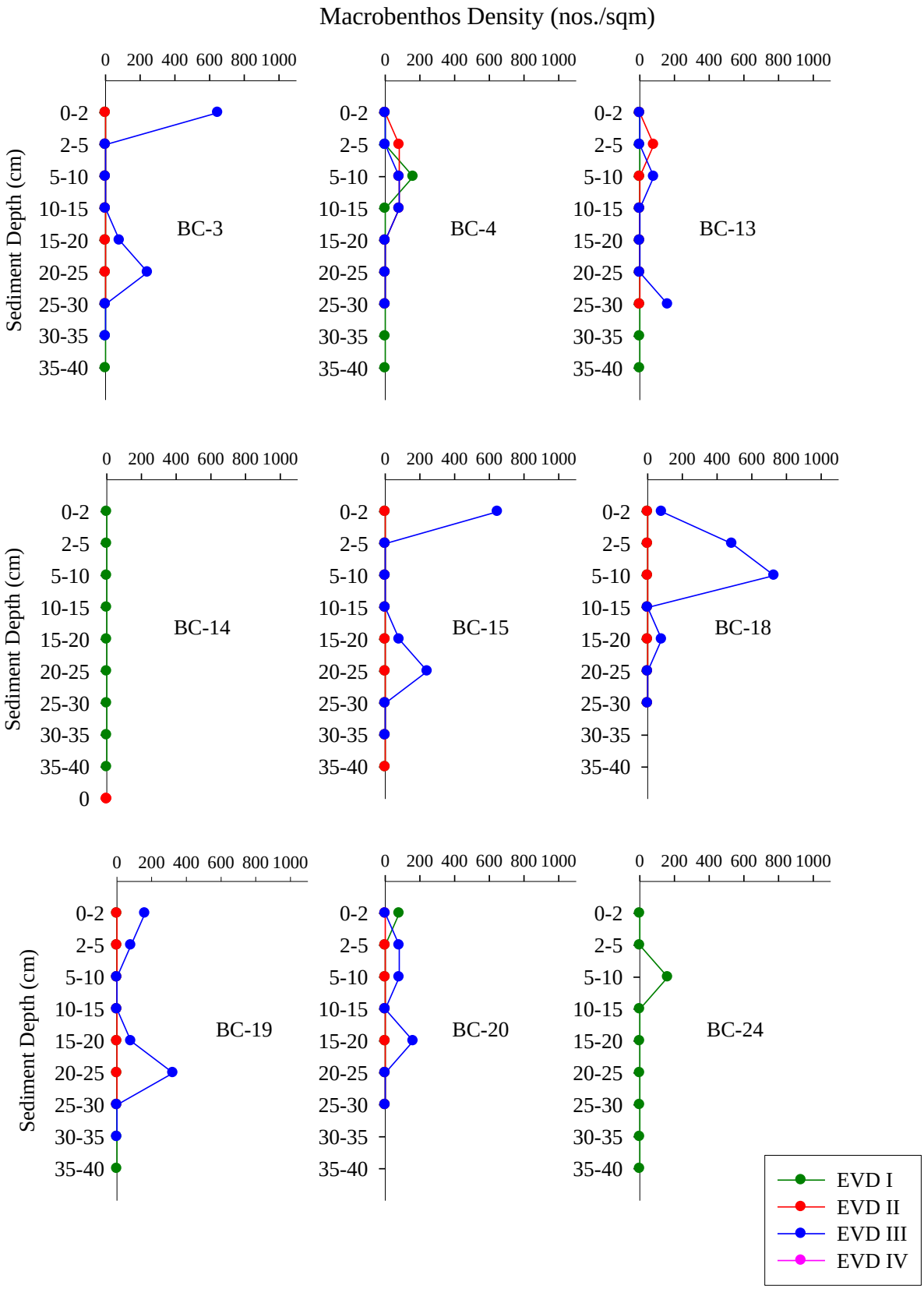

Fig 5.4.2.3.1: Vertical distribution of Macrofauna density (no.m-^{2})

5.4.3 Meiofauna

5.4.3.1 Composition

Meiofauna comprised of 9 groups (Fig. 5.4.3.1.1). Nematode was the dominant group (46%), followed by Ostracoda (15%), Halacarida (14%), Harpacticoida (11%), Turbellaria (9%), Crinoid (2%), nauplii (2%) and Tardigrada and Nemertina with 0.3% each. The dominant taxa of nematode were commonly present from top to deeper core depth (35cm) of entire sample. Out of 9 taxa, five taxa nematode, ostracod, halacarida, harpacticoida and turbellaria were abundantly present in top 10cm the core section.

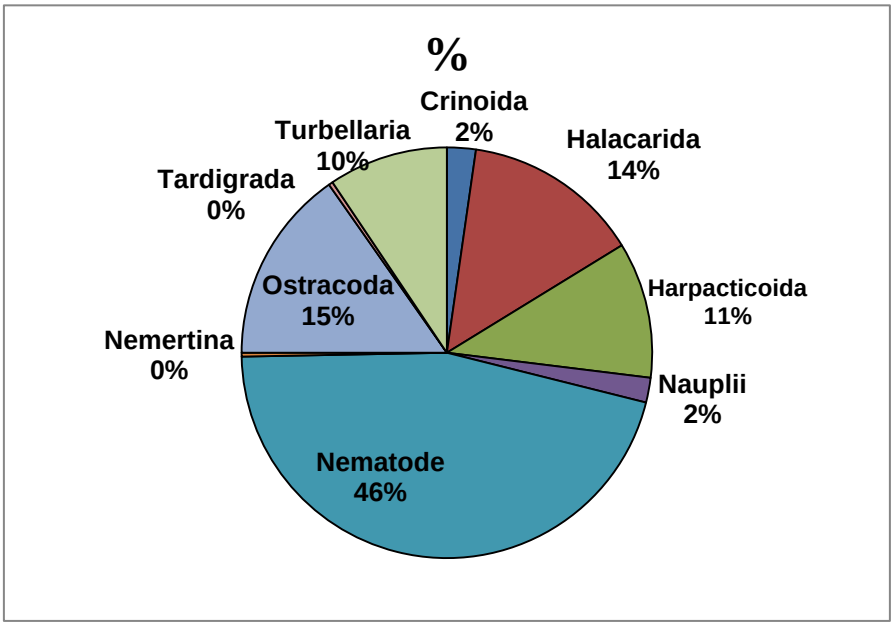

Fig. 5.4.3.1.1: Composition (%) of meiofauna in the core samples

5.4.3.2 Abundance

The average density of meiofauna varied from 12 no. $10cm^{-2} \pm 5$, n=26 in a length of 35cm core sample (Fig. 5.4.3.2.1). Spatial variability the maximum density was noticed in stations BC-22 (28 no. $10cm^{-2}$) and lowest in the station BC-4, 26 (3 no. $10cm^{-2}$). Further, least amount of meiofauna distributed in the 74.5°E longitude covered stations.

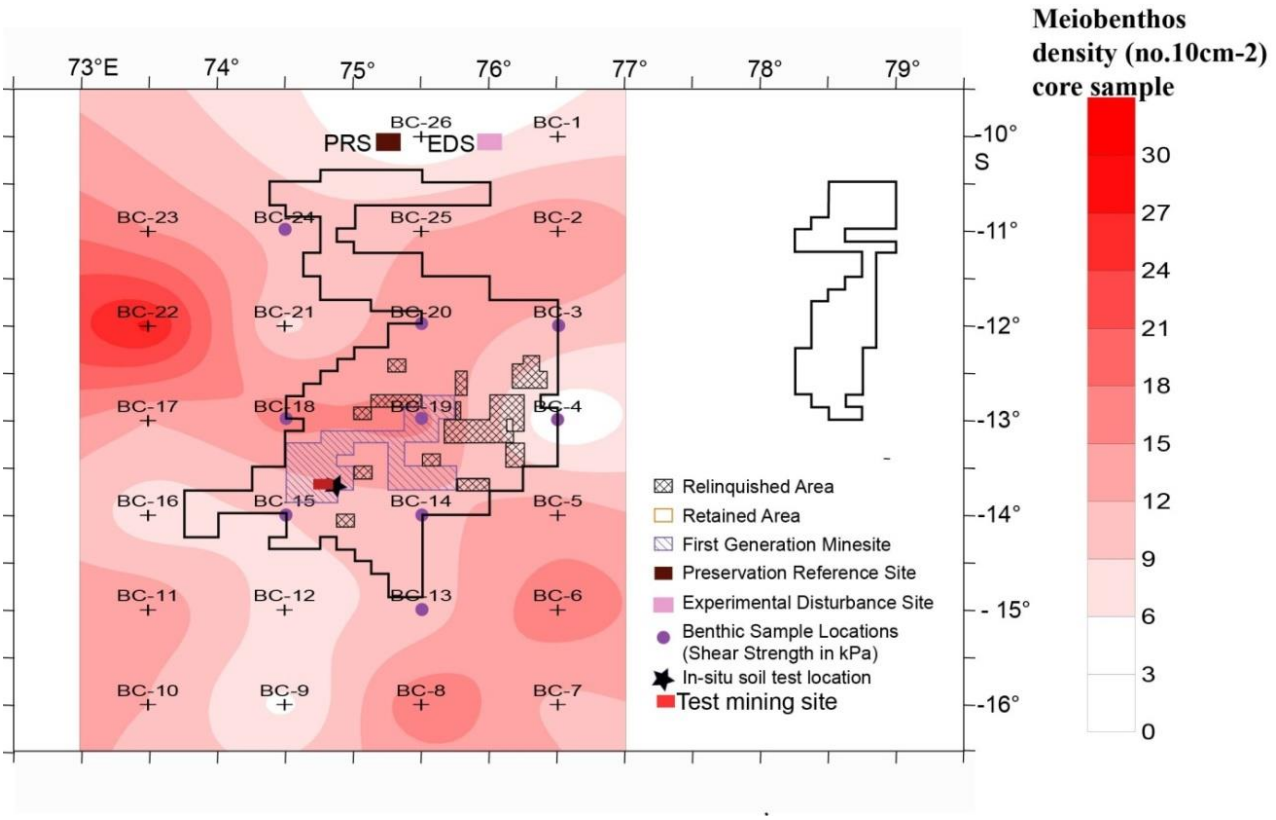

Fig. 5.4.3.2.1: Distribution of meiofauna (no. per 10cm^{-2})

5.4.3.3 Vertical Distribution

The abundance of meiofauna shows a decreasing concentration towards the deeper sections of core samples (Fig. 5.4.3.3.1). Even though meiofauna was observed in the entire core sections (0-35 cm), the top core section of 0 to 1.5 cm sample alone consists of 53% of total faunal abundance. Further, 0 to 5 cm (69%) and 5-10cm (17%) of core sections covers 87% of the total faunal abundance and the supplementary depth of 10-35 cm had relatively less fauna (13%). This confirms the highest concentration of meiofauna is in the top layers of core samples (0 to 5 cm).

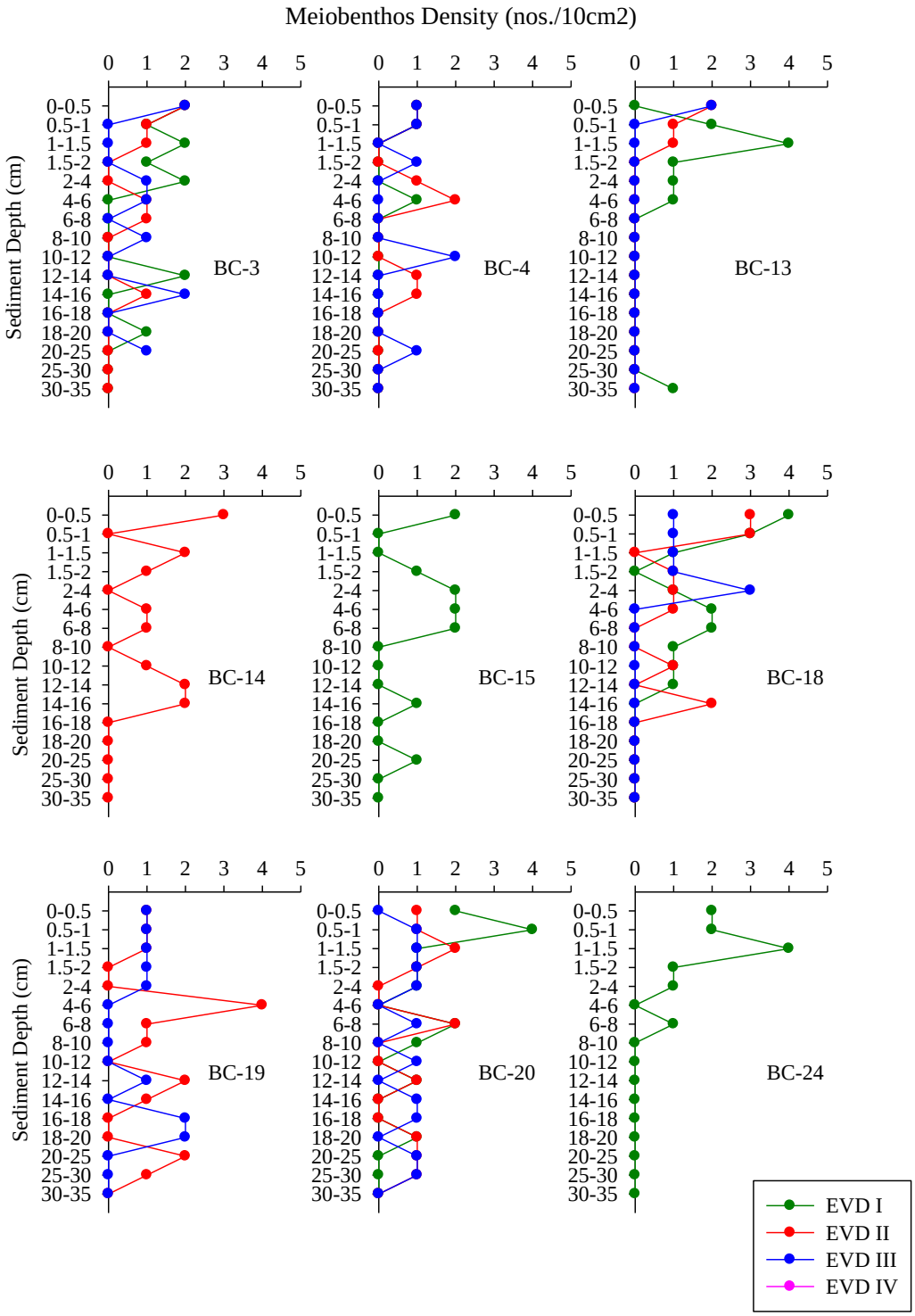

Fig. 5.4.3.3.1: Vertical distribution of meiofauna density (no.s/10cm^2)

5.5 Biological communities in IRZ and PRZ

The present report is based on the biological sampling conducted during cruise SK-120 onboard RV Sagar Kanya in1997-98 for surface productivity (Matodkar et al., 2001), whereas the benthic data was largely acquired from the Impact Reference Zone (IRZ) and Preserved Reference Zone (PRZ) in CIOB during cruise SSD-13 onboard RV Sindhu Sadhana during July-August 2015. In addition, a detailed comparison is also provided with the earlier long-term data collected from the CIOB (Ingole et al., 2001; 2003; 2005; Pavitran et al., 2007; 2009; Singh et al., 2016; 2018).

5.5.1 Preserved Reference Zone

5.5.1.1 *Chlorophyll a* and primary production in surface waters

Chlorophyll a (Chl a) was measured in top 0-150 from at one stations located at 75^{o} E and 11^{o} S latitude. Chrolophyll a concentration was generally low in the euphotic zone and higher in the subsurface layers (Fig. 5.4.1.1.1). The *chlorophyll a* maxima of 0.45 mgm-^{3} was observed around the 50m water depth. The values decreased sharply bellow 50m water depth. However, the lowest Chl a value of 0.033mgm-^{3} was in the surface water. The values for simulated insitu primary production were measured during day time (12 hrs incubation). The surface productivity was maximum (4.38 mgCm^{-3}-d^{-1}) and this phenomenon was also observed at most of the stations. Minimum value of 0.01mgCm-^{3}-d-1 was estimated at the water depth of 80m. As indicated in Fig. 3.4.5.1 the secondary peak in the primary productivity coincided with Chl a maxima at around 40m water depth. The integrated column productivity varied was relatively high around 10^{o} S and 75^{o} E. The high *chlorophyll a* at 75^{o} E and 12^{o} S latitude was found matching with high primary productivity and at 14^{o} S and 73^{o} E low Chl a matched with low primary productivity in the same area.

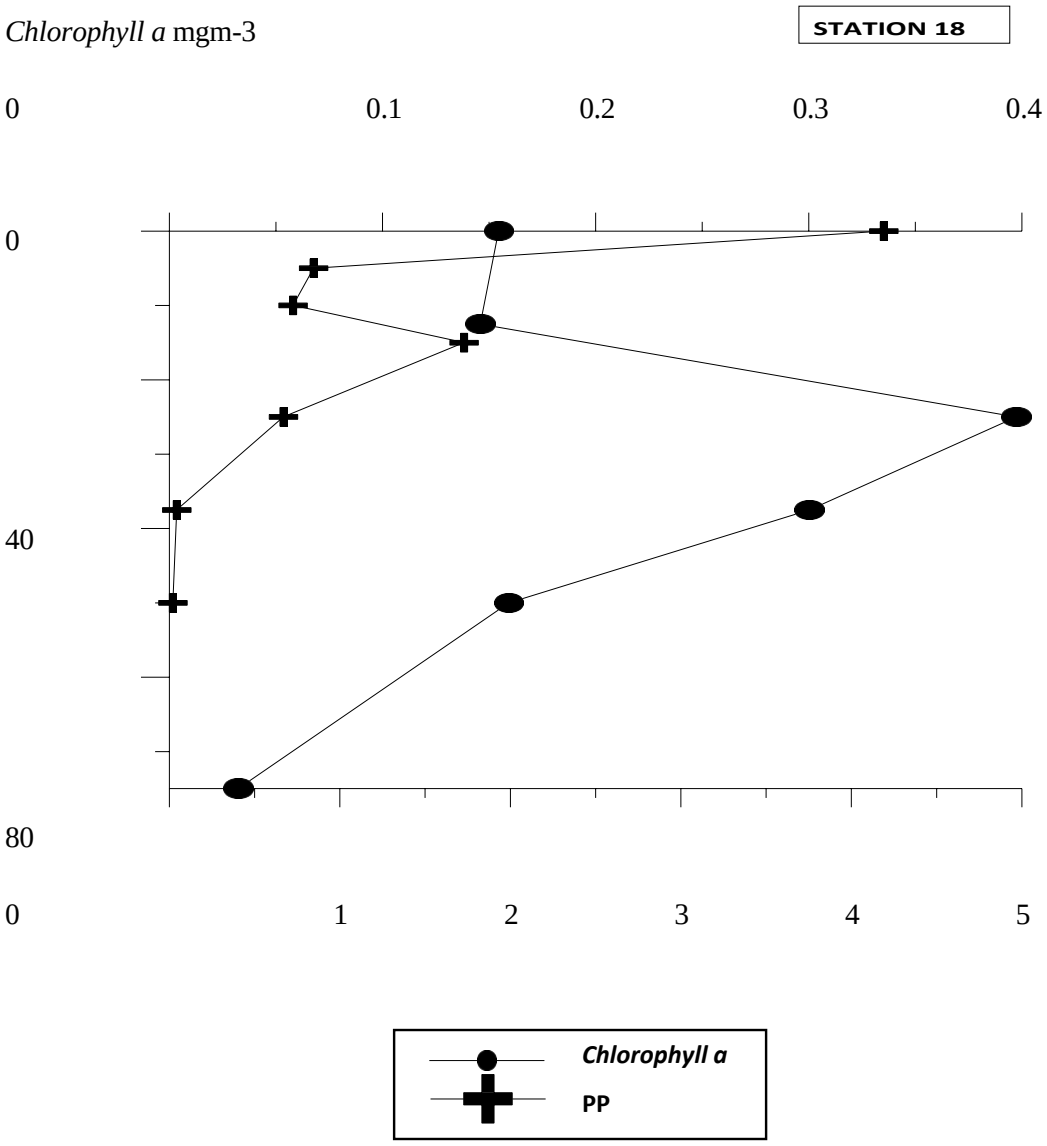

Fig. 5.5.1.1.1: *Chlorophyll a* (mgm^{-3}) and Primary productivity (mgCm^{-3}d^{-1}) distribution in PRZ (Stn 18) area of Central Indian Ocean Basin.

5.5.1.2 Phytoplankton

Diatoms and dinoflagellates are generally the dominant groups of phytoplankton in the PRZ area (Fig. 5.5.1.2.1). The phytoplankton cell counts at surface and bottom water were low. The population of phytoplankton comprised of Nitzschia sp. and Navicula sp. Chaetoceros sp and Octactis sp. were toctonaria, Nitzschia sp. Chaetoceros sp, Nitzschia sp. Among the dinoflagellets, Protoperidinium sp, Gymnodinium sp, Prorocentrum sp were present but in very low numbers. (Fig. 5.5.1.2.2)

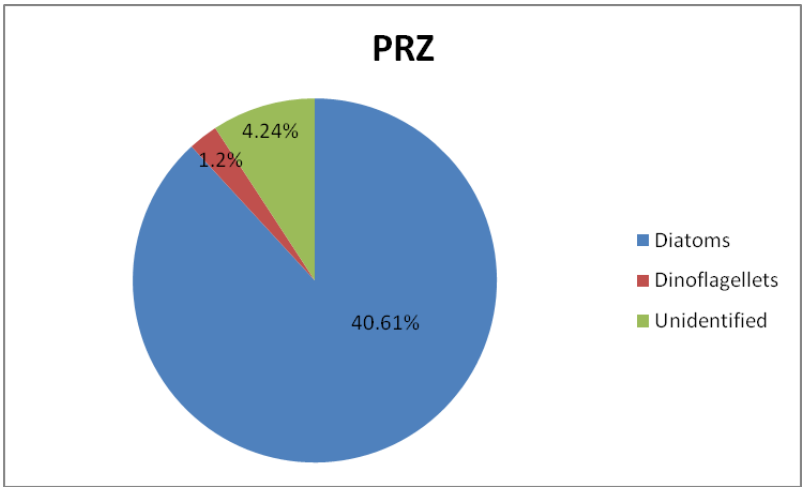

Fig. 5.5.1.2.1: Composition (%) of phytoplankton in the surface waters of PRZ

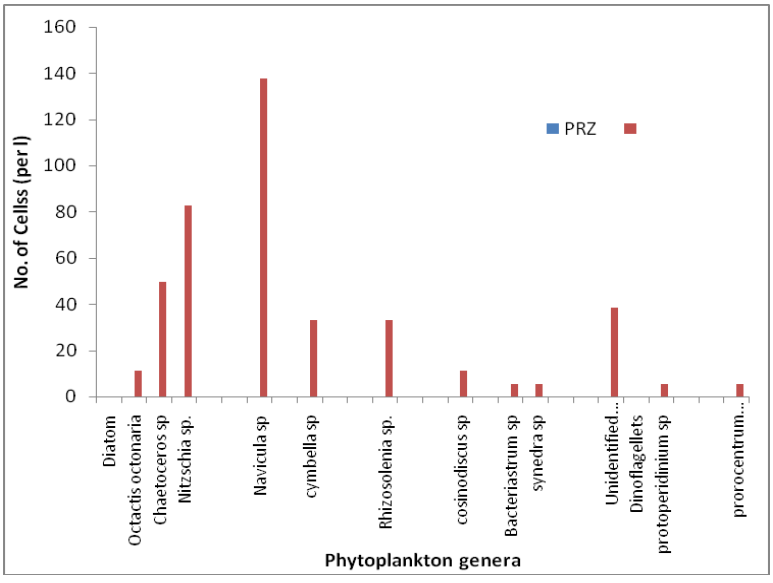

Fig. 5.5.1.2.2 Composition abundance of phytoplankton (No. of cellL^{-1}) in the surface waters of PRZ area

5.5.1.3 Zooplankton

The zooplankton biomass measured at three depths (0-50, 50-200, 200-300 m) covering the isothermal layer and thermocline are presented in Fig. 5.5.1.3.1. The study area has rich and varied assemblage of zooplankton organisms with a total of 32 groups identified. Calanoid copepods (>80%) were the dominant groups of zooplankton in the study area. This was followed by Cheatognaths (5%), ostracods (1%), decapod larvae (1.0%), amphipods (1%), molluscs (< 1%). The euphausids (0.7%) and fish larvae (0.3%) were also observed but with low abundance. Among the dominant copepod fauna, Calanus sp. constituted the bulk of population in terms of density and diversity. It was followed by Eucalanus sp, Calocalanus sp, Clausocalanus sp, and Pluromama sp. in the order of dominance. Decapod larvae were mostly of the deep sea Caridian prawns.

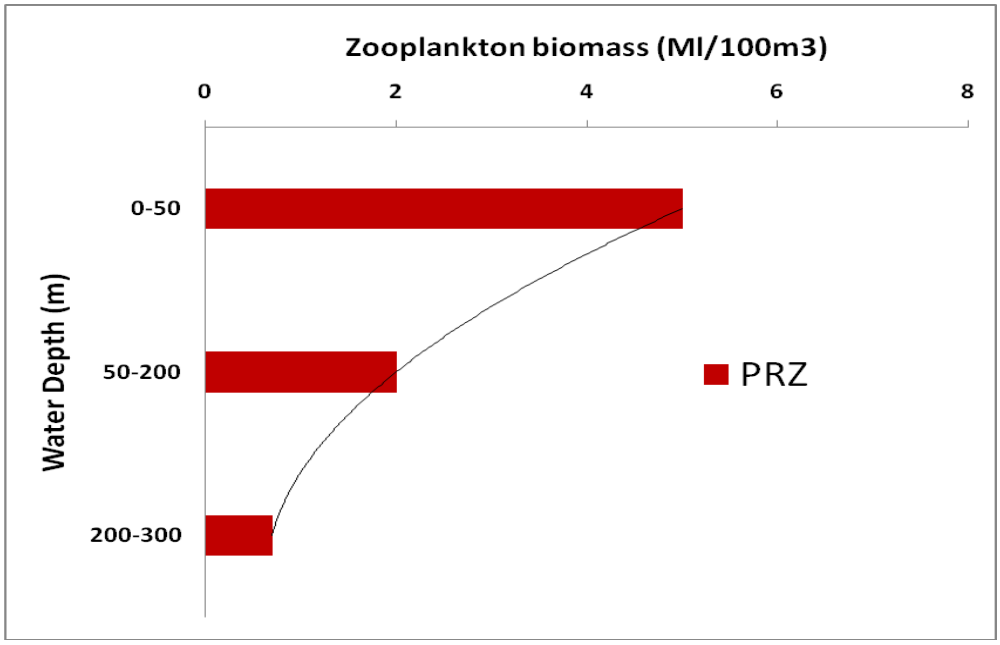

Fig. 5.5.1.3.1: Zooplankton biomass at 0-50, 50-200 and 200-300 m depth in PRZ area in Central Indian Ocean Basin.

5.5.1.4 Macrofauna

5.5.1.4.1 Composition

A total of 7 macrofauna groups were present in the PRZ area. Nematodes were the dominant taxa and constituted 38% of faunal abundance. It was followed by Foraminifera (28%) and Polychaeta (13%). The remaining 21% percent of macrofauna was contributed by other fauna such as Tanid (6%), Harpcticoida (3%), Isopoda (3%) and unidentified forms (9%), (Fig. 5.5.1.4.1.1). Here nematodes are considered among macrofauna because when the sediment samples were sieved on 300 µm mesh sieves, nematodes were found to be equally dominant in macrofauna as well, and some time also exceed the polychaetes in terms of group density. Some larger sized nematodes found in the CIOB sediment are shown in Fig. 5.5.1.4.1.2.

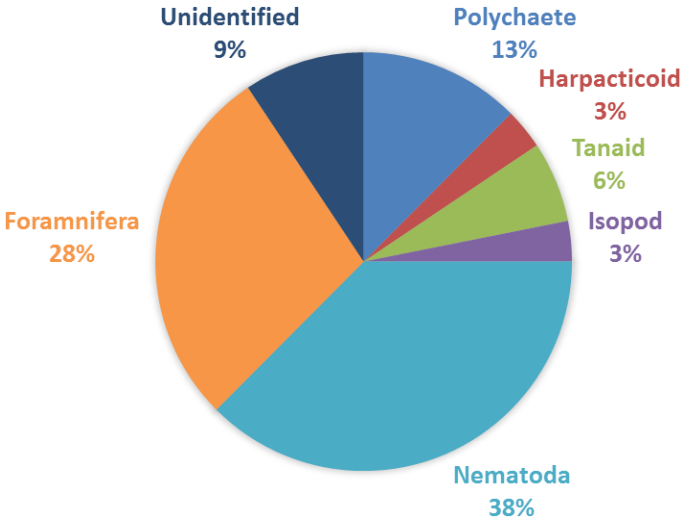

Fig. 5.5.1.4.1.1: Composition of macrofauna in the PRZ area

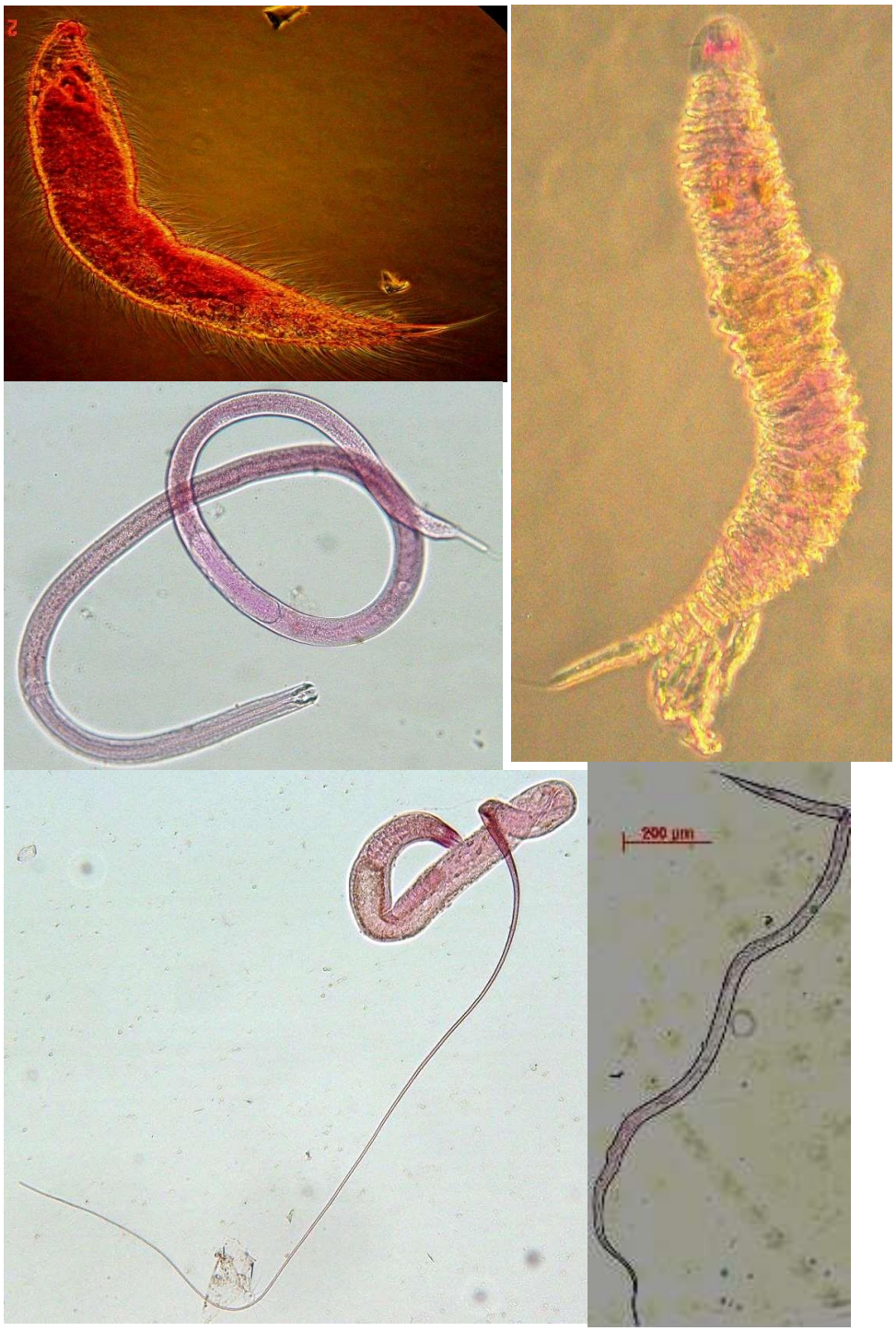

Fig. 5.5.1.4.1.2: Representative of large size nematodes collected from CIOB nodule experimental area. (Odantanticoma sp.; Quadricoma sp.; Adoncholaimus sp.; Halalaimus sp)

5.5.1.4.2 Abundance

The macrofauna were identified from individual cores and calculated in terms of number per square meter (no/m^2). The density of macrofauna varied from 113 to 624 no/m^2 (Mean: 363 ± 199 sd, n=5). The maximum faunal density of 624 no/m^2 was recorded at station BC06 and the minimum density of 113 no/m^2 was at station BC3 (Fig. 5.5.1.4.2.1).

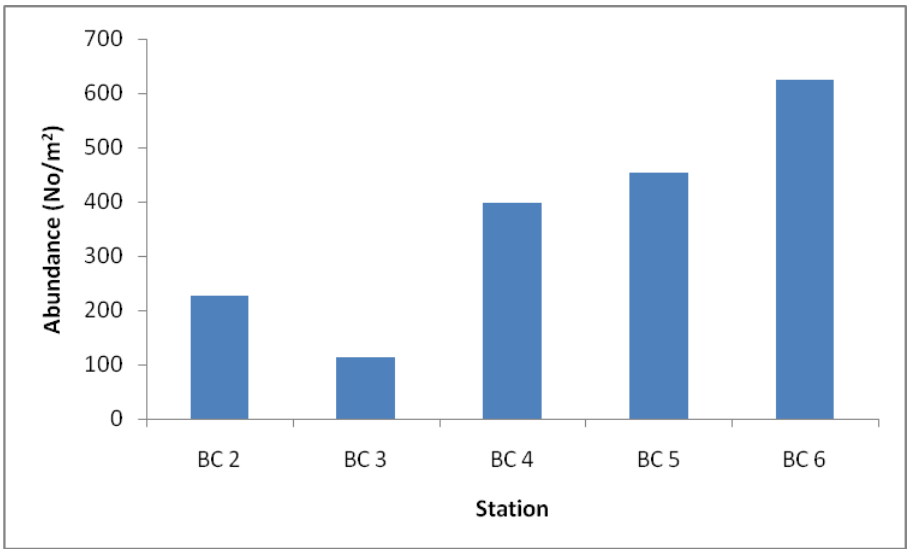

Fig. 5.5.1.4.2.1: Station-wise macrofaunal abundance (No/m2) in PRZ

5.5.1.4.3 Vertical distribution

Macrofaunal density decreased sharply down to a sediment depth of 10 cm and very little or no fauna was recorded below 30 cm (Fig. 5.5.1.4.3.1). Vertical distribution suggests the presence of 84.4% macrofauna in the upper 10 cm layer and remaining 15.6% fauna in lower sediment layer (below 10 cm). The upper sediment layer that was sectioned at an interval of 2 cm down to 10 cm depth had the presence of all 6 macrofaunal groups whereas only two taxa (i.e Nematoda and Foraminifera) were present below 10 cm.

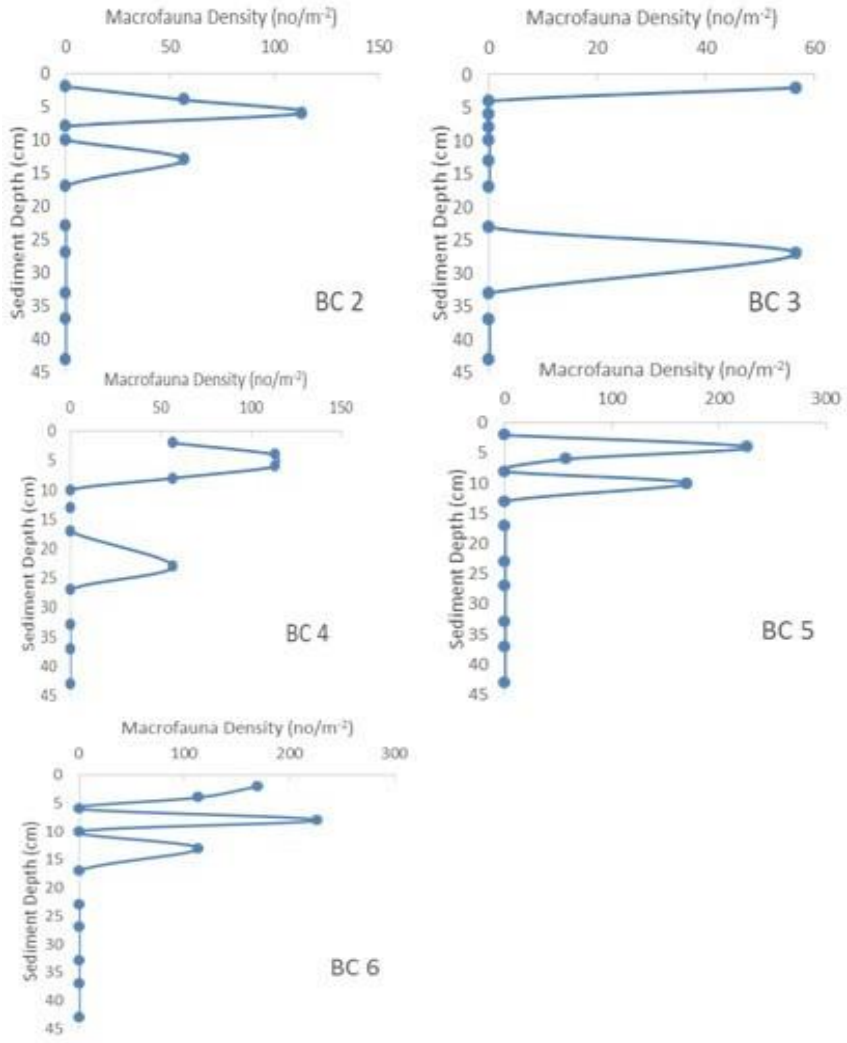

Fig. 5.5.1.4.3.1: Vertical distribution of macrofauna in the PRZ

5.5.1.5 Meiofauna

5.5.1.5.1 Composition

Meiofauna comprised of 10 groups of which nematoda was the most dominant comprising 73% of the meiofauna, followed by Tintinida (8%) and Harpacticoida (7%) (Fig. 5.5.1.5.1.1). Nematodes were mainly present in entire sediment section of 0-6 cm, however their abundance was higher (>80%) in the top 0-2 cm layer.

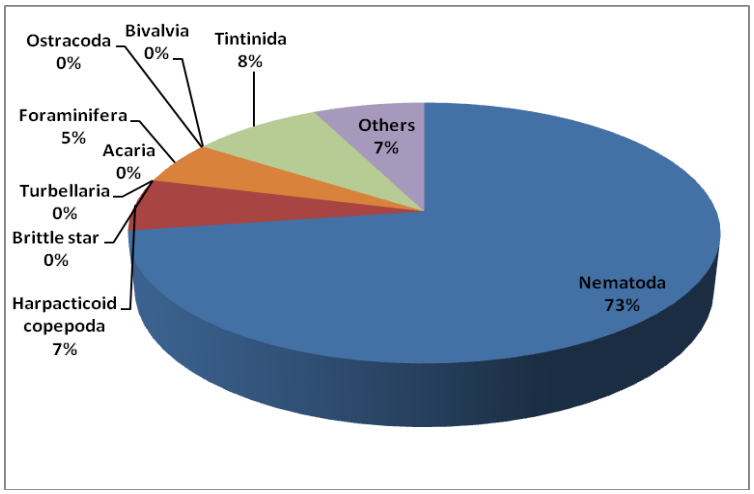

Fig. 5.5.1.5.1.1: Composition (%) of meiofauna in PRZ

5.5.1.5.2 Abundance

The density of meiofauna varied from 76 to 99 ind/10cm^2 with a mean value of 87±9 sd (n=5). High meiofauna abundance was seen in BC4 (99 ind/10cm^2) whereas the low abundance (76 ind/10cm^2) was observed at BC3 (Fig. 5.5.1.5.2.1).

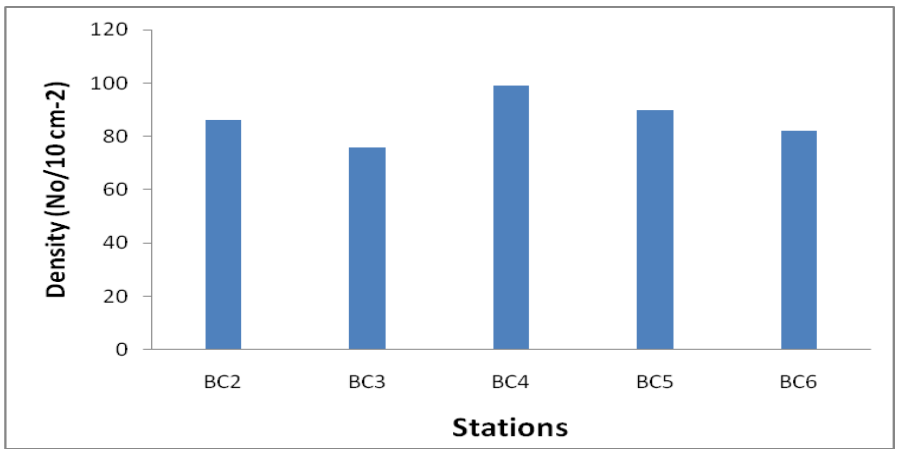

Fig. 5.5.1.5.2.1: Total meiofaunal abundance (ind/10cm^2) in PRZ

5.5.1.5.3Vertical distribution

It has been reported by numerous researchers that 80% of the deep sea meiofauna is generally concentrated in top 0-6 cm layer of soft sediment (Shirayama, 1984, 1999; Radziejewska et al., 2001; Ingole et al., 1999; 2005). Hence the distribution of meiofauna was studied only in top 0-6 cm sediment layer. Almost 50% (47.5 to 56.8%) of meiofauna was present in top 0-2 cm sediment layer in PRZ (Fig. 5.5.1.5.3.1) followed by 2-4 cm which also had relatively higher meiofaunal concentration (27 to 42%). It is interesting to note that 4-6 cm sediment section also had high meiofauna abundance (9.8 to 23.5%). Other studies on vertical distribution of meiofauna in CIOB (Ingole et al., 1999; 2001; 2005) have reported presence of some meiofauna (~5%) in deeper sections up to 30 cm. The percent contribution of nematodes varied from 81.4 to 89.5% with an average of 85.5 %. Maximum abundance of 85 ind. per 10 cm^2 (85.6%) was in the central region (BC4).

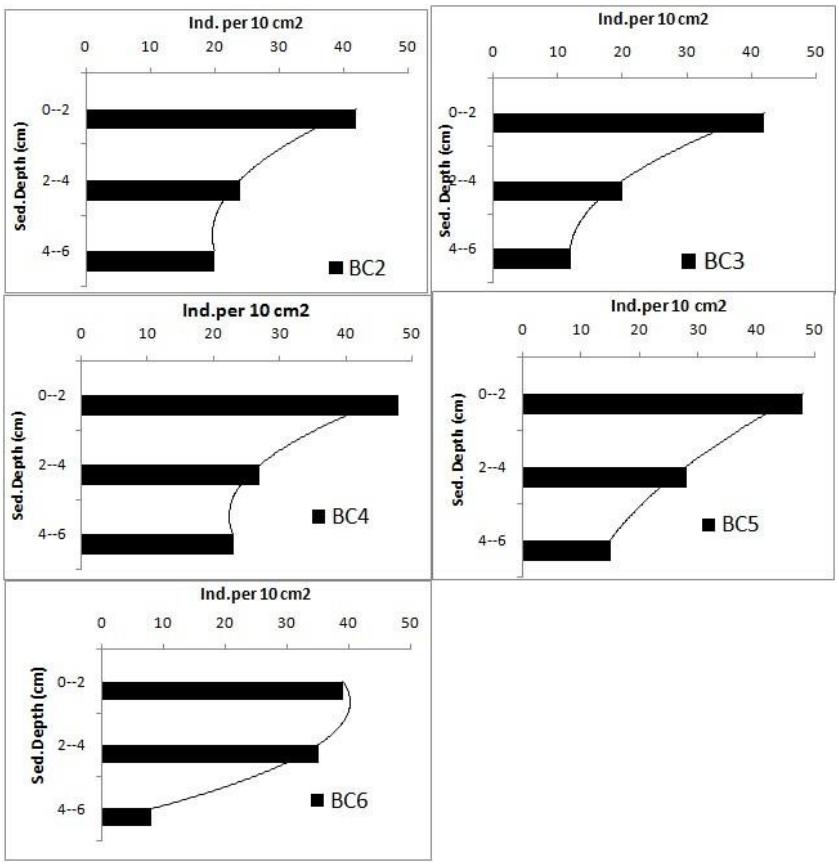

Fig. 5.5.1.5.3.1: Vertical distribution of meiofauna in the PRZ

5.5.2 Impact Reference Zone (IRZ)

5.5.2.1 *Chlorophyll a* and primary production

Chlorophyll a (Chl a) concentration in the top 0-150 m water column showed moderate value. Chl a was generally low in euphotic zone with increased values below 50m. The maximum Chl a concentration of 0.22 mgm^{-2} was recorded in the water depth of 80 to100 m. (Fig. 5.5.2.1.1). Chl a value was significantly higher (factor of 5) in the subsurface compared to the surface concentration. The values decreased sharply below the 100 m. However, the lowest value of Chl a of 0.06mgm-3 was in the sub-surface water at the depth of 20m. Surface primary productivity production measured during the day time for top 150 m water showed maximum production of 0.18 mgC $m^{-3}d^{-1}$ in the surface water (Fig. 5.5.2.1.1). The integrated column productivity varied and values decreased sharply below the 20m. Minimum production of 0.05 mgC m-3-d-1 was measured in the water depth of around 60 m with more or less same production in 100m.

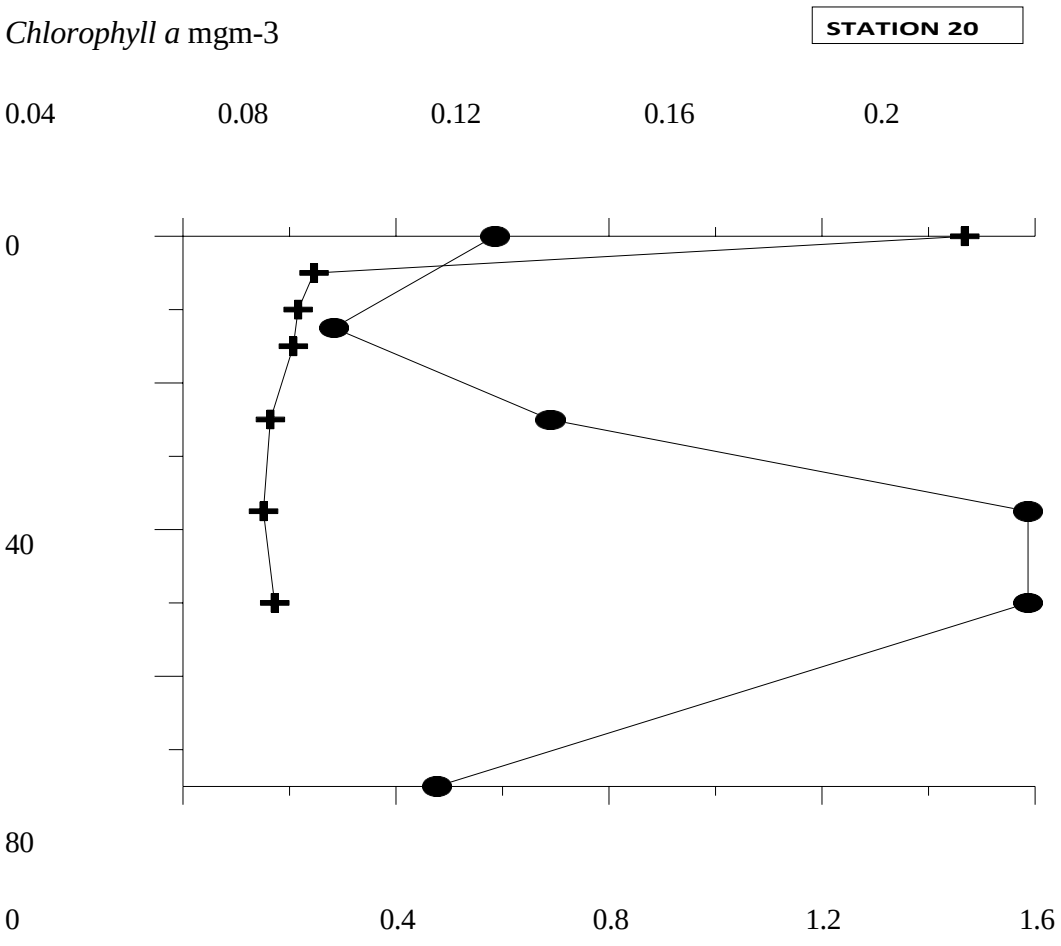

Fig. 5.5.2.1.1: *Chlorophyll a* (●) (mgm-3) and Primary productivity (+) ($mgCm^{-3}d^{-1}$) distribution in IRZ (Stn 20) area of Central Indian Ocean Basin.

5.5.2.2 Phytoplankton

Diatoms and dinoflagellates were the main groups of organisms in the area. Phytoplankton cell counts at surface and bottom water were low. The population of phytoplankton was largely dominated by Chaetoceros sp (24%), Navicula sp (13%) and Nitzschia sp (8%) (Fig. 5.5.2.2.1). Odentella sp (5%), Octactis (4%) spp and Rhizosolenia sp. (4%) were the other dominant diatoms. Among the Dinoflagellets, Protoperidinium sp (8%), Prorocentrum sp (4%) and Gymnodinium sp (3%) were present in all the samples (Fig. 5.5.2.2.2).

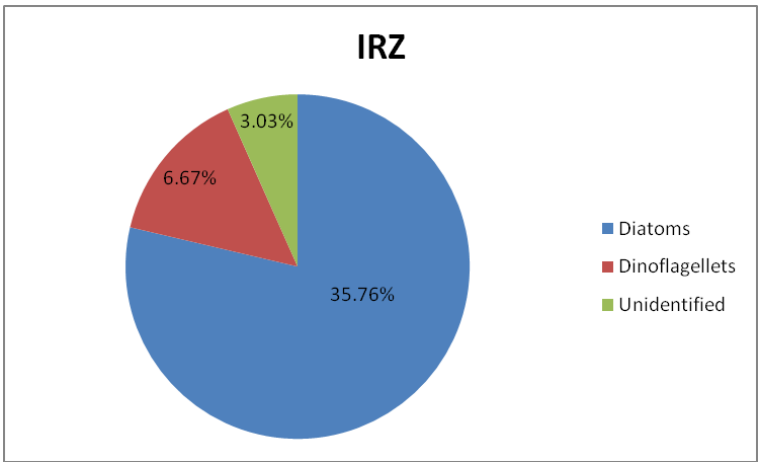

Fig. 5.5.2.2.1: Composition (%) of phytoplankton in the surface waters of IRZ

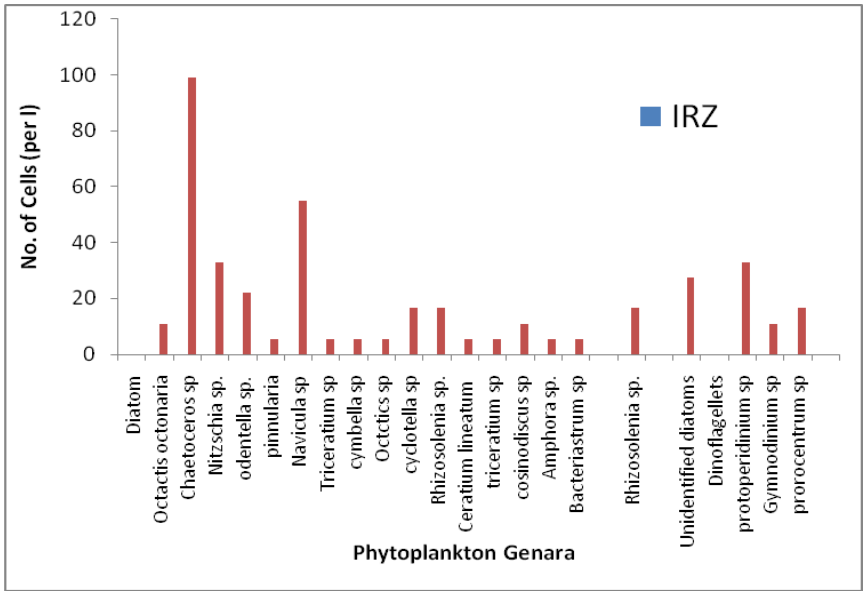

Fig. 5.5.2.2.2 Composition and abundance of phytoplankton (No. of cellL^{-1}) in the surface waters of IRZ area

5.5.2.3 Zooplankton

The zooplankton biomass in the top surface was much higher in the isothermal layer (0-50m) as compared to the thermocline layer (50 –200m) (Fig. 5.5.2.3.1). The biomass values were higher

by a factor of 6 in surface waters suggesting concentration of zooplankton in upper layer and that the study area has rich and varied assemblages of zooplankton. A total of 32 groups were identified. Calanoid copepods (>80%) being the dominant followed by Cheatognaths (5%), ostracods (1%), decapod larvae (1.0%), amphipods (1%), molluscs (< 1%). The euphausids (0.7%) and fish larvae (0.3%) were also observed but with low abundance.

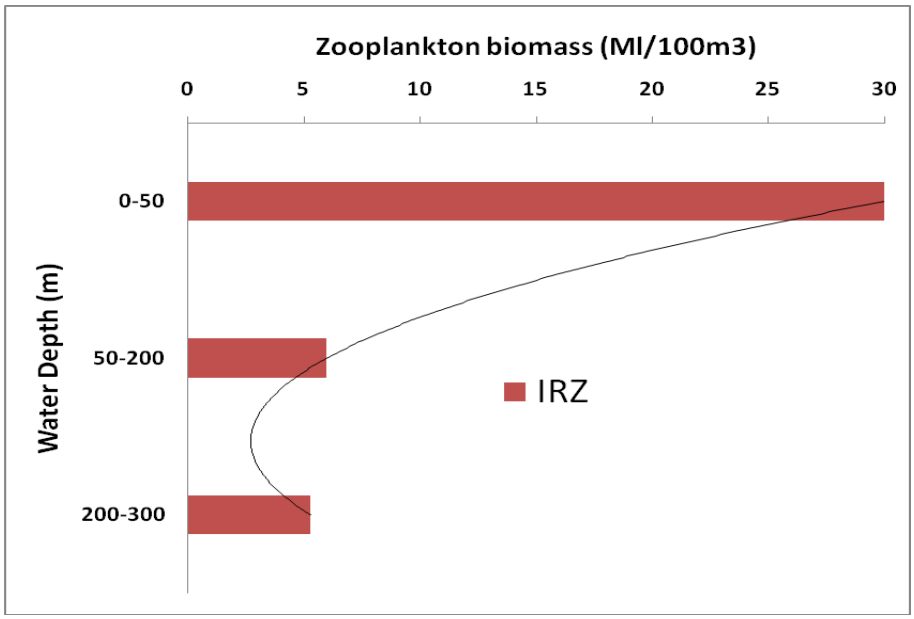

Fig. 5.5.2.3.1: Zooplankton biomass at 0-50, 50-200 and 200-300 m depth in IRZ area of the Central Indian Ocean Basin.

5.5.2.4. Macrofauna

5.5.2.4.1 Composition

A total of 7 macrofauna groups were recorded of which 6 could be identified (Fig. 5.5.2.4.1.1). Nematoda was the most dominant with 57% of the total composition followed by foraminifera (15%) and Crustacea (14%). The crustaceans were dominant in area. Generally, annelid polychaetes are the dominant taxa in macrofauna of CIOB (Ingole et al., 2003; Ingole et al., 2001; 2005; Pavitran et al., 2007). As recommended by the International Seabed Authority, foraminifera were also considered as a part of macrofauna in the present study and hence the percentage of nematode was somewhat reduced. However, nematoda percentage increased from 57% to 67% when we excluded the data on foraminifera.

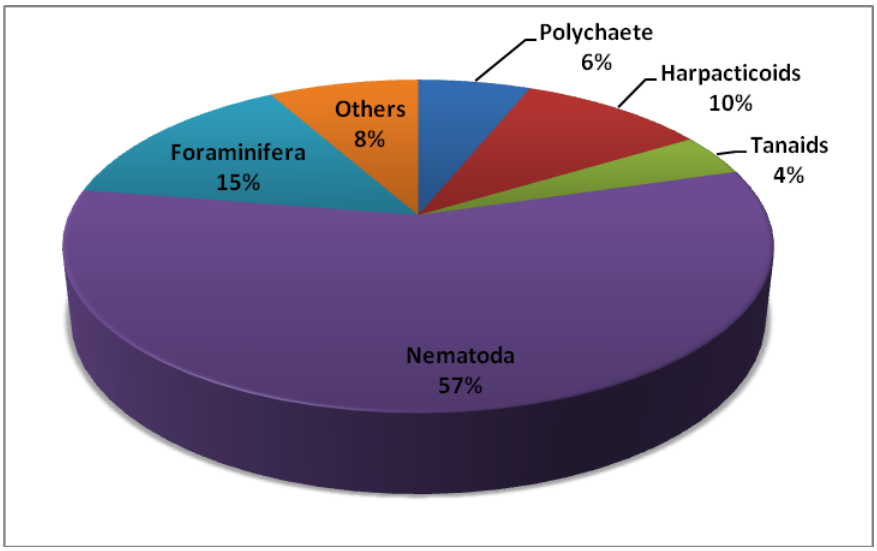

Fig. 5.5.2.4.1.1: Composition (%) of Macrofauna in IRZ

5.5.2.4.2 Abundance

The density of macrofauna in IRZ area varied from 283 and 794 no./m^{-2} with a mean of 556 and sd of ± 648 no/m^2 , n=5. Five replicate cores were collected from the IRZ area. Most of the fauna (93.9%) was concentrated in the top 10 cm sediment layer. The density of macrofauna was marginally higher in IRZ compared to the PRZ (Fig. 5.5.2.4.2.1).

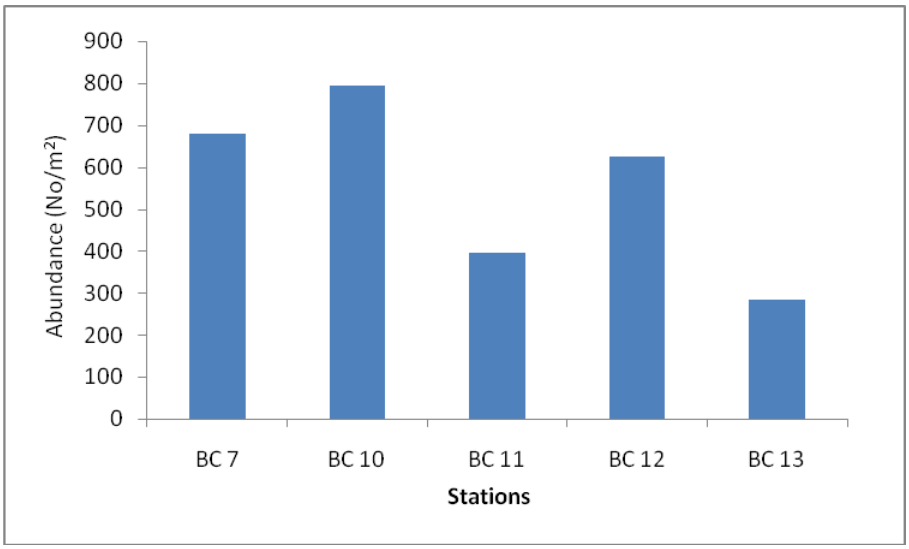

Fig. 5.5.2.4.2.1: Station-wise macrofaunal abundance (No/m^2) in IRZ

5.5.2.4.3 Vertical distribution

The vertical distribution of macrofauna was studied up to a depth of 45 cm. The macrofauna were present upto the sediment depth of 15 cm. Macrofauna was not observed between 15-25 cm sediment sections but fauna was again seen in 25-30 cm section where only nematodes were present. Similar to the PRZ, the faunal abundance decreased below the depth of 10 cm (Fig. 5.5.2.4.3.1).

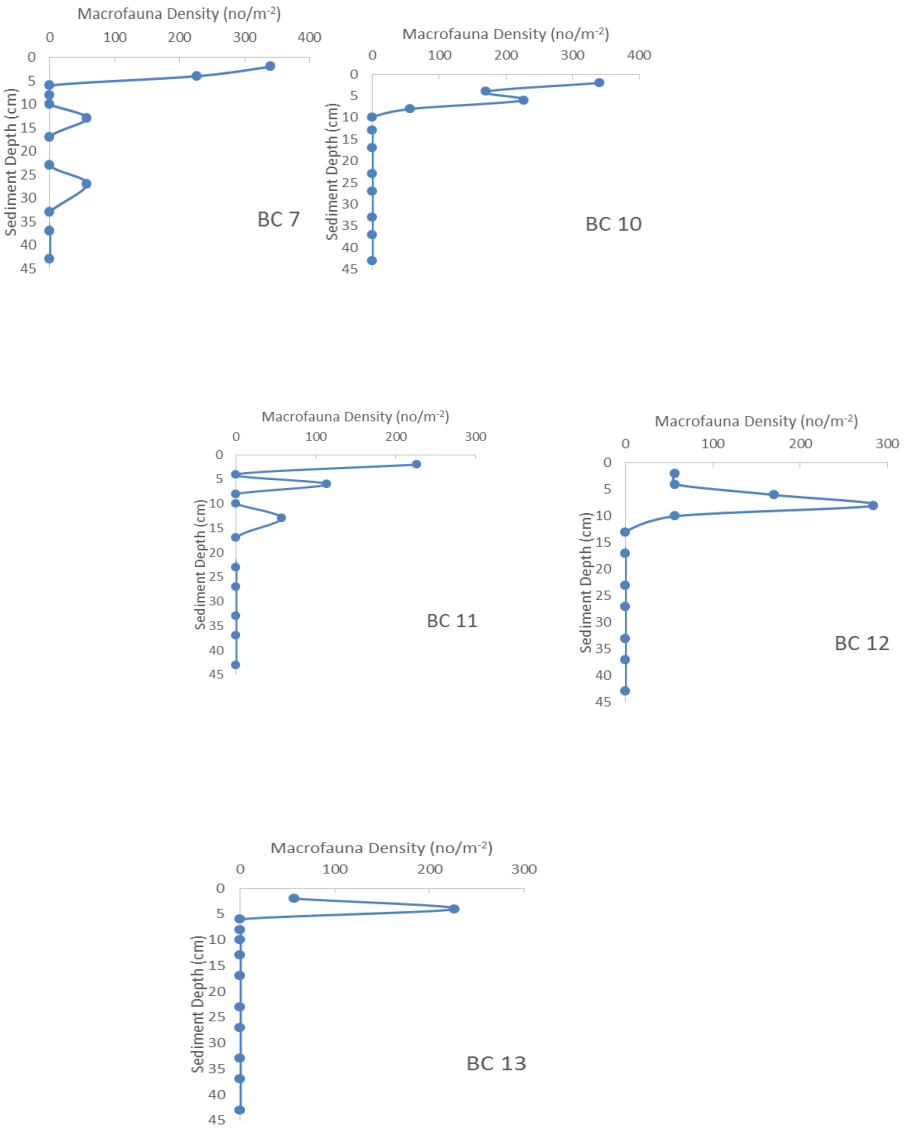

Fig. 5.5.2.4.3.1: Vertical distribution of macrofauna in IRZ

Representative photographs macrofauna from IRZ and PRZ are given in Plates 1-4.

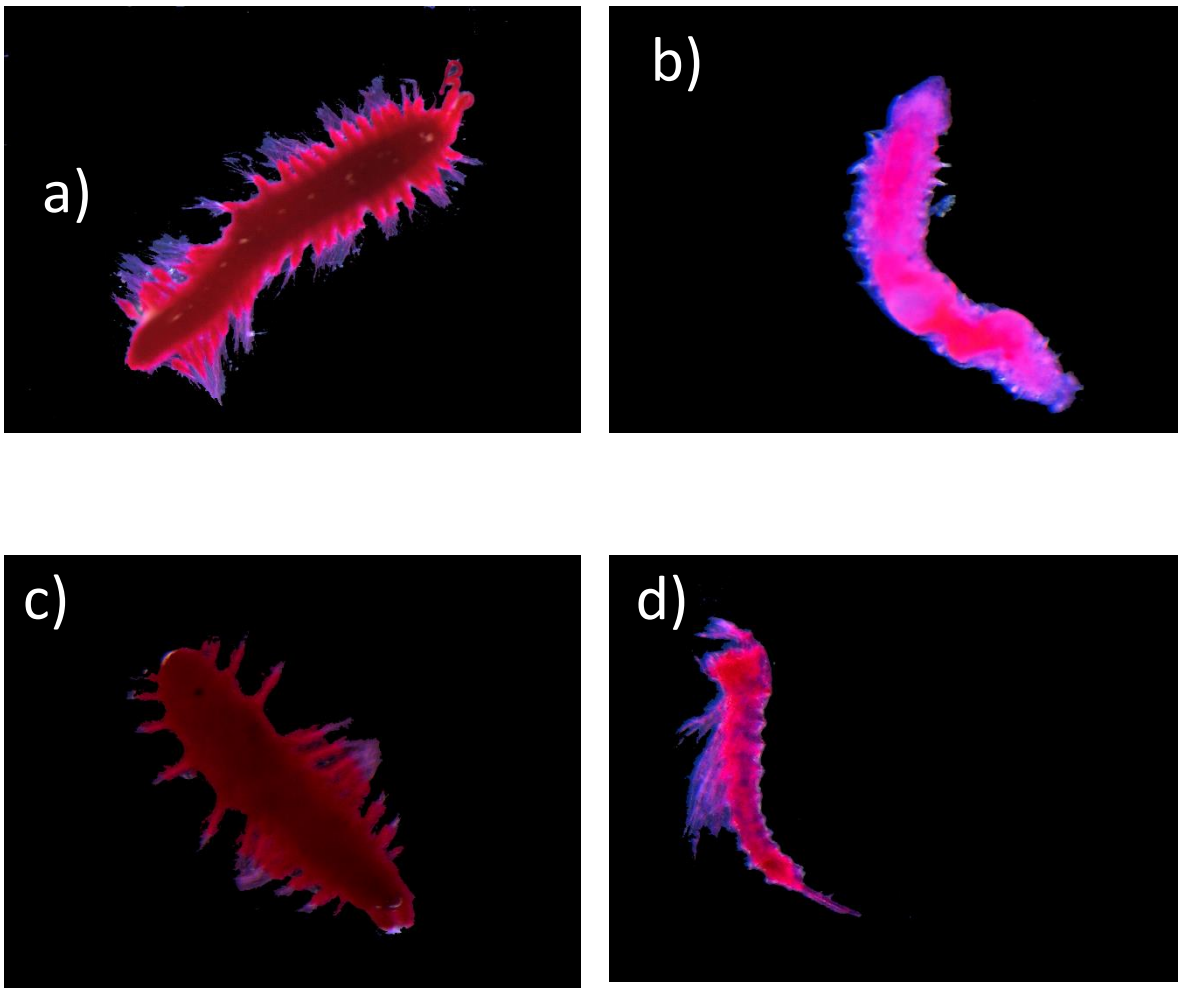

Plate 1: (a), (b), (c), Polychaeta; (d) Harpacticoida

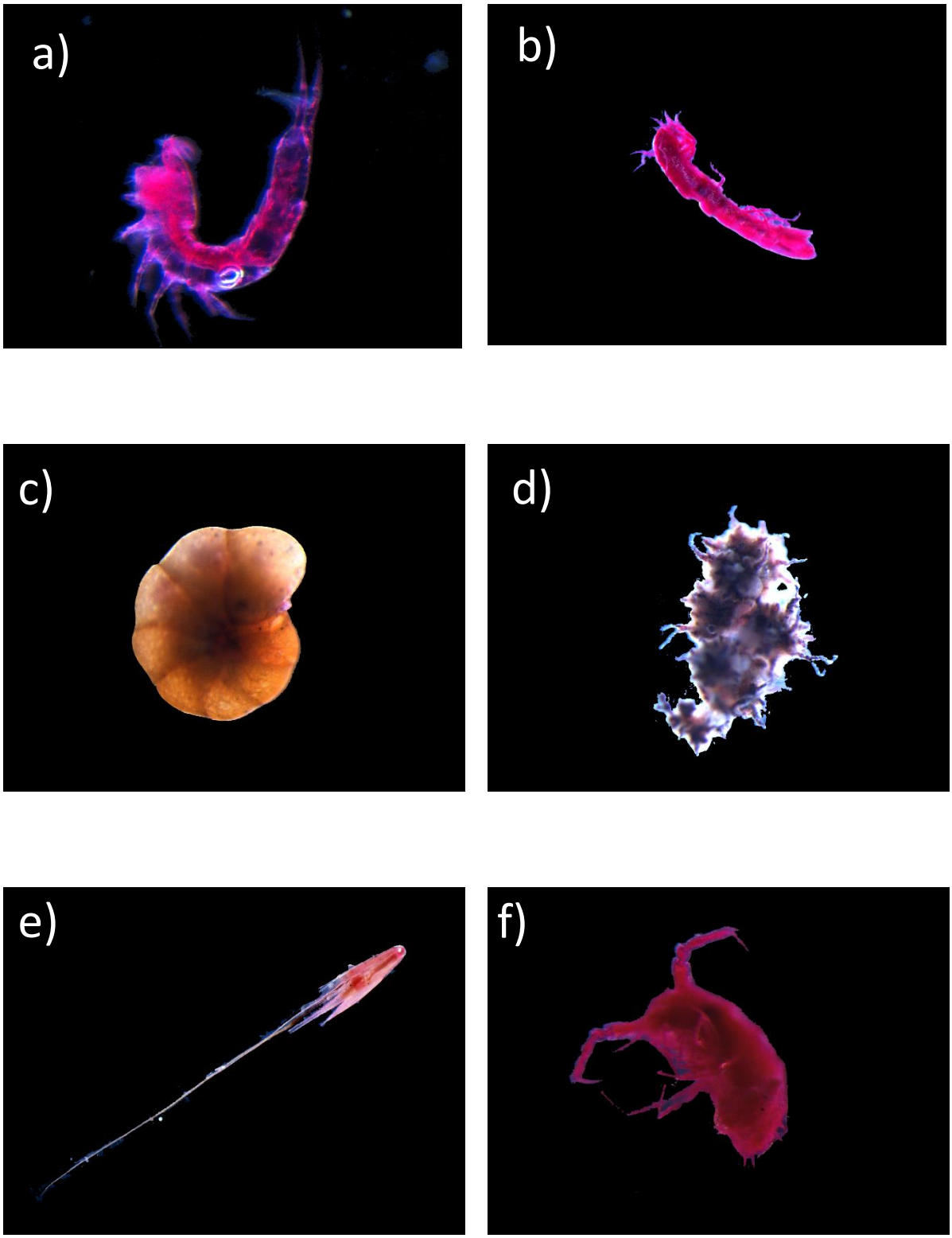

Plate 2: (a) Harpacticoida, (b) Isopoda, (c), (d) Foraminifera,(e), (f) Unknown

Plate 3: Different types of harpacticoid Copepodes from the CIOB

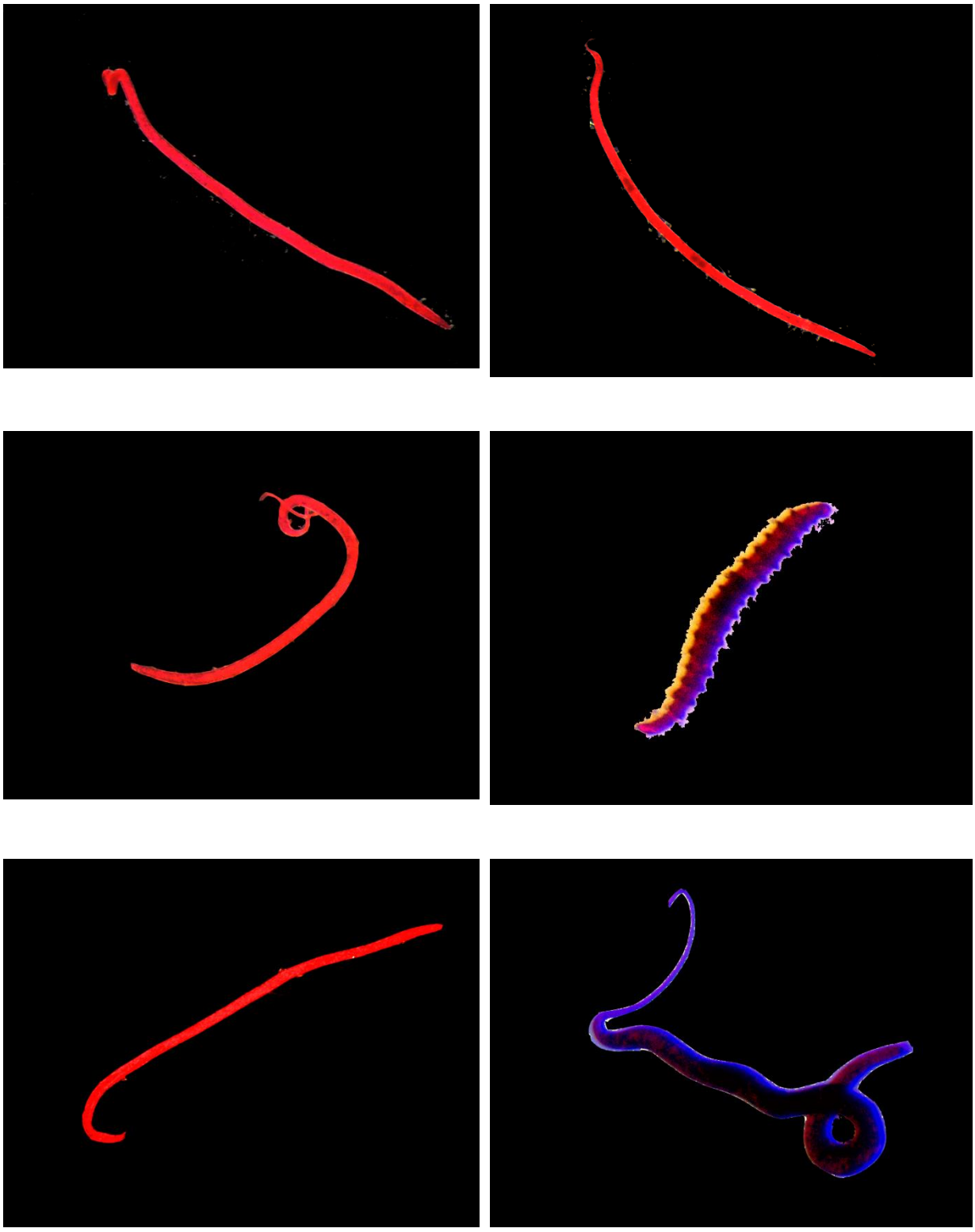

Plate 4: Different types of nematodes from the CIOB

5.5.2.5 Meiofauna

5.5.2.5.1 Composition

Meiofauna comprised of 10 groups out of which 9 were identified and one could not be identified due to broken body parts. Nematoda was the dominant group (49.5%), followed by Tintinida (15%), Foraminifera (12%), Harpacticoida (5%). The dominance of nematodes were generally evident in the top 0-2 cm sediment layer (Fig. 5.5.2.5.1.1).

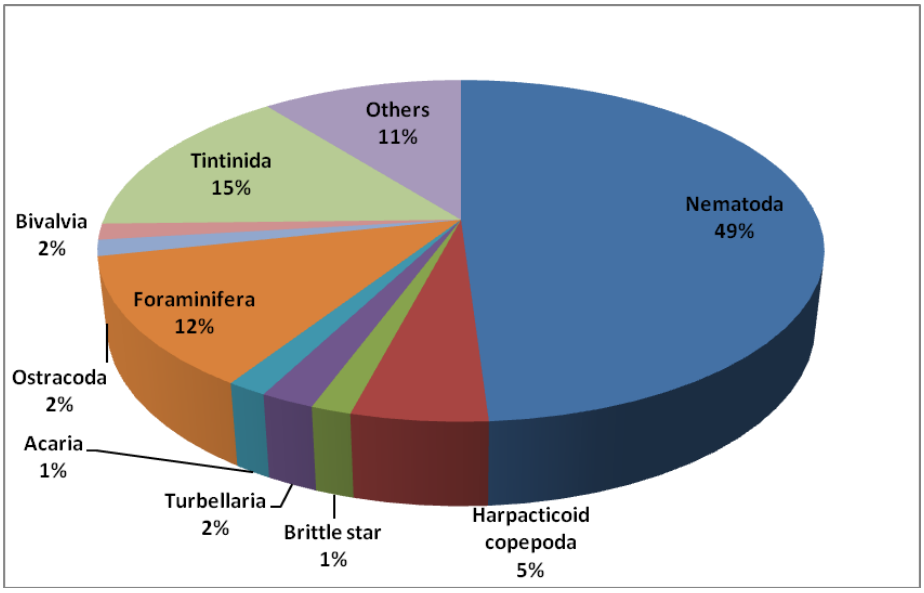

Fig. 5.5.2.5.1.1: Composition (%) of meiofauna in IRZ

5.5.2.5.2 Abundance

Highest meiofaunal abundance of 122 ind/10 cm^2 was seen in BC13, whereas the lowest abundance of 79 ind/10 cm^2 was observed in BC11 (Fig. 5.5.2.5.2.1). The mean abundance of meiofauna in IRZ was 102 with an SD of ±15, (n=5). Nematoda was the most abundant group comprising 48.44% of fauna in top 0-2 cm sediment layers of all the samples.

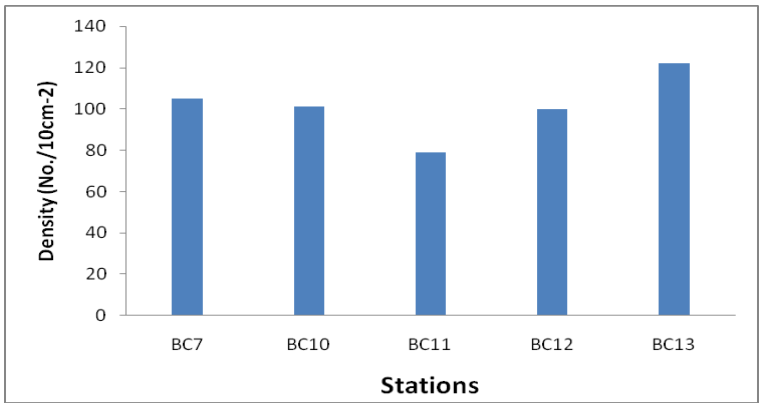

Fig. 5.5.2.5.2.1: Abundance of meiofauna in the IRZ area

5.5.2.5.3 Vertical distribution

Maximum meiofaunal abundance was observed in the top 0-2 cm sediment section and the percent abundance varied between 43 to 57%. About 30 to 37% fauna was observed in 2-4 cm sediment layer and 4-6 cm sediment layer had 10 to 23% fauna (Fig. 5.5.2.5.3.1). Nematodes were the most dominant and their percent contribution in IRZ area varied between 77.2 to 91.1 % with an average of 84.22 %. Nematodes were evenly distributed in the study area, however relatively higher value of 92 ind. per 10 cm2 (91%) and 107 ind. per 10 cm2 (87%) were observed respectively in the southern sector and central sectors. Different types of meiofauna are shown in Plate 5.

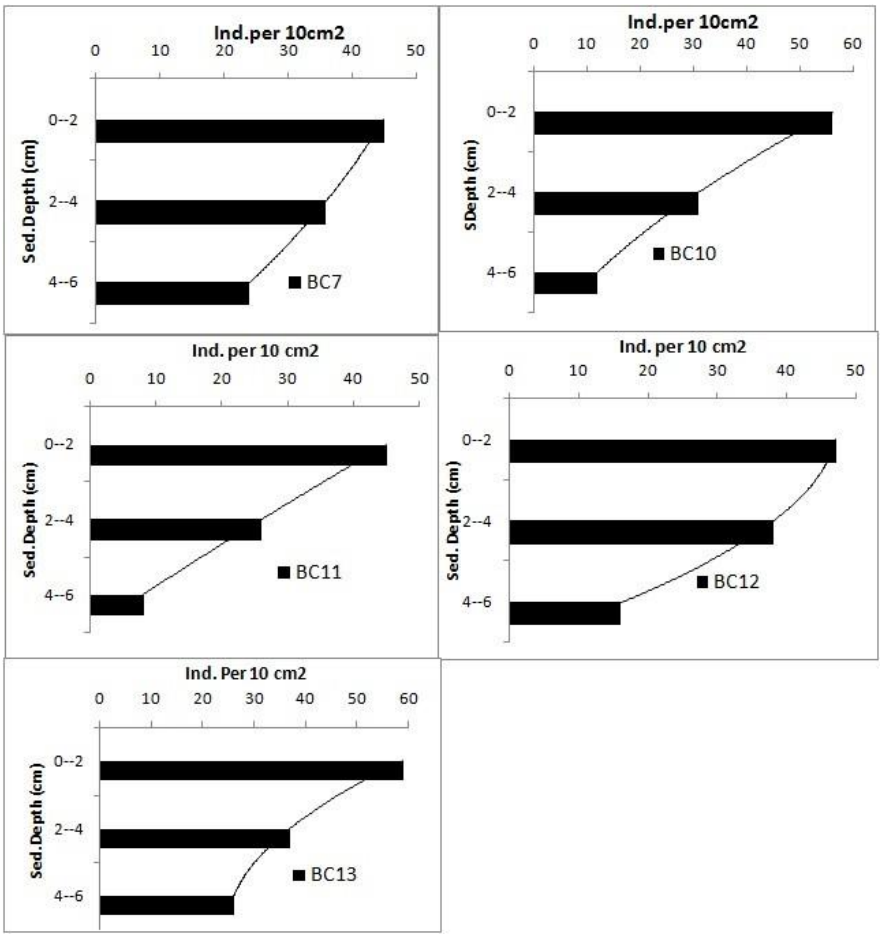

Fig. 5.5.2.5.3.1: Vertical distribution of meiofauna in the IRZ area

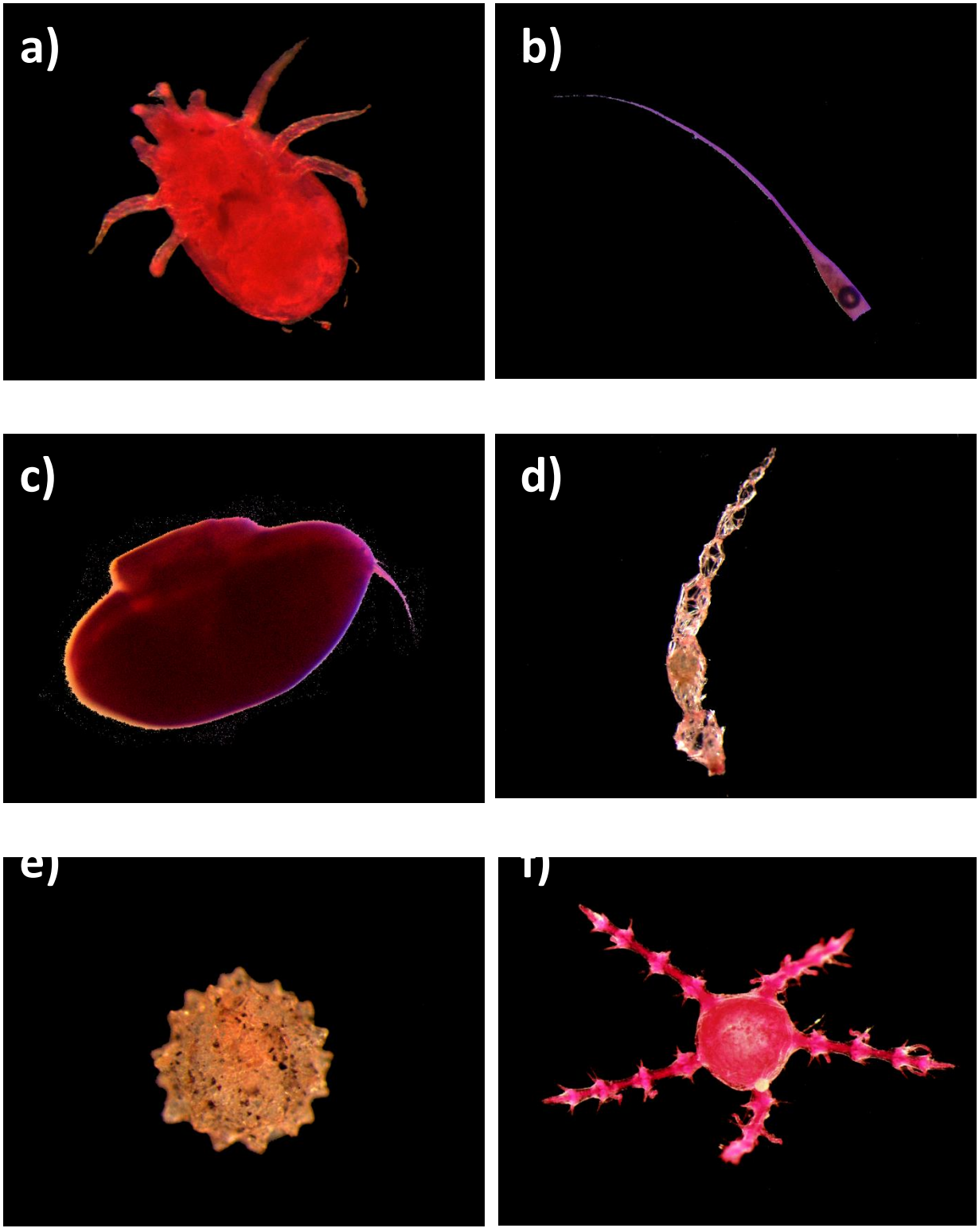

Plate 5: Meiofauna from the CIOB a) Acarina, b) Tintinid, c)Ostracoda, d) –e) Foraminifera, f) Ophiuroidea.

5.6 Nodule fauna

The nodule samples were obtained during the cruise of R. V. Akademic Boris Petrov (Cruise no. ABP 38) conducted in the CIOB during September- October 2009.The study area lies between 12º20' to 13º 00' S latitudes and 74º 18' to 75º 30' E longitudes in the depth range of 5000 to 5300 m (Table 5.6.1) using a modified USNEL spade box corer of 50 x 50 x 50 cm dimension (sampling area of 0.25 m^2). All the nodules were carefully removed from the sediment surface; photographed and preserved individually in 5% neutralized formalin rose Bengal solution and stored in containers for further laboratory analyses. Altogether 109 nodules were collected from six deep sea operations. In the laboratory, all the nodules were examined and then washed on 25µ sieve. The material retained on the sieve was scrutinized under stereo-microscope and all the faunal material were sorted and mounted on temporary glass slides to facilitate the taxonomic identification. Individual nodules were then classified according to the shape, size and were subjected for various morphometric measurements. To calculate the nodule surface area, measurement was done on for three axes using a Vernier calliper and weighed to obtain the individual weight. Nodules were classified based on their morpho-types and they were dominated by ellipsoidal, botryoidal and polynucleated (Fig. 5.6.1). The nodules were of varied shapes and sizes and the surface area varied between 19 to 475 cm^2. The weight of the individual nodule varied from 1-185 g. The major surface texture was rough and gritty, but smooth textured nodules were also recovered at few stations. Majority of nodules were ellipsoidal, botryoidal and polynucleated. Few were rounded, flat, irregular and broken.

Table 5.6.1: Location and depth of the sampling stations

Stn. Nos.	Position of sampler Lat (ºS)	Long (ºE)	Water depth(m)
IVBC-18 A	12 57.679	74 18.520	5041
IVBC-18 B	12 58.842	74 29.693	5164
IVBC-18 C	12 59.210	74 26.847	5220
IVBC- 18 D	12 50.934	74 29.648	5164
IVBC- 18 E	12 59.133	74 28.748	5148
IVBC- 18 F	12 59.132	74 29.77	5165
IVBC-19 D	12 59.881	75 29.918	5148
IVBC- 19 F	13 00.073	75 29.802	5113

Fig. 5.6.1: Different type of nodules used for the study (A- B: Botryoidal type, C: Ellipsoidal type, D-E: Polynucleated nodule type, F: Smooth surface nodule type).

Abundance and diversity of meiofauna associated with each nodule analyzed is given in Table 5.6.2. The associated fauna comprised of ten major groups of which nematodes were found most dominant and they contributed 30% of the total population (Fig. 5.6.2, 5.6.3) followed by harpacticoid copepods (12-25%), polychaetes (15%), orbitads, (8-15%), bivalves (8-15%), isopods (10-16%), kinorhynchs (10-12%), foraminiferans (11-12%), tanaids (10%), cnidarians (10%). Overall density of associated meiofauna per nodule varied from 1 to 14 (Fig. 5.6.4). The abundance of nematodes and harpacticoid copepod per nodule varied from 2-3; whereas that of isopods ranged from 1-2. The abundance of rest of the fauna was low and remained around 2 ind. per nodule.

Table 5.6.2: Details of the nodule size, weight and associated meiofauna						
Stn. Nos.	Details of the Nodule samples				Associated meiofauna	
	Individual nodule number	Size (cm)	Wt. (g)	Surface area (cm^2)	Abundance (Nos. per nodule)	Diversity (Nos. of groups)
IVBC-18 B	1	7-8	138	442	1	1
	2	5-6	69	245	NF	NF
	3	5-6	72	230	NF	NF
	4	4-5	38	167	NF	NF
	5	3-4	30	141	NF	NF
	6	3-4	25	126	NF	NF
	7	2-3	11	69	NF	NF
IVBC-18 C	1	3-4	35	169	5	3
	2	3-4	26	133	7	3
	3	4-5	34	168	5	2
	4	4-5	20	125	NF	NF
	5	3-4	23	131	NF	NF
	6	3-4	9	79	1	1
	7	2-3	8	55	NF	NF
	8	2-3	5	45	NF	NF
IVBC-18 D	1	2-3	5	53	6	4
	2	1-2	3	32	1	1
	2	1-2	3	32	1	1
IVBC-18 F	1	3-4	15	108	NF	NF
	2	2-3	11	75	NF	NF
	3	4-5	29	131	2	2
	4	2-3	6	52	1	1
	5	2-3	10	73	NF	NF
	6	3-4	4	52	NF	NF
	7	7-8	113	441	NF	NF
	8	3-4	15	102	NF	NF
IVBC-19 D	1	3-4	34	172	NF	NF
	2	3-4	49	202	NF	NF

	3	2-3	25	125	9	3
	4	2-3	11	76	NF	NF
	5	1-2	2	19	4	1
	6	2-3	33	174	NF	NF
	7	1-2	4	43	NF	NF
	8	0-1	1	21	8	7
	9	2-3	47	204	10	3
	10	3-4	40	167	4	2
	11	3-4	32	152	NF	NF
	12	2-3	12	96	NF	NF
	13	4-5	91	347	NF	NF
IVBC-19 F	1	4-5	30	129	1	1
	2	2-3	8	61	7	3
	3	2-3	6	64	1	1
	4	6-7	88	315	2	1
	5	2-3	7	54	2	2
	6	3-4	21	115	1	1
	7	9-10	185	475	3	3
	8	2-3	4	45	3	1
	9	1-2	2	26	4	2
	10	3-4	16	107	1	1
	11	4-5	15	103	1	1
	12	2-3	3	34	6	2
	13	3-4	11	81	4	1
	14	2-3	6	52	NF	NF
	15	2-3	13	81	13	5
	16	3-4	18	97	2	1
	17	2-3	10	71	5	2
	18	3-4	19.	146	14	3
	19	2-3	4	60	1	1
	20	2-3	2	25	NF	NF
	21	2-3	6	49	4	1
	22	2-3	3	34	NF	NF
	23	2-3	6	46	1	1

	24	3-4	6	59	NF	NF
	25	6-7	83	296	2	2
	26	1-2	4	47	1	1
	27	1-2	4	36	2	1
	28	2-3	9	59	2	1
	29	2-3	11	68	2	1
	30	4-5	57	178	NF	NF
	31	3-4	21	122	6	1
	32	2-3	7	44	NF	NF
	33	3-4	8	57	NF	NF
	34	2-3	3	29	NF	NF
	35	3-4	9	90	NF	NF
	36	6-7	40	209	NF	NF
	37	2-3	8	70	NF	NF
	38	4-5	78	273	NF	NF
	39	2-3	4	39	NF	NF
	40	2-3	2	36	NF	NF
	41	1-2	4	29	NF	NF
NF=Not found						

Table 5.6.3: Details of the nodule samples used for the faunal study.					
Stn Nos.	No. of nodules collected	No. of faunal groups	Mean faunal abundance	Faunal diversity (%)	% nodule with fauna
18C	17	5	6.70	50	52.94
18D	5	4	5.50	40	40.00
18E	6	3	4.00	40	16.67
18F	6	2	2.00	20	66.67
19D	40	8	10.17	80	37.50
19F	35	8	22.00	80	25.71
Mean	18.17	5	8.40	51.67	39.92

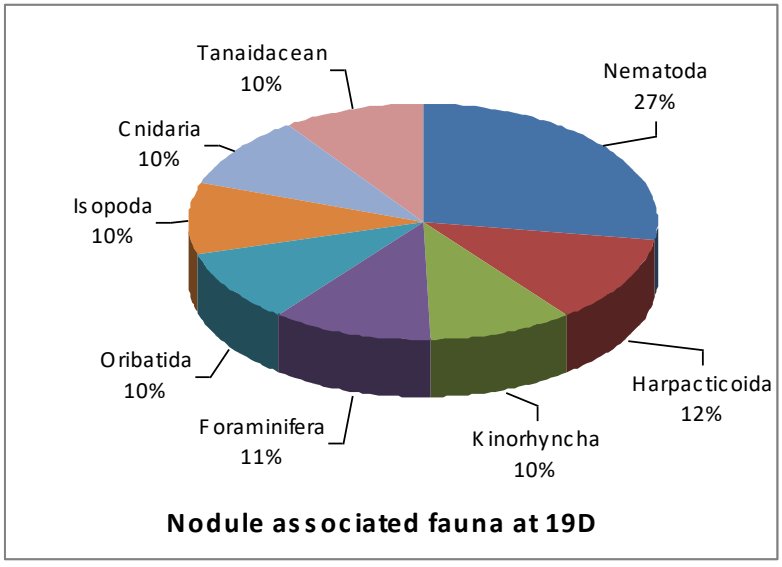

Fig. 5.6.2: Composition (%) of nodule associated fauna

Fig. 5.6.3: Nodule associated faunal communities (A- Tanaid; B- Nematoda, C- Harpacticoida, D- Orbitadea, E- Polychaeta, F- Ostracoda).

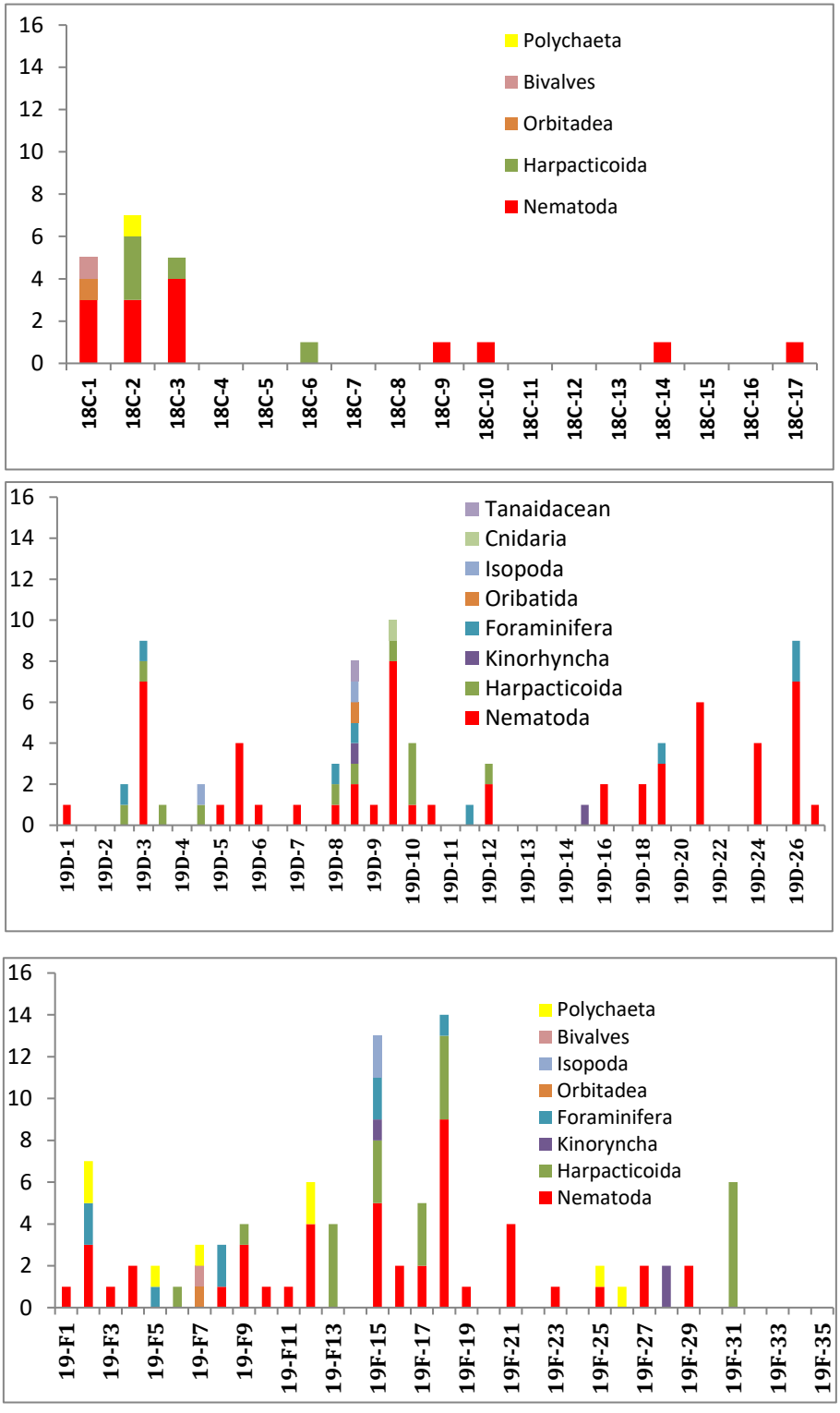

Fig. 5.6.4 Abundance of fauna with individual nodules at different stations

In present study when all nodules were included in the statistical analysis, there was positive correlation between faunal abundance and exposed surface area (Fig. 5.6.5). Moreover, correlation between the total number of meiofauna taxa per nodule and surface area coverage also showed positive relationship (Fig. 5.6.6). Thus, nodules provide suitable habitat for mobile meiofauna (Fig. 5.6.7).

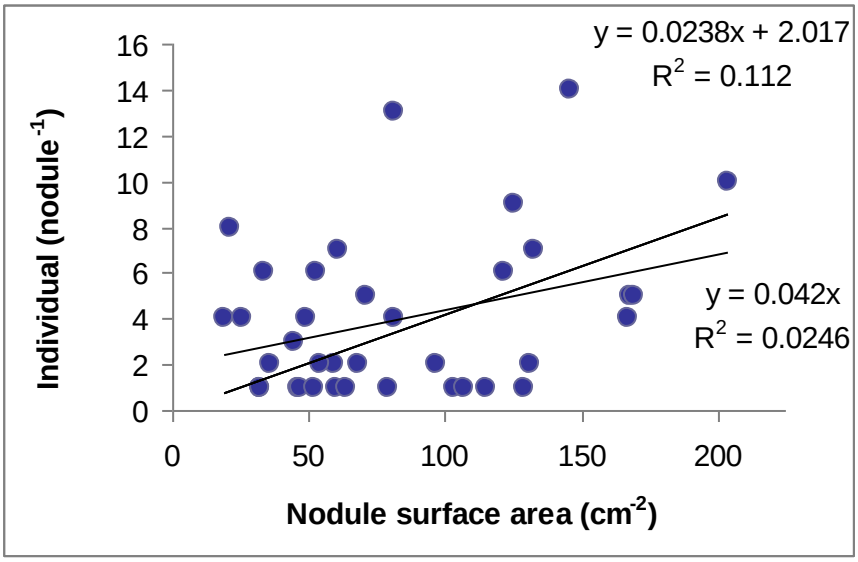

Fig. 5.6.5: Correlation between the nodule surface area and abundance of associated meiofauna.

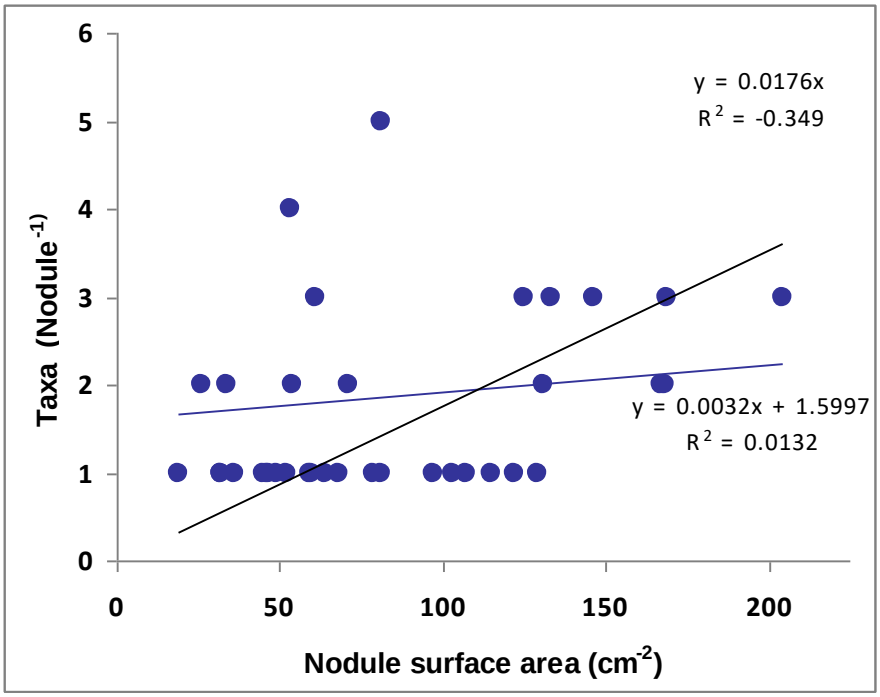

Fig. 5.6.6: Correlation between the nodule size and number of associated taxa

Fig. 5.6.7: Nodules from the CIOB with associated sessile fauna

Recently Singh et al. (2018) addressed very critical issue of whether or not free-living meiobenthic nematode assemblages inhabiting the bare sediment (soft sediment without nodules) in abyssal nodule fields of CIOB are unique and differ from those found in the crevices of polymetallic nodules. There were fewer numbers of nematode genera recorded from the crevices with the differences being found in the dominant genera and families (Fig. 5.6.8). Thalassomonhystera, Acantholaimus and Desmoscolex were noted as characteristic of the bare

sediment while Leptolaimus and Camacolaimus showed the highest likelihood in nodule crevices. Hard nodule crevice substratum does favour some species level morphotypes of the genus Leptolaimus and Camacolaimus since these morphotypes were found exclusively in nodule crevices. However, owing to the still limited sampling effort in the deep sea, it may be premature to conclude if they are endemic to nodules.

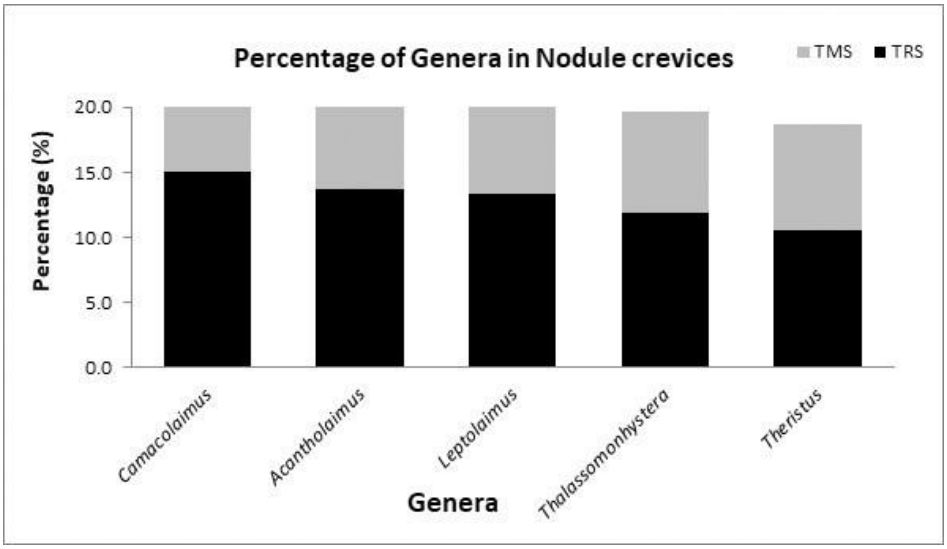

Fig. 5.6.8: Nematode genera/species (%) in nodule crevices in IRZ (TMS) and PRZ (TRS) (Singh et al., 2018).

5.7 Ecosystem functioning

Fore most important aims of marine ecological study are to improve our understanding about the processes that produce and maintain biodiversity in the deep sea and how these processes operate. The deep-sea floor contains a broad array of habitats such as sediment-covered slopes and plains, rocky mid-ocean ridges and seamounts, and island-like chemoautotrophic communities ranging from hydrothermal vents to whales. Communities in many of these habitats are likely to be very susceptible to anthropogenic disturbance due to low rates of productivity, growth, colonization, and delicate habitat structure. In fact, the benthic ecosystem of the abyssal depth is a desert deprived of local primary production and is considered as food limited environment (Smith et al. 2008; Sherman and Smith, 2009).Consequently the organisms living in abyssal habitats have to depend on supply of particulate organic matter (POM) from the surface waters (Radziejewska, 2002).It is generally predicted that heterogeneous habitats allow more species to co-exist in a given area (Zeppilli et al., 2016).

However, as depth increases, food becomes limited for the deep-sea organisms, therefore microbes are the most important in recycling the organic matter.

6. Potential impacts of nodule collector trial on physico-chemical environment

This section describes the potential impacts that could occur during a full scale mining operation for polymetallic nodules on the physico-chemical environment. Although all possible impacts will be described in this section, it should be recognised that since the nodule collector trials will be restricted to the activity close to the seafloor, many of the potential impacts will not be applicable to it and also the scale of the activity is going to be miniscule either in terms of commercial mining or even the benthic impact experiments conducted earlier simulate mining on a small scale.

6.1 Types of likely impacts

6.1.1 Emissions to air

The emissions to air could be from the mining/research vessels that will be in used in the activity either during mining or exploration. However, as the nodule collection trial, does not involve any additional generation of pollutants except for normal operation of the research vessel, no serious harm is expected. Moreover, the IMO regulations regarding safety and environmental practice at sea, including the Convention for the Prevention of Pollution (MARPOL) from Ships, 1973 (as modified by the Protocol of 1997) will be followed.

6.1.2 Water column impacts

In case of collector test, pumping of seawater to the surface or discharge of midwater plume is not planned and hence no impact in water column is expected.

6.1.3 Effects of nodule removal

Collection of nodules from the associated sediments that are mainly clay sized particles could disturb the benthic habitat in the mining area causing changes in the seabed habitat. This could lead to alterations in seafloor micro-topography as well as physico-chemical conditions of the sediments. However in the case of the collector trials, the maximum impacted area from where the nodules will be removed will only be 0.0016 km^2 (1.6 m pickup width x 1000 m length of track = 1600 m^2) in which the maximum quantity of sediment picked up could vary between 1600 kg for 20% of sediment adhering by weight of nodule at 50% expected

efficiency of the nodule collector (see Table 6.4.1 for details) which is not likely to have a significant effect on the physico-chemical environment of the area.

6.1.4 Effects of plume dispersal

It is expected that due to the locomotion and sucking up action of the nodule miner / collector, a sediment plume will be generated due to the digging and churning of sediments which will be resuspended in the near bottom water column, either from the mining machine or from the slurry discharge locally 80 m above the seabed. Likely impacts from sediment plume formation during deep-sea mining include mixing, resuspension and redeposition of sediments blanketing in the vicinity of the mine site that could lead to burial of benthic organisms and clogging of their filter feeding organs, oxygen depletion in the resedimented seafloor and the water column within the plume due to changes in labile organic matter or reduced metal, and release of toxic metals from leaching and bioaccumulation of contaminants.

The above effects can be measured through collection of environmental data in the near bottom waters as a reference before the collector operation as well as analysing water and sediment samples at regular intervals through time series observations using sensors mounted on moorings or physical sampling. It is proposed to deploy moorings around the test area with sediment traps and current meters to collect real time data on movement of sediment particles during the collector trials.

However during the trials, the activity is restricted to collection of nodules on the seafloor and discharging them immediately behind the collector, which is not likely to create a sediment plume except for a minor disturbance about 0.5-1 m above the seafloor that would settle within the tracks. The other operation involves pumping the collected nodules with sediments adhering to it, to a height of 50-80 m and releasing it causing resettlement of the particles around the collector track. As the calculations (section 6.4) show, the concentration of solids in water that would be released during this activity will be $\leq$ 0.03% of the total volume of water extending up to 100 m (50 m on either side) of the 1000m track. If the lateral extent is more than 100 m as expected here, the dilution will be much more and concentration of suspended particles be still smaller. Hence, it is not expected to cause any harm to the biota or changes on the sediment deposition patterns on the seafloor.

6.1.5 Effects of noise and light

Noise and vibration generated by nodule collection machine, the riser pipe and the ship can affect the auditory senses and systems of some of the marine animals and such noise can also interfere with communication between animals or limit their ability to detect prey (Popper et al., 2003). Many of the deep-sea fishes depend on underwater sound for communication during mating and also for navigation (https://news.agu.org/press-release/new-research-reveals-sound-of-deep-water-animal-migration/) and noise generated at the base of the thermocline in the "deep-sound channel" has the potential to travel long distances (see https://dosits.org/wp-content/uploads/ 2017/07/DOSITS-Booklet-2015-web.pdf). Hence the positioning of pumps along the vertical transport or riser pipe may need to avoid the deep sound channel as well as the deep scattering layer where large concentrations of fish and invertebrates as well as deep diving marine mammals that feed on them are found (Weaver and Billet, 2019).

It is expected that seafloor mining operations may require lights on the support ship as well as on the collector for photography purpose. Light can penetrate a few hundred metres in the ocean and as most deep-sea fishes are sensitive to light, it could have an impact on their vision. That is why, depending on the species, deep-sea fishes either avoid or are attracted by artificial light. Bright artificial light can also obscure or completely block the function of bioluminescence, which is fundamental to deep-sea organisms for e.g. orientation (especially in rough terrain), communication, finding food, mating, and defence against predation Weaver and Billet, 2019). However in contrast to the long-term continuous mining operation, the nodule collection trials are not expected to cause any serious harm.

The ensuing sections provide detailed estimations of the area likely to be impacted, as well as volume and weight of sediment and nodules to be disturbed during nodule collection trials, followed by the results of the benthic impact experiment conducted by India in CIOB and the development of sediment plume model. The last section deals with the likely impacts of the collector trials on physico-chemical environment based on detailed environmental variability data as well as the impact assessment carried out during the Indian Deep-sea Environment Experiment.

6.2 Results of benthic impact experiment

6.2.1 Background of benthic impact experiments

Several Benthic Impact Experiments (BIEs) have been carried out so far to assess the potential impact of nodule mining on the seafloor conditions. The first impact assessment study for deep-

sea mining was during two of the pilot mining tests under the Deep Ocean Mining Environment Study (DOMES, 1972-81) conducted by Ocean mining Inc (OMI) and Ocean mining Associates (OMA) in the Pacific Ocean. Subsequently, several experiments have been conducted by different research groups (Table 6.2.1.1) for assessing the potential impacts using devices such as the plough-harrow as well as a hydraulic sediment re-suspension system in the Pacific and Indian Oceans.

Table 6.2.1.1: Basic data of Benthic Impact Experiments (BIEs) for assessing potential environmental impact of nodule mining

Experiment	Conducted by	Area	Tows	Duration	Area/ Distance	Discharge
DISCOL	Hamburg University, Germany	Peru Basin	78	~12 days	10.8 km^2	--
NOAA -BIE	National Oceanographic & Atmospheric Administration, USA	Clarion Clipperton Fracture Zone	49	5290 mins	141 km	6951 m^3
JET	Metal mining Agency of Japan	Clarion Clipperton Fracture Zone	19	1227 mins	33 km	2495 m^3
IOM -BIE	InterOceanMetal – consortium of East Europen Countries	Clarion Clipperton Fracture Zone	14	1130 mins	35 km	2693 m^3
INDEX	Govt. Of India / National Institute of Oceanography,	Central Indian Ocean Basin	26	2534 mins	88 km	6015 m^3

Note: It is important to note that all these studies were conducted prior to the environmental guidelines issued by International Seabed Authority.

6.2.2 The Indian Deep-sea Environment Experiment (INDEX)

This program has been conducted as follows:

1995-1997 - Baseline data collection for identification of experimental disturbance site (EDS-Test area) and preservation reference site (PRS-Reference area)

1997- Benthic impact experiment

2001-2005 - Long-term monitoring of impact and restoration of environmental conditions in EDS and PRS

6.2.3 Baseline data collection in proposed candidate sites

Five areas of 10kmx10 km were selected to carry out baseline studies for selection of test and reference areas for the benthic impact experiment.

The coordinates of these areas (Fig. 6.2.3.1) were as follows:

A1 : 10 00 - 10 10 S, 75 55 - 76 05 E

T1 : 10º00' - 10º10'S, 75º10' - 75º20' E

R1 : 10º00' - 10º10'S, 75º35' - 75º45' E

T2 : 12º15' - 12º25'S, 75º45' - 75º55' E

R2 : 11º55' - 12º05'S, 76º00' - 76º10' E

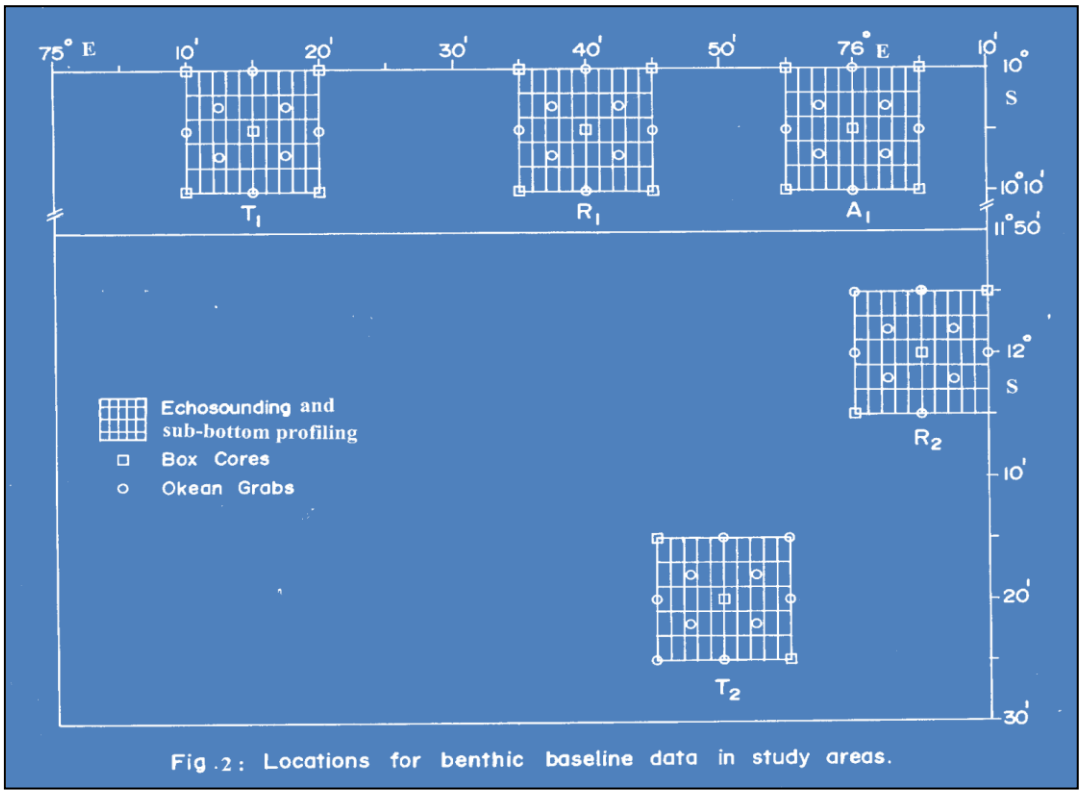

Fig. 6.2.3.1: Study areas for selection of test and reference areas for BIE

For this purpose the quantum of work done was as follows:

- Number of cruises = 2
- Number of study areas of 10 x 10 miles = 5
- Bathymetric and sub-bottom profiling = 1500 km
- Box core and grab samples = 64
- Bottom photographs obtained = ~300

6.2.4 Selection of Test and Reference areas

Based on the geological and environmental data collected for 5 sites in the CIOB, Area A1 was selected as the test site or Experimental Disturbance Site (EDS) and Area T1 was selected as the reference site or Preservation Reference Site (PRS) (Fig. 6.2.4.1). The average nodule abundance, water depth and slopes in these areas are given in Table 6.2.4.1.

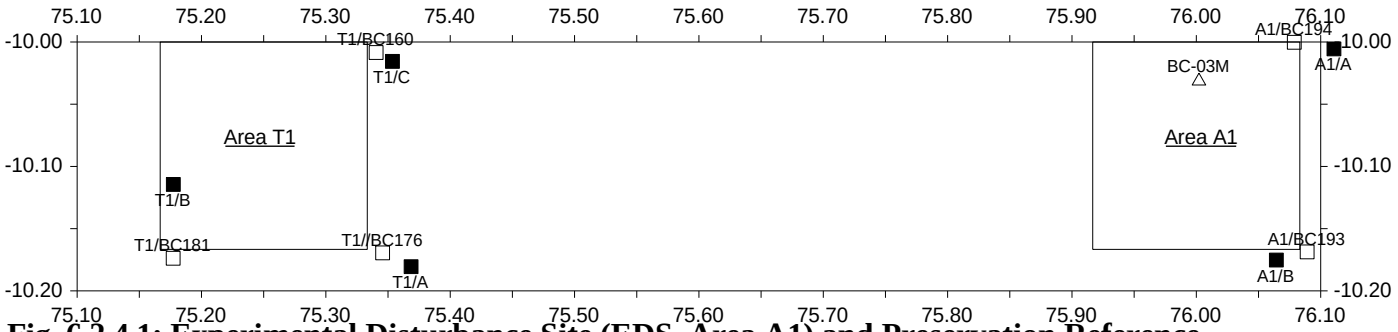

Fig. 6.2.4.1: Experimental Disturbance Site (EDS, Area A1) and Preservation Reference Site (PRS, Area T1)

Table 6.2.4.1: Selection of test & reference areas for impact experiment

Area	Av. Abundance (kg/m^2)	Av. Depth (m)	Av. Slope	Remarks
A1	2.10	5327	1.1	Test area (EDS)
T1	1.94	5217	1.1	Reference area (PRS)
R1	1.14	5330	1.4	-
T2	3.41	5217	1.7	-
R2	5.05	5297	1.7	-

6.2.5 Benthic disturbance experiment

This section describes the Indian Deep-Sea Environment Experiment (INDEX) in the Central Indian Ocean Basin and reports the migration trends of suspended sediments in and around the disturbed area. The experiment was conducted as a part of the Indian programme on 'Environmental impact assessment of nodule mining funded by the Ministry of Earth Sciences (Govt. of India) and executed by CSIR-National Institute of Oceanography, Goa (India).

6.2.5.1 Study area

A test site of 3.5 km x 5.4 km, with a disturbance strip of 3 km x 200 m in NW–SE direction was selected, which lies between 10101°S and 75159°E and 10103°S, 76102°E and depth ranges between 5300 and 5400 m (Fig. 6.2.5.1.1). The disturbance zone has even topography, no rock outcrops and low nodule abundance. as per the requirements for operation of the benthic disturber. The total relief around this site is 20–40 m, with low nodule abundance (<2 kg/m2).

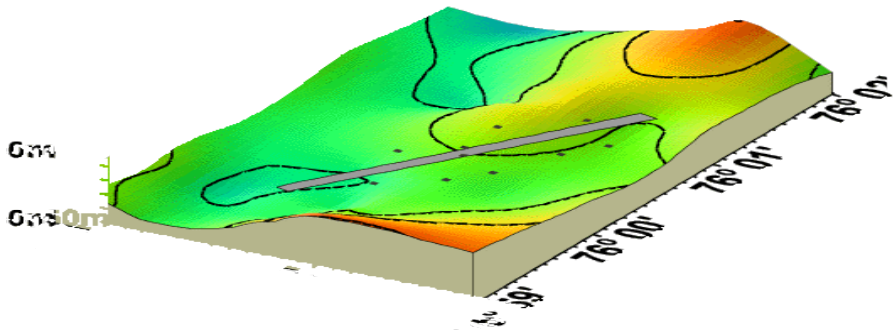

Fig. 6.2.5.1.1: Experimental disturbance area

The site was surveyed by deep-towed sub-bottom profiling (5 kHz) equipment along 3 profiles. The sediment thickness in the area varies from 40 to 90 m, with 4 distinct layers of sediment. The upper two layers are very thin (mean thickness 3.5 and 5 m) and lower two layers are thicker (mean thickness 22 and 35.5 m). The sediment type is siliceous ooze, mainly consisting of clay minerals such as smectite, illite, chlorite and kaolinite, as well as authigenic assemblages, such as Fe-rich smectites, phillipsites, other zeolites, and Fe–Mn oxides.

6.2.5.2 Systems deployed for benthic disturbance experiment

The experiment was conducted during two cruises of R.V. Yuzhmorgeologiya: (i) pre-disturbance cruise (27 May–8 July 1997); and (ii) disturbance and post-disturbance impact assessment cruise (22 July–5 September 1997). A 6-channel Magnavox MX 200 receiver was used to obtain Global Position System (GPS) fixes. ASMOD (underwater positioning system) was used for underwater positioning of the survey equipment. ASMOD consists of four

acoustic transponders that were deployed and calibrated during the pre-disturbance cruise. GPS and ASMOD fixes were integrated to enable maneuvering of underwater survey and sampling equipment. The position data in both GPS and ASMOD were computed on WGS-72 spheroid to enable integration with previous survey data base in the site. GPS was used for the ship's position, and ASMOD was used for all the operations (such as disturber, deeptow camera and coring) in and around the disturbance area. During sediment sampling, precise positioning was obtained with the help of pinger along with the ASMOD data.

Deep-sea moorings with sediment traps were deployed close to the bottom (7 m above the seafloor) at 10 locations around the disturbance zone (Fig. 6.2.5.2.1) to record the time series data on fluxes before, during and after the disturbance. These were retrieved in the post-disturbance cruise after conducting the disturbance experiment and collecting data on the post-disturbance effects. The effects were also studied by deep-towed cameras and box corer samples (Fig. 6.2.5.2.1) in the pre- as well as post-disturbance phases.

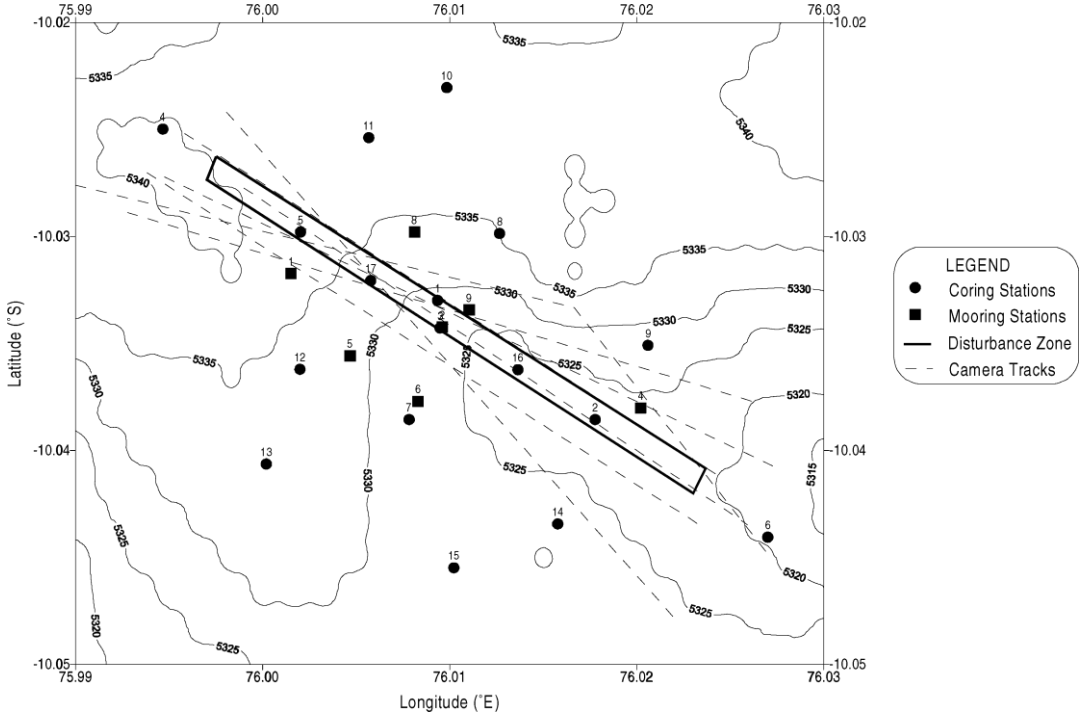

Fig. 6.2.5.2.1: Locations of camera profiles, sediment traps, box cores in the experiment site (Depths in meters)

6.2.5.3 Equipment for benthic disturbance experiment

The experiment was conducted with a benthic disturber (Fig. 6.2.5.3.1), named 'Deep-Sea Sediment Resuspension System (DSSRS)', developed by the Sound Ocean System Inc. (SOSI), USA. The disturber creates an artificial disturbance on the seafloor by fluidising the bottom sediment as it moves on the seafloor, and pumps and discharges the sediment through a 5 m-

high stack. The plume created by the resuspended sediment was studied to assess the impact of such a disturbance on the benthic ecosystem. The same disturber was used earlier for three of the deep sea disturbance experiments conducted by NOAA (USA), MMAJ (Japan) and IOM (consortium of Eastern European countries).

Fig.6.2.5.3.1: Deep-sea sediment resuspension system

6.2.5.3.1 Components of the disturber

Main unit

The tow frame, which weighs 3.2 t is hydrodynamically designed to house the subsystems of the disturber and has dimensions of 4.8 m x 2.4 m x 5.0 m. The frame is connected with a coaxial cable that tows as well as transmits signals and power to the disturber unit. The frame consists of a discharge stack, 5 m high, with a diameter of 30 cm and is bell-shaped at the bottom, where the sediment is sucked up and discharged from the top. There are two pumps on the disturber, one for fluidising the sediment by water jets with 16 nozzles and another to suck the sediment slurry and raise it through the discharge stack. The pumps are controlled from the deck unit. A rosette of 12 bottles of 1.7 l capacity is attached near the discharge stack to collect samples of water with resuspended sediments at select intervals and used to quantify the

resuspension rate. A TV camera is attached to the frame to view the functioning of the disturber, which is monitored from the deck unit.

Depressor and cable

This unit weighs about 1 t and is attached to the cable, about 200 m ahead of the disturber, to help dampen the ship motion. A 21-mm coaxial cable is used for deploying, operating and transmitting power and signals to and from the system.

Deck unit

This is a PC-based system with custom made software and hardware to monitor and control the operation of the system. Clogging of the pumps can be sensed through the current level from the monitor and corrective measures can be taken. The camera, lights, and rosette can be operated from this unit. Also the video image transmitted by slow scan camera can be seen on the TV monitor.

Operation of the disturber

The disturber is attached to the coaxial cable in front of the frame and has a transponder for acoustic positioning. Once the disturber touches the bottom, its functioning can be monitored from the altitude, roll, pitch and heading displays on the deck unit, where the functioning of the pumps also can be controlled. Plume generation can be seen on the video monitor, and the average sediment pumped can be estimated by taking intermittent water samples in the rosette on the disturber. The position of the disturber was observed real time on the acoustic navigation system (ASMOD).

Quantum of disturbance in the study area

Salient features of the disturbance are as follows (Sharma et al., 2000):

- Total number of tracks=26,
- Total days of disturbance=9,
- Disturbance time=42 h 14 min,
- Estimated sediment resuspension=3555 t (6023 m3),
- Total dry sediment resuspended=580 t,
- Total distance covered=88.3 km.

6.2.6 Results of benthic impact experiment

6.2.6.1 Seafloor disturbance from photo and video data

Observations were made by deep-towed TV and photo system to evaluate the seabed features in and around the disturbance area in order to assess the impact of benthic disturbance on the

seafloor. The deep-tow system was operated 4–5 m above the seafloor, during which continuous online observations were made onboard from the video data, and a 35-mm still camera was operated remotely in the areas of interest. The survey profiles were carried out up to 750 m on either side as well as across the disturbance site. Pre-disturbance photographic data show typically undisturbed conditions, with extensive biological activity in the form of benthic organisms, their fecal casts, burrows, tracks and trails (Fig. 6.2.6.1.1a). In contrast, immediate post-disturbance observations show tracks of disturber as pairs of depressions of the sleds and fluidised sediment surface between them (Fig. 6.2.6.1.1b). These areas are devoid of any biological activity except for an occasional megabenthic organism. Sediment piled up on the sides of the disturber tracks due to its motion could be observed in areas adjacent to the tracks. The camera profiles parallel to the disturber tracks showed lumps of sediment that had been redeposited from the discharge stack either on the track or besides them during the tow (Fig. 6.2.6.1.1c). The other areas showed a very fine layer of sediment cover resulting in smooth microrelief (Fig. 6.2.6.1.1d) and no burrows, fecal casts or animal trails. The areas away from the tow zone do not show any effects of disturbance and have fecal casts, burrows, trails as well as megabenthic organisms.

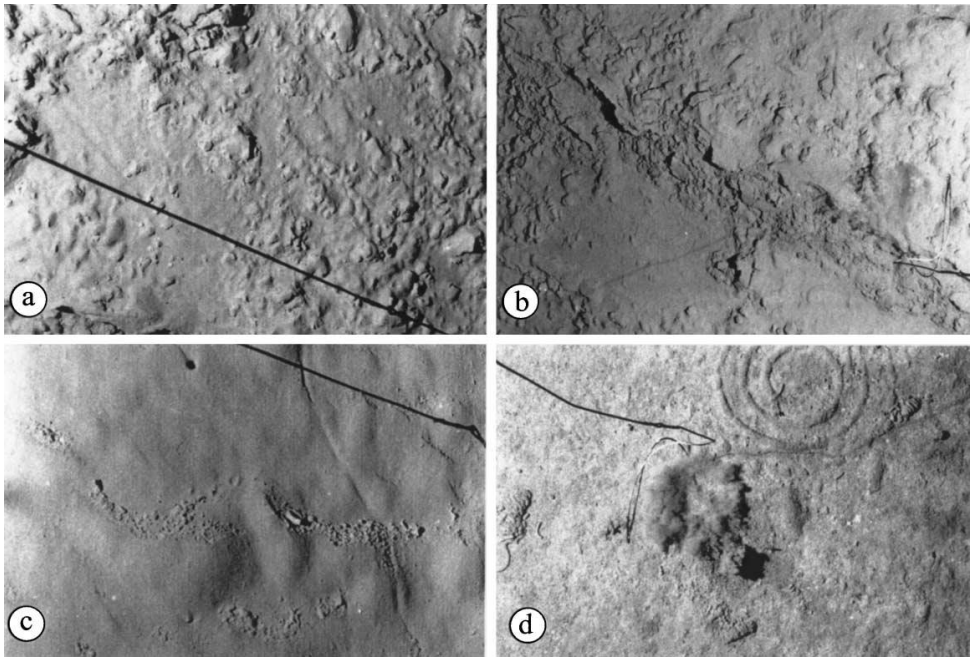

Fig. 6.2.6.1.1: Disturbance features from seabed photos (a) disturber tracks, (b) piles of sediment, (c) resedimentation,(d) undisturbed seafloor.

In order to evaluate the areal extent of the impact, frequency distributions of different disturbance features noted in photographs were plotted with respect to the distance from the center of the disturbance track (Fig. 6.2.6.1.2). Most of the tracks of the disturber (87%) as well

as sediment piles (91%) generated due to the disturber movement are concentrated within 100 m on either side. This is expected because the width of the disturbance site is 200 m. Mostly (57%) the effect of resedimentation is observed within the disturbance site (i.e. 100 m on either side). Many of the (89%) resedimentation features are observed up to a distance of 200 m, and few (11%) up to a distance of 250 m on either side, which means that the sediment has travelled up to 150 m away from the disturbance site. Consequently, most of the undisturbed areas (75%) are concentrated beyond 100 m on either side of the disturbance site and extend up to more than 750 m on either side, which is the limit of the photographic data. Of all these data, the most interesting is the area of influence due to resedimentation, which extends up to 150 m from the edge of the disturbance site.

The highest intensity is shown by the locations within disturbance tracks, followed by those with lumps and piles of sediment, the resedimented areas and the undisturbed seafloor representing the least disturbance in the area. The intensity of impact is the highest within the disturbance zone and decreases away from this zone (Fig. 6.2.6.1.3). Image analyses methods have been used to determine the intensity of disturbance, from the variation in colour intensity of the sediment in deeptowed photographs. This photographic and colour intensity data can be used to compare the photos of subsequent observations, during monitoring, to assess the restoration of seafloor features over a period of time.

6.2.6.2 Sediment resettlement from flux data

Particle fluxes in the near bottom water before, during and after the disturbance, were estimated from time series sediment traps at 7 m height above the seafloor, moored at 10 locations around the disturbance site. Each mooring consisted of one sediment trap (a Russian-made Lotus time series sediment trap with 12 sampling cups). The collection area of the traps is 0.5 m^2. In all, 8 moorings could be retrieved after the disturbance. Out of these, 5 moorings (DMS-1, 2, 4, 8 and 9) collected samples during most part of the experiment. The moorings DMS-5 and 6 functioned only partially, collecting particles only during pre-disturbance phase. Hence, the flux data are based on 7 traps.

Observations from sediment traps deployed around the disturbance area (Fig. 6.2.6.2.1) show that the near-bottom particle fluxes in the pre-disturbance phase (~40 days) range from 41 to 55 mg/m^2/ day in different traps, with an average of 48 mg/m^2/day for the experiment site. During the disturbance phase (8.5 days), the particle fluxes increased by 3–4 times in different traps, with an average of 150 mg/m2/day. The average fluxes in the post-disturbance phase (5–6 days) dropped to 95 mg/m^2/day. This means that the fluxes, which had increased by 300% from

the background value during the disturbance phase, reduced to 200% (or by 33%) within 5–6 days of the last disturbance. So it is expected that the remaining particles suspended in the near-bottom water column, would either settle very fast, or the finer particles may remain in suspension for a longer time and get transported to the adjacent areas. Therefore, the silty sized sediments being relatively coarser (and heavier) may settle down soon after the disturbance, whereas the clay sized sediment may remain in suspension for a longer period.

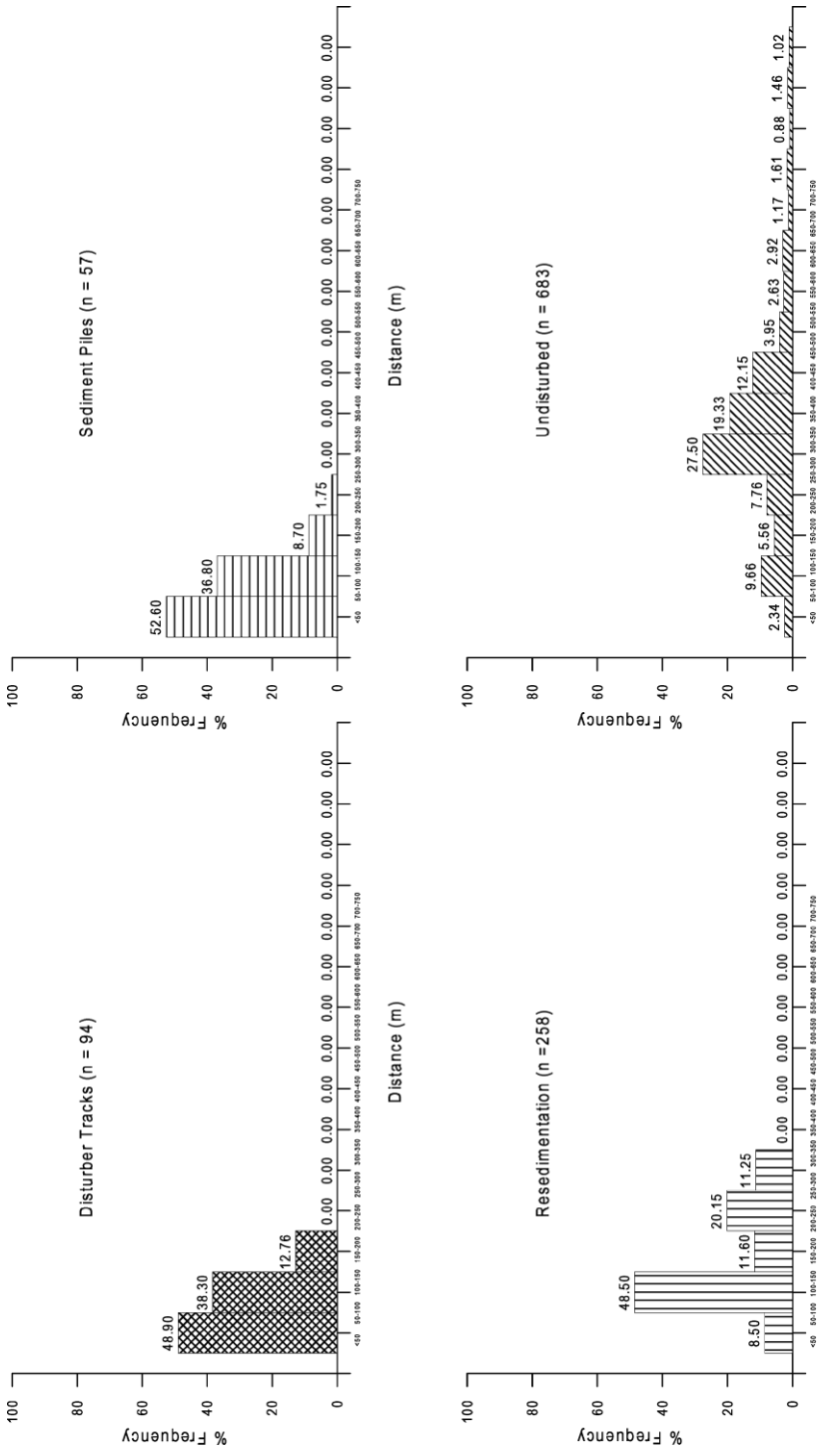

Fig. 6.2.6.1.2: Frequency distribution of disturbance features.

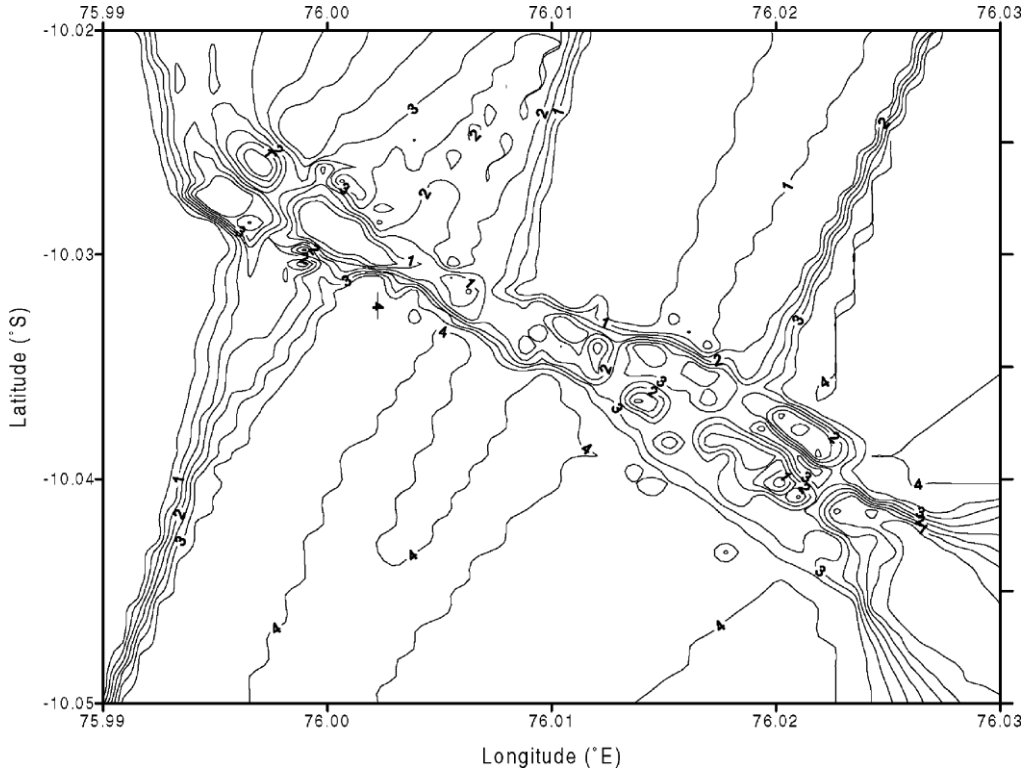

Fig. 6.2.6.1.3: Contour diagram of intensity of disturbance from photographic data: (1) Highest disturbance, (2) moderate disturbance, (3) low disturbance, (4) no disturbance.

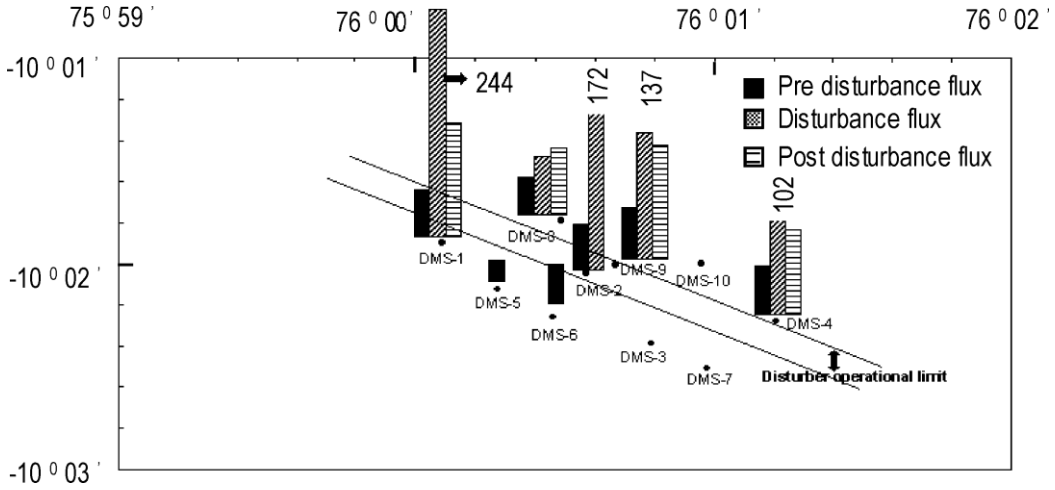

Fig. 6.2.6.2.1: Relationship between particle fluxes and locations of traps.

Particle fluxes recorded in different cups during the disturbance period were compared (Fig. 6.2.6.2.2) to analyze the resettlement of particles during this period. Out of the two cups that collected particles during the disturbance period, the first cup contained marginally fewer particles compared to the second cup, at two out of three locations. The rate of sediment pumped being almost the same during the entire 8.5-day period, it appears that some of the

sediment from the first part of disturbance remained in suspension, and subsequently settled into the second cup, increasing the collection in the later period. This probably indicates that some of the sediment particles remain in suspension for sometime after the disturbance. The higher collection in the post-disturbance phase, as compared to background values, also indicates the subsequent settling down of some of the resuspended particles. However, the increase is seen in the traps closer to the disturbance zone (within 100 m) compared to one slightly farther away (200 m). Duration of each cup is 5 days, hence it can be presumed that during this period the resuspended particles reach up to 100 m, and may take more time to get transported to more distant areas.

In order to evaluate the transportation pattern of the suspended particles, the fluxes were plotted with respect to distance from the center of the disturbance site for all the three phases (Fig. 6.2.6.2.3). In the pre-disturbance phase, the collection is almost uniform irrespective of the distance, as the traps collect the particles that are settling under natural conditions. During the disturbance phase, the traps closest to the disturbance track (DMS-2 and DMS-9) collected higher amounts of resuspended sediment, compared to others away from the site. However, one trap (DMS-1) had anomalously high sediment flux, which may correspond to the general deep-sea current circulation in the area. In the post-disturbance phase, particle fluxes were lower than that during the disturbance period. The other trap closest to the disturbance site (DMS-9) continued to record very high fluxes, but in general the fluxes decreased with distance from the disturbance site. Once again, one trap (DMS-1) showed anomalously high collection during this phase as well, although it was away from the site.

Collection of higher quantities of particles may be related to general current direction in the area during the period of disturbance. Observations from current meters deployed at 5100 m depth close to the site indicate the current direction to be S–SW during this period (NIO, 1997). Preferential deposition of sediment in a particular direction (north of tow zone) was observed during NOAA's Benthic Impact Experiment, as well (Trueblood, 1993). This indicates that although the sediment particles are resuspended very close to the seafloor (B5 m) where the intensity of currents is very low, they do follow the prevailing currents at these abyssal depths. This also indicates that the impact of resedimentation will not only be in the disturbed zone, but also will spread to adjacent areas, the intensity of which will depend upon various factors such as the strength of the currents, size of the particles, volume of sediment discharged as well as the altitude of discharge. Consideration of all these parameters will determine the potential impact of sediment redistribution on the seafloor environment.

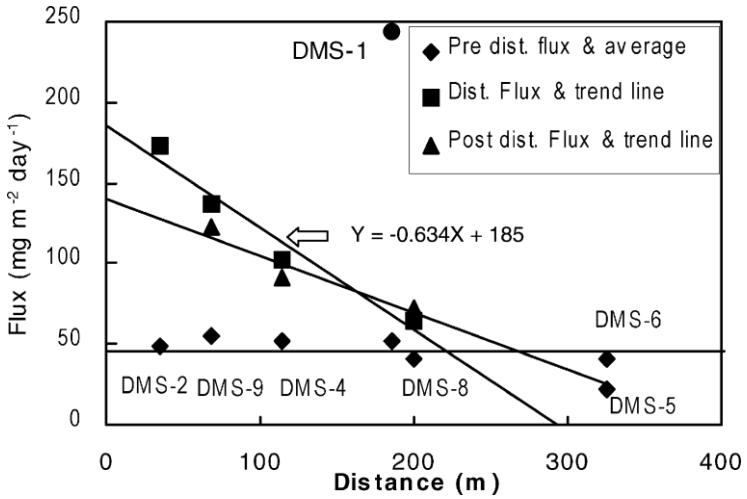

Fig. 6.2.6.2.2: Comparison of particle fluxes recorded by traps during the disturbance period.

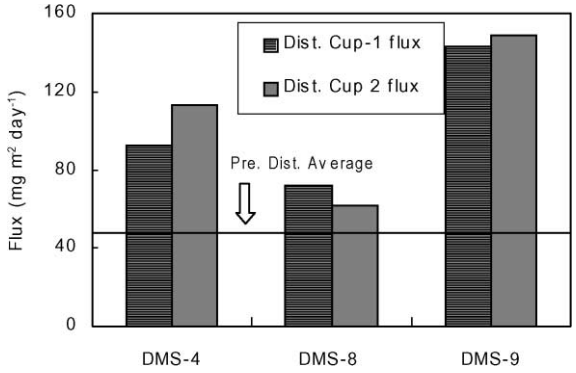

Fig. 6.2.6.2.3: Relationship between particle fluxes with respect to distance from disturbance site.

6.2.6.3 Sediment movement deciphered from organic carbon data

Sediment sampling was carried out with spade/box cores (50 cm x 50 cm x 50 cm) at the locations within the disturbance track, adjacent to the disturbance area and at locations away from the disturber track (Fig.6.2.6.3.1). Cores were obtained by inserting the acrylic core liners, which were sub sampled for the sedimentological, geochemical, mineralogical, biostratigraphic and geotechnical studies. Sub sampling was carried out at 2 cm intervals, and organic carbon was determined by wet oxidation method for sediment cores representing pre- and post-disturbance phases. Analyses of the sediments from both the phases were carried out on the same day to avoid any errors, and precision was checked by repeating the analyses of some of the samples.

Particulate organic carbon or sedimentary organic matter is an important parameter in benthic ecosystem sustenance. The benthic biomass is directly related to both the quantity and quality of the available organic matter.

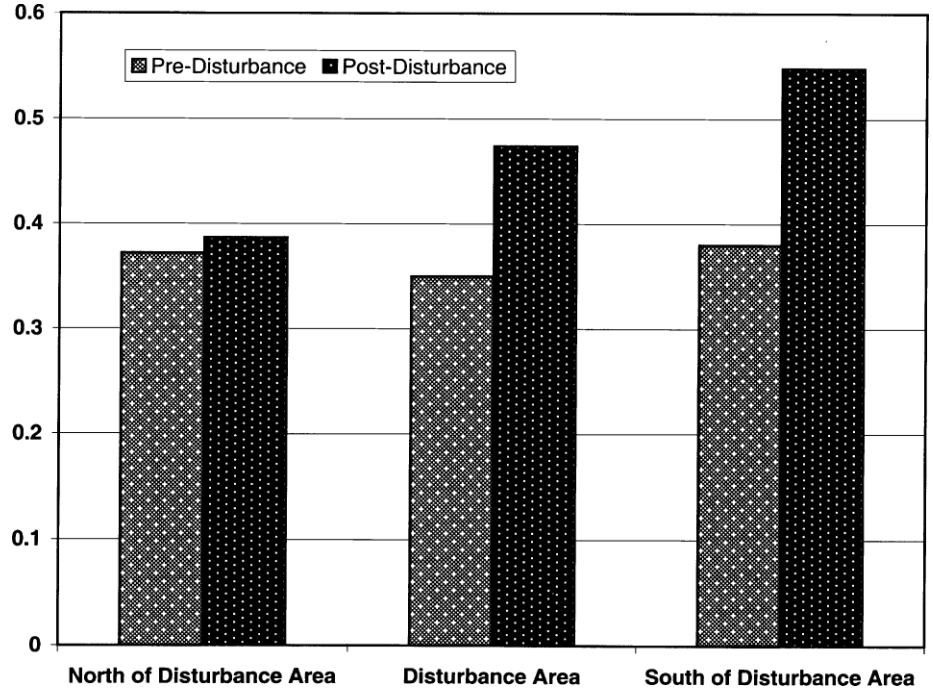

Fig.6.2.6.3.1: Comparison of average organic carbon contents (%) in surface sediments of pre- and post-disturbance phases of different areas.

The organic carbon levels were studied in the sediments representing both the pre- and post-disturbance phases. Within the accuracy levels of bottom transponder based acoustic navigation system, the same location could be sampled in both the phases. Post-disturbance sediments in general showed an increase in organic carbon levels, but varying horizontally (Fig. 6.5.3.2). No changes are observed for average organic carbon values in the area to the north of the disturbance site, unlike an increase (by 30%) in the disturbance site, and an even higher increase (45%) in the area to the south of the disturbance site (Fig. 6.2.6.3.2). It appears that the condition of surface sediment in the area to the north remained stable during the pre- and post-disturbance phases, in comparison to other two areas. This may be due to redeposition of suspended sediments within the site and transportation of organic carbon-rich surface sediments to the south. Further, the distribution of organic carbon in surface sediments plotted for pre- disturbance phase (Fig. 6.2.6.3.2) shows that the trend is gradual (from 0.28% to 0.4%) from NW to SE end of the site. The distribution in post-disturbance phase shows a significant increase within the site and also in the reverse direction, i.e. from SE to NW. The values are

also significantly high (up to 0.64%) in the SW direction. Due to the prevailing currents, the fines may have been removed and deposited in the general direction of the bottom currents. The dominant benthic current direction during June–August is towards S–SW and the spatial distribution map of organic carbon has clearly shown an increase in this direction (Fig. 6.2.6.3.2), indicating the direction of resedimentation.

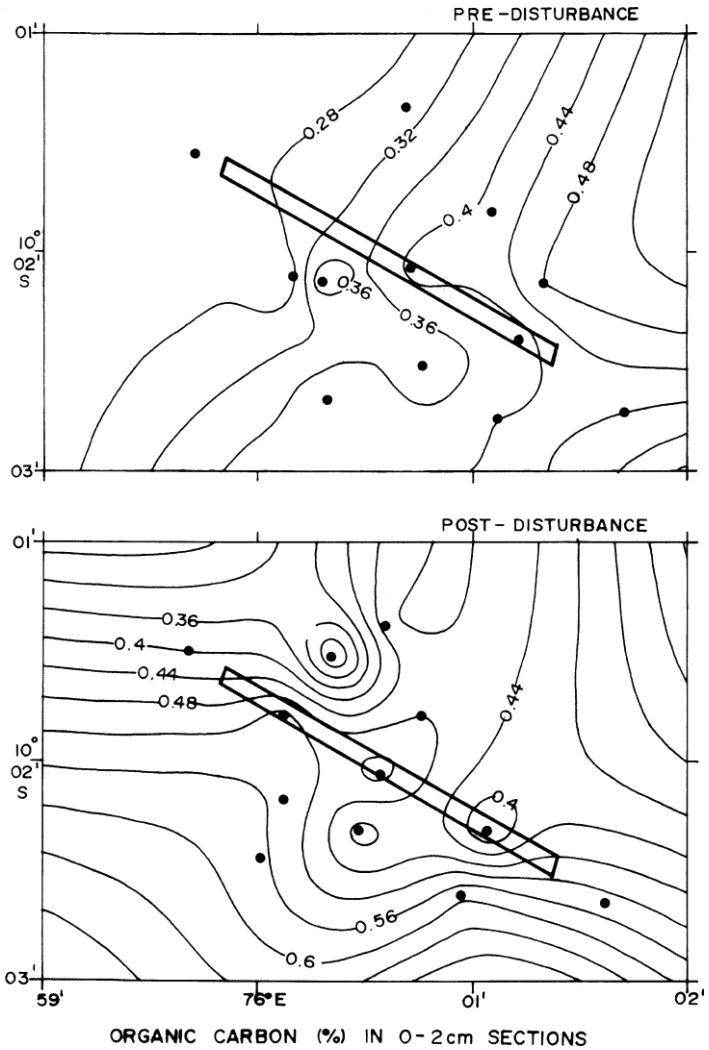

Fig. 6.2.6.3.2: Distribution of organic carbon in surface sediments in pre- and post disturbance phases. A clear increase in post-disturbance organic carbon contents is noticed in the S–SW direction.

6.2.7 Salient observations of impact assessment and monitoring of disturbance

In order to monitor the processes of restoration of benthic environment and re-colonization by the organisms, the first set of observations on all parameters were undertaken onboard RV AA Sidorenko during March-April 2001. The data was collected at the same locations as in the pre-disturbance and post disturbance phases, as well as at reference locations where the baseline data was collected earlier. The second cruise for monitoring the recolonisation and

restoration of the benthic environment was undertaken during May-June 2002 onboard RV AA Sidorenko which was followed by the third monitoring cruise onboard RV AA Sidorenko during March-April 2003 and the fourth cruise of RV Akademik Boris Petrov to Central Indian Ocean Basin was organized from 26 March to 2 May 2005. Salient observations of key environmental parameters in EDS and PRS are given in Tables 6.2.7.1 and 6.2.7.2. Key findings of these observations are as follows:

i. Clay concentrations continued to remain higher than the pre- and post-disturbance levels, including at the reference locations, indicating natural influx of clay possibly from distal/proximal sources.

ii. After the initial drop in shear strength and minor increase in water content in post-disturbance phase, shear strength and water content vary in a narrow range in different phases of the study. Also slight change in water content appears to result in large variation in shear strength values.

iii. Nutrient profiles and organic carbon content in sediment have shown natural variation following the restoration of the conditions immediately after the experiment.

iv. The macrofaunal and meiofaunal density show that although restoration was initiated after the experiment, their numbers have been very low subsequently, not only in the experimental area but in the reference area as well probably due to natural underwater disturbances.

v. Substantial increase in carbohydrates, proteins and lipids suggest that the benthic environmental conditions are amenable to growth of fauna, but the bacterial numbers are taking longer time to get restored.

From the above observations, it can be inferred that although the environmental conditions have not been restored to the pre-disturbance / baseline levels, the different parameters appear to be under the influence of natural variability and the initial effect of the disturbance experiment has waned off.

Table 6.2.7.1: Salient features of environmental data during monitoring at EDS

Parameters*	**Pre-dist. (June97)**	**Post-dist. (Aug. 97)**	**Monit. I (Apr. 01)**	**Monit. II (June 02)**	**Monit. III (Apr. 03)**	**Monit. IV (Apr. 05)**
Clay (%)	35	40	62	62	56	68
Water Content (% dry)	544	563	463	567	616	503
Shear Strength (kPa)	2.08	0.75	3.47	3.35	2.47	3.00
Organic Carbon (%)	0.35	0.46	0.28	0.35	0.37	0.31
Macrofauna (No. m^{-2})	229	179	177	--	66	64
Meiofauna Abund. (No. 10 cm^{-2})	46	23	17	6	11	6
Meiofauna (Groups)	11	4	9	6	10	4
Microbes (Total counts)	10^9	10^7	10^8	10^6	10^7	10^7

*****Average concentrations of key parameters for surface samples of 3 cores in the experimental site.

Table 6.2.7.2: Salient features of environmental data at preserved reference site (PRS)

Parameters*	**Pre-dist. (June 97)**	**Post-dist. (Aug. 97)**	**Monit. I (Apr. 01)**	**Monit. II (June 02)**	**Monit. III (Apr. 03)**	**Monit. IV (Apr. 05)**
Clay (%)	53	53	49	56	52	68
Water Content (% dry)	525	588	561	552	582	545
Shear Strength (kPa)	2.8	4	7.1	4.8	2	1.95
Organic Carbon (%)	0.36	0.55	0.26	0.36	0.45	0.26
Macrofauna (No. m^{-2})	197	96	225	NA	74	60
Meiofauna Abundance (No. 10 cm^{-2})	35	32	25	3	18	5
Meiofauna (Groups)	7	7	5	3	7	3
Microbes (Total counts)	10^9	10^7	10^7	10^6	10^6	10^7

*****Average concentrations of key parameters for surface samples in cores in the reference site**.**

6.3 Development of sediment plume dispersion model

Dispersion characteristics of the sediment plume that is generated on account of any sediment disturbance activity such as mining largely depend upon the current velocities and their vertical structures in the benthic layer. Therefore information on the variability of the ocean currents in the benthic layer is very much essential to model the dispersion of sediment plume. During the benthic disturbance experiment conducted during August 1997, it was observed that the sediment plume migrated in different directions after it was discharged at 10m above from the seafloor. This has resulted in different changes in the benthic environment, its biogeochemical processes and the distribution of benthic organisms. The effects of similar discharge in case of nodule mining will depend on various factors, such as, the height of discharge, the density of sediments and their composition, the discharge rate, the *in situ* currents as well as the structure of the water column.

In order to predict the dispersion of sediment plume in the water column under different conditions, modeling studies have been initiated since 2003. For this purpose, the baseline data collected on water column characteristics, sediment types and bottom topography are used as inputs to simulate sediment dispersion at different levels and to predict its migration in the mining area.

As a part of this study, a 3-dimentional model for sediment dispersion has been developed with the following objectives.

- Development of 3D hydrodynamic model and its applications to the INDEX area of CIOB
- Development of sediment transport model to simulate re-suspended sediment dispersion
- Model simulation of morphological changes of sea bed and blanketing due to sediment deposition
- Calibration and validation with the observed data on sediment fluxes

6.3.1 Model Development

A 3D hydrodynamic model and sediment transport model have been developed and integrated with the graphical user interface. Initial runs of the model have been carried out for testing the model setup using current flux along the open boundaries. In order to simulate the currents during the disturbance period the currents measured at MS5 (Lat: 10 º 01.0’S, Long.

75°59.8'E; Depth = 5330 m) and MS1 (Lat: 9 ° 57.27'S, Long. 74°56.56'E; Depth = 5176 m) have been selected as forcing boundary conditions.

Salient features of hydrodynamic model are

- Solves the basic governing equations of flow momentum, continuity, suspended sediment transport and bed transport numerically in a coupled way.
- 3D BFC grid for irregular topography of flow domain using built-in grid generator.
- Sigma-coordinate system vertically to take into account bottom/bed topography undulations.
- Wind forcing over the computational domain

Salient features of sediment transport model are

- Bottom bed representation through contours of bed grain size distribution.
- Blanket thickness
- Deposition, re-entrainment of sediment particles
- Bed consolidated model based on layer approach
- Sediment sources, like point, line and area
- Pre- and post- processor activities
- On line help facilities

6.3.2 Model capabilities

- Predict suspended and bed load sediment movement for any geographical locations including deep sea.
- Sediment sludge disposal into sea water, dispersion of plume and settling
- The model can be used for either continuous or instantaneous plume sedimentation sources and the model takes into account processes including advection, dispersion·
- It includes many specialized features of graphics and menu driven pre/postprocessor for setting up the input, running the calculation, and selecting and obtaining graphical output for the analysis and for presentation

Salinity transport equation for the model is as follows:

$$\frac{\partial s}{\partial t}+\frac{\partial us}{\partial x}+\frac{\partial vs}{\partial y}+\frac{\partial ws}{\partial z}=\frac{\partial}{\partial z}\left(k_v\frac{\partial s}{\partial z}\right)+\frac{\partial}{\partial x}\left(k_h\frac{\partial s}{\partial x}\right)+\frac{\partial}{\partial y}\left(k_h\frac{\partial s}{\partial y}\right)$$

Temperature equation for the model is as follows:

$$\frac{\partial T}{\partial t}+\frac{\partial uT}{\partial x}+\frac{\partial vT}{\partial y}+\frac{\partial wT}{\partial z}=\frac{\partial}{\partial z}\left(k_v\frac{\partial T}{\partial z}\right)+\frac{\partial}{\partial x}\left(k_h\frac{\partial T}{\partial x}\right)+\frac{\partial}{\partial y}\left(k_h\frac{\partial T}{\partial y}\right)$$

Sediment transportequation for the model is as follows:

$$\frac{\partial c}{\partial t}+\frac{\partial uc}{\partial x}+\frac{\partial vc}{\partial y}+\frac{\partial (w+ws)c}{\partial z}=\frac{\partial}{\partial z}\left(k_v\frac{\partial c}{\partial z}\right)+\frac{\partial}{\partial x}\left(k_h\frac{\partial c}{\partial x}\right)+\frac{\partial}{\partial y}\left(k_h\frac{\partial c}{\partial y}\right)\pm Sc$$

Vertical co-ordinate system (s - co-ordinate system in z-direction)

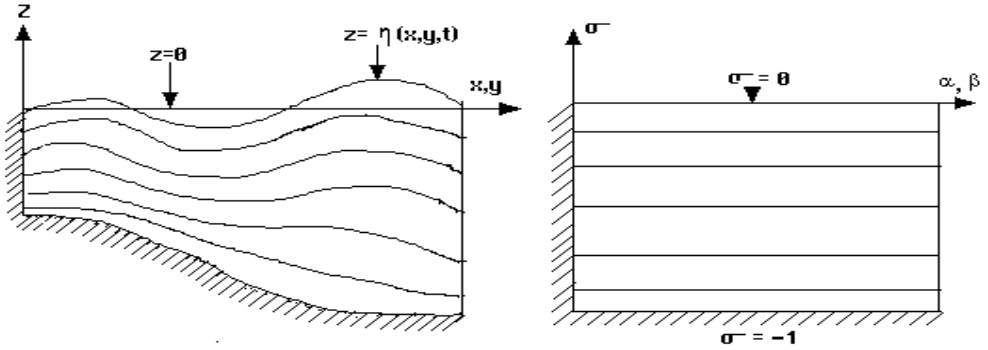

$$\frac{\partial \eta}{\partial t}+\frac{1}{J}\left(y_\eta\frac{\partial (UH)}{\partial \varsigma}-y_\varsigma\frac{\partial (UH)}{\partial \eta}+x_\varsigma\frac{\partial (VH)}{\partial \eta}-x_\eta\frac{\partial (VH)}{\partial \varsigma}\right)+\frac{\partial (WH)}{\partial \sigma}=0$$

Topographic features considered in the model are

- bathymetric map (hydrographic chart)
- bed roughness contours (d50 grain size contours)

Boundary conditions of the model are

- Flux at open boundaries
- Sediment sources location and concentration
- Period of benthic disturbance, quantity of resuspension

Model outputs are

- Hydrodynamic parameters
- Suspended sediment conc. at various locations
- Sediment dispersion pattern

- Blanket thickness, settling
- Sea bed changes due to sedimentation processes.

The software has been tested for its efficacy in the prediction of sediment plume with the available bathymetry (obtained from ETOP-2) and observed currents at MS1 and MS5 locations. The details of implementation of the input data into the model are discussed in the following sections.

Input data used for the model is as follows:

The currents measured at 4, 8, 15, 30, 50, 100 and 500 meters above sea bottom (mab) during October 1996 - May 1997 were analyzed using Tidal Analysis Software Kit (TASK). This was used to prepare the flux boundary conditions along the open boundaries in the model for the disturbance period (August 1997).

6.3.3 Model Implementation

The computation domain (Fig. 6.3.3.1) has been selected between 75° and 77°E longitudes and between 9° and 11°S latitudes for carrying out various model runs. The computational grid is shown in Fig. 6.3.3.2. Since the observed currents are available at two locations (MS1 and MS5), these data (Fig. 6.3.3.3) have been used separately as option 1 (MS1) and option 2 (MS5) for considering as open boundary condition. The predicted currents from the two options at MS5 have been compared with the observed currents at the same location and the results are shown in Fig. 6.3.3.4 and 6.3.3.5 respectively. It is found from Fig. 6.3.3.4 that there is a discrepancy between the observed and predicted currents with option 1. The model simulations using the option 2 are compared well with the observed currents at MS5 (Fig. 6.3.3.5). This highlights the better performance of the model with the option 2 as the open boundary condition. The predicted velocities for various time intervals are shown in Fig. 6.3.3.6 to 6.3.3.8.

The computational domain (Fig. 6.3.3.9) selected for sediment plume simulation is between 75°55'- 76°01'E and 10°04'-10°09'S. The domain has been discretised by 40, 30 and 8 in x, y and z directions respectively. The actual bathymetry (Fig. 6.3.3.9) has been selected for this study and the currents data at MS5 are used as open boundary conditions and the sediment concentration (79.2 mg/l) as a sediment boundary condition at 10 mab. The computed bathymetry is shown in Fig. 6.3.3.10. The software has been run for 2 days and the

dispersion of plume in space (vertical as well as horizontal direction) is shown from Fig. 6.3.3.11 to Fig. 6.3.3.15.

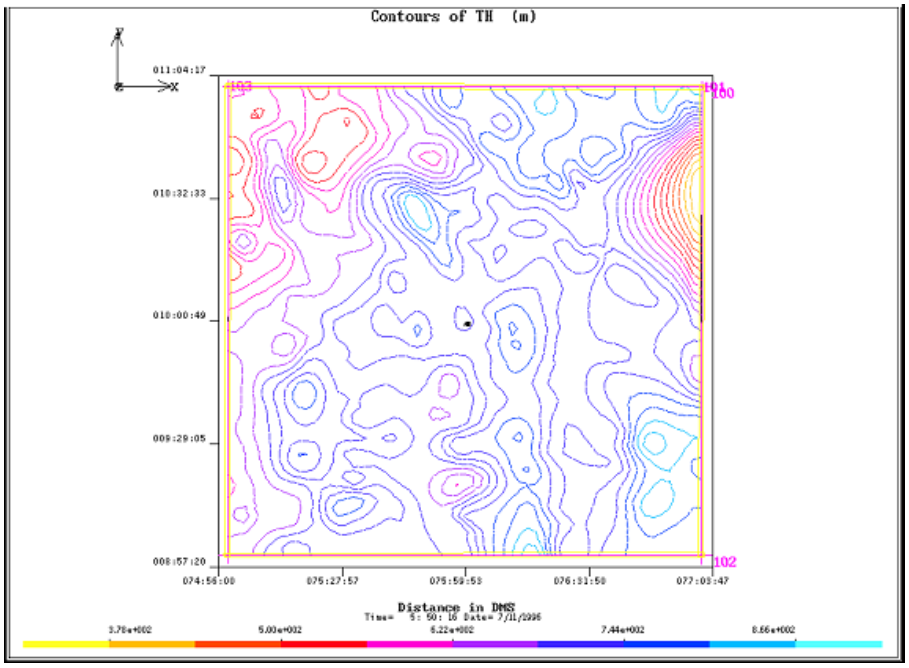

Fig. 6.3.3.1: Model domain with the bathymetry (Obtained from etopo-2)

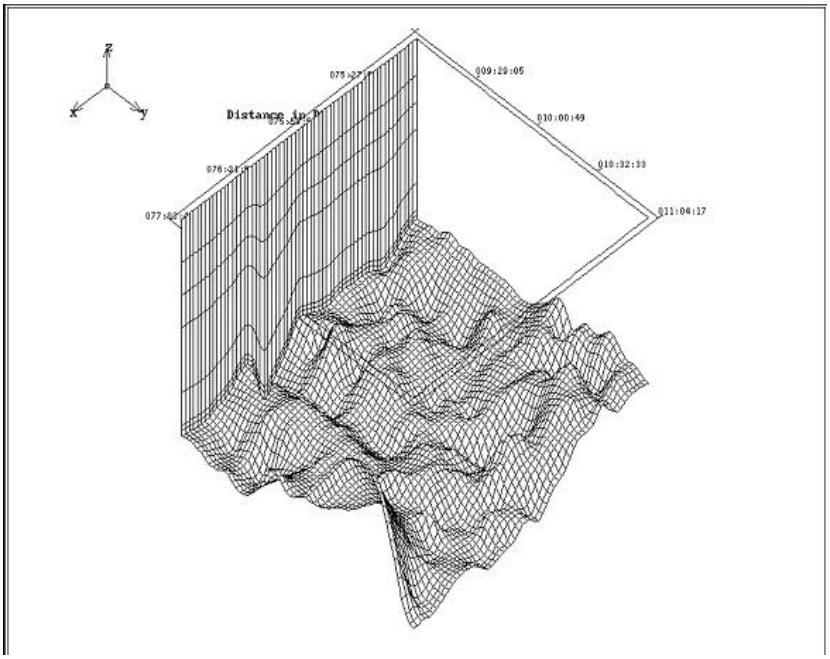

Fig. 6.3.3.2: Computational Grid in Physical plane

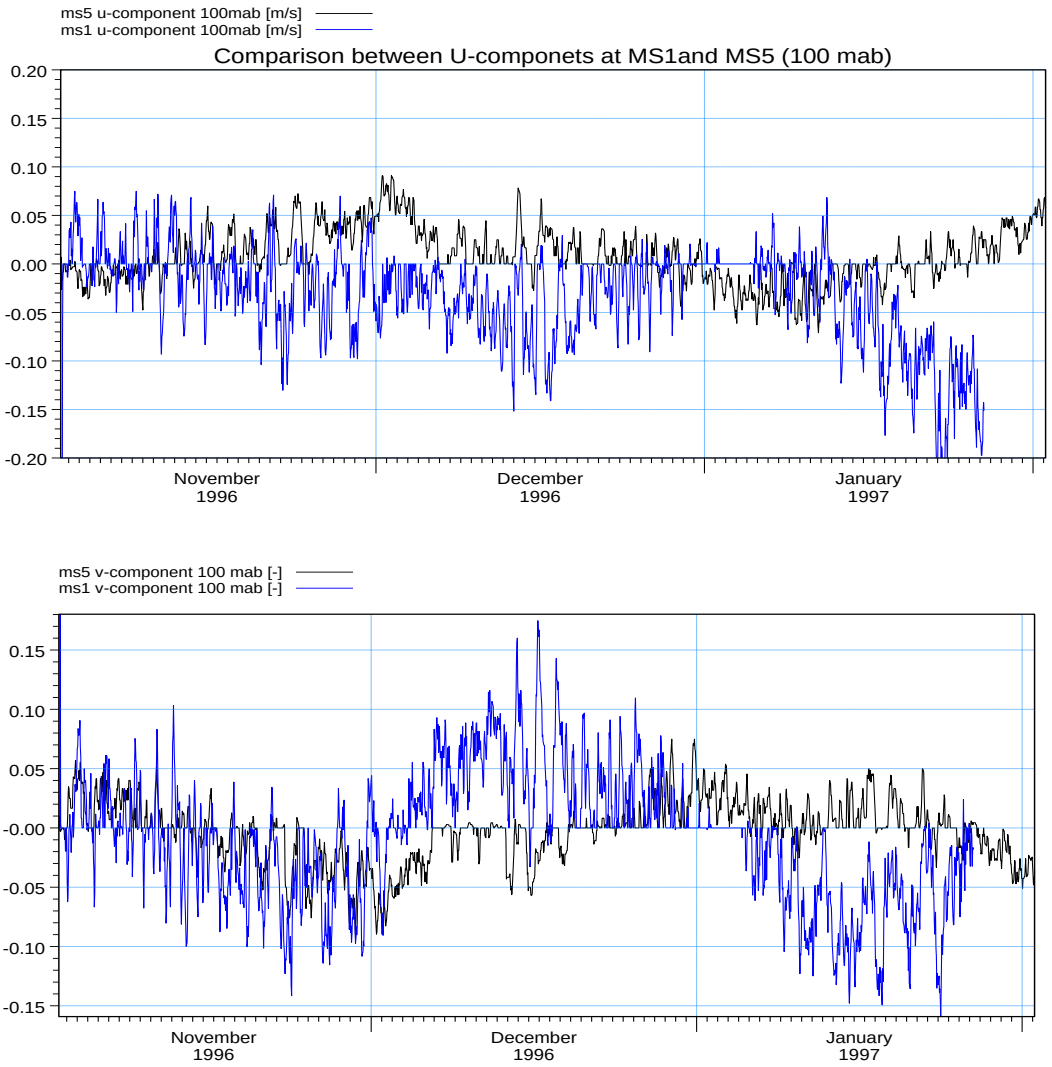

Fig. 6.3.3.3: Observed current data at MS1 and MS5 Locations

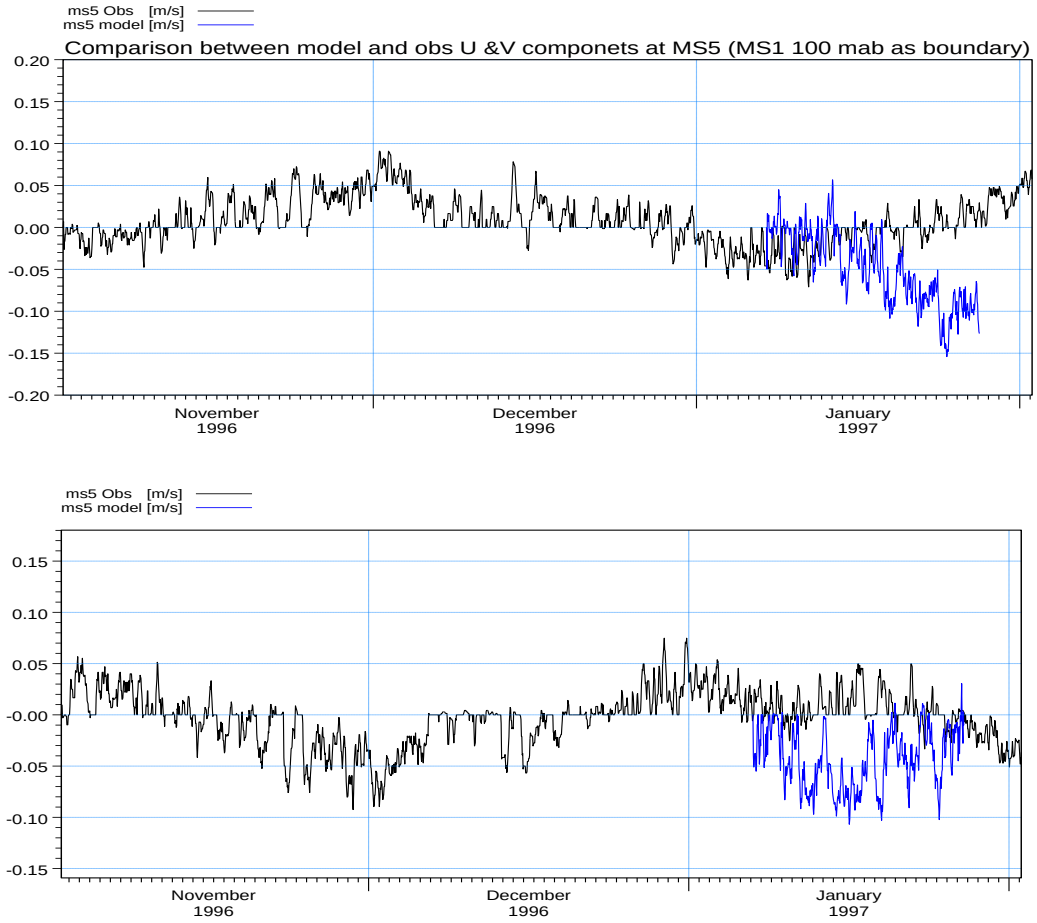

Fig. 6.3.3.4: Comparison of model and observed u and v components at MS5 location (100mab) (boundary conditions: observed currents of location MS1)

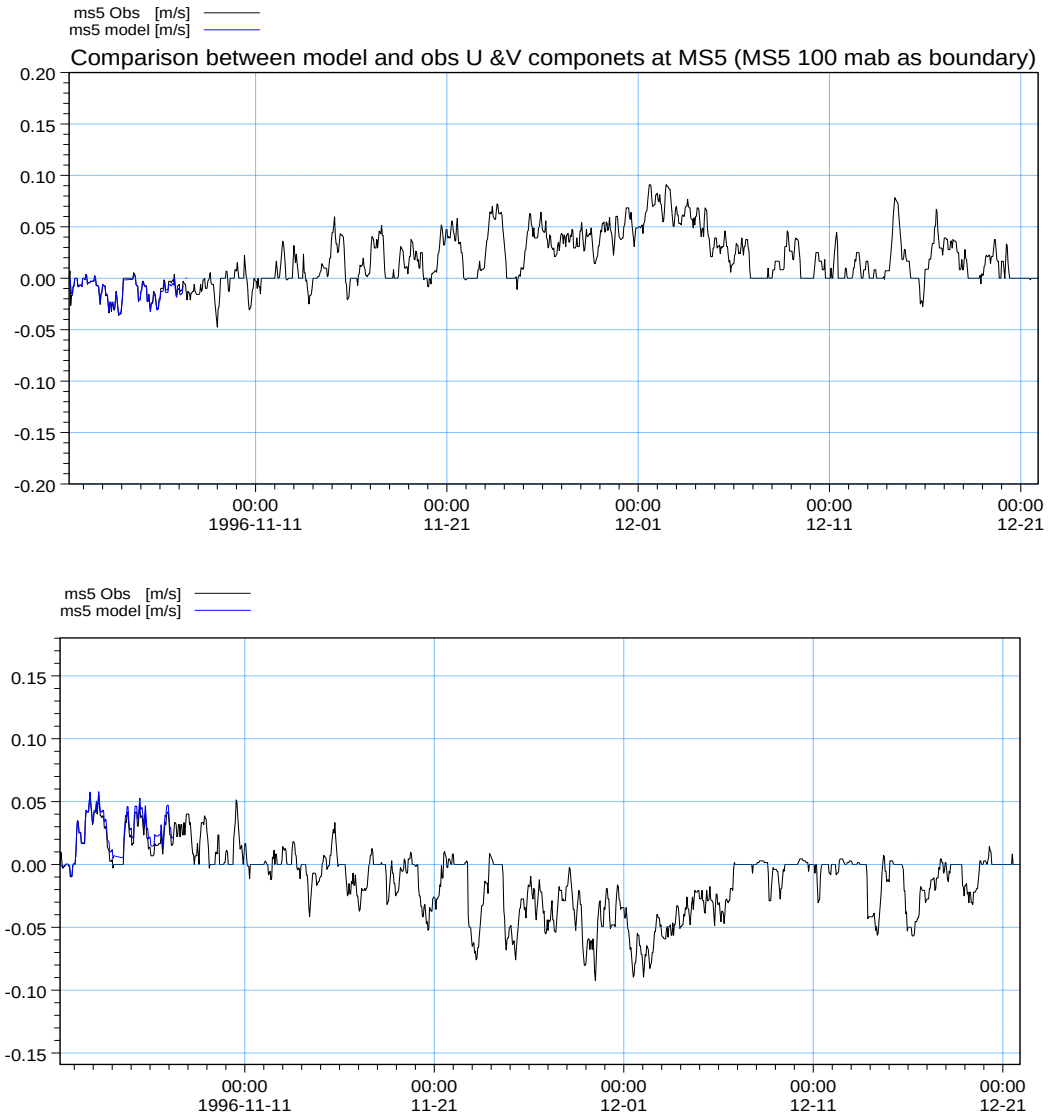

Fig. 6.3.3.5: Comparison of model and observed u and v components at MS5 location (100 mab) (boundary conditions: observed currents of location MS5).

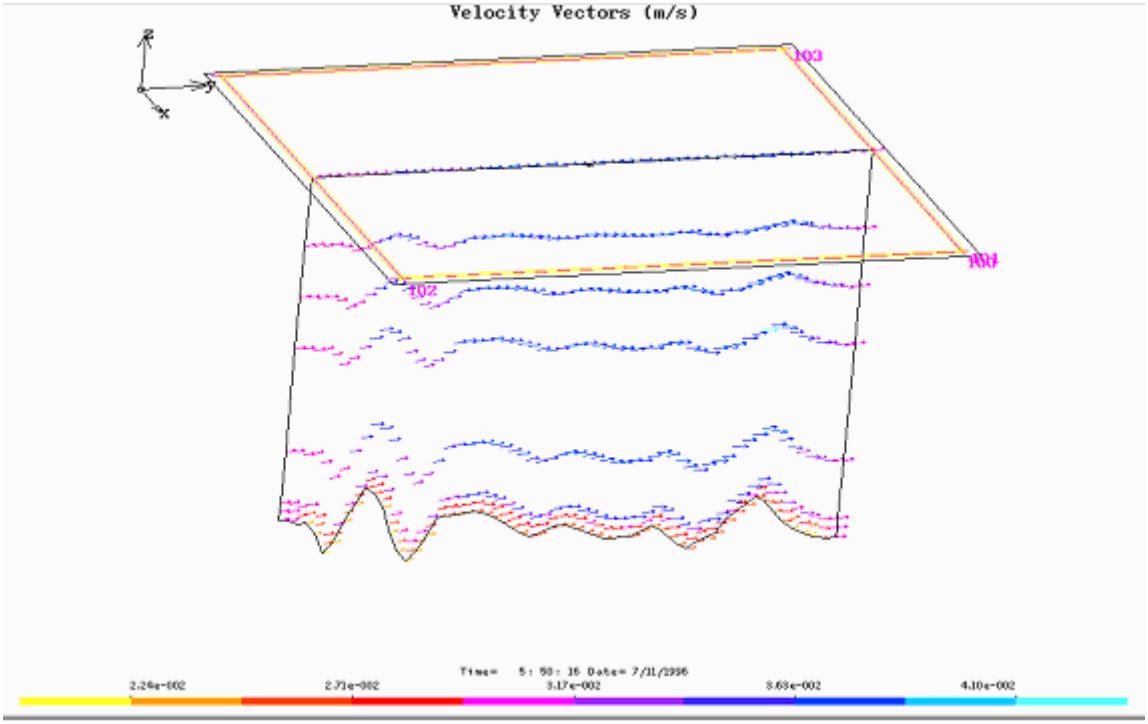

Fig.6.3.3.6: Velocities at 6 hrs of 7th Nov. 1996

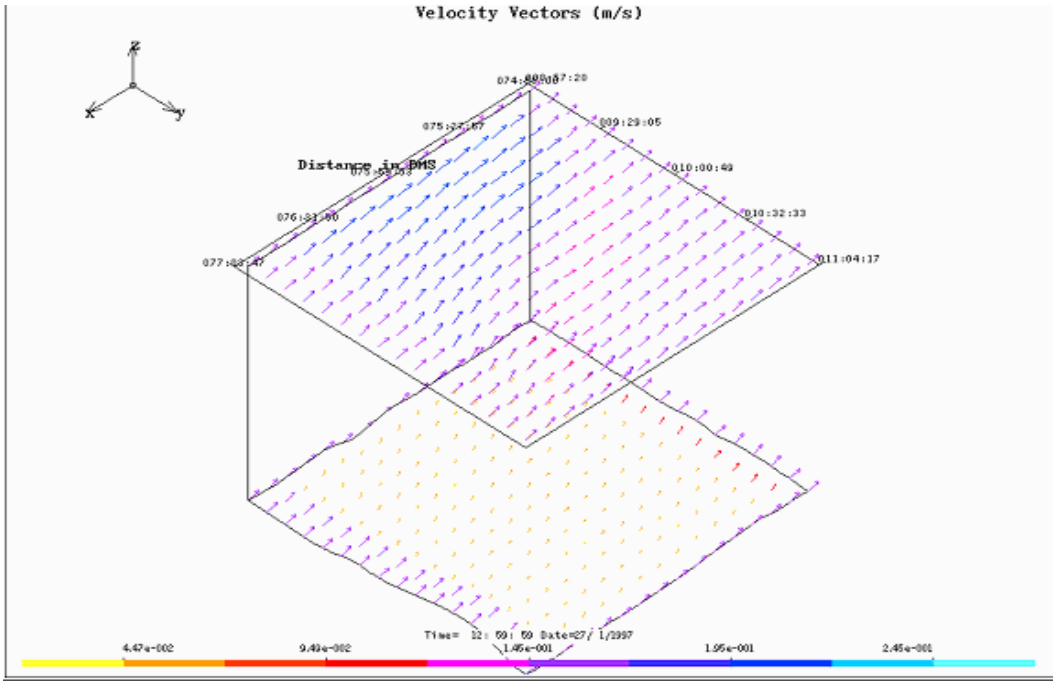

Fig.6.3.3.7: Velocities at 12 hrs of 7th Jan. 1997 (Free surface model)

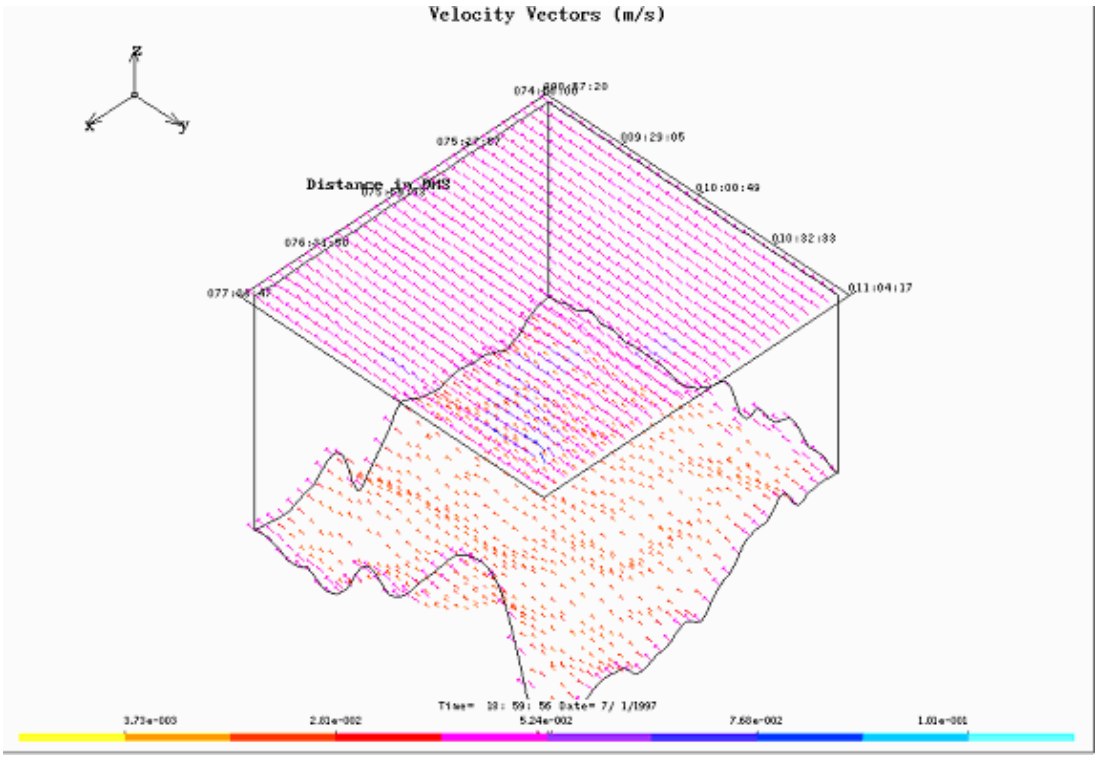

Fig. 6.3.3.8: Velocities at 18 hrs of 7th Jan. 1997 (Rigid lid model)

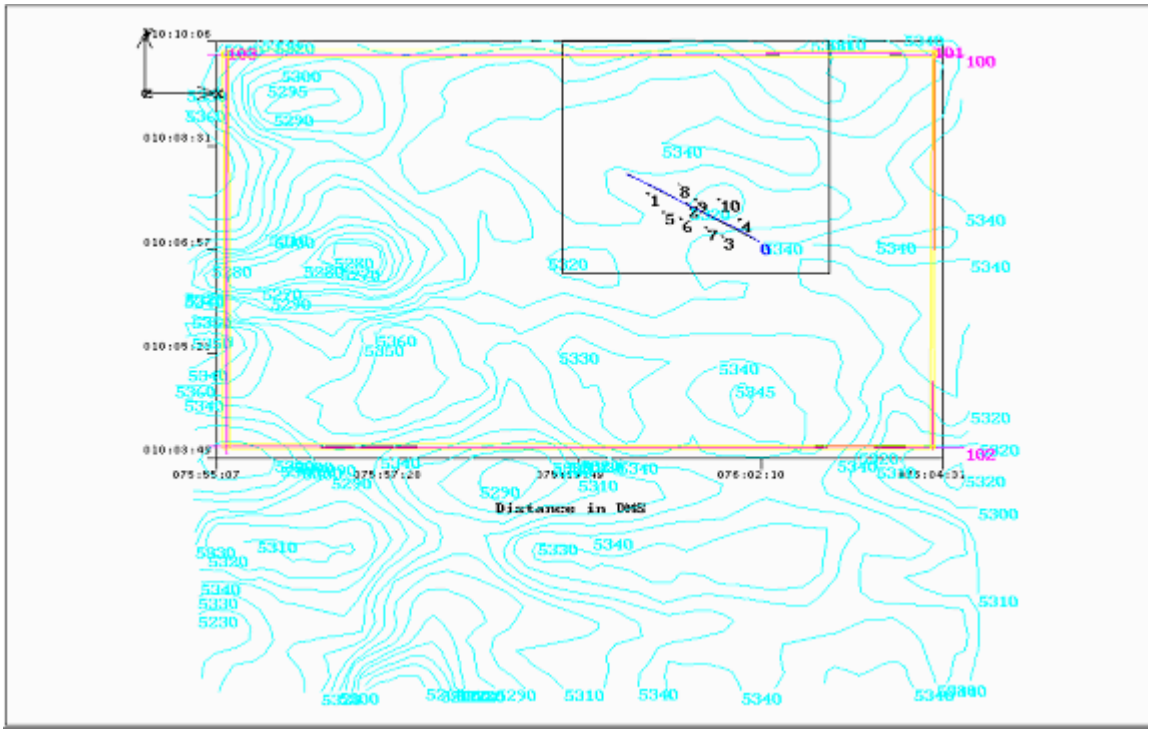

Fig. 6.3.3.9: Bathymetry and location of BIE

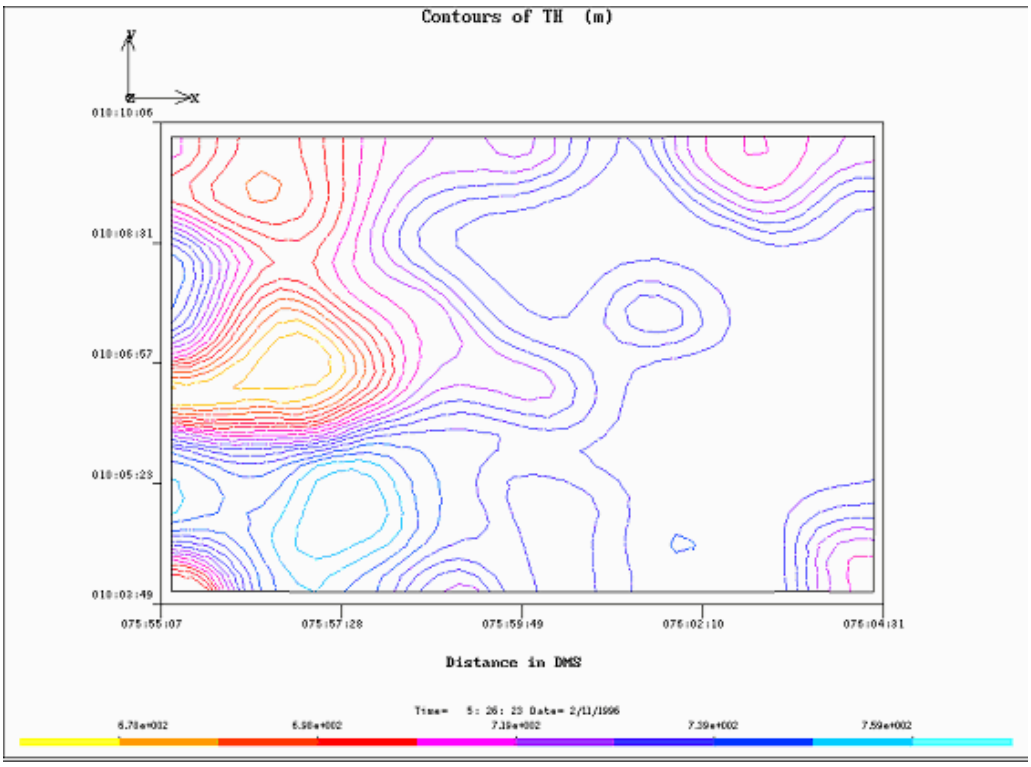

Fig. 6.3.3.10: Interpolated bathymetry

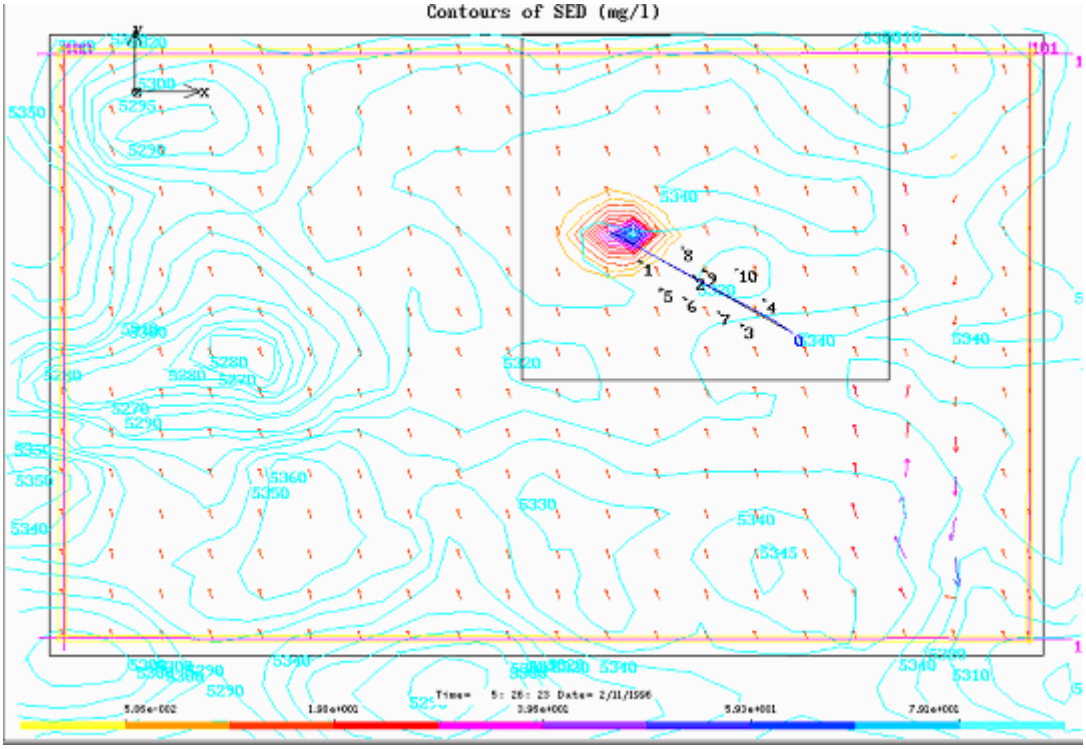

Fig. 6.3.3.11: Sediment plume dispersion during towing at 10mab (5hrs on 2nd Nov. 1996)

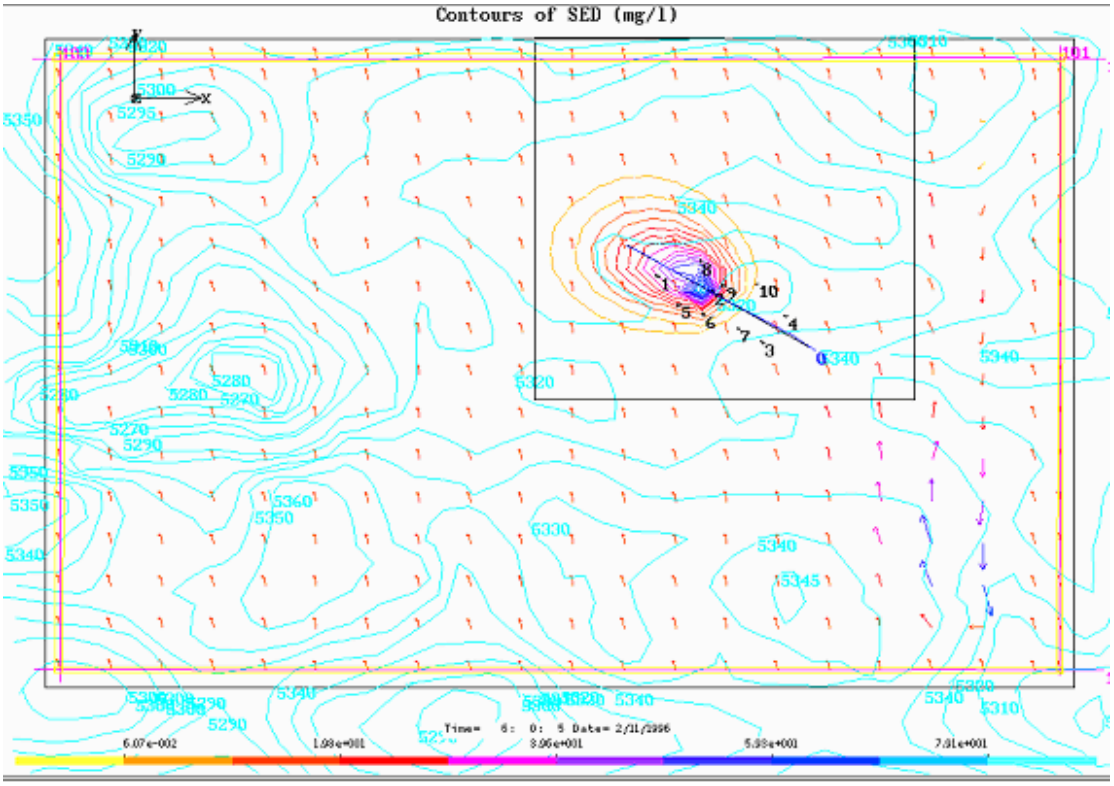

Fig. 6.3.3.12: Sediment plume dispersion during towing at 10mab (6hrs on 2nd Nov. 1996)

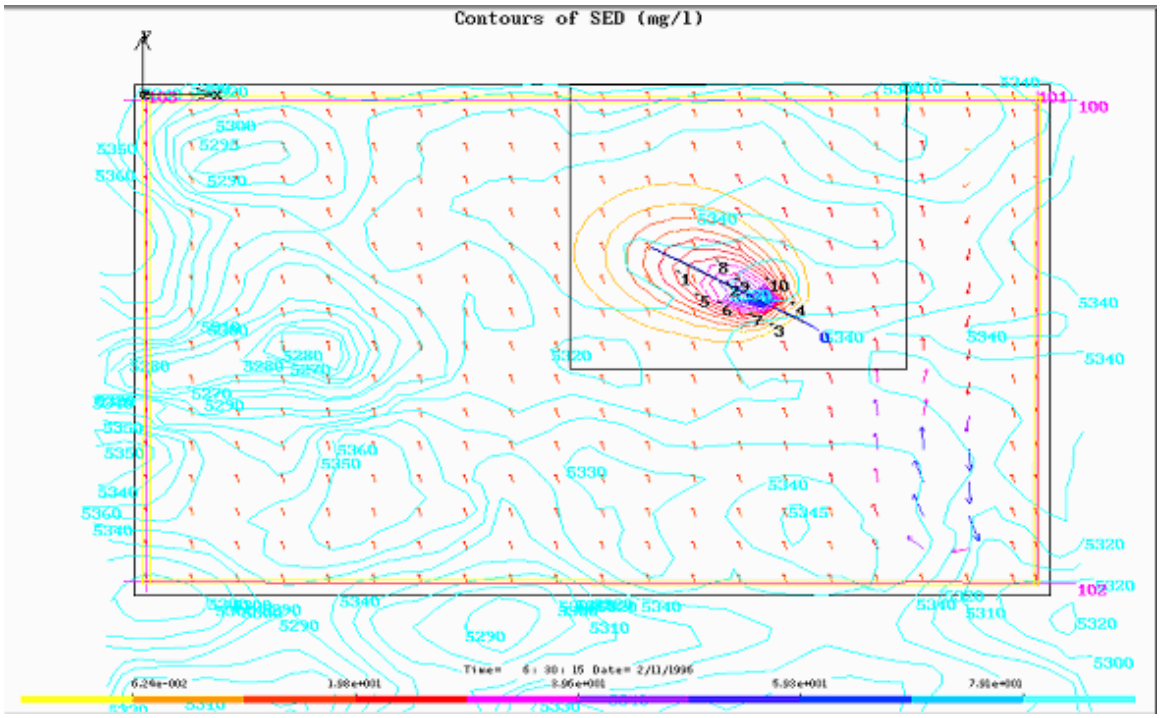

Fig. 6.3.3.13: Sediment plume dispersion during towing at 10 mab (6 hr 30 min on 2nd Nov. 1996)

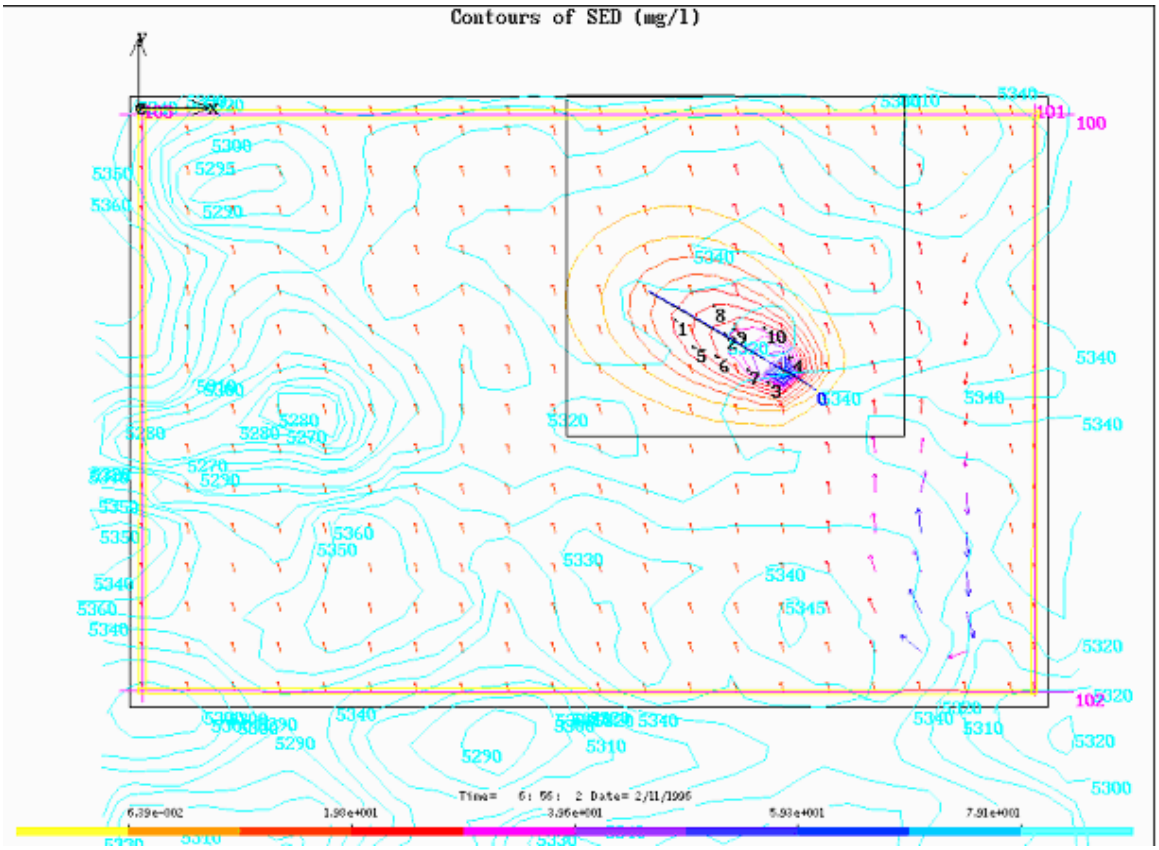

Fig. 6.3.3.14: Sediment plume dispersion during towing at 10 mab (6 hr 56 min on 2nd Nov. 1996)

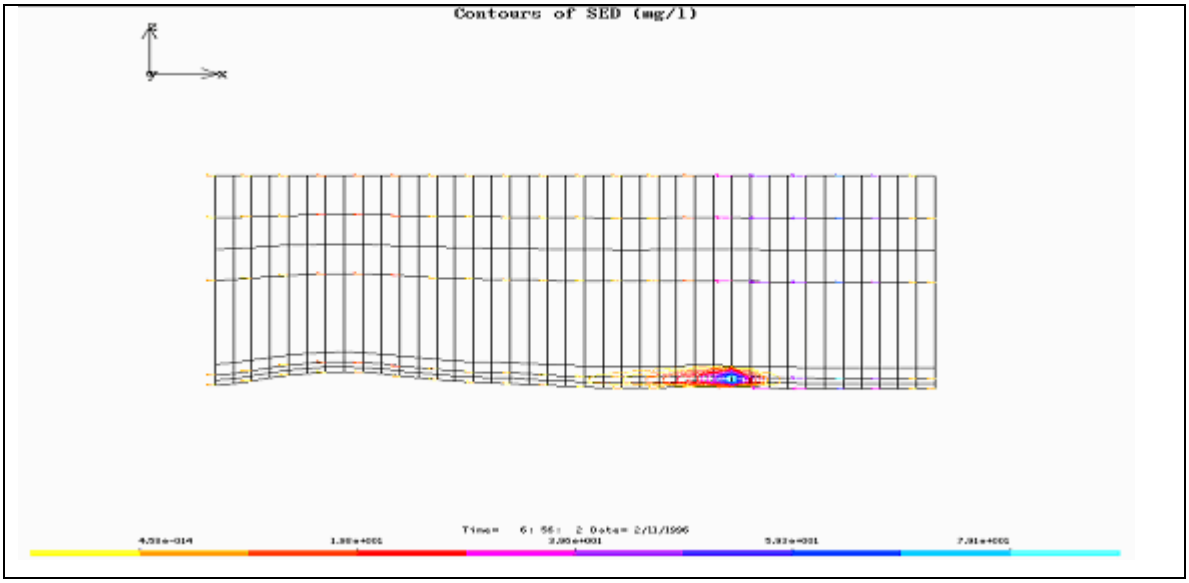

Fig. 6.3.3.15: Sediment plume dispersion during towing at 10 mab (6 hr 56 min on 2nd Nov. 1996)

Based on the above, sediment plume dispersion was computed at different times during the disturbance experiment as shown in Fig. 6.3.3.16.

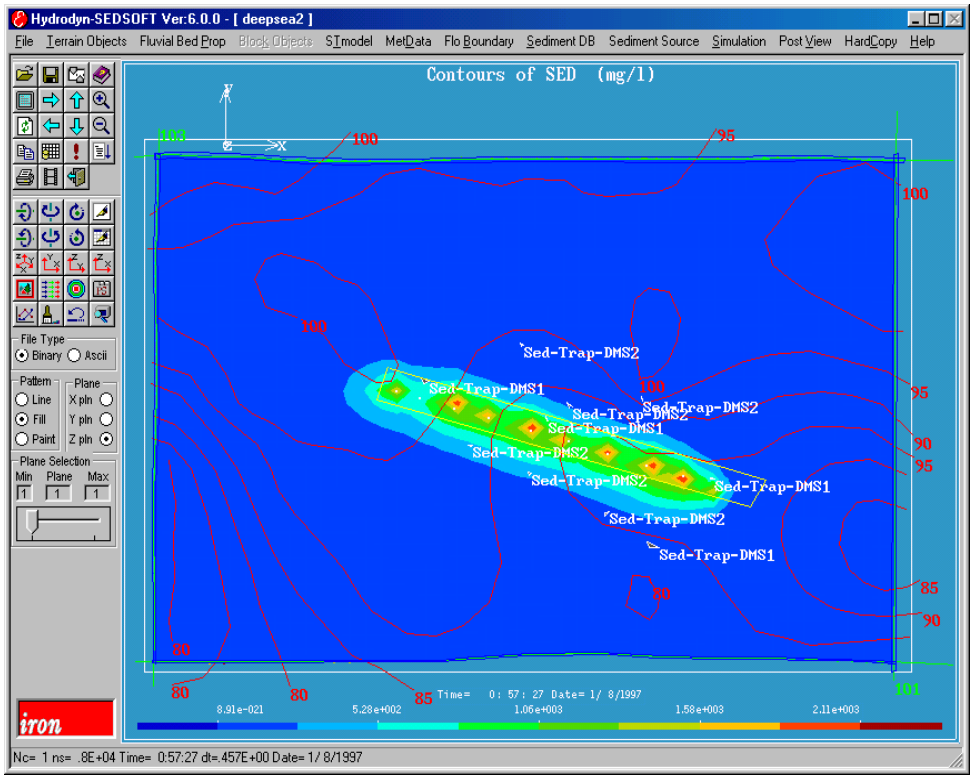

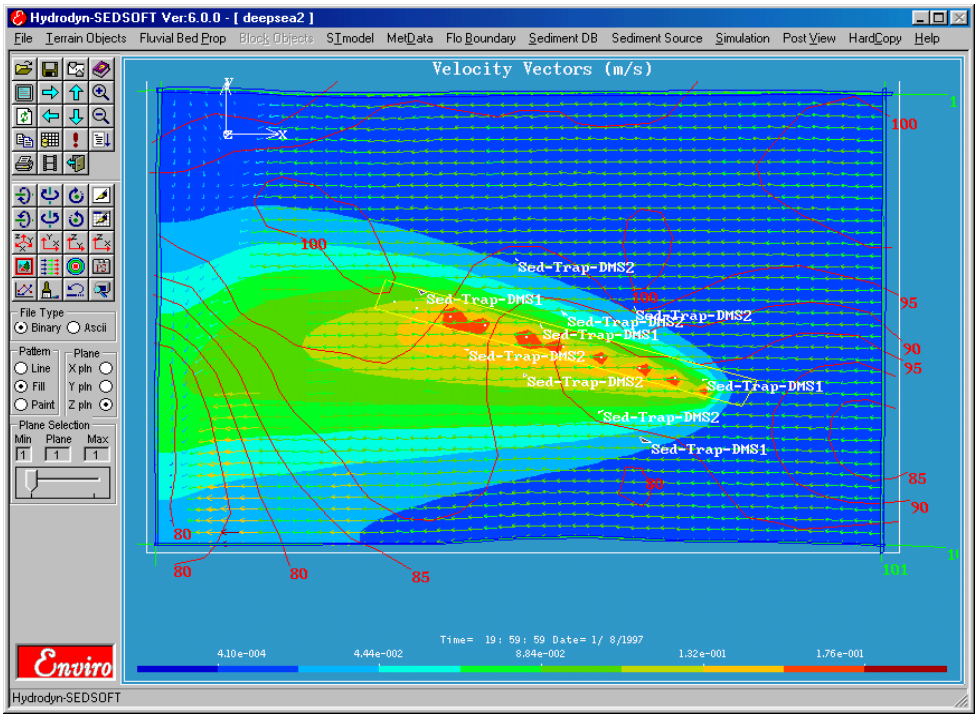

Fig. 6.3.3.16: Sediment plume dispersion within 1 hour of disturbance (above) and 20 hours of disturbance (below)

The model predicted that the plume could move about 100m to 500m on either side of the disturbance strip 20 hours (at a height of 10m above seafloor) after the disturbance. The model also predicted that the concentration of suspended matter in plume has reduced exponentially from $1.32e^{-001}$at 500m to $4.1e^{-004}$ mg/l at a distance of 3km. The earlier current measurements have shown that the currents are very weak in the abyssal areas which will keep the sediment plume in suspension in a restricted area.

6.3.4 Modification of the model

The earlier developed Hydrodyn-SEDPLUM hydrodynamic model for the CIOB was further improved based on the present technology and integrating the suspended sediment transport, sea bed transport modules for predicting the currents, turbidity, sediment plume concentration and changes in the bed morphology. The earlier model was developed based on the explicit finite difference technique and also no data were available for calibration. The Hydrodyn-SEDPLUM was modified using the implicit finite difference scheme formulation to speed up the computation and obtained improvement in software efficacy in computational 3D flow field.

6.3.4.1 Long-term currents data for validating the Hydrodyn-SEDPLUM model

Long-term time series currents data was collected from 5 locations in the CIOB by deploying 5 current meter moorings at depths of above 5 km during 4 April – 5 May 2011, and recovered these moorings during 20 September 2012 – 11 October 2012. The arrangement of 5 moorings is shown in Fig. 6.3.4.1.1. Four moorings occupied the four corners of the 2x2 degree (220 km x 220 km) box and the 5th mooring occupied the centre of the box.

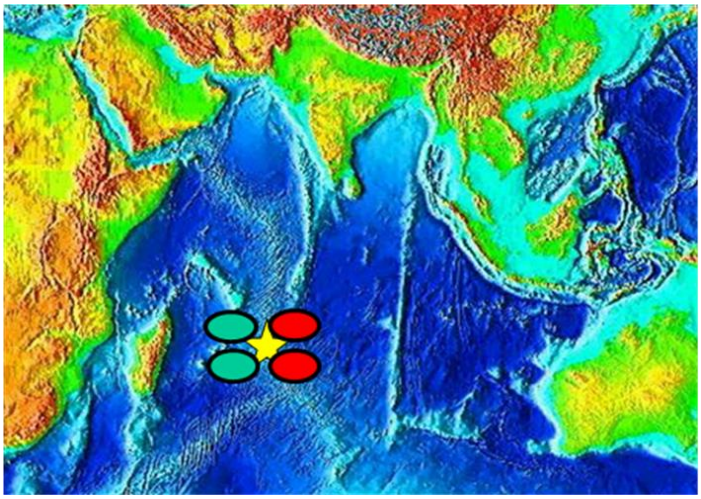

Fig. 6.3.4.1.1: Deep-sea current meter moorings in the CIOB

6.3.4.2 Observed currents variability at 5155 m depth in the CIOB

The observed time-series of zonal and merdional current velocities as measured by the Current Meters are subjected to smoothening with 36 hour low pass filtering and further smoothened by daily averages, 5 day averages and monthly averages. These smoothened time-series zonal and meridional current velocities are then compared with the corresponding daily averaged, 5 day averaged and monthly averaged HYCOM simulated zonal and meridional current velocities at 5000 m depth at the deeper depths in the deep-sea or near-bottom depth levels. Time variation of observed zonal and meridional currents at 5155 m depth is presented in Fig. 6.3.4.2.1.

The time variation of Current Meter measured zonal currents at 5155 m are large up to ±12 cm.s-1 during May-August 2011 and up to 4-8 cm.s-1 in February 2012 and for the rest of 2012 the zonal current attained weaker magnitudes. The observed meridional currents are also stronger with higher magnitudes (-12 cm.s-1) of southerly flow in September 2011 and higher magnitudes (14 cm.s-1) of northerly flow during July 2011. In April-May, the southeasterly flow prevails.

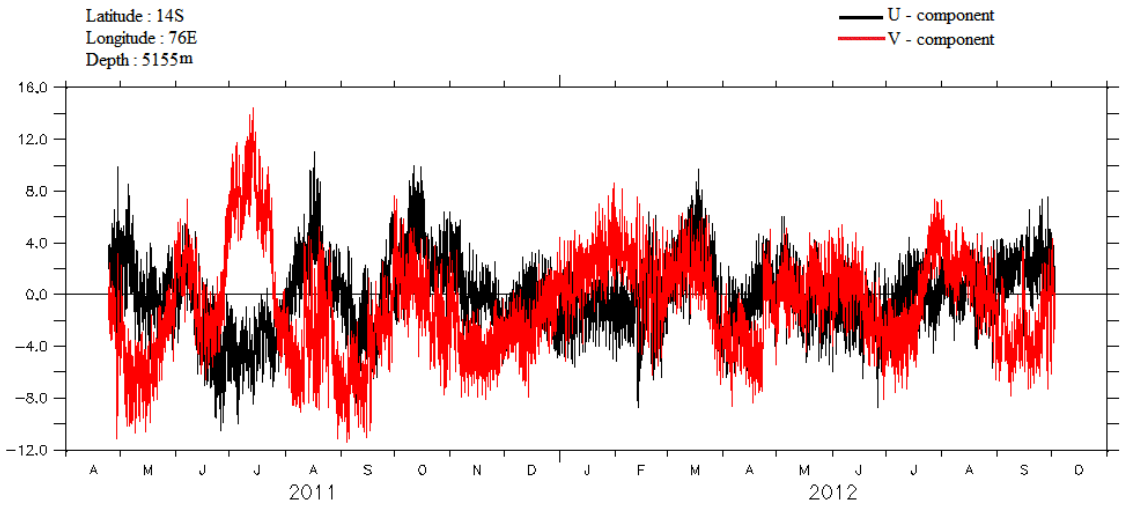

Fig. 6.3.4.2.1: Time series of observed zonal (U – red curve) and meridional (V – black curve) currents at a location 14°S, 76°E at 5155 m depth during April 2011- August 2012. Units are in cm.s^{-1}.

By June-July, the flow is northwesterly with 13 cm.s^{-1} speed. During August, southeasterly flow prevails with 10 cm.s^{-1} speed. During September – October, the flow is southwesterly. During November-December 2011, the flow becomes southwesterly. During January-

February 2012, zonal currents are weak (5 $cm.s^{-1}$) westerly and meridional currents are also weak northerly (7 $cm.s^{-1}$), constituting a weak northwesterly flow. During March 2012, the flow is northeasterly (8 cm.s-1) and reverses to southwesterly by April. During May-June, the flow is northwesterly, and changes to southwesterly with 7 $cm.s^{-1}$ speed by July. During August, the flow is weak (7 $cm.s^{-1}$) southeasterly and persists till September 2012, as that at the beginning of the time series (April 2011).

6.3.4.3 Seasonal variation of HYCOM model simulated currents at 5000 m depth

The HYbrid Coordinated Ocean Model (HYCOM) simulated daily currents data were downloaded from the website [*http://ncss.hycom.org/thredds/catalog.htm*/] and used for comparing with the observed currents in the CIOB. The HYCOM simulated daily currents were obtained at 1/12 degrees (or) 9 km interval during the period from 01 January 2011 to 31 December 2012. The HYCOM daily currents are then 5 day averaged and monthly averaged and used for comparison with the respective time-series observed currents. The comparisons of HYCOM simulated daily averaged, 5 day averaged and monthly averaged currents with the corresponding observed time-series currents data were made at the depths of 100 m, 200 m, 300 m and 400 m in the upper ocean, at intermediate depth of 1000 m and at 5000 m depth in the deep-sea. These HYCOM model deep-sea currents at 5000 m depth were compared with the observed currents at 5155 m depth. The HYCOM simulated currents were used to understand the horizontal circulation variability at sea surface, 100 m depth, 1000 m depth and 5000 m depth levels in the domain of 10°S -20°S and 72°E-80°E during 2011-2012 period.

We have included the HYCOM derived horizontal circulation at 5000 m depth in the study area of 10°S-20°S and 72°E-80°E for the seasons of January, April, July and September in 2011 and 2012 (Fig. 6.3.4.3.1 and Fig. 6.3.4.3.2). The HYCOM simulated currents reveal the presence of the broad westward flowing South Equatorial Current (SEC) as documented earlier by many researchers. The high spatial resolution (1/12° degree, equivalently 9 km grid size) in HYCOM simulations captured the high spatial variations in the horizontal circulation and reveals the presence of meso-scale eddies and large scale meandering in the westward flow of the SEC. This large scale anticyclonic and cyclonic meanders covered the study box of 14°-16°S and 76°-78°E and led to large zonal and meridional current fluctuations in the observed currents and model simulations. The meanders were conspicuous south of 14°S at all the depth levels, and currents were relatively strong in these meanders. It was noticed that the horizontal circulation at 100 m depth was characterized by strong westward flow passing

through the study location (14°S, 76°E) in April 2011, July 2011, and September 2011 compared to the weaker westward flow at this depth in 2012. The large meanders in the broad westward flowing SEC appear to be responsible for the existence of intraseasonal variability at 50-60 day period oscillations. It is interesting to note the consistency in the time variations of meridional currents from sea surface to abyssal depths. This shows that the large-scale meanders extend up to deeper depths over the water column, and brings in strong horizontal shear instability in the westward flowing SEC.

The HYCOM derived deep-sea circulation at deeper depth of 5000 m is interestingly reversed between 10°S and 14°S even at this great depth in January 2012 from that of January 2011. The large scale anticyclonic flow (anticlockwise rotation) with the embedded meandering meso-scale eddies in January 2011 changed to cyclonic (clockwise rotation). The strong southward flow at 74°E in January 2011 was shifted to 78°E in January 2012. At the study location (marked by red star in these figures) the flow was towards southwest and weak in January 2011 and changed towards northwest in January 2012 at the same depth. Along 15°S, the flow was towards west in both January 2011 and January 2012. The deep-sea circulation at this depth in April 2011 and 2012 remains the same and is anticyclonic (clockwise circulation) within the box between 14°S and 16°S. There is a strong southward flow at 77°E in April in both these years of 2011 and 2012 (Fig. 6.3.5.4.1). In July 2011 and July 2012, the circulation at this depth was westward along 15°S within the box and eastward at 14°S. The flow was towards northeast at the study location (marked red star). North of 13°S, the flow remained the same in July 2011 and July 2012 with a strong northwestward over the central region to 10°S, 74°E (Fig. 6.3.4.3.2). By September 2011 and 2012, the deep-sea circulation constituted with meso-scale eddies between 15°S and 14°S and circulation reversed near 15°S. At the study location, flow remained the same and was towards south with the same magnitude of 5 $cm.s^{-1}$ (Fig. 6.3.4.3.2 bottom panel) in September 2011 and 2012.

Thus HYCOM simulated horizontal circulation at 5000 m depth consisted of meso-scale eddies and seasonal flow reversal occurred from 2011 to 2012 north of 14°S, and the year-to-year consistency in flow circulation is also evident within the chosen box in the study area. The HCYOM simulated abyssal currents at 5000 m during austral winter (July 2011 and 2012) constituting the meso-scale clockwise circulation eddy between 9°S and 12°S and between 75° and 77°E agrees very well with that reported by Ramesh Babu et al. (2001) at 5000 db level (Fig. 6.3.3.9) based on the analysis of the hydrographic data collected in the CIOB. Further, the observed currents at 5155 m depth, i.e., 30 m above seabed, did not match with the HYCOM model currents at 5000 m depth, but also exhibited out of phase with these

model currents. This mismatch was more prominent in 2012. This mismatch suggests that there exists a Bottom Ekman Layer (BEL) in the CIOB study area as the currents experience friction in the bottom Ekman layer. The HYCOM model currents at 5000 m depth represent the free flow away from the bottom. Murty et al. (1999) reported the presence of Bottom Ekman Layer (BEL) at 10°S, 76°E below 50 m above seabed, wherein the flow was strongly south-southeastward.

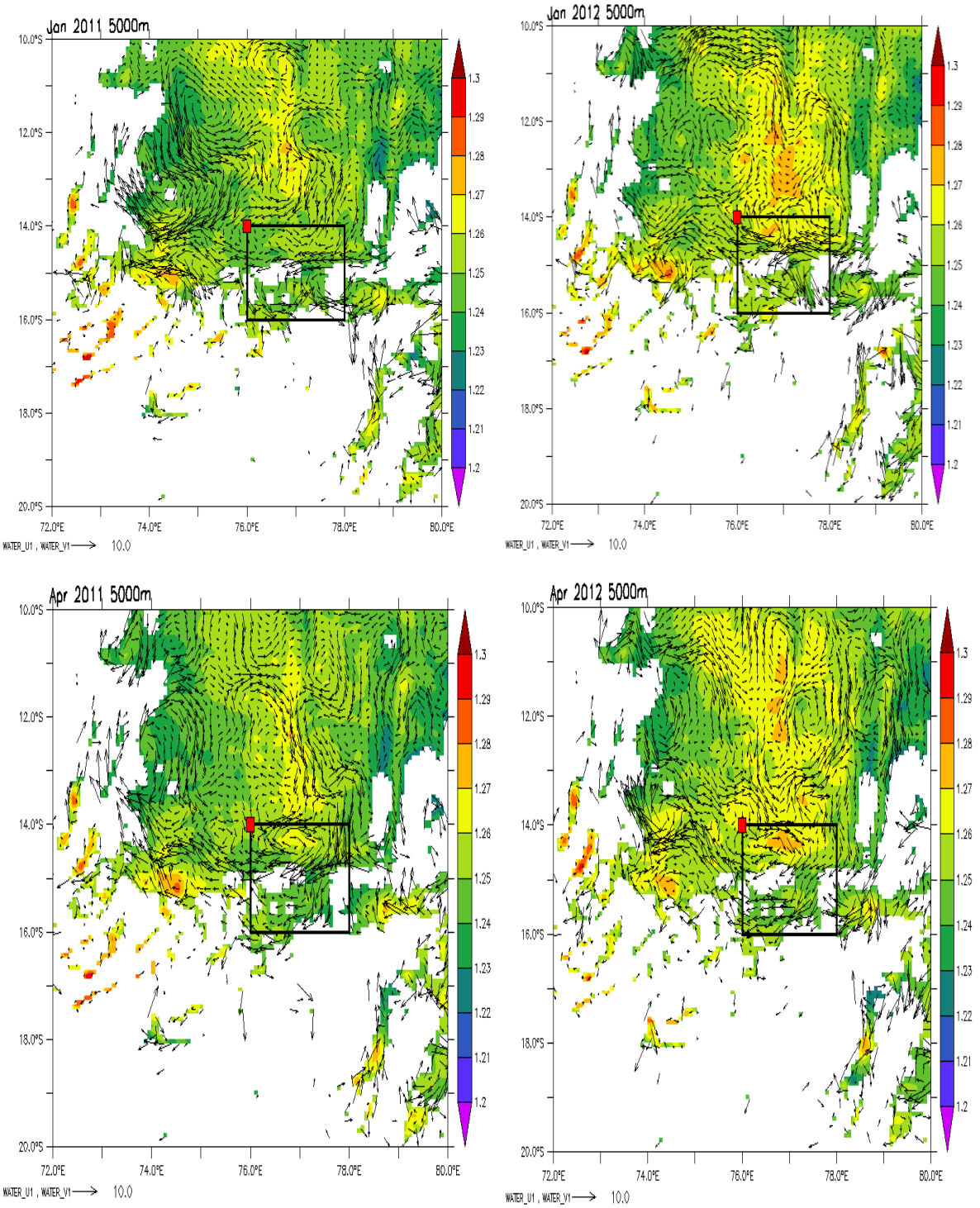

Fig. 6.3.4.3.1:HYCOM simulated seasonal circulation at 5000 m depth in January (top) and April (bottom) in the year 2011 (left panel) and year 2012 (right panel). The black box represents CIOB deep-sea moorings and the red star the study location.

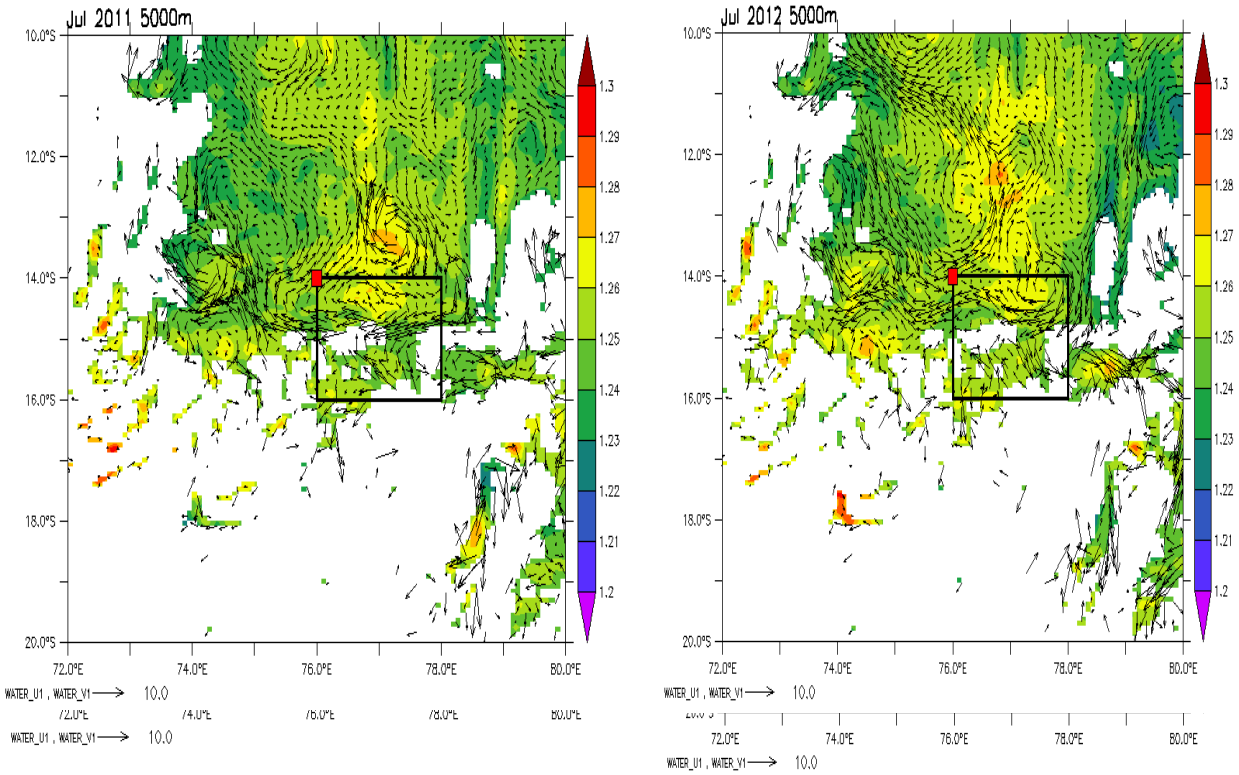

Fig. 6.3.4.3.2: HYCOM simulated seasonal circulation at 5000 m depth in July (top) and September (bottom) in the year 2011 (left panel) and year 2012 (right panel). The black box represents the CIOB deep-sea moorings and the red star the study location.

6.3.5 Comparison of observed and computed currents with the Hydrodyn-SEDPLUM model

In this section, a comparison of the observed currents and Hydrodyn-SEDPLUM model derived meridional (north-south flow) and zonal currents (east-west flow) at the depth of 5071 m are compared at the central location of 14S, 77E and is shown in Fig. 6.3.5.1. It can be seen that the model predicted currents are well matching with the observed currents over the period of May 2011 to January 2012.

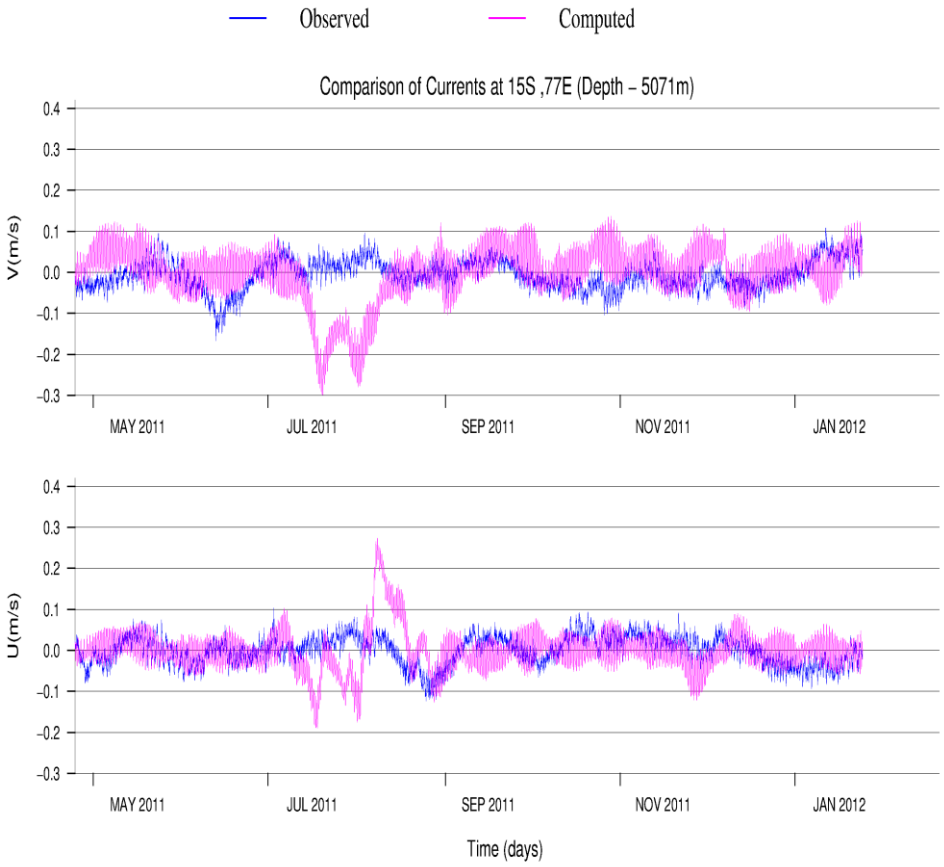

Fig. 6.3.5.1: Comparison of observed and CIOB plume model computed variation of U & V velocity (m/s) in case of coarse mesh for various seasons at the central location of the Box at 77E, 15S at depth of 5071 m.

From the above analysis, the following observations regarding the performance of the Hydro-SEDPLUM model can be drawn:

- The observed long-term ADCP and RCM currents data collected from CIOB during April 2011 – August 2012 show variability of currents in the water column and in the abyssal layer.

- The HYCOM simulated currents also showed large spatial variability in the flow characteristics and circulation in the water column and in the abyssal layer in the CIOB domain.
- For the Hydrodyn-SEDPLUM, a unique technique for bathymetric depth computation in CIOB is developed using triangulation method for Cardosat / Zebco data.
- Numerical runs were made for testing the efficacy in computation scheme of plume dispersion at different locations in the CIOB domain.
- Numerical runs were made for various oceanographic conditions forpredicting the environmental impacts in the CIOB domain.
- Incorporated the data of bed soil characteristics.
- Calibrated the Hydrodyn-SEDPLUM with the observed CIOB currents from the abyssal depths.
- Validated the model with the observed field data.
- The Hydrodyn-SEDPLUM model predicted the suspended sediment concentrations and changes in sea bed sediment characteristics at different time intervals.
- The Hydrodyn-SEDPLUM model predicted the suspended sediment spread area at different time scales to estimate risk.
- The Hydrodyn-SEDPLUM model predicted the sediment plume dispersion and blanket thickness for various sea bed mining operations.

The summary of the study is as follows:

- The Hydrodyn-SEDPLUM model predicted currents are well compared with observed currents even at abyssal depths.
- The model concept confirms that the model can be used at any locations in the CIOB.
- The plume dispersion model was run with hypothetical source information (line source, moving source and point source) in the CIOB flow field.
- The model predicted well the sediment plume dispersion, deposition and blanket thickness at various time levels and at different depths.
- The Hydrodyn-SEDPLUM model developed performed satisfactory and can be used in the CIOB for the dispersion of sediment plume during the processes of mining of polymetallic modules.

6.4 Estimations of area, volume and weight of sediment and nodules to be disturbed during nodule collection trials

This section describes the calculations of area, volume and weight of sediment and nodules expected to be disturbed during nodule collection trials. As described in sections 3.3 and 3.4, the nodule collector machine is likely to have 4 moving tracks (each of 0.75 m width), with 2 pickup units (each of 0.8 m width). During the trials, the machine is expected to cover a total distance of 1000 m, with a penetration from 0.15 m. Hence, the calculations of area, volume and weight of sediment and nodules (Table 6.4.1) to be disturbed are based on the following variables:

1. Nodule collector machine with 4 moving tracks (0.75mx4=3m) and 2 pickup units (2x0.8m=1.6m) = total width 4.6 m
2. Distance covered 1000 m cumulative
3. Depth of penetration 0.15 m
4. Wet density of sediment – 1.2 kg/m^3

Table 6.4.1: Estimations of area, volume and weight of sediments and nodules to be disturbed

a. Volume and weight of sediment disturbed per sq. m

i. Volume of sediment impacted (1m x 1m x depth of penetration) For penetration of 0.15 m	0.15 m^3
ii. Weight of sediment disturbed (volume x density of sediment 1.2 kg/m^3) For penetration of 0.15 m	0.18 kg

b. Volume and weight of sediment lifted within pickup width of 1.6 m (2x0.8 m) only

i. Volume of sediment lifted (width x depth x length of track) For penetration of 0.15 m (1.6mx0.15mx1000m)	240 m^3
ii. Weight of sediment lifted (volume x density of sediment 1.2 kg/m^3) For penetration of 0.15 m (240m^3x1.2)	288 kg

c. Area, volume and weight of sediment disturbed for entire width of collector (moving tracks + pickup unit)

Collector with 4 moving tracks (4 x 0.75m=3m) and 2 pickup units (0.8mx2=1.6m) = Total width of collector 4.6 m

i. Area covered (width of miner x length of track)	4600m^2
ii. Volume of sediment disturbed (area x depth) For penetration of 0.15 m	690 m^3
iii. Weight of sediment disturbed (volume x density of sediment=1.2 kg/m^3 For penetration of 0.15 m	828 kg

d. Quantity of nodules and adhered sediment expected to be lifted

i. Area to be swept (@ 1.6 m width of pickup units)	1600 m^2	
ii. Quantity of nodules picked (@10 kg/m^2xarea) - At 50% pickup efficiency	8000 kg	
iii. Sediment to be lifted with nodules at 50 % efficiency of nodule collector# - If sediment is 20% by weight of nodule	Weight 1600 kg	Volume 1333.3 m^3
# that will go into suspension when it is released either at the top of the pickup unit or riser pipe		

e. Concentration of sediments in water after suspension considering immediate width (100m) of dispersion

i. Volume of water - moving point dispersion at 80 m altitude (lxbxh= 1000x100mx80m)	80,00,000 m^3	
ii. For 50% efficiency of nodule collector, add sediment volume from 'd(iv)'	Total volume	Sediment (%) concentration
- If sediment is 20% by weight of nodule	80,01,333.3	0.0166

The volume of sediment expected to be impacted over 1m^2 for penetration of 0.15 m , is estimated to be 0.15 m^3 . Considering a wet density of 1.2 kg/m^3, the weight of sediment to be disturbed would be 0.18 kg for penetration of 0.15 m. Estimates also show that the volume of sediment lifted within the pickup width of 1.6 m along 1000 m track would be 240m^3 for a penetration of 0.15 m, which translates into a weight of 288 kg. The area expected to be covered with a collector with 4 moving tracks would be 4600 m^2 for a cumulative distance of 1000 m. For this area, the volume of sediment to be disturbed by the collector would be 690 m^3 by volume with a corresponding weight of 828 kg.

For a total pickup width of 1.6 m, average nodule abundance of 10 kg/m^2, the quantity of nodules expected to be picked up is estimated to be . 8000 kg for 50% of pickup efficiency which is considered optimum for such devices.The estimates show that 1600 kg of sediment could get disturbed by the collector movement with a corresponding volume of 1333.3 m^3if the adhered sediment is 20% by weight of nodules at 50 % pick up efficiency of nodule collector.

Estimations also show that in case of discharge at 80 m altitude along 1000 m track considering immediate width (100mon either side) of dispersion,the concentration of solids (sediments) would be 0.0166% of the total volume of water in case of 20% of solids in the water columnfor 50 % efficiency of nodule collector. It must be noted that, higher the area (or

width) of dispersion, lower will be the concentration of sediment in the corresponding volume of water.

In order to evaluate the scale of the proposed collection trials with respect to that of the Indian Deep-sea Environment Experiment (INDEX) conducted by India in 1997, a comparison between selected parameters of the two has been carried out (Table 6.4.2). Although there is some difference in the mechanism of the two, the data suggests that the area covered during the proposed collection trials would be 0.766% of INDEX, the distance covered would be 1.14%, and the volume of sediment disturbed would be 0.00232% of INDEX, which are much smaller in proportion to the previous experiment and so it is expected that the impact of nodule collector trials would also be extremely small as compared to those observed during the benthic impact experiment.

Table 6.4.2: Comparison of maximum impact of collection trials with INDEX results

Variable	Collection trial	INDEX	% of INDEX
Area	4600 m^2	600,000 m^2 (3000x200m)	0.766 %
Distance	1000 m	88,000 m (88 km)	1.14 %
Volume of sediment disturbed	1380 m^3	29,625,000 m^3	0.00232 %

Salient points of the above calculations are summarized as follows:

1. Volume of sediment impacted per sq. m. will be 0.15 $m^3$for penetration of 15 cm
2. Weight of sediment disturbed per sq. m. will be 0.18 kg for penetration of 15 cm
3. Volume of sediment lifted within pickup width of 1.6 m for a track length of 1000 m will be 240-for penetration of 15 cm
4. Weight of sediment lifted within pickup width of 1.6 m a track length of 1000 m will be 288 kg for penetration of 15 cm
5. Area covered by the collector with 4 moving tracks and 2 pickup units will be 4600 m^2 for 1000 m distance
6. Volume of sediment disturbed by the collector with 4 tracks and 2 pickup units will be 690 m^3 with corresponding weight of 828kg .

7. For pickup width of 1.6 m along 1000 m track with nodule abundance of 10 kg/m^2, weight of nodules to be lifted would be 8000 kg for 50% pickup efficiency of nodule collector.
8. In case of 50 % efficiency of nodule collector, the sediment adhered to nodules during pickup would bebe1600 kg considering that the weight of sediment to nodules is 20%. 9. Concentration of sediments in water after being released at 80 m altitude along 1000 m track will be 0.0166 % in terms of volume if theweight of sediments to nodules is 20 %. 10. In terms of area, distance, and volume of sediment, the scale of proposed trials is extremely small (≤ 1%) than of those in case of the previous experimental disturbance (INDEX), which in itself was considered to be a fraction of commercial mining. Hence, it could be expected that the overall impact of the proposed trials would be negligible on the marine environment.

6.5 Likely impacts of nodule collector trial

The locomotion wheels of the nodule collector to be deployed will either sink into the top 10-15 cm or create a ploughing effect and have a scouring effect. Data analyzed from deep-sea photos of a suction device during the INDEX experiment in CIOB has shown tracks of the disturber operation as pairs of depressions of the sleds 10–15 cm deep with fluidized sediment surface between them. These areas were devoid of any biological activity except for occasional megafauna. Sediment, piled up on the sides of the disturber tracks because of the depression caused by the motion of the disturber, which could be observed in areas adjacent to the tracks (Sharma et al., 2000). The camera profiles parallel to the disturber tracks showed lumps of sediment that had been redeposited from the discharge stack either on the tracks or beside them during the tow. The other areas showed a very fine layer of sediment cover, resulting in smooth microrelief and no burrows, fecal casts, or animal trails, which are usually common in undisturbed areas. The areas away from the tow zone did not show any effects of disturbance and contained fecal casts, burrows, trails, and megabenthic organisms. Similar effects are likely to occur, but on a much smaller scale, as the area of operation is only about 100 m^2 compared to a large area of 3000 x 200 m disturbed before.

The nodule collector will put some bottom sediments into suspension while crawling on the seabed. In addition, the crushed nodule and accompanying sediments will be discharged at a height of 80 m above the seafloor. In comparison to the settling time of particles separated into individual grains which may travel for longer distances and stay in suspension for longer periods, the crushed nodule and sediment aggregates are expected to settle much faster. In

natural conditions, particles rarely occur as individual grains in oceans. A sediment sample from the DISCOL experimental site was analysed for grain size after mechanical agitation equivalent to seafloor disturbance during mining (Oebius et al., 2001), which has settled much faster than the experiments on individual grains. In the INDEX experiment, the sediment traps deployed in and around the disturbed zone have found that most (57%) of the resedimentation is observed within the disturbance site. The bottom currents measured with current meters moored close to the bottom (described in previous section) were found to be weak and have low frequency variability with a 40-60 day period. The mean flow at the planned depth of discharge is low and the flow tends to veer towards the seabed (Murty et al., 1999), which means that the solids discharged at 80m above seafloor tend to be directed towards to the seafloor. A low frictional velocity was also found (Murty et al., 1999) which implies that the bed stress is usually low to cause local re-suspension of sediments. As it would take less than one day (higher estimate) to settle, the particles are not likely to be involved in the scavenging (thus not affecting the dissolved constituents) and plankton growth (see Rolinski et al., 2001 for the possibilities of sediment discharge and the long-term propagation of tailings from deep-sea mining).

The experimental results of INDEX have shown that the grain size of majority of the samples retained their original sediment texture (silty clay) and are not significantly affected by the disturbance (Valsangkar et al., 1999). Some of the sediments from the disturbed zone, however, have changed to clayey silt after the disturbance (Valsangkar et al., 1999) suggesting that the grain size is reduced to some extent possibly due to the crushing effect. Similar impact is likely to be taking place now in a very small area, the size itself may not have clouding effect because of the resultant texture is still silt sized (>4 to 63 μm)

As per the calculations presented in Section 6.4, concentration of solids in water after suspension will be 0.0166% in terms of volume. Consider that the solids will be a mixture of nodule pieces and sediments. If the plume is fully composed of nodule pieces, only the seawater adsorbed portion is likely to be leached out. It is unlikely that even the loosely bound metals will be leached out. The laboratory experiments found that even for extracting the loosely bound metals to oxide surfaces will require a change in pH of the medium and it is unlikely that the pH will be reduced in the seawater on discharge of solid waste.

Particulate organic carbon brought in with the tailings would not be different from the organic carbon values of suspended matter at the depths of discharge (~80m above seafloor) and thus the oxygen demand from its degradation is not expected as it would be in surface waters (Chan and Anderson, 1981). Nutrient concentrations of discharged water are also

likely to be similar in bottom waters, but the nutrient concentrations in porewater can be slightly higher than the bottom water. However with the kind of dilution, the moderately higher concentrations of nutrients are not likely to affect the ambient environment. Investigations of trace metal reactions between artificial seawater, tailings, and manganese micro- or crushed nodules (Benjamin and Felmy, 1981) found that Cu, Cd and other metals were not released at natural pH of ambient seawater in the mining region. The experiments also found that in the range of 5 - 25°C, dissolution or sorption to sediment particles are not changed significantly (see Shriever and Thiel, 2013 for the description of tailings and their disposal in deep-sea mining). The bottom water and the seawater at 80 m above seafloor (the depth of discharge) have nearly same cooler temperatures (~4-5°C), and thus the desorption of metals is unlikely.

The ploughing effect of nodule collector could lead to mortality of some of the benthic biota and could change the organic matter concentrations of bulk sediments (Nath et al., 2012). Artificial sediment mixing can take place which can affect the benthic fauna and alter the mixing depth temporarily. The geochemistry of sediments in effect may not change, except the effect of crushed nodules increasing the elemental concentration of sediments. An additional change can be due to resedimentation of particles removed and deposited elsewhere. During the INDEX experiment, the majority of the sediment cores from within the disturbed area and areas towards the south showed a 30% increase in organic carbon content as well as an increase in carbon burial rates after disturbance, though with a reduction in carbon/phosphorus ratios. The increased organic carbon values were probably due to the organic matter from dead biota and the migration and redeposition of fine-grained, organic-rich particles. A positive relationship was observed between total and labile organic carbon and macrobenthos density and total bacterial numbers prior to disturbance, whereas a negative relationship was seen after disturbance owing to drastic reduction in the density of macrofauna and bacteria. As regards to the inorganic geochemistry of sediments, the surficial sediments in and around the disturbed track during the INDEX experiment were studied for metal variation in three phases: (1) before the disturbance, (2) immediately after the disturbance, and (3) during monitoring of restoration after ~44 months, from the same locations (Nath et.al., 2005). Most of the elements analyzed showed reduced average concentrations immediately after the disturbance suggesting physical removal and resedimentation in other areas with the migration of the plume. All the elements showed positive relation and coherence in the sediments collected after the disturbance, irrespective of their differences in provenance and depositional environment, whereas elemental

associations during the pre-disturbance and monitoring periods can be explained by the known geochemical processes. A possible transformation of clay mineral type due to the benthic disturbance that would involve changes in surface chemistry of clays was envisaged. Inter-element relations among redox-sensitive elements have also changed with time. This includes decoupling of Co from Mn after 44 months, probably due to the varying oxidation kinetics of two major oxides, Fe and Mn. Model calculations suggest increased diagenetic remobilization rates of Mn during the monitoring phase. Substantial increase in redox-sensitive elements, especially Fe and Mn indicate oxygenation of bottom water due either to reduced activity of benthic burrowing organisms or to renewal of oxygen-rich Antarctic Bottom water (AABW). The pre-disturbance values in terrigenous component were found to be restored with time, likely due to influence of shifts in the direction of bottom flow and suggests that bottom currents would play a major role in restoring the lithogenic component by transporting it from other locations (Nath et al., 2005).

6.5.1 Likely impacts on seafloor conditions

A fair idea of likely restoration can be gauged from the results obtained from previous experiment. However, the scale of the proposed operation is much smaller in case of the collector trial. The immediate changes of physical and chemical properties of sediments around the disturbed site, during the INDEX experiment, soon after the disturbance (in 1997) are compared with the data of 4 subsequent monitoring observations (from 2001 to 2005). In addition, the changes took place in reference area far removed from the disturbed area are also compared in the following paragraphs. The contours and bar diagrams represent the changes taking place in core tops. The clay content in monitoring phases (4 to 8 years after the disturbance) of both the disturbed and reference areas has increased substantially (Fig. 6.5.1.1) over the pre- and post-disturbance periods, which can only be due to additional clay supply not related to disturbance. Bottom currents and possibly eddies were found to be responsible for restoration of lithogenic component (Nath et al., 2005), is probably because of additional clay-sized material.

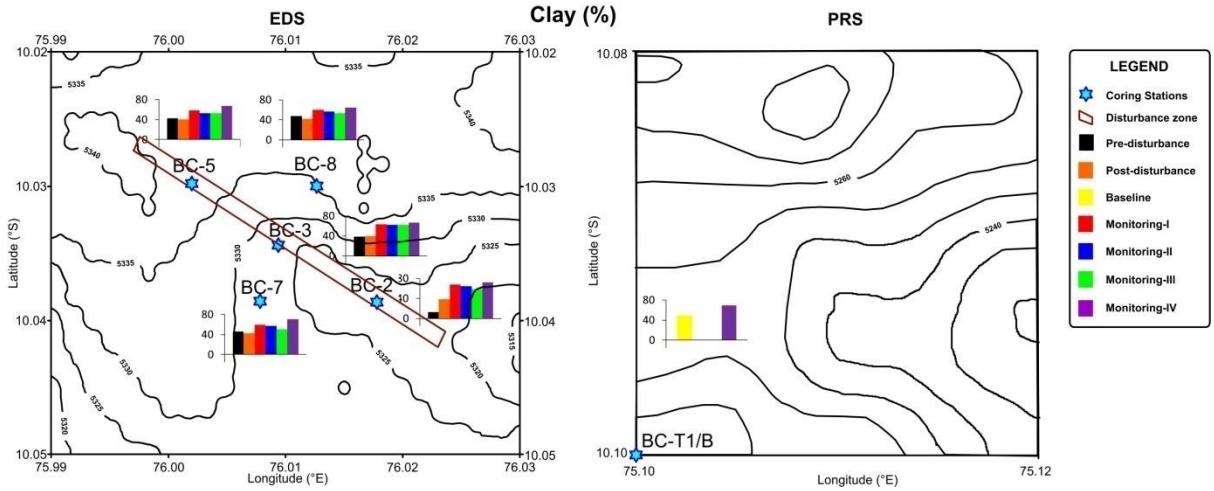

Fig. 6.5.1.1: Changes in clay content (%) in surface sediments in and around disturbed site (on left) and the reference area (on right) with time (disturbance, post-disturbance and 4 phases of monitoring)

Porosity of the surface sediments in all the five phases (Fig. 6.5.1.2) has remained within the narrow range. Slight increases in monitoring phases II, III and IV of disturbed area are also reflected in the reference area.

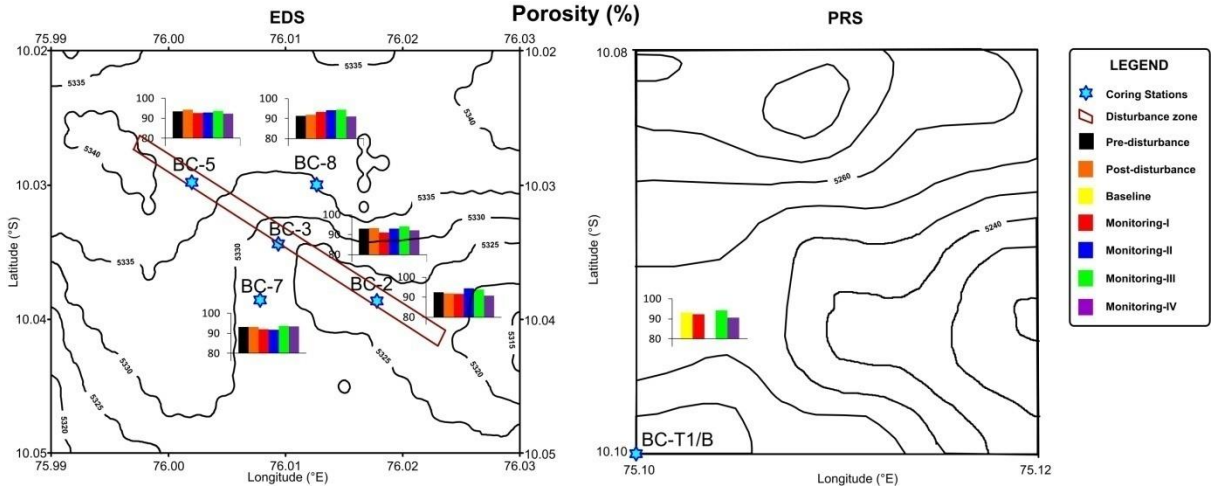

Fig. 6.5.1.2: Changes in Porosity (%) in surface sediments in and around disturbed site (on left) and the reference area (on right) with time (disturbance, post-disturbance and 4 phases of monitoring)

While immediate changes in shear strength of surface sediments of the disturbed area (BC-2, BC-3 and BC-5) was seen after the disturbance, increases were seen in the areas which were not disturbed (Fig. 6.5.1.3). Varying degrees of restoration was seen in different areas.

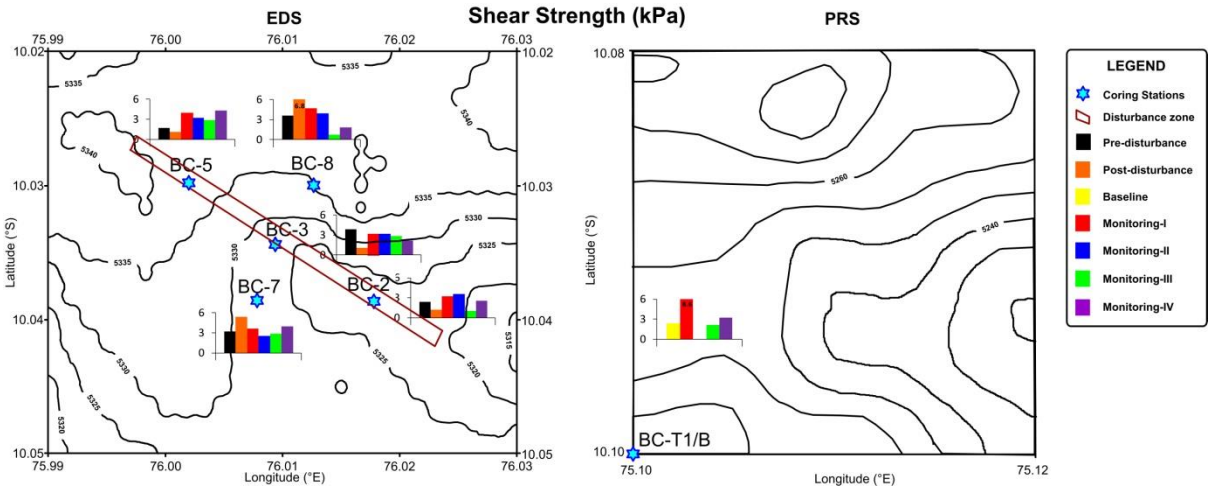

Fig. 6.5.1.3: Changes in shear strength (kPa) in surface sediments in and around disturbed site (on left) and the reference area (on right) with time (disturbance, post-disturbance and 4 phases of monitoring)

Porewater nutrient (nitrate and phosphate) values in the surface sediments in all the phases of disturbance and monitoring (Figs. 6.5.1.4; 6.5.1.5) were within the range of natural variability.

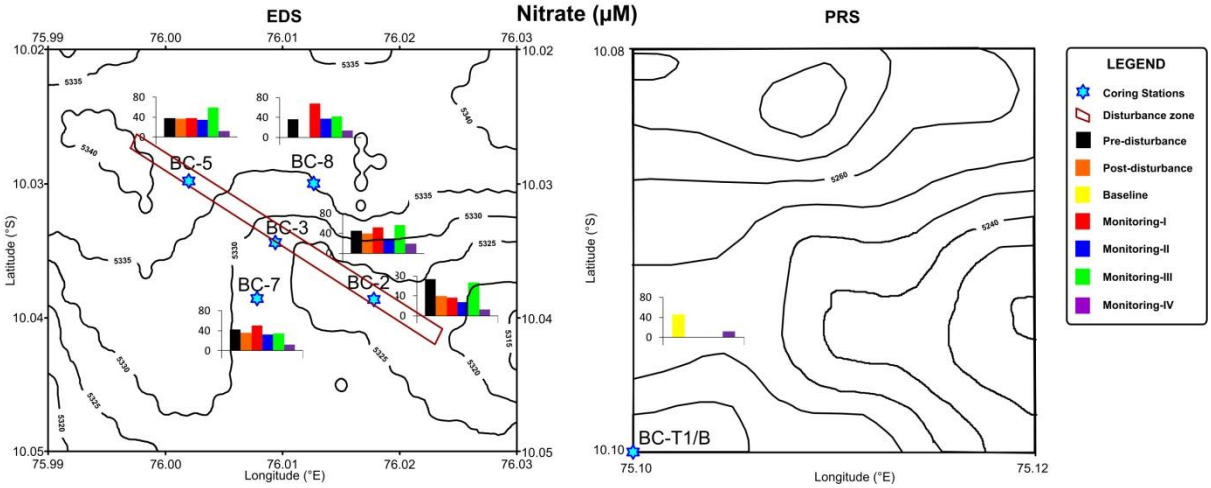

Fig. 6.5.1.4: Changes in porewater nitrate in sediment core tops in and around disturbed site (on left) and the reference area (on right) with time (disturbance, post-disturbance and 4 phases of monitoring)

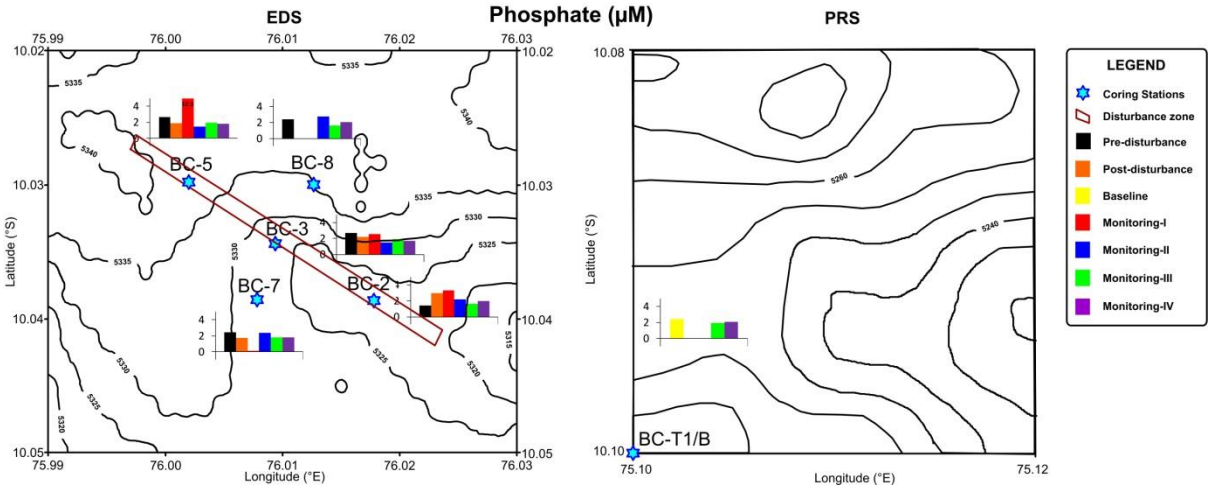

Fig. 6.5.1.5: Changes in porewater phosphate in sediment core tops in and around disturbed site (on left) and the reference area (on right) with time (disturbance, post-disturbance and 4 phases of monitoring)

Organic carbon content in two stations within the disturbed strip (BC-3 and BC-5) have shown an increase after the disturbance (Fig. 6.5.1.6), which was attributed to the carbon from dead biota. Organic carbon in the later phases were found to be locally variable.

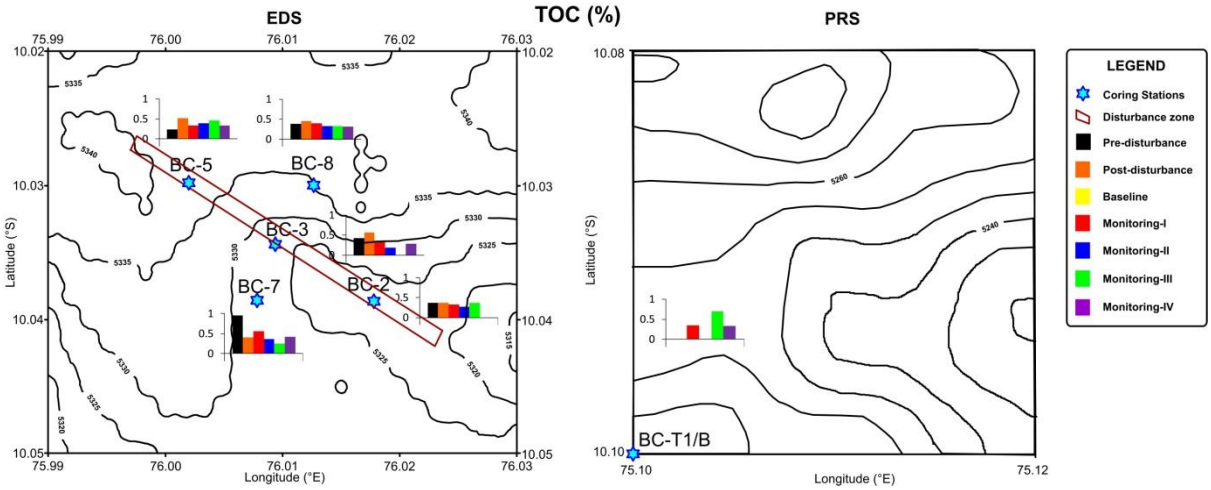

Fig. 6.5.1.6: Changes in organic carbon (%) in sediment core tops in and around disturbed site (on left) and the reference area (on right) with time (disturbance, post-disturbance and 4 phases of monitoring)

In effect, while some of the physical and chemical properties of sediments have undergone some change soon after the disturbance at surface, the natural conditions seem to have taken over soon after that.

6.5.2 Likely impacts on sub-seafloor conditions

Downcore variation in physical and chemical properties of sediments can be indicative of biogeochemical changes taken place recently, benthic mixing and the paleodeposition as well. While the pre- and post-disturbance downcore profiles of clay content are nearly similar, increased clay content in the monitoring phases (Fig. 6.5.2.1) is similar to that seen in surface reiterating the interpretation of additional clay supplies to the area.

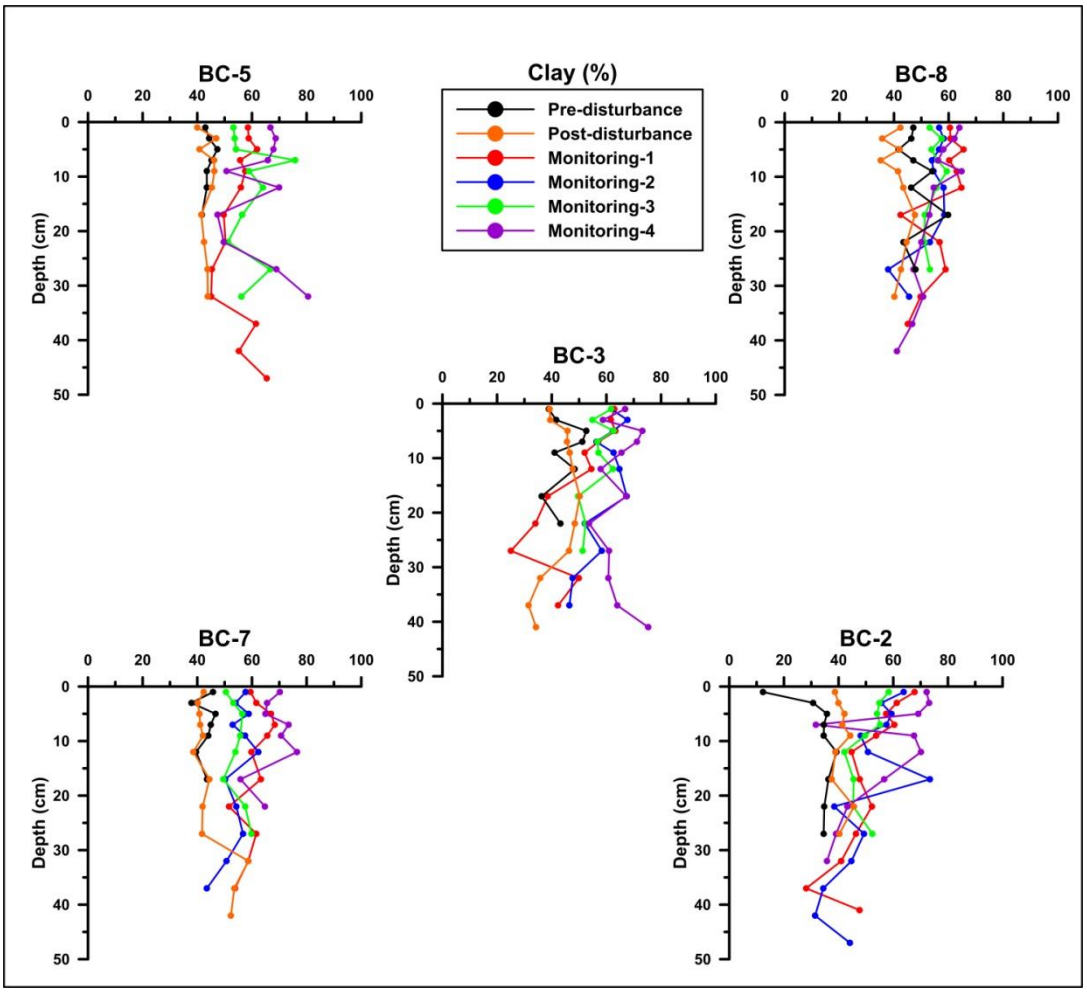

Fig. 6.5.2.1: Downcore changes in clay content (%) in the disturbed area with time (disturbance, post-disturbance and 4 phases of monitoring). Cores BC-2, 3 and 5 are from the disturbed strip, BC-7 is on the south and BC-8 is on the north of disturbed strip.

While the top 10 cm shows the variability in water content, sediments deeper than 10 cm vary in a very narrow range in all the monitoring phases (Fig. 6.5.2.2). Significant changes in the top 10 cm could reflect the mixing depth of burrowing biota.

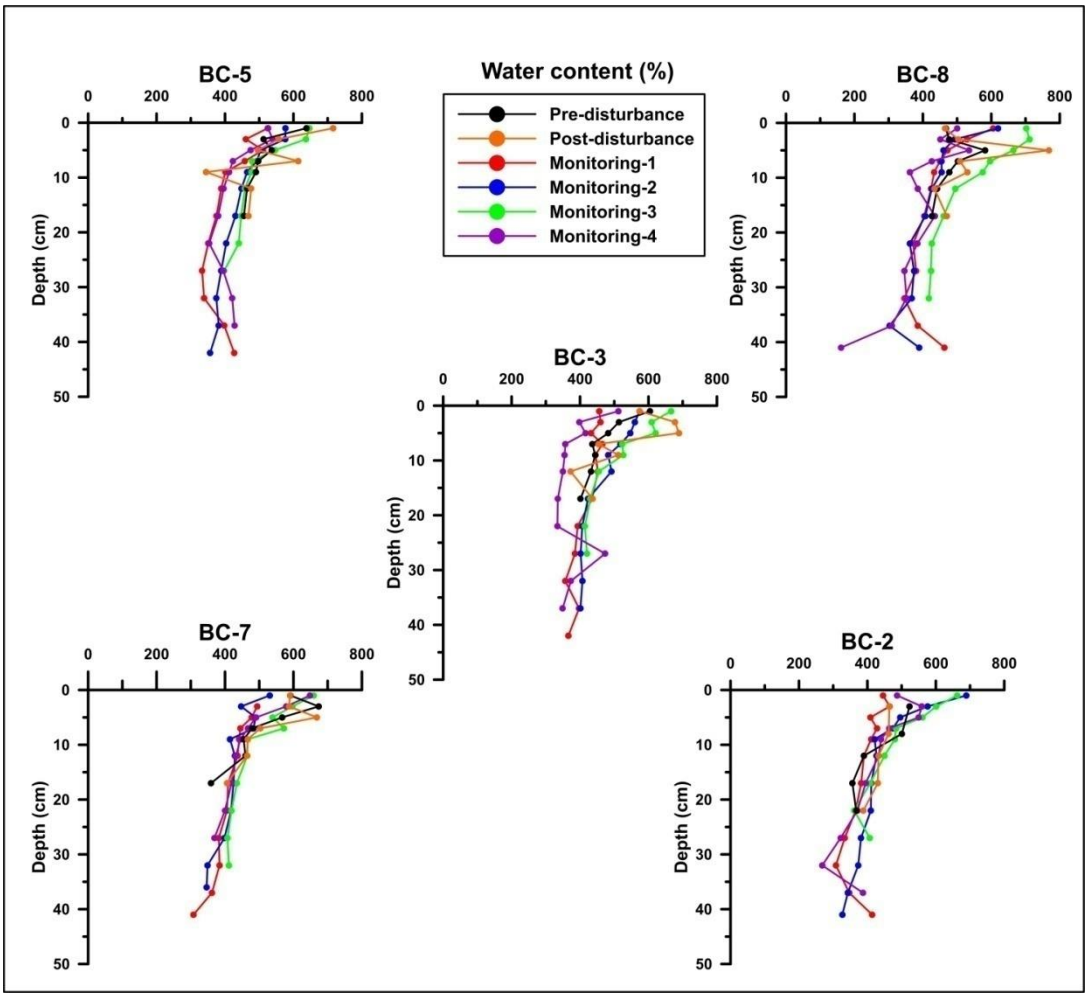

Fig. 6.5.2.2: Downcore changes in water content (%) in the disturbed area with time (disturbance, post-disturbance and 4 phases of monitoring). Cores BC-2, 3 and 5 are from the disturbed strip, BC-7 is on the south and BC-8 is on the north of disturbed strip.

Though, the shear strength shows a large variability within the time periods observed (Fig. 6.5.2.3), a consistent feature is the increasing shear strength values with depth in all the phases.

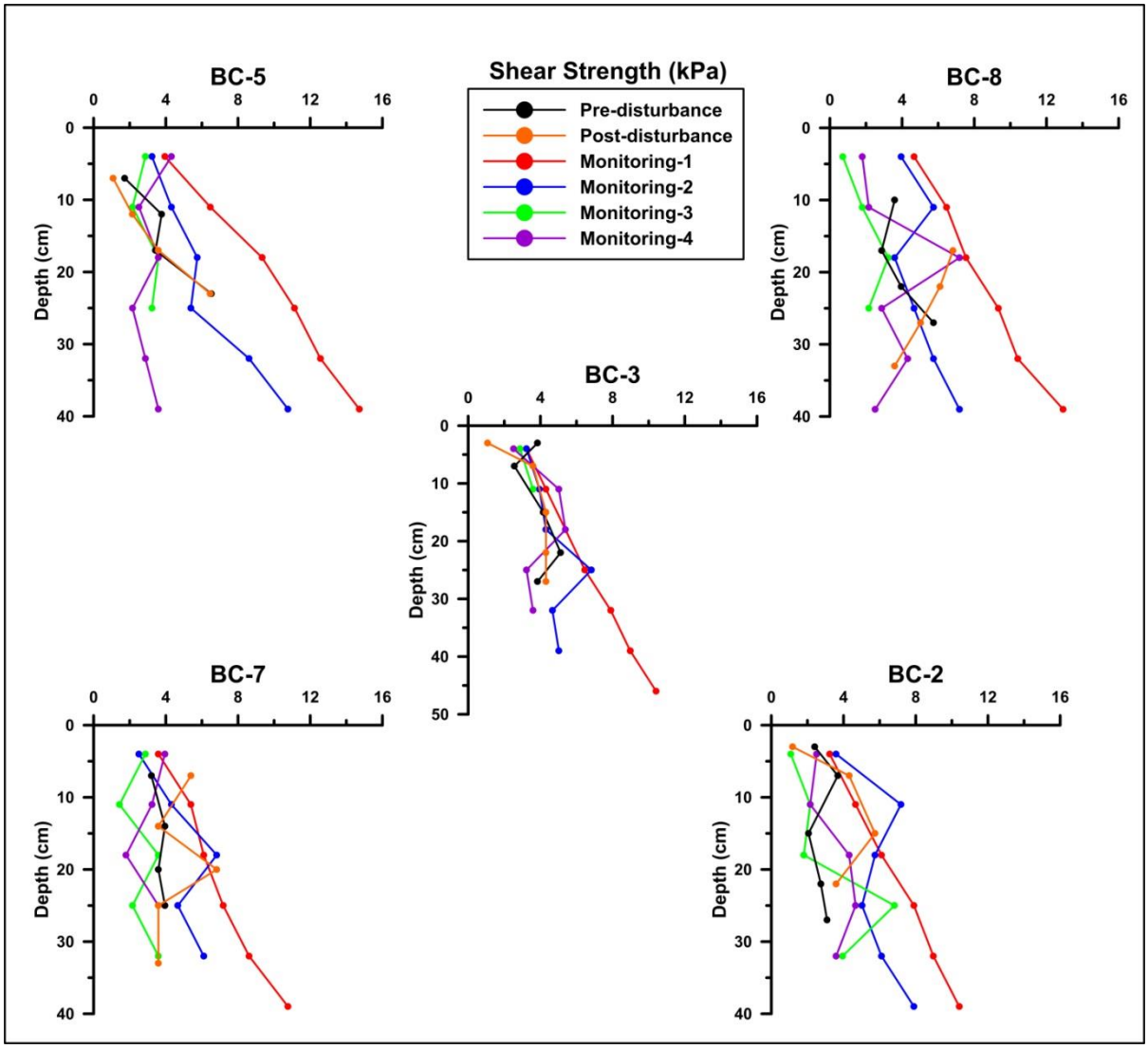

Fig. 6.5.2.3: Downcore changes in shear strength (kPa) in the disturbed area with time (disturbance, post-disturbance and 4 phases of monitoring). Cores BC-2, 3 and 5 are from the disturbed strip, BC-7 is on the south and BC-8 is on the north of disturbed strip.

While the downcore porewater nitrate concentrations and profiles of pre- and post-disturbance phases are nearly similar, the subsequent monitoring phases have shown different values which were either decreased or increased (Fig. 6.5.2.4), possibly reflecting the prevalent natural benthic biogeochemical conditions. Porewater phosphate values (Fig. 6.5.2.5) remained within 2-4 µM in all the phases and the disturbance values were within this range.

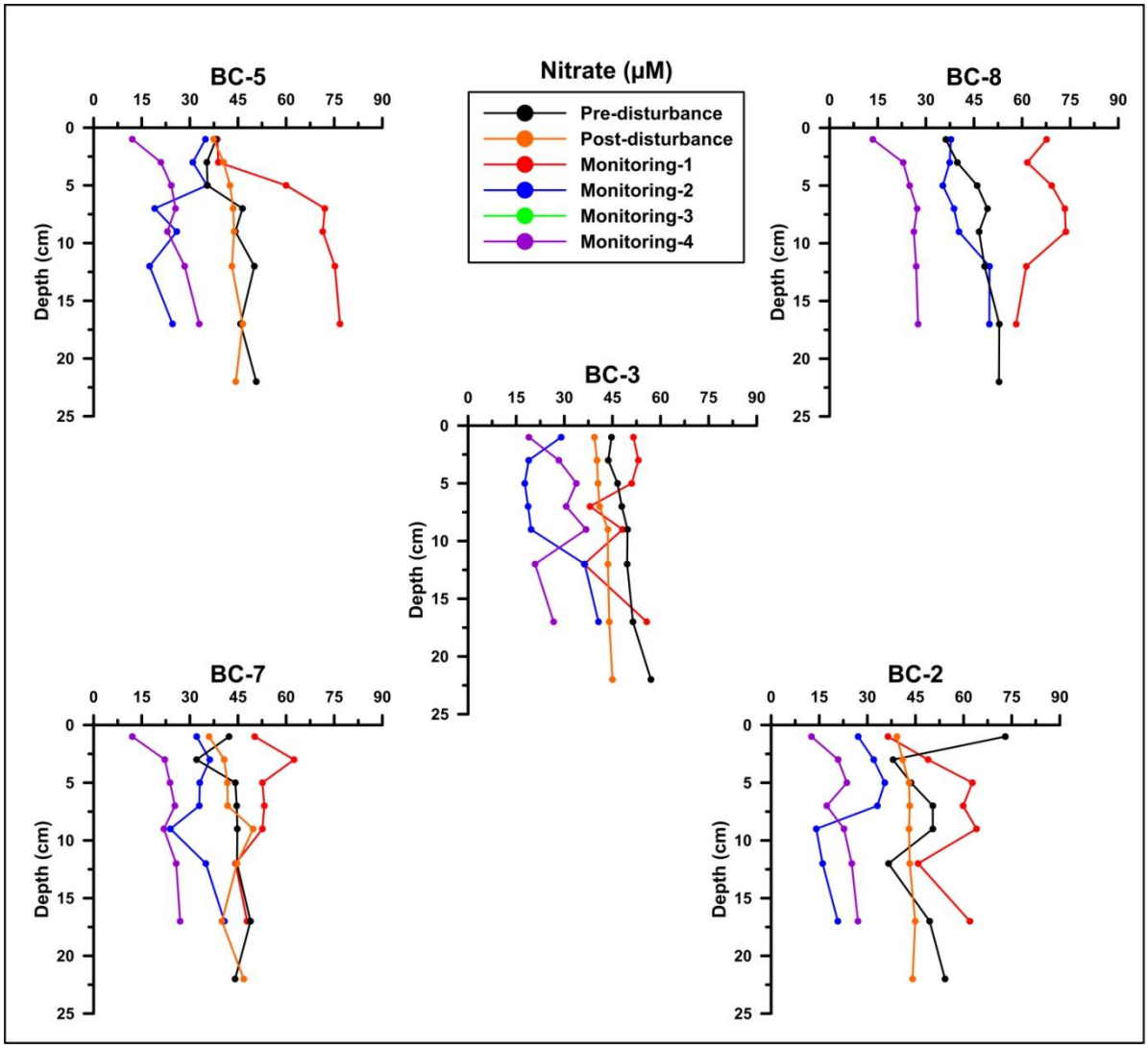

Fig. 6.5.2.4: Downcore changes in porewater nitrate in the disturbed area with time (disturbance, post-disturbance and 4 phases of monitoring). Cores BC-2, 3 and 5 are from the disturbed strip, BC-7 is on the south and BC-8 is on the north of disturbed strip

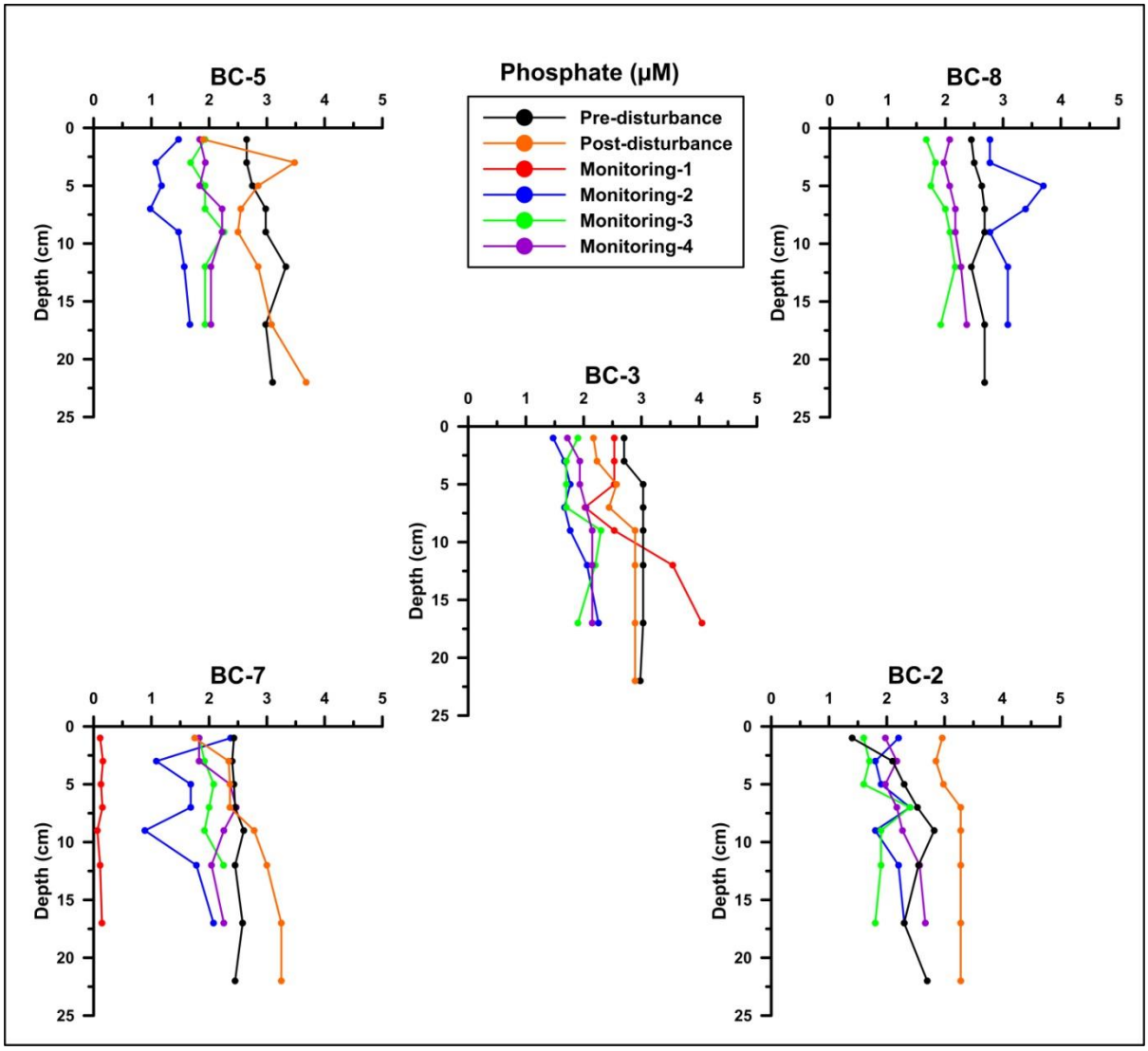

Fig. 6.5.2.5: Downcore changes in porewater phosphate in the disturbed area with time (disturbance, post-disturbance and 4 phases of monitoring). Cores BC-2, 3 and 5 are from the disturbed strip, BC-7 is on the south and BC-8 is on the north of disturbed strip

As seen in the surface sediments, the total organic carbon has shown an increase in the top 5-10 cm in the post-disturbance phase. The TOC values in general are very low (Fig. 6.5.2.6) and vary within a narrow range and mostly show gradual reduction within the top 5 cm. Subsurface peaks/increases in monitoring phases could reflect the benthic mixing depths. In the reference area which is far removed from the disturbed area, similar reduction in top 5 cm is generally seen with the development of occasional subsurface peaks (Fig. 6.5.2.7) reflecting the natural changes.

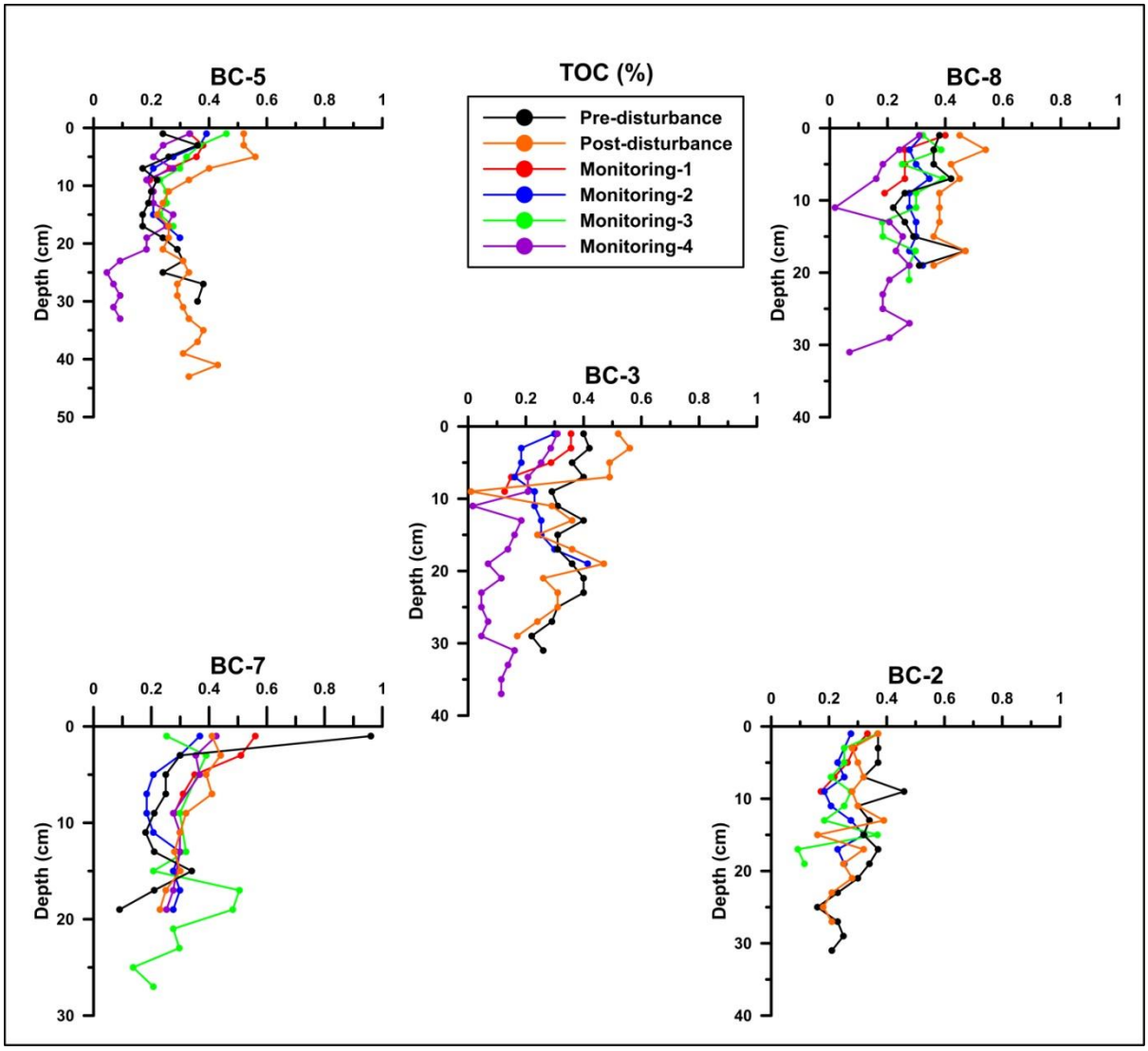

Fig. 6.5.2.6: Downcore changes in total organic carbon in sediments in the disturbed area with time (disturbance, post-disturbance and 4 phases of monitoring). Cores BC-2, 3 and 5 are from the disturbed strip, BC-7 is on the south and BC-8 is on the north of disturbed strip

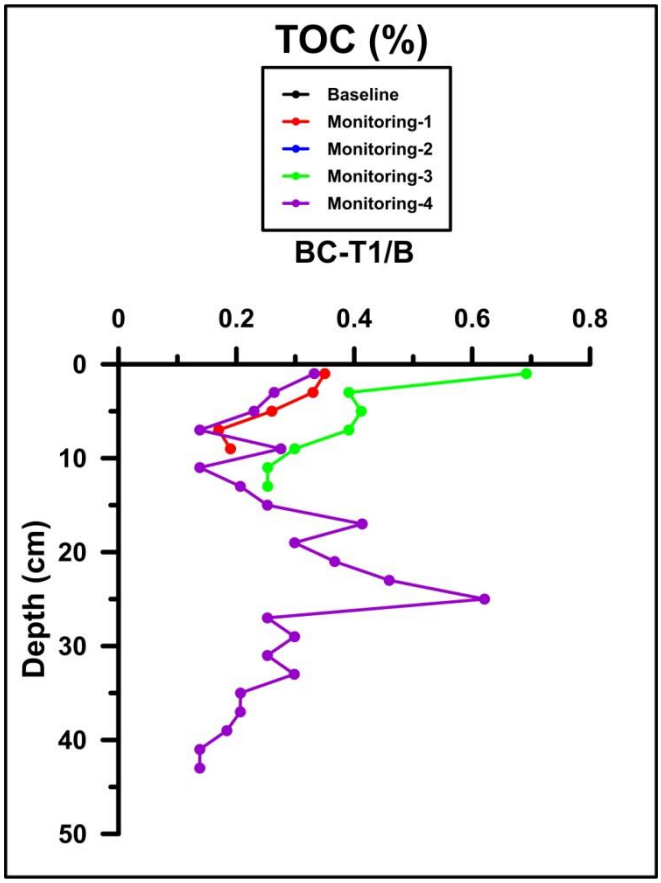

Fig. 6.5.2.7: Downcore changes in total organic carbon in sediments in the reference area with time (3 phases of monitoring over a period of 7 years).

6.5.3 Likely impacts with respect to natural variability

In addition to monitoring the disturbed area and the reference area for assessing the restoration of benthic environment, environmental variability data was also collected in the nodule bearing areas covering the entire contract area (which is presented in Section 4). The deep-sea is traditionally considered to be lacking significant temporal variation in the physic-chemical environment. But the studies during the last two to three decades have shown variation in deep-sea processes such as eddy kinetic energy, seasonality in settling fluxes and the physiological response to seasonally changing organic matter in the deep-sea (e.g., Tyler, 1988; Corliss et al., 2009). Thus, in addition to studying the regional variation in environmental parameters, sampling campaign was carried out four times in the Indian contract area for studying the temporal and seasonal changes over a period of 7 years. Here, some of the physical and chemical parameters (clay content, porosity, shear strength, dry bulk density, porewater nutrient and sedimentary organic carbon concentration), in the core tops (mainly the top 2-5 cm) are presented in order to ascertain the limits of variability in natural conditions in the context of assessing the changes that may take place during nodule collector

operation. The temporal variation in surface sediment values for clay content, porosity, shear strength, dry bulk density, porewater phosphate, organic carbon are compared to the post-disturbance changes of INDEX (Table 6.5.3.1), which show that the post-disturbance changes are generally well within the range of natural / temporal changes.

Table 6.5.3.1: Post-disturbance changes of INDEX Experiment compared to temporal changes in the surface sediments in and around the contract area

Parameter	Temporal variation	Post-disturbance change
Clay content (%)	19.74	0.35 to 26.31
Porosity (%)	4.9	0.19 to 0.93
Shear strength (kPa)	2.87	0.64 to 2.76
Wet bulk density (g/cm^3)	0.06	0.005 to 0.016
Porewater phosphate (µM)	4	0.53 to 1.56
Organic carbon (%)	0.32	0 to 0.28

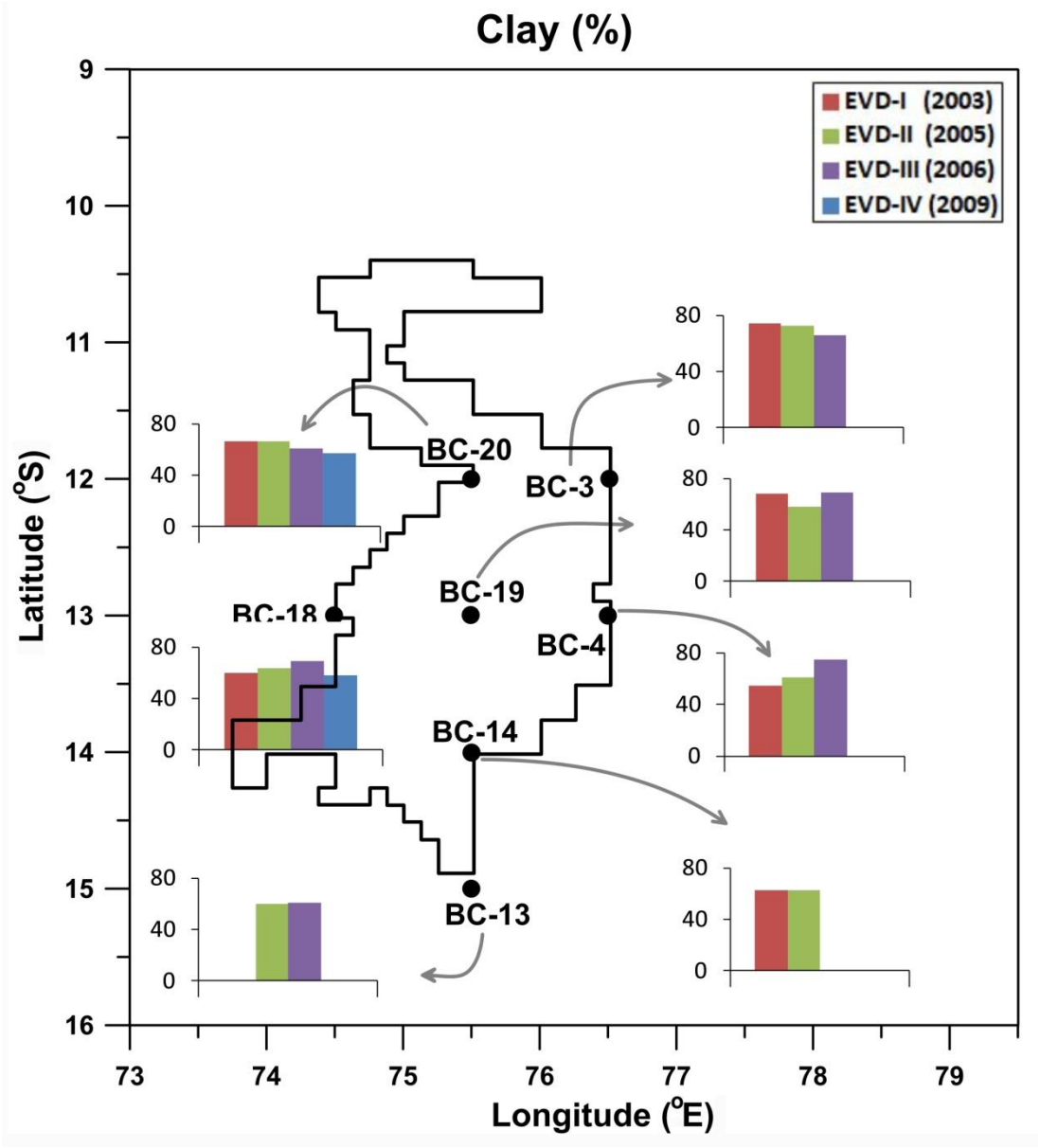

Fig. 6.5.3.1: Temporal variation in clay content (%) in surface sediments in the nodule bearing areas of CIOB over a period of six years.

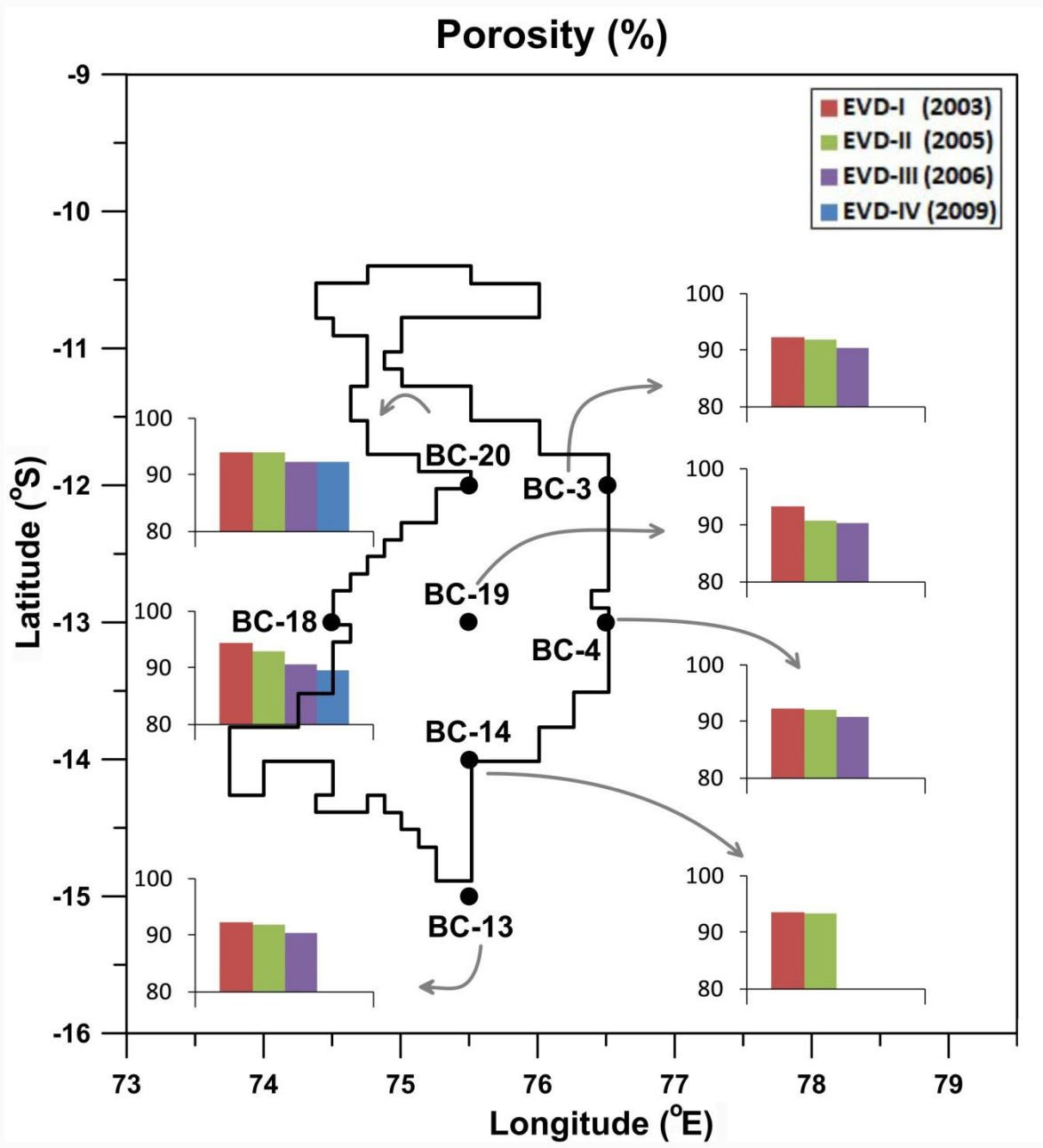

Fig. 6.5.3.2: Temporal variation in porosity (%) in surface sediments in the nodule bearing areas of CIOB over a period of six years

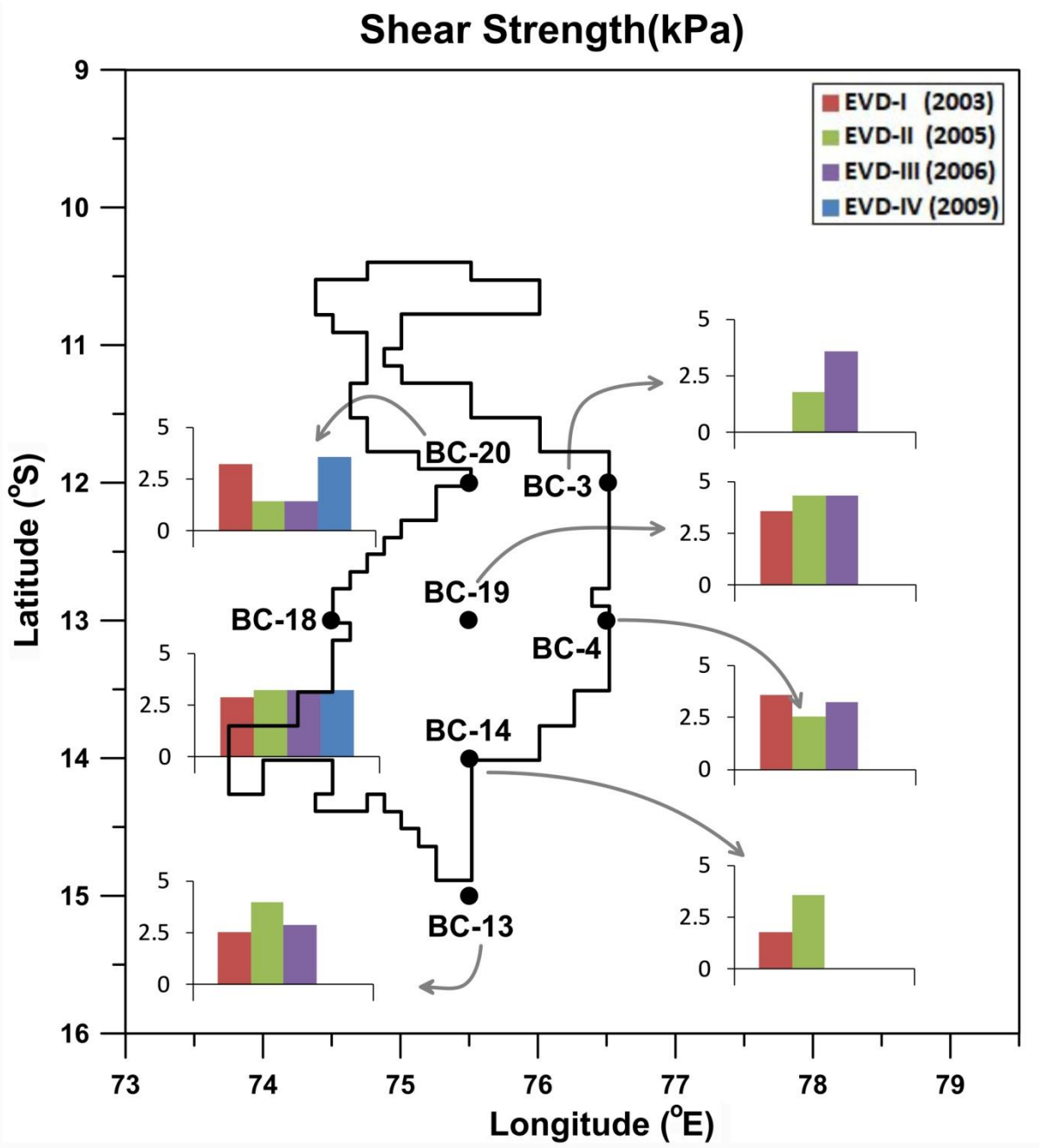

Fig. 6.5.3.3: Temporal variation in shear strength (kPa) in surface sediments in the nodule bearing areas of CIOB over a period of six years

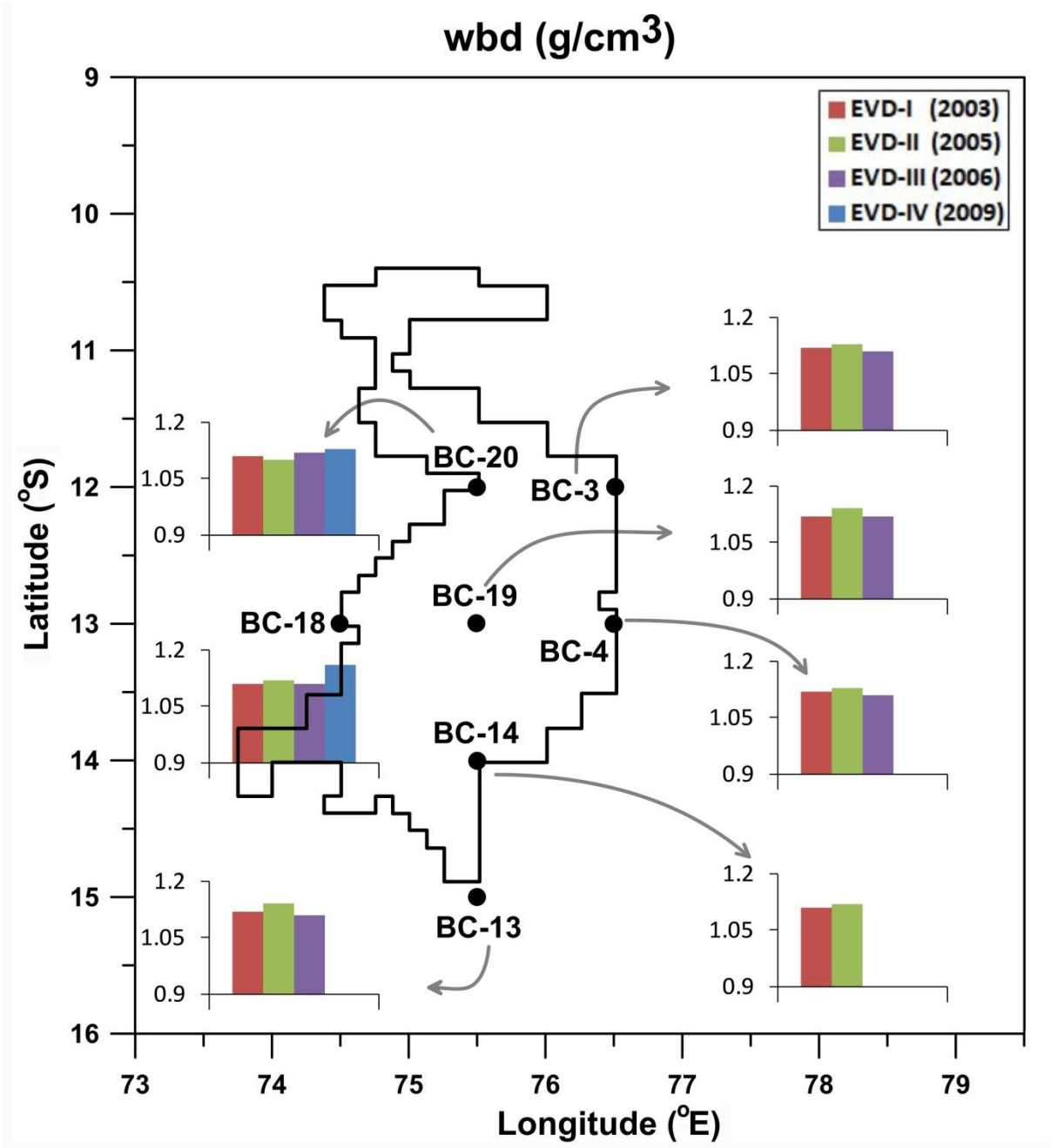

Fig. 6.5.3.4: Temporal variation in wet bulk density (g/cm^3) in surface sediments in the nodule bearing areas of CIOB over a period of six years

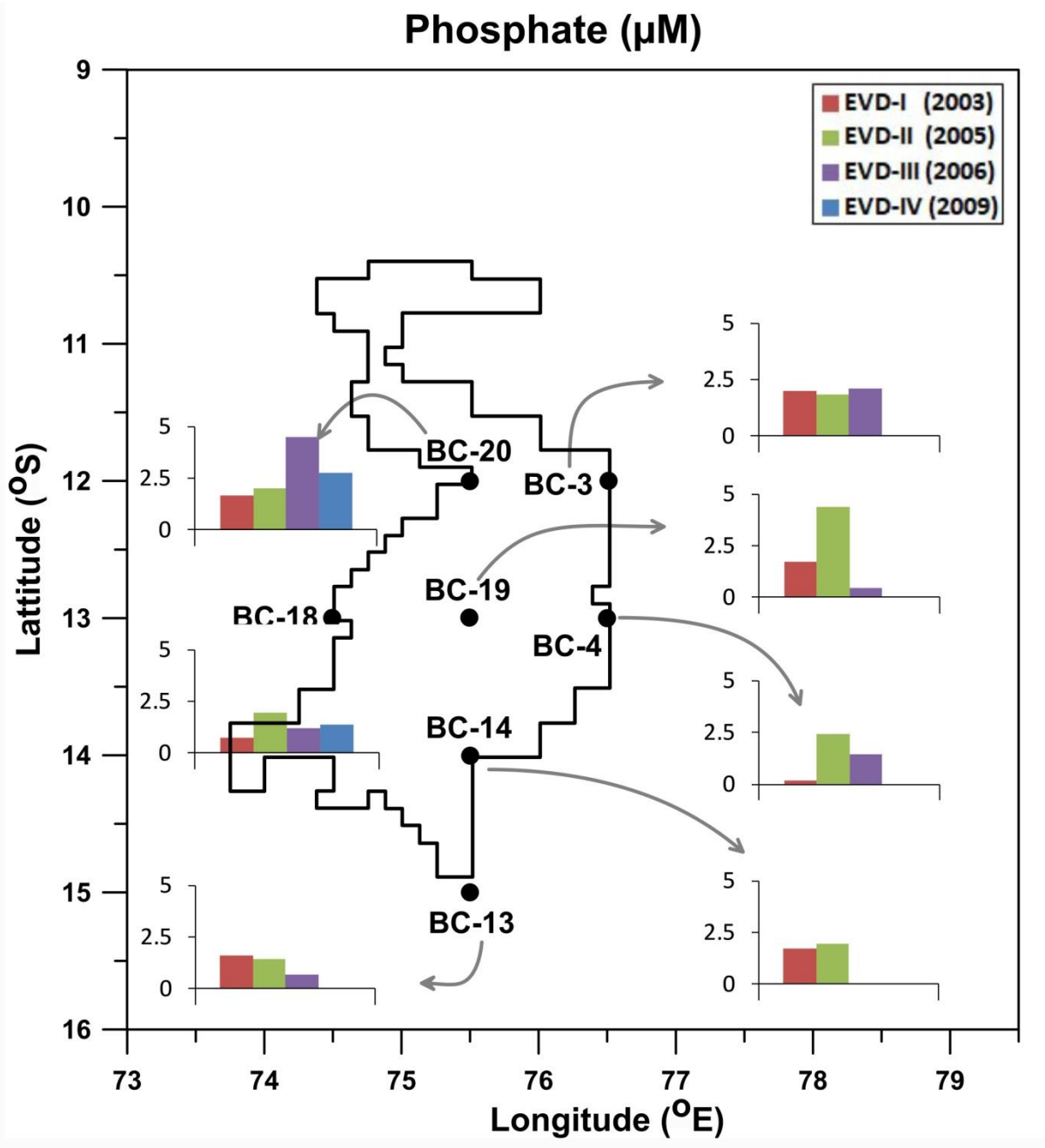

Fig. 6.5.3.5: Temporal variation in porewater phosphate (µM) in surface sediments in the nodule bearing areas of CIOB over a period of six years

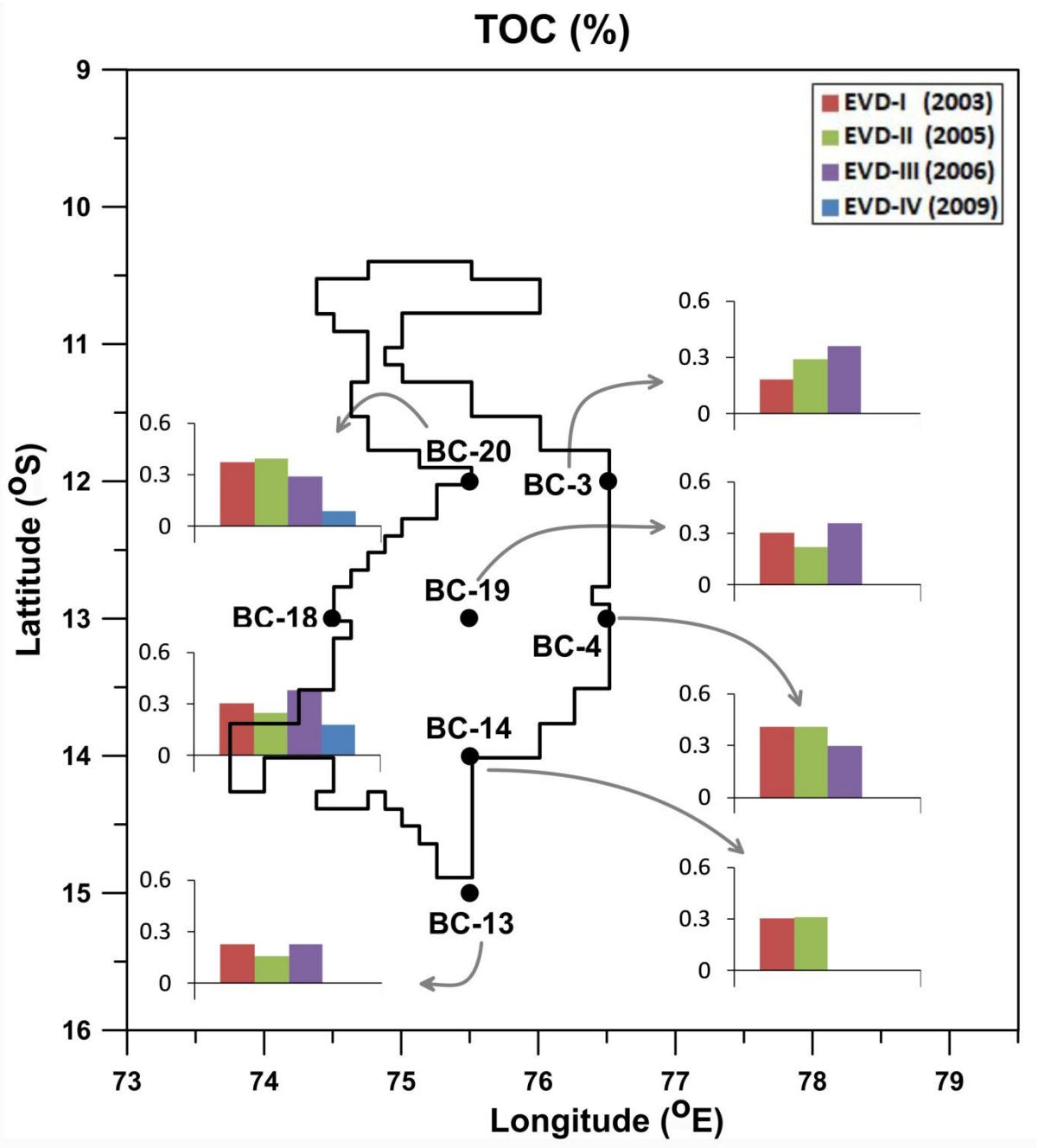

Fig. 6.5.3.6: Temporal variation in sedimentary organic carbon (%) in surface sediments in the nodule bearing areas of CIOB over a period of six years

Temporal variation in down core profiles of geochemical parameters was also studied to assess the benthic biogeochemical changes with time in natural conditions. There is a clear north south variation in pore water nitrite content at 13°S latitude. The southern stations show a lower concentration of nitrite at a given station, as compared to the northern stations. The down core profile patterns are nearly similar after a year but with a change in magnitude in the two regions. The magnitude of changes in the northern stations is more pronounced than the minor changes noticed in the southern stations.

Down core organic carbon profiles in nearly all the stations show that organic carbon values are maximum at the surface, which is similar to the disturbed area. Changes in organic carbon content were seen at some stations, either reflecting the temporal change in organic carbon fluxes or change in community structure or feeding behaviour in the benthic community at this site. In some cores, subsurface peaks are seen indicating burrowing activity in those areas. The subsurface lows and highs in organic carbon are ascribed to benthic burrowing and bioturbation activity, which seems to become shallower with time. The northern stations seem to have similar surficial as well as down core profiles of organic carbon indicating some sort of relation to the sediment type. Lower organic carbon in the surface layers has remained unchanged after two years indicating no change in the overall structure of the feeding community and that surface and suspension feeders dominate over burrowing organisms. Distinct changes in the down core profiles are seen between the two year data in the southern and eastern areas.

In summary, the physical and chemical changes of sediments expected during the nodule collector trial are within the range of natural changes. In the experiment (INDEX) carried out, the restoration of physical and chemical changes was observed after a period of 44 months when the first monitoring expedition was carried. Hence, there is a strong possibility that restoration would have occurred anytime during this period of 44 months. Moreover, as the area, distance, and volume of sediment to be disturbed during the proposed trials is extremely small ($\leq$ 1%) than that in case of the previous experimental disturbance (INDEX), a much smaller impact is expected due to the collector trials that would possibly restore in much shorter time.

7. Potential impacts of nodule collector trial on the biological environment

7.1 Types of likely impacts

The likely impacts that might affect biological communities during the nodule collector trials are (1) removal of benthic biota associated with sediments and nodules, (2) sediment disturbance and plume deposition, (3) smothering due to sediment particles onbottom water dwelling biota, (4) biogeochemical alterations of the sediment, and (5) potential release of toxic sediments and/or substances into the lower water column. The likely impacts at surface, mid-water and seafloor are described below in the context of knowledge gained from the impact experiments carried out earlier.

7.2 Impacts at surface

In the proposed nodule collector test, there is no plan to bring either the nodules or the associated sediments and bottom water to the surface, and thus there will be no discharge at the sea surface. The vessels routinely follow the international guidelines regarding safety and environmental practice at sea. No pollutants will be discharged as per the international laws.

7.3 Impacts in midwater

The water column below 500 meters from surface is considered to host extreme conditions to support life. As a result, existence of biota depends on the little organic matter sinking from the productive upper ocean. Because this organic matter is consumed and degraded as it sinks, zooplankton abundance and biomass decrease exponentially with increasing depth. However, just at the base of mid-water oxygen minimum zone, at the interface of OMZ-oxidizing conditions contains a very narrow zone of unusually high zooplankton biomass (https://www.gso.uri.edu/maritimes/BackIssues/00%20Summer/Text(htm)/zooplankton.htm). Among the few studies carried out on zooplankton in full depths in abyssal areas, the individual concentration of zooplanktonin the North Atlantic decreases drastically from 4000 ind. 1000 m^{-3} at 1000 m to 200 ind. 1000 m^{-3} at 4500 m (Koppelmann and Weikert, 1992). As no operations are planned in midwater, no biological impacts are expected in the entire water column except at ~80 m above the seafloor, which is the altitude for discharge of crushed nodules and sediments during the trial. However, as the occurrence of zooplankton population under the extreme conditions is very small, no harm is expected due to the discharge of sediment and nodules at this depth. Moreover, as shown in Table 6.4.1, the

concentration of sediment discharges is miniscule (0.0083-0.0333%) in the water column, no impact is expected on the biological communities in this reqion.

7.4 Impacts at the seafloor

It is expected that the maximum area covered during the collector tests would be 4600$m^2$and the depth of disturbance would be 15-30 cm of sediments only. The abundance of both epi and in-faunal organisms in surface sediment layer is relatively moderate (between 80 to 250 individuals m^{-2}) in the proposed experimental area. Previous experiments have shown that the magnitude of impacts on sediment associated fauna varies widely with the faunal abundances as well as scale and intensity of disturbance (e.g., Jones et al., 2017; Miller et al., 2018). Also, long term monitoring of disturbance show varying degrees of recovery of different components of benthic ecosystem (e.g., Miljutin et al., 2011, Vanreusel et al., 2016).

The meiofaunal abundance in nodule-free areas in general are higher than that in nodule-bearing areas (e.g., Renaud-Mornant and Gourbault, 1990; Miljutina et al. 2010). In the nodule-bearing areas, meiofaunal abundance may be influenced by geological features such as sediment type, clay content, water content, porosity and other environmental parameters. The meiofaunal densities in CIOB are lesser than those in other deep-sea regions including that in the largest nodule bearing area of Clarion-Clipperton Zone (CCZ)(Table 7.4.1) to the tune of tens to even hundreds of times higher than in CIOB (Zeng et al., 2018). Low meiobenthic abundances in CIOB could be due to the substratum type. Higher meiofaunal abundance in the eastern area of the COMRA than that in their western area (Gao et al. 2002; Wang et al. 2013), both in CCZ, have been attributed to different sediment types, with the eastern area having siliceous ooze which can be softer, contain more water and rich organic debris in large pores (Chen, 2004). Siliceous clays, on the other hand as in case of CIOB, have coarser and harder particles, with lower water content and smaller pores.

Table 7.4.1: Comparisons among metazoan meiofaunal abundance from World Oceans areas and polymetallic nodule areas (Zeng et al., 2018)

	Location	Longitude/°E	Latitude/°S	Depth/m	Sediment Depth/cm	Nematodes Abundance/ (ind/10cm^2)	Metazoan Meiofauna Abundance/ (ind/10cm^2)
Central Indian Ocean							
Ingole et al. (2000)	Central Indian Basin	76.0	10.0–10.1	5300–5330	10	20–24	35–45
Wang (2012)	Central Indian Basin	85	10	4944	10	6.35	7.76
Singh et al. (2014)	Central Indian Basin (nodule area)	74.5–75.5	13.0	5041–5164	10	23.99 ± 2.7	-
Atlantic Ocean							
Tietjen et al. (1989)	Hatteras abyssal plain, NW Atlantic Ocean	−70.4	−32.5	5411	15	85 ± 20	114 ± 26
Kalogeropoulou et al. (2010)	Porcupine abyssal plain, NE Atlantic Ocean	−16.5	−48.8	4850	at least 10	301.3–935.5	346.6–1073.5
Arctic Ocean							
Soltwedel et al. (2003)	Molloy Deep, Arctic Ocean	2.6–3.0	-(79.1–79.2)	5416–5569	5	875–1201	935–1295
Hoste et al. (2007)	Hausgarten, Arctic Ocean	4.0	−79.1	1200–5500	5	135–3211	149–3409
Pacific Ocean							
Renaud-Mornant and Gourbault (1990)	NE Pacific Basin, CCNP (nodule-free area)	−130.7	-(14.6–14.7)	5000–5140	2.5	36–87	66–157
Renaud-Mornant and Gourbault (1990)	NE Pacific Basin, CCNP (nodule-bearing area)	-(130.7–131.0)	-(14.0–14.6)	4905–5020	2.5	25–101	45–189
Bussau (1993)	Peru Basin, nodule area, NE Pacific Ocean	−88	7	4100–4200	1	75	100
Gao et al. (2002)	Eastern area of the COMRA's Contract Area	-(145.3–145.4)	−8.4	5000–5300	6	23.15	32.47
Gao et al. (2002)	Western area of the COMRA's Contract Area	-(154.0–154.1)	-(10.0–10.1)	5000–5300	6	11.56	18.05
Shimanaga et al. (2007)	Philippine Sea, Western Pacific Ocean	130.0	−7.0	5569	3	30–126	31–133
Miljutina et al. (2010)	NE Pacific Basin, CCNP (nodule-free area)	−130.1	-(14.0–14.1)	5013–5046	5	136.5 ± 9.9	-
Miljutina et al. (2010)	NE Pacific Basin, CCNP (nodule-bearing area)	−130.1	-(14.0–14.1)	4877–5000	5	69.5 ± 6.3	-
Wang et al. (2013)	Eastern area of the COMRA's Contract Area	-(145.6–145.7)	-(8.5–8.7)	5236–5329	6	97. 23 ± 19. 51	104.40 ± 20.48
Wang et al. (2013)	Western area of the COMRA's Contract Area	-(154.0–154.1)	-(10.0–10.1)	5074–5159	6	36. 78 ± 25. 08	40.26 ± 25.84
This study	Central Indian Basin (nodule-free area)	80.0–84.2	7.1–14.1	4738–5418	6	2.40–17.28	2.96–19.11
This study	Central Indian Basin (nodule-bearing area)	80.0	12.5–13.5	5049–5407	6	6.07–6.42	6.70–7.97

During INDEX, the distribution, composition and abundance of meiobenthos and macrobenthos were studied before and after the disturbance in the 3000 x 200m disturbance track as well as outside the disturbance track. Characteristic changes in the spatial and vertical distribution of macrobenthos were discernable after the disturbance particularly in the disturbance track (Ingole et al.,1999). The changes were not similar within and outside the disturbance track. While a significant decrease in density was noticed inside the track, outside track was either not affected or showed a marginal increase in the numerical count. Significant reduction in the vertical distribution was also recorded. Similarly the abundance of meiofauna, in particular, nematodes and copepods showed reduction up to 40% in the disturbed track. The meiofaunal densities outside the disturbance track showed no significant changes. Interestingly, increase in density at some stations, similar to macrobenthos was noticed (Ingole et al., 1999). Total meiofauna density that rangedbetween 35 and 45 organisms per 10 cm^2 during the predisturbance period, reduced moderately to 21-32 organisms per 10 cm^2 during the postdisturbance period in the test and reference sites respectively (Ingole et al., 2000). Nematoda was the most abundant metazoan group, on an average representing 55% of the meiofaunal population. The abundance of nematodes and harpacticoid copepods as well as total meiofauna showed decrease during post-disturbance sampling (Table 7.4.2). The reduction in metazoan density after physical disturbance could

have been due to either mortality of fauna accompanied by dispersal to other areas with the help of bottom water currents (Ingole et al., 2000). Vertical distribution of meiofauna in the sediment cores revealed that 75% to 90% of the metazoan population was confined to the top 2-cm layer of the sediment.

Table 7.4.2

Mean values of meiofaunal density (no./10 cm^2) during pre- and postdisturbance studies (n = 12 each).

	Predisturbance		Postdisturbance	
	Outside the track	Inside the track	Outside the track	Inside the track
Nematoda	20 ± 7	24 ± 11	17 ± 8	12 ± 7
Harpacticoida	8 ± 5	11 ± 5	7 ± 4	4 ± 3
Other groups	7 ± 9	10 ± 7	8 ± 5	5 ± 6
Total	35	45	32	21

Source: Ingole et al., (2000)

The restoration process was monitored four times subsequently between years 2001 and 2005.The macrofaunal density in the test site showed a significant increase (x:400 ind.m^{-2}) in the first monitoring observation 44 months after the post-disturbance sampling (x:320 ind.m^{-2}) (Ingole et al., 2005a). Overall macrofaunal density has in fact increased in the disturbed strip as well as in the areas north and south of the disturbed strip (Fig. 7.4.1), which suggests that the recovery of benthic fauna is possible in the disturbed zone. Moreover, as this increase and reduction in meiofunal density in subsequent phases was observed in the reference area as well, it can only be due to natural changes occurring in the area, implying that the effects of artificial disturbance had waned off by then.

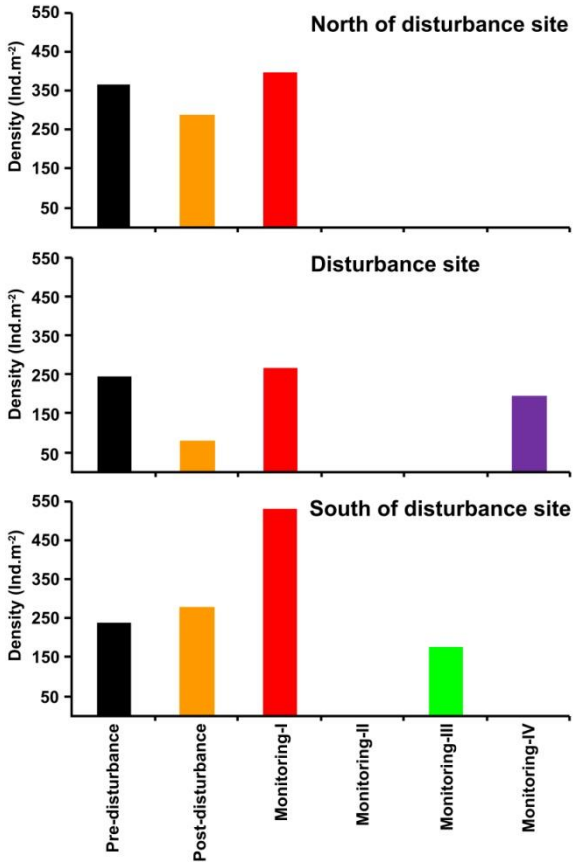

Fig. 7.4.1: Changes in macrofaunal density in the disturbed strip, north and south of disturbed strip during the disturbance and subsequent monitoring phases

The population of nematodes and oligochaetes was restored after 44 months, in fact, more than what was seen before, but the crustaceans did not reach the baseline populations measured in June 1997 (Fig. 7.4.2). Soon after the disturbance, while there was a reduction in certain groups, an increase was seen in some other groupsas observed immediately after as well as during monitoring phases.The comparison of pre- and post-disturbance data with the monitoring phase showed improvement in the polychaete density, especially the juvenile population, signifying the possibilityof polychaete recruitment in the test area (Ingole et al., 2005a). Most of the cores showed presence of oval structures and mottled surfaces suggesting variable degrees of bioturbation in deeper (25 cm) sediment layers. The textural and biochemical analysis of the CIOB sediment showed considerable increase in clay content, labile organic matter, carbohydrates and proteins in 44 months (Nath et al. 2005). Thus, the sediment analysis suggests an improvement in the biochemical parameters and likely enhanced food conditions for the benthos. Since the deep-sea polychaetes are known to respond quickly to the improved food supply (Vanreusel et al. 2001), the recruitment of

benthic polychaete in CIOB may have been stimulated due to the augmented availability of food material (Ingole et al., 2005a).

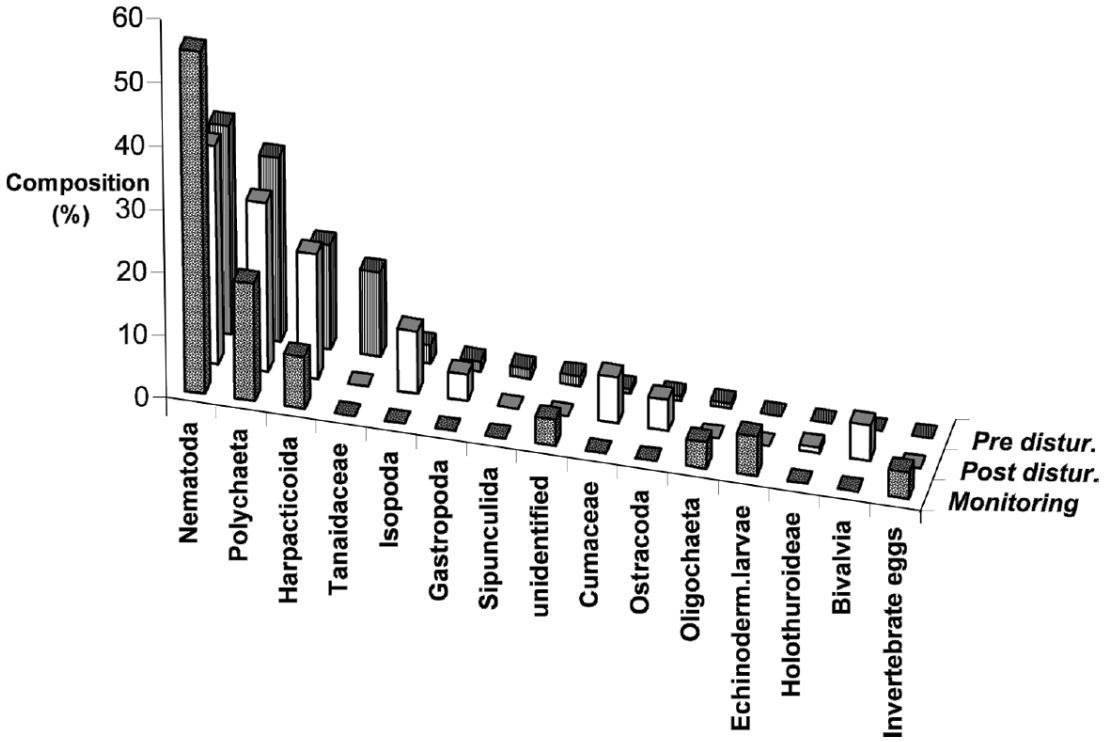

Fig. 7.4.2:Macrofaunal composition (%) during three INDEX phases (Ingole et al., 2005a)

A comparison of the depth integrated meiofauna abundance in the test and reference areas during the monitoring phase with that of the pre- and post-disturbance phases is given in Figs. 7.4.3 and 7.4.4 (Ingole et al., 2005b). The density of meiofauna decreased from 45 no. 10 cm^{-2} to 21 no. 10 cm^{-2} soon after the disturbance, and the maximum reduction was in the test area (Stn. 2, 3, and 5; Figs.7.4.3 and 7.4.4). The monitoring study conducted after 44 months, showed wider variation in mean meiofaunal density with overall increase not only in the test area (Stn. 2, 3, and 5; Fig. 7.4.3) but also on either side of the test area (Fig. 7.4.4).

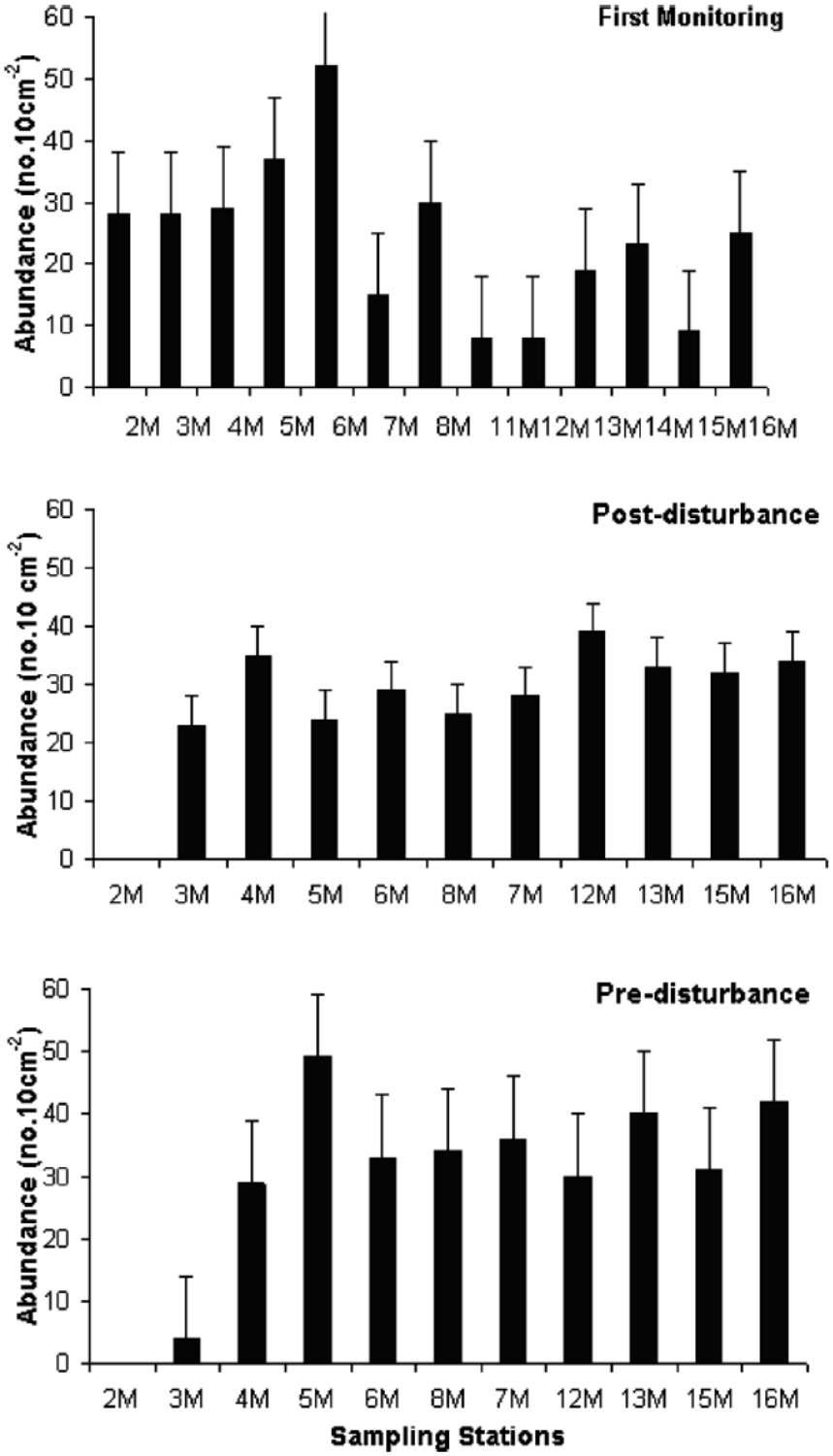

Fig. 7.4.3: Meiobenthic abundance (no. 10 cm^{-2}) in individual cores during three INDEX phases (Ingole et al., 2005b).

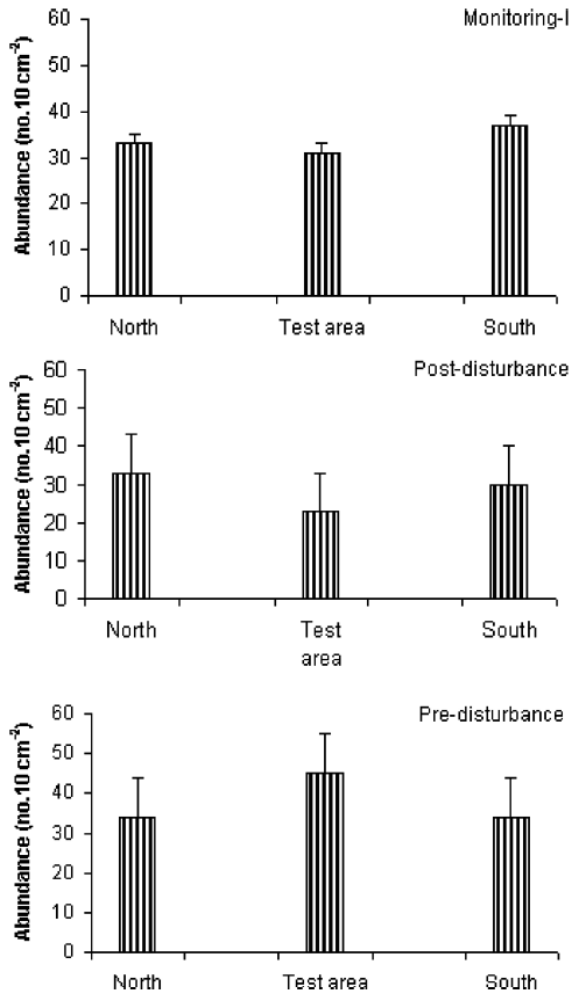

Fig. 7.4.4: Meiofaunal abundance (no. 10 cm^{-2}) in CIOB during different INDEX phases (Ingole et al., 2005b)

The nematode:copepod (N:C) ratio, which had increased from 2.18 (pre-disturbance) to 3.00 in post-disturbance probably with the reduction of copepods. But in the monitoring phase, the ratio drastically increased to 30 (Ingole et al., 2005b) suggesting changes in community structure. The increased meiofaunal population and enhanced N;C ratio in favour of copepods, in the test area as well as in the adjacent area was mainly due to the augmented food supply (Nath et al.2005; Nath et al., 2012; Raghukumar et al, 2001). Nevertheless, occurrence of some portion of the meiofaunal population in deeper layers of some of the sediment cores collected during the monitoring phase, suggests a possible influence of higher sediment reworking by larger macro- and megabenthic organisms (Soetaert et al. 1997; Nath et al. 2005).Presence of live polychaete burrows as deep as 25 cm (Ingole et al. 2005a) further support the fresh bioturbation activity in the sediment layer, both in the referenceand test areas (Ingole et al., 2005b).Later monitoring phases have shown mixed results in down-core in meiobenthic fauna (Fig. 7.4.5) suggesting that the natural conditions have taken over.

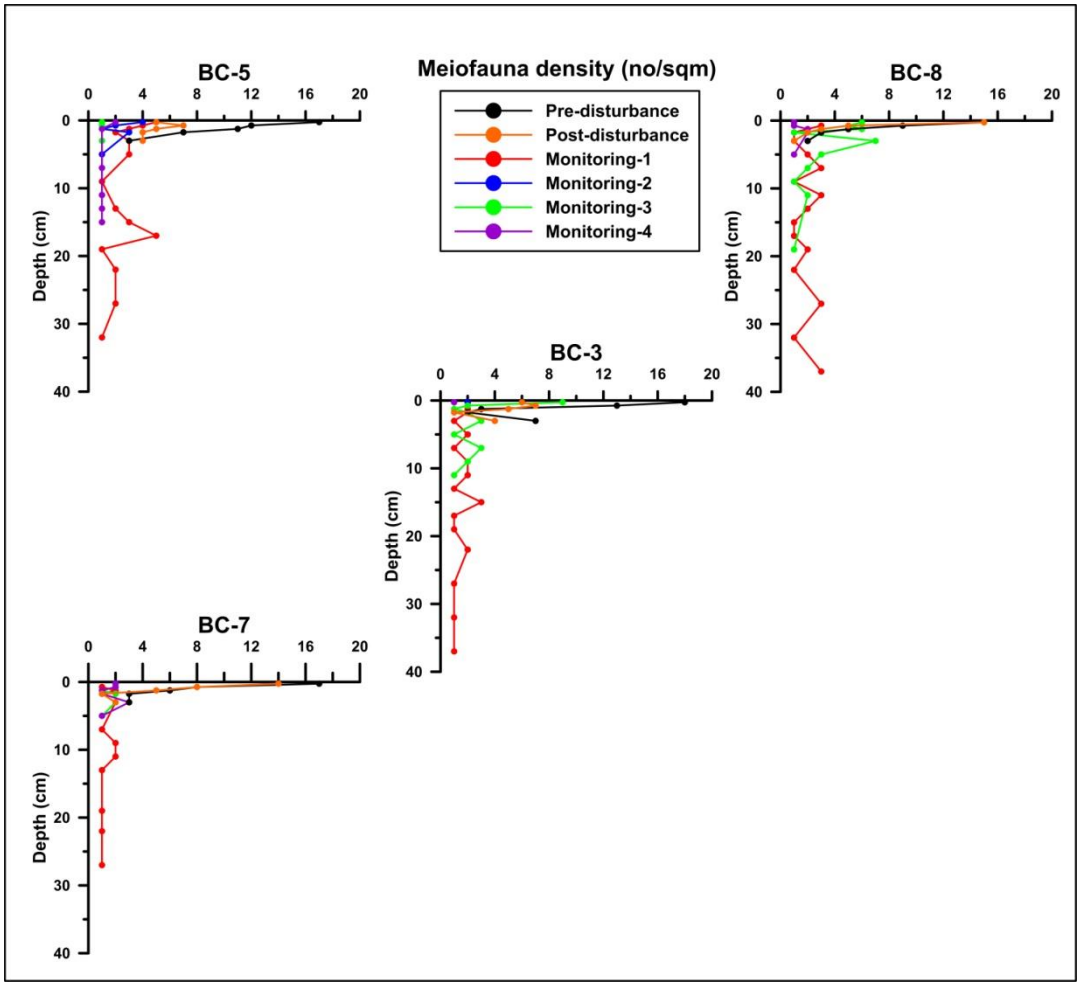

Fig. 7.4.5: Changes in downcore meiofaunal density in the disturbed area over a period of 9 years. Cores BC3 and BC5 are from the disturbed strip, BC7 and BC8 represent the south and north of disturbed strip.

In addition to monitoring the effects of disturbance in the test and reference areas, a basin-wide environmental study was also carried out in and around the Indian contract area. The detailed regional variability in benthic fauna has been described in the Section 5. Temporal and seasonal variability of benthic biogeochemistry was studied for a period of six years (four sampling campaigns) in areas with varying topography, sediment type and substratum characters. This probably is one of the few deep-sea sites where a seasonal study has been conducted. A large spatial and temporal variability is seen both in the macrofaunaland meiofaunaldensities (Figs.7.4.6 and 7.4.7)with no particular trend. Temporal changes in major groups were also not consistent possibly because of variation in topography, physical properties of sediments and the settling fluxes of organic matter. The changes in faunal densities and diversity that were observed due to the benthic disturbance experiment are well within the range of natural variability on local as well as regional scales. The diversity of

benthic fauna in the IRZ (see Section 5), where the nodule collector test will be carried out, is similar to that commonly found in the entire nodule bearing area in and around the Indian contract area. It is expected that this genetic and biogeographic continuity of fauna would helpthem sustain and recover in the area to be disturbed bynodule collector tests.

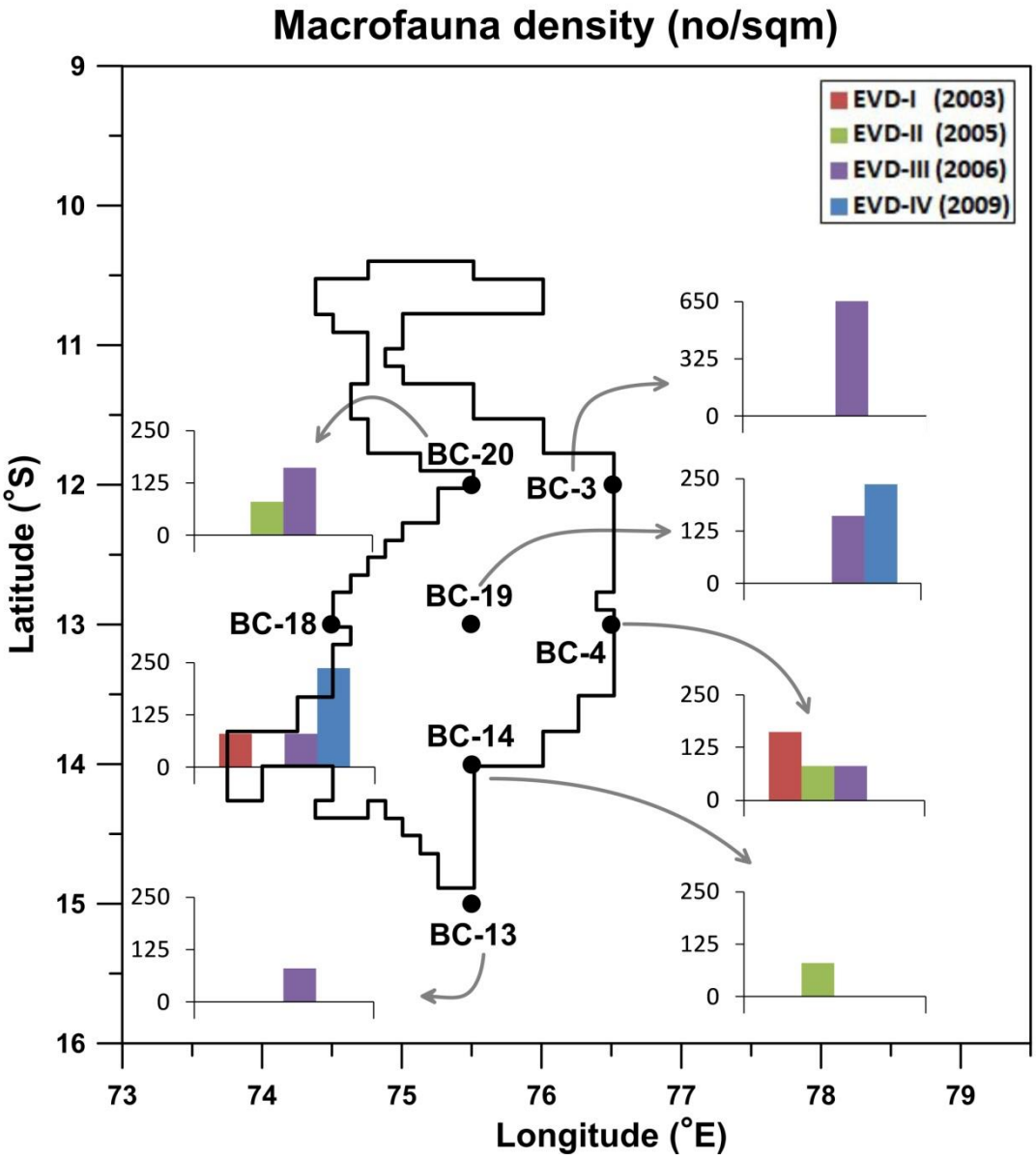

Fig. 7.4.6: Temporal variation in macrobenthic density over a large nodule bearing area in CIOB

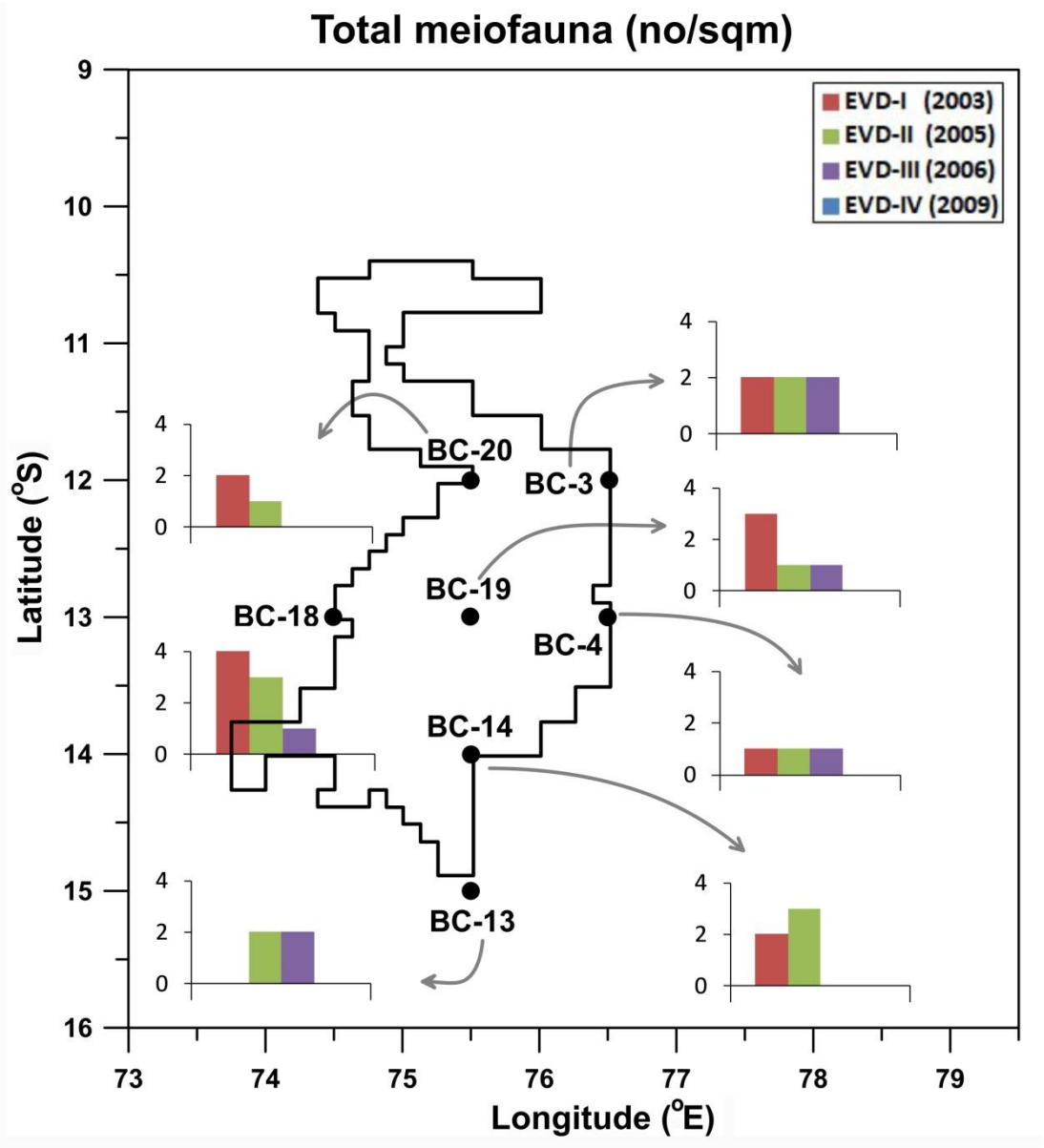

Fig.7.4.7: Temporal variation in meiobenthic density over a large nodule bearing area in CIOB

7.5 Faunal abundance changes related to plume deposition (blanketing)

The removal of topmost sediments in the experimental area and the re-deposition of these sediments after discharge and dispersion to distal areas could lead to the smothering of organisms, the clogging of respiratory or filter-feeding organs of some of the organisms. During the INDEX experiment, an increase in suspended particles of 300% (from 49 to 150 mg m^2 day^{-1}) was observed during the disturbance (Sharma et al., 2001). This value is an average from 10 sediment traps deployed 10m above the seabed around the disturbance site. The effects of this plume were observed to a maximum distance of 250 m from the tracks,

where the disturbed area had dimensions of 3000 x 200m and the discharge at a height of 5-6m above was estimated to be 580 tonnes over a period of 9 days. The area affected by resedimentation during this experiment was mainly south-southwest of the disturbed area which was the direction of prevailing currents during that period. However, the resedimentation effects were not noticed on larger fauna, as increased macrofaunal abundance was observed in the south of the test site after the disturbance (Ingole et al., 2005a). A marginal decrease in meiofaunal abundance (from 35 to 30 nos. 10 cm^{-1}) was seen in the south of disturbance area (Ingole et al., 2005b). In most of the benthic impact experiments, a general reversal, mainly in density of meiofauna, towards control levels over a period of time has been observed (see Jones et al., 2017 for a review). The proposed area to be disturbed during the collector trials is not intended to create large plume as most of the nodules picked up will be discharged at the bottom itself.

7.6 Effects of plume on demersal scavengers and fish

In one of the trials, sediment and crushed nodules are expected to be discharged 50-80m above the seafloor. For the short temporal and low spatial scale of the planned activity, we assume that larger mobile epifaunal organisms and demersal scavengers and fish will move out of the area of impact, as the mobility of nodule collector will be seen as a threat. Resuspension of sediment within disturber-tracks in one of the benthic disturbance experiment has attracted fish as a potentially increased food source was made available, similar to the situation when a dredging takes place.

7.7Effects of toxic discharges on faunal organisms

There are no plans to introduce any chemicals during the planned nodule collector trials. The discharged material will be the fine particles of bottom sediments and crushed nodules which are occurring in the ecosystem itself. A recent article by Hauton et al., (2017) has synthesized the toxic impacts of metals potentially released during deep-sea mining. Of direct relevance to abyssal polymetallic nodule mining is a consistent avoidance behavior in echinoderms presented with copper contaminated sediments reported by Brown et al., (2017). In a 96-h laboratory exposures at 4°C the shallow-water holothurian *Holothuriaforskali* consistently avoided sediments contaminated with copper at concentrations of 5 mg l^{-1} by climbing onto the side of the treatment tank (Brown et al., 2017). These behaviors were also mirrored by the abyssal holothurian *Amperima* sp. exposed to copper-contaminated sediments at a depth of 4,167 m in the Peru Basin (Brown et al., 2017b). And it is pertinent to quote

Hauton et al., (2017) who state that "these data demonstrate that macro- and megafaunal species have the sensory capacity to detect metals in the environment and that, in at least some species, this can result in the expression of avoidance behavior to help protect the organism from toxic effects. Hence, it can be expected that mobile species exposed to contaminated plumes have the potential to demonstrate chronic impacts by moving away from areas of contamination during exploitation".

In summary, the area and duration of expected impact is much less than ($\leq$1%) in terms of area, distance covered, volume and weight of sediment than the benthic impact experiments (BIEs) in the 1990s, where the recovery has taken place over a time period. The maximum area to be impacted by the nodule collector will have an approximate size of 4600 m² which is an extremely small fraction of the seafloor that is normally sampled during any exploration activity conducted for deep-sea minerals. The nodule collector to be deployed is comparable to dragging an epi-benthic sledge over the seafloor and not similar in size or scale to the mining systems involving suction techonologies. Even though some of the faunal communities associated with sediments and nodules might either temporarily migrate or get destroyed, this however is, unlikely to affect the gene flow or connectivity of species due to the small size of the area. Moreover, endemic species of faunal communities associated with nodules have not be observed in the CIOB as most of the faunal groups/species are found in the sediments associated with nodules as well as those without nodules. As compared to other Benthic Impact Experiments (Jones et al., 2017), at the INDEX site, macrofaunal numbers were not significantly different from control samples in either of the post impact studies (30 days and 1395 days), but total numbers of individuals were very low (<6 individuals per sample). INDEX meiofauna increased in density over time, becoming similar to control conditions by1395days (Jones et al., 2017). However, the restoration during the previous benthic disturbance experiment would have taken place before the first monitoring campaign carried out 1395 days after the experiment. Thus, it is envisaged that the benthic ecosystem with low faunal abundances such as that in CIOB, in an experiment which is going to be for a maximum of few hours in a very small area, would restore more quickly than the earlier areas.

8. Plan for environmental impact assessment and monitoring of proposed activity

8.1Environmental data collection

As described in section 3.3 and 3.4, the pre-prototype nodule collector will be tested over a cumulative distance of 1000 m during which seafloor sediment down to 15-30cm depth may be impacted in IRZ. This section describes the plan of work to be carried out to assess the following:

a) Change in geomorphology due to collector trial in the area.
b) Changes in physico-chemical characteristics of seafloor sediment
c) Changes in abundance and diversity of benthic communities and recolonization.
d) Thickness of redeposited sediment due to locomotion and discharge plume
e) Changes in benthic community structure due to smothering by sedimentation.
f) Changes in water column physico-chemical characteristics due to discharge plume.
g) Changes in metals in dominant fauna due to resettled sediments and discharge plume.

8.1.1 Impact assessment of benthic conditions

Analyses of various parameters essential for environmental studies and monitoring will be carried out before, during, and after the collector test.The Impact Reference Zone (IRZ) of 7.5x7.5 nautical miles was selected which corresponds to block no. 109D in the Contract area for the purpose of conducting the nodule collector test. Simultaneously, based on the geological and environmental variability data collected earlier in the area, a Preserved Reference Zone (PRZ) also of same size corresponding to block no. 90B was selected having similar nodule abundances and metal grade to IRZ and also the environmental data over four seasons was collected at locations close to it. The IRZ and PRZ are separated by ~60 nautical miles (Fig. 8.1.3.1). The IRZ will be used to conduct the collector test whereas the PRZ will be used as a reference site in order to study the changes in natural environmental conditions in the contract area.

Baseline benthic conditions in IRZ and PRZ have been studied by collecting environmental data in two cruises during 2015 and 2019 as listed below,

i. Grain size distribution –sand, silt and clay content
ii. Geotechnical properties - water content, shear strength, wet bulk density
iii. Geochemistry of sediment (organic carbon), elemental concentration of key elements (ex. V, Cr, Cu, Ni, Co, Zn, Pb) and pore water(pH, nutrients).

iv. Benthic community structure – Abundance and composition of meiofauna, macrofauna and megafauna.
v. Biochemistry of sediment – Protein, Carbohydrates, lipids to estimatelabile organic matter, Adenosine Triphosphate
vi. Microbiology of sediment - Total bacterial count, Microbial mass and diversity
vii. Bioturbation studies
viii. Molecular biology: Molecular taxonomy identification and diversity/ Gene connectivity.

8.1.2 Impact assessment in water column

Collection of data in the water column is importantfor assessing the influence of the activity on the composition of the water and its impact on ecosystem processes. This is proposed by evaluating the following

i. Chemical – pH, dissolved oxygen, suspended particulate matter, nutrients, metals, dissolved organic matter
ii. Biological – Phytoplankton, primary productivity and zooplankton
iii. Microbiology – Total bacterial count, Adenosine Triphosphate, Microbial mass and diversity, Bacterial productivity
iv. Physical - Variability of temperature, salinity, turbidity

8.1.3 Hydrodynamic studies using deep sea moorings and current meters

For baseline oceanographic data collection from IRZ and PRZ, deployment of three deep sea moorings with sediment traps and current meters (Figure 8.1.3.1) is planned. The configuration for moorings is shown in Fig 8.1.3.2.These moorings will be deployed for a period of 1 year for collection of data on current velocity and direction, and the sediment traps at different depths for estimating biogenic and lithogenic fluxes to the seafloor. . The data will be useful for plume modelling during to collector test as well.

The proposed mooring locations are as follows:

1) Centre of IRZ (13° 33’S, 75° 33’E)
2) Centre of PRZ (12° 56’S, 74° 41’E)
3) North of IRZ (11° 30’S and 75° 30’E)

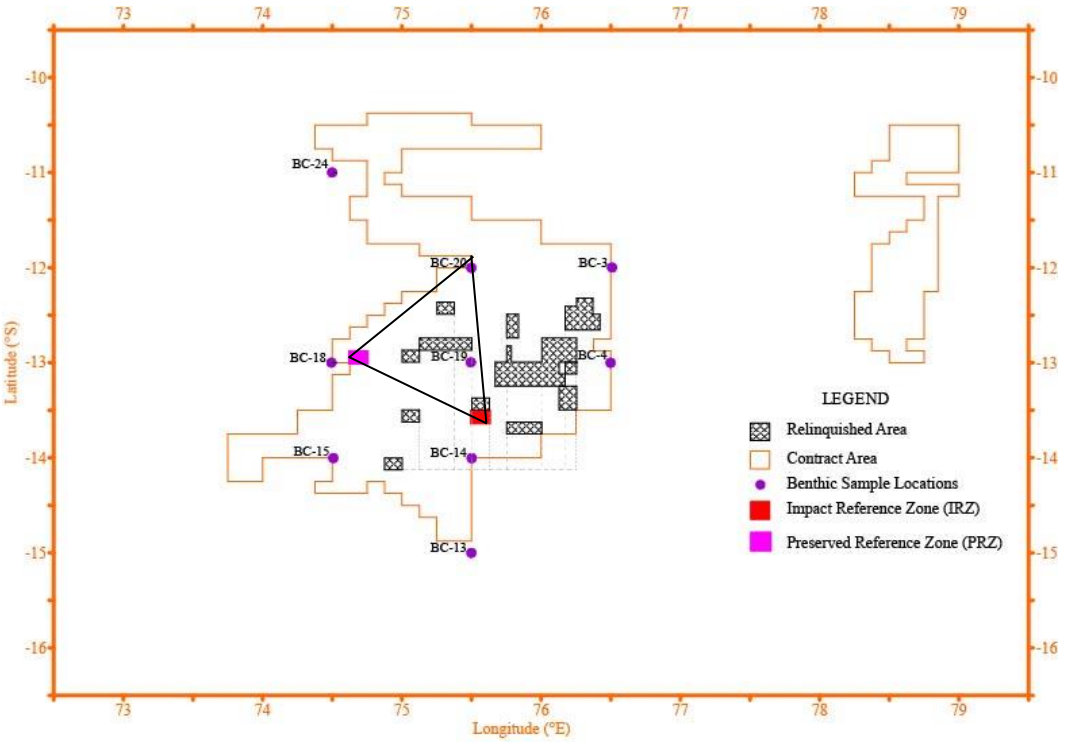

Fig. 8.1.3.1 Proposed locations of deployment of 3 deep sea moorings (Triangle) in the Indian Contract Area

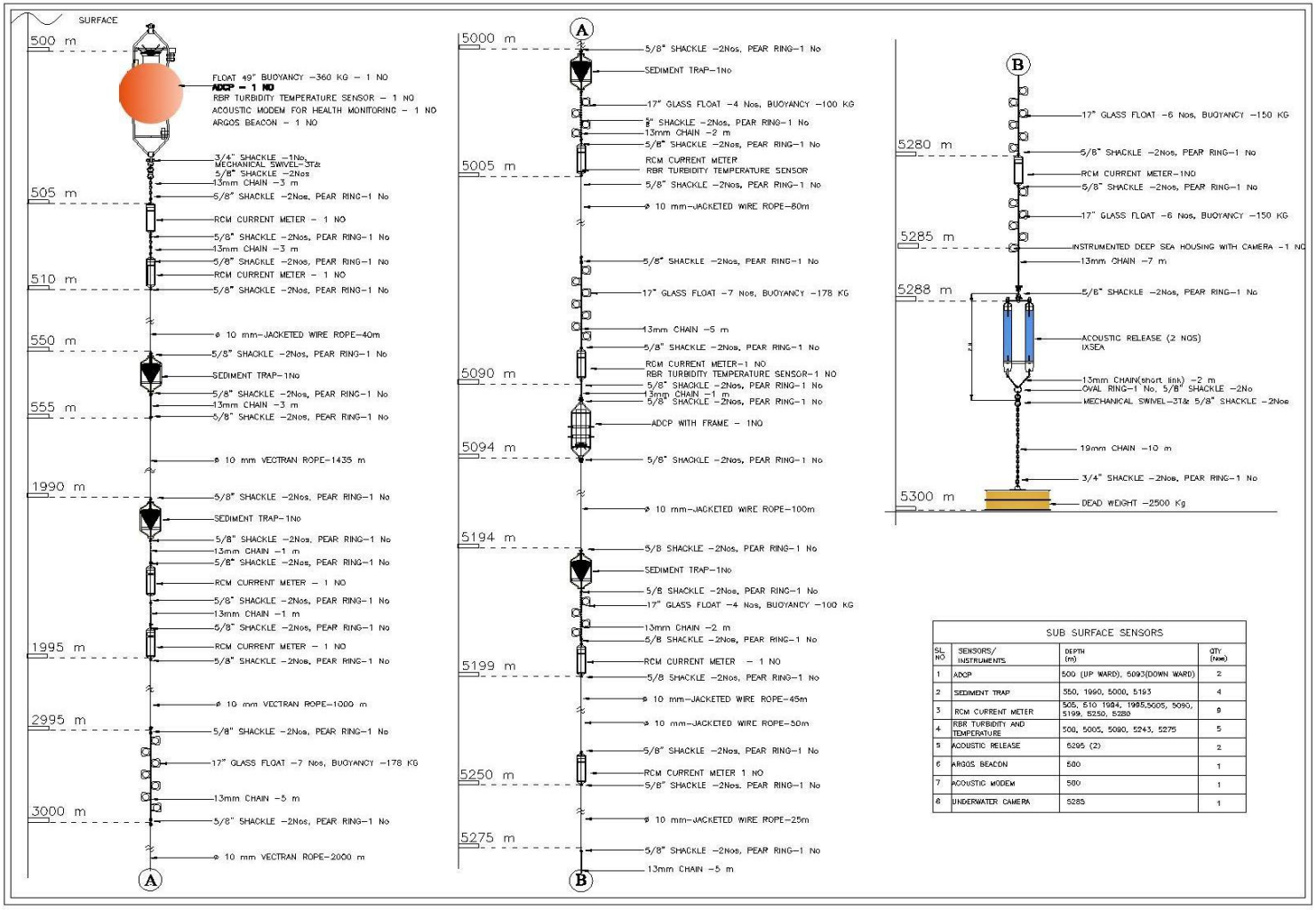

Fig. 8.1.3.2 Configuration of deep sea moorings to be deployed in IRZ and PRZ (Source: NIOT).

8.1.4 Sea surface conditions using satellite imageries

Satellite images from the IRZ and PRZ areas will be used for data analysis of sea surface temperature, chlorophyll and productivity for different seasons.

8.1.5 Seafloor disturbance and restoration using deep tow/AUV/ROV systems

In order to evaluate the seafloor disturbance due to collector movement as well as restoration of environmental conditions and recolonisation in test area, it is planned to carry out deep tow or AUV / ROV surveys in IRZ and PRZ. This high resolution bathymetric data from IRZ and PRZ will be collected in before and after the collector test.The photo images and /or videos from the collector system will be also used to study plume intensity and penetration in sediments.

As the collector test will be carried out in a small area, the navigation using acoustic transponders is proposed to maintain accuracy of positioning during and after the test. About 3-4 transponders will be deployed around area of collector test which will be used for positioning of sediment sampling, mooring, deep tow survey from ship.

8.1.6 Sediment plume dispersion during collector test

About 4-5 short moorings along with sediment trap and current meter (Fig. 8.1.6.1)will be deployed at about 100m above seafloor in and around collector test area in IRZ to study the sediment plume movement. Similarly 1 short mooring with sediment trap and current meter will be deployed in the PRZ to record the natural environmental conditions.

8.2 Impact assessment and monitoring plan

Environmental data collection campaigns will be carried out, before and after the nodule collector trials, at selected locations in IRZ and PRZ to evaluate the impact as well as to monitor the same over a period of time for restoration of the benthic conditions on parameters collected during baseline studies. To monitor the effect of the collector test on water column and seafloor, the data on all parameters as baseline studies will be collected after 1 year from the collector test. This will give an idea about the restoration of impact of disturbance. The water and sediment samples will be collected from 5 locations around the area of collector test in IRZ (Fig. 8.2.1) and at the centre location in PRZ in all phases of the study.

It is expected that due to collector test a sediment plume will be generated,and sediments will be resuspended in the near bottom water column, either from the mining machine or from the slurry discharge locally 80m above the seabed. The likely area to be impacted during collector test, can be visualized from the results of the earlier disturbance experiment carried out in 1997 in the CIB. The sediment trap data showed that the sediment plume moved about 150m to 250m on either side of the disturbance strip. Photographic data showed that the effect of resedimentation is observed within the disturbance site only (i.e. 100m on eitherside). The resedimentation features,however, are observed up to a distance of 200m, andfew up to a distance of 250m on either side, which means that the sediment has travelled up to 150m away from the disturbance site.

Hydrodynamic model was generated to predict the movement of plume dispersal during the disturbance experiment in 1997 for the area that is 3 degrees north of the IRZ. The model predicted that the plume could move about 100m to 500m on either side of the disturbance strip 20 hours (at a height of 10m above seafloor) after the disturbance. The model also predicted that the concentration of suspended matter in plume has reduced exponentially from $1.32e^{-001}$at 500m to $4.1e^{-004}$ at a distance of 3km. The earlier current measurements have shown that the currents are very weak in the abyssal areas which will keep the sediment plume in suspension in a restricted area. Therefore, the monitoring stations are proposed to be occupied within 500m to 1000m on either side of the collector test track.

It is proposed to develop the hydrodynamic model of plume dispersal for the IRZ. This model will be generated using the new data collected from long and short moorings to be deployed in 2020 in IRZ, PRZ, BC20.

A detailed cruise plan for environmental data collection in different phases is also prepared for the purpose (Table 8.2.1).

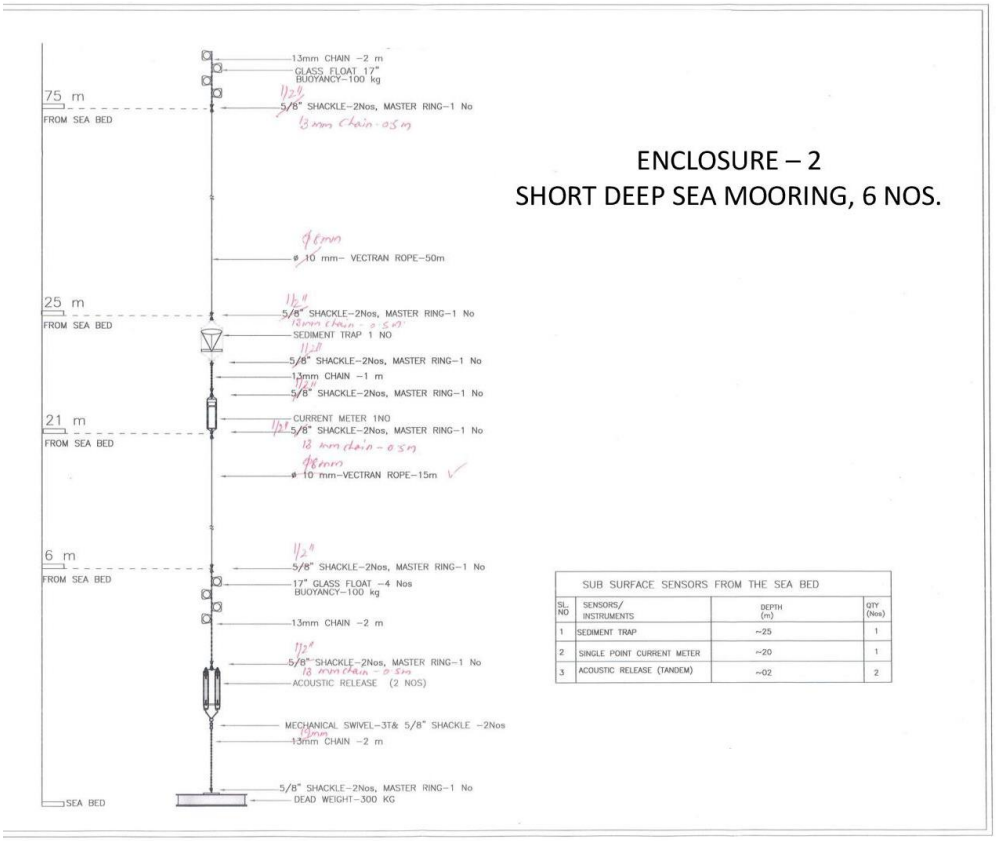

Figure 8.1.6.1: Short mooring configuration to be deployed in the CIOB (Source: NIOT)

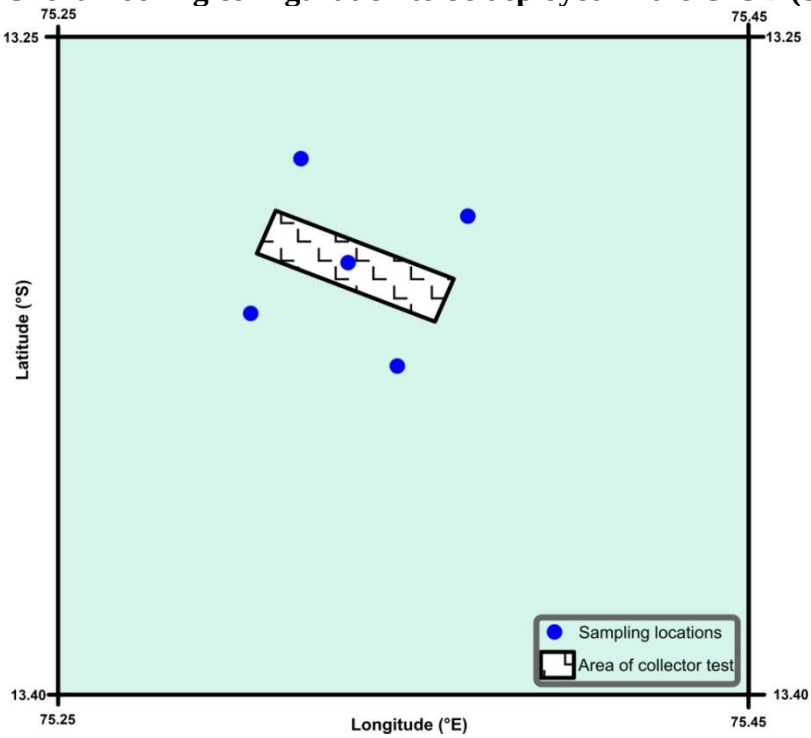

Figure 8.2.1: Schematic diagram of area of collector test (not to scale) in IRZ and sampling locations.

Table 8.2.1 Cruise plans for environmental data collection in different phases

Cruse no.	Purpose	Duration	Remark
1	Baseline data collection in IRZ & PRZ	30 days	Completed in 2015
2	Baseline data collection in IRZ & PRZ (for additional parameters)	30 days	Completed in 2019
3	Deployment of long term moorings in pre-selected locations	30 days	To be conducted in 2020-21
4	Pre collector test environmental data collection and deployment of short moorings in PRZ &IRZ	30 days	To be conducted just before the test
5	Post collector test environmental data collection for impact assessment in PRZ & IRZ and retrieval of short moorings	30 days	To be conducted just after the test
6	Monitoring of restoration of environmental conditions in IRZ and natural conditions in PRZ	30 days	To be conducted after ~1 year of the test

Note: Further observations / cruises will be planned based on the results of the monitoring cruise.

8.3 Reporting, data management and dissemination

The results of the baseline studies, impact assessment and monitoring will be submitted to the Authority through the Annual Reports along with data. The huge data in different scientific disciplines generated out of these studies will be stored on Project's data base. The data will include multibeam bathymetry, sediment and water column characteristics, faunal diversity and microbial parameters. Periodical evaluation of the progress of different activities in the project will be conducted by a high level committee of experts appointed by the Ministry of Earth Science. The results of the study will also be disseminated to the scientific community in the form of conference presentations as well scientific publications in peer reviewed journals.

References

Allen, M.B., 1961. Our knowledge of the kinds of organisms in Pacific phytoplankton In: M.S. Doty (Ed.) Primary productivity measurement, marine and freshwater. IGY World Data Center, Natl., Acad., Sci., Washington, D.C. 58-60.

ASTM 1995. Annual book of ASTM Standards, 04.08 Soil and Rocks (I) D420-D4914, ASTM, Philadelphia, USA, 981.

Babu V. R., Suryanarayana A., Murty V. S. N., 2001. Indian Basin (CIB) during austral summer and winter periods of 1997, Deep Sea Research Part II: Topical Studies in Oceanography, 48, 3327-3342.

Banakar, V.K., Gupta, S.M., Padmavati, V.K., 1991. Abyssal sediment erosion from the Central Indian Basin: Evidence from radiochemical and radiolarian studies. Mar. Geol., 96, 167–173.

Benjamin, M. M. and A. Felmy, 1981. Trace metal exchange between ferromanganese nodules and artificial seawater. Marine Mining 3, 151 – 183.

Bennett, R.H., Lambert, D.N., 1971. Rapid and reliable technique for determining wet density and porosity of deep-sea sediments. Marine Geology, 11, 201-207.

Borole, D.V., 1993. Late pleistocene sedimentation: a case study of the Central Indian Ocean Basin. Deep-Sea Research I 40, 761-775.

Brown, A., Thatje, S., and Hauton, C., 2017a. The effects of temperature and hydrostatic pressure on metal toxicity: insights into toxicity in the deep sea. Environ. Sci. Technol. 51, 10222–10231. doi: 10.1021/acs.est.7b02988.

Brown, A., Wright, R., Mevenkamp, L., and Hauton, C., 2017b. A comparative experimental approach to ecotoxicology in shallow-water and deep-sea holothurians. Aquat. Toxicol. 191, 10–16. doi: 10.1016/j.aquatox.2017.06.028.

Bull, W. B.,1990. Stream-terracgenesis Implications for soildevelopment, Geomorphology 3, 351-367.

Byrne, R.H. and Breland, J.A., 1989. High precision multiwavelength pH determinations in seawater using cresol red. Deep-Sea Res., 36, 803-810.

Chen X. L., 2004. The physical properties of surface sediments in oceanic polymetallic nodule. Donghai Mar Sci 22, 28–33

Cochran, J.R., 1990. Himalayan uplift, sea level, and the record of Bengal Fan sedimentation at the ODP Leg 116 sites, in Cochran, J. R., et al., Proceedings of the Ocean Drilling Program, Scientific results, vol 116: College Station, Texas, Ocean Drilling Program, 397–414.

Curray, J.R., Emmel, F.J., Moore, G.F., Kieckhefer, R.M., 1981. Sediment budget and accretionary prism volume variations around the Sunda Arc.Proc. Symp. on Convergence and Subduction, College Station TX.

Curray, J.R., Munasinghe, T., 1989. Timing of intraplated deformation, Northeastern Indian Ocean, Earth Planet. Sci. Lett., 94, 71-77.

Das, A., Krishnaswami, S., 2007. Elemental geochemistry of river sediments from the Deccan Traps, India: Implications to sources of elements and their mobility during basalt–water interaction. Chem. Geol., 242, 232-254.

Das, B.M., 1998. Principles of geotechnical engineering. PWS Publishing, Boston, 712p.

DeSousa, S.N., Sardessai, S.D., Rameshbabu, V., Murty, V.S.N., Gupta, G.V.M., 2001. Chemical characteristics of Central Indian Basin waters during the southern summer. Deep Sea Res. Part II., 48, 3343–3352.

El-Sayed, S.Z., Taguchi, S., 1979. Phytoplankton standing crop and primary productivity in the Tropical Pacific. Marine Geology and Oceanography of Pacific Manganese Nodule Province, Prenum press, New York and London, 241-286.

Eppley, R., Renger, W.E.H., Venrick, E.L., Mullin, M.M., 1973. A study of plankton dynamics and nutrient cycling in the central gyre of the North Pacific Ocean. Limnol. Oceanogr., 18, 534-551.

Felix, D., 1980. Some Problems in Making Nodule Abundance Estimates from Seafloor Photographs. Marine Mining, 2, 293–302.

Fewkes, R.H., Mcfarland, W.D., Reinhart, W.R., Soram, R.K. 1979. Development of a Reliable Method for Evaluation of Deep Sea Manganese Nodule Deposits. In:Bureau of Mines Open File Report 64-80, US Department of the Interior Bureau of Mines, Washington, DC, pp. 91.

Fieux, M., Andrié, C., Charriaud, E., Ilahude, A.G., Metzl, N., Molcard, R., Swallow, J.C., 1996. Hydrological and chlorofluoromethane measurements of the Indonesian throughflow entering the Indian Ocean. J. Geophys. Res., 101 (C5), 12433–12454.

Fisk, M.R., Duncan, R.A., Baxter, A.N., Greenough, J.D., Hargraves, R.B., Tatsumi, Y., Shipboard Scientific Party, 1989. Reunion hotspot magma chemistry over the past 65 m.y.: Results from Leg 115 of the Ocean Drilling Program. Geology. 17, 934-937.

Folk, R.L., 1968. Petrology of sedimentary rocks. Univ. Texas, Austin, Teaxas, 170.

Fryxell, G.A., Taguchi, S., El-Sayed, S.Z., 1979. Vertical distribution of diverse phytoplankton communities in the central Pacific. Marine Geology and Oceanography of Pacific Manganese Nodule Province, Prenum press, New York and London, 203-239.

Gao A. G., Wang C. S., Yang J. Y., Wang Z. P., He D. H., 2002. Distribution of deep-sea meiobenthos of the eastern and western portions of the COMRA's Pioneer area. Donghai Mar Sci., 20, 28–35.

Glasby, G.P., Mountain, B., Vineesh, T.C., Banakar, V., Rajani, R., Xiangwen, R., 2010. Role of Hydrology in the formation of Co-rich Mn Crusts from the Equatorial N Pacific, Equatorial S Indian Ocean and the NE Atlantic Ocean. Resource Geology, 60, 165-177.

Gordon, R.G., DeMets, C., Royer, J.–Y., 1998. Evidence for long–term diffuse deformation of the lithosphere of the equatorial Indian Ocean. Nature 395, 370–374, doi: 10.1038/26463.

Grass, H., Jost, V., Ramesh Kumar, M.R., Schulz, J., Bauer, P., Schluessel, P., 2000. The Hamburg Ocean Atmospheric Parameters and Fluxes from Satellite Data (HOAPS): A climatological ATLAS of satellite derived air- sea interaction parameters over the oceans. Max Planck Report. No. 312, 130pp.

Grasshoff, K., Ehrhardt, M., Kremling, K., 1983. Methods of Sea water Analysis, 2nd edtn, Verlag Chemie, Weinheim.

Hasle, G.R., 1959. A quantitative study of phytoplankton from the equatorial Pacific. Deep-Sea Research, 6, 38-59.

Hauton, C., Brown, A., Thatje, S., Mestre, N.C., Bebianno, M.J., Martins, I. Bettencourt, R., Canals, M., Sanchez-Vidal, A., Shillito, B., Ravaux, J., Zbinden, M., Duperron, S. Mevenkamp, L., Vanreusel, A., Gambi, C., Dell'Anno, A., Danovaro, R., Gunn, V., Weaver P., 2017. Identifying toxic impacts of metals potentially released during deep-sea mining—a synthesis of the challenges to quantifying risk,Front. Mar. Sci., 4.

Hogben, N, Lumb, F.E., 1967. Ocean Wave Statistics, National Physical Laboratory, London, D.R.Hillman and Sons Ltd., Frome., 263.

Holmes, R.W., 1961. Summary of productivity measurements in the southeastern pacific ocean, In: M.S. Doty(Ed.), Primary productivity measurement :Marine and Freshwater IGY World data center, Natl. Acad. Sci., Washington, D.C., 18-57.

Ingole B. S., Ansari Z. A., Matondkar S. G. P., et al, 1999. Immediate response of meio and macrobenthos to disturbance caused by a benthic disturber. Proceedings of the Third ISOPE OceanMining Symposium., 191–197.

Ingole B. S., Ansari Z. A., Rathod V., Rodrigues N., 2000. Response of meiofauna to immediate benthic disturbance in the Central Indian Ocean Basin. Mar Georesour Geotechnol, 18, 263–272.

Ingole, B., Ansari, Z.A., Rathod, V., Rodrigues, N., 2001. Response of deep-sea macrobenthos to a small-scale environmental disturbance. Deep-Sea Research II,48, 3401–3410.

Ingole B.S., 2003. Macrobenthic abundance in the vicinity of spreading ridge environment in Central Indian Ocean. Current Science, 85, 328-333.

Ingole, B. S., Pavithran, S., and Ansari Z. A., 2005a. Restoration of Deep-Sea Macrofauna after Simulated Benthic Disturbance in the Central Indian Basin, Mar. Georesources and Geotechnology, 23, 267–288.

Ingole, B. S., Goltekar, R., Gonsalves, S. and Ansari, Z. A., 2005b. Recovery of Deep-sea Meiofauna after Artificial Disturbance in the Central Indian Basin, Marine Georesources and Geotechnology, 23, 253–266.

Iyer, S.D., Sudhakar, M., 1993. A new report on the occurance of zeolitites in the abyssal depth of the Central Indian Ocean Basin. Sediment. Geol., 84, 169–178.

Jamart, B.M., Winter, D.F., Banse, G.C.A., Lam, R.K., 1977. A theoretical study of phytoplankton growth and nutrient distribution in the Pacific Ocean off the north-western U.S. Coast. Deep-Sea Research, 24., 753-773.

Jauhari, P., Pattan, J.N., 2000. Ferromanganese nodules from the Central Indian Ocean Basin, in Cronan, D.S., ed., Handbook of marine mineral deposits: Boca Raton, FL, CRC Press, p. 171–195.

Jones, D.O.B., Kaiser, S., Sweetman, A.K., Smith, C.R., Menot, L., Vink, A., et al., 2017. Biological responses to disturbance from simulated deep-sea polymetallic nodulemining. PLoS ONE, 12(2).

Kamesh Raju, K.A., Ramprasad, T., 1989. Magnetic lineation in the Central Indian Basin for the period A24–A21: A study in relation to the Indian Ocean Triple Junction. Earth Planet. Sci. Lett., 95, 395–402.

Kamesh Raju, K.A., 1990. Magnetic and bathymetric studies in the vicinity of the 73oE fracture zone, Central Indian Basin. Mar. Geol., 95, 147–153.

Kamesh Raju, K.A., 1993. Magnetic lineation, fracture zones and seamounts in the Central Indian Ocean Basin. Mar. Geol., 109, 195–201.

Kessarkar, P.M., 1998. Tectonic reorganization in the Indian Ocean: Evidences from seafloor crenulations. Curr. Sci., 74, 472–476.

Khadge, N.H., 2005. Changes in the geotechnical properties of sediments from the Central Indian Basin induced by disturbance experiment. Marine Georesources and Geotechnology, 23, 401-417.

Khadge, N.H., 2008. Geotechnical properties of sediments. In: Benthic environmental variability in the CIOB Report. MOES (DOD), New Delhi, pp 66-76.

Khadge, N.H., 2015. Sedimentology and geotechnical properties of sediments. In Comprehensive report on baseline environmental conditions in the area retained by India for nodule mining in the CIB. MoES, New Delhi, pp 16-59.

Khadge, N.H., Shirodker, P., 2018. Grain size analysis and geotechnical properties of sediments. In Baseline environmental conditions in IRZ and PRZ in the CIOB. MoES, report New Delhi, 32-55.

Kodagali, V.N., 1991. Morphologic investigations of `uncharted' seamount from the Central Indian Ocean Basin revisited with multibeam sonar system Mar. Geod., 15, 47-56

Kodagali, V.N., 1995. Influence of bathymetry in manganese nodule pilot mine site selection: A case study from the Central Indian Basin, in Yamazaki, T., Aso, K., Okano, Y., Tsurusaki, K., eds., Proceedings, the First (1995) ISOPE Ocean Mining Symposium: ISOPE Ocean Mining Symposium, Tsukuba, Japan., 99–104.

Kolla, V., Hendersaon, L., Biscaye, P.E., 1976. Clay mineralogy and sedimentation in the western Indian Ocean. Deep-Sea Research, 23, 949-961.

Koppelmann, R., and H. Weikert. 1992. Full-depth zooplankton profiles over the deep bathyal of the NE Atlantic. Mar. Ecol. Prog. Ser. 86, 263–272.

Krey, J., 1973. Primary production in the Indian Ocean. In : the Biology of the Indian Ocean, B. Eitzschel, editor, Springer-Verlag, Berlin,115-126.

Krey, J., Babenerd, B., 1976. Phytoplankton production atlas of the International Indian Ocean Expedition, Institute Meereskunde, Kiel,70.

Krishna, K.S., Ramana, M.V., Gopala Rao, D., Murthy, K.S.R., Malleswara Rao, M.M., Subrahmanyam, V., Sarma, K.V.L.N.S., 1998. Periodic deformation of oceanic crust in the central Indian Ocean. J. Geophy. Res., 103, 17,859–17,875.

Krishna, K.S., Bull, J.M., Scrutton, R.A., 2001. Evidence for multiphase folding of the central Indian Ocean lithosphere. Geol., 29, 715–718.

Krishna, K.S., 2003. Structure and evolution of the Afanasy Nikitin seamount, buried hills and 85°E Ridge in the northeastern Indian Ocean. Earth Planet. Sci. Lett., 209, 379–394.

Linsy, P., Nath, B.N., Mascarenhas-Pereira, M.B.L., Teena Chauhan., Tyson Sebastian, C., Prakash Babu., Kurian, S., Miriyala, P., Armoury Kazip., Borole, D.V., Khadge, N.H., 2018. Distribution and Diagenesis of Phosphorus in the Deep-Sea Sediments of the Central Indian Basin. JGR 123, 7963-7982.

Malone, T.C., 1971. The relative importance of netplankton and nanoplankton as primary production in neric and oceanic tropical waters. Limnol. Oceanogr., 26, 633-639.

Mascarenhas–Pereira, M.B.L., Nath, B.N., Borole, D.V., Gupta, S.M., 2006. Nature, source and composition of volcanic ash in sediments from a fracture zone trace of Rodriguez Triple Junction in the Central Indian Basin. Mar. Geol., 229, 79–90.

Mascarenhas–Pereira, M.B.L., Nath, B.N., 2010. Selective leaching studies of sediments from a seamount flank in the Central Indian Basin: Resolving hydrothermal, volcanogenic and terrigenous sources using major, trace and rare–earth elements. Marine Chemistry doi: 10.1016/j.marchem.2010.03.004.

Mascarenhas-Pereira, M.B.L., Nath, B.N., Iyer, S.D., Borole, D.V., Parthiban, G., Jijin, R., Khedekar, V.D., 2016. Multiple ash layers in late Quaternary sediments from the Central Indian Basin. J. Volcanol. Geotherm. Res., 316, 85-100.

Matondkar, S.G.P., Nair, K.K.C., Ansari, Z.A., 2005, Biological characteristics of Central Indian Basin waters during the southern summer. Marine Georesources and Geotechnology, 23, 299-314.

McKenzie, D.P., Sclater, J.G., 1971. Evolution of Indian Ocean since Late Cretaceous. Geophy. J. R. Astron. Soc., 25, 437–528.

Miljutina, M. A., Miljutin, D. M., Mahatma, R., and Galerón, J., 2010. Deep-sea nematode assemblages of the Clarion-Clipperton Nodule Province (Tropical North-Eastern Pacific), Mar. Biodivers., 40, 1-15.

Miljutin, D.M., Miljutina, M.A., Arbizu, P.M., GaleronJ., 2011.Deep-sea nematode assemblage has not recovered 26 years after experimental mining of polymetallic nodules (Clarion-Clipperton Fracture Zone, Tropical Eastern Pacific) Deep-Sea Res. Part I, 58, 885-897.

Miller, A., Thompson, K. F., Johnston, P., and Santillo, D., 2018, Overview of Seabed Mining Including the Current State of Development, Environmental Impacts, and Knowledge Gaps, Front. Mar. Sci., 17, 237–251.

Mukhopadhyay, R., Khadge, N.H., 1990. Seamounts in the Central Indian Ocean Basin: indicators of the Indian plate movement. Proc. Indian Acad. Sci. (Earth Planet. Sci.), 99, 357–365.

Mukhopadhyay, R., Batiza, R., 1994. Basinal seamounts and seamount chains of the Central Indian Ocean: probable near axis origin from a fast spreading ridge. Mar. Geophys. Res., 16, 303–314.

Mukhopadhyay, R., Batiza, R., Iyer, S.D., 1995. Petrology of seamounts in the Central Indian Ocean Basin: Evidence for near-axis origin: Geo-Marine Letters, 15, 2, 106–110.

Mukhopadhyay, R., George, P., Ranade, G., 1997. Spreading rate dependent seafloor deformation in response to India–Eurasia collision: results of a hydrosweep survey in the Central Indian Ocean Basin. Mar. Geol., 140, 219–229.

Mukhopadhyay, R., Iyer, S.D., Ghosh, A.K., 2002, The Indian Ocean Nodule Field: Petrotectonic evolution and ferromanganese deposits. Earth Science Review, 60, 67-130.

Murphy, J., and Riley, J. P., 1962. A modified single solution method for determination of phosphate in natural waters. Anal. Chim. Acta. 27, 31-36.

Murty, V.S.N., Babu, V.R., Rao, A.S., Beena, B.S., 1999. Current structure and kinetic energy of the abyssal waters in the central Indian Ocean basin. Proceedings of the Third 1999 Ocean Mining Symposium, Goa, India, November 8–10, 216–223.

Murty, V.S.N., Savin, M., RameshBabu, V., Suryanarayana, A., 2001. Seasonal variability in the vertical current structure and kinetic energy in the Central Indian Ocean Basin. Deep-Sea Res. (II: Top. Stud. Oceanogr.), 48(16), 3309-3326.

Nath, B.N., Iyer, S.D., 1989. Basalt microlapilli in deep sea sediments of Indian Ocean in the vicinity of Vityaz fracture zone J. Geol. Soc. India., 34, 303-309.

Nath, B.N., Mudholkar, R.V., 1989. Early diagenesis processes affecting nutrients in the pore waters of the central Indian Ocean cores. Mar. Geol., 86, 57-66.

Nath, B.N., Rao, V.P.C., Becker, K.P., 1989. Geochemical evidence of terrigenous influence in deep–sea sediments up to 8^{o} S in the Central Indian Basin. Mar. Geol., 87, 301–313.

Nath, B.N., Roelandts, I., Sudhakar, M., Plueger, W.L., 1992. Rare earth element patterns of the Central Indian Basin sediments related to their lithology. Geophys. Res. Letts., 19, 1197–1200.

Nath, B.N., Balaram, V., Sudhakar, M., and Pluger, W.L., 1992, Rare earth element geochemistry of ferromanganese deposits of the Indian Ocean. Marine Chemistry, 38, 185–208.

Nath, B. N., Gupta, S. M., Mislankar, P. G., Rao, B. R., Parthiban, G., Roelandts, I., Patil, S. K., 2005. Evidence of Himalayan erosional event at approx. 0.5 Ma from a sediment core from the equatorial Indian Ocean in the vicinity of ODP Leg 116 sites. Deep–Sea Res. II., 52, 2061–2077.

Nath, B.N., Borole, D.V., Aldahan, A., Patil, S.K., Mascarenhas–Pereira, M.B.L., Possnert, G., Ericsson, T., Ramaswamy, V., Gupta, S.M., 2008. ^{210}Pb, ^{230}Th, and ^{10}Be in Central Indian Basin seamount sediments: Signatures of degassing and hydrothermal alteration of recent origin, Geophys. Res. Lett., 35, L09603, doi:10.1029/2008GL033849.

Nath, B. N., Khadge, N. H., Nabar, S., Raghukumar, C., Ingole, B. S., Valsangkar, A. B., Sharma, R., Srinivas, K., 2012. Monitoring the sedimentary carbon in an artificially disturbed deep–sea sedimentary environment. Environmental Monitoring Assessment 184, 2829–2844.

Noorany, I., 1985. Shear strength properties of some deep-sea pelagic sediment In: Strength testing of marine sediments: Laboratory and in situ measurements, R.C. Chaney and K.R. Demars (Editors) ASTM STP 883, 251-257.

Oebius, H.U., Becker, H.J., Rolinski, S. & Jankowski, J. (2001)Parametrization and evaluation of marine environmental impactsproduced by deep-sea manganese nodule mining. Deep-SeaResearch II 48: 3453–3467.

Patriat, P., 1987. Reconstitution de I'&olution du systeme de dorsales de I'Gcean Indien par les methodes de la Cidmatique des Plaques. Terres Aust. Antarct. Fr. (Mission Rech.), Paris, 308.

Patriat, P., Stgoufin, J., 1988. Reconstruction of the Central Indian Ocean. In: Scotese, C. R., Sager, W. W. (Eds.), Mesozoic and Cenozoic Plate Reconstructions. Tectonophysics, 155, 211–234.

Pattan, J.N., Gupta, S.M., Mudholkar, A.V., Parthiban, G., 1992. Biogenic silica in space and time in sediments of Central Indian Ocean. Ind. J. Mar. Sci.,21, 116–120.

Pavithran S., Ingole B.S., Nanajkar M., Nath B.N. (2007) Macrofaunal diversity in the Central Indian Ocean Basin. Biodiversity, 8, 11–16.

Pavithran, S., Ingole, B.S., Nanajkar, M., Raghukumar, C., Nath, B.N., Valsangkar, A.B., 2009. Composition of macrofauna from the Central Indian Ocean Basin. Journal of Earth System Science, 118 (6), 689-700.

Popper, A. R., Fewtrell, J., Smith, M. E., & McCauley, R. D. (2003). Anthropogenic sound: Effects on the behaviour and physiology of fishes. Marine Technology Society Journal, 37(4), 35–40.

Radziejewska, T., Modlitba, I., 1999. Vertical distribution of meiobenthos in relation to geotechnical properties of deep-sea sediment in the IOM Pioneer Area (Clarian-Clipperton Fracture Zone, NE Pacific). Proceedings of the third IOSOPE Ocean Mining Symposium, Goa, India, 126-130.

Radziejewska, T., 2002. Responses of Deep-Sea Meiobenthic Communities to Sediment Disturbance Simulating Effects of Polymetallic Nodule Mining. Int. Rev. Hydrobiol.

Raghukumar, C., Loka Bharathi, P.A., Ansari, Z.A., Nair, S., Ingole, B., Sheelu, G., Mohandass, C., Nagender Nath, B., Rodrigues N., 2001. Bacterial standing stock,meiofauna and

sediment–nutrient characteristics: indicators of benthic disturbance in the Central Indian Basin. Deep-Sea Research II 48, 3381–3399.

Ramana, M.V., Subrahmanyam, V., Krishna, K.S., Chaubey, A.K., Sarma, K.V.L.N.S., Murty, G.P.S., Mittal, G.S., Drolia, R.K., 1994. Magnetic studies in the northern Bay of Bengal. Mar. Geophys. Res., 16(3), 237-242.

Ramesh Babu, V., Suryanarayana, A., Murthy, V.S.N. 2001. Thermohaline circulation in the central Indian basin (CIOB) during austral summer and winter periods of 1997. Deep-Sea Research I, 48:3327-3342.

Rao, V.P., Nath, B.N., 1988. Nature, distribution and origin of clay minerals in grain size fractions of sediments from manganese nodule field, Central Indian Ocean Basin. Indian J. Mar. Sci., 17, 202-207.

Rao, V.K., Chandrasekhar, K., Murty V.S.N., 2016. Analysis of Sea Surface Temperature, Surface Winds, Surface Currents and Sea Surface Height and in the Southern Tropical Indian Ocean during 2010 – 2012. MSc Dissertation, Andhra University, Visakhapatnam, 58

Renaud-Mornant, J. and Gourbault, N., 1990. Evaluation of abyssal meiobenthos in the eastern central Pacific (Clarion-Clipperton fracture zone), Progress in Oceanography 24, 317-329.

Richardson, M.D., Briggs, K.B., Young, D.K., 1985. Effects of biological activity by abyssal benthic macroinvertebrates on sedimentary structures in the Venenzuela Basin. Marine Geology, 68, 243-267.

Roden, A.A., Jago C.F., Jones, S.E., 1998. Influence of benthic macrofauna on the geotechnical and geophysical properties of surficial sediments, North Sea. Continental Shelf Research, 18, 1347-1363.

Royer, J.Y., Patriat, P., Bergh, H.W., Scotese, C.R., 1988. Evolution of the Southwest Indian Ridge from the Late Cretaceous (anomaly 34) to the Middle Eocene (anomaly 20). Tectonophysics 155, 235–260.

Royer, J.–Y., Gordon, R.G., 1997. The motion and boundary between the Capricorn and Australian plates. Science 277, 1268–1274.

Ryther, J.H., 1969. Photosynthesis and fish production in the sea. Science, 166:72-76.

Sagar, K.N.V., Murty, V.S.N., 2016. Variability of Currents and Temperature in the Central Indian Ocean Basin of the Southern Tropical Indian Ocean during May 2011- August 2012. MSc Dissertation, Andhra University, Visakhapatnam, 90

Schriever G., Thiel H., 2013. Tailings and their disposal in deep-sea mining. In: Proceedings of the 10th (2013) ISOPE ocean mining and gas hydrates symposium. Szczecin, Poland, 5–17.

Sclater, J.G., Detrick, R., 1973. Elevation ofmid-ocean ridges and the basement age of Joides deep sea drilling sites. Geol. Soc.Amer. Bull., 84, 1547-1554,

Sclater, J.G., Fisher, R.L., 1974. The evolution of the East Central Indian Ocean with emphasis on the tectonic setting of the Ninety East Ridge. Geol. Soc. Am. Bull., 85, 681–702.

Sclater, J.G., Luyendyk, B.P., Meinke, L., 1976. Magnetic lineations in the southern part of the Central Indian Basin. Geological Society of American Bulletin, 87, 371- 378.

Sclater, J.G., Ritter, U., Hilton, W., Meinke, L., Fisher, R.L., 1971. Charts of residual magnetic field plotted along track for the Indian Ocean. Scripps Institute of Oceanography, Special Report. No. 71–77.

Segoufin, J., Patriat, P., 1981. Reconstructions del'océan Indian occidental pour les époques des anomalies M21, m2 et 34, paléoposition de Madagascar. Bulletin of Geological Society, France, 23, 603-607.

Sharma, R. and Nath, B. N., 2000. Selection of test and reference areas for the Indian Deepsea Environmental Experiment (INDEX). Marine Georesources & Geotechnology 18, 177-187.

Sharma, R., B. N. Nath, G. Parthiban, and S. Jaisankar. 2001. Sediment redistribution duringsimulated benthic disturbance and its implications on deep-sea bed mining.Deep-seaResearch, 48, 3363–3380

Sharma, R., Khadge, N.H., Jai Shankar, S., 2013. Assessing the distribution and abundance of seabed minerals from seafloor photographic data in the Central Indian Ocean Basin, International journal of remote sensing, 34, 1691-1706.

Sharma, R., 2019.Environmental factors for design and operation of deep-sea mining system. In: Sharma, R. (Ed.) Deep-sea mining and environment – impacts, consequences and management. Springer International Publishers AG (In press).

Sherman A. D., and Smith, K. 2009, Deep-sea benthic boundary layer communities and food supply: A long-term monitoring strategy. Jr., Deep Sea Res., Part II, 2009, 56, 1754–1762.

ShyamPrasad, M., 2005. Exploration for nodules in the Central Indian Ocean Basin: Past present and the future. Eds. by: Anand, S.; Sanjay, K. (Natl. Semin. on Polymetallic Nodules (PMN 2005); Regional Research Laboratory, Bhubaneswar, Orissa; India; 29-30 Sep 2005). 22-25

Singh, R., Ingole, B.S., 2016. Structure and function of nematode communities across the Indian western continental margin and its oxygen minimum zone. Biogeosciences 13, 191–209.

Singh, R., Sautya, S., Ingole, B.S., 2018. The community structure of the deep-sea nematode community associated with polymetallic nodules in the Central Indian Ocean. Deep-Sea Res., Part II, 161, 16-28.

Small, C., 1998. Global systematics of mid-ocean ridge morphology. In: Faulting and Magmatism at Mid-Ocean Ridges. Buck, W.G., Delaney, P.T., Karson, J.A., Lagabrielle, Y., (Editors), American Geophysical Union, Washington, DC, 12–25.

Smith, C.R., De Leo, F.C., Bernardino, A.F., Sweetman, A., 2008a. Abyssal food limitation, ecosystem structure and climate change. Trends in Ecology and Evolution, doi: 10.1016/j.tree.2008.05.002

Soetaert, K., Vanaverbeke, J., Heip, C., Herman, P. M. J., Middelburg, J. J., Sandee, A. and Duineveld,G., 1997. Nematode distribution in ocean margin sediments of the GobanSpur (Northeast Atlantic) in relation to sediment geochemistry.Deep-Sea Research, 44, v1671–1683.

Tapscott, C., Patriat, P., Fisher, R.L., Sclater, J.G., Hoskins, H., Parsons, B., 1980. The lndian Ocean Triple Junction. J. Geophys. Res., 85, 4723–4739.

Toole, J.M., Warren, B.A., 1993. A hydrographic section across the subtropical South Indian Ocean. Deep–Sea Res. I., 40, 1973–2019.

Tyler, P.A., 1988. Seasonality in the deep sea. Oceanography and Marine Biology: An Annual Review26, 227–258.

Valsangkar, A.B., Khadge, N.H., 1989. Size analyses and geochemistry of ferromanganese nodules from the Central Indian Ocean Basin. Marine Mining, 8, 3, 325–347.

Valsangkar, A. B., Ambre, N. V., & Rodrigues, M, 1999. Sedimentological impacts of INDEX experiment. In Proceedings of the third ISOPE-ocean mining symposium (pp. 131–137). Goa, India.

Valsangkar, A.B., 2011. Spatial distribution and longitudinal variation of clay minerals in the Central Indian Basin. Act. Geologica Sinica, 85, 814-825.

Vanreusel, A., N. Cosson-sarradin, A. J. Gooday, G. L. J. Paterson, J. Galeron, M. Sibuet,and M. Vinex., 2001. Evidence for episodic recruitment in a small opheliid polychaete spe-cies from the abyssal NE Atlantic.Progress in Oceanography50: 285–301.

Vanreusel, A., Hilario, A., Ribeiro, P. A., Menot, L., Martinez Arbizu, P., 2016.Threatened by mining, polymetallic nodules are required to preserve abyssal epifauna, Sci. Rep. 6.

Veillette, J., Sarrazin, J., Gooday, A.J., Galéron, J., Caprais, J.-C., Vangriesheim, A., Etoubleau, J., Christian, J.R., Juniper, S.K., 2007a. Ferromanganese nodule fauna in the Tropical North Pacific Ocean: species richness, faunal cover and spatial distribution. Deep-Sea Research I, 54, 1912–1935.

Veillette, J., Juniper, S.K., Gooday, A.J., Sarrazin, J., 2007b. Influence of surface texture and microhabitat heterogeneity in structuring nodule faunal communities. Deep-Sea Research I, 54, 1936–1943.

Vineesh, T.C., Nath, B.N., Banerjee, R., Jaisankar, S., Lekshmi, V., 2009. Manganese Nodule Morphology as Indicators for Oceanic Processes in the Central Indian Basin. International Geology Review, 51, 27–44.

Wang X. G., Zhou Y. D., Zhang D. S., Hong L. S., Wang C. S., 2013. A study of meiofauna in the COMRA's contracted area during the summer of 2005. Acta Ecol Sin 33, 492–500.

Warren, B.A., 1981a. Trans–Indian hydrographic section at latitude 18°S: property distributions and circulations in the South Indian Ocean. Deep–Sea Res., 28, 759–788.

Warren, B.A., 1981b. The shallow oxygen minimum of the South Indian Ocean. Deep–Sea Res., 28, 859–864.

Warren, B.A., 1982. The deep water of the Central Indian Basin. J. Mar. Res., 40 (Supplement), 823–860.

Weaver, P., Billet, D. 2019. Environmental impacts of nodule, crust and sulphide mining. In: Sharma, R. (Ed.) Deep-sea mining and environment – impacts, consequences and management. Springer International Publishers AG, 27-62.

Weissel, J.K., Anderson, R.N., Geller, C.A., 1980. Deformation of the Indo–Australian plate. Nature 287, 284–291.

Yatheesh, V., Bhattacharya, G.C., Mahender, K., 2006. The terrace like feature in the mid-continental slope region off Trivandrum and a plausible model for India Madagascar juxtaposition in immediate pre-drift scenario. Gondwana Research, 10, 179-185.

Zeng, Q., Huang D., Lin, R., Wang., 2018. Deep-sea metazoan Meiofauna from a Polymetallic nodule area in the Central Indian Ocean Basin, Mar Biodiv., 48, 395–405.

Zeppilli, D., Pusceddu ,A., Trincardi, F., Danovaro, R., 2016. Seafloor heterogeneity influences the biodiversity–ecosystem functioning relationships in the deep sea. Scientific Reports, 6, 26352.